



CONFERENCE PROCEEDINGS



UGC Sponsored
National Conference on

Recent Advancements in Science and Technology

VOLUME II : Physics



:: Organized by ::

Vidya Bharati Shaikshanik Mandal's

Vidya Bharati Mahavidyalaya, Amravati

Re-accredited with Grade 'A' by the NAAC (CGPA 3.23 - Third Cycle)
College with Potential for Excellence (CPE Status Thrice by the UGC)
Star College Status by DBT, New Delhi, Mentor College under Paramarsh by UGC
Identified as Lead College by S.G.B. Amravati University, Amravati

:: In Collaboration with ::

S.S.S.K.R. Innani Mahavidyalaya

Karanja (Lad), Dist. Washim 444105 (M.S.), India
NAAC Re-Accredited 'A+' Grade (CGPA 3.28)
C.P.E. Status Awarded by UGC, New Delhi
Affiliated to Sant Gadge Baba Amravati University, Amravati

ISBN : 978-81-19931-25-5



CONFERENCE PROCEEDINGS



UGC Sponsored
National Conference on

Recent Advancements in Science and Technology

VOLUME II : Physics



:: Organized by ::

Vidya Bharati Shaikshanik Mandal's

Vidya Bharati Mahavidyalaya, Amravati

Re-accredited with Grade 'A' by the NAAC (CGPA 3.23 - Third Cycle)
College with Potential for Excellence (CPE Status Thrice by the UGC)
Star College Status by DBT, New Delhi, Mentor College under Paramarsh by UGC
Identified as Lead College by S.G.B. Amravati University, Amravati

:: In Collaboration with ::

S.S.S.K.R. Innani Mahavidyalaya

Karanja (Lad), Dist. Washim 444105 (M.S.), India
NAAC Re-Accredited 'A+' Grade (CGPA 3.28)
C.P.E. Status Awarded by UGC, New Delhi
Affiliated to Sant Gadge Baba Amravati University, Amravati

SAI JYOTI PUBLICATION, NAGPUR

UGC Sponsored
National Conference on

Recent Advancements in Science and Technology

VOLUME II : Physics

Chief Editor

Dr. Pradnya S. Yenkar

Principal, Vidya Bharati Mahavidyalaya, Amravati

ISBN : 978-81-19931-25-5

Date : 10th Feb., 2024

Publisher :

Sai Jyoti Publication

Itwari, Nagpur

E-mail : sjp10ng@gmail.com

Type Setting & Printing

LASER POINT,

Gadge Nagar, Amravati

No part of this book shall be reproduced, stored in retrieval system, or translated in any form or by any means, electronic, mechanical, photocopying and/or otherwise without the prior written permission of the publishers.

• **Disclaimer :**

- The publishers, The Principal, Vidyabharti Mahavidyalaya, Amravati and the organizers are not responsible for the content of any of the research paper/article published in this conference proceedings.
- The authors/Co-authors are responsible for the plagiarism
- For any conflict of interests, the Author/Co-Authors are responsible.
- For any query/issue/ethical aspects contact the corresponding Author.

CONFERENCE PROCEEDINGS

UGC Sponsored National Conference on
Recent Advancements in Science & Technology

Date : 10th Feb, 2024

:: Organized by ::

Vidya Bharati Shaikshanik Mandal's

Vidya Bharati Mahavidyalaya, Amravati

:: In Collaboration with ::

S.S.S.K.R. Innani Mahavidyalaya

Karanja (Lad), Dist. Washim 444105 (M.S.), India

Editorial Board

VOLUME II : Physics

Chief Editor

Dr. Pradnya S. Yenkar
Principal,
Vidya Bharati Mahavidyalaya, Amravati

Editors

Dr. R. A. Patil, Associate Editor
Dr. G. T. Lamdhade, Member
Dr. K. B. Raulkar, Member
Dr. A. O. Chauhan, Member
Mr. R. B. Butley, Member
Mr. C. C. Jadhav, Member
Mr. S. K. Kokate, Member

CONTENTS

Physics

S.No.	Title	Author/s	Page No.
1	Green Synthesis of ZnO NPs using Capping Agent: Ultra-Sonication Treatment	S. D. Charpe P.P. Raut G.T. Lamdhade Rohit Agrawal Vijay Rahangdale	1-3
2	Electrical and Sensing Applications of ZnO doped with PPy to study Ammonia Gas	R. P. Ikhar A. J. Atram G. T. Lamdhade R. R. Mistry S. M. Yenorkar K. B. Raulkar	4-10
3	Emission Spectrum Analysis of Several Lighting and Display Devices Using USB650-UV-VI-SPI Mini Portable Spectrometer	Shailesh R. Jaiswal Rupali G. Korpe Pankaj A. Nagpure	11-15
4	Effect on Polymer blend of Proton Doner Polymer Electrolyte	S. P. Bakde S. R. Jadhao	16-18
5	Photovoltaic applications of SnO ₂ gas sensor	B.H.Bhatti K.B.Raulkar G. T. Lamdhade A. O. Chauhan R. B. Butley C. C. Jadhao A. B. More	19-23
6	Green Synthesis of Zinc Oxide Nanoparticles using Neem Leaf Extract and their Characterization	R. M. Agrawal K M Heda S D Charpe P P Raut G T Lamdhade	24-27
7	Luminescence in SrMgAl ₁₀ O ₁₇ :Eu,Cr for downshifting the solar spectrum	P.K.Tawalare	28-30
8	Synthesis, Structural, Optical and Morphological Characterization of Graphene Oxide	Pravin Rathod Vishnudas Bhosle Ashok Ubale	31-34
9	A review on synthesis and applications of nanomaterials	V. U. Rahangdale S. D. Charpe	35-38
10	Ammonia Gas Sensing Application of Nano-composites of SnO ₂ Doped with ZnO & Polypyrrole	A. J. Atram R. P. Ikhar G. T. Lamdhade B. M. Mude K. M. Mude K. B. Raulkar	39-44

11	Fabrication of Nano-structured SnO ₂ Powder by Sol-Gel Method	S. R. Bijwe G. T. Lamdhade P. S. Bodkhe K. B. Raulkar	45-51
12	Study of Doping Metal Oxides Gas Sensor for Efficient CO ₂ Gas Sensing	R. S. Bhuyar K. B. Raulkar S. R. Bijwe G. T. Lamdhade	52-56
13	Synthesis and Characterization of PANI Doped ZnO-SnO ₂ for Humidity Sensing Application	T. R. Ingle, G. T. Lamdhade	57-63
14	A Review of Polymer and Their Blends: Classifications & Applications	P.P. Raut G.T. Lamdhade S. D. Charpe	64-67
15	Synthesis of ZnO Nanoparticles by Chemical Precipitation Method	N. B. Thakare G. T. Lamdhade V. S. Kalyamwar Y S. Tamgadge D. N. Bhojar	68-71
16	Fabrication and Application of SnO ₂ doped ZnO to sense CO ₂ Gas	Rita S. Bhuyar G. T. Lamdhade K. B. Raulkar	72-78
17	Review on Nanocrystalline perovskite (ABO ₃): A potential material for solid state gassensor	Manisha S. Pande V. D. Kapse S.V.Agnihotri T.R.Tatte	79-81
18	Electrical and Dielectric Properties of EC-PMMA Polymers and their Blends	Kajal Sirtawar	82-91
19	Brief Insights into Synthesis Methods and Applications of Nanostructured Metal Oxides	S. P. Patil R. B. Pedhekar V. S. Kalyamwar V. D. Wankhade V. R. Hiranwale	92-94
20	Humidity Sensors: AlCl ₃ -Dipped Nanocrystalline Magnesium Oxide	R B Butley R V Joat G T Lamdhade K B Raulkar A O Chauhan C C Jadhao B.H. Bhatti	95-102
21	Advances and Perspectives in Nanotechnology: A Short Review	R B Butley R V Joat G T Lamdhade K B Raulkar A O Chauhan C C Jadhao B.H. Bhatti	103-107

22	Synthesis and Optically Stimulated Luminescence (OSL) Properties of CaSiO ₃ : Ce, Al Phosphor for Radiation dosimetry	C. B. Palan A.O.Chauhan N.S. Sawala S. K. Omanwar	108-110
23	Synthesis and Characterization of NB-UVB emitting Yttrium phosphate phosphor	A. O. Chauhaan C. B. Palan N. S. Sawala G. T. Lamdhade K. B. Raulkar R. B. Butley C. C. Jadhao	111-114
24	Photoluminescence Studies of Eu (III) activated YBaB ₉ O ₁₆ phosphor	A. O. Chauhan G. T. Lamdhade K. B. Raulkar R. B. Butley C. C. Jadhao B. H. Bhatti	115-118
25	Recent Developments in the Study of Three-dimensional Spin Structure of the Proton	Dr. Bipin Sonawane	119-123
26	Luminescent Properties of Borate Based Phosphors Review	M. P. Jmabhale C. B. Palan S. P. Hargunani R. P. Sonekar	124-126
27	Synthesis and Photoluminescence (PL) Properties of LaB ₃ O ₆ :Eu ³⁺ Phosphor	M. P. Jmabhale S. P. Hargunani R. P. Sonekar	127-130
28	Thermally Stimulated Discharge Current (TSDC) Study of 4:1 PS PMMA Polyblend Thin Films doped with 10% Oxalic Acid	Anant S. Wadatkar	131-134
29	A Review on Carbon based Nanomaterial. Properties, Characteristics and Applications	Ms. S. T. A. Khan Mr. P.S. Wagh Ms. S. P. Dharmey Ms. S. A. Amale	135-141
30	Comparative Assessment of Zirconia as a Biomaterial Synthesized Via Two Different Methods	V.G. Thakare R. K. Watile	142-144
31	Piezoelectric Materials for Energy Harvesting Technology	J.M.Bodulwar Dr. A.B. Lad Dr. K.R. Nemade	145-148
32	Mechanism and Classification of supramolecular gels	Sakharam B. Sangale	149-154
33	Recent Advances in Natural Dyes for Dye Sensitized Solar Cell	Sanjay Takpire Sandeep Waghuley	155-158

34	Investigation on effect of Cd ²⁺ and K ⁺ doping on upconversion luminescence in Y ₂ O ₃ : YbEr phosphor	Harsha S. Deshmukh Dr. Gajanan G. Muley	159
35	Synthesis and Characterization of Nano-composites decorated by Graphene for the advanced applications	Vaishnavi V. Pandhe Suraj V. Tayade Sandeep A. Waghuley	160-162
36	Investigation of AC electrical analysis of EC/PVC blend films	Welekar N.R. Raulkar K.B. Lamdhade G. T.	163-167
37	Synthesis and Structural properties of lead titanate by wet chemical method	N. V. Galande A. U. Bajpeyee S. H. Shamkuwar	168-171
38	Gas sensing properties of Co surface modified SmFeO ₃ thick film	R. B. Mankar V. D. Kapse	172-175
39	Synthesis Methods and Applications of Cadmium Ferrite Nanoparticle: An Overview	T. R. Tatte V. D. Kapse S. V. Agnihotri M. S. Pande	176-178
40	A Short Review on feature, Properties and application of Nanowire	Miss S.A. Amale Mr.P.S. Wagh Miss.S.P. Dharme Miss S.T. Khan	179-183
41	Review On Polyindole Composites For Supercapacitor Application	Akshay P. Bangar Suraj V. Tayade Sandeep A. Waghuley	184-189
42	Nonlinear I–V characteristics and thermal stability of nanocrystalline Titanium oxide	Balkhande V.M. Lamdhade G.T. Daware A.S.	190-194
43	Humidity Sensors: A Comprehensive Review	Daware A.S., Rewar G.D., Lamdhade G.T. Balkhande V.M.	195-197
44	Copper Oxide Nanoparticles for Solar Cell Application	Ambika P. Anbhore Suraj Tayade Sandeep A. Waghuley	198-200
45	Synthesis and Thermoluminescence (TL) Properties of NaLi ₂ PO ₄ :Ce Phosphor for Radiation dosimetry	Vikas S. Punse C. B. Palan P. A. Nagpure A. O. Chauhan Bhushan Dhabekar S. K. Omanwar	201-203
46	Investigation of DC electrical properties of EC/PVC blends	Welekar N.R. Raulkar K.B. Lamdhade G. T.	204-209

47	Comparative Analysis of ZnO Zinc Oxides Synthesized via Chemical Bath Deposition and Other Deposition Methods	Miss. D. D. Bonte	210-218
48	Study of Thermal Properties of Solid Polymer Complexes doped with TiO ₂ and GDC	R. Risodkar	219-221
49	Chemical Synthesis of Polyaniline Nanocomposites for Advanced Applications	Vaishnavi D. Nagmote Suraj V. Tayade Sandeep A. waghuley	222-224
50	Synthesis and Photoluminescence Properties of Tb ³⁺ doped KSrPO ₄ Phosphor	N. S. Sawala C.B. Palan A. O. Chauhan S.K. Omanwar	225-227
51	Nanocrystalline Spinel Cobalt Aluminate Prepared By Co precipitation Method	S.V. Agnihotri V. D. Kapse T.R. Tatte P.V. Tumram M. S. Pande	228-231
52	Dynamics of Coupled Circle Map on Diffusion Limited Aggregate	Pratik M. Gaiki Parag A. Bramhankar	232-236
53	Evaluating the Impact of Material Composition on Photovoltaic Property: A Spectroscopic Investigation	Mr. Y. R. Mankar Mr. S. K. Kokate	237-246
54	Review on Fabrication of Cds Based Efficient Solar Cell Incorporated With SiO ₂	Priya U. Sah Akshay P. Bangar Sandeep A. Waghuley	247-249
55	A Study Kinematical Variable in the Detector Technology	Bhadra Binesh Dr. Bipin Sonawane	250-253
56	Electron Temperature as well as Radial Profile of Spectral Emission also Change due to Formation of a Laser Pulse	A.P. Pachkawade	254-257
57	Investigated as tunneling behavior of electrolytic solution using DC glow discharge	A.P.Pachkawade	258-261
58	Green synthesis of Zinc Oxide nanoparticles using Plant - A review	B. S. Agrawal G. T. Lamdhade	262-269
59	Conducting Polymer Based Anticorrosion Materials	D. J. Bhagat K. R. Nemade K. A. Koparkar	270-272
60	AC electrical characterization of PTh-PVAc thin films using Iodine as A dopant	Dhananjay P. Deshmukh	273-275
61	A Review - Metal Oxide Gas Sensor	Farhan Ahmad Sanjay Devade	276-278

62	Optical and structural property of YBO ₃ :Tb ³⁺ phosphor synthesized by novel Aldo-Keto gel method	K. K. Rathod K. A. Koparkar	279-281
63	Review on Improving Photoluminescence Emission in Borate Phosphors Activated by Gd ³⁺	Mohammad Jived R. P. Snooker Sanjay Hargonani R. M. Chavan Sapna Rajankar	282-286
64	Recent Progresses in Gas Sensors Based on Reduced Graphene Oxide-ZnO Composites	N. B. Thakare G. T. Lamdhade D. N. Bhoyar G. S. Warade	287-293
65	Synthesis and characterization of SnO ₂ nanoparticles by Sol-gel Method	C.C. Jadhao G.T. Lamdhade K.B. Raulkar A.O. Chauhan R.B. Butley	294-297
66	Synthesis and Luminescent Behavior of Europium-Infused Barium Alumino-Borate Phosphors	R. S. Palaspagar	298-301
67	Synthesis and Characterization of Conducting Polyaniline-Tin Oxide Thin film Nanocomposites	Shrikant H. Nimkar	302-305
68	A Review On TiO ₂ Nanoparticle: Structure, Properties & Applications	Dharme S.P. Wagh P.S. Khan S.T. Amale S.A.	306-309
69	Green synthesized TiO ₂ nanoparticles for antimicrobial properties:Review	P. S. Wagh S. T. Khan S. P. Dharme S. A. Amale	310-316
70	Review of synthesis of nanoparticles by various methods	C.C. Jadhao G.T. Lamdhade K.B. Raulkar A.O. Chauhan R.B. Butley	317-320
71	Synthesis and Luminescence Characteristics of Eu ³⁺ activated LiSr ₄ (BO ₃) ₃ Phosphor	S.S.Rajankar R.M.Chavan Mohammad Javed S.P.Hargunani R.P.Sonekar	321-323
72	Feynman Diagrams and Rules in QED	Shrusti Kothari Dr. Bipin Sonawane	324-327
73	TiO ₂ nanoparticles synthesized by sol-gel and green synthesis method for antimicrobial properties: Mini Review	P. S. Wagh S. T. Khan S. P. Dharme S. A. Amale	328-330
74	Review on Metal Oxides Based CO ₂ Gas Sensors	Mankar S.S. Lamdhade G.T. Raulkar K.B	331-334

75	A Review on SnO ₂ Nanoparticle: synthesis, Structure, Property and it's applications	Miss. S. A. Amale Mr. P.S.Wagh Miss. S.P.Dharme Miss.S.T.Khan	335-339
76	Review on Nanofabrication Techniques	Ms.S.T.Khan Mr.P.S.Wagh Ms.S.P.Dharmey Ms.S.A.Amale	340-345
77	A Review on Supercapacitor: Types and Applications	Dharme S.P. Wagh P.S. Khan S.T. Amale S.A.	346-350
78	Synthesis and Characterization of PEO: PVP: NaNO ₃ Based Polymer Electrolyte	P. A. Fartode V. G. Farkunde	351-354
79	A Study of TiO ₂ Thin Films: From Synthesis to Property Enhancement through Chemical Bath Deposition and Annealing	Mr.A.B.Tayde Mr.S.K.Kokate	355-363
80	Fabrication and characterization of CdO-MgO nanocomposite based thick films	V. D. Kapse Rajikshah Chandshah	364-368
81	Study of Sensing Mechanism of PPy and MgO Metal Oxide for CO ₂ Gas	M.N.Pawar P.S.Deole A.V.Rajgure G.T.Lamdhale	369-375
82	Copper Oxide Nanoparticles for Solar Cell Application	Ambika P. Anbhore Suraj Tayade Sandeep A. Waghuley	376-378
83	A Comprehensive Review on the Synthesis of Semiconductor Nanomaterials and Their Diverse Applications	Ranjana Wakade P.P. Nalawade	379-383
84	Frontier Developments in Optical Material: A Review	R.A. Gandhare A.R. Kadu J. T. Ingle	384-386

CONFERENCE PROCEEDINGS

UGC Sponsored National Conference on
Recent Advancements in Science & Technology

Date : 10th Feb, 2024

:: Organized by ::

Vidya Bharati Shaikshanik Mandal's

Vidya Bharati Mahavidyalaya, Amravati

:: In Collaboration with ::

S.S.S.K.R. Innani Mahavidyalaya

Karanja (Lad), Dist. Washim 444105 (M.S.), India

Editorial Board

VOLUME II : Physics

Chief Editor

Dr. Pradnya S. Yenkar
Principal,
Vidya Bharati Mahavidyalaya, Amravati

Editors

Dr. R. A. Patil, Associate Editor
Dr. G. T. Lamdhade, Member
Dr. K. B. Raulkar, Member
Dr. A. O. Chauhan, Member
Mr. R. B. Butley, Member
Mr. C. C. Jadhav, Member
Mr. S. K. Kokate, Member

1

Green Synthesis of ZnO NPs using Capping Agent: Ultra-Sonication Treatment

S. D. Charpe^{1*}, P.P. Raut², G.T. Lamdhade³, Rohit Agrawal⁴, Vijay Rahangdale⁵

^{1*}Assistant Professor, Department of Physics, J.D. Patil Sangludkar Mahavidyalaya, Daryapur, Dist. - Amravati,

²Research Scholar, Department of Physics, Vidya Bharti Mahavidyalaya, Amravati, India

³Professor & Head of Department of Physics, Vidya Bharti Mahavidyalaya, Amravati, India

⁴Assistant Professor, Department of Physics, Shri R.L.T. College of Science, Civil Lines, Akola

⁵Assistant Professor, Department of Physics, Jagat Arts, Commerce and I.H.P. Science College, Goregaon,

E-mail of Corresponding Authors: sushildeo8@gmail.com

Abstract:

Nano-sized ZnO metal oxide was prepared by Green Synthesis method using capping agent, further synthesized material was assisted with ultra-sonication treatment. This material has been investigated for their structural properties. X-ray diffraction pattern reveals that pure zinc oxide was synthesized successfully. Also, calculated average particle size found to be 85.46 nm. Also synthesized powder contains Zn and O elements only without any impurity.

Keywords: Nano-size ZnO, Ultra –Sonication, X-ray Diffraction (XRD).

1. Introduction

In the new era of materials science and electronic devices semiconductor materials have great potential to enhance electronic devices different passive properties. Green synthesis approach of nano-sized particle is dependent upon green chemistry principles which include the structure and morphological of nanoparticles using non-toxic chemicals, reusable material, environmentally friendly solvents and finally product that is synthesized nano material should be a degradable waste product. Green synthesis will be done using biological systems like bacteria, fungi, algae, plants, yeasts and actinomycetes [1]. Among these systems; plant extract systems are more appropriate methods to synthesize nano-sized metal oxide materials like ZnO and etc. As green synthesized metal oxides (MO_x) nano-particles like ZnO, SnO₂, WO₃, etc. have high surface area-to-volume ratio, high reactivity, and good size distribution. This type of metal oxides is used in many applications like gas sensor technology, antimicrobial, biomedical, targeted drug delivery, etc. [2-5].

Among the many semiconductor materials Zinc Oxide (ZnO) is extensively used material. This material is used because ZnO is a wide-band gap semiconductor of the II-VI semiconductor group of the periodic table and zinc, a transition metal. The native doping of the semiconductor (causes are as yet unknown) is n-type [6-9]. This semiconductor has several favorable properties, including good transparency, high electron mobility, wide band gap, and strong room-temperature luminescence. Those properties are used in emerging applications for transparent electrodes in liquid crystal displays, in energy-saving or heat-protecting windows, and in electronics as thin-film transistors and light-emitting diodes.

To acquire these properties material has a unique structure and this unique structure is easily achieved using novel synthesis methods. ZnO was synthesized by many chemical synthesis methods also ZnO was synthesized using Green synthesis technology [10]. Particles sized of nanosized ZnO material should be controlled by using Ultra- Sonication treatment [11-12].

2. Materials and Methods

2.1 Collection and Preparation of Neem Leaves Solution

Neem leaves called as *Azadirachta indica* collected from College campus. For cleaning purpose, clean Neem leaves using distilled water after washing kept these leaves in sunlight

for drying purpose further on dried Neem leaves in Oven at 30°C for 24 hr. Furthermore, dried Neem leaves crushed into mortar pestle to get fine power of Neem leaves. Add 2 gram fine powder of Neem leaves into 50 mL of chilled distilled water, stirred it continuously for 5 hr, further the mixture was ultra –sonicated for 10 min to dissolve the Neem leaves fine powder [13]. The obtained solution of Neem leaves was filtered to remove any residue or contaminants. The obtained stock solution stored at 5°C at further experimental use.

2.2 Green Synthesis of Nano-size Zinc Oxide (ZnO) from Neem Leaves Solution

For preparation of ZnO nanosized particles (ZnO NPs), initially zinc nitrate hexahydrate [Zn (NO₃)₂ 6H₂O] was mixed into Neem leaves (capping agent) solution and sodium hydroxide [NaOH] followed by continuously 3 hr stirring [14]. The white precipitate was centrifuge at 1200 rpm for 10 min and precipitate was settled done at bottom at solution container. Further, precipitate washed with distilled water and ethanol to get fine powder paste. Then, a solid white powder obtained was dried in an oven at 60°C for 5 hr. The product was calcined in a muffle furnace at 450°C for 6 hr. Finally get ZnO NPs powder.

3. Characterization of Nano-sized ZnO

In order to investigate various properties of the synthesized sample, it is necessary to characterize this sample by various characterization techniques like X-ray Diffraction (XRD) Technique. This helps to obtain the information about the different structural properties and particle size of sample.

3.1 X-ray Diffraction (XRD) Technique

In order to get information about crystal structure, crystalline size, purity of sample etc. of synthesized Zinc Oxide, X-ray diffraction was carried out. XRD pattern of the synthesized sample was obtained at room temperature. The scanning angle 2 θ was varied from 20-80 degree in step of 0.06° and the step time is fixed at 0.2 sec using Cu-K α radiation.

Figure 1 Shows the XRD pattern of S₀. The recorded XRD pattern confirmed that synthesized ZnO is highly crystalline in nature. The higher peak intensities of an XRD pattern are due to the better crystallinity.

Using PDXL software which provided with Rigaku Miniflex 600 model, it is confirm that synthesized powder contains Zn and O elements only without any impurity.

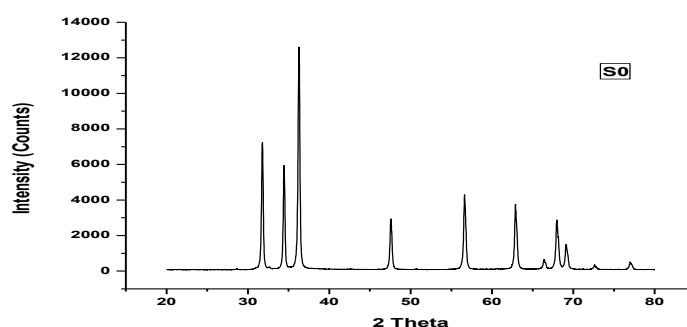


Fig. 1: XRD pattern of 0 min ZnO (S₀).

The domain size of the crystal can be estimated from the full width at half maximum (FWHM) of the peaks by means of the Scherrer formula [15]. Particle size of the synthesized Zinc Oxide was found to be 85.46 nm.

4. Conclusion

Nano-sized Zinc Oxide (ZnO) was successfully synthesis using Neem leaves called as *Azadirachtaindica* using zinc nitrate hexahydrate as capping agent. From XRD, calculated average particle size found to be 85.46 nm also synthesized powder contains Zn and O elements only without any impurity.

Reference:

- [1] Annu, A. A., & Ahmed, S. (2018). Green synthesis of metal, metal oxide nanoparticles, and their various applications. *Handbook of Ecomaterials, 2018*, 1-45.
- [2] Jeevanandam, J., Kiew, S. F., Boakye-Ansah, S., Lau, S. Y., Barhoum, A., Danquah, M. K., & Rodrigues, J. (2022). Green approaches for the synthesis of metal and metal oxide nanoparticles using microbial and plant extracts. *Nanoscale, 14*(7), 2534-2571.
- [3] Das, M., & Chatterjee, S. (2019). Green synthesis of metal/metal oxide nanoparticles toward biomedical applications: Boon or bane. In *Green synthesis, characterization and applications of nanoparticles* (pp. 265-301).
- [4] Yulianto, B., Septiani, N. L. W., Kaneti, Y. V., Iqbal, M., Gumilar, G., Kim, M., & Yamauchi, Y. (2019). Green synthesis of metal oxide nanostructures using naturally occurring compounds for energy, environmental, and bio-related applications. *New Journal of Chemistry, 43*(40), 15846-15856.
- [5] de Jesus, R. A., de Assis, G. C., de Oliveira, R. J., Costa, J. A. S., da Silva, C. M. P., Iqbal, H. M., & Ferreira, L. F. R. (2024). Metal/metal oxide nanoparticles: A revolution in the biosynthesis and medical applications. *Nano-Structures & Nano-Objects, 37*, 101071.
- [6] Fan, Z., & Lu, J. G. (2005). Zinc oxide nanostructures: synthesis and properties. *Journal of nanoscience and nanotechnology, 5*(10), 1561-1573.
- [7] Kumar, S. S., Venkateswarlu, P., Rao, V. R., & Rao, G. N. (2013). Synthesis, characterization and optical properties of zinc oxide nanoparticles. *International Nano Letters, 3*, 1-6.
- [8] Zafar, M., Iqbal, T., Afsheen, S., Iqbal, A., & Shoukat, A. (2023). An overview of green synthesis of zinc oxide nanoparticle by using various natural entities. *Inorganic and Nano-Metal Chemistry, 1-18*.
- [9] Orek, C., Keser, S., Kaygili, O., Zuchowski, P., & Bulut, N. (2023). Structures and optical properties of zinc oxide nanoclusters: A combined experimental and theoretical approach. *Journal of Molecular Modeling, 29*(8), 227.
- [10] Shafey, A. M. E. (2020). Green synthesis of metal and metal oxide nanoparticles from plant leaf extracts and their applications: A review. *Green Processing and Synthesis, 9*(1), 304-339.
- [11] Bhuyan, A., & Ahmaruzzaman, M. (2024). Ultrasonic-assisted synthesis of highly efficient and robust metal oxide QDs immobilized-MOF-5/Ni-Co-LDH photocatalyst for sunlight-mediated degradation of multiple toxic dyes. *Journal of Alloys and Compounds, 972*, 172781.
- [12] Tang, L., Wang, B., Bai, S., Fan, B., Zhang, L., & Wang, F. (2024). Preparation and characterization of cellulose nanocrystals with high stability from okara by green solvent pretreatment assisted TEMPO oxidation. *Carbohydrate Polymers, 324*, 121485.
- [13] Noorjahan, C. M., Shahina, S. J., Deepika, T., & Rafiq, S. (2015). Green synthesis and characterization of zinc oxide nanoparticles from Neem (*Azadirachta indica*). *Int. J. Sci. Eng. Technol. Res, 4*(30), 5751-5753.
- [14] Vijayakumar, S., Saravanakumar, K., Malaikozhundan, B., Divya, M., Vaseeharan, B., Durán-Lara, E. F., & Wang, M. H. (2020). Biopolymer K-carrageenan wrapped ZnO nanoparticles as drug delivery vehicles for anti MRSA therapy. *International journal of biological macromolecules, 144*, 9-18.
- [15] Brito, P. S. D., Patricio, S., Rodrigues, L. F., Santos, D. M. F., & Sequeira, C. A. C. (2010). Electrodeposition of Zn-Mn alloys from recycling battery leach solutions in the presence of amines. *The Sustainable World-WIT Transactions on Ecology and the Environment; Brebbia, CA, Ed, 367-378*.

Electrical and Sensing Applications of ZnO doped with PPy to study Ammonia Gas

R. P. Ikhara¹, A. J. Atram², G. T. Lamdhade³, R. R. Mistry⁴,
S. M. Yenorkar⁵, K. B. Raulkar³

¹Vidya Bharati Madhyamik Vidyalaya, Patrakar Colony, Amravati

² Department of Physics, Lokmanya Tilak Mahavidyalaya, Wani

³Department of Physics, Vidya Bharati Mahavidyalaya, Amravati, 444602

⁴Department of Physics Deogiri College Aurangabad, Maharashtra 431005, India

⁵Department of Physics/Electronics Shri Shivaji College, Parbhani 431401, India

* Corresponding Author e-mail: kbraulkar2016@gmail.com

ABSTRACT

Nanocomposites of PPy (polypyrrole)-ZnO were prepared by chemical oxidative polymerization technique using an anhydrous ferric chloride (FeCl_3) as an oxidizing agent. The characterization of prepared sensor was done using XRD and SEM (Scanning electron microscope) to determine the crystal size and porosity, respectively. Thick films of the sample were prepared on clean glass plate with the help of screen printing technique. Then sensors were studied by measuring resistance in air and ammonia environments at room temperature (300 K).

Sensitivity of the sensors was determined at different concentrations of ammonia gas. It was found that PZ3 sensor (85% PPy + 15 % ZnO) was best among the others as it showed maximum sensitivity at 90 ppm of NH_3 gas. Also from dynamic response, response time and recovery times were found to be 3 min and 17min. respectively.

Keywords: PPy- ZnO nanocomposites, sensitivity, dynamic response, screenprinting technique.

1. Introduction:

In present environment, we face with toxic, volatile and combustible gases in the environment. Detecting these harmful gases is vital in order to control air pollution, prevent human life, and protect nature from being damaged. Ammonia is widely used in industrial process and medical diagnoses. Hence its detection is very impotent [1-6].

NH_3 sensors based on conducting polymers have shown better sensing responses among various sensors based on different materials. Polypyrrole (PPy) is one of the most stable conducting polymers under ambient conditions. It has attracted more attention as an NH_3 sensor because of its unique conducto-metric response to NH_3 [7-8].

Zinc Oxide (ZnO) has been extensively studied for various applications in sensing, acoustic wave resonator, acoustic optic modulator. The origin of various applications the lies in its crystal structure, in which the oxygen atoms and zinc atoms are tetrahedral, bonded. In such anon-Centro symmetric structure, the center of positive charge and negative charge can be displaced due to external pressure induced lattice distortion. In fact, among the tetrahedrally bonded semiconductors, ZnO has the highest wide band gap semiconductor with a band gap ~ 3.2 eV at room temperature which provides a large electro-mechanical coupling. This property of ZnO nanostructures was also investigated for their potential applications in nano systems [9-11]. The present study deals with the synthesis, characterization of PPy-ZnO nano-composites, sensitivity and dynamic response.

2. Experimental:

A. Synthesis of ZnO Nanoparticles:

GR grade, sd-Fine, India (purity 99.99%) chemicals were used for the preparation of ZnO

nanoparticles. Zinc acetate dehydrate $Zn(O_2CCH_3)_2(H_2O)_2$, sodium hydroxide, Methanol and de-ionized water was used. In the preparation of Zinc Oxide (ZnO), 0.2M Zinc Acetate dehydrates dissolved in 100 ml de-ionized water, was ground for 15 min and then mixed with 0.02 M solution of NaOH with the help of glass rod. After the mixing the solution was kept under constant magnetic stirring for 15 min. and then again it was grinded for 30 min. The white precipitate product was formed at the bottom. Then abundant liquid was discarded and the product was washed many times with the deionized water and methanol to remove byproducts. The final product was then filtered by using Watt-man filter paper to obtain precipitate in the form of white paste. Now this paste was kept in a vacuum oven at $80^\circ C$ for 4 hrs. so that the moisture will be removed from the final product and we will get dryproduct. Then this dry product was crushed into a fine powder by using grinding machine and finally this fine nano-powder of ZnO was calcinated at temperature $800^\circ C$ for 6 hrs. in the auto controlled muffle furnace (Gayatri Scientific, Mumbai, India.) so that the impurities from product will be completely removed and got a final product of ZnO nanoparticles.

B. Synthesis of Polypyrrole (PPy):

The Py monomer, anhydrous iron (III) chloride ($FeCl_3$) and methanol were used as received for synthesis of PPy. The solution of 7 ml methanol and 1.892 g $FeCl_3$ was first prepared in round bottom flask. Then 8.4 ml Py monomer was added to ($FeCl_3$ + methanol) solution with constant stirring in absence of light. The amount of Py monomer added to the solution (1/2.33 times of $FeCl_3$) was in such a way to get maximum yield. The resulting black precipitates are filtered and washed with copious amount of distilled water until the washings are clear. PPy so obtained is dried by keeping in oven at $600^\circ C$ for 3 h. The synthesized material was characterized by using XRD and SEM.

C. Preparation thick films:

Synthesized nanomaterials of ZnO, and PPy were mixed with different weight percentage. The binder was prepared by using 8 wt% butyl carbitol and 92 wt% ethyl cellulose. On chemically cleaned glass plate, paste of Al_2O_3 was screen printed and it was kept for 24 hr to dry it at room temperature and then heated at $100^\circ C$ for 2 hrs to remove the binder. Paste or ink of PPy+ZnO was then screen printed on Al_2O_3 layer. Again plate was dried at room temperature for 24 h and binder was removed by heating it at $150^\circ C$ for 4 hrs. Finally integrated electrons (fig. 1) were made using silver paint for electrical connections (fig. 2). Sample codes are given in table 1.



Fig. (1)

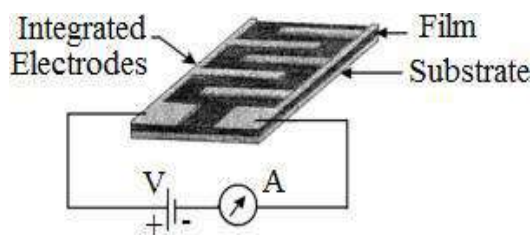


Fig. (2)

Table 1: Sample Codes

Sr. No.	Composites	Codes
1	95 % PPy + 5 % ZnO	PZ1
2	90 % PPy + 10 % ZnO	PZ2
3	85 % PPy + 15 % ZnO	PZ3

4	80 % PPy + 20 % ZnO	PZ4
5	75 % PPy + 25 % ZnO	PZ5
6	70 % PPy + 30 % ZnO	PZ6

3. Result and Discussion:

(i) XRD (X-Ray Diffraction):

XRD patterns of all the composites of PPy and ZnO are as shown in Fig. 3.

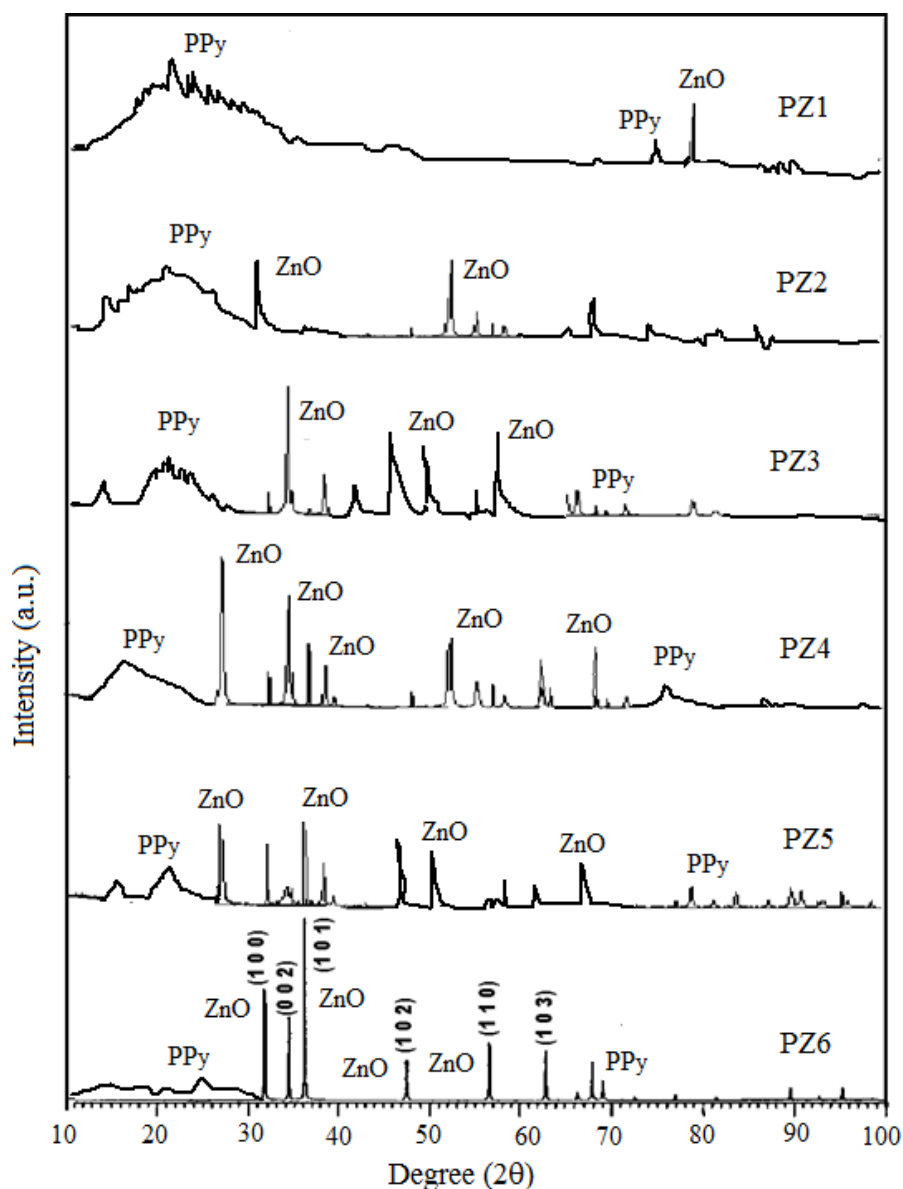


Fig. 3: XRD of PPy and ZnO composites

XRD pattern of PPy manifested amorphous nature of PPy. At 27° broad peak occurred which is the characteristics of amorphous nature of polypyrrole. Occurrence of this broad peak is due to the scattering of X-Rays from polymer chains at the interplaner spacing. The maximum intensity position of amorphous also depends on monomer to oxidant ratio [12]. The average grain size, determined from XRD pattern using Scherrer formula is about 87 nm [13]. The main diffraction peaks for the ZnO, which are located at $2\theta = 31.4^\circ; 34.2^\circ; 36.7^\circ; 47.6^\circ; 56.1^\circ; 63.4^\circ$ and correspond to Bragg reflections (100), (002), (101), (102), (110), (103), respectively, allowed us to identify a hexagonal wurzita type structure ($a = 3$).

25 Å and $c = 5.21$ Å) for ZnO. These peaks are in agreement with the data obtained for ZnO [14]. From XRD pattern of composites, it is observed that average crystallite size of PZ3 sensor (85% PPy + 15% ZnO composition) is least (92 nm) as compared to other compositions and hence PZ3 sensor has large active area which tends to increase the sensitivity of PZ3 sample.

(ii) SEM Analysis:

The surface morphology of composites of PPy and ZnO materials were studied by SEM and its pictures are shown in the following figures.

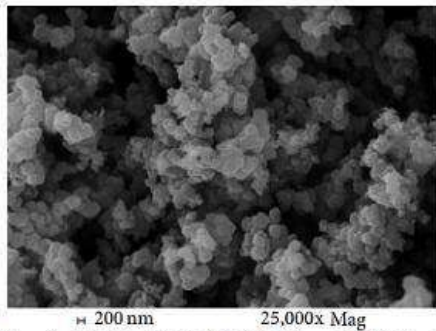


Fig. 4: SEM of PZ1 (95 % PPy + 5 % ZnO)

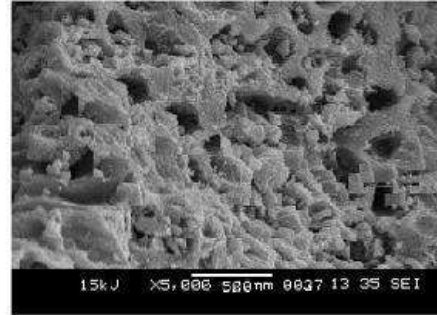


Fig. 5: SEM of PZ2 (90 % PPy + 10 % ZnO)

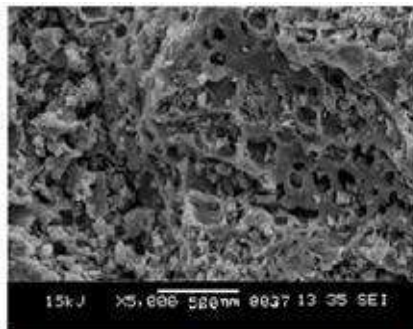


Fig. 6: SEM of PZ3 (85 % PPy + 15 % ZnO)



Fig. 7: SEM of PZ4 (80 % PPy + 20 % ZnO)

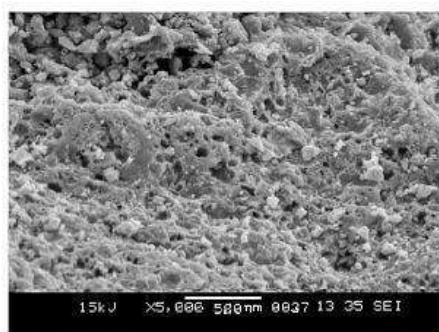


Fig. 8: SEM of PZ5 (75 % PPy + 25 % ZnO)

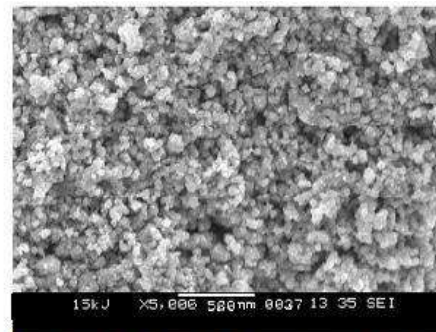


Fig. 9: SEM of PZ6 (70 % PPy + 30 % ZnO)

From the SEM photos, it is observed that in every inch of the region, number of pores was different and an average numbers of pores were taken for comparative study. From every photo, porosity was calculated for one inch square area. From figures, it is found that porosity of PZ3 sample is more among the samples. Due to high porosity, surface area increases and hence it tends to more response of the gas.

(iii) Sensitivity Measurement:

The sensitivity is expressed by the formula:

$$S = \frac{\text{Change in resistance}}{\text{Original resistance}} = \frac{R_{\text{gas}} - R_{\text{air}}}{R_{\text{air}}}$$

Where,

R_{gas} = Resistance of the sensor in presence of NH_3 gas environment

and R_{air} = Resistance of the sensor in presence of air.

When PPy is exposed to electron donating gases like NH_3 , a redox reaction occurs and its effective number of charge carrier decreases, thus reducing its conductance i.e. resistance increases during NH_3 exposure, indicating a p-type-like gas sensing behavior [15]. PPy-ZnO sensors exhibit good dependence on NH_3 gas concentration up to 90 ppm, where it reaches a saturation level at room temperature (300K). By keeping surface area fixed, a lower gas concentration implies a lower coverage of gas molecules on the surface. An increase in the gas concentration raises the surface coverage eventually leading to saturation level and thus determining the upper limit of detection. Amongst the prepared sensors, PZ3 sensor showed more sensitivity as 15 % of ZnO mixed with 85 % of PPy produces more porosity (Fig. 6) and hence enhanced surface area thereby increasing gas sensitivity. The variation of sensitivity with NH_3 gas concentration is shown in the figure 10.

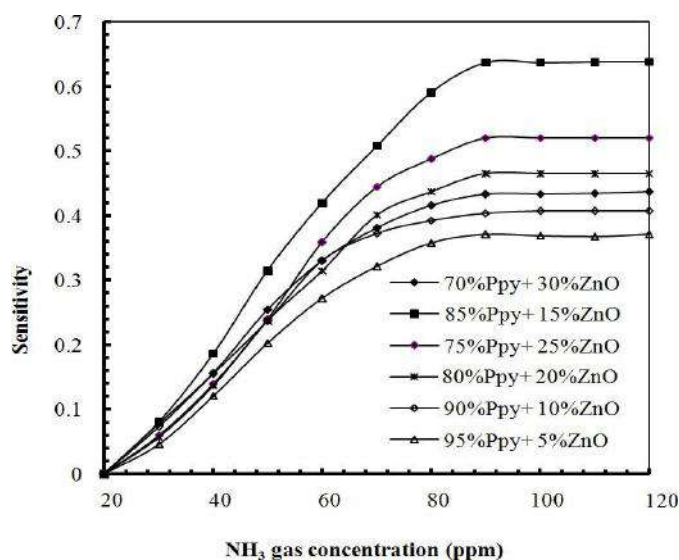


Fig. 10: Variation of sensitivity with concentration of NH_3 gas for different sensors

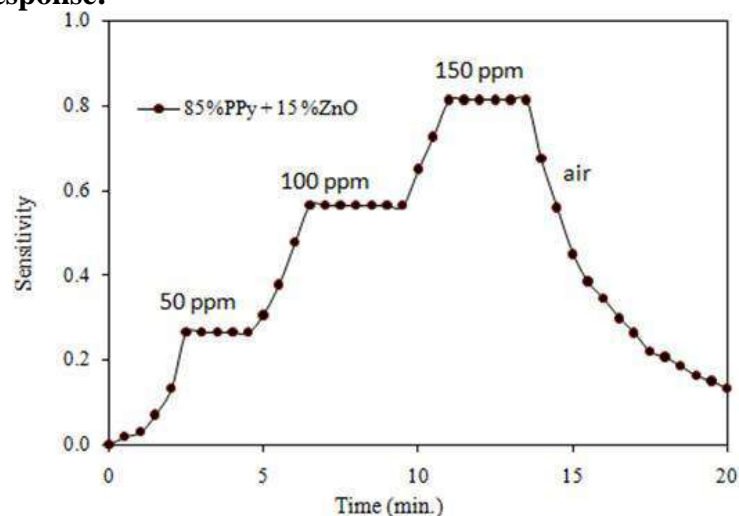
(iv) Dynamic Response:

Fig. 11: Dynamic response of PZ3 sensor for 50, 100, 150 ppm of NH_3 gas

Figure 11 shows the dynamic response of PZ3 (85%PPy + 15%ZnO) sensor for 50, 100, 150 ppm of NH_3 gas at room temperature (300 K). Time required to attain 90 % of maximum resistance change due to exposure of gas. The recovery time is defined as the time taken to reach 90% of the recovery when gas is turned off. Response time was found to be about 3 min and recovery time was found to be nearly 17 min. This shows that PZ3 sensor is fast i.e.it shows quick response but slow in recovery.

The gas sensing mechanism for the prepared sensors may be explained on the basis of interactions between the sensing film and adsorbed gas. It has been proposed that NH_3 can adsorb and donate a lone pair of its electrons to PPy. Electrons will recombine with existing holes in the p-type PPy, leading to a resistance increase in agreement with the observed NH_3 response. By adding unloaded ZnO nanoparticles (ZnO NPs), the response is enhanced. This could reasonably be explained by interaction of gas with increased specific area of ZnO nanoparticles. From the SEM image, ZnO NPs addition results in considerable increase of film porosity and hence the surface area.

4. Conclusion:

Porosity of PZ3 sample was found to be more and its average crystalline size was found to be 90 nm, from XRD pattern. PZ3 sensor showed more sensitivity (about 0.624) at 90 ppm concentration of NH_3 gas among the remaining sensor. From dynamic response, response time and recovery times were found to be 3 min and 17 min. respectively. It showed that PZ3 sensor is fast in action.

5. References:

- [1] Jafarpour M.M., Foolad A., Mansouri M.K., Nikbakhsh Z. and Saeedi Zade H. (2010). Ammonia Sensing Properties of $(\text{SnO}_2\text{-ZnO})/\text{Polypyrrole}$ coaxial nanocables, World Acad Sci. Eng. Technol, 70, 940-945.
- [2] Raulkar K.B, Wasnik T.S, Joat R.V., Wadatkar A.S. Agrawal, R.M. and Lamdhade G.T., (2019). Study on DC Conductivity of PPy-ZnO Nanocomposites, Materialstudy Proceedings, 15(3), 595-603.
- [3] Jorgensen T.C. and Weatherley L.R. (2003). Ammonia removal from wastewater by

- ionexchange in the presence of organic contaminants, *Water Research* 37, 1723–1728.
- [4] Chougule M.A., Dalavi D.S., Sawanta Mali, Patil P.S., Moholkar A.V., Agawane G.L., Shashwati Sen and Patil V.B. (2012). Novel method for fabrication of room temperature polypyrrole–ZnO nanocomposite NO₂ sensor, *Elsevier-Measurement*, 45(8), 1989- 1996.
- [5] Mahaja C., Chaudhari P. and Mishra S. (2018). RGO–MWCNT–ZnO based polypyrrolenanocomposite for ammonia gas sensing, *Journal of Material Science*, 29, 8039–8048.
- [6] Chatterjee S., Shit A. and Nandi A.K. (2013). Nanochannel morphology of polypyrrole–ZnO nanocomposites towards dye sensitized solar cell application, *Journal of Materials Chemistry A*, 1, 12302–12309.
- [7] Abdolmajid B.M., Tayebe N., Badraghi J. and Kazemzad. (2009). Synthesis of ZnO Nanoparticles and Electrodeposition of Polypyrrole/ZnO Nanocomposite Film, *Int. J. Electrochem Sci.*, 4, 247–257.
- [8] Yeolea B., Sena T., Hansoraa D., Mishra S. (2016). Polypyrrole/Metal Sulphide Hybrid Nanocomposites: Synthesis, Characterization and Room Temperature Gas Sensing Properties, *Materials Research*, 19(5), 37-42.
- [9] A shour A., Kaid M.A., El-sayed N.Z. and Ibrahim A.A. (2006). Physical properties of ZnO thin films deposited by spray pyrolysis technique, *Applied surface Science*, 52,7844-7848.
- [10] Mohammad M.T., Hashim A.A. and Al-Maamory M.H. (2006). Highly conductive and transparent ZnO thin films prepared by spray pyrolysis technique, *Materials Chemistry and Physics*, 99, 382-387.
- [11] Chakraborty A., Mondal T., Bera S.K., Sen S.K., Ghosh R. and Paul G.K. (2008). Effects of Al and In incorporation on the structural and optical properties of ZnO thin films synthesized by spray pyrolysis technique, *Materials Chemistry and Physics*, 112,162-168.
- [12] Nemade K.R. and Waghuley S.A. (2012). V₂O₅-P₂O₅ Glass Ceramic As A Resistive Solid-State CO₂ Gas Sensor, *Asian Journal of Chemistry*, Vol. 24, No. 12, , 5947-5948.
- [13] Klug H.P. and Alexande L.E., (1974). X-ray Diffraction Procedure for Polycrystalline Materials, Wiley Online library,125-127.
- [14] Hamed A.K., Aryan Eghbali, Mansoor Keyanpour-Rad, Mohammad R.V. and Mahmoud Kazemzad. (2014). Ammonia sensing properties of (SnO₂–ZnO)/polypyrrole coaxial nanocables, *J. Mater Sci.*, 49, 685–690.
- [15] Shao H., Qian X.F. and Huang B.C., (2007). Fabrication of single crystal ZnO nanorods and ZnS nanotubes through a simple ultrasonic chemical solution method. *Materials Letters*, 61(17):3639-3643.

3

Emission Spectrum Analysis of Several Lighting and Display Devices Using USB650-UV-VI-SPI Mini Portable Spectrometer

Shailesh R. Jaiswal^{1*}, Rupali G. Korpe², Pankaj A. Nagpure²

¹Department of Physics, Shri R. L.T. College of Science, Akola. 444001(INDIA)

²Department of Physics, Shri Shivaji Science College, Amravati. 444602 (INDIA)

Abstracts

This study reports an analysis of emission spectra of various lighting and display devices using a USB650-UV-VI-SPI mini portable spectrometer with 'Spectra Suite Ocean Optic' computer software. This study also shed light on the biological effects of lighting devices on human health. The fourth new eco-friendly and health-friendly alternatives for lighting and display technology such as mercury-free fluorescent lamps (MFFLs) and organic LEDs have been put.

1. Introduction

Humans are exclusive animals on the planet that produces lighting using external sources. In olden eras, the sun light is one of the natural sources of light in day time but at night, lighting was obtained by burning dry vegetation. Progressively open fires were replaced by candles, fuel lamps and natural gas. In 1880, Thomas Edison invented an electric light appropriate for commercialization and today electric lighting predominates and our cities are covered in light well into the night. Over time due to the large development in lighting technology, it possible for lighting to be providing at lesser price to more numbers of individuals.

The commercial incandescent lamp which was developed by Edison's, operates by heating a tungsten filament to emit light. But in the incandescent lamp most of the energy is loss in to heat i.e., energy emitted in the infrared, outside the range of human vision. Over time electric lighting types expanded, a process driven by demand for cost efficiency, large area lighting, visual attractions and the preference for high color renderings that are similar to daylight [1]. However, over time incandescent lamp were replace by the gas discharge lamps (e.g., fluorescent, high-pressure sodium and metal halide). Gas discharge lamps are a light source that generates light by sending an electrical discharge through an ionized gas, plasma. Some lamps convert ultraviolet radiation (emitted photons of characteristics energy from gas discharge/ionized gas) to visible light with the help of phosphor coating on the inside of the lamp's glass surface. Such type of lamps is called low-pressure gas discharge lamps. The classic fluorescent lamp and compact fluorescent lamp (CFL) are the best examples of Low-pressure gas discharge lamps.

Fluorescent lamps are inexpensive, have a long life, have good luminous efficacy, and very good CRI but it contains mercury. All fluorescent lamps contaminate the environment with mercury when broken or disposed of after use. Because of their shapes and the structure of the materials, the collection and recycling of the lamps do not apply to every situation. Apart from that it contains ambient temperature affects the switch-on and output, and need auxiliary ballast and starter or electronic ballast. These are the major disadvantages of fluorescent lighting [2].

Nowadays replacement of fluorescent lamps with environmentally benign light sources such as light-emitting diodes (LEDs). The use of LEDs seems to be the most environmentally benign way of lightning. A characteristic method to producing "white" light from LEDs is to combine a blue LED (peak wavelength ~ 460 nm) with a phosphor coating to produce a broad spectrum in the green-yellow-red range. The manufacturer is able adjust the balance between

these two components to produce a range of correlated-color temperatures (CCTs) for "white" LEDs [1].

But W-LED still suffers from a poor color rendering index (CRI) [2] and a comparatively low luminous intensity (especially when a good CRI is attempted). Secondly it is found that most of the new commercial LED light bulbs emit a high proportion of the blue region reaching up to 35% of the total emitted light. Therefore, the biggest disadvantage of LED is the suppression of melatonin in humans due to blue light. From the literature survey, it is reported that blue light from light-emitting diodes elicits a dose-dependent suppression of melatonin in humans [3].

The fig.1 shows the history of lighting technologies which have been adopted by the human being.

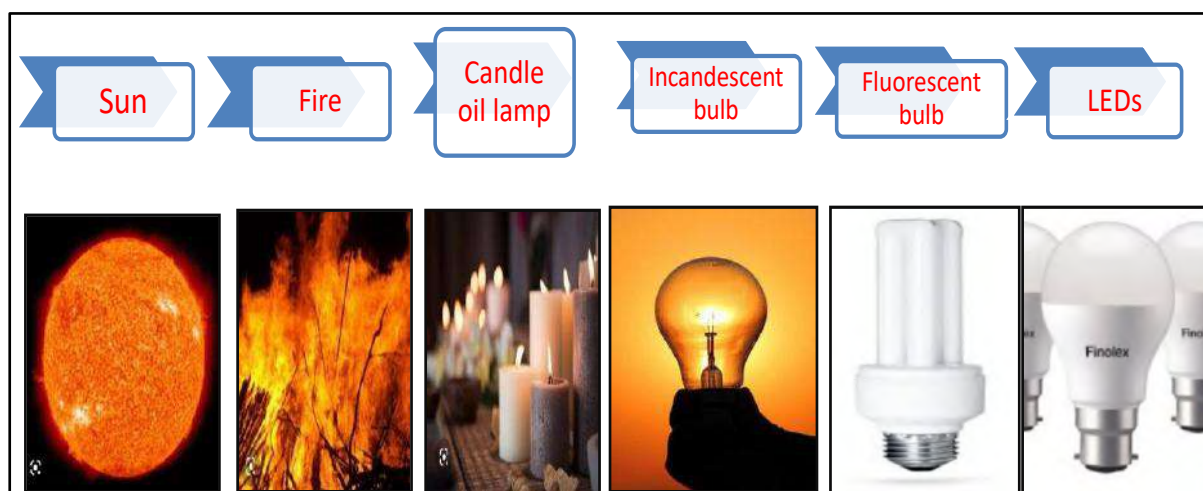


Fig.1: History of Lighting Technology [4]

In this report, we investigate the emission spectrums of different light sources (lighting and display devices) and also studies their biological effects on human health. For that we adopted directed method of reading, in which we identify the spectra of various lighting and display devices using USB650-UV-VI-SPI mini portable spectrometer with 'Spectra Suite Ocean Optic' computer software. Compare all the emission spectra (other sources of light, lighting and display devices) with daylight (Sun) spectra. Also put idea of forth new eco-friendly and health-friendly alternatives for lighting and display technology such as mercury-free fluorescent lamps (MFFLs) and organic LEDs.

2. Working Method

Emission spectra of various lighting and display devices were acquired using USB650-UV-VI-SPI mini portable spectrometer with 'Spectra Suite Ocean Optic' computer software. It has a wavelength range of 200-850 nm, and utilizes a detector with 650 active pixels; that's 650 data points in one full spectrum, or one data point per nanometer. The spectrometer is a low-cost, small- footprint lab spectrometer that's ideal as a general-purpose instrument for budget-conscious teaching and research labs. The innovativeness of this spectrometer is to directly measure the emission spectrum of any natural and artificial light sources. No need to collect the samples/phosphors of the devices for monitoring the spectra. Diagrammatic representation of the system is shown in the fig.2

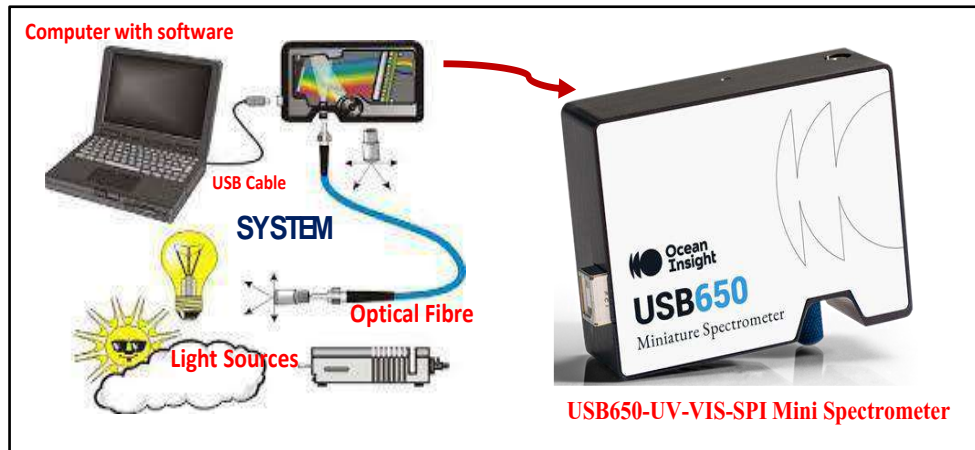


Fig.2: Complete System with USB650-UV-VI-SPI mini portable spectrometer [5]

3. Result

3.1 Spectral Power Distribution (SPD) of the Lighting Sources:

Sun Light Spectrum: Spectra were acquired from direct sunlight. The emission spectra of sun having all types of wavelengths starts with violet and blue colors, with a wavelength of 380 nanometers. It spans the range of visible light colors, including green, yellow and orange and ends at the bottom with red colors with a wavelength of 750 nm as shown in fig. 3 (a).

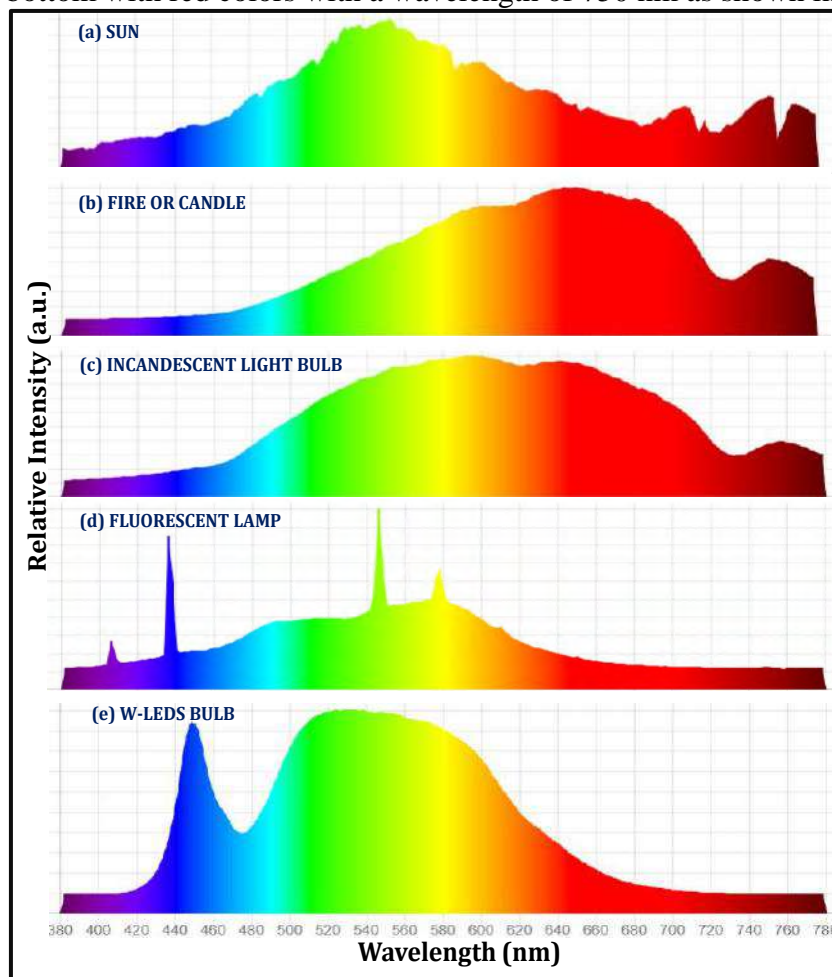


Fig.3: Spectral Characteristics of the Different Light Sources

Fire or Candle: Spectra were acquired from direct burning of fire or candle. The spectra have a flattened appearance, with the short wavelength and an upward swing in emission from 550 to 700 nm as shown in fig. 3 (b).

Incandescent Lamps: Spectra were acquired from incandescent lamp. The emission spectra of incandescent lamps have blackbody shapes. It is a thermal radiator that emit a continuous spectrum of light extending from about 380 nm to 780 nm as shown in fig. 3 (c).

Fluorescent Lamps: Spectra were acquired from fluorescent lamp. The fluorescent lamp is a low-pressure gas discharge lamp that generates light predominately by phosphors excited by UV emissions. The fluorescent lamp spectra show broad band spectra with consist of a set of sharp emission lines at wavelength of 408, 436, 544, 574 and 611 nm as shown in fig. 3 (d). The red emissions are found to be quite low.

Light Emitting Diodes (LED): Spectra were acquired from LED lamps. These are solid state light sources that generate light by electroluminescence, moving electrons from a high energy state to a lower energy state on a semi-conductor substrate. Fig. 3 (e) shows two spectra from white LED bulb containing the primary emission at 420–460 nm and the phosphor induced secondary emission in the green to red. The second emission peak in the W-LED spectrum is induced by a phosphor coating on the LED which absorbs a portion of the blue emission and reradiates at longer wavelengths.

3.2. Discrimination of Lighting Types

We compare the spectrum of various light sources such as sun light, fire, or candle, incandescent bulb, fluorescent tube and LED as shown in the fig. 4.

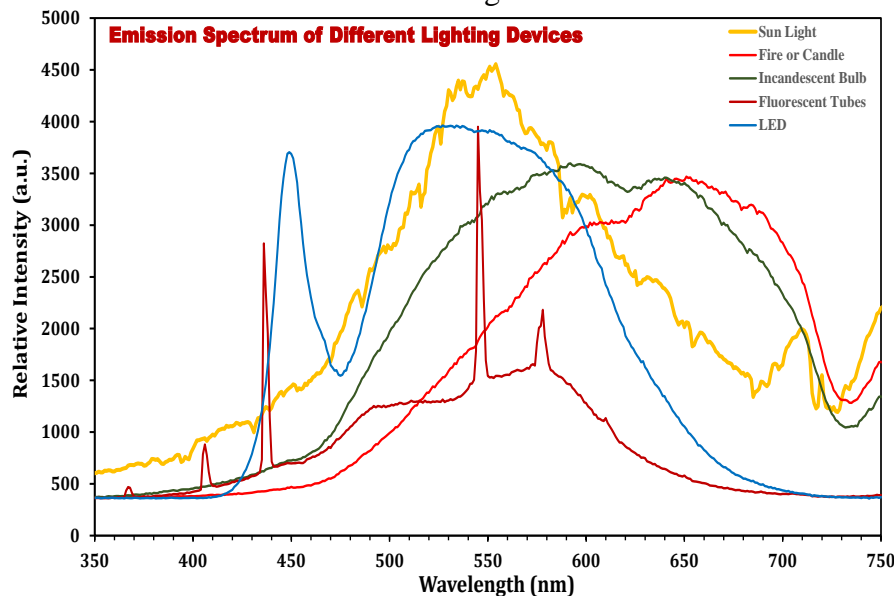


Fig. 4. Comparison of emission spectrum of different light sources

From the graph results in fig. 4, the emission of blue light spectra is more in LED. The blue spectrum element of W-LED spectrum accounts for a larger amount, thus creating the blue light problem. In most of the countries LED widely used both indoors (lighting and display devices) and outdoors (streetlight, automobile headlights etc.). Fig.5 shows emission spectrum of different flat LED display (Cell Phones/Laptops Screen/TVs Screen).

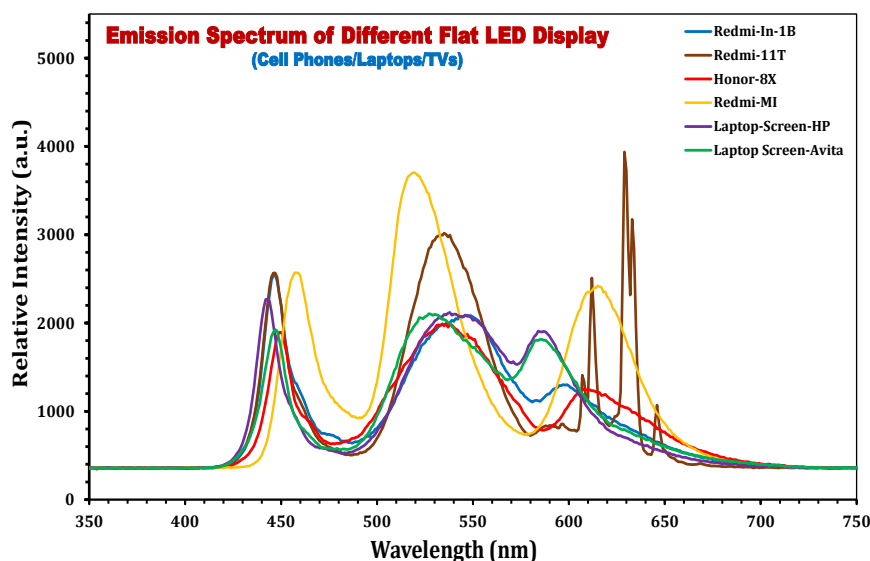


Fig.5 Emission spectrum of different flat LED display/ Screen

Many reports said that exposure to an intense and powerful (LED) light is ‘photo-toxic’ and can lead to irreversible loss of retinal cells and diminished sharpness of vision [6]. From the literature survey, it is reported that blue light from light-emitting diodes elicits a dose-dependent suppression of melatonin in humans [3].

4. Conclusion

In fact, artificial lighting is an integral part of our everyday life. We spend an average of 10-12 hours under these lights. It was observed that as compared to the emission spectrum of other light sources, LED emits blue light most so it causes melatonin suppression due to which sleeping pills can occur. Also, white LEDs still suffer from a poor color rendering index (CRI) due to comparatively low luminous intensity. It is, therefore, important that LED lights need the photobiological safety standards prescribed internationally. In fluorescent lamps, low-pressure mercury vapor is used, and this mercury caused an adverse effect on human health. It is concluded that this lighting technology may have two alternatives one is mercury-free fluorescent lamps in which we can use Xe discharge rather than Hg & other may be organic LED in which we can suppress the blue color. The future will show if this developing technology will take market shares in the lighting field. We hope that their use will favor the design of new eco-friendly and health-friendly lighting technologies.

Acknowledgement

One of the authors is very thank full to the department of Physics, Shri Shivaji Science College, Amravati for providing the facilities of mini spectrometer. The authors thank all those who helped them in this work.

References:

1. C. D. Elvidge, D. M. Keith, B. T. Tuttle, and K. E. Baugh, *Sensors* **10** (2010) 3961-3988
2. N. C. George, K. A. Denault and R. Seshadri, *Annual Review of Materials Research* **43** (2013) 481–501.
3. K. E. West and et al, *Journal of Applied Physiology* **110** (2011) 619–626.
4. G. Zissis, *Light Sources and Lighting* **7** (2013) 333-374.
5. <https://whitebearphotonics.com/products/usb-650>
6. F. Falchi, P. Cinzano, C. Elvidge, D. Keith, and H. Haim. *Journal of Environmental Management* **92** (2011) 2714

4

Effect on Polymer blend of Proton Doner Polymer Electrolyte**S. P. Bakde¹, S. R. Jadhao²**¹Department of Physics, Shri R. R. Lahoti Science College Morsh, Dist. Amravati, Maharashtra, India.²Department of Physics, Nehru Mahavidyalaya , Arts, Commerce, Science College, Nerpersopant, Dist. Yavatmal, Maharashtra, India.**Abstract:**

Solid polymer blend electrolytes of polyvinyl alcohol (PVA) and Polyethylene glycol (PEG) complex with ammonium nitrate (NH₄Br) salt in different compositions have been prepared by solution cast technique using distilled water as a solvent. The complexation of these flim has been studied by AC electrical conductivity. The dielectric constant, dielectric loss and ac conductivity of PVA:PEG has been observed to increase along with the addition of ammonium bromide at the different frequency and temperature range. The AC conductivity was measured using 4284 LCR meter in frequency range of 20Hz to 1MHz and at different temperature.

Keywords: Polymer blends, Ammonium salts, AC conductivity.

Introduction:

Many researchers have been carried out for prepared environment friendly biodegradable materials. These materials have been found useful for drug delivery, pharmaceuticals, paints, textiles, and tissue engineering applications. They have many uses, with many new applications involving blends of these polymers with other polymers and other materials [1]. The selection of polymers for blending plays a major role in attaining good mechanical, thermal and electrical properties. PEG are synthetic water soluble polymers having a wide range of applications, including use in pharmaceutical experiments, food additives and plasticizers [2-3]. PVA is a nontoxin and water soluble polymer having good charge storage capacity [4]. To increase the ionic conductivity depend on the addition of some dopant (ammonium salts) in polymer. Ammonium salts have been a very good proton doner to the polymer matrix system and to increase the conductivity [5-7]. In this paper the attempt has been made to investigate effect of dopent on ac conductivity of PVA-PEG blends.

Experimental technique:

The solid polymer electrolyte of pure (PVA + PEG) with Ammonium Bromide were prepared in different concentration (95:05), (85:15), (75:25) by solution casting technique. In this technique, PVA and PEG were dissolving in water separately. After dissolving same concentration of PAV + PEG mix with ammonium bromide salt then stirred well by using magnetic stirred for 10-12 hr to obtained homogenous mixture. The obtained mixture is casted in petri dish. The whole assembly was placed in dust free chamber. The solvent was allowed to evaporate slowly at room temperature for 3-4 days. The dried blend solid polymer electrolyte films were formed. The AC conductivity were measured using 4284 LCR meter in frequency range of 20Hz to 1MHz and at different temperature.

Result and Discussion:

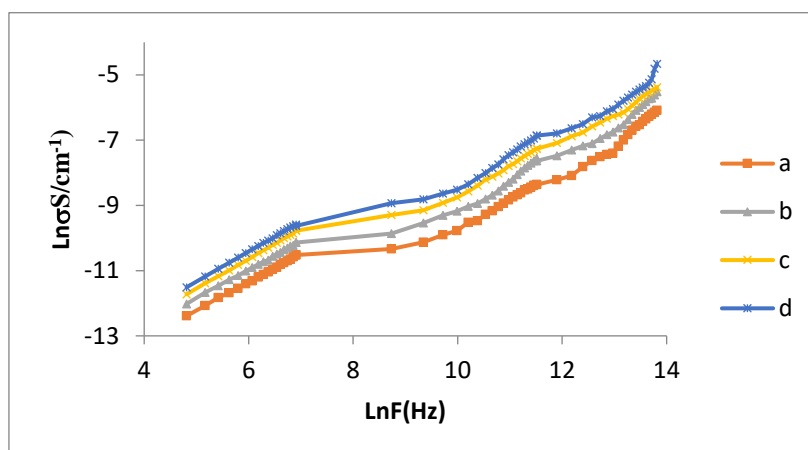


Fig 1: Variation of AC conductivity with frequency (a) PVA-PEG (b) 5 mole %, (c) 15 mole %, (d) 25 mole % of NH_4Br .

The fig. 1 shows that the variation between AC conductivity with frequency for (a) PVA:PEG, (b) PVA:PEG: NH_4Br (95:05) and (c) PVA:PEG: NH_4Br (85:15), PVA:PEG: NH_4Br (75:25). It is observed that the conductivity increases with an increase of frequency in all composition due to more number of free ions. This will increase mobile of charge carrier. [8-9]. It found that conductivity of PVA:PEG blend increases with increase in salt concentration upto 25 mol% due to enhancement of ionic mobility and the large number of carrier ions being introduced into the complex [10-11].

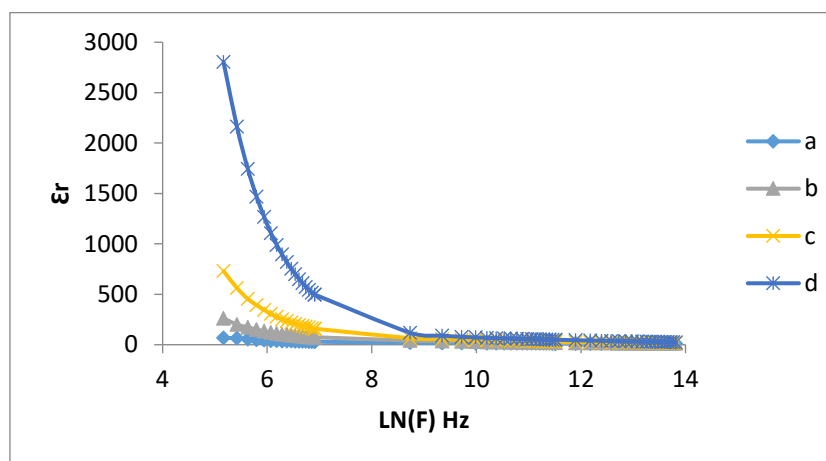


Fig 2: Variation of Dielectric constant with frequency (a) PVA-PEG (b) 5 mole %, (c) 15 mole %, (d) 25 mole % of NH_4Br .

The frequency dependent dielectric constant of PVA-PEG- NH_4Br mole % as shown in (figure 2). It is observed that dielectric constant is high at low frequency. Due to contribution of charge accumulation at electrode-electrolyte interface. But in high frequency dielectric constant decreases and nearly constant value with increases in frequency. This is due to the dipole not being able to follow opposite of electric field variation at higher frequency [12-13].

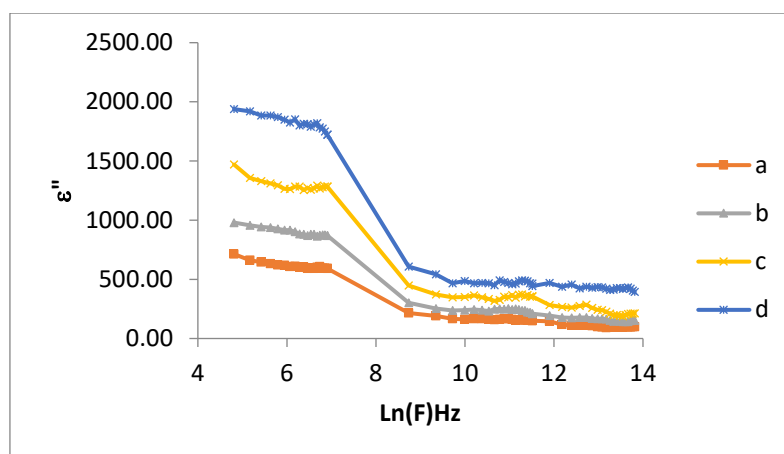


Fig 3: Variation of Dielectric loss with frequency (a) PVA-PEG (b) 5 mole %, (c) 15 mole %, (d) 25 mole % of NH₄Br.

The dielectric loss as a function of frequency is shown in fig 3 shows the dependence of (ϵ'') on the frequency at room temperature. It is found that the dielectric loss is high at low frequencies and decreases with increase in the frequency. The origins of the dielectric losses are the conduction of losses [14].

Conclusion:

Solid polymer blend electrolytes of polyvinyl alcohol (PVA) and Polyethylene glycol (PEG) complex with ammonium nitrate (NH₄Br) salt in different compositions have been prepared by solution cast technique. The conductivity of PVA:PEG complexed with ammonium bromide (NH₄Br) increase with increasing frequency and concentration of ammonium salt. The frequency dependant dielectric constant and dielectric loss decreases with increase in frequency. It is reveal that electrical conductivity of PVA-PEG doped with NH₄Br increases with increasing salt concentration as well as temperature, which is attributed to the formation of charge transfer complexes.

References:

1. G. Swift, Polymer Degradation and Stability, 45 (2), 215–231, (1994).
2. D. B. Braun & D. J. Delong, Kirk-Othmer Encyclopedia of Chemical Technology, 3rd edn, 18, 616-32, (1982).
3. Y. R. Gowrikar, N. Y. Yishwanathan & Sreedhar Jayadev, Polymer Science (Wiley Eastern Limited, New Delhi), (1986).
4. Jr. F. Billmeyer, Text book of polymer Science , Eiley Singapore, (1984).
5. M. Kumar, S. S. Sekhon Eur polymer J 38, 1297-1304, (2002).
6. M. Hema, S. Svasekarapandian, A. Sakunthala, D. Arunkumar, H. Nithiya, Physica 403, 2740-2747, (2008).
7. A. M. Stephan, Eur. Polym. J. 42, 21-40, (2006).
8. S. Ramesh, A. K. Arof, Mater Sci Eng B, 85, 11-15, (2001).
9. D. K. Pradhan, R. N. P Chaudhary, B. K. Samantaray, Mater Chem. Phys., 11, 557-561, (2009).
10. N. Vijaya, S. Selvasekarapandian, G. Hirankumar, S. Karthikeyan, H. Nithya, C. S. Ramya, M. Prabhu, Ionics, 18, 91-99, (2011).
11. S. L. Palaa, S. N. Varmaa, N. Krishna Jyothib and K. V. KumarcJ. Indian Chem. Soc., 96, 182-184, 2019.
12. S. Ibrahim, S. M. M. Yasin, N. M. Nee, R. Ahamad, M. R. Johan, solid state commun, 426-434, (2012).
13. S. Ramesh, A. H. Yahana, A. K. Arof, solid state Ionics, 291-294, (2002).
14. E. H. Zareh, P. N. Moghadam, E. Azarian, I. Sharifia, Iranian polymer Journal, 20 (4), 319-328, (2011).

Photovoltaic applications of SnO₂ gas sensor

B.H.Bhatti^{1*}, K.B.Raulkar², G. T. Lamdhade³, A. O. Chauhan⁴, R. B. Butley⁵,
C. C. Jadhao⁶, A. B. More⁷

¹Department of Physics, Indira Gandhi Mahavidyalaya, Ralegaon District- Yavatmal (445402), Maharashtra, India.

^{2,3,4,5,6,7}Department of Physics, Vidya Bharati Mahavidyalaya, C. K. Naidu Road, Camp, Amravati (444602), Maharashtra,

*Corresponding Author: bhushanbhatti80@gmail.com

Abstract

Tin oxide is a remarkable chemical in today's research because to its unique electrical and optical properties. Because of its huge band gap (3.6 eV), it is used as a core material in a wide range of important applications, including optoelectronics, spintronics, photovoltaics, thin-film transistors, photocatalysis, dielectrics, sensors, and transparent electronics. Thin film technology provides various advantages in the solar industry, including low cost, low material and energy consumption, and ease of use. Solar cells made from SnO₂ thin films have the potential to open up new technical paths for power production, with conversion efficiencies ranging from 15% to 20%. The authors examine and outline potential areas of SnO₂ research for photovoltaic and gas sensor applications. The data obtained will indicate the possibility of designing physical, chemical, magnetic, and optical characteristics of SnO₂ for sensing and photovoltaic applications.

Keywords: Tin oxide, Photovoltaic, Thin film, Gas sensors.

1. Introduction

Material science is the systematic investigation of any material to determine its varied characteristics and qualities. It covers a wide variety of applications, from manufacturing nanoscale gadgets to developing novel materials at the atomic level. In the current context, we are dealing with a number of difficulties linked to traditional energy sources, global warming, soil and water contamination, climate change, sanitation, and so on. Our primary objective is to alleviate these issues by bringing new technologies and advanced materials. Nanotechnology and thin films play an essential role in dealing with such challenges. As stated by [1], this can be used to enhance the performance of currently used materials and develop new functional materials. This is because they not only offer good opportunities to study the optical, electrical, and thermal properties in quantum confinement, but they also provide crucial understandings of the functional units involved in the fabrication of nanoscale electronic, optoelectronic, and magnetic devices.

ZnO, TiO₂, and SnO₂ are the most studied metal oxides due to their unique global uses. Tin oxide is the best option for photovoltaic investigations since it is plentiful, affordable, and non-toxic. The primary goal of this research is to learn more about the functioning of SnO₂ and to identify potential research topics for future applications in photovoltaics and gas sensors [2].

2. Overview of Tin Oxide and its Properties

From the past several decades semiconducting (Metal) oxides such as ZnO, TiO₂ and SnO₂ have been demonstrated to be an essential class of transparent conducting oxides (TCO) for use in solar cells and gas sensors. Tin oxide is the most common material used in optoelectronics because to its low electrical resistance and high transmittance in the visible range [3]. Tin oxide is a good option for these uses due to its large band gap (3.6 eV) and strong excitation binding energy (130 MeV). It is the only group-IV oxide that exhibits transparent properties and excellent conductivity in the visible range of (300–800 nm). Bulk

SnO_2 is unable to achieve effective UV emission because of the dipole-forbidden rule. Structural morphology, tetragonal structure of pure and SnO_2 thin films doped with TM of material is clearly visible by AFM measurements as shown in Fig.1.

3. Methodology

SnO_2 films may be grown using a variety of deposition processes, including chemical vapor deposition, spray pyrolysis, thermal evaporation, sol-gel, and sputtering. Recently, the Sol-Gel process was employed to create several high-quality thin films for photovoltaics and gas sensors.

3.1 Chemical deposition technique

3.1.1 Chemical vapor deposition (CVD)

CVD is a chemical approach for vacuum deposition in which gaseous precursors are transferred into a chamber with the substrate. At high temperatures, the chemical interaction between the precursor and the substrate can provide the needed thin layer thickness. This is a prominent method in the semiconductor industry for producing high-quality, high-performance semiconductors [4]. There are numerous CVD methods for producing thin films, including thermal chemical vapor deposition, APCVD (Atmospheric-pressure CVD), MOCVD (Metalorganic chemical vapor deposition), PECVD (Plasma-enhanced chemical deposition), LCVD (Laser Assisted Vapor Deposition), and PACVD (Photo-assisted chemical vapor deposition).

3.1.2 Atomic layer deposition (ALD)

The atomic layer deposition process is also known as vapor phase deposition. In this approach, the reactions between gaseous precursors and substrate occur one at a time. This process uses two or more gaseous precursors to produce a thin coating of the appropriate thickness. ALD is a step-by-step method in which precursors react exclusively with the available substrate and no further reactions occur after the surface is saturated. As a result, it is a slower process, but it allows for fine thickness control of the film even at lower temperatures [5,6].

3.1.3 Sol- Gel Method

Sol-Gel is a chemical solution deposition process in which precursor materials generate a solution known as 'sol'. This 'sol' was placed on the substrate using a carefully regulated method. The Sol-Gel approach comprises a gelation process in which the precursor material converts from a liquid 'sol' to a solid 'gel' form [6]. This solution is known as a sol-gel, which is a continual mixture of suspended precursor particles and substrate. The sol-gel process includes spin coating, dipping, and spraying. Table 1 is a brief summary of various ways for synthesizing a thin film for practical applications.

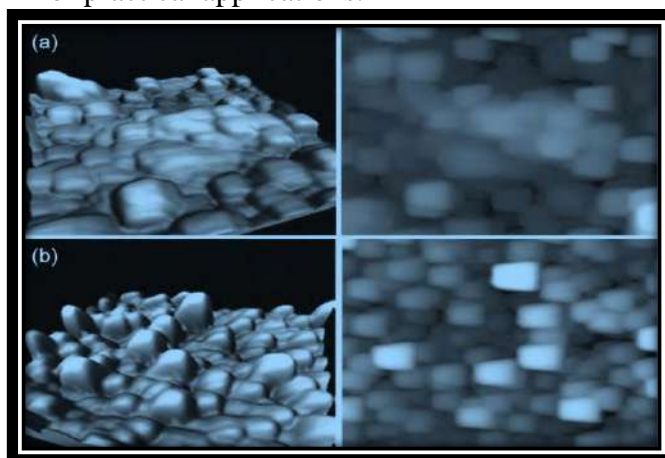


Fig. 1 — 3D AFM images of (a) pure SnO_2 and (b) doped $\text{Sn}_{0.095}\text{Mn}_{0.005}\text{O}_2$ thin films.

3.2 Physical deposition technique

3.2.2 Sputtering

Sputtering is a physical thin film deposition process in which surface atoms are liberated by blasting the surface of a target material with ions before coming to rest on the substrate. At low temperatures, the target material for this deposition process is Nobel gas Argon. Normally, Nobel gas is less reactive, thus it acts neutrally during any chemical reaction in the chamber, making it a quick and reliable approach. Sputtering is obviously an etching method, making it suitable for surface cleaning applications [7]. We grouped the sputtering process into four types: diode sputtering, reactive sputtering, bias sputtering, and ion beam sputtering.

3.2.3 Thermal evaporation

In thermal evaporation, the material is heated in a vacuum chamber until its surface atoms have sufficient energy to leave the surface. The evaporated material then condensed on the substrate for synthesis of thin film of desired thickness.

3.2.4 Spray pyrolysis deposition

Spray pyrolysis involves spraying a solution over a heated surface to form a thin layer. Spray pyrolysis is the chemical dissociation or evaporation of droplets containing a solute of the desired nanomaterial [8]. As a result, it has been adopted by both gas-phase and liquid-phase approaches. The spray pyrolysis technique works by creating an aerosol from a variety of precursor solutions, such as a metallic salt solution or a colloidal solution²⁵. It is a non-reversible method that achieves great efficiency.

4. Tin Oxide as Photovoltaic Cell

PV materials for photovoltaic applications work via the photoelectric effect. In this process, the exposed PV material turns electromagnetic energy (sunlight) into electrical energy. Photovoltaic cells are the most demanding renewable energy sources [9]. It offers several benefits over other sources of energy such as fossil fuels and petroleum. It is a viable and sustainable energy source that will meet growing energy demand without harming our environment. Zhu et al.[10] successfully used solution-processed SnO₂ nanocrystals to build an effective ETL for inverted thin film photovoltaic solar cells.

Table 1 — A glance of various preparation methods of thin film deposition of SnO₂ material.				
Thin Films Deposition Techniques				
Chemical Process (Non-equilibrium reaction)		Physical Process (Equilibrium reaction)		
	↓			↓
Plating	Sol Gel	CVD	Evaporation	Sputtering
Electroplating	Dipping	MOCVD	Ion Plating	RF
Electrolysis	Spraying	PECVD	MBE	DC
Flame Hydrolysis deposition (FHD)	Spin Coating	ALD	Laser ablation & Electron Beam	Magnetron

They proposed that due to several unique features, SnO₂ is more suitable than ZnO and TiO₂. In their article, Dong et al. [11] investigated compact SnO₂ ESL and compact TiO₂ ESL, as well as their PCEs. Fabrication of thin films using the sol-gel technique. They characterized the films using SEM, J-V curves, PL, XRD, and IPCE. In their article, Roose et al. [12] detailed the UV instability of a perovskite solar cell employing my TiO₂. They came to the conclusion that employing a thin coating of m- SnO₂ may solve this instability. In their trials, they reached a high efficiency of around 16.4%. The solar cell is made from Ga doped SnO₂ film. The authors reported an approximate PCE of up to 23% for perovskite solar cells using the spin

coating and single gel procedures for deposition of SnO₂ thin films and examination of their characteristics by comparing thermally annealed SnO₂ TF (T-SnO₂) and P- SnO₂ TF [13-14].

5. Tin Oxide as Gas Sensors

Nowadays, gas sensors are the most exciting study topic because they are effective in monitoring environmental concerns based on the needs of physical, chemical, and biological processes in the Earth's atmosphere. Researchers want to increase its durability, responsiveness, and sensitivity. Gas sensors have an essential role in environmental monitoring, medical applications, breath analysis for medical diagnostics, industrial applications, food processing, and so on [15]. Gas sensors are primarily used to differentiate odors, detect gases, and monitor changes in specific gases in the atmosphere. Material selection has a significant impact on gas sensor performance.

Beniwal A et al. [15] explored a SnO₂ sensor for detecting low-concentration ammonia at ambient temperature. They synthesized SnO₂ thin films using the sol-gel process and characterized them using XRD, AFM, XPS, and SEM. They concluded

that it is a highly promising sensor for detecting Ammonia concentration at extremely low temperatures, and that it would have a wide range of applications in the future due to its outstanding stability, adequate recovery time, and good responsiveness. Gupta P et al. [16] proposed that doping Zn improves the gas sensing characteristics of SnO₂, such as surface shape, crystallinity, crystal size, and so on. They found that SnO₂ has higher sensitivity for O₂ gas sensing than pure and Zn doped SnO₂. Khuspe G D et al. [17] found in their investigation that SnO₂ is more sensitive and stable to NO₂ gas. They reported a higher sensor response of 19% and stability of 77.90%. Zhou Q et al. [18] found that Ni and Zn doped SnO₂ gas sensors recovered and responded more quickly than specific Zn or Ni doped SnO₂ nanomaterials did. They conducted several studies on the concentration of harmful CO gas and discovered improved sensitivity and stability.

6. Results and Discussion

The authors of the current study looked into recent improvements in tin oxide. A study on alternate methods for producing SnO₂ thin films in pure, composite, and doped with transition metals to exhibit structural and electrical properties has been presented. This article describes many methods of synthesizing SnO₂ films to highlight their merits and drawbacks, as well as numerous advances and their different effects and potential applications, notably in photovoltaics and gas sensors. With so many fascinating applications for SnO₂ thin films, we are concentrating on the most demanding ones: photovoltaics and sensors. Excellent charge collecting qualities in solar cells and a promising future for green energy technology are two of SnO₂'s many advantages. Pure SnO₂ thin films produced using a variety of techniques, including sol-gel, ALD, spin coating, PLD, and sputtering, had the highest PCE of 19.56% [14]. The PCEs of Nb doped SnO₂ thin film, Mg doped SnO₂ thin film, and Ga doped SnO₂ thin film, with doping of transition metals, are 17.57%, 14.60%, and 16.40%, respectively [35–37]. According to the inquiry, the Composite thin film of SnO₂-TiO₂ acquired the greatest PCE of 40% of all the studies, 21.10%. Comparably, pure SnO₂ thin films made using the Sol-gel process respond to ammonia (NH₃) gas with a 28% reaction and NO₂ gas with a 19% response [15, 17]. The authors have reported an enhanced high response and sensitivity of 37.6% for the monitoring of O₂ gas by doping of Zn in SnO₂ thin film [16]. Researchers used Ni and Zn doping in their studies to monitor CO gas, and they discovered that the responses were 7.28 and 5.90, respectively.

7. Conclusions

The fabrication of SnO₂ thin films using the Sol gel technique still has a lot of untapped potential. It is worth noting that, among the alternative synthesis technologies, the Sol gel technique is the most appropriate due to its clear advantages of precision, simplicity, flexibility, homogeneity, and uniformity. However, one of its advantages is that the manufacture of SnO₂ thin films by sol gel allows for essential characterizations such as XPS and VBS studies on SnO₂ materials. We hope that the study of this characterization technique may explore the new path of photovoltaic and gas sensor applications, which can be useful to achieve the desired efficiencies of solar cells for future aspects as well as excellent performance (gas response, selectivity, stability, sensitivity) in gas sensor.

8. References

1. Brinker C J & Ginger D, *Nanotechnol Res Dir Soc*, 2020 (2011) 261.
2. Das S & Jayaraman V, *Prog Mater Sci*, 66 (2014) 112.
3. Kim H & Pique, *Appl Phys Lett*, 84 (2004) 218.
4. Wang J T, *Modern Inorg Synth Chem*, 7 (2011)151.
5. George S M, *Chem Rev*, 110 (2010) 111.
6. Shim E, *Smart Text Protect*, 3 (2013) 87.
7. Kern W & Schuegraf K K, (Eds) *Handbook of thin film deposition, Process and Tech*, (Intel Corporation Santa Clara, California) 2002.
8. Ashik U P M, Kudo S & Hayashi J, *Synth Inorg Nanomater*, 2 (2018) 19.
9. Grama S, Massachusetts Institute of Technology, System Design and Management Program, (2007).
10. Zhu Z, Bai Y, Liu X, Chueh C, Yang S & Jen A, *Adv Mater*, 28 (2016) 6478.
11. Dong Q, Shi Y, Wang K, Li Y, Wang S, Zhang H, Xing Y, Du Y, Bai X & Ma T, *J Phys Chem C*, 119 (2015) 10212.
12. Roose B, Johansen C M, Dupraz K, Jaouen T, Aebi P, Steiner U & Abate A, *J Mater Chem A*, 6 (2018) 1850.
13. Ganchev M, Katerski A, Stankova S, Eensalu J S, Terziyska P, Gergova R, Popkirov G & Vitanov P, *IOP J Phys Conf Ser*, 1186 (2019) 01202.
14. Yu H, Yeom H I, Lee J W, Lee K, Hwang D, Yun J, Hwang D, Yun J, Ryu J, Lee J, Bae S, Kim S K & Jang J, *Adv Mater*, 30 (2018) 1704825.
15. Beniwal A, Srivastava V & Sunny, *Mater Res Express*, 6 (2019) 4.
16. Gupta P & Sharma S K, *Mater Res Express*, 4 (2017) 065010.
17. Khuspe G D, Sakhare R D, Navale S T, Chougule M A, Kolekar Y D, Mulika R N, Pawar R C, Lee C S & Patil V B, *Ceram Int*, 39 (2013) 8673.
18. Zhou Q, Chen W, Xu L, Kumar R, Gui Y, Zhao Z, Tang C & Zhu S, *Ceram Int*, 44 (2018) 4392.

6

Green Synthesis of Zinc Oxide Nanoparticles using Neem Leaf Extract and their Characterization

R. M. Agrawal*, K M Heda, S D Charpe, P P Raut, G T Lamdhade

Department of Physics, Shri RLT College of Science, Civil Line Road, Akola 444001(M.S.) Department of Physics, J.D. Patil Sangludkar Mahavidyalaya, Daryapur Dist. Amravati, Maharashtra-444803

Department of Physics, Vidya Bharati Mahavidyalaya Camp, C.K. Naidu Road, Amravati,(M.S.) 444602

*Corresponding author. Tel: (+91) 9422917514; E-mail: agrawal195@gmail.com, sushildeo86@gmail.com.

Abstract

Zinc oxide (ZnO) nanoparticles was synthesized by using (*Azadirachta Indica*) Neem leaf extract. In these different parts of neem tree such as leaves, bark, twigs and fruits are used for synthesis ZnO nanoparticles mainly by two methods: one by soaking and another by boiling. It also provides an unconventional and fresh approach which shows that it is a reliable, non-toxic in nature, eco-friendly and also low-cost method. The synthesized Zinc oxide nanoparticle was then characterized by using X-ray diffraction technique, Ultra violet (UV) and FTIR technique. The particle size was found to be 32 nm. It also exhibits the synthesized nanoparticle are in crystalline in nature. This method offers a biological technique to synthesize ZnO nanoparticles in controlled and precise manner with well-defined diverse sizes and shapes. Also, the band gap energy was found to be 4.5 eV. The green synthesized method can be used as an alternative to the existing chemical and physical methods.

Key Words: *Neem Leaf, Zinc Nitrate.*

1. Introduction

Over last few decades, nanotechnology has established as the great innovation in modern science and technology. Nanoparticle is well-defined as a small object that behaves as a whole part in terms of its transport and properties. (1). As Green synthesis of nanoparticle is an advanced and innovative branch of nanotechnology it has gained more significant importance and become one of the most useable methods (2). The biosynthesis method of plant extracts has drawn attention as a simple and viable substitute to chemical procedures and physical methods [3]. Zinc oxide, is a crystalline yellowish-white powder and is almost completely soluble in water. It shows hexagonal Wurtzite crystalline structure. The Zinc Oxide Nanoparticles is a type of inorganic compound and due to the unique physical, chemical, and biological properties it has widespread application as an additive in a wide variety of materials and products, including ceramics, glass, cement, and rubber, amongst others (4,5). *Azadirachta indica* commonly known as Neem belongs to *Meliaceae* family. Each part of the tree has been used as a traditional medicine for various household remedy. The major advantage of using the neem leaves is that it is a normally available medicinal plant and the biosynthesized ZnO nanoparticle might have been enhanced as it was capped with the neem leaf extract [6].

2. Experimental

Synthesis of Zinc Oxide Nanoparticles

Preparation of Neem Leaves (*Azadirachta Indica*) Extract

Zinc oxide (ZnO) nanoparticles were synthesized from neem (*Azadirachta indica*) and leaf extracts using zinc nitrate ($Zn(NO_3)_2$) as the precursor. The leaves were washed with water to remove dirt and dust and dried. The leaves were then oven dried at 30 °C for 6-8 days. After

complete drying, the leaves were ground to powder using a mixer grinder by using moter pestel. The powder is then mixer grinder and add 250 ml of distilled water and stirred to obtained Neem leaf extract.

After that 150 ml neem leaf extracts were boiled on a hot water bath. when the leaf extract started boiling, 20 g zinc nitrate was added and stirred constantly. The mixture was boiled till paste was obtained. The paste was then transferred to silica crucible and heated at high temperature of 600 °C for one hours in a muffle furnace. A white colour Zinc oxide nanoparticles obtained.

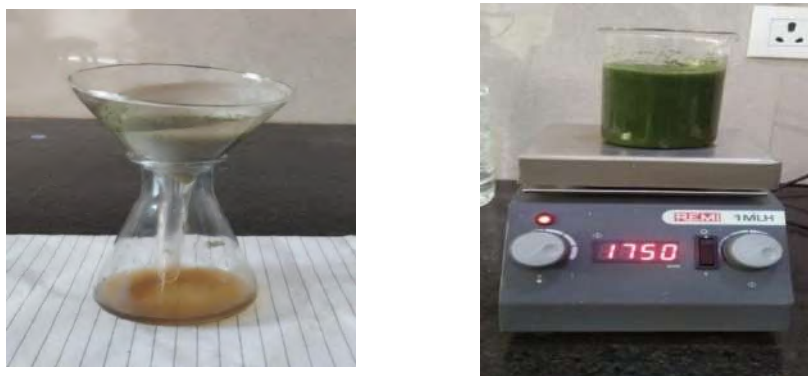


Figure 3.1 : Preparation of Neem leaves (*Azadirachta Indica*) extract

3. Characterization

Zinc oxide nanoparticle was synthesized by using green synthesis method from zinc nitrate $Zn(NO_3)_2 \cdot 6H_2O$, using Neem (*Azadirachta Indica*) Leaf Extract. The obtained material was calcinated at 600 °c in muffle furnace.

3.1. X-ray diffraction analysis

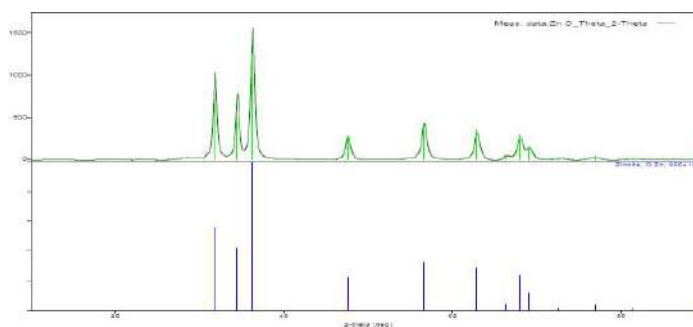


Figure 3.2 : X Ray Diffraction

The XRD pattern of pristine zinc oxide (ZnO) nanoparticle synthesized by green synthesis method and calcinated at 600°C as shown in figure 4.1.(a).The crystalline nature with 2 θ peak lying at (100), (002), (101), (102), (110) and (103) planes. All the peaks match well the standard hexagonal wurtzite structure of zinc oxide (ZnO) with lattice constants $a = b = 0.3249$ nm and $c = 0.5206$ nm [JCPDS card no. 36-1451]. All the peaks are perfectly match with pure ZnO structure, which indicates the high purity of the obtained ZnO nanoparticle. The average crystalline size was found to be 21 nm calculated by Deye-Scherrer formula [7].

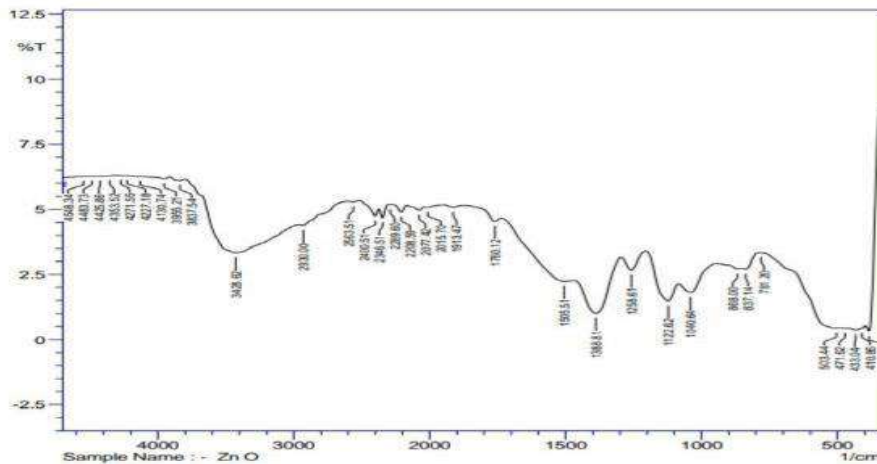
3.2 Fourier Transform Infrared

The FTIR spectrum of ZnO nanoparticles is shown in Figure 3. The major peak for the Neem plant extract shifting from 3428.62 cm^{-1} ZnO was assigned to the O-H of the phenol groups and -NH_2 stretching vibrations. $837\text{-}805 \text{ cm}^{-1}$ for the aromatic compound (C-H) and stretching for the amine group C-N, C=C and N-H at the range of 1505 cm^{-1} . ZnO nanoparticles showed a sharp and intense at 433.04 cm^{-1} [8]

Figure 3.3 FTIR Spectroscopy of ZnO NPs

3.3 UV-Visible spectroscopy

UV-phototypesetter analysis was done for preliminary confirmation of green synthesized



nanoparticles. Absorbance peak of green synthesized ZnO NPs obtained in UV wavelength

range (200-375nm), which confirmed their size in nano range. ZnO NPs synthesized using Neem extract exhibited absorbance peaks at 272 nm.[9]

The band gap for the nanoparticle is calculated by the formula = $E = hc/\lambda$ calculated band gap value is 4.5 eV.

where,

E = band gap

h = Planck's

constant c =

velocity of the light

λ = wavelength

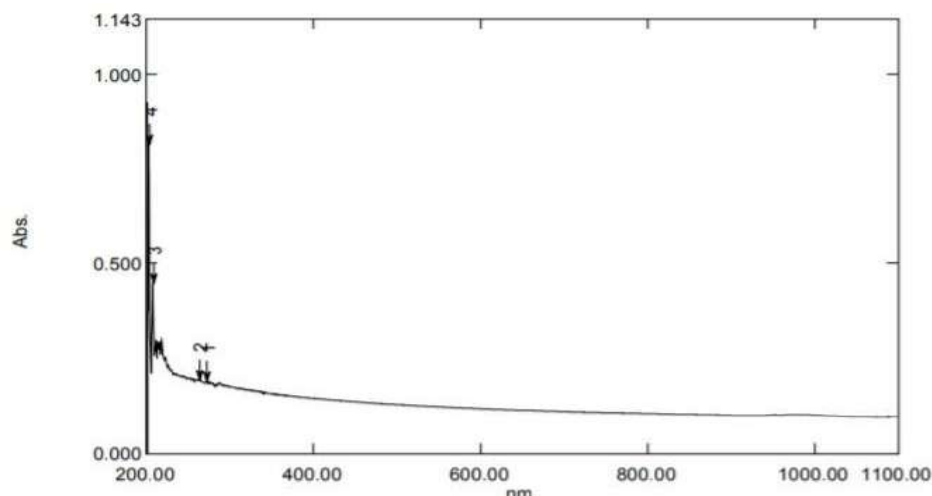


Figure 3.4. UV -Vis spectrum of ZnO NPs.

4. Conclusion

Zinc oxide nanoparticle was synthesised by a simple, efficient, cheap, environment-friendly and green protocol by using $\text{Zn}(\text{NO}_3)_2 \cdot 6\text{H}_2\text{O}$ with neem (*Azadirachta Indica*) Leaf extract. The material was characterised by using X Ray diffraction method and particle size was found to be 21 nm. The synthesis of ZnO NP was measured using the UV- Visible spectroscopy at a maximum absorbance of 272 nm. The FTIR analysis shows the presence of some reducing biomolecules associated with some organic functional (O=H) groups responsible for the encapsulation and stabilization of the NPs. The band gap of prepared ZnO nanoparticle is found to be 4.5 eV.

References

- [1]. Prathna, T.C., Chandrasekaran, Ashok, M., Raichur and Amitava Mukherjee. 2012. Biomimetic synthesis of nanoparticles. *Science, Technology & Applicability*, 20(2): 76-80.
- [2]. Barnali Ashe. 2011. A Detail investigation to observe the effect of zinc oxide and Silver nanoparticles in biological system, Ph.D. Thesis, Department of Biotechnology & Medical Engineering, National Institute of Technology, Rourkela, India: p.2.
- [3]. Nagajyoti, P.C., Prasad, T.N.V.K.V., Sreekanth, T.V.M., KapDuk Lee. (2011). Biofabrication of silver nanoparticles using leaf extract of *Saururus chinensis*. *Digest J.Nanomat. Biostruct.* 6(1):121-133.
- [4]. Sabir, S.; Arshad, M. and Chaudhari, S.K. (2014). Zinc oxide nanoparticles for revolutionizing agriculture: synthesis and applications. *J. Scientific. Worl.*, 8: 2014
- [5]. Alwan, R.M.; Kadhim, Q.A.; Sahan, K.M.; Ali, R.A.; Mahdi, R.J.; Kassim, N.A. and Jassim, A.N. (2015). Synthesis of zinc oxide nanoparticles via sol-gel route and their characterization. *Nanoscience. and Nanotech.*, 5(1): 1-6.
- [6]. Asmita J.Gavhane., P. Padmanabhan, Suresh P. Kamble and Suresh N. Jangle. (2012). Synthesis of silver nanoparticles using extract of neem leaf and triphala and evaluation of their Antimicrobial activities. *Inter. J.Pharma.Bio Sci.* 0975-6299
- [7]. S. Azizi, R. Mohamad, A. Bahadoran, S. Bayat, R. A. Rahim, A. Ariff and W. Z. Saad, (2016), Effect of annealing temperature on antimicrobial and structural properties of bio- synthesized Zinc Oxide nanoparticles using flower extract of *Anchusa italic.* *J Photochem Photobiol B*, 161, 441-449.
- [8]. S. Yedurkar, C. Maurya, P. Mahanwar, (2016) Biosynthesis of zinc oxide nanoparticles using *Ixora coccinea* leaf extract a green approach, *Open J. Synth. Theory Appl.* 5 ,1-14.
- [9]. K. Akhil and S. S. Khan, (2017), Effect of humic acid on the toxicity of bare and capped ZnO nanoparticles on bacteria, algal and crustacean systems. *J Photochem Photobiol B*, 167, 136-149.

Luminescence in SrMgAl₁₀O₁₇:Eu,Cr for downshifting the solar spectrum

P.K.Tawalare,

Department of Physics, Jagadamba Mahavidyalaya, Achalpur City, 444806, India.

Abstract

New results on luminescence of Cr³⁺ are reported in SrMgAl₁₀O₁₇ host prepared by combustion synthesis. SrMgAl₁₀O₁₇:Cr (SAM:Cr) was prepared by combustion synthesis. SAM:Eu²⁺,Cr³⁺ exhibits excitation in a broader range down to 320 nm. A downshifting phosphor which will absorb light in 350-450 nm and emit in the green region can improve the performance of the cell.

1. Introduction

In the system SrO-MgO-Al₂O₃ two compounds viz. SrMgAl₁₀O₁₇ (SAM II) and Sr₂MgAl₂₂O₃₆ (SAM I) are known. Both crystallize in hexagonal system, space groups being P-6m2 for (SAM I) and P6₃/mmc for (SAM II). Besides these, Iyi and Gobbels have mention some non-stoichiometric phases as well. There have been number of investigations related to luminescence in SAM II. Luminescence of Eu²⁺, Ce³⁺, Mn⁴⁺ had been documented in the literature.

2. Experimental

SrMgAl₁₀O₁₇:Cr (SAM:Cr) was prepared by combustion synthesis. Strontium nitrate, Magnesium nitrate, aluminum nitrate and urea were thoroughly mixed in molar ratio 1:1:10:28.33. Crucible containing the mixture was inserted at 500 C in a preheated furnace. In few minutes the mixtures wells with evolution of gases and finally a flame appears. The flame lasts for about a minute. The crucible is removed from the furnace after the flame extinguishes. The foamy product is crushed to powder and used for further characterization. For preparing Eu²⁺, Cr³⁺ doped samples; Europium and/or Chromium nitrate in the desired quantities were added to the starting mixture.

3. Result and Discussion

Fig.1 shows XRD pattern of the SAM:Cr prepared by combustion synthesis. Intensity is rather low and pattern appears noisy. This is due to small particle size of the powders prepared by combustion synthesis. A reasonable match with the ICDD file 26-0879 is seen all the same. SAM crystallizes in hexagonal space group P 6₃mmc. The structure of SAM consists of two spinel blocks of SrMgAl₁₀O₁₇ separated by one mirror plane (SrO). There are four types of Al³⁺ sites. Highest coordination is 6 for Al1. Sr ions are 9 coordinated and lie at the D_{3h} sites of local symmetry. The coordination number of Sr is 9 shown in Fig.2

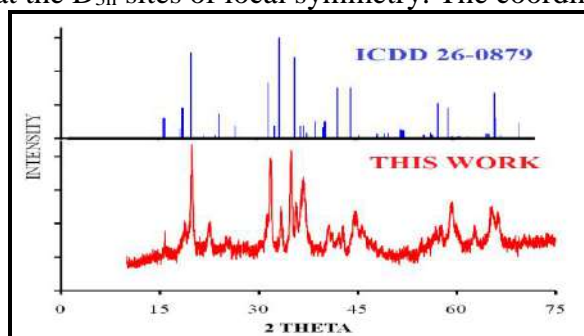


Figure 1 XRD pattern for SAM prepared by combustion synthesis

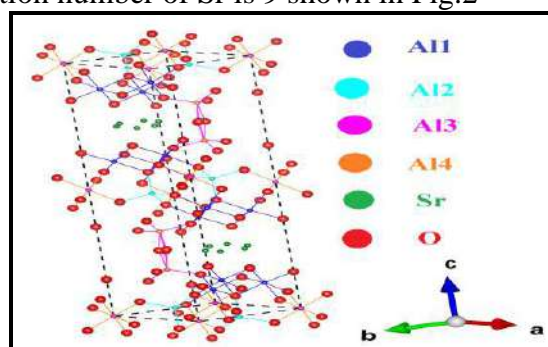


Figure 2 Unit cell of SrMgAl₁₀O₁₇ showing different Al sites.

PL emission spectra for SAM:Cr are shown in Fig.3. A line emission attributable to the ${}^2E_g \rightarrow {}^4A_{2g}$ transition around 699 nm is observed. There are several components due to splitting. This is in good agreement with the previous reports. Inset shows dependence of PL intensity on Cr^{3+} concentration. Highest intensity is observed for 2 mol.% and there is moderate quenching for higher values. From this data, critical distance for $Cr^{3+} - Cr^{3+}$ energy transfer is calculated as 14.3 Å. Excitation spectrum (Fig.4, curve a) for 699 nm emission consists of two strong, broad bands around 408 and 554 nm attributable to ${}^4A_{2g} \rightarrow {}^4T_{1g}$, ${}^4A_{2g} \rightarrow {}^4T_{2g}$ transitions, respectively.

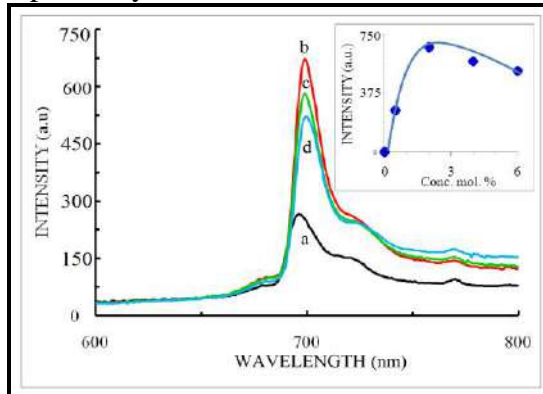


Figure 3 PL emission spectrum of SAM:Cr³⁺ for 420 nm excitation. Cr³⁺ concentrations a> 0.5, b> 1.0, c> 2.0 and d> 4 mol.%.

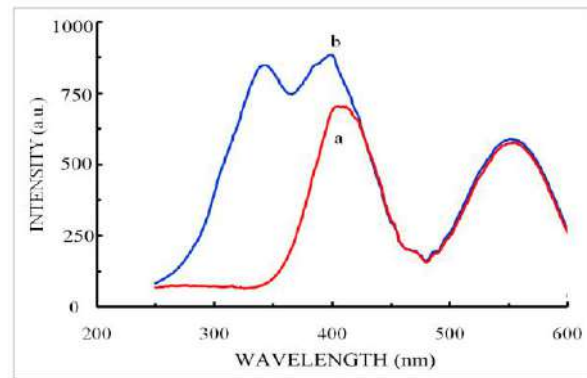


Figure 4 Excitation spectra for Cr³⁺ PL emission in a> SAM:Cr³⁺ for and b> SAM:Eu²⁺,Cr³⁺

For extending the excitation in near UV region, we attempted Eu²⁺-Cr³⁺ energy transfer. Eu²⁺ is known to absorb in near UV region and emit in the blue region. Excitation spectrum indeed showed additional features after Eu²⁺ co-doping. An additional band attributable to Eu²⁺ is observed in the excitation spectrum for Cr³⁺ emission at 699 nm (Fig. 5, curve b). Cr³⁺ emission also increases in doubly doped samples (Fig. 6). Eu²⁺ concentration taken as 10 mol.% and Cr³⁺ concentration was varied between 0.5-2.5 mol.%. Maximum Cr³⁺ emission is observed for 1.5 mol.% of Cr³⁺ (Fig. 5 inset). Increase in Cr³⁺ emission is accompanied by decrease in Eu²⁺ emission (Fig. 6). Inset shows decrease in Eu²⁺ emission as a function of Cr³⁺ concentration. Data of Figures 4-6 show energy transfer from Eu²⁺ to Cr³⁺ which results in broadening of the excitation spectrum for Cr³⁺ which covers broad region of the spectrum from nUV to visible.

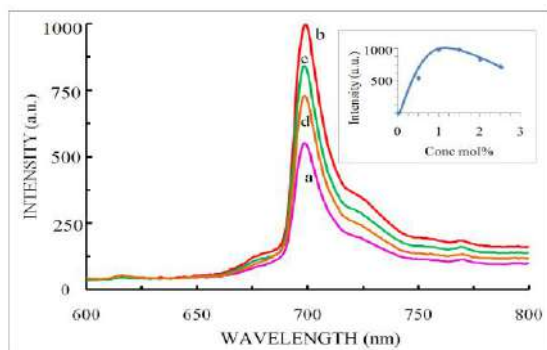


Figure 5 PL emission spectrum of SAM:Eu²⁺,Cr³⁺ in the range 600-800 nm. Excitation wavelength was 340 nm (Eu²⁺ excitation).

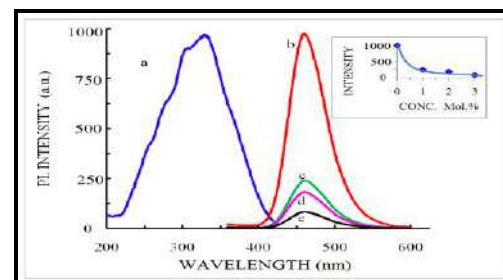


Figure 6 PL excitation and emission spectra (in the range 400-600 nm) of SAM:Eu²⁺,Cr³⁺ Excitation wavelength was 340 nm.

Eu²⁺ concentration is 10 mol.%. Cr³⁺ concentrations a> 0.5, b> 1.5, c> 2.0 and d> 2.5 mol.%,
Inset shows dependence of intensity of 699 nm line on Cr³⁺ concentration.

a> Excitation spectrum for SAM: Eu²⁺,Cr³⁺ for 460 nm (Eu²⁺) emission
Eu²⁺ concentration is 10 mol.%. Cr³⁺ concentrations b> 0.5, c> 1.5, d> 2.0 and e> 2.5 mol.%,
Inset shows dependence of intensity of 460 nm band on Cr³⁺ concentration.

Figure. 7 shows results on lifetime measurements for Cr³⁺ emission in SAM:Cr³⁺ phosphor. Decay can be fitted to a single exponential with $\tau = 3.35$ ms as shown in inset. This is of the same order as reported in the literature.

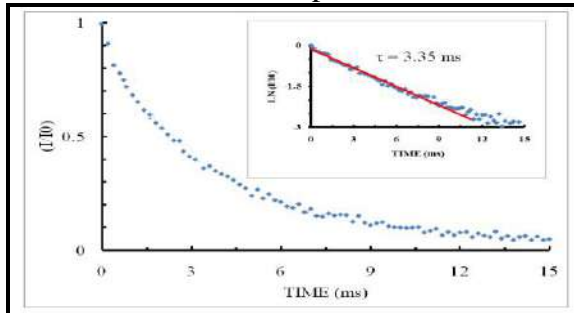


Figure 7 Luminescence decay of 699 nm emission in SAM:Cr³⁺
Decay can be fitted to a single exponential with $\tau = 3.35$ ms as shown in inset. 408 nm excitation was used for recording the decay.

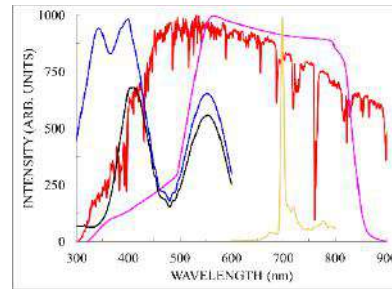


Figure 8 Modification of Solar Spectrum using Cr³⁺ doped phosphors.
a> AM1.5 solar spectrum, b> spectral response of CdS-CdTe solar cell, Cr³⁺ excitation spectrum for c> Al₂O₃:Cr³⁺ d>SAM:Cr³⁺ and e>SAM: Eu²⁺,Cr³⁺, f> Typical Cr³⁺ emission spectrum.
Shaded portion shows the portion of solar spectrum adequate for downshifting.

Conclusions

SrMgAl₁₀O₁₇:Cr³⁺ shows emission close to 700 nm. SAM:Eu²⁺,Cr³⁺ exhibits excitation in a broader range down to 320 nm. It is thus suitable for downshifting the solar spectrum in the region 320 to 430 nm (Figure 8). An ideal phosphor should absorb in the entire 300-500 nm and convert to longer wavelengths. SAM:Eu²⁺,Cr³⁺ is quite close to this.

References

1. Nobuo Iyi and Matthias Gobbels J.Solid State Chem. 122 (1996) 46
2. Tanno Hiroaki, Shuxiu Zhang, Shinoda Tsutae and Kajiyama Hiroshi J. Lumin. 130 (2010) 82
3. Ju.Guifang, Hu.Yihua, Li .Chen, Wang, Xiaojuan J. Lumin. 132 (2014) 1792
4. Le Wang, Hong Zhang, Yang Hui Li, Pei Liang, Ye Shen, Feng Jio Appl. Ceram. Tech. 13 (2016) 185
5. Shalinta Tigga Nameeta Brahme D. P. Bisen J. Mater. Sci. Materials in Electronics 28 (2017) 4750
6. Lili Meng, Lifang Liang and Yanxuan Wen J.Mater. Sci. Materials in Electronics 25 (2014) 2676
7. R.Cao, H.Xue, X.Yu, F.Xiao, D.Wu, F.Zhang J Nanosci. Nanotechnol. 16 (2016)3489
8. N.Iyi and M Goebbels J. Solid State Chem. 122 (1996) 46
9. Li-Ming Shaoa, Jin-Qiu Zhaob, Zhi-Guo Xiab and Xi-Ping Jing, J. Electrochem. Soc. 158 (2011) J300
10. Le Wang, Hong Zhang, YangHui Li, Pei Liang and Ye Shen Int. J. Appl. Ceram. Technol. 13 (2016) 185
11. Guifang Ju, Yihua Hu, Li Chen and Xiaojuan Wang, J. Lumin 132 (2012) 1792
12. Xiaoyu Luo, Xiaoliang Yang and Siguo Xiao, Mater. Res. Bull. 101 (2018) 73

8

Synthesis, Structural, Optical and Morphological Characterization of Graphene Oxide

Pravin Rathod^{*1}, Vishnudas Bhosle¹, Ashok Ubale²,

^{*1}Department of Physics and Electronics, Government Vidarbha Institute of Science and Humanities (An autonomous), Amravati , Maharashtra, India
rathodpp11iyc@gmail.com¹

¹Department of Physics and Electronics, Government Vidarbha Institute of Science and Humanities (An autonomous), Amravati , Maharashtra, India
mulikar.vk@gmail.com

³Department of Forensic Science, Government Institute of Forensic Science, Chhatrapati Sambhajnagar, Maharashtra, India
ashokuu@yahoo.com

ABSTRACT

Here, in this report we have followed a well-known modified Hummer's method for the synthesis of graphene oxide. In this method we have completely removed the presence of NaNO₃. Graphite powder was oxidized using concentrated H₂SO₄ and KMnO₄ which is resulted into high yield of the product. Structural investigation of synthesized product was studied using X-ray powder diffraction (XRD). X-ray powder diffraction pattern of the product showed the diffraction peak at ($2\theta = 10.64^\circ$) with an inter space distance of 0.839 nm, crystallite size of 5.31 nm and lattice strain of 0.0710. Optical characterization was done using UV-Visible spectrophotometer, Fourier Transform infrared spectroscopy (FTIR) and morphological study was performed using Scanning electron microscope (SEM).

Keywords: Hummer's Method, Graphene Oxide, XRD, FTIR, SEM

INTRODUCTION

In recent years, carbon based nanomaterials has generated enormous interest in the field of nanomaterials. Carbon based nanomaterial such as graphene, carbon nanotubes and activated carbon have unique pore structure¹, adsorptive capacity², electronic properties³ and acidity⁴. In the realm of carbon based nanomaterials graphene has rapidly gained prominence for its exceptional properties and versatile applications across various industries. Graphene is a one-atom-thick planar sheet of sp²-hybridized carbon atoms arranged in honeycomb structure. Out of the other carbon based nanomaterials graphene have many distinctive properties such as enhanced hole field-effect mobility up to the 48000 cm²/Vs [5], higher thermal conductivity 40 to 90 W/mK [6], higher intrinsic mobility up to 5600000 cm²/Vs at T = 50 K [7], the Young's modulus of G can reach 1100 GPa [8], excellent optical transmittance 97.7% [8] and large surface area- 2630 m²g⁻¹ [9]. The high surface area of graphene has been effectively utilized in various application such as nanoelectronics¹⁰, hydrogen production and storage¹¹, drug delivery¹², gas sensing¹³, catalysis¹⁴ and photovoltaics¹⁵. Single-layer of graphene nanosheets were first obtained by mechanical exfoliation (Scotch-tape method) of bulk graphite¹⁶ and another method to obtained grapheme nanosheets is epitaxial chemical vapour deposition.¹⁷. These routes are not preferred for the bulk production of graphene and these routes are not used for large scale manufacturing so scalable synthesis approaches from structurally similar compounds are of prominent scientific interest. The large scale synthesis is an important factor for the synthesis of graphene and one of the most admired approach is to use of strong oxidizing agents to obtained graphene oxide (GO). Graphene oxide is one of the form of graphene which

is a nonconductive hydrophilic carbon material.¹⁸ The very first GO synthesis process were enlarged by Brodie¹⁹, Staudenmeier²⁰ and Hummer's²¹. Out of these methods, modified Hummer's method is widely used because KClO_3 was replaced by KMnO_4 as the oxidation agent. In this method, the byproducts of toxic gas were terminated and the safety of experiments were enhanced. Furthermore, the oxidation time was reduced. In this paper, modified Hummers' method was employed to prepare GO.

Experiments and Method

Chemicals and Materials: Graphite powder (100 μm size), KMnO_4 , H_2SO_4 , H_2O_2 , HCl and orthophosphoric acid were purchased from SD Fine chemicals. All chemicals were of analytical grade and used as received.

Synthesis of Graphene Oxide (GO): In this investigation, a modified Hummers' method²² was employed to prepare GO. In this method, we completely removed sodium nitrate (NaNO_3) and initiation of orthophosphoric acid. 3.0 g of graphite powder (100 μm) was added to 120 ml solution of sulphuric acid (H_2SO_4) and orthophosphoric acid (H_3PO_4) in a 500 ml conical flask in ratio 9:1. The mixture was stirred vigorously and maintained at 100°C for 2 hours. The mixture was then allowed to cool to room temperature and kept below 10°C by placing the mixture in an ice bath. 15.0 g of potassium permanganate (KMnO_4) was added gradually over a period of one hour after which it was continuously stirred for another hour in order to obtain homogeneous mixture. It was then removed from ice-water bath, placed in a warm-water bath maintained at 60°C and stirred for an hour. After this, the mixture was allowed to cool to room temperature. Later on 250 ml of distilled water was added to the mixture. For the purpose of to stop the reaction, 20 ml of hydrogen peroxide (H_2O_2) was added to the mixture until the color changed from reddish brown to dark brown. The obtained mixture was left overnight. The mixture was re-dispersed in dilute hydrogen chloride and ultrasonicate for 15 minutes. After this, it was repeated two times and washed in distilled water. In the end, the mixture was filtered and dried at 100°C for 4 hours in air on hot plate.

Characterization: The structural study of GO was performed by X-ray diffractometer (Model: Mini flex-II, Rigaku, Japan) with $\text{Cu K}\alpha$ radiation ($\lambda = 1.5406 \text{ \AA}$) operating at 40 kV and 30 mA. Surface morphology was studied using Scanning Electron Microscope (SEM, Model: JEOL JSM-6360, Japan). Fourier transmission infrared (FTIR) spectra of the GO were recorded using FT-IR Spectrometer (Shimadzu, Japan) in the range of $4000\text{-}400 \text{ cm}^{-1}$. The optical absorption spectra were measured in the range of $300\text{-}800 \text{ nm}$ by using UV-Visible spectrometer (UV-1800 Spectrophotometer, –Shimadzu, Japan).

RESULTS AND DISCUSSION

The Structural properties of GO: XRD analysis was used to determine the structural properties of the GO. XRD spectra is as shown in Figure 1 (a). The synthesized GO exhibit a very strong peak at $2\theta = 10.64^\circ$ with an inter space distance of 0.839 nm, crystallite size of 5.31 nm and lattice strain of 0.0710. The calculated structural parameters are as shown in table 1.

FTIR Spectroscopy Analysis of GO: FTIR spectra analysis was performed to investigate the structure and functional groups of the materials, as shown in Figure 1 (b). The GO sheet showed apparent adsorption bands for the carboxyl $\text{C}=\text{O}$ (1733 cm^{-1}), aromatic $\text{C}=\text{C}$ (1626 cm^{-1}), epoxy $\text{C}-\text{O}$ (1238 cm^{-1}), alkoxy $\text{C}-\text{O}$ (1048 cm^{-1}), and hydroxy $-\text{OH}$ (3333 cm^{-1}) groups. The exhibition of oxygen-containing functional groups, such as $\text{C}=\text{O}$ and $\text{C}-\text{O}$, further confirmed that the graphite in fact was oxidized into GO.

The Optical Absorption of GO: The analysis of UV-Visible spectra of the GO was shown in Figure 1 (c). The UV-Visible spectrum is a plot of the absorbance as a function of wavelength

λ . The absorbance peak of GO dispersion is in the range of 300-325 nm. It is indicated that graphene oxide possessed a good absorption in the visible range 323~800 nm. The results exhibit the good photoresponse of GO sheet not only in ultraviolet range but also in visible range, which implied the enormous potential for application of light.

Morphological study: Scanning electron microscope was employed for the detailed morphological studies as shown in fig 1 (d). The SEM images of GO show the characteristic wrinkles and folds of GO nanosheets. This result confirmed that two dimensional nanosheets of GO can be produced from exfoliation of Graphite oxide.

Figures and Tables

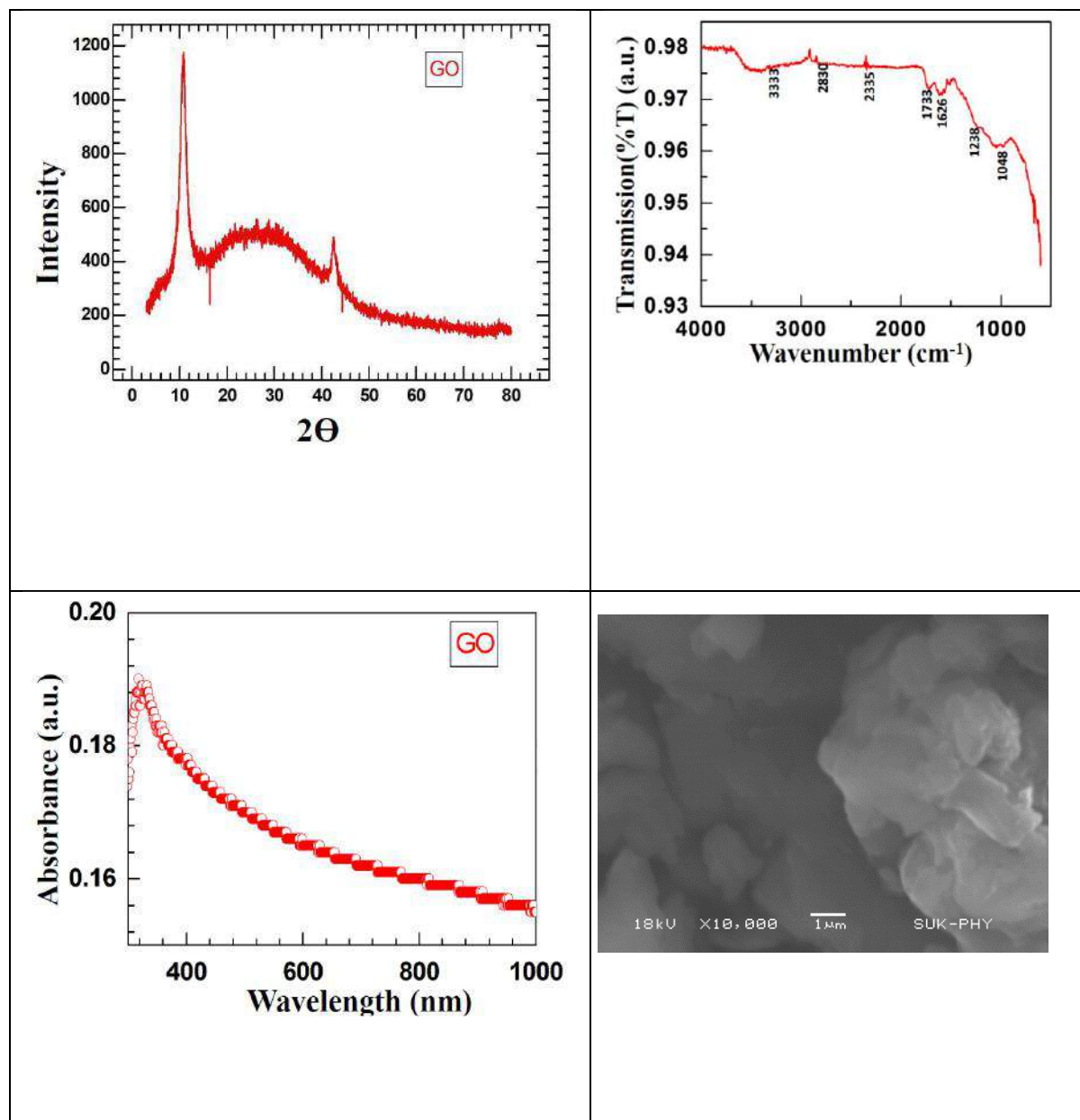


Table 1. Structural parameter of GO

2θ	Plane	FWHM (β)	Crystalline size D in nm	Dislocation in crystal δ	Lattice strain ε	Interspace distance d (nm)
10.53	(001)	1.5	5.3165	0.0353	0.0710	0.8391
42.47	(002)	1.13	7.5395	0.0175	0.0126	0.2125

CONCLUSION

GO nanostructure were successfully prepared via modified Hummer method. The SEM analysis showed successful preparation of GO nanostructure at nanoscale. The exfoliation of graphene sheets is confirmed

by SEM image. The presence of oxygen-containing groups and characteristic peaks in FT-IR and XRD analysis further determined the successful preparation of GO nanostructure. The presence of oxygen-containing functional groups provided more opportunities for potential applications of GO in many areas. These data will provide a reference to further study the nature of graphene oxide.

REFERENCES

- [1] Simon, P., Gogotsi, Y. "Materials for electrochemical capacitors." *Nat. Mater.* 7, 845–854, 2008.
- [2] Gu, Zonglin, Zaixing Yang, Yu Chong, Cuicui Ge, Jeffrey K. Weber, David R. Bell, and Ruhong Zhou. "Surface curvature relation to protein adsorption for carbon-based nanomaterials." *Sci. rep.* 5, 10886, 2015.
- [3] Dubois, SM-M., Zeila Zanolli, Xavier Declerck, and J-C. Charlier. "Electronic properties and quantum transport in Graphene-based nanostructures." *Eur. Phys. J. B.* 72, 1–24, 2009.
- [4] Garg, Bhaskar, Tanuja Bisht, and Yong-Chien Ling. "Graphene-based nanomaterials as heterogeneous acid catalysts: a comprehensive perspective." *Mol.* 19, 14582-14614, 2014.
- [5] Thodkar, Kishan, and Fabian Gramm. "Enhanced Mobility in Suspended Chemical Vapor-Deposited Graphene Field-Effect Devices in Ambient Conditions." *ACS Appl. Mater. Interfaces.* 15, 37756-37763, 2023.
- [6] H. Malekpour, K.-H. Chang, J.-C. Chen, C.-Y. Lu, D. L. Nika, K. S. Novoselov, and A. A. Balandin. *Nano Letters.* 14, 5155-5161, 2014.
- [7] Hirai, Hideki, Hideaki Tsuchiya, Yoshinari Kamakura, Nobuya Mori, and Matsuto Ogawa. "Electron mobility calculation for graphene on substrates." *J. Appl. Phys.* 116, 8, 2014.
- [8] Li, Qingzhong, Fei Fan, Yang Wang, Wei Feng, and Peijun Ji. "Enzyme immobilization on carboxyl-functionalized graphene oxide for catalysis in organic solvent." *Ind. Eng. Chem. Res.* 52, 6343-6348, 2013.
- [9] Liu, Jun, Yuhua Xue, Yunxiang Gao, Dingshan Yu, Michael Durstock, and Liming Dai. "Hole and electron extraction layers based on graphene oxide derivatives for high performance bulk heterojunction solar cells." *Adv. Mater.* 24, 2228–2233, 2012.
- [10] Radsar, Tahereh, Hassan Khalesi, and Vahid Ghods. "Graphene properties and applications in nanoelectronic." *Opt. Quantum Electron.* 53, 1-38, 2021.
- [11] Aksoy, Burcu Topaloğlu, and Bunyemin Çoşut. "Graphene/graphene oxide-based nanomaterials for hydrogen production and storage applications." *Nanomater. Hyd. Storage Appl.* Elsevier, 97-116, 2021.
- [12] Song, S., Shen, H., Wang, Y., Chu, X., Xie, J., Zhou, N., and Shen, J. "Biomedical application of graphene: From drug delivery, tumor therapy, to theranostics." *Colloids Surf. B.* 185, 110596, 2020.
- [13] Kwon, B., Bae, H., Lee, H., Kim, S., Hwang, J., Lim, H., Lee, J.H., Cho, K., Ye, J., Lee, S. and Lee, W.H. "Ultrasensitive N-channel graphene gas sensors by nondestructive molecular doping." *ACS nano.* 16, 2176-2187, 2022.
- [14] Fan, X., Zhang, G., and Zhang, F. "Multiple roles of graphene in heterogeneous catalysis." *Chem Soc Rev.* 44, 3023-3035, 2015.
- [15] Das, Sonali, Deepak Pandey, Jayan Thomas, and Tania Roy. "The role of graphene and other 2D materials in solar photovoltaics." *Adv. Mater.* 31, 1802722, 2021.
- [16] Novoselov, Kostya S., Andre K. Geim, Sergei V. Morozov, De-eng Jiang, Yanshui Zhang, Sergey V. Dubonos, Irina V. Grigorieva, and Alexandr A. Firsov. "Electric field effect in atomically thin carbon films." *Science.* 306, 666-669, 2004.
- [17] Yu, Q. K.; Lian, J.; Siriponglert, S.; Li, H.; Chen, Y. P.; Pei, S. S. "Graphene Segregated on Ni Surfaces and Transferred to Insulators." *Appl. Phys. Lett.* 93, 113103, 2008.
- [18] H. Chen, M. B. Muller, K. J. Gilmore, G. G. Wallace, D. Li. "Mechanically strong, electrically conductive, and biocompatible graphene paper." *Adv. Mater.* 20, 3557–3561, 2008.
- [19] B. C. Brodie. "On the atomic weight of graphite." *Philos. Trans. R. Soc. London.* 149, 249–259, 1859.
- [20] Staudenmaier, L. "Method for the preparation of graphitic acid." *Ber Dtsch Chem Ges.* 31, 1481-1487, 1898.
- [21] S. Hummers, R. E. Offeman, *J. Am. Chem. Soc.* 1958, 80, 1339–1339.
- [22] Eluyemi, M. S., M. A. Eleruja, A. V. Adedeji, B. Olofinjana, O. Fasakin, O. O. Akinwunmi, O. O. Ilori, A. T. Famojuro, S. A. Ayinde, and E. O. B. Ajayi. "Synthesis and characterization of graphene oxide and reduced graphene oxide thin films deposited by spray pyrolysis method." *Graphene.* 5, 143-154, 2016.

A review on synthesis and applications of nanomaterials

V. U. Rahangdale*, S. D. Charpe¹

Jagat Arts, Commerce and I.H.P. Science College, Goregaon, Dist. Gondia, Maharashtra- 441801 India

¹Department of Physics, J. D. Patil Sangludkar Mahavidyalaya, Daryapur Dist. Amravati, Maharashtra-444803,

E-mail address of corresponding author: vijayrahangdale11@gmail.com

Abstract

Nanotechnology has very broad range of potential applications in the field of physics, biology and medicine on nanoscale. Nanomaterials are the group of materials that have at least one dimension in the range of 1 to 100 nm. As these materials possess exceptionally important properties at nanoscale level, it is important to study the different synthesis methods related to nanomaterials to explore them. This review article gives deep inside about the physical methods of synthesis of nanomaterials and their applications, which may be helpful for researchers.

Keywords: History, classification, synthesis methods, applications of nanomaterials.

1 Introduction

From the beginning of 19th century nanotechnology branch is flourishing to a great extent. Today lot of research is going on related to the nanotechnology. Nanotechnology can be stated as the developing application of materials and devices by modifying their dimensions in nanoscale. "Nano" word is derived from the Greek word nanos or Latin word nanus which means "dwarf". Materials are said to be nanomaterials if their size or one of their dimensions is in the range of 1 to 100 nm [1].

Although nanotechnology is new, but research on nanometer scale is done in very early time. Colloidal dispersions and metallic quantum dots have been in the nanometer scale for centuries. Chinese people were using gold nanoparticles as an inorganic dye for applying red color in ceramic porcelains more than thousand years ago [2, 3]. The nanomaterials show different properties compared to the bulk material which depends on their size and shape. So to introduce a new characteristic in a material it must be modified with its shape and size at the nanoscale level. Nanomaterials may be of different shapes like nanorods, nanoparticles, nanosheets which are characterized based on dimensions. Nanomaterials with zero-dimensional are nanoparticles, one dimensional is nanorods or nanotubes and two dimensional are in the form of films and layers type. The nanomaterials are of different types based on their morphology, size, properties and the constituent in it. They are carbon-based nanomaterials, metal nanoparticles, semiconductor nanomaterials, polymeric nanomaterials, lipid-based nanomaterials.

It is not easy to cover all the synthesis methods of nanomaterials and applications, Therefore this review attempts to provide information about the physical methods for the synthesis and applications of nanomaterials by referring important papers from history and the current literature.

2 Synthesis Methods of Nanomaterials

The synthesis of nanoparticles can be done by following methods

- (1) Physical methods
- (2) Chemical methods and
- (3) Biological methods

In this review article only physical methods for the synthesis of nanomaterials have been discussed.

2.1 Synthesis of nanomaterials by Physical route

The physical methods are categorized to “top-down” and “bottom-up” approaches. In “top-down” approach the larger materials are crushed into smaller particles by mechanical milling. The problem with top-down approach is the imperfection of the surface structure and difficulty in getting desired particle size and shape [4, 5].

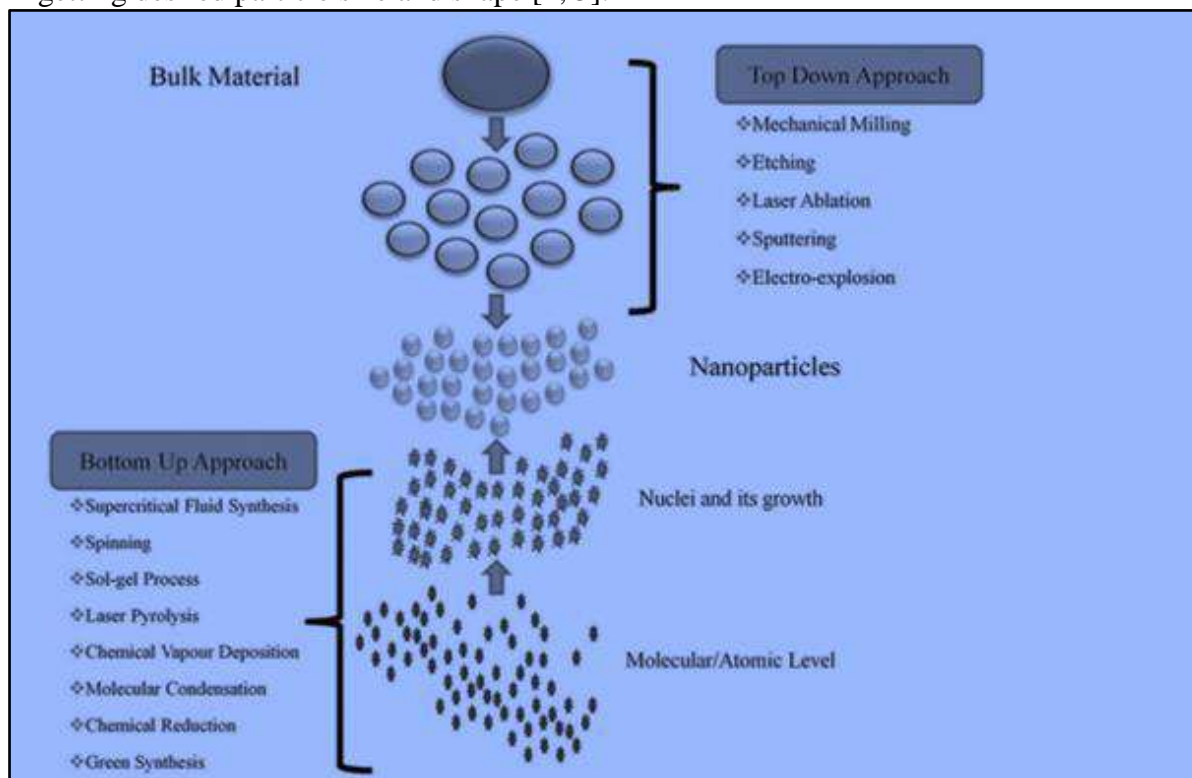


Fig. 1 Synthesis of nanomaterials via top-down and bottom-up approaches [6]

It is well known that the conventional top-down techniques such as lithography can cause substantial crystallographic damage to the processed patterns and additional defects may be introduced even during the etching steps [7, 8]. Bottom-up approach is often emphasized in nanotechnology literature, though bottom-up is nothing new in materials synthesis. In the “bottom-up” method either liquid or gaseous phase, nanoparticles are condensed in which the larger materials are formed by the chemical combination of the smaller ions.

2.1.1 Top-down approaches

In top-down approaches, bulk materials are divided to produce nanostructured materials. Top-down methods include mechanical milling, etching, and sputtering and laser ablation. In this article mechanical milling process for the synthesis of nanomaterials has been discussed.

Mechanical milling

Mechanical milling is a cost-effective method for producing materials at the nanoscale level from bulk materials. Mechanical milling is an effective method for producing blends of different phases, and it is helpful in the production of nanocomposites. The principle of the ball milling method is shown in Fig. 2

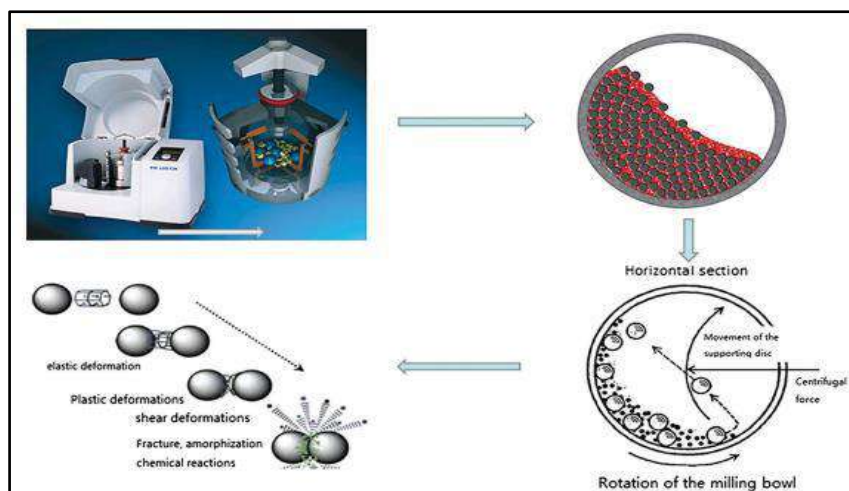


Fig. 2 The principle of the ball milling method [9]

Mechanical milling is used to produce wear-resistant spray coatings, aluminum and copper-based nanoalloys, and many other nanocomposite materials [10]. Ball-milled carbon nanomaterials are considered a novel class of nanomaterial, which provides the opportunity to satisfy environmental remediation, energy storage, and energy conversion demands [11].

2.1.2 Bottom-up approaches

Bottom-up approaches includes chemical vapor deposition, sol-gel method, and soft & hard templating method. Here chemical vapor deposition for the synthesis of nanomaterials has been discussed.

Chemical vapor deposition (CVD)

Chemical vapor deposition is more difficult than physical vapor deposition but it has benefits including the capacity to create pure thin films or nanoparticles, high manufacturing yield, and simplicity in scaling up. Chemical vapor deposition method is generally used in the synthesis of carbon-based nanomaterials. In CVD, a thin film is formed on the substrate surface via the chemical reaction of vapor-phase precursors [12]. A precursor is considered suitable for CVD if it has adequate volatility, high chemical purity, good stability during evaporation, low cost, a non-hazardous nature, and a long shelf-life. Moreover, its decomposition should not result in residual impurities [12]. For instance, in the generation of carbon nanotubes via CVD, a substrate is placed in an oven and heated to high temperatures. Subsequently, a carbon-containing gas is slowly introduced to the system as a precursor. At high temperatures, the decomposition of the gas releases carbon atoms, which recombine to form carbon nanotubes on the substrate [13]. However, the choice of catalyst plays a significant role in the morphology and type of nanomaterial obtained.

3. Applications of Nanomaterials

Nanotechnology and nanomaterials can be applied in all kinds of industrial sectors. They are usually found in these areas:

- A) **Electronics:** Carbon nanotubes are close to replacing silicon as a material for making smaller, faster and more efficient microchips and devices, as well as lighter, more conductive and stronger quantum nanowires. Graphene's properties make it an ideal candidate for the development of flexible touchscreens.
- B) **Energy:** A new semiconductor developed by Kyoto University makes it possible to manufacture solar panels that double the amount of sunlight converted into electricity. Nanotechnology also lowers costs, produces stronger and lighter wind turbines, improves fuel efficiency and, thanks to the thermal insulation of some nanocomponents, can save energy.

C) Biomedicine: The properties of some nanomaterials make them ideal for improving early diagnosis and treatment of neurodegenerative diseases or cancer. They are able to attack cancer cells selectively without harming other healthy cells. Some nanoparticles have also been used to enhance pharmaceutical products such as sunscreen.

4. Conclusion

In recent days the synthesis of nanomaterials are increasing with novel and advanced technology. The nanomaterials with mixed compositions are also synthesizing to apply in different fields. Synthesis methods discussed in this article will produce the nanoparticles of desired size, shape and property which will be used for various applications. Therefore, the present review article will provide an opportunity to make general information about the nanoparticles. Nanotechnology can be used in recycling and removing contamination from the wastewater. Nowadays wide research in going into the fields of electronics and storage devices, sensors and medicine but still there is a scope for the development of research in nanotechnology.

References:

1. Nanostructure and Nanomaterials by Guozhong Cao, Imperial College Press 57 Shelton Street Covent Garden London 2004.
2. J. Ayers, in *Ceramics of the World: From 4000 BC to the Present*, eds. L. Camusso and S. Bortone, Abrams, New York, p. 284, 1992.
3. H. Zhao and Y. Ning, *Gold Bull.* 33, 103 (2000).
4. Thakore Sonal et al., *Mater. Sci. Eng.: C* 44 (2014) 209–215.
5. S. Dutz, R. Hergt, J. Mürbe, R. Müller, M. Zeisberger, W. Andrä, J. Töpfer, M.E. Bellemann, *J. Magn. Magn. Mater.* 308 (2007) 305–312.
6. P. Khanna, A. Kaur and D. Goyal, *J. Microbiol. Methods*, 2019, 163, 105656
7. B. Das, S. Subramaniam, and M.R. Melloch, *Semicond. Sci. Technol.* 8, 1347 (1 993).
8. C. Vieu, E Carcenac, A. Pepin, Y. Chen, M. Mejias, L. Lebib, L. Manin Ferlazzo, L. Couraud, and H. Launois, *Appl. Surf: Sci.* 164, 11 1 (2000).
9. S. Zhuang, E. S. Lee, L. Lei, B. B. Nunna, L. Kuang and W. Zhang, *Int. J. Energy Res.*, 2016, 40, 2136–2149.
10. Prasad Yadav, R. Manohar Yadav and D. Pratap Singh, *Nanosci. Nanotechnol.*, 2012, 2, 22–48.
11. H. Lyu, B. Gao, F. He, C. Ding, J. Tang and J. C. Crittenden, *ACS Sustainable Chem. Eng.*, 2017, 5, 9568–9585
12. A. C. Jones and M. L. Hitchman, in *Chemical Vapour Deposition*, ed. A. C. Jones and M. L. Hitchman, Royal Society of Chemistry, Cambridge, 2008, pp. 1–36.
13. K. A. Shah and B. A. Tali, *Mater. Sci. Semicond. Process.*, 2016, 41, 67–82.

Ammonia Gas Sensing Application of Nano-composites of SnO₂ Doped with ZnO & Polypyrrole

A. J. Atram¹, R. P. Ikhar², G. T. Lamdhade³, B. M. Mude⁴,
K. M. Mude⁵, K. B. Raulkar³

¹Department of Physics, Lokmanya Tilak Mahavidyalaya, Wani

²Vidya Bharati Madhyamik Vidyalaya, Patrakar Colony, Amravati

³Department of Physics, Vidya Bharati Mahavidyalaya, Amravati, 444602

⁴Ramnarain Ruia College, Matunga (E) Mumbai -400019, India

⁵Department of Physics, Bhavan's College, Andheri (W) Mumbai-400058, India

* Corresponding Author e-mail: kbraulkar2016@gmail.com

Abstract:

(SnO₂-ZnO)/polypyrrole(PPy) coaxial nanocables sensor had been fabricated and used to check the response for ammonia gas sensing. (SnO₂-ZnO) coaxial nanocables having narrow diameter size about 60 nm were fabricated via electroplating technique. Using vapor-phase polymerization of pyrrole monomer, on the surface of SnO₂-ZnO nanofibers, PPy shell, as a conducting polymer had been polymerized. The important part is that the fabricated sensor manifested linear sensing response to ammonia gas at room temperature (300 K). This method had made easy and feasible detection and determination of NH₃ gas concentration. The synthesis material exhibited quick response, recovery time and high sensitivity. The materials characteristics under study exhibited good potential in the industrial applications such as high response to ammonia gas. The response time is 12 s and recovery time is 38 s. Hence the sensor under study was best among the known sensors. Due to low operating temperature i.e. 300 K (room temperature), its durability is more.

Keywords: SnO₂-ZnO sensor, PPy, electroplating technique, sensitivity, response and recovery times.

I. Introduction:

Day by day, the environment is being uncomfortable for breathing due to the many dangerous gasses present in the atmosphere. Therefore, it is vital to detect such harmful gases in order to control air pollution, prevent human life, and protect nature from being damaged. Many people are facing problems with toxic, combustible and volatile gases in the atmosphere including domestic, laboratorial, and industrial places. One such hazardous and toxic gas is ammonia and hence its detection is very important task. This gas, in general is used in many places and in many applications, such as for cooling purposes in the industries [1-3] and medical diagnoses [4-6]. Thus, many researchers are developing affordable and reliable techniques and methods for the detection of ammonia as well as other toxic gases [7-8].

Conducting polymer ammonia gas sensors, at room temperature (300 K) have shown better detection responses among the various material used sensors which work at high temperatures [9]. At low temperature, sensor life will be more and power consumption is less which makes easier operation of the sensor [10-15]. Many notable features, such as low energy optical transitions, controllable electrical conductivity, low ionization potential, and high electron affinity have been shown by conducting polymers, which can be synthesized either by electro-chemical or polymerization of pyrrole (Py) monomer [16-20]. Polypyrrole (PPy), being most stable conducting polymer under ambient conditions has attracted attentions in sensing NH₃ gas due to its unique conducto-metric response to ammonia [21-23]. When surface to

volume ratio is higher, more potential places are there for reactions to occur then this causes the best and more accurate sensing mechanism of PPy as chemical reactions which take place on the surface.

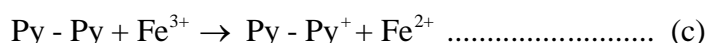
In the present work, (SnO₂-ZnO)/PPy nanocables had been synthesized via electrospinning method and vapor-phase polymerization of Py on the surface of SnO₂-ZnO nanofibers. The core-sheath structure of prepared nanocables was confirmed by Transmission electron microscopy (TEM). The fabricated sensor could detect ammonia gas with fast response and recovery time. It also manifested linear response to ammonia concentration. The determination of NH₃ gas concentration becomes more feasible due to linear behavior of graph.

II. Experimental

A. Synthesis of (SnO₂-ZnO)/PPy nanocables:

To synthesize SnO₂-ZnO composite nanofibers, 2g polyvinyl alcohol (PVA) was dissolved in 18 ml distilled water, followed by adding 1g Zinc Acetate and 1g Stannous Chloride to prepare electrospinning solution. This mixture was kept at 60⁰C for 4h under constant stirring at 400 rpm speed. The electrospinning process was performed with a constant feeding rate of 0.3 ml/h and 8 cm distance between the tip of the syringe and the Al plate collector while the 16 kV electric potential was maintained. The calcination of electrospun nanofibers was done in the furnace at 700⁰C for 3 h which resulted in the formation of SnO₂-ZnO composite nanofibers.

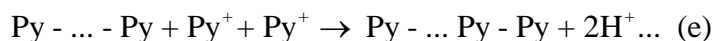
On the template of SnO₂-ZnO composite nanofibers, Py monomers in a vapor-phase were polymerized. The soaked template of nanofibers in 0.1 molarity ethanolic FeCl₃ solution for 30 min was left in the air for 15 min. This nanofibers template, for about 3h was exposed to saturated Py vapor, due to which, iron (III) ions absorbed on the surface of the nanofibers. Py monomer was oxidized by an iron (III) ion (a). Py dimer and two hydrogen ions will be liberated by bonding two of oxidized Py monomers together (b). By reaction (c), Py dimer will be oxidized using an iron (III) ion and finally a Py trimer resulted by bonding with another oxidized Py (d). This oxidation reaction (e) is given below:



.....

.....

.....



The template was kept hanging up from the vessel containing Py placed on a stirrer which was used for polymerization of Py. For a time about 4 h, Py was heated through stirring. The slow production of black colored precipitates on the template confirmed the PPy formation.

B. Preparation of (SnO₂-ZnO)/PPy nanocables Sensor and its measurements:

On 10 mm x 5 mm x 1 mm alumina substrate, nanofibers were electrospun by electrospinning procedure. SnO₂-ZnO nanofibers layer was resulted after electrospun nanofibers calcination at 700⁰C for 3h. Finally PPy layer was developed on SnO₂-ZnO nanofibers layer. In this way, (SnO₂-ZnO)/PPy nanofibers sensor was fabricated.

By the silver paste, thin Pt wires were cemented to the sample area with a gap of about 1mm [24]. The sample was mounted on thick walled borosilicate glass tubing to form sensor probes. The sensing response of (SnO₂-ZnO)/PPy were recorded at 300 K temperature (Room Temperature) by using two insulated cables connected to the impedance measurement device. 15 ppm to 90 ppm range ammonia gas concentrations were used for the measurement. Sensitivity is defined as the ratio of resistance of the sensor due to presence of gas to the resistance in air environment and is given by

$$S = \frac{\text{Resistance in presence of gas}}{\text{Original resistance in air}} = \frac{R_{\text{gas}}}{R_{\text{air}}}$$

Where,

R_{gas} = Resistance of the sensor in presence of NH₃ gas environment and

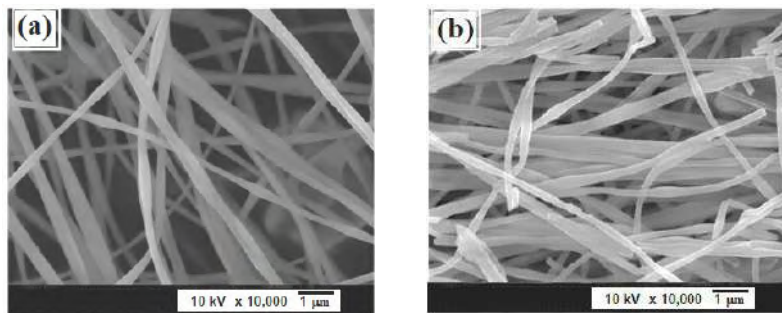
R_{air} = Resistance of the sensor in presence of air.

For achieving 90 % of total resistance change, the time taken by the sensor is known as the response time in case of absorption and in case of desorption, this time is referred as recovery time.

III. Results and Discussions:

A. Characterization study:

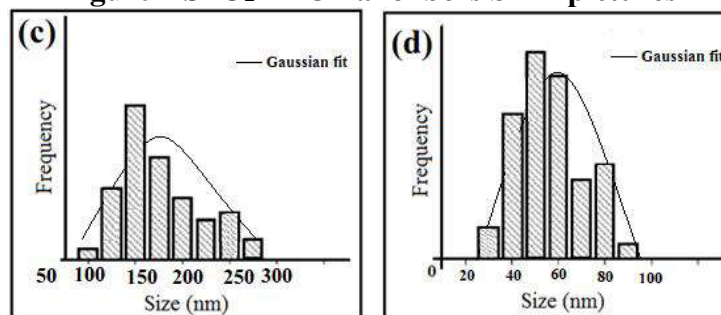
The nano-scale dimensions of the fibers and its porosity provided higher accessible surface region, because of which, higher rate of reaction initiated by the diffusion of ammonia gas. The SEM pictures are shown below:



(a) Before calcination

(b) After calcination

Figure 1 SnO₂-ZnO nanofibers SEM pictures



(c) Before calcination

(d) After calcination

Figure 2 SnO₂-ZnO nanofibers SEM pictures

From figure (1) (a) & (b), it is exhibited that, due the removal of volatile species, diameter sizes of nanofibers reduced. As shown in figure 2 (c) and (d), before calcinations, average nanofibers size is about 165 nm and that after calcination, it is 60 nm.

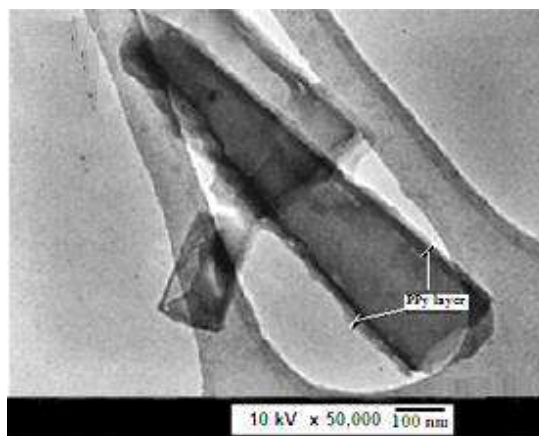
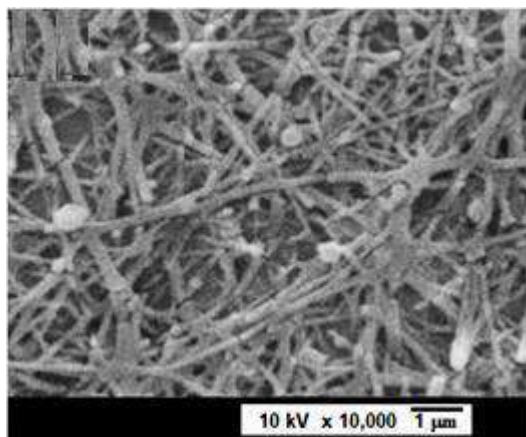


Figure 3 SEM image of (SnO₂-ZnO)/PPy **Figure 4 TEM image of (SnO₂-ZnO)/PPy**

Morphology of PPy-coated nanofibers showing similar texture with those of electrospun nanofibers before and after calcination is depicted in figure 2. Figure 4 depicted the TEM of PPy-coated nanofiber which manifested core shell type structure with thin PPy layer. In the study of TEM, nanocables peeled off from the substrate, dispersed in ethanol and exposed to ultrasonic environment of 30 s which causes the shorter length of nanocables. Though the SnO₂-ZnO nanofibers have white colour, they becomes yellowish in FeCl₃ ethanolic solution. Further when exposed this solution with pyrrole vapour, it becomes black, which manifested formation of PPy layer on the SnO₂-ZnO nanofibers. TEM, also exhibited nanofiber's diameter size which was also derived from SEM pictures.

B. Sensitivity Measurement:

At different concentration of ammonia gas (15 ppm to 90 ppm), the variation of sensing behavior of resistor type (SnO₂-ZnO)/PPy nanofibers sensor with time is shown in the following figure 5.

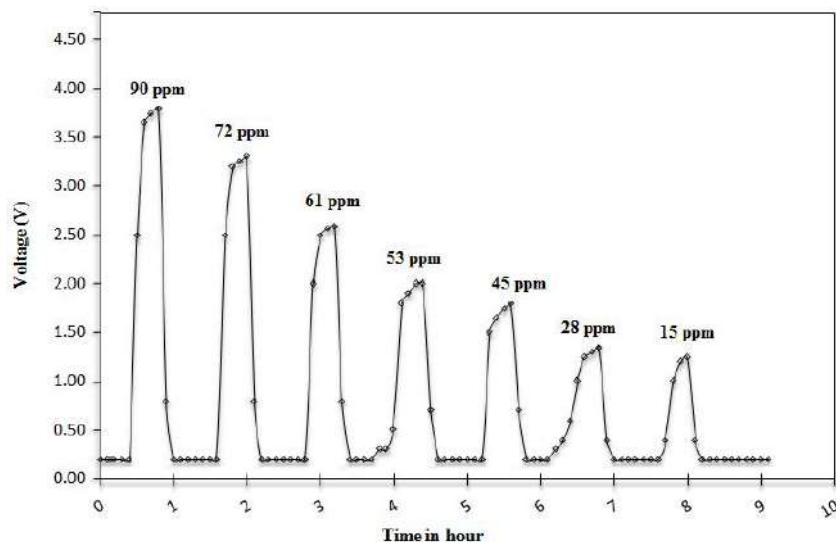


Figure 5 response/recovery features of (SnO₂-ZnO)/PPy nanofibers sensor to NH₃ gas at 300 K

As shown in figure (5), the response of sensor to the varying concentration of ammonia gas is due to the interactions between positive charge along the PPy chains and surrounding environment of NH₃ gas. Redox reaction occurs when PPy is exposed to the NH₃ gas, an electron donating gas. Due to this, decrease in effective number of charge carriers causing reduction of its conductance [25]. At different NH₃ concentration, typical response/recovery

features of nanocables versus time are depicted in figure (5) at constant current. As shown in response, voltage increases at higher ammonia concentration (say 90 ppm), after about 45 s, it reaches constant value, exhibiting saturation of sensor. Then sensing probe is exposed to air to get recovery of voltage to initial minimum value (0.2 V). for different concentration of NH_3 , sensor showed different saturation levels. This feature of sensor can be used to evaluate the sensor response for different gas concentrations. The minimum response time is determined to be 38 s, hence this sensor showed fast response as its surface to volume ratio is large.

Different sensing measurements were carried out and average sensing response is graphed with ammonia gas concentrations which are shown in figure 6.

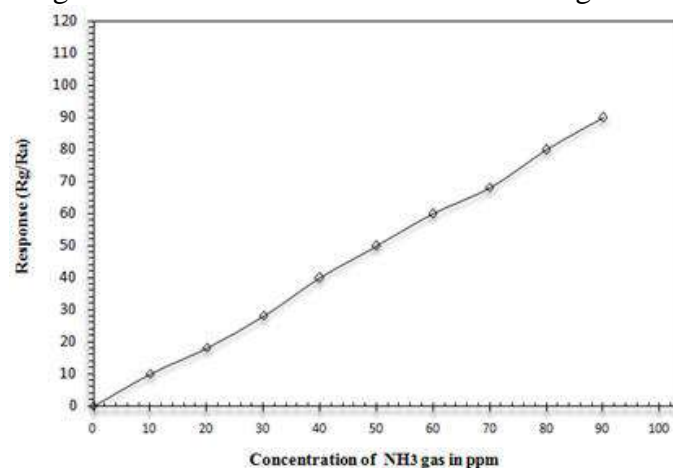


Figure 6 Linear response of $(\text{SnO}_2\text{-ZnO})/\text{PPy}$ nanofibers sensor to NH_3 gas

As shown in figure 6, as ammonia gas concentration increases, amount of reaction occurring between NH_3 and PPy increases, exhibiting involvement of more free electrons along the PPy chains and raising of resistance of the sensor i.e. more response. This linear response is useful to determine the unknown ammonia gas concentration.

IV. Conclusion:

$\text{SnO}_2\text{-ZnO}$ electrospun nanofibers were prepared via vapor-phase polymerization to use as porous template for polymerizing thin PPy layer and $(\text{SnO}_2\text{-ZnO})/\text{PPy}$ nanofibers sensor was fabricated to sense NH_3 gas at room temperature (300 K). The fabricated sensor exhibited linear response to ammonia gas which allows for the determination of unknown ammonia gas concentration. SEM and TEM pictures, after calcination exhibited decrease of diameter sizes of nanofibers. Due to high porosity of nanofibers structure, more reactions between NH_3 and the positive charges along PPy chains occur and sensing is enhanced. This more porosity also led to easier diffusion of ammonia gas which exhibit decrease of response and recovery times. The response time is 12 s and recovery time is 38 s. Hence the sensor under study was best among the known sensors. Due to low operating temperature i.e. 300 K (room temperature), its durability is more.

V. Acknowledgement:

The authors would like to acknowledge Department of Physics, Vidya Bharati Mahavidyalaya, Amravati (India) for providing Research center to carry on this work.

VI. References:

- [1] Wang C., Lei S., Li X., Guo S., Cui P., Wei, X., Liu W. and Liu H., (2018), A Reduced GO-Graphene Hybrid Gas Sensor for Ultra-Low Concentration Ammonia Detection, *Sensors (Basel)*, 18(9), 3147.
- [2] Devi R.S., Venkatesh R. and Sivaraj R., (2014), Synthesis of Titanium Dioxide Nanoparticles by Sol-Gel Technique, *IJRSET*, 10, 15206-211.

- [3] Dighore N., Dhonde S., Gaikwad S. and Rajbhoj A., (2016), Synthesis of conducting polymer Polypyrrole-MoO₃ nanocomposites, *Mor. J. Chem.*, 4, 797-804.
- [4] Ly A., Luo Y., Cavailles G., Olivier M.G., Debliquy M. and Lahem D., (2020). Ammonia Sensor Based on Vapor Phase Polymerized Polypyrrole, *Chemosensors*, 8, 30.
- [5] Tai H., Wang S., Duan Z. and Jiang Y., (2020). Evolution of breath analysis based on humidity and gas sensors: Potential and challenges, *Sens. Actuators B Chem.*, 318, 128104.
- [6] Nakhleh, M.K., Amal H., Jeries R., Broza Y.Y., Aboud M., Gharra A., Ivgi H., Khatib S., Badarneh S. and Har-Shai, L., (2017). Diagnosis and Classification of 17 Diseases from 1404 Subjects via Pattern Analysis of Exhaled Molecules, *ACS Nano*, 11, 112–125.
- [7] Hua B. and Gaoquan S., (2007). Gas Sensors Based on Conducting Polymers, *Sensors*, 7, 267-307
- [8] Shanga Y., Wanga X., Xu E., Tong C. and Wu J., (2011). Optical ammonia gas sensor based on a porous silicon rugate filter coated with polymer-supported dye, *Analytica Chimica Acta*, 685, 58-64
- [9] Hamouma O., Kaur N., Oukil D., Mahajan A. and Chehimi, M. M., (2019), Paper strips coated with polypyrrole-wrapped carbon nanotube composites for chemi-resistive gas sensing, *Synth. Met.*, 258, 116223.
- [10] Sachan, A., Castro, M., Choudhary V. and Feller J.F., (2018). Influence of Water Molecules on the Detection of Volatile Organic Compounds (VOC) Cancer Biomarkers by Nanocomposite Quantum Resistive Vapor Sensors vQRS, *Chemosensors*, 6, 64.
- [11] Li W., Liu H., Xie D., He Z. and Pi X., (2017). Lung Cancer Screening Based on Type-different Sensor Arrays, *Sci. Rep.*, 7, 1969.
- [12] Guntner A.T., Righettoni M. and Pratsinis S.E. (2016). Selective sensing of NH₃ by Si-doped -MoO₃ for breath analysis, *Sens. Actuators B Chem.*, 223, 266–273.
- [13] Chitte H. K., Bhat N.V. and Vasant E., (2011), Synthesis of Polypyrrole Using Ferric Chloride (FeCl₃) as Oxidant Together with Some Dopants for Use in Gas Sensors, *Journal of Sensor Technology*, 1, 47-56.
- [14] Wang Y., Jia W., Strout T., Baikun Z., Cui J. and Lei Y., (2011), Ammonia Gas Sensor Using Polypyrrole-Coated TiO₂/ZnO Nanofibers, *Electroanalysis*, 21, 1432
- [15] Tang X., Raskin J.P., Kryvutsa N., Hermans S., Slobodian O., Nazarov A.N. and Debliquy M. (2020). An ammonia sensor composed of PPy synthesized on reduced graphene oxide by electropolymerization, *Sens. Actuators B Chem.*, 305, 127423.
- [16] Dai M.Z., Lin Y.L., Lin H.C., Zan H.W., Chang K.T., Meng H.F., Liao J.W., Tsai M.J. and Cheng H. (2013). Highly sensitive Ammonia sensor with organic vertical nanojunctions for noninvasive detection of hepatic injury, *Anal. Chem.*, 85, 3110–3117.
- [17] Chartuprayoon N., Hangarter C.M., Rheem Y., Jung H. and Myung N.V. (2010), Wafer-scale fabrication of single PPy nanoribbon-based ammonia sensor, *J. Phys. Chem.*, 114, 11103–11108.
- [18] Capone S., Forleo A., Francioso L., Rella R., Siciliano P., Spada- vecchia J., Presicce D.S. and Taurino A.M. (2003), Solid state gas sensors: state of the art and future activities, *Journal of Optoelectronics and Advanced Materials* 5, 5, 1335 – 1348.
- [19] Garg R., Kumar V., Kumar D., and Chakarvarti S.K., (2015). Polypyrrole Microwires as Toxic Gas Sensors for Ammonia and Hydrogen Sulphide, *Columbia International Publishing Journal of Sensors and Instrumentation*, 3, 1-13.
- [20] Shao Q., Chen W., Wang Z., Qie L., Yuan L., Zhang W., Hu X., Huang Y., (2011). SnO₂-based composite coaxial nanocables with multi-walled carbon nanotube and polypyrrole as anode materials for lithium-ion batteries, *Electrochem. Commun.* 13, 1431-1434.
- [21] Lin C.W., Chen H.L., Chen T.Y., Huang C.C., Hsu C.S., Liu R.C. and Liu W.C. (2011), Ammonia Gas Sensing Performance of an Indium Tin Oxide (ITO) Based Device with an Underlying Au-Nanodot Layer, *Sens Actuators B* 160:1481.
- [22] Shang Y., Wang X., Xu E., Tong C. and Wu J. (2015), Porous Silicon Structures as Optical Gas Sensors, *Anal Chim Acta*, 15(8), 19968–19991.
- [23] Wang Y., Jia W., Strout T., Schempf A., Zhang H., Li B., Cui J. and Lei Y., (2009), Preparation, Characterization and Sensitive Gas Sensing of Conductive Core-sheath TiO₂-PEDOT Nanocables, *Sensors (Basel)*, 9(9), 6752–6763.
- [24] Vaezi M.R. and Sadrezhaad S.K., (2007). Nanopowder synthesis of zinc oxide via solchemical processing, *Mater Sci. Eng B* 140, 73.
- [25] Hernandez S.C., Chaudhuri D., Chen W. and Myung N.V., (2007). Maskless electrodeposited contact for conducting polymer nanowires, *Appl. Phys. Lett.* 92, 073104.

Fabrication of Nano-structured SnO₂ Powder by Sol-Gel Method

S. R. Bijwe¹, G. T. Lamdhade², P. S. Bodkhe³, K. B. Raulkar²

¹Department of Physics, Shri. Shivaji College of Arts, Commerce & Science, Akola

²Department of Physics, Vidya Bharati Mahavidyalaya, Amravati, 444602

³Department of Chemistry, Vidya Bharati Mahavidyalaya, Amravati, 444602

* Corresponding Author e-mail: sarikashirbhate2013@gmail.com

Abstract:

SnO₂ powder was efficiently produced through the sol-gel method, followed by washing and calcination at 400°C to yield SnO₂ nano-powder. X-ray diffraction (XRD) analysis demonstrated the formation of a rutile structure in the SnO₂ nanocrystalline powder. Scanning Electron Microscopy (SEM) revealed a uniform distribution of small grains across the analyzed area. UV-Vis spectroscopy was employed to assess optical properties, showing a characteristic absorbance peak at 312 nm corresponding to SnO₂. The energy band gap of the SnO₂ thin film, determined from the $(\alpha h\nu)^2$ versus $h\nu$ graph, was measured at 3.78 eV. The synthesized SnO₂ film exhibited a transmittance of 78% in the spectral range of 350 nm to 800 nm. Overall, the XRD analysis confirmed the rutile structure, SEM analysis illustrated homogeneity, UV-Vis absorbance spectrum verified SnO₂ presence, and the measured band gap indicated the semiconductor nature. The high visible range transmittance (78%) underscores SnO₂'s potential for transparent conductive applications. Overall, the results indicate successful synthesis and characterization of SnO₂ nanocrystalline powder with promising optical and structural properties.

Keywords – Band gap, Metaloxide, Tin oxide, nanocrystallites, Sol-gel

1. Introduction

Nano-crystals of semiconductor metal oxides, particularly Tin Oxide (SnO₂), have gained attention for their unique properties distinct from their bulk forms. SnO₂ is noteworthy for its wide bandgap ($E_g = 3.64$ eV at 330K), n-type conductivity, and high transparency (>80%) in the visible range. It crystallizes in a rutile structure and can be synthesized in various shapes and sizes using cost-effective methods. These properties make SnO₂ suitable for applications such as solid-state gas sensors, flat-panel displays, and solar energy cells. Thin films of SnO₂ exhibit a high free carrier density, primarily due to factors like oxygen vacancies, excess interstitial tin, and unintentional chlorine doping, often originating from glass substrates during high-temperature processes [1-3].

Various methods have been employed to prepare SnO₂ nanostructures, aiming for better control over particle size and physical properties. These methods include the hydrothermal method, polymeric or organo-metallic precursor synthesis, sonication, microwave-assisted synthesis, and surfactant-mediated methods. However, these techniques often come with drawbacks such as complexity, high cost, energy or time consumption, and low throughput. For instance, the hydrothermal method typically requires at least 24 hours to synthesize SnO₂ nanoparticles. Polymeric and sonication techniques, while effective, are complex and yield fewer throughputs, making them unsuitable for large-scale production. In contrast, the sol-gel method offers a simple and efficient approach to produce homogeneous nanoparticles with high purity and crystallinity at relatively low temperatures. In the sol-gel process, the precursor solution undergoes two main steps: dispersion of colloidal particles in a liquid (sol) and

conversion of the sol into a rigid phase (gel) through hydrolysis and condensation reactions. This method is known for its simplicity and its ability to facilitate the synthesis of nanostructures with desirable properties.

The sol-gel method typically results in the synthesis of amorphous precipitates, and subsequent heat treatment becomes necessary to induce particle growth through re-crystallization and to alter the particle morphology. However, when it comes to the preparation of tin oxide, the sol-gel method stands out due to several advantages over alternative approaches. It offers benefits such as lower processing temperatures, improved homogeneity, controlled stoichiometry, and the flexibility to form dense monoliths, thin films, and nanoparticles [4-5].

In our current study, we delved into the structural, morphological, and optical properties of SnO₂ nano-powder and thin films, synthesized through a straightforward and convenient sol-gel technique. The characteristics of these SnO₂ nanocrystallites were explored using various characterization techniques, including X-ray diffraction (XRD), Scanning Electron Microscopy (SEM), and UV-Vis spectroscopy.

2. Experimental

2.1 Materials:

For the synthesis of SnO₂ nanoparticles, we utilized high-quality Analytical Reagent (A.R.) grade chemicals, specifically tin tetrachloride penta-hydrate (SnCl₄·5H₂O), ethylene glycol, and ammonia, all sourced from Loba Chemie Pvt. Ltd. in Mumbai, India. These chemicals were employed without undergoing any additional purification steps. Double distilled water served as the solvent during the synthesis, facilitating the dissolution of precursors like SnCl₄·5H₂O, ethylene glycol, and liquid ammonia.

2.2 Method:

The sol-gel technique was used for the synthesis of tin oxide nano-powder. A 0.1 molar solution of tin tetrachloride penta-hydrate was prepared by dissolving 3.51 g in 50 ml of double-distilled water. To this, 50 ml of ethylene glycol was added, creating a 100 ml precursor mixture. The mixture was stirred at 300 RPM on a magnetic stirrer, and a 0.1M aqueous ammonia solution was added drop-wise at a rate of 10 drops per minute. After about 50 drops, a sol-gel formed within 5 minutes. The resulting gel was filtered, washed, and the content was transferred to a crucible or onto a glass substrate using a 1 μm commercial applicator to form a thin film. Both the precipitate and the thin film were dried at 150°C for 2 hours to remove water molecules. After the completion of the synthesis process, the crucible sample and the thin film on the glass substrate, both initially displaying a black-brown colored tin oxide nano-powder, underwent a subsequent step of calcination. This involved heating at 400°C for a duration of 2 hours. Calcination is a crucial thermal treatment process that aids in enhancing crystallinity, promoting particle growth, and influencing the final morphology of the synthesized material [6-8].

The resulting material from the calcination process is expected to exhibit improved structural and morphological properties, contributing to the desired characteristics of SnO₂ nanocrystallites. The entire synthesis process, including the drying and calcination steps, is depicted in detail in Fig. 1, providing a comprehensive visual representation of the different stages involved in achieving the final SnO₂ nanocrystallite products through the sol-gel method.

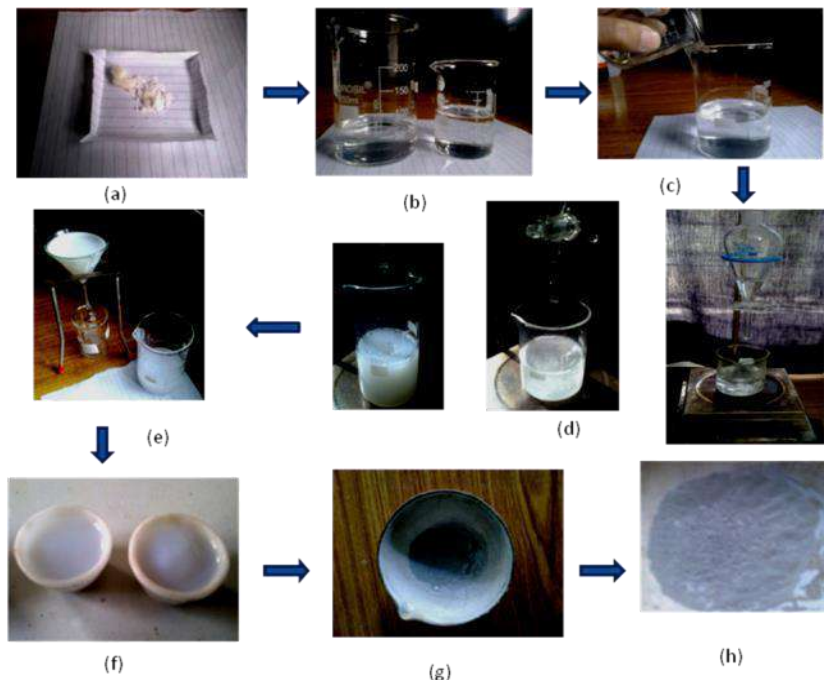


Fig.1 Stepwise photographic illustration of synthesis process of SnO₂ nanocrystallites (a) precursor, SnCl₄, 5H₂O, (b) solutions in beakers contain from left to right SnCl₄, 5H₂O, ethylene glycol, (c) simultaneous addition (d) gel formed by drop-wise addition aqueous ammonia under constant magnetic stirring, (e) filtration and washing, (f) gel of SnO₂ nanocrystallites, (g) dried SnO₂ nanocrystallites at 150°C for 2 hrs. and (h) calcinated at 400°C to obtain SnO₂ nanocrystallites in powder form.

2.3 Characterization:

The structural properties of SnO₂ nano-powder were studied by X-ray diffraction measurements (Bruker D-8 advance diffractometer, Billerica, MA) using the Cu K α ($\lambda = 1.5406 \text{ \AA}$) as a radiation source, operated at 40 kV and 30 mA with a scan rate of 0.02°/s over the range of 10°-80°. The average crystallite size (hkl) of all crystal planes for SnO₂ powder was estimated from the classical Scherrer formula [9-10]

$$D = \frac{K\lambda}{\beta \cos \theta} \quad \dots \dots \dots (1)$$

Where K is the shape factor usually has a value 0.9, λ is the X-ray wavelength and θ the Bragg's angle and β gives the full width of the half maxima (FWHM).

The study involved examining the surface structure of SnO₂ powder using a scanning electron microscope (SEM). Additionally, spectral transmittance and absorbance measurements were conducted using a UV-Vis spectrometer (Shimadzu 1650PC) in the wavelength range of 250 nm to 800 nm. The X-intercept was determined by extrapolating the linear portion of the exponential curve in the graph of $(\alpha h\nu^2)$ versus photon energy ($h\nu$). This X-intercept represents the bandgap energy of the SnO₂ material. In simpler terms, it identifies the energy required to transition electrons from the valence band to the conduction band in the material.

3. Results and Discussions

3.1 Structural and Morphological Properties:

The X-ray diffraction analysis of the SnO₂ powder sample, synthesized through the sol-gel technique, was conducted to determine its phase, crystal structure, and estimate the average grain size. The recorded X-ray diffraction pattern presented in Fig. 2 indicates the formation of

SnO₂ nanoparticles with a polycrystalline phase featuring a rutile structure [JCPDS Card No: 41-1445, with lattice parameters $a = 4.743 \text{ \AA}$ and $c = 3.1859 \text{ \AA}$]. The XRD pattern displays distinct crystal planes such as (110), (101), (211), (002), (310), and (301), highlighting the polycrystalline nature of the powder. The average lattice constant was determined by considering the values obtained from different (hkl) planes, reflecting the average spacing between atoms in the crystal lattice.

The average lattice constant, denoted by 'a', was determined by utilizing the formula

$$a = d\sqrt{h^2 + k^2 + l^2} \dots\dots\dots (2)$$

Where, 'd' represents the interplanar distance and (hkl) are the Miller indices. Through this calculation, the average lattice constants were found to be $a = 4.7470 \text{ \AA}$ and $c = 3.1854 \text{ \AA}$. The absence of any impurity phase was confirmed in the X-ray diffraction (XRD) spectra.

Furthermore, the average crystallite size ('D'), determined using Scherer's formula based on the XRD spectra, was found to be 52 nm. This provides information about the average size of the crystalline domains in the material. The respective angles of peak positions (2θ), Miller indices (hkl) corresponding to different crystal planes, and interplanar distances ('d') are detailed in Table 1. These results collectively contribute to a comprehensive understanding of the structural properties of the SnO₂ powder synthesized through the sol-gel technique [11].

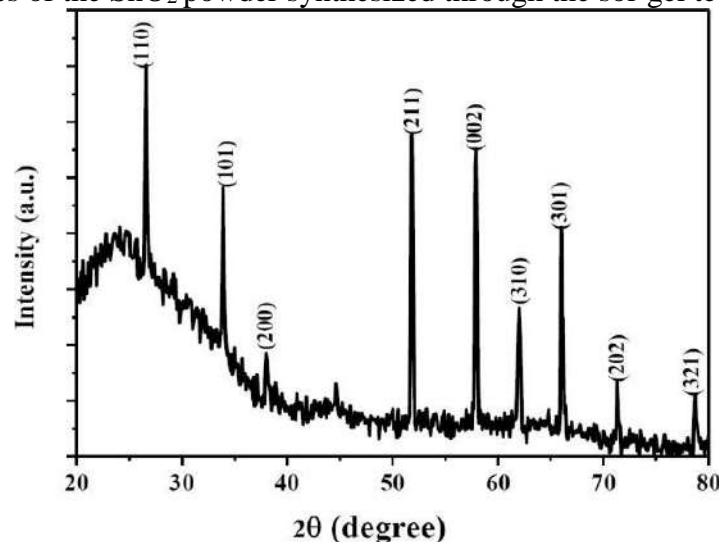


Fig.2 XRD pattern of SnO₂ nanocrystallites

Table1: XRD analysis of SnO₂ nanocrystallites

2θ	(hkl)planes	Inter-planardistances(d) in nm
26.6 ⁰	(110)	58.9
33.9 ⁰	(101)	55.3
38.0 ⁰	(200)	43.6
51.8 ⁰	(211)	59.3
57.9 ⁰	(002)	57.7
62.0 ⁰	(310)	49.3
66.0 ⁰	(301)	51.7
71.3 ⁰	(202)	47.5
78.7 ⁰	(321)	44.4

SEM analysis was performed to reveal morphological features of the sample. SEM micrograph of nano-crystalline SnO₂ thin film is shown in Fig.3 this shows a homogeneous, uniform distribution of SnO₂ nanocrystallites over a scanned area.

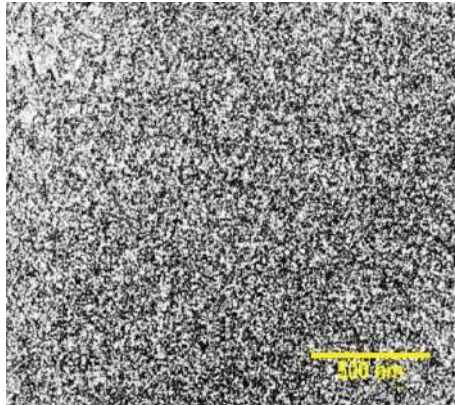


Fig.3 SEM micrograph of SnO₂ nanocrystallites

3.2 Optical Properties:

The UV-Vis absorbance spectra for SnO₂ nanocrystallites are depicted in Fig. 4 and Fig. 5. A distinctive absorption peak was observed at approximately 312 nm within the wavelength range of 275 nm to 350 nm. The substantial reduction in transmittance near the band edge suggests improved crystallinity and a lower defect density in the synthesized thin film.

Specifically, the SnO₂ thin film exhibited a transmittance of 78% in the spectral range from 350 nm to 800 nm. This information indicates that the thin film allows a significant amount of light to pass through within this wavelength range, highlighting its transparency and suggesting potential applications in optoelectronic devices or other technologies where controlled light transmission is essential. The analysis of the transmission Fig.4 (thin film) and absorbance spectra (absorbance for SnO₂ nanocrystallites) in the vicinity of the fundamental absorption edge shows that the variation of the absorption coefficient is in accordance with following relation which implies the direct transitions.

$$(\alpha h\nu)^2 = A(h\nu - E_g) \dots\dots\dots (3)$$

Here, α is an absorption coefficient, h is Planck constant, ν is the frequency and $h\nu$ is the incident photon energy.

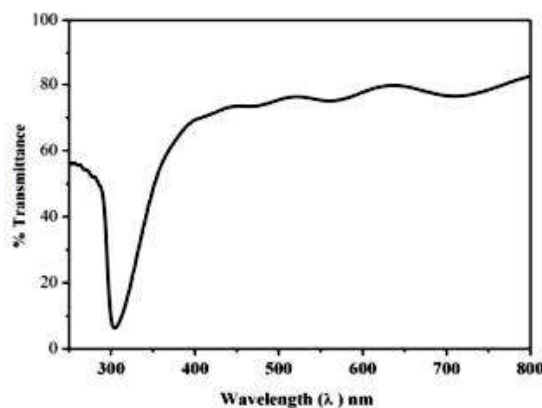


Fig.4 Transmittance spectrum of SnO₂ thin film

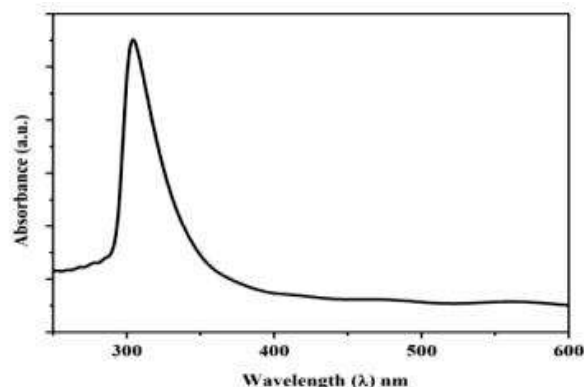


Fig.5 UV-Vis absorption spectrum of SnO₂ nanocrystallites

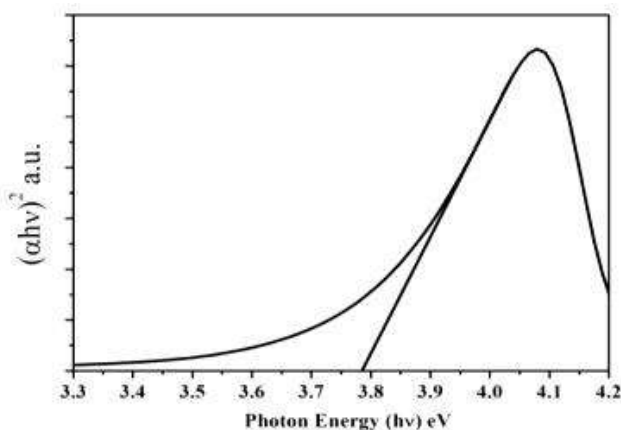


Fig.6 The plot of $(\alpha h\nu)^2$ vs $h\nu$ for SnO₂ nanocrystallites

The direct band gap (E_g) of our sample was determined by analyzing the absorption coefficient data as a function of wavelength, using the Tauc relation. This involved extrapolating the straight line of the $(\alpha h\nu)^2$ vs. $h\nu$ plot to intercept on the horizontal photon energy axis. The measured band gap was found to be 3.78 eV, as illustrated in Fig. 6.

It's noteworthy that the obtained tin oxide (SnO₂) exhibits an optical band gap larger than the reported value of 3.64 eV for bulk SnO₂. This difference is attributed to the quantum confinement effect. Essentially, the quantum confinement effect refers to the phenomenon where the electronic and optical properties of materials are altered when their dimensions are reduced to nanoscale dimensions. In the case of our sample, the smaller size of nanocrystallites contributes to the observed increase in the optical band gap, highlighting the impact of quantum confinement on the material's optical properties.

4. Conclusions

Tin oxide (SnO₂) nanocrystallites and thin film were synthesized successfully by Sol-Gel method. Here, we concluded from XRD analysis that particles are polycrystallized with tetragonal rutile structure. Morphological characteristics of SnO₂ nano crystallines thin film are obtained from SEM image, shows uniform distribution of quite small grains with average crystallite size of 52 nm. The absorbance and transmittance spectra indicate that the synthesized tin oxide nano-crystallites are small and uniform. UV-Vis analysis reveals a characteristic absorbance peak at $\lambda=312$ nm for SnO₂. The bandgap, determined from the plot of $(\alpha h\nu)^2$ versus $h\nu$, is measured at 3.78 eV. Transmittance analysis demonstrates 78% transmittance for the as-synthesized SnO₂ thin film in the spectral range 350 nm to 800 nm.

5. Acknowledgements

The authors are thankful to the reviewers for the careful inspection of the manuscript also a big thanks to department of physics, Vidyabharati Mahavidyalaya Amravati for providing facilities to carry out research work.

References

- [1] Devi R.S., Venckatesh R. and Sivaraj R., 2014, Synthesis of Titanium Dioxide Nanoparticles by Sol-Gel Technique, *IJIRSET*, **10** 15206-211.
- [2] Dighore N., Dhonde S., Gaikwad S. and Rajbhoj A., 2016, Synthesis of conducting polymer Polypyrrole-MoO₃ nanocomposites, *Mor. J. Chem.*, **4** 797-804.
- [3] Chartuprayoon N., Hangarter C.M., Rheem Y., Jung H. and Myung N.V. 2010, Wafer-scale fabrication of single PPy nanoribbon-based ammonia sensor, *J. Phys. Chem.*, **114** 11103–11108.
- [4] Hernandez S.C., Chaudhuri D., Chen W. and Myung N.V., 2007. Maskless electrodeposited contact for conducting polymer nanowires, *Appl. Phys. Lett.* **92** 073104.
- [5] Sachan, A., Castro, M., Choudhary V. and Feller J.F., 2018. Influence of Water Molecules on the Detection of Volatile Organic Compounds (VOC) Cancer Biomarkers by Nanocomposite Quantum Resistive Vapor Sensors vQRS, *Chemosensors*, **6** 64.
- [6] Hamouma O., Kaur N., Oukil D., Mahajan A. and Chehimi, M. M., 2019, Paper strips coated with polypyrrole-wrapped carbon nanotube composites for chemi-resistive gas sensing, *Synth. Met.*, **258** 116223.
- [7] Nakhleh, M.K., Amal H., Jeries R., Broza Y.Y., Aboud M., Gharra A., Ivgi H., Khatib S., Badarneh S. and Har-Shai, L., 2017. Diagnosis and Classification of 17 Diseases from 1404 Subjects via Pattern Analysis of Exhaled Molecules, *ACS Nano*, **11** 112–125.
- [8] Shang Y., Wang X., Xu E., Tong C. and Wu J. 2015, Porous Silicon Structures as Optical Gas Sensors, *Anal Chim Acta*, **15(8)** 19968–19991.
- [9] Wang Y., Jia W., Strout T., Schempf A., Zhang H., Li B., Cui J. and Lei Y., 2009, Preparation, Characterization and Sensitive Gas Sensing of Conductive Core-sheath TiO₂-PEDOT Nanocables, *Sensors (Basel)*, **9(9)** 6752–6763.
- [10] Hua B. and Gaoquan S., 2007. Gas Sensors Based on Conducting Polymers, *Sensors*, **7** 267-307.
- [11] Raulkar K B, 2021. Fabrication and applications of (SnO₂-ZnO)/polypyrrole(ppy) coaxial nanocables to response NH₃ gas, *Vidyabharati International Interdisciplinary Research Journal*, **12(1)** 209–214

Study of Doping Metal Oxides Gas Sensor for Efficient CO₂ Gas Sensing

R. S. Bhuyar¹, K. B. Raulkar², S. R. Bijwe¹, G. T. Lamdhade²

*1 Department of Physics, Shri Shivaji College of Arts, Comm. & Science, Akola, MS, India

2 Department of Physics, Vidyabharti Mahavidyalaya, Amravati, MS, India

Corresponding: ritabhuyar1984@gmail.com

ABSTRACT

In present studies the efforts are made to improve gas sensing properties by doping of mixed metal oxide and the result indicates substantial increase in gas sensing properties of CO₂ gas sensor. The gas response of SnO₂:TiO₂ doping observed substantial increase in porosity over pure metal oxide. The metal oxides used for the designing of gas sensor were first calcinated at 600⁰C for 6 hr. Sensors of SnO₂:TiO₂ were prepared by screen printing technique with Al₂O₃ as substrate on clean glass plate. The surface morphologies of doping of SnO₂:TiO₂ were analyzed by SEM. Static and dynamic responses also studied, it was found that response of optimized sample 92SnO₂:08TiO₂ shows enhancement in gas sensing properties as compared to pure SnO₂ and TiO₂.

Keywords: Metal Oxide nanoparticles, screen printing technique, Gas sensing.

1. Introduction:

Currently, electronics is a fast developing field; we observed that the sensor plays a very important and vital role for controlling, monitoring, analyzing and in all era. There are multiple type of sensors, depending upon their working. Among the sensors, the chemical sensor is the best one and is preferred due to its high performance [1]. The chemical sensor has made great advances and has taken root in human life and industry as a feature of modern technology and also remarkable progress is expected in the future [2-5]. We have multiple types of sensors, depending upon their working. Among these, the chemical gas sensor is preferred due to its high sensitivity. The sensor has countless advances and has taken origin in industry and human life as a feature of recent modern technology and also notable progress is expected in the prospect. In the last decade, it had an increasing attention in the electronic industry for those aspects related to semiconducting gas sensor (SGS) materials. Semiconductor gas sensors having good benefits related to other sensor devices, due to its low price, simple implementation, and good reliability for real-time control systems and easy make. The gas sensor is electronic noses, because sensing devices are able to capture and process signals generated by surface interaction processes with gas molecules, in one or multiple built-in sensitive layers. Most of the industries are using such type of sensors due to their wide applications. As per previous studies the sensing properties of metal oxide-based material depend upon its chemical and physical characteristics, which are strongly hooked in to the preparation conditions, doping and grain size, which indicates that the synthesis of the sensing material is crucial within the preparation of high-performance Metal oxide semiconductor (MOS) gas sensors. SnO₂, TiO₂ powders and films can be prepared by a spread of synthesis methods [6-10]. The electrical resistance of the sensors prepared by TiO₂ doping with SnO₂ was measured in presence of CO₂ gas. The study revealed that 92SnO₂:08TiO₂ sensor showed more sensitivity for CO₂ gas concentration at room temperature.

2. Material and Method

2.1 Synthesis of SnO₂ Nanoparticles

In order to carry out the experiment described above, GR grade chemicals with a purity level of 99.99% were purchased from Sd-fine in India. In order to produce stannous dioxide (SnO₂), 2 grams (0.1 millimetres) of stannous chloride dehydrate (SnCl₂.2H₂O) were dissolved in 100 milliliters of water. After the aqueous solution that was previously used had finished dissolving entirely, 4 cc of an ammonia solution was added while magnetic stirring was performed. A time period of spinning for twenty-five minutes led to the beginning of the formation of a white gel precipitate. After that, it was allowed to rest for ten to fourteen hours before being examined again. After that, it was cleansed in deionized water after passing through four or five filters in the previous process. A total of 0.27 grammes of charcoal-activated carbon black powder was added to the precipitate that was produced as a consequence. After about one day of being ground into powder in a vacuum oven at a temperature of 80 degrees Celsius, the mixer was removed. The dry material was broken up into smaller pieces and then milled into a powder. In order to purge impurities from the end product, the ultrafine SnO₂ nanopowder was calcined in an auto-controlled muffle furnace at a temperature of 700 degrees Celsius for up to seven hours [11].

2.2 Synthesis of TiO₂ Nanoparticles

Iso-propanol [(CH₃)₂CHOH] and nitric acid [HNO₃] were both utilised straight from their respective containers when they were prepared. Titanium tetra iso propoxide [Ti(OCH(CH₃)₂)₄]. To a solution that was 22 millilitres in size, drop by drop additions of 20 millilitres of titanium tetra isopropoxide, 10 millilitres of isopropanol, and 12 millilitres of deionized water were made while the temperature was maintained at 80 degrees Celsius. After an hour, 0.80 millilitres of highly concentrated HNO₃ and 0.8 millilitres of deionized water were added to the TTIP solution. After six hours of continuous stirring at 60°C, a very viscous sol-gel was created. Two hours at 300°C were spent heating the prepared sol-gel outside. After annealing, 2g of TiO₂ nanocrystalline powder was created. The produced powder was mixed with the iso-propanol solution in a 1:10 ratio. To acquire thoroughly dried powder, the obtained powder was stored in a vacuum oven at 70 °C for 24 hours.

2.3 Preparations of thick films

The obtained samples were used for screen printing, which resulted in the creation of thick films. Sintered fine powders of pure and composite nano-powders of SnO₂ and TiO₂ in different weight ratios were first mixed with ethyl cellulose as a temporary binder in order to form the thixotropic paste for screen printing. This paste was then used to print on screens. In order to get the desired results, this solution is combined with organic solvents such as terpineol, butyl cellulose, and butyl carbitol acetate. The production of the paste consisted of inorganic chemicals 75 percent of the time and organic ingredients 25 percent of the time. Screen printing was used to apply thick sheets of pure and composite SnO₂ and TiO₂ materials formed from the paste onto a clean glass substrate. Al₂O₃ served as the base for the printing process. The created films were baked for an hour at 90–100°C to completely evaporate all of the organic materials (in the form of binders) and organic pollutants. Electrodes are made to measure surface conductivity on the thick film's opposing sides, and the silver paint is then dried by heating the film at 70°C for 0.5 hours. The table below displays the samples in order

Table 1: Sample code

Sr.No.	Sample doping	Sample code
01	Pure SnO ₂	S1
02	98SnO ₂ : 02TiO ₂ /Al ₂ O ₃ /GP	S2
03	96 SnO ₂ :04 TiO ₂ /Al ₂ O ₃ /GP	S3

04	94 SnO ₂ :06 TiO ₂ /Al ₂ O ₃ /GP	S4
05	92 SnO ₂ :08 TiO ₂ /Al ₂ O ₃ /GP	S5
06	90 SnO ₂ :10 TiO ₂ /Al ₂ O ₃ /GP	S6
07	Pure TiO ₂	S7

3. Result & Discussion

3.1 X-ray Diffraction Study

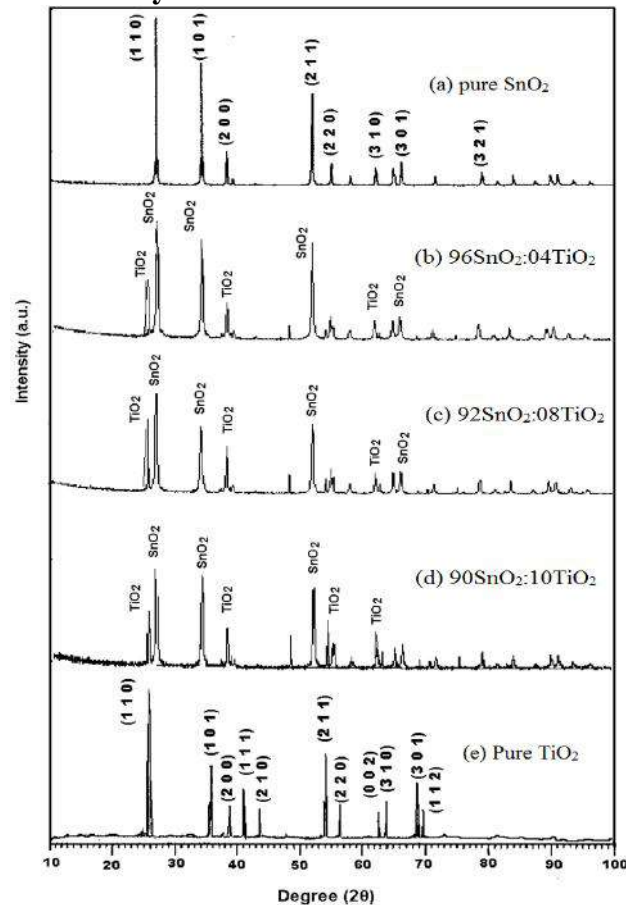
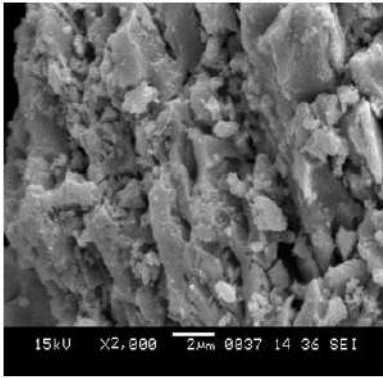
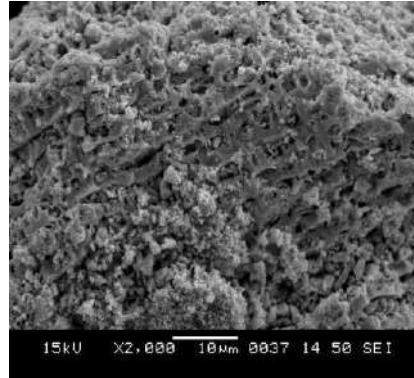
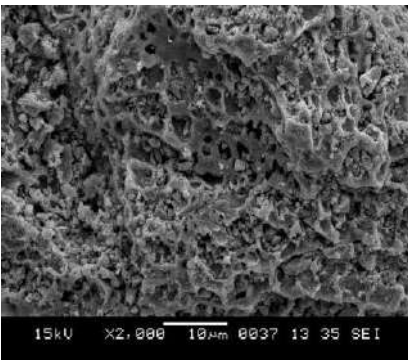
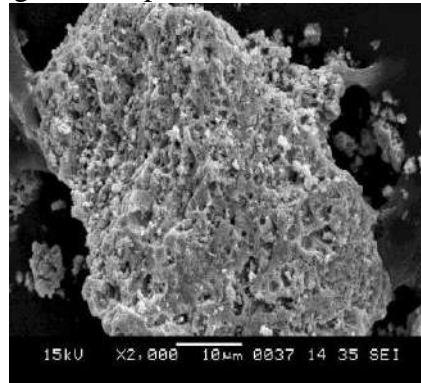


Fig.1. XRD pattern of SnO₂ -TiO₂ System

Fig. 1 shows the pure SnO₂ and TiO₂ X-ray diffraction patterns and doping of SnO₂ and TiO₂. It is recorded in terms of 2θ in the range 10 to 100°. Prominent peaks of SnO₂ and TiO₂ are observed. It was manifested that the associated peak's intensity rose and peaked for 92SnO₂:08TiO₂ doping. All planes corresponding to the Anatase-tetragonal phase of TiO₂ with space group number 141 are formed. The unit cell parameters $a = b = 3.2320$, $c = 6.6430$, $\alpha = \beta = \gamma = 90^\circ$. FWHM was used to compute the "crystallite size (D)" from Scherer's formula and was found to be 93.23 nm for 92SnO₂:08TiO₂ doping. It was observed that average crystallite size of 92SnO₂:08TiO₂ doping is least as compared to other compositions and pure materials and hence 92SnO₂:08TiO₂doping surface large active surface area for sensing the gas.

3.2 SEM (Scanning Electron Microscope) study

The SEM images (Fig. 2-4) showed that the number of pores varied in every square inch of the region, and hence to compare, an average number of pores was used. For an area of one inch on each shot, porosity was determined

Fig. 2 SEM picture of TiO₂Fig. 3 SEM pictures of 96 SnO₂:04 TiO₂Fig. 4 SEM pictures of 92SnO₂:08TiO₂Fig. 5. SEM picture of SnO₂

According to SEM images, SEM pictures of 92SnO₂:08TiO₂ showed more porosity as compared to pure SnO₂, pure TiO₂ and doped SnO₂ + TiO₂ sensors. This showed the increased effective area of S5 sensor for absorption of CO₂ gas.

3.2 Sensitivity measurement

It was shown that sensitivity increases linearly up to 550 ppm for all doping samples then becomes saturated for further increase in CO₂ gas concentration. Variation of sensitivity is also shown in the bar graphs at 600 ppm CO₂ gas concentration [12-14]. It was found that S5 sensor (92SnO₂:08TiO₂) has maximum sensitivity 1.554 at 600 ppm CO₂ gas among the prepared sensor.

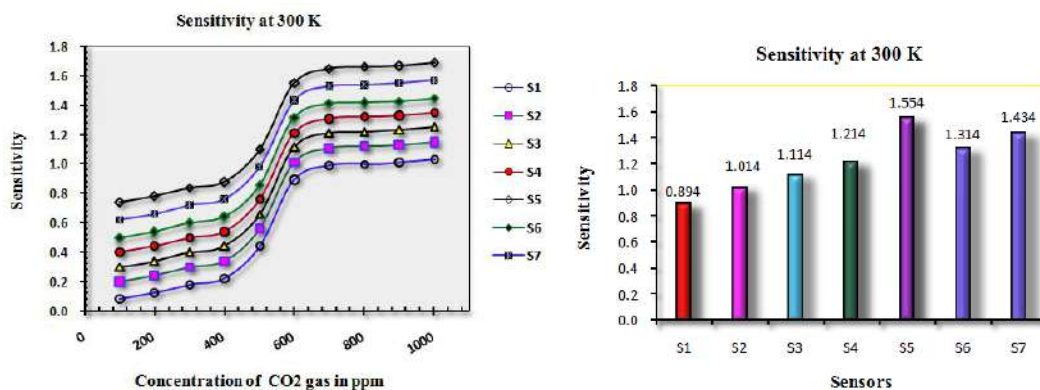


Fig. 6 Sensitivity of the SnO₂:TiO₂ system changes as CO₂ concentration (ppm) increases at 300 K.

4. Conclusion

Sensors were prepared by using pure SnO₂, pure TiO₂ and TiO₂ doped with SnO₂ with different percentage of doping. The series consists of sensors S1, S2, S3, S4, S5, S6, S7. Among these seven prepared sensors, S5 sensor showed less crystalline size from XRD study, to be 93.23 nm, from SEM study, it showed more porosity and more active absorption surface area. Hence sensitivity of S5 sensor is enhanced and found to be 1.554 at 600 ppm CO₂ gas concentration.

5. Acknowledgement:

Author of this research paper expressed sincere thanks to Department of Physics, Vidya Bharti Mahavidyalaya, Amravati, India, for constant support to carry out this research work and also thanks to Karmavir Bhaurao patil College, Washi, Navi Mumbai for SEM analysis.

Reference:

- [1] Raulkar K.B, Wasnik T.S, Joat R.V., Wadatkar A.S. Agrawal, R.M. and Lamdhade G.T., (2019). Study on DC Conductivity of PPy-ZnO Nanocomposites, *Materialstudy Proceedings*, 15(3), 595-603.
- [2] Jafarpour M.M., Foolad A., Mansouri M.K., Nikbakhsh Z. and Saeedi Zade H. (2010). Ammonia Sensing Properties of (SnO₂-ZnO)/Polypyrrole coaxial nanocables, *World Acad Sci. Eng. Technol*, 70, 940-945.
- [3] Jorgensen T.C. and Weatherley L.R. (2003). Ammonia removal from wastewater by ion exchange in the presence of organic contaminants, *Water Research* 37, 1723–1728.
- [4] Chougule M.A., Dalavi D.S., Sawanta Mali, Patil P.S., Moholkar A.V., Agawane G.L., Shashwati Sen and Patil V.B. (2012). Novel method for fabrication of room temperature polypyrrole–ZnO nanocomposite NO₂ sensor, *Elsevier-Measurement*, 45(8), 1989-1996.
- [5] Mahaja C., Chaudhari P. and Mishra S. (2018). RGO–MWCNT–ZnO based polypyrrole nanocomposite for ammonia gas sensing, *Journal of Material Science*, 29, 8039–8048.
- [6] Chatterjee S., Shit A. and Nandi A.K. (2013). Nanochannel morphology of polypyrrole–ZnO nanocomposites towards dye sensitized solar cell application, *Journal of Materials Chemistry A*, 1, 12302–12309.
- [7] Abdolmajid B.M., Tayebe N., Badraghi J. and Kazemzad. (2009). Synthesis of ZnO Nanoparticles and Electrodeposition of Polypyrrole/ZnO Nanocomposite Film, *Int. J. Electrochem Sci.*, 4, 247–257.
- [8] Yeolea B., Sena T., Hansoraa D., Mishra S. (2016). Polypyrrole/Metal Sulphide Hybrid Nanocomposites: Synthesis, Characterization and Room Temperature Gas Sensing Properties, *Materials Research*, 19(5), 37-42.
- [9] A shour A., Kaid M.A., El-sayed N.Z. and Ibrahim A.A. (2006). Physical properties of ZnO thin films deposited by spray pyrolysis technique, *Applied surface Science*, 52,7844-7848.
- [10] Mohammad M.T., Hashim A.A. and Al-Maamory M.H. (2006). Highly conductive and transparent ZnO thin films prepared by spray pyrolysis technique, *Materials Chemistry and Physics*, 99, 382-387.
- [11] Chakraborty A., Mondal T., Bera S.K., Sen S.K., Ghosh R. and Paul G.K. (2008). Effects of Al and In incorporation on the structural and optical properties of ZnO thin films synthesized by spray pyrolysis technique, *Materials Chemistry and Physics*, 112, 162-168.
- [12] Nemade K.R. and Waghuley S.A. (2012). V₂O₅-P₂O₅ Glass Ceramic As A Resistive Solid-State CO₂ Gas Sensor, *Asian Journal of Chemistry*, Vol. 24, No. 12, , 5947-5948.
- [13] Klug H.P. and Alexande L.E., (1974). X-ray Diffraction Procedure for Polycrystalline Materials, *Wiley Online library*, 125-127.
- [14] Shao H., Qian X.F. and Huang B.C., (2007). Fabrication of single crystal ZnO nano-rods and ZnS nanotubes through a simple ultrasonic chemical solution method. *Materials Letters*, 61(17):3639-3643.

Synthesis and Characterization of PANI Doped ZnO-SnO₂ for Humidity Sensing Application

T.R.Ingle, G.T.Lamdhade¹

1) Department of Physics, VidyaBharatiMahavidyalaya, Camp, C.K.Naidu Road, Amravati (M.S.) India
Corresponding Authors: Email: ingletr@rediffmail.com (T.R.Ingle), gtlamdhade@rediffmail.com,
oumgajanan@gmail.com (G.T.Lamdhade) Mob.+919403000509

Abstract:

Polyaniline (PANI) based Metal oxide nanocomposites were prepared by using the screen printing technique. The films were fired and optimized temperature of 60°C for 30 minutes in an air atmosphere. In the present work Polyaniline is prepared by polymerization of aniline under acidic conditions. Zinc Oxide (ZnO) nanoparticles and Tin Oxide (SnO₂) prepared by the Precipitation method at room temperature. The films were showing a decrease in resistance with an increase in temperature indicating semiconducting behavior. It is observed that PANI doped Metal oxide nanocomposite sensor shows a high response and sensitivity with good repeatability as compared to that of pure PANI and Metal oxide nanoparticle. The crystallinity and the crystallite size were examined by X-Ray Diffraction technique (XRD), and Scanning Electron Microscopy (SEM). Also confirms that the properties of pure polyaniline can be improved by the synthesis of Polyaniline - Metal oxide nanocomposites

Keywords: Polyaniline, Metal Oxides Nanocomposites, Humidity sensor, XRD, SEM

1. Introduction: Humidity control and monitoring are of great interest to a wide area; these include moisture sensitive products, fresh and pack-age food, drug storage and environmental control for valuable Antiques or paintings etc. [1, 2]. Humidity sensors that are available in the market include dew point, infrared, catalytic and tin oxide-based sensors, which may be expensive, or require high temperature operation and consume significant amount of power and high cost of maintenance [3]. Much research has been focused on the development of humidity sensitive material [4–6]. Among these are the investigation of using conducting polymers such as polyaniline, polypyrrole, and polythiophene for humidity and gas sensing [7–9]. Advantages with polymers as sensing materials are light weight, flexible, low cost and simple fabrication process [10]. Pure polymer, polymer blends and polymer–inorganic composites have also been studied for the purposes, resulting in different degree of advancements in this area [11–16].

2. Synthesis of Material:

A) Synthesis of Polyaniline (PANI): In general is synthesized using two major polymerization approaches: electronic and chemical polymerization. In the present work polyaniline is synthesized by chemical polymerization method in which 0.2 M aniline hydrochloride is used as monomer unit. The synthesis is done by oxidative polymerization with 0.25 M ammonia peroxy sulphate in aqueous medium. Both solution kept 1 hour at room temperature then mixed in beaker, briefly stirred. And left at rest to polymerize, next day, the PANI precipitate was collected on a filter, washed with three 100 ml portion of 0.2 M HCL and similarly with acetone. Polyaniline hydrochloride powder was dried in air and then in vacuum at 60°C. Polyaniline prepared under these reactions and processing condition are further referred to as standard sample.

B) Synthesis of Tin oxide (SnO₂): In preparation of SnO₂, 2 g (0.1 M) of stannous chloride dehydrate (SnCl₂·2H₂O) is dissolved in 100 ml water. After complete dissolution, about 4 ml

ammonia solution is added to above aqueous solution with magnetic stirring. Stirring is continued for 20 minutes. White gel precipitate is immediately formed. It is allowed to settle for 12 hrs. Then it is filtered and washed with water 2-3 times by using deionized water. The obtained precipitate were mixed with 0.27 g carbon black powder (charcoal activated). The obtained mixer is kept in vacuum oven at 70 °C for 24 hours so that the mixer gets completely in to dried powder. Then this dry product was crushed into a fine powder by grinder. Now obtained product of fine nanopowder of SnO₂ was calcinated at 600°C up to 6 hours in the auto controlled muffle furnace (*Gayatri Scientific, Mumbai, India.*) so that the impurities from product will be completely removed

C) Synthesis of Zinc oxide (ZnO): It is prepared by the aqueous solution of zinc nitrate. And is prepared by dissolving 0.2M of zinc nitrate hexahydrate in 100 ml of distilled water. To this aqueous zinc nitrate solution 0.2 M sodium hydroxide is added and the reaction mixture was heated at 80°C along with stirring and the process is carried out for four hour after which the white precipitate was obtained. The formed oxide wet precipitate is centrifuged. Then the wet precipitate is washed with de-ionized water to remove impurity ions present in it and further heated in the oven at 150°C to dry the precipitate formed.

4. RESULT AND DISCUSSIONS:

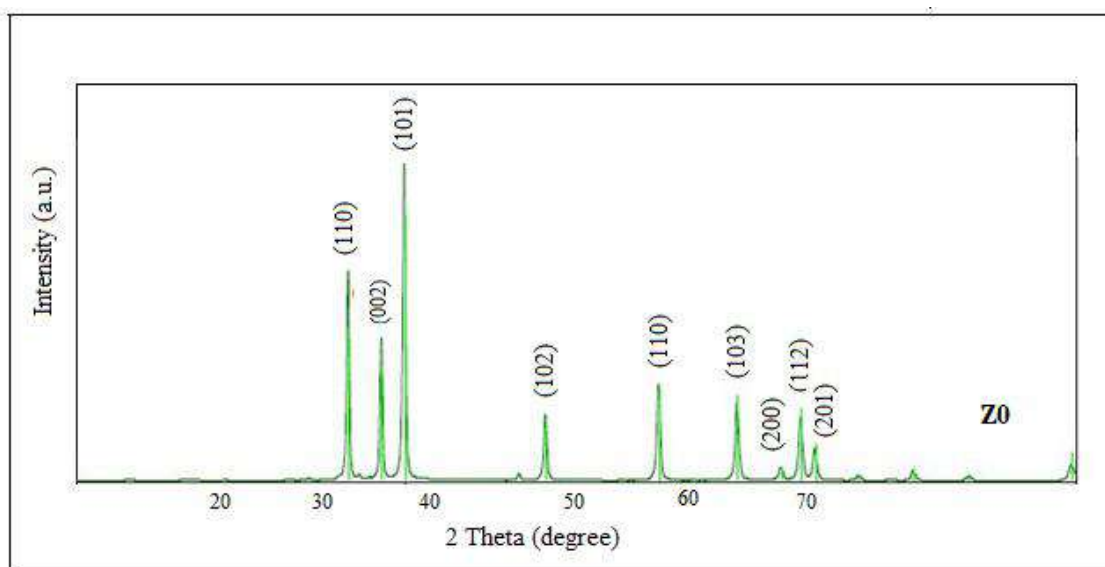


Figure 1. XRD of pristine ZnO (Z-0)

Figure 1,2,3 shows XRD pattern of pristine material ZnO, SnO₂ and Polyaniline (PANI) nanocrystalline materials respectively. The XRD pattern of pristine zinc oxide (ZnO) nanostructure synthesized by liquid phase method via solid state method calcinated at 700°C as shown in figure 4.1.(a). The crystalline nature with 2θ peak lying at (100), (002), (101), (102), (110) and (103) planes. All the peaks match well the standard hexagonal wurtzite structure of zinc oxide (ZnO) with lattice constants $a = b = 0.3249$ nm and $c = 0.5206$ nm its unit cell volume ($V=47.49\text{Å}^3$) [JCPDS card no. 36-1451]. All the peaks are perfectly match with pure ZnO structure, which indicates the high purity of the obtained ZnO nanoparticle. The average crystalline size was found to be 37.33 nm calculated by Deye-Scherrer formula [17].

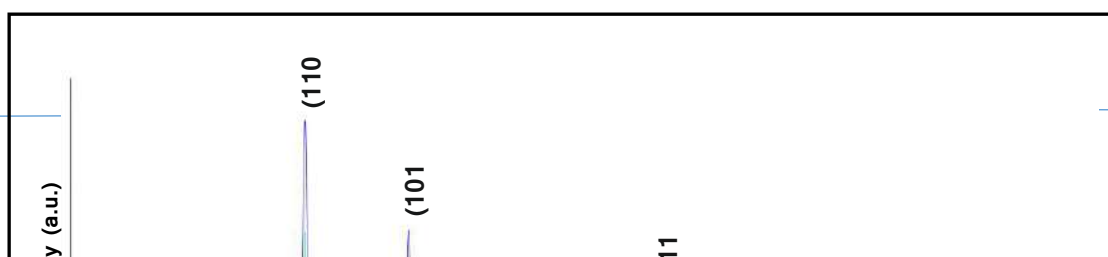


Figure 2. XRD of pristine (SnO₂) (S-0)

Figure 2. shows the XRD pattern of pristine stannic oxide (SnO₂) nanostructure synthesized by liquid phase via co-precipitation method calcinated at 600°C it is clearly observed that the highest intensity peak is obtained at (110) crystal planes and other peaks lying at (101), (200), (211), (220) and (002) of SnO₂. All the peaks match well with the standard tetragonal structure of SnO₂ with lattice constant $a = b = 4.723$ nm and $c = 3.18$ nm and its unit cell volume ($V=71.48\text{Å}^3$) with JCPDS card no. 71-0652. All the peaks are perfectly match with pure SnO₂ nanostructure, which indicates the high purity of obtained SnO₂ nanoparticles. The average crystalline size was found to be 28.95 nm calculated by using Debye-Scherer formula [18].

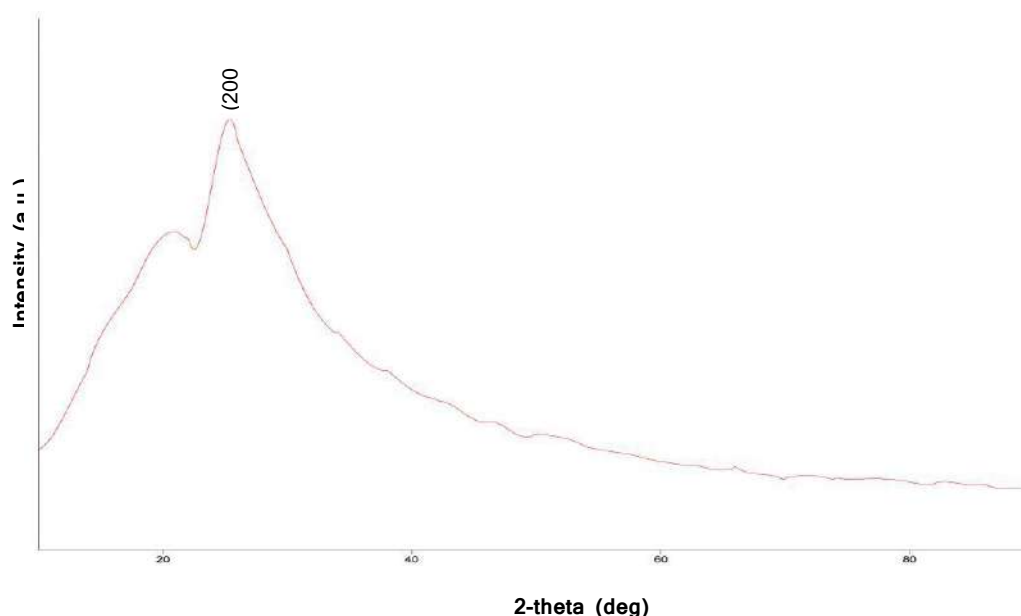


Figure 3. XRD of pristine (Polyaniline) (P-0)

Figure 3. shows the XRD pattern of pristine Polyaniline (P0) nanostructure synthesized by precipitation method and calcinated at 70°C was studied by XRD spectrometer using $\text{CuK}\alpha$ lines the spectra indicates the almost amorphous nature of sample as shown in fig- 4.1(c) the film prepared at higher thickness show polyaniline nature having peak for polyaniline at $2\theta = 25.58$. Similar observations on polyaniline sample have been reported by previous worker [19]

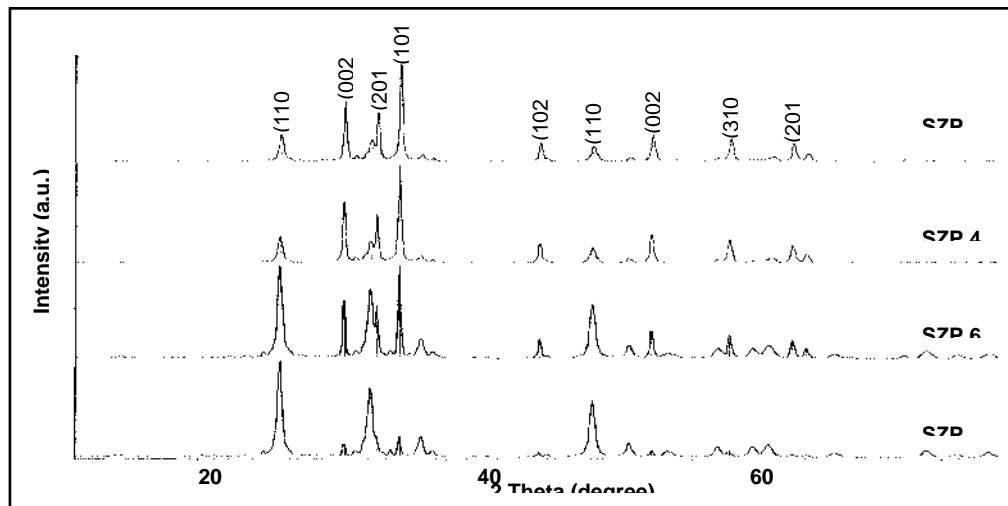


Figure 4. XRD Pattern of Polyaniline (PANI) Doped Metal Oxide Nanocomposites

Figure. 4. shows the XRD pattern of nanocomposite of Series (SZP) having four samples SZP-2(20SnO₂ - 70ZnO - 10 PANI), SZP-4 (40SnO₂-50ZnO-10PANI), SZP-6 (60SnO₂ - 30Zn -10PANI),and SZP-8 (80SnO₂ -10ZnO-10PANI), It is observed that from XRD pattern for SZP-4 sample shows crystalline nature with 2 θ peaks lying at (110),(002),(201),(101),(102),(110) and (002) (310) and (201) planes. The observes peaks are the mixed combination of SnO₂ and ZnO semiconducting metal oxides and Polyaniline (PANI). It is seen from crystal quantization plot, that more peaks about are corresponds to SnO₂ nanomaterial and very few about of them are corresponds to ZnO and polyaniline (PANI) nonomaterials. For the XRD pattern of the sample such as SZP-8, SZP-6, SZP-2 also shows crystalline nature and crystalline planes are obtained due to SnO₂ ZnO, and polyaniline. The average crystalline size is obtained by using scherrer formula and has been found to be 38.44 nm, 29.33 nm, 52.58 nm, 61.26 nm, for sample SZP-2, SZP-4, SZP-6, and SZP-8 respectively.

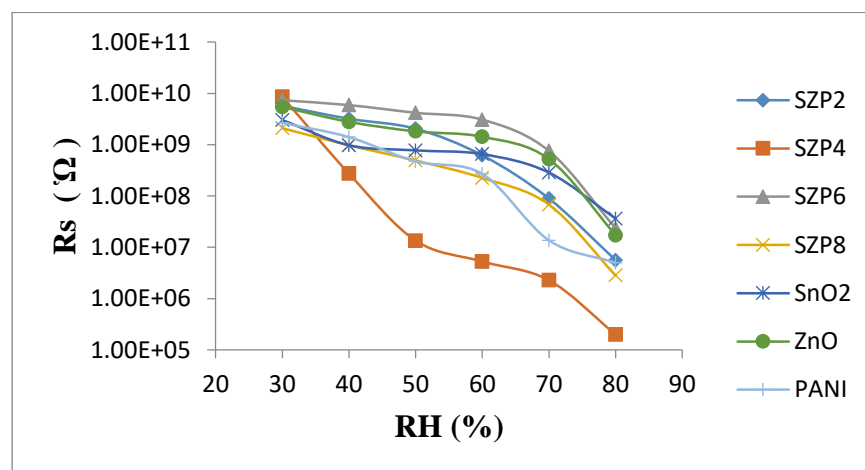


Fig. 5. Hysteresis plot

Hysteresis plot shows the variation between resistances of sample with respect to the relative humidity in increasing and decreasing order from 30 to 80 % RH as shown in the fig. 5. A very small hysteresis present during forward and reverse cycle of relative humidity, where as a very significant average change observed in the value of resistance of sample, in the sample SZP-4 (40SnO₂-50ZnO -10PANI) the change in value of resistance is near about from 10¹⁰ Ω

to $10^5 \Omega$, these is a remarkable change in the value of resistance. Therefore, by the addition of 10 %

Molar Polyaniline in the combination of ZnO and SnO₂, in different molecular weight concentration the adsorption and desorption process are much faster in the samples. it is also noted that ,by increasing the sensor temperature from 30° C to 80 ° C, its resistance decreases at a particular constant humidity due to process of adsorption and deadsorption.

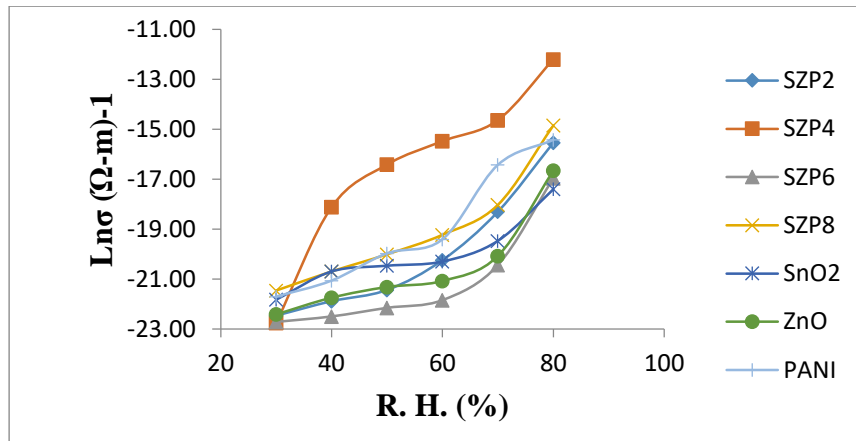


Fig. 6. Variation of Conductivity with Relative Humidity

it is observed that in fig .6 The conductivity increases perfectly linearly with relative humidity from 30 to 80 % RH and decreasing relatively on same path from 80 to 30 % RH. In this case also the conductivity increases with increase in temperature and it is highest at temperature 80°C and lowest at temperature 30°C. the conductivity difference between temperature 30°C and other ones are minimizes and the conductivity curves are not seen mixed so as seen in the group of sample. This behavior is obtained due to the addition of small amount of PANI in the SnO₂ and ZnO.the conductivity get stabilized through the resistance to near in the range of Megaohm (MΩ) . Hence the stability, linearity and equality are obtained in the samples

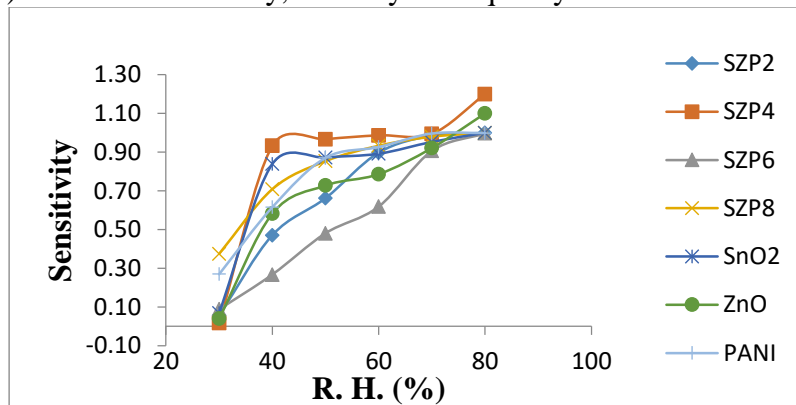
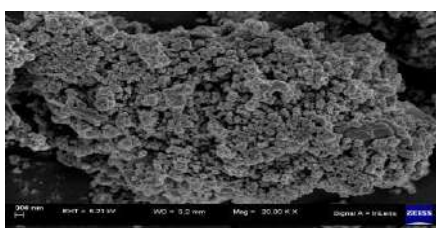


Fig. 7. Variation of Sensitivity with Relative Humidity

In the above samples the sensitivity is found to be increasing with the RH for all the samples of thick films and it is increasing up to some particular RH and then afterward it remains constant as shown in fig. 7 For higher RH the sensitivity is found to be higher in case of all samples of thick films. The sensitivity of SZP-4 (40 SnO₂ -50 ZnO -10 PANI) is more than



SZP-2, SZP-6, and SZP-8 samples and also from the pristine samples S-0 , Z-0 and P-0. The (SnO₂-ZnO-PANI) composite sensors exhibits significantly higher sensitivity than sensor constructed specially from SnO₂, ZnO nanoparticles and PANI itself due to the formation of heterogeneous interface between

them and more adsorption site was created to absorbed more water vapours.

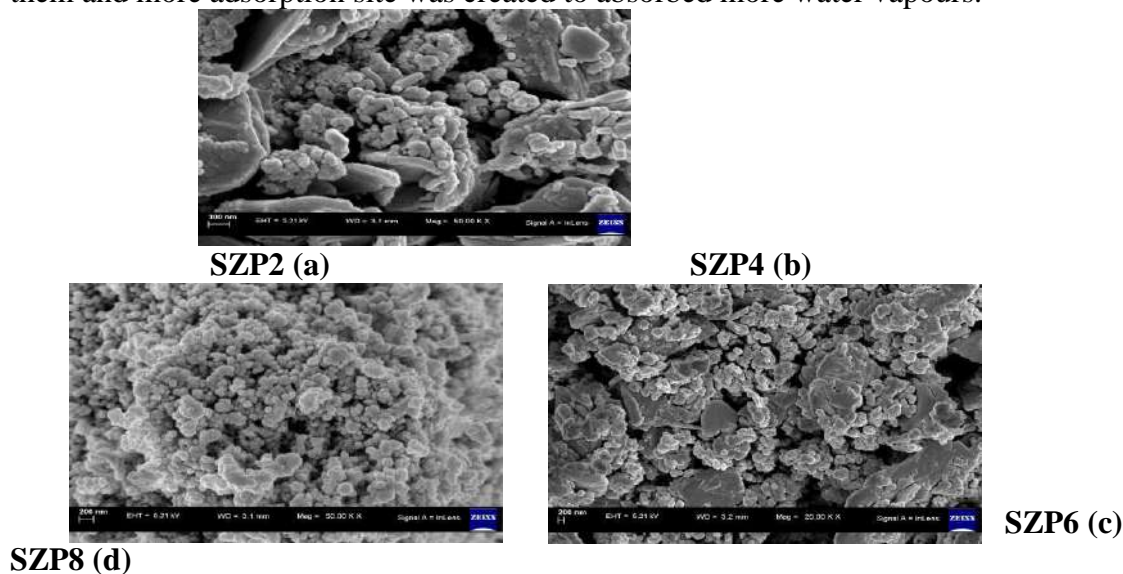


Fig. 8. FESEM Image of PANI Doped Metal Oxide Nanocomposites

The FE-SEM morphology of nanocomposites shows the particles are small sized, almost spherical flower like, rod like structure. The micrograph of SZP-4 (figure.8.(b).) One can see that nanocrystalline and porous SnO_2 , ZnO , is formed on the surface of SZP4 .By using crystalline quantization plot , these more peaks correspond to SnO_2 , than ZnO , and Polyaniline .The average crystalline size is obtained by using scherrer formula and it has been found to be 38.17nm, 35.20 nm, 38.25 nm, 41.31nm , Each grain seems to be like a bead of different shape and reveals that they possess the grain size of nanometer order and shows nanoporous structure. It means that the structure is likely to facilitate the adsorption and condensation processes of water molecules because of the capillary pore and having large surface area. This porosity leads to an effective response and recovery towards humidity.

5. CONCLUSIONS:

Nanostructured SnO_2 , ZnO , was successfully prepared via chemical precipitation method and PANI with IUPAC polymerization technique. Minimum crystallite size was found to be for SnO_2 (S0) is 28.95 nm , ZnO (Z0) is 37.33 nm and Polyaniline 25.58 nm.The Hysteresis plot shows very significant average change in the value of the resistance from near about $10^{10}\Omega$ to $10^5\Omega$ during forward and reversed cycles of sample SZP-4(40 SnO_2 -50 ZnO -10PANi). The sensitivity is found to be increasing with the RH for all the samples of thick films and it is increasing up to some particular RH and then afterward it remains constant. Amongst all the prepared samples.

References:

- [1] Traversa E. Sens. Actuators B 23, 135-136., 1995
- [2] C.Y. Lee, G.B. Lee, Humidity sensors: a review, Sens. Lett. 3, 1–15. 2005
- [3] D. Hodgins, The electronic nose using conducting polymer sensors, Sens. Rev. 14 (4) (1994) 28–31.
- [4] V. K Khanna, V. K. and R.K., Nahar , Sens. Actuators 5, 187-198. 1984
- [5] D. Goram., And T., Marija., Sens. Actuators 18,407-414. 1989
- [6] S.G Ansari., Z. A Ansari, M.R Kadam., Sens. Actuators B 21,159-163. 1994
- [7] U Dellow. P. Keller. and Meyer J., Sens. Actuators A 61,298-302. 1997
- [8] E Kan-Senchou. Kunaglee T. Jiin Liu F, Sens. Actuators B56, 106-111. 1999

-
- [9] F Kock. and T Kockel., *Chemical Engineering Journal*, 76, 49-60. 2000.
- [10] R. Niranjana . and S Sathaye., *Sens. Actuators B*, 81, 64-67. 2001
- [11] W. Tai and J-H. Oh, *Sens. Actuators B*, 85, 154-157. 2002
- [12] K. Ogura, T. Saino, M. Nakayama, H. Shiigi, *J. Mater. Chem.* 7, 2363–2366., 1997
- [13] N. Parvatikar, S. Jain, C.M. Kanamadi,,M.V, *J. Appl. Polym. Sci.* 103,653– 658., 2007
- [14] S.T. McGovern, G.M. Spink, G.G. Wallace, *Sens. Actuators B* 107, 657–665. 2005
- [15] M.L. Singla,, S. Awasthi, A. Srivastava,, *Sens. Actuators B* 127, 580–585., 2007
- [16] M. Wan, Z.X. Wei, Z.M. Zhang, L.J. Zhang, K. Huang, *Synth. Met.*135 175–176. 2003
- [17] Nagarajan S and Kuppusamy K A, *Journal of Nanobiotechnology.*, 11,1-11, (2013).
- [18]Patil G E, Kajale D D, Gaikwad V B, Jain G H, *Int. Nano Lett.*, 2, 46-51 ,(2012).
- [19] Farrukh M A, B T Heng, R Adnan., *Turk J Chem*, 34, 537 – 550, (2010).

A Review of Polymer and Their Blends: Classifications & Applications

P.P. Raut^{1*}, G.T. Lamdhade¹, S. D. Charpe²

^{1*}Research Scholar, Department of Physics, Vidya Bharti Mahavidyalaya, Amravati, India

¹Professor & Head of Department of Physics, Vidya Bharti Mahavidyalaya, Amravati, India

²Assistant Professor, Department of Physics, J.D. Patil Sangludkar Mahavidyalaya, Daryapur, Dist. - Amravati,

E-mail of Corresponding Authors: paranlisush29@gmail.com

Abstract:

Polymer and their blends are a very important class of materials. As these materials plays vital role in day today life so it is necessary to study. Polymer material classified according to the mechanical response and basis of electrolytes system. Variation in polymeric properties mainly depends upon there synthesis methods and deposition techniques. So, various synthesis methods and deposition techniques are mention. USP (unique selling point) of polymeric materials are there application in various sector such as Electronic devices and batteries applications, in membranes such a range of industrial applications and also polymers are essential components of many drug delivery systems and biomedical products.

Keywords: Polymer, Polymer blends, Electrolytes, Applications

1. Introduction

Polymer material plays vital role in day today life. Polymer materials and their blends has varies applications in many areas e,g electrochemical devices batteries, fuel cells, super capacitor, sensors and insulating materials [1-4]. So, it is important to study ice-break material like solid polymer and polymer electrolytes. To study the basic of the polymers and their polyblends is essential.

2. Polymer

Polymers form a very important class of materials without which the life seems very difficult. They are all around us in our everyday use e.g. in rubber, in plastic, in resins, and in adhesives and adhesives tapes. The word polymer is derived from Greek words, poly = many and mers = parts or units of high molecular mass each molecule of which consist of a very large number of single structural units joined together in a regular manner. In other words polymers are giant molecules of high molecular weight, called macromolecules, which are build up by linking together of a large number of small molecules, called monomers. The reaction by which the monomers combine to form polymer is known as polymerization [5]. The polymerization is chemical reaction in which two or more substances combine together with or without evolution of anything like water, heat or any other solvents to form a molecule of high molecular weight. The product is called polymer and the starting material is called monomer.

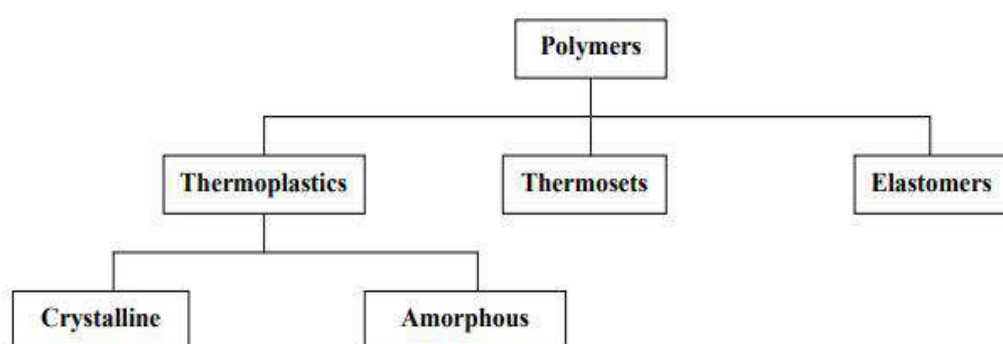
Every polymer has its own characteristics, but most polymers have the following general properties. They have low density, low coefficient of friction, good corrosion resistance, good mouldability, economical, poor tensile strength, low mechanical properties, and poor temperature resistance. It can be resistant to chemicals and also to both thermal and electrical insulators. Generally, polymers are light in weight with varying degrees of strength. Polymers can be processed in various ways to produce thin fibers or intricate parts.

Polymer electrolytes are plastic materials that can be modified and processed by conventional techniques. If the polymer chains are helped for a charge transport of the ionic type, often called "polymer electrolyte". In general, polymer electrolytes are used as separator and they are used for ionic transport. In recent years, Polymer electrolytes have attracted

scientific and technological importance because of their potential applications. The idea of preparation of polymer electrolytes was first proposed by Wright [6, 7] and Fenton *etal* in 1973 [8, 9] but their technological significances are fulfilled and appreciated by Armand *etal* [10] few years later. Poly (ethylene oxide) was the first solvating polymer to be proposed and studied in solid polymer electrolyte (SPE) Li-rechargeable batteries [11, 12]. Most of the solid polymer electrolytes (SPEs) are prepared by dissolving lithium salts in a solvating polymer in a common solvent or by diffusion in the solid (or) molten state. An effort is also made to fix or immobilize the anion on the polymer matrix by covalent bonding (or) another chemical or physical process [13]. In the present work, an attempt has been made to develop the polymer electrolytes based on PVAc.

2.1 Classification of Polymer on Basis of Mechanical Properties

Polymers may be classified as follows, according to the mechanical response at elevated temperatures [6].



Flow-chart 1. Classifications of Polymer

2.2 Classification of Polymer on Basis of Electrolytes System

The polymer electrolyte systems [14] could be classified into three categories, namely, Polyelectrolyte, Solvent swollen polymer electrolyte and Solvent free polymer electrolytes. Solvent free polymer electrolytes means that polymer –salt complexes which are formed by complexes between salts of alkali metals and polymer containing solvating heteroatoms such as O, N, S, etc. The most common examples are complexation between poly (ethylene oxide) (PEO) and alkali metal salts. The polymer salt complexes are further classified into: a) Solid polymer electrolytes b) Blend polymer electrolytes c) Gel polymer electrolytes d) Composite polymer electrolytes.

2.3 Synthesis and Deposition Methods for Polymers and Polyblends

Methods for synthesis and deposition of polymer thin films and their polyblends are: Langmuir Blodgett (LB) Technique [15], Gas phase deposition technique [16], Solvent evaporation [17], Vacuum evaporation technique [18], Isothermal evaporation technique [19-20], Spin Coating [21-22], Plasma Polymerization [23], Laser lithography [24] and etc.

3. Applications of Polymers and Their Blends

3.1 Electronic Devices and Batteries

Polymers are already playing a critical role in saving energy and resources across a variety of applications, such as transport, packaging, healthcare, and buildings [25]. Polymer scientists are conducting a great deal of research into the potential for polymers to provide cutting-edge renewable energy technologies. Such avenues are photovoltaic, fuel cell, polymer semiconductors, LED (light-emitting diode), etc. Polymer and polymer blends elucidates some important polymers thoughtful effort of elaborating various such energy application schemes in line with the energy assembly, energy storage, dye sensitized electric cell, light emitting and sensing, perovskite electric cell, thermoelectrical generator, polymer composite for

thermoelectrical generator, piezoelectric, triboelectric generator, and supercapacitor have been discussed for better understanding of the readers [26].

3.2 Polymer Blends in Membranes

It is intended to highlight here possible ways of improvement the properties of polymeric membranes, by modifying with other polymers, functional groups, compounds, drugs, bioactive components, and nanomaterials. Polymeric membranes are widely used in a range of industrial applications, such as desalination, wastewater treatment, bio-purification/separation, solvent purification/recovery, gas and liquid phase pollutant capture, and gas separations [27].

3.3 Polymer Blends in Drug Delivery

Polymers are essential components of many drug delivery systems and biomedical products [28].

4. Conclusion

Polymer and polymer blended material are an effectively synthesis and deposited. These fabricated new versatile materials have potential applications in various sectors such as drug delivery, electronic devices and batteries and etc.

References:

- [1] Davoodi, S., Al-Shargabi, M., Wood, D. A., & Rukavishnikov, V. S. (2024). Recent advances in polymers as additives for wellbore cementing applications: A review. *Fuel*, 357, 129692.
- [2] Gupta, R. K., Shaikh, H., Imran, A., Bedja, I., Ajaj, A. F., Aldwayyan, A. S., & Ayub, R. (2024). Electrical transport properties of [(1- x) succinonitrile: x poly (ethylene oxide)]-LiCF₃SO₃-Co [tris-(2, 2'-bipyridine)]₃ (TFSI)₂-Co [tris-(2, 2'-bipyridine)]₃ (TFSI)₃ solid redox mediators. *RSC advances*, 14(1), 539-547.
- [3] Baskaran, R., Selvasekarapandian, S., Kuwata, N., Kawamura, J., and Hattori, T., AC impedance, DSC and FT-IR investigations on (x) PVAc-(1- x) PVdF blends with LiClO₄, *Mater. Chem. Phys.*, 98, 55-61. (2006).
- [4] M. Armand, The history of polymer electrolytes, *Solid State Ionics*, 69, 309-319, (1994).
- [5] Lin, S., Semiao, A. C., Zhang, Y., Lu, S., & Lau, C. H. (2024). Interfacial polymerization using biobased solvents and their application as desalination and organic solvent nanofiltration membranes. *Journal of Membrane Science*, 692, 122281.
- [6] Saldívar-Guerra, E., & Vivaldo-Lima, E. (2013). Introduction to polymers and polymer types. *Handbook of polymer synthesis, characterization, and processing*, 1-14.
- [7] P.V.Wright *Brit.Polym.J.*, 7, 319, (1975).
- [8] G.S.Misra, *Introductory Polymer Chemistry*, Wiley Eastern Limited, (1993).
- [9] D.E.Fenton, J.M.Parker, P.V.Wright, *Polymer*, 14,589, (1973).
- [10] M.B.Armand, J.M.Chabagno, M.Duclot, in: P.Vashishta, J.N.Mundy, G.K.Shenoy (Eds.), *Fast Ion Transport in solids*, North Holland, Amsterdam, vol.131 (1979) pp.131.
- [11] J.P.Gabango, *Proceedings of the symposium on lithium batteries Honolulu*, 88-1, (1987), (Eds). A.N.Dey, The Electrochemical society, Pennington, NJ, (1988).
- [12] A.Hooper, J.M.North, *Solid State Ionics*, 1161, 9-10 (1983).
- [13] F.M.Gray in *polymer Electrolytes Reviews-1*, (Eds). J.R.MacCallum, C.A.Vincent, Elsevier Applied Science, London, 139-172, (1987).
- [14] Di Noto, V., Lavina, S., Giffin, G. A., Negro, E., & Scrosati, B. (2011). Polymer electrolytes: Present, past and future. *Electrochimica Acta*, 57, 4-13.

-
- [15] M. Petty, Langmuir– Blodgett Films: An Introduction, Cambridge University Press, 1996, p. 256, (1999).
- [16] A. Ulman, An Introduction to Ultrathin Organic Films From Langmuir–Blodgett to Self-assembly, Academic Press, Inc., San Diego, (1991).
- [17] Nongyi Cheng, Lushuai Zhang, Jae Joon Kimac and Trisha L. Andrew, Vapour phase organic chemistry to deposit conjugated polymer films on arbitrary substrates, Journal of Materials Chemistry C 5, 5787, (2017).
- [18] Catalina Natalia, Cheaburu-Yilmaz, Hatice Yesim Karasulu, Onur Yilmaz, Polymeric Nanomaterials in Nanotherapeutics, Micro and Nano Technologies, 437-468, (2019).
- [19] K.Sangwal, Growth from Solution, Encyclopedia of Materials: Science and Technology (Second Edition), 3671-3680, (2001).
- [20] J.Koskinen, Cathodic-Arc and Thermal-Evaporation Deposition, Comprehensive Materials Processing, 4, 3-35, (2014).
- [21] Peng Geng, Ashish Zore and Michael R. Van De Mark, Investigation of the Evaporation Rate of Water from Colloidal Unimolecular Polymer (CUP) Systems by Isothermal TGA, Polymers, 12(11), 2752, (2020)
- [22] R. G. Larson and T. J. Rehg, ed. S. F. Kitsler and P. M. Schweizer, Book: Liquid Film Coating, Chapman & Hall, 1st edition, chapter, 14, 709-734, (1997).
- [23] H.Yasuda, Y.Iriyama, Comprehensive Polymer Science and Supplements, 4, 357-375, (1989).
- [24] John Monte Hudson, Laser Lithography of Thin Polymer Films, 1-2, (2004).
- [25] Katz, H. E., Searson, P. C., & Poehler, T. O. (2010). Batteries and charge storage devices based on electronically conducting polymers. *Journal of Materials Research*, 25(8), 1561-1574.
- [26] Liang, Y., Zhao, C. Z., Yuan, H., Chen, Y., Zhang, W., Huang, J. Q., ... & Zhang, Q. (2019). A review of rechargeable batteries for portable electronic devices. *InfoMat*, 1(1), 6-32.
- [27] Marta J. Woźniak-Budych, Polymeric membranes for biomedical applications, Journal of Physical Sciences Reviews, (2021).
- [28] Nyamweya, N. N. (2021). Applications of polymer blends in drug delivery. *Future Journal of Pharmaceutical Sciences*, 7, 1-15.

Synthesis of ZnO Nanoparticles by Chemical Precipitation Method

N. B. Thakare¹, G. T. Lamdhade^{2*}, V. S. Kalyamwar³, Y S. Tamgadge⁴, D. N. Bhojar¹

¹Department of Physics, Shri Shivaji Science & Arts College, Chikhli, Dist. Buldhana, (MS), India-443201

²Department of Physics, Vidhya Bharti Mahavidyalaya, Amravati, (MS), India- 444602

³Department of Physics, Bhartiya Mahavidyalaya, Amravati, (MS), India- 444602

⁴ Department of Physics, Shri Shivaji college Motala, Dist. Buldhana (MS), India-443103

*Corresponding author email: gtlamdhade@rediffmail.com

Abstract:

ZnO nanoparticles were synthesized by a simple cost-effective chemical precipitation method technique using L-histidine as a capping agent. The X-ray diffraction pattern (XRD) has been utilized to investigate various structural parameters of ZnO nanoparticles. XRD pattern confirms purity and phase formation of ZnO nanoparticles. Particle size has been calculated using XRD data and have found to be 24 nm and 19 nm for pure and L-histidine capped ZnO nanoparticles. These nanoparticles have also been characterized by UV-visible (UV-vis) spectroscopy. The blue shift evident from the absorption spectra clearly indicate formation of ZnO nanoparticles.

Keywords: ZnO nanoparticles, X-ray diffraction, UV-visible spectra.

1. Introduction:

Zinc oxide (ZnO), a transition metal oxide material, has been recognized as a promising semiconductor material due to its direct band gap (3.37 eV) and relatively high exciton binding energy (60 meV) at room temperature [1]. With its exceptional physical and chemical properties, this versatile material has great potential for applications in electronics, optoelectronics, spin electronics and sensing devices [2-5]. Several techniques have been used to prepare ZnO nanostructures, including sol-gel, including SILAR [6] sol-gel [7], hydrothermal [8], solvothermal [9], chemical bath deposition [10], pulse laser deposition [11], spray pyrolysis [12], DC magnetron sputtering [13]. Among these synthesis routes, the precipitation approach, compared with other conventional strategies, provides a facile way for low-cost and large-scale production that does not require expensive raw materials and complicated equipment [14]. To avoid agglomeration of the nanoparticles capping agents play important role.

In the present study, we report the synthesis of ZnO nanoparticles using cost-effective and simple chemical precipitation method employing with the biocompatible amino acid L-histidine as a capping agent. Powder X-ray diffractometry (XRD) and UV-visible spectroscopy have been utilized to investigate the structural evaluation and optical properties of as-synthesized ZnO nanoparticles.

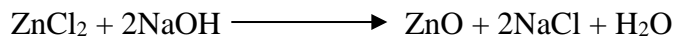
2. Experimental:

2.1 Synthesis Of ZnO Nanoparticles

All chemicals used were of analytical reagent grade and used without further purification. Zinc chloride (ZnCl₂) AR grade and Sodium Hydroxide pellets (NaOH) AR grade was purchased from Sigma Aldrich, USA while L-histidine was procured from TCI Chemicals, Japan. To begin, stock solutions of 1M ZnCl₂, 2M NaOH, and 0.1M L-histidine in double distilled water were prepared in separate beakers.

To synthesized pure ZnO nanoparticles, firstly 10 ml of 1M ZnCl₂ was dissolved in 100 ml distilled water and stirred for 30 minutes. Then, 10 ml of 2M sodium hydroxide was added, and the mixture was stirred continuously for 2h at room temperature. L-histidine-capped ZnO

nanoparticles were synthesized by taking 10 ml of 1M ZnCl₂ was dissolved in 100 ml distilled water and stirred for 30 minutes. Then 6 ml of 0.1M L-histidine was added dropwise into this solution and stirred for another 60 minutes at room temperature. Thereafter, 10 ml of 2M sodium hydroxide was added, and the mixture was stirred continuously for 2h at room temperature. The two samples were termed as S-1 and S-2. The chemical reaction can be summarized as follows:



The precipitate was then centrifuged in both cases for 20 minutes at 4000 rpm (REMI Model-8RC) and rinsed with ethanol 2-3 times. The white precipitate was subsequently dried for four hours at 80 °C in an electric oven. The solid precipitate was then finely ground in an agate mortar to get fine powder and then thermally treated at 450 °C in a muffle furnace for 4 h to remove residuals.

2.2 Characterization:

Powder XRD measurements were performed using by using Rigaku X-ray diffractometer Miniplex II with nickel filtered CuK α radiation ($\lambda=1.5406 \text{ \AA}$). For optical properties the product was characterized by UV-visible spectrophotometer (Model-Black-C-SR, Stellarnet Inc. USA) in the spectral range 300 -900 nm.

3. Result and Discussion:

3.1 XRD Studies

The X-ray-diffraction pattern of ZnO powder samples S-1 and S-2 after calcination at 450°C is shown in Fig. 1. The presence of different peaks such as (100), (002), (101), (102), (110), (103), (200), (112), (201), (004), and (202) confirm the hexagonal wurtzite structure of ZnO powder [15,16]. No other peaks related to impurities are observed, which proves the high purity of the wurtzite phase. The average crystallite size of the ZnO NPs was estimated from X-ray line broadening of the diffraction peaks using Debye-Scherrer's relation. The average particle size for samples S-1 and S-2 was obtained to be 24 nm and 19 nm, which clearly indicate that the capping agent has played a role in controlling the size and size distribution.

Different parameters unit cell volume (V) [17], Atomic Packing Fraction (APF) [18], X-ray density (d_x) [19], Bulk density (d_B) [20] and porosity [21] of ZnO nanoparticles are listed in table1.

Table 1: Different parameters of unit cell

Sample	Lattice Constant (\AA)			Volume V (\AA^3)	APF	X-ray density (d_x)	Bulk density (d_B)	Porosity %	D (nm)
	a	b	c						
S-1	3.2494	3.2494	5.2038	47.584	0.7547	11.3598	6.529	42.5214	24
S-2	3.2342	3.2342	5.1772	46.899	0.7550	11.2508	6.366	44.7652	19

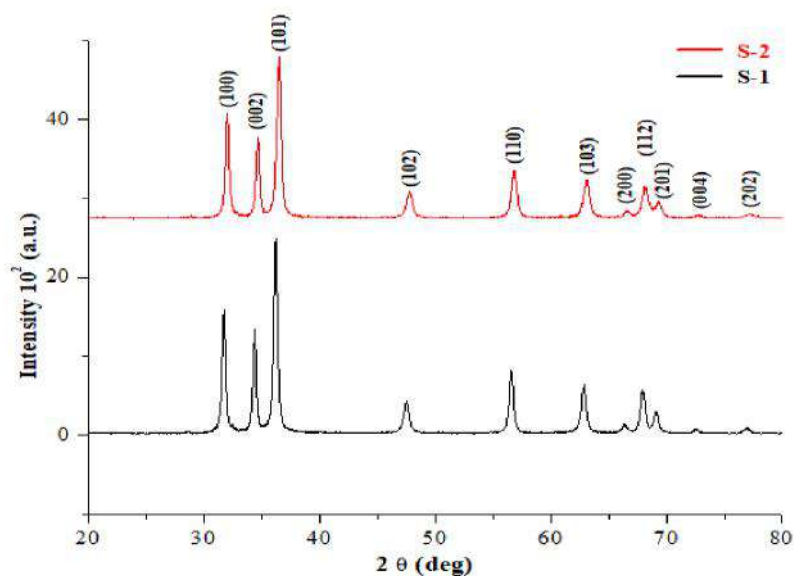


Figure 1: XRD Pattern of pure and L-histidine capped ZnO nanoparticles

3.2 UV- Visible Study:

Figure 2 depicts the UV-Vis absorption spectra of pure and L-histidine capped ZnO nanoparticles. For pure ZnO, the absorption starts at 381 nm, while for the capped ZnO nanoparticles, the absorption starts at 372 nm. There is a window of UV absorption of width 29 nm for capped sample. Compared to pure ZnO, the absorption spectrum shows a blue shift which suggests that surface modification has enabled the formation of nanoparticles of lesser size. The capping agent has played a role in controlling the size and size distribution.

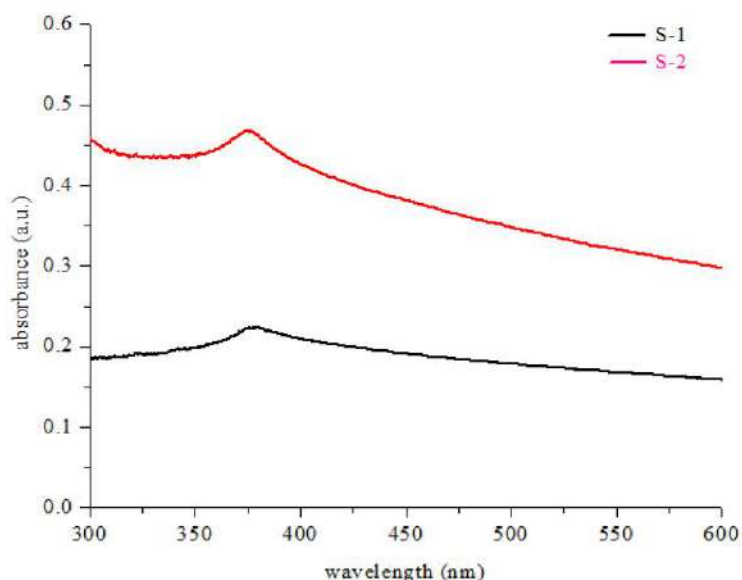


Figure 2: UV-visible spectra of different samples of ZnO

4. Conclusion:

ZnO nanoparticles were effectively synthesized by a simple chemical precipitation method. With a proper concentration of L-histidine, ZnO nanoparticles with particle sizes up to 19 nm can be obtained when calcined at 450 oC. The X-ray diffraction (XRD) pattern provides confirmation of the phase, purity, and particle size of ZnO nanoparticles. The reduction in particle size, caused by the presence of a capping agent, leads to an increase in the

porosity of the nanostructure. UV-visible spectroscopy provides evidence of a blue shift, indicating that the surface modification has facilitated the formation of smaller nanoparticles.

5. References:

- [1] K.V. Gurav, V.J. Fulari, U.M. Patil, C.D. Lokhande, Oh-Shim Joo, *Appl. Surf. Sci.*, 2010, 256, 2680–2685, <https://doi.org/10.1016/j.apsusc.2009.09.080>.
- [2] Ümit Özgür; Daniel Hofstetter; Hadis Morkoç, *Proceedings of the IEEE*, 2010, 98, 1255-268, <https://doi.org/10.1109/JPROC.2010.2044550>.
- [3] Kausar Harun, Fayaz Hussain, Agus Purwanto, Bouchta Sahraoui, Anna Zawadzka and Ahmad Azmin Mohamad, *Mater. Res. Express*, 2017, 4, 122001, <https://doi.org/10.1088/2053-1591/aa9e82>.
- [4] J. B. K. Law, J. T. L. Thong, *Appl. Phys. Lett.*, 2006, 88, 133114, <https://doi.org/10.1063/1.2190459>.
- [5] M. W. Ahn, K. S. Park, J. H. Heo, J. G. Park, D. W. Kim, K. J. Choi, J.-H. Lee, S.-H. Hong, *Appl. Phys. Lett.*, 2008, 93, 263103, <https://doi.org/10.1063/1.3046726>.
- [6] Vithoba L. Patil, Sharadrao A. Vanalakar, Pramod S. Patil, Jin H. Kim, *Sens. Actuators B Chem.*, 2017, 239, 1185-1193, <https://doi.org/10.1016/j.snb.2016.08.130>.
- [7] Ameer Azam, Faheem Ahmed, Nishat Arshi, M. Chaman, A.H. Naqvi, *J. Alloys Compd.*, 2010, 496, 399-402, <https://doi.org/10.1016/j.jallcom.2010.02.028>.
- [8] Sunandan Baruah and Joydeep Dutta, *Sci. Technol. Adv. Mater.*, 2009, 10, 013001, <https://doi.org/10.1088/1468-6996/10/1/013001>.
- [9] Sirachaya Kunjara Na Ayudhya, Parawee Tonto, Okorn Mekasuwandumrong, Varong Pavarajarn, and Piyasan Prasertdam, *Crystal Growth & Design*, 2006, 6(11), 2446–2450, <https://doi.org/10.1021/cg050345z>.
- [10] Huihu Wang, Shijie Dong, Ying Chang, Xiaoping Zhou, Xinbin Hu, *Appl. Surf. Sci.*, 2012, 258, 4288-4293, <https://doi.org/10.1016/j.apsusc.2011.12.080>.
- [11] T. Ohshima a, R.K. Thareja b, T. Ikegami a, K. Ebihara, *Surf. Coat. Technol.*, 2003, 169–170, 517-520 [https://doi.org/10.1016/S0257-8972\(03\)00164-6](https://doi.org/10.1016/S0257-8972(03)00164-6).
- [12] Sang Duck Lee, Sang-Hun Nam, Myoung-Hwa Kim, Jin-Hyo Boo, *Phys. Procedia*, 2012, 32, 320-326 <https://doi.org/10.1016/j.phpro.2012.03.563>
- [13] Jian-Wei Hoon, Kah-Yoong Chan, Jegenathan Krishnasamy, Teck-Yong Tou, Dietmar Knipp, *Appl. Surf. Sci.*, 2011, 257, 2508-2515, <https://doi.org/10.1016/j.apsusc.2010.10.012>.
- [14] Rania E. Adam a, Gallia Pozina b, Magnus Willander a, Omer Nur, *Photonics Nanostructures - Fundam. Appl.*, 2018, 32, 11-18, <https://doi.org/10.1016/j.photonics.2018.08.005>.
- [15] J. Zhou, F. Zhao, Y. Wang, Y. Zhang, L. Yang, *J. Lumin.*, 2007, 122–123 195–197, <https://doi.org/10.1016/j.jlumin.2006.01.089>.
- [16] Z.M. Khoshhesab, M. Sarfaraz, M.A. Asadabad, *Synth. React. Inorg., Met.-Org., Nano-Met. Chem.* 2011,41, 814–819, <https://doi.org/10.1080/15533174.2011.591308>.
- [17] G. Vijayaprasath, R. Murugan, T. Mahalingam, G. Ravi, *J Mater Sci Mater Electron*, 26 (2015) 7205-7213, <https://doi.org/10.1007/s10854-015-3346-z>
- [18] S.D. Birajdar, V. Bhagwat, A. Shinde, K. Jadhav, *Mater Sci Semicond Process*, 2016, 41, 441-449, <https://doi.org/10.1016/j.mssp.2015.10.002>.
- [19] V. Mote, Y. Purushotham, B. Dole, *Cryst. Res. Technol.*, 2011, 46, 705-710, <https://doi.org/10.1002/crat.201100107>
- [20] Shinde, T.J., Gadkari, A.B., Vasambekar, P.M.: *J. Mater. Sci. Mater. Electron.*, 2010, 21, 120-124, <https://doi.org/10.1007/s10854-009-9878-3>.
- [21] Lakhani, V.K., Pathak, T.K., Vasoya, N.H., Modi, K.B.: *Solid State Sci.*, 2011, 539, 201113, <https://doi.org/10.1016/j.solidstatesciences.2010.12.023>.

Fabrication and Application of SnO₂ doped ZnO to sense CO₂ Gas

Rita S. Bhuyar¹, G. T. Lamdhade², K. B. Raulkar²

*1 Department of Physics, Shri Shivaji College of Arts, Comm. & Science, Akola, MS, India

2 Department of Physics, Vidyabharati Mahavidyalaya, Camp, Amravati, MS, India

Corresponding: ritabhuyar1984@gmail.com

ABSTRACT

In the present work, ZnO is doped in SnO₂ with the percentage 2%, 4%, 6% & 8% and prepared sensors are labeled as T1, T2, T3, T4, T5 & T6. Chemicals used are first calcinated at 700⁰C for 6 hours then mixed the given proportion and screened out on the plane glass plate using screen printing technique. Prepared materials are characterized by XRD and SEM. The X-ray diffraction (XRD) pattern indicates a small crystalline size for the T4 material, which consists of 94% SnO₂ and 6% ZnO. The SEM study reveals increased porosity in the T4 sensor. The resistance of the T4 sensor, with a polypyrrole (PPy) layer on top, decreases at room temperature with an increase in CO₂ gas concentration. This leads to higher sensitivity due to the presence of surface oxygen vacancies in ZnO and SnO₂, which act as donors. The sensor with a PPy rooftop layer on 94% SnO₂: 6% ZnO doping exhibited the highest sensitivity 1.638 at 1200 ppm among all the prepared sensors.

Keywords: Tin dioxide, Zinc Oxide, screen printing technique, Multilayer sensor, CO₂ gas

1. Introduction:

In the rapidly evolving field of electronics, sensors play a crucial role in controlling, monitoring, and analyzing various processes. Chemical sensors, known for their high performance, are particularly noteworthy in this regard. Their advancements have become integral in both daily life and industrial applications, with expectations of further progress in the future. Metal oxide sensors, especially those based on SnO₂, are popular for gas detection due to their stability and selectivity. This work focuses on the sensing process of SnO₂-based sensors and explores techniques such as doping, dynamic responsiveness, and sensor array improvements to enhance their gas detection capabilities. The integration of composite sensors is anticipated to significantly improve the detection of hazardous gases. Polypyrrole (PPy) stands out as an intelligent material with applications in optical, electrical, and electro-chromic devices, as well as sensors. In recent years, PPy has gained prominence in detecting volatile organic compounds (VOCs) due to its selectivity and sensitivity to target gas molecules. The study aims to develop PPy-based sensors with reliable mechanical and electrochemical performance for improved sensing devices. Given the presence of harmful chemicals in the air, gas sensors have garnered attention in both academic and industrial settings. The study underscores the health risks associated with poisonous gases and emphasizes the need for effective gas sensors to detect such hazards. Various metal oxides, including SnO₂, TiO₂, ZnO, In₂O₃, and WO₃, offer stability benefits. While SnO₂ is crucial in semiconductor sensors, it has limitations in detecting low-concentration biogas and odors for gas alarms. The study delves into the preparation conditions, dopants, and grain sizes of SnO₂-based materials, as these factors significantly influence their chemical and physical qualities, impacting their sensing capabilities. The primary objective is to construct a multi-layer CO₂ gas sensor utilizing a combination of polypyrrole and SnO₂-doped ZnO [1-3]. While SnO₂-based chemiresistors

exhibit faster gas sensing responses than conducting polymer-based counterparts, they require higher operating temperatures ($>200\text{ }^{\circ}\text{C}$).

2. Materials and Method

2.1 Synthesis of SnO_2 Nanoparticles

To conduct the described experiment, high-purity GR grade chemicals (99.99%) were procured from Sd-fine in India. Stannous dioxide (SnO_2) was synthesized by dissolving 2 grams (0.1 millimeters) of stannous chloride dehydrate ($\text{SnCl}_2 \cdot 2\text{H}_2\text{O}$) in 100 milliliters of water. Following complete dissolution of the aqueous solution, 4 cubic centimeters of ammonia solution were added with magnetic stirring. A twenty-five-minute stirring period initiated the formation of a white gel precipitate. Subsequently, the mixture was left undisturbed for ten to fourteen hours before further examination. Afterward, the precipitate underwent cleansing with deionized water, passing through four or five filters as part of the previous process. The resulting precipitate was combined with 0.27 grams of charcoal-activated carbon black powder. Following a day of grinding into powder in a vacuum oven at 80 degrees Celsius, the mixture was removed. The dry material was then broken into smaller pieces and milled into a powder. To eliminate impurities, the ultrafine SnO_2 nano powder underwent calcination in an auto-controlled muffle furnace at 700 degrees Celsius for duration of seven hours [4-5].

2.2 Synthesis of Polypyrrole

Chemical polymerization was employed to prepare powder polypyrrole, utilizing a high weight ratio of 4.290 for the pyrrole (Py) monomer and the oxidant (FeCl_3). The synthesis maintained a constant concentration of FeCl_3 , with methanol serving as the solvent. The synthesis involved the use of Py monomer, anhydrous iron (III) chloride (FeCl_3), and methanol. In a round-bottom flask, a solution of 7 ml methanol and 1.892 g FeCl_3 was prepared, and then 8.4 ml Py monomer was added to the (FeCl_3 + methanol) solution with continuous stirring in the absence of light. The addition of Py monomer to achieve maximum yield was carefully controlled. The polymerization of Py, initially suppressed in the solution, progressed rapidly due to an increase in oxidation potential resulting from solvent evaporation. During the polymerization reaction, the solution's color changed to dark green/black immediately upon the addition of Py monomer. The reaction was exothermic, evidenced by a rise in solution temperature at the reaction's onset. The reaction was conducted at room temperature for duration of 4 hours. The final precipitated polymer was filtered using conventional methods, and the polymer underwent multiple washes with distilled water until the filtrate became colorless. To eliminate any remaining traces of unreacted pyrrole and residual ferric and ferrous chloride formed during polymerization, the polymer was washed with methanol. The resulting polypyrrole, obtained in powder form, was first dried at room temperature for a few hours and then further dried in an oven at 80°C for 5-6 hours. This synthesized polypyrrole was subsequently utilized for the active layers of Semiconductor Gas Sensors [6-9].

2.3 Synthesis of Zinc Oxide

In this study utilized chemicals of GR grade obtained from Sd-Fine, India, with a purity of 99.99%. These chemicals were used as-is without any additional purification. The key reagents included Zinc Acetate Dihydrate ($\text{Zn}(\text{O}_2\text{CCH}_3)_2 \cdot (\text{H}_2\text{O})_2$), sodium hydroxide (NaOH), methanol, and deionized water. To prepare the ZnO, 0.2 M Zinc Acetate Dihydrate was dissolved in 100 ml of deionized water and ground for 15 minutes. Subsequently, this solution was mixed with a 0.02 M NaOH solution using a glass rod. The resulting mixture underwent constant magnetic stirring for 15 minutes and was then ground for an additional 30 minutes. A white precipitate formed at the bottom. Excess liquid was discarded, and the product was thoroughly washed with deionized water and methanol to eliminate by-products. The final product, a white paste, was filtered using Whatman filter paper. This paste was then placed in

a vacuum oven at 80°C for 4 hours to remove moisture and obtain a dry product. The dry product was further crushed into a fine powder using a grinding machine. Finally, this fine ZnO nano-powder was subjected to calcination at 800°C for 6 hours in an auto-controlled muffle furnace (Gayatri Scientific, Mumbai, India). This step aimed to eliminate impurities and yield the final product of ZnO nanoparticles [10-12].

2.4 Preparations of thick films

The collected samples were employed for screen printing to generate thick films. Initially, finely sintered powders of pure and doped nano-powders of SnO₂ and ZnO, in various weight ratios, were mixed with ethyl cellulose as a temporary binder to create a thixotropic paste suitable for screen printing. This paste was applied to screens, and to achieve the desired consistency, it was combined with organic solvents like terpineol, butyl cellulose, and butyl carbitol acetate. The paste formulation comprised 75 percent inorganic chemicals and 25 percent organic ingredients. Screen printing was utilized to deposit thick layers of both pure and doped SnO₂ and ZnO materials, derived from the paste, onto a clean glass substrate. The printing process was conducted on an Al₂O₃ base, as illustrated in Figure 1.

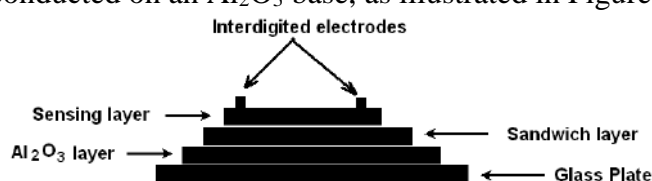


Fig. 1. The structure of SnO₂/ZnO multilayer sensor.

The produced films underwent baking for one hour at temperatures ranging from 90 to 100°C to ensure the complete evaporation of all organic materials, including binders, and eliminate any organic contaminants. Electrodes were constructed to measure surface conductivity on both sides of the thick film. Subsequently, silver paint was applied to the electrodes, and the film was dried by heating at 70°C for 0.5 hours. The table below presents the samples in sequential order.

Table 1: Sample code

Sr.No.	Sample doping	Sample code
1.	Pure SnO ₂	T1
2.	98SnO ₂ : 2 ZnO/Al ₂ O ₃ /GP	T2
3.	96 SnO ₂ : 4 ZnO/Al ₂ O ₃ /GP	T3
4.	94 SnO ₂ : 6 ZnO/Al ₂ O ₃ /GP	T4
5.	92 SnO ₂ : 8 ZnO/Al ₂ O ₃ /GP	T5
6.	Pure ZnO	T6

3. Result & Discussion

3.1 X-ray Diffraction Study

The X-ray diffraction pattern of Polypyrrole (PPy) is illustrated in Figure 2, revealing its amorphous nature. The XRD analysis demonstrated a wide peak at 26°, indicative of PPy's amorphous structure. This broad peak is attributed to the scattering of X-rays by polymer chains within the inter-planar gaps. The intensity and location of this amorphous peak were influenced by the monomer-to-oxidant ratio.

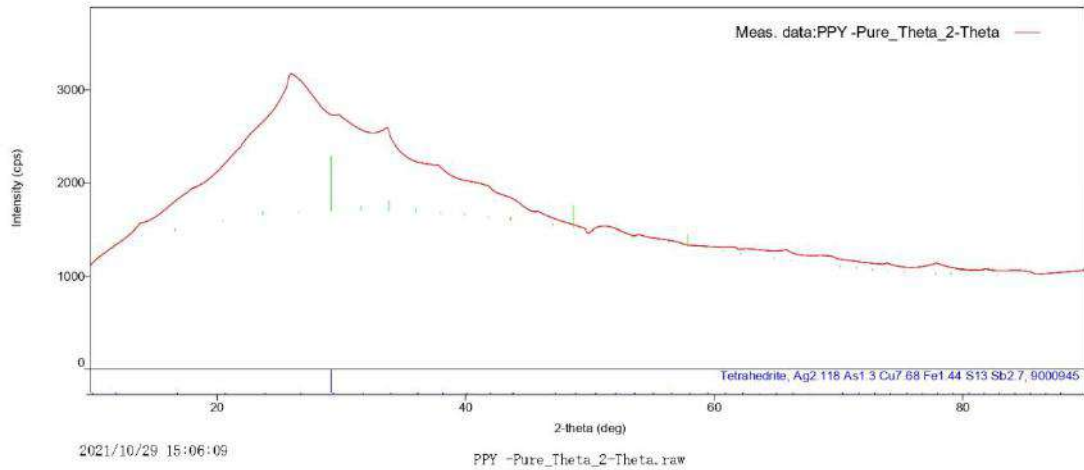
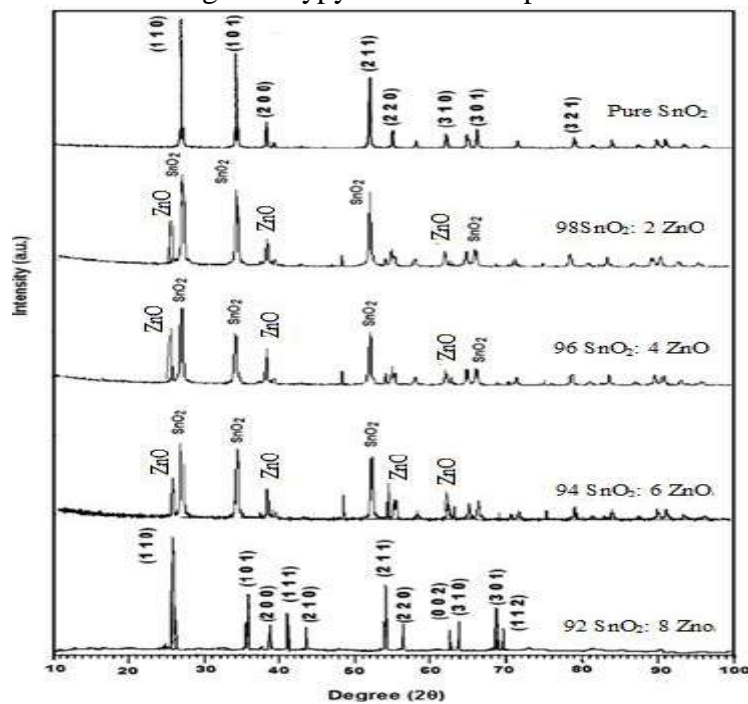


Fig.2. Polypyrrole's XRD spectra

Fig. 3. XRD pattern of SnO₂-ZnO System

It was observed from XRD that the average crystallite size of the 94SnO₂:06ZnO doping composition is the smallest compared to other compositions and pure materials. Consequently, this doping combination exhibits a larger active surface area, making it more effective for gas sensing applications.

3.2 SEM (Scanning Electron Microscope) Study

The SEM images (Fig. 4-6) exhibited variations in pore density across different regions, and an average pore count per square inch was calculated for comparison. The porosity was determined for an area of one square inch in each image. The prepared pure samples showed higher porosity compared to other compositions. Increased porosity contributes to enhanced gas absorption or sensing capabilities.

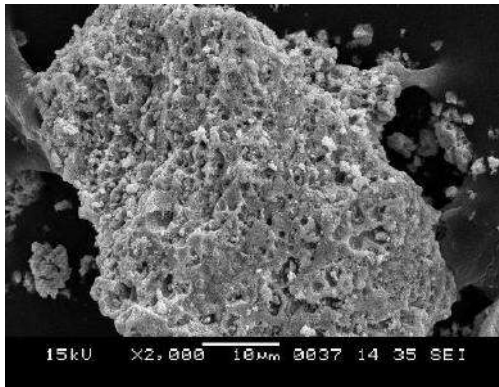


Fig. 4. SEM picture of SnO₂

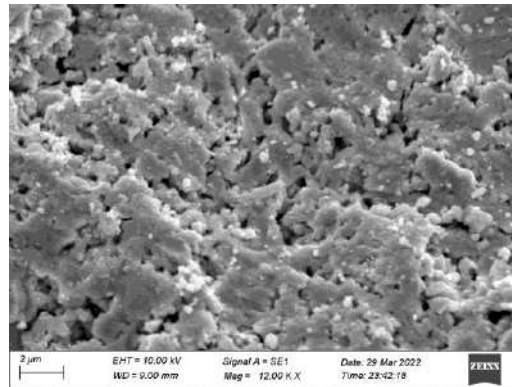


Fig. 5. SEM picture of ZnO

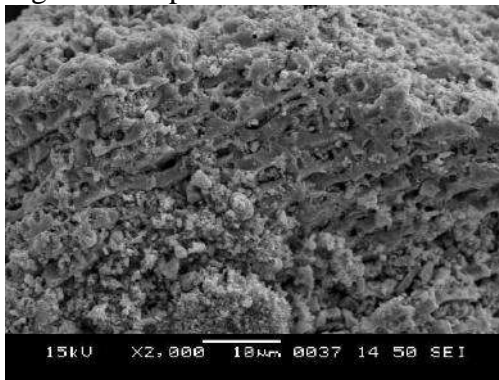
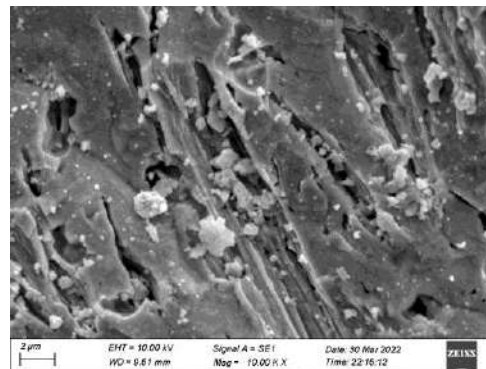


Fig. 6. SEM picture of 94 SnO₂:6ZnO/Al₂O₃/GP (sensor T4)



From SEM study, it is manifested that porosity of T4 sensor is more porous as compared to other prepared sensor. Therefore T4 sensor has more active surface area for CO₂ gas absorption.

3.3 Resistivity measurement

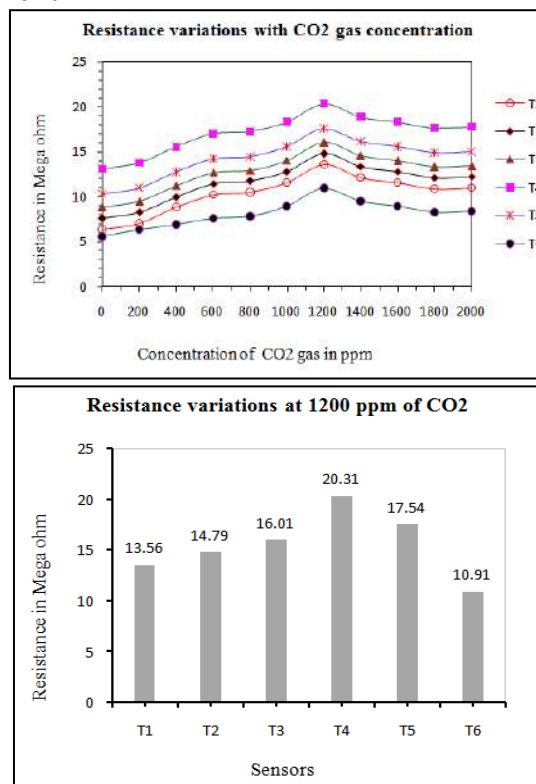


Fig.:7 variation of resistance with CO₂ gas concentration

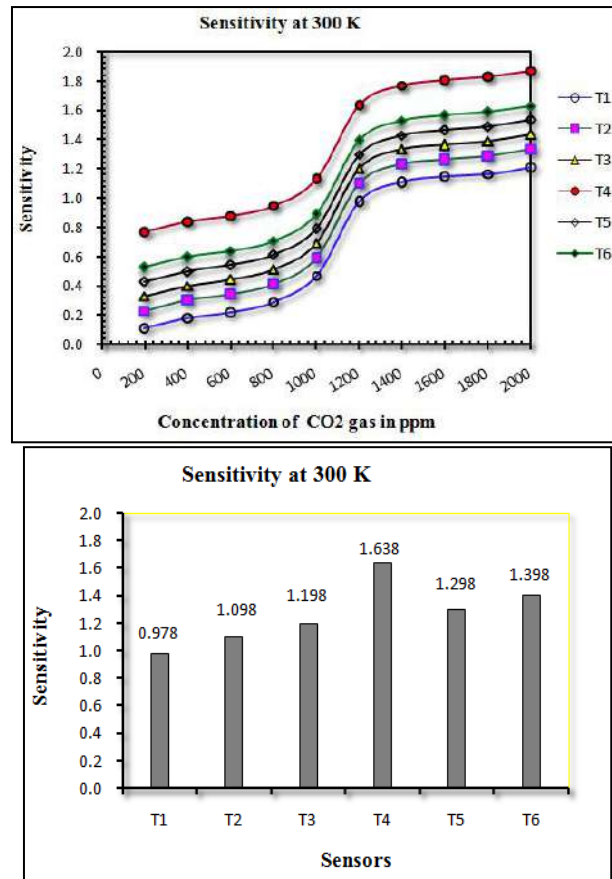


Fig.:8 variation of Sensitivity with CO₂ gas concentration

As shown in Fig. 7, resistance increases with increase in concentration of CO₂, becomes maximum resistance for T4 sensor, 20.31 MΩ and resistance decreases with further increase in concentration of CO₂ at room temperature (300 K). From Fig. 8, sensitivity first increases by little amount and suddenly increase at 1200 ppm CO₂ gas concentration then remain nearly constant. T4 sensor showed maximum sensitivity to be 1.638 at 300 K and at 1200 ppm [13-14].

4 Conclusion

XRD showed small crystalline size for T4 sensor, SEM exhibited T4 sensor is more porous as compared to other prepared sensor. Therefore T4 sensor has more active surface area for CO₂ gas absorption. Maximum resistance for T4 sensor was recorded to be 20.31 MΩ at 1200 ppm concentration of CO₂ gas at room temperature (300 K). Sensitivity of T4 sensor recorded to be maximum 1.638 at 300 K and at 1200 ppm. Thus T4 sensor is best to sense CO₂ gas.

5. Acknowledgement:

Author of this research paper expressed sincere thanks to Professor and Head, Department of Physics, Vidyabharati Mahavidyalaya, Amravati, India, for constant support to carry out this research work and also thanks to Karmavir Bhauraopatil College of Engg. Washi, Mumbai for SEM analysis.

References

1. Rakhymzhan Zhumadilo¹ et al (2024) Carbon nanowall-based gas sensors for carbon dioxide gas detection, *Nanotechnology*, Accepted Manuscript online 3 January 2024 IOP Publishing Ltd, DOI 10.1088/1361-6528/ad1a7e
2. Fraden J., (1997). Handbook of Modern Sensors: Physics, designs and applications. AIP Press, American Journal of Physics, 66, 4, 357.
3. Barsan N., Kozicj D., and Weimar U., (2007). Metal Oxide Based Gas Sensors Research: Sensors and Actuators B- Chemical, 121 , 18-35.
4. Mitra P., and Mukhopadhyay A. K., (2007). Bulletin of Polish Academy of Sciences and Technical Sciences, 55(3).
5. Gopel W., Hesse J. and Zemel J. N., (1989). Fundamentals and General Aspects. Sensor: A Comprehensive Survey, 1, 117-118.
6. Gopel W., Hesse J. and Zemel J. N., (1990). Thermal sensors. sensor : A comprehensive survey, 4, 117-118.
7. Mude, B.M., Mude, K.M., Raulkar, K.B, Zade, R.N.,Yenorkar, S.M. and Yawale, S.P, (2017). Study of CO₂ gas detection by multilayer SnO₂-ZnO-PPy sensor, Int. Res. J. of Science & Engineering, Special Issue A1 :143-148
8. Waghuley, S.A., Yenorkar, S.M., Yawale, S.S., &Yawale, S.P. (2008). Application of chemically synthesized conducting polymer-polypyrrole as a carbon dioxide gas sensor. Sensors and Actuators B: Chemical, 128(2), 366-373.
9. Moseley, P. T. (1997). Solid state gas sensors. Measurement Science and technology, 8(3), 223.
10. Yawale, S. P., Yawale, S. S., &Lamdhade, G. T. (2007). Tin oxide and zinc oxide based doped humidity sensors. Sensors and Actuators A: Physical, 135(2), 388-393.
11. Ly A., Luo Y., Cavailles G., Olivier M.G., Debliquy M. and Lahem D., (2020). Ammonia Sensor Based on Vapor Phase Polymerized Polypyrrole, Chemosensors, 8, 30.
12. Tai H., Wang S., Duan Z. and Jiang Y., (2020). Evolution of breath analysis based on humidity and gas sensors: Potential and challenges, Sens. Actuators B Chem., 318, 128104.
13. Nakhleh, M.K., Amal H., Jeries R., Broza Y.Y., Aboud M., Gharra A., Ivgi H., Khatib S., Badarneh S. and Har-Shai, L., (2017). Diagnosis and Classification of 17 Diseases from 1404 Subjects via Pattern Analysis of Exhaled Molecules, ACS Nano, 11, 112–125.
14. Hamouma O., Kaur N., Oukil D., Mahajan A. and Chehimi, M. M., (2019), Paper strips coatedwith polypyrrole-wrapped carbon nanotube composites for chemi-resistive gas sensing, Synth. Met., 258, 116223.

Review on Nanocrystalline perovskite (ABO₃): A potential material for solid state gassensor

Manisha S. Pande^{a*}, V. D. Kapse^b, S.V.Agnihotri^c, T.R.Tatte^d

^{a*} Department of Physics, Shri Sant Gajanan Maharaj College Of Engineering, Shegaon-444203, India.
manisha031082@gmail.com

^b Department of Physics, Arts, Science and Commerce College, Chikhaldara-444807, India.
vdk.nano@gmail.com

^c Department of Physics, Amolakchand Mahavidyalaya, Yavatmal-445001, India.
drsva205@gmail.com

^d Department of Physics, Shri Dr. R. G. Rathod Arts & Science College, Murtizapur-444107, India.
truptitatte21@gmail.com

ABSTRACT

This paper concentrates on nanocrystalline powders of ABO₃ structure were synthesized by the various. Solid state gas sensor is a very effective sensor compared to other sensors because it can detect different harmful gases and it can be used in variety of applications. Given the intense market rivalry, it would be ideal for gas sensors to become more dependable and of higher quality. High sensitivity, high precision, and cost-effective compatible gas sensors have garnered a lot of interest. Research on sensing materials has been broadly targeted in order to provide good gas sensing. This paper review on solid state gas sensor. The creation of effective and efficient gas sensors is the result of advancements innanotechnology and the use of various materials.

Keywords: Nanomaterials, gas sensors, perovskite, etc.

1. Introduction

In day today modern life detection of different gases play a vital role. The significant area of research towards gas sensing that leads to the fabrication of gas sensing devices which detect various harmful gases. Human body suffers from different diseases due to the emission of various toxic and hazardous gases. Solid-state sensors are among the most versatile of all sensors, as they detect a wide variety of gases, and can be used in many different applications. Among the unique attributes of the solid-state sensor are the abilities of the sensor to detect both low ppm levels of gases, as well as high combustible levels. Solid state gas sensors, are the excellent candidates to the fabrication of commercial gas sensors for a wide range of applications [1-5]. The development of high precision gas sensors is crucial for the monitoring of harmful (exhaust) gases in the environment. A variety of dangerous gases, such as CH₄, NO₂, LPG, NH₃, SO₂, CO, H₂S, NO₂, Acetone, H₂, ethanol, and methanol, are constantly released by industry, transportation, and agricultural activities. Many of these gases are hazardous to human health as well as the environment, even at levels measured in parts per million, or ppm. Some of these gases, like H₂, are naturally explosive when exposed to air.

In recent years, nanomaterials based on perovskite have been used in a variety of sustainable applications. Their structural properties enable researchers to investigate functionalities in a variety of directions, including solar cells, LEM devices, transistors and sensors, etc. Perovskite nano-materials have been shown to have remarkable sensing performance to a wide range of chemical and biological species, both in solids and solutions. In particular, they are able to detect small molecules (e.g., oxygen, nitrogen dioxide, carbon dioxide, etc.). In addition, Solid-state gas sensors are emerging as a viable substitute for the intended real-

time functions in light of recent developments in the materials sciences and advancements in processing and downsizing techniques. The greatest options for the development of commercial gas sensors for a broad range of such applications are solid state gas sensors, which are based on a variety of concepts and materials. [6-10].

2. Structure, Stability and Properties of Perovskites

Perovskite is the name given to the compounds that have the formula type ABX_3 with different sized 'A' and 'B' cations bonded to anion X [11]. ABO_3 Perovskites exhibit good thermal stability with an eV band gap of 3–4, which is why they were used in a lot of gas sensing studies [12]. Perovskite materials can be employed as sensors for gaseous species because their stability was significantly disrupted when exposed to gaseous environments, such as NO_2 , CH_4 , NH_3 , C_2H_5OH , acetone, etc. [13]. The chemiresistive I–V, phosphorescence, and fluorescence responses of these perovskite materials can be used to record the sudden changes in them. However, in these sensing investigations, the opto- electronic characteristics of perovskites are crucial. Renowned contenders with remarkable attributes including electrical conductivity, ferroelectricity, superconductivity, catalytic activity, etc. are perovskite oxides. There are several ways to synthesis the nanocrystalline perovskite material, including the hydrothermal, sol-gel, and chemical co-precipitation processes, etc. Because of the remarkable stability of the perovskite structure, structural flaws can be created when one or both of the cations in the A and B sites are partially substituted with other metals that have a different oxidation state.

3. Review of solid state gas sensor

Soil, water, and air pollution are the three categories into which environmental contamination falls. Of these three categories, air and water pollution are the main contributors to disasters since they spread quickly over a wide area in a short amount of time. Since industrial progress has dramatically expanded environmental pollution to such a level that public concern is now so great that it cannot be ignored any longer, environmental monitoring and management are absolutely necessary. Therefore, in order to address these environmental issues, thorough study has been done to quickly identify these contaminants and lower their levels to within the regulatory allowed concentrations. These factors have contributed to the advancement of solid-state gas sensor research and development in recent years. Gas sensors with metal oxides as the sensing medium have been widely used in gas detection applications. In fact, there is growing interest in gas sensing for nanocrystalline semiconducting metal oxides with regulated compositions, which also represent an intriguing new area of fundamental research [14]. Because of its oxide stability, high response, low production cost, and ability to respond to a wide spectrum of chemicals, semiconductor metal oxide nanostructures are the most preferred of all the solid state gas sensing materials. They respond quickly, are robust, dependable, and reasonably priced. Different types of solid state gas sensors are semiconductor gas sensor, optical gas sensor, electrochemical gas sensor, etc. Semiconductor gas sensors (SGS), known sometimes as chemoresistive gas sensors, are typically based on metal oxides (e.g. SnO_2 , TiO_2 , In_2O_3 , WO_3 , NiO , etc.). Recent applied research and product releases in this sector of gas sensors have revealed some noteworthy developments regarding the use of nanotechnologies and gas-sensing layers. In the sensing industry, optical gas sensors are crucial for measuring chemical and biological quantities. Changes in the absorption spectrum were used to measure the first optical chemical sensors. Chemical sensors and biosensors currently employ a wide range of optical techniques, such as ellipsometry, surface plasmon resonance (SPR), spectroscopy (luminescence, phosphorescence, fluorescence, Raman), interferometry (white light, modal, and optical waveguide structures), spectroscopy of guided modes in optical waveguide structures (grating coupler, resonant mirror), and interferometry (white light,

phosphorescence, and fluorescence). Electrochemical gas sensors use an electrochemical cell, which is made up of two terminals (an anode and a cathode) of the same composition and a casing that holds a collection of chemical reactants (electrolytes or gels) in contact with the environment. A membrane on the top of the gas sensor enclosure allows the gas sample to pass through it. At the anode, oxidation happens, and at the cathode, reduction happens.

4. Conclusion

In this review study, the materials chosen for the construction of such gas sensors, and the sources of emission and regulatory standards of air pollutants are briefly reviewed. It has been addressed how advances in material science have led to the development of potential solid-state gas sensors, with the aim of comprehending the underlying technology and offering targeted functionality for a particular application.

References

- [1] P. T. Moseley, B. C. Tofield (eds.), *Solid State Gas Sensors*, Adam Hilger, Bristol and Philadelphia (1987).
- [2] M. J. Madou, S. R. Morrison (eds.), *Chemical Sensing with Solid State Devices*, Academic Press, New York, 1989.
- [3] A. Mandelis, C. Christofides (eds.), *Physics, Chemistry and Technology of Solid State Gas Sensor Devices*, Wiley (1993).
- [4] P. T. Moseley, *Meas. Sci. Technol.* 8, 223 (1997).
- [5] I. Lundström, *Sensors and Actuators B* 35-36, 11 (1996).
- [6] P. T. Moseley, B. C. Tofield (eds.), *Solid State Gas Sensors*, Adam Hilger, Bristol and Philadelphia (1987).
- [7] M. J. Madou, S. R. Morrison (eds.), *Chemical Sensing with Solid State Devices*, Academic Press, New York, 1989.
- [8] A. Mandelis, C. Christofides (eds.), *Physics, Chemistry and Technology of Solid State Gas Sensor Devices*, Wiley (1993).
- [9] P. T. Moseley, *Meas. Sci. Technol.* 8, 223 (1997).
- [10] I. Lundström, *Sensors and Actuators B* 35-36, 11 (1996)
11. T.M., Fthenakis, V.M., Eds.; Academic Press: Cambridge, MA, USA, 2018; pp. 233–254.
12. Varignon, J.; Bibes, M.; Zunger, A. Origin of band gaps in 3d perovskite oxides. *Nat. Commun.* 2019, 10, 1658.
13. Zhu, Z.; Sun, Q.; Zhang, Z.; Dai, J.; Xing, G.; Li, S.; Huang, X.; Huang, W. Metal halide perovskites: Stability and sensing-ability. *J. Mater. Chem. C* **2018**, 6, 10121–10137.
14. N. Barsan, M. Schweizer-Berberich, W. Göpel, *Fresenius J. Anal. Chem.* 365, 287(1999).

Electrical and Dielectric Properties of EC-PMMA Polymers and their Blends

Kajal Sirtawar¹

Department of Physics, Vidya Bharti Mahavidyalaya Camp, Amravati 444 602, India

Email: kajalsirtawar.ks@gmail.com

Abstract

Electrical and dielectrical properties of EC, PMMA and their polyblends doped with THF, have been investigated as a function of temperature, electric field and frequency, to study the mechanism of electrical conduction. The most important of the cellulose ethers is ethyl cellulose (EC). Its electrical, mechanical and weathering properties are good in comparison with other cellulose. Poly Methyl Methacrylate (PMMA) is a hard, rigid, transparent thermoplastic, which has good outdoor weatherability and is more impact resistant than glass. Poly Methyl Methacrylate (PMMA) is weakly polar. Polymers like Ethyl Cellulose (EC) and Poly Methyl Methacrylate (PMMA) being essentially insulating materials, the number of free charge carriers is very small and their mobility is very low. In present study the current was measured by applying the frequency in the range 1 KHz -1 MHz at various constant temperatures (323-373 K). Dielectric constant increases with increase of temperature. AC electrical conductivity of Ethyl Cellulose (EC), Poly Methyl Methacrylate (PMMA) and their blend (EC/PMMA) is increasing with increasing frequency of applied electric field. Dielectric constant increases with increase of temperature.

Keywords Tetrahydrofuron; ethyl cellulose; poly methyl methacrylate

1. Introduction

The physical mixing or blending of two polymers produces an alloy with quite different properties, which can be potentially useful [1]. The a.c. and d.c. electrical conductivity studies are aimed at understanding the origin of the charge carrying species, their numbers and the way in which they move through the bulk of the material. These parameters are related to the chemical composition, microstructure and morphology of the material [2]. The most important of the cellulose ethers is ethyl cellulose (EC). Its electrical, mechanical and weathering properties are good in comparison with other cellulosic's, but not generally outstanding. Poly methyl methacrylate (PMMA) is a hard, rigid, transparent thermoplastic, which has good outdoor weatherability and is more impact resistant than glass. PMMA is weakly polar [3]. The electrical conduction in iodine doped polystyrene (PS) and poly methyl methacrylate (PMMA) has already been reported by Chakraborty et al [4]. Keller et al reported the thermally stimulated discharge current (TSDC) study of poly blends of PS and PMMA [5]. Deshmukh et al [6] reported electrical conduction in semiconducting PVC– PMMA thin film. The electrical conductivity of polyaniline doped polyvinylchloride (PVC) and poly methyl methacrylate (PMMA) thin films has been measured by studying the I–V characteristics at various temperatures in the range 323–363 K by DESHMUKH et al [7]. In the present investigation, the a.c. conductivity of EC, PMMA and their blend was measured to identify the mechanism of electrical conduction. The dielectric constants have been measured for different temperatures. A good number of reports [8, 9, 10] on the theory of electrical conduction and experimental findings have appeared in a number of such blends. Polymers like EC and PMMA being essentially insulating materials, the number of free charge carriers is very small and their mobility is very low.

2. Experimental

In the present work, Isothermal Evaporation Technique has been used, as it is best suited to the laboratory. Polymers of Ethyl Cellulose (EC) and Poly Methyl Methacrylate (PMMA) were obtained from S.d. Fine Chem Ltd, Mumbai, India. The different quantities of given substances have been used for preparing film of thickness. The two polymers PMMA or Ethyl Cellulose (EC) were pure were taken in 1:1 ratio were dissolved in the common solvent THF (10 ml). And their blends were taken in 1:3 ratio dissolved in the common solvent THF (15 ml). The solution was kept for 3-4 days to allow polymers to dissolve completely to yield uniform solution. A glass (15 cm X 15 cm) thoroughly cleaned with water and later with was used as a substrate. To achieve perfect levelling (and uniformity in thickness of the film), a pool of mercury was used in a plastic tray. It was, thereafter, allowed to evaporate in air at room temperature. Further, it was dried for 48 h to remove any traces of solvent. The dry film was removed from the plate and cut into pieces (samples) of desired size. The films of other samples were prepared by the same method.

2.1 AC Conductivity Measurement

The film sample was loaded into the sample holder in oven. The a. c. frequencies were applied (in the range 1KHz-1MHz) across the sample by using the 4284 A precision LCR meter (20Hz-1MHz) supplied by Agilent Technologies, Singapore. The corresponding dielectric constants were measured by using LCR meter. From the dielectric data, the a. c. conductivity of the samples was calculated by using relation,

$$\sigma_{ac} = f \epsilon' \tan\delta / 1.8 \times 10^{10}$$

Supplied by Mitutoyo Corporation Japan, was for the measurement of thickness of sample thin film. It is measuring range is 0-25mm with resolution 0.001mm. And the thickness of the EC and PMMA blend film is 0.002mm.

3. Results and discussion

In our study, we observed for Ethyl Cellulose (EC) and Poly Methyl Methacrylate (PMMA) there is decrease of dielectric constant with increase in frequency. The dielectric constant of Ethyl Cellulose (EC) and Poly Methyl Methacrylate (PMMA) for pure sample is increases at lower frequency range and as frequency get increases the dielectric constant suddenly decreases and then remains same as the frequency increases up to 1 M Hz. Here we noticed that the range of dielectric constant of polymer blends of Ethyl Cellulose (EC) with Poly Methyl Methacrylate (PMMA) increases as compare to the pure samples as shown in Figure. This is the expected behaviour in most dielectric material. This is due to the dielectric relaxation. From a structural point of view the dielectric relaxation involves the orientation polarization, which in turn depends upon the molecular arrangement in to the dielectric. So at higher frequencies the rotational motion of polar molecules of dielectric is not sufficiently rapid for the attainment of equilibrium with the field. As a result dielectric constant decreases with frequency. Also there is the increase of dielectric constant with increase in temperature as shown in Figure. Thus the increase in dielectric constant is due to the greater freedom of moment of dipole molecular chains within the polymer blends.

Conductivity plots

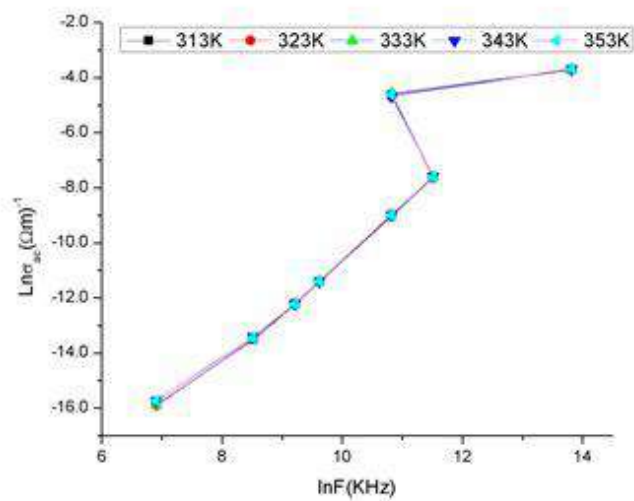


Fig. 3.1 Variation of conductivity with frequency at various constant temperatures (For Pure EC)

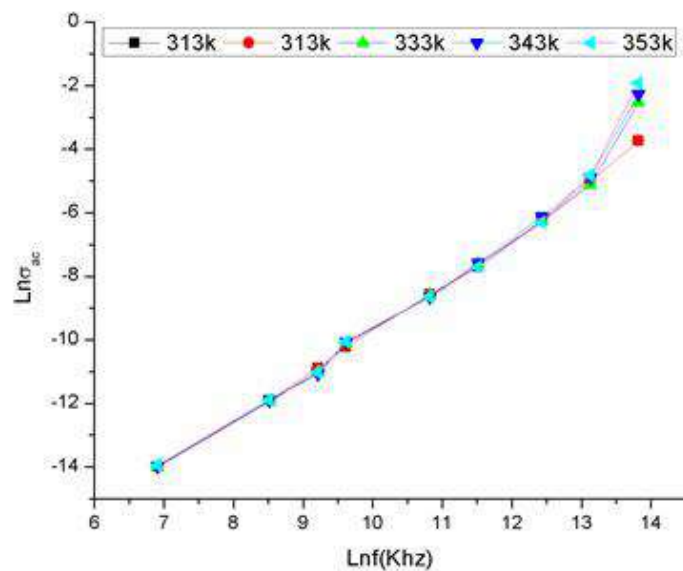


Fig.3.2 Variation of conductivity with frequency at various constant temperatures (For Pure PMMA)

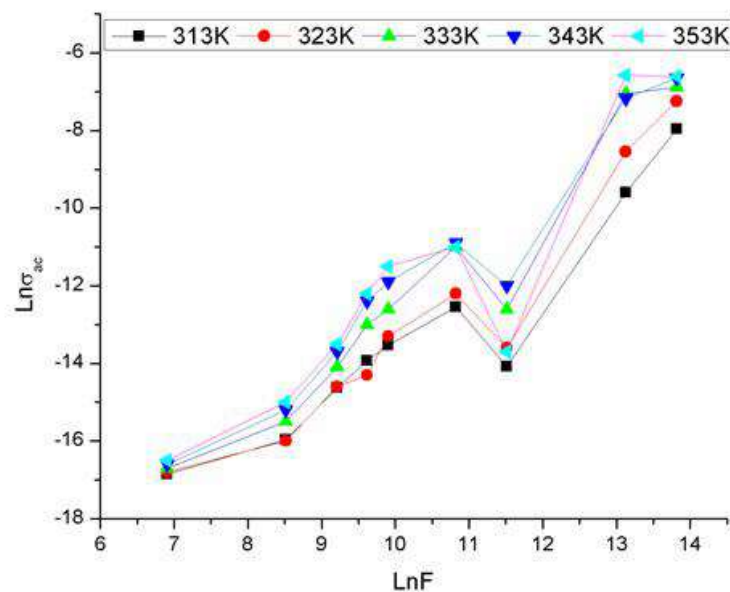


Fig.3.3 Variation of conductivity with frequency at various constant temperatures (For EC/ PMMA)

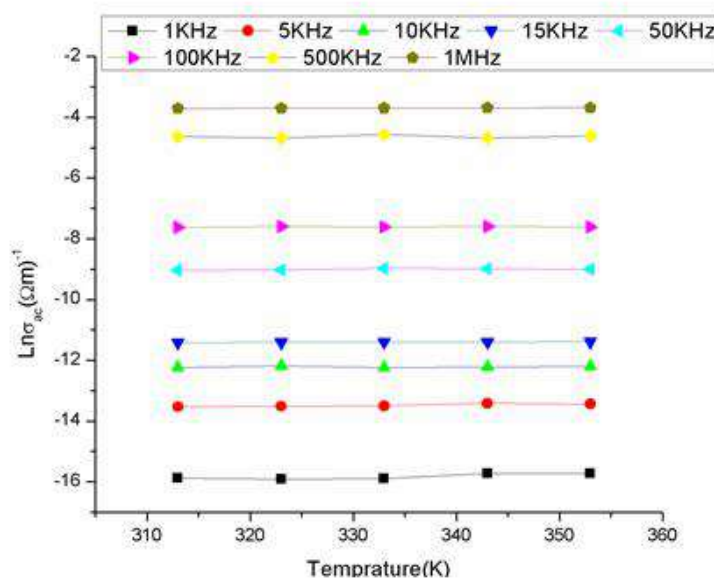


Fig.3.4 Variation of conductivity with Temperature at different constant frequencies (For Pure EC)

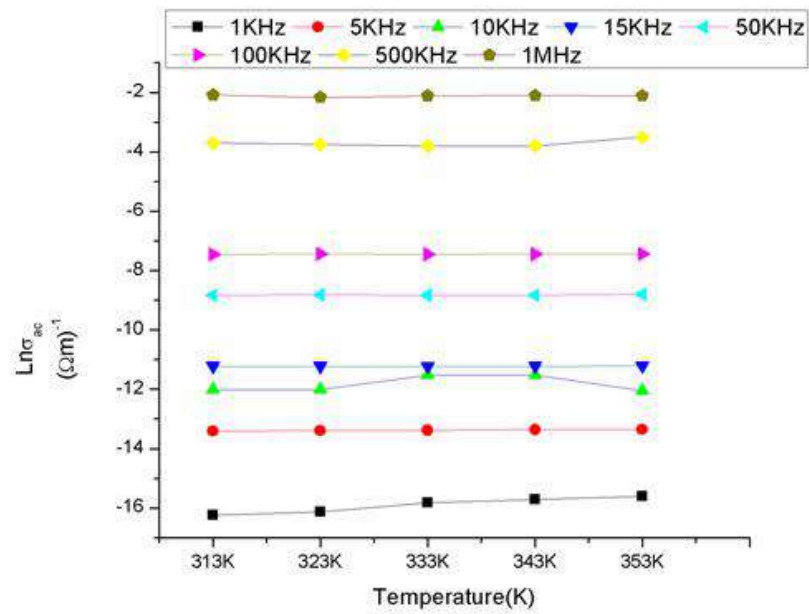


Fig.3.5 Variation of conductivity with Temperature at different constant frequencies (For Pure PMMA)

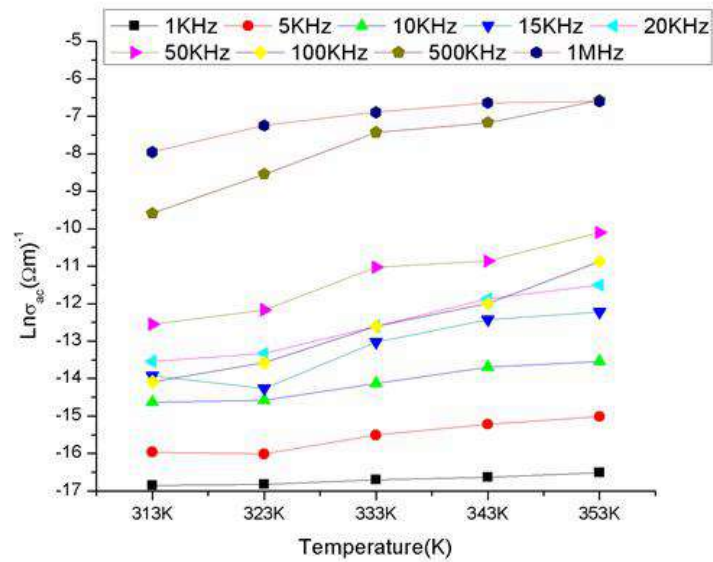


Fig. 3.6 Variation of conductivity with Temperature at different constant frequencies (For EC/PMMA blend)

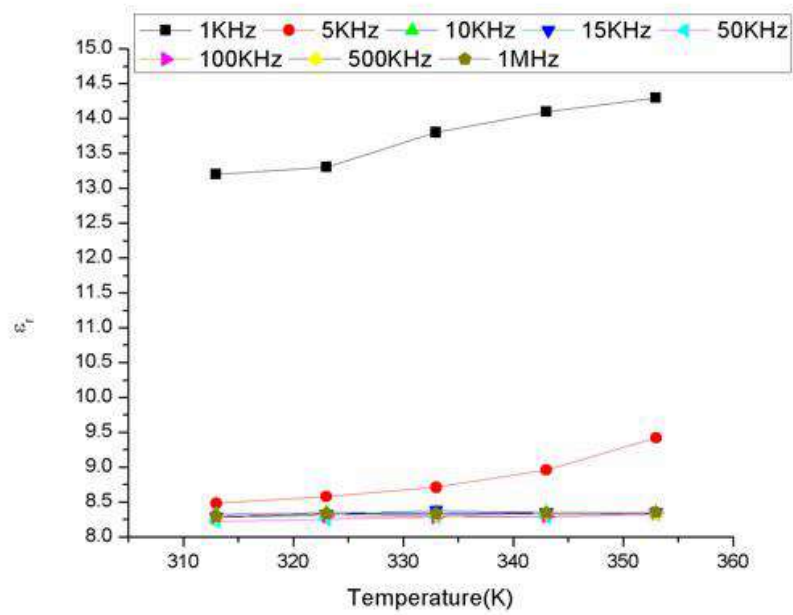


Fig.3.7 Variation of Temperature with dielectric constant (ϵ_r) at various frequencies (For Pure EC)

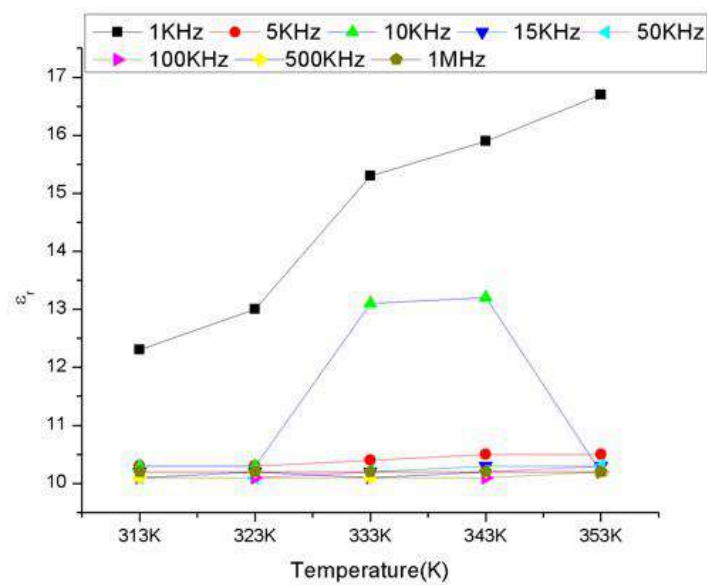


Fig.3.8 Variation of Temperature with dielectric constant (ϵ_r) at various constant frequencies (For Pure PMMA)

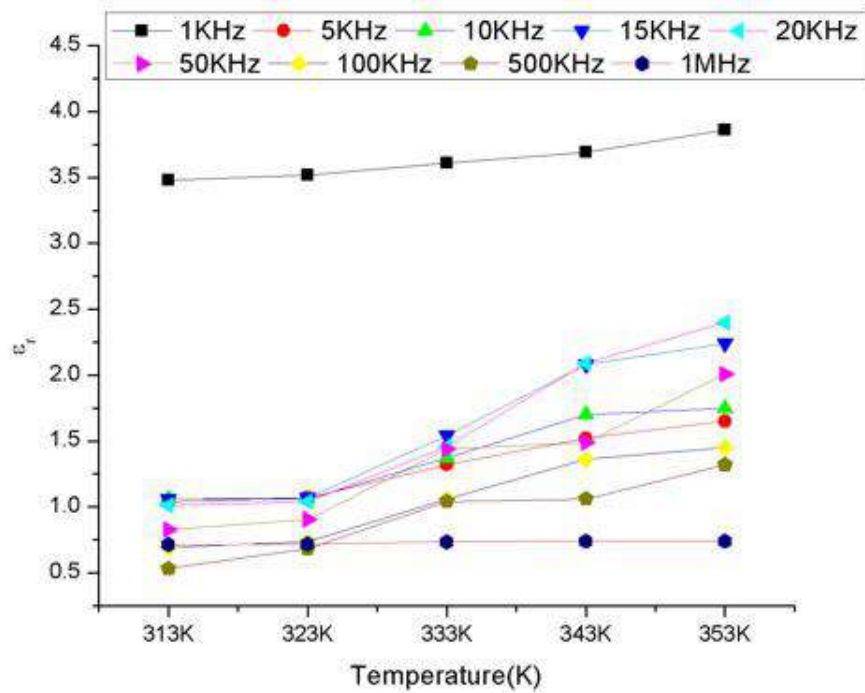


Fig.3.9 Variation of Temperature with dielectric constant (ϵ_r) at various constant frequencies (For EC/PMMA blend)

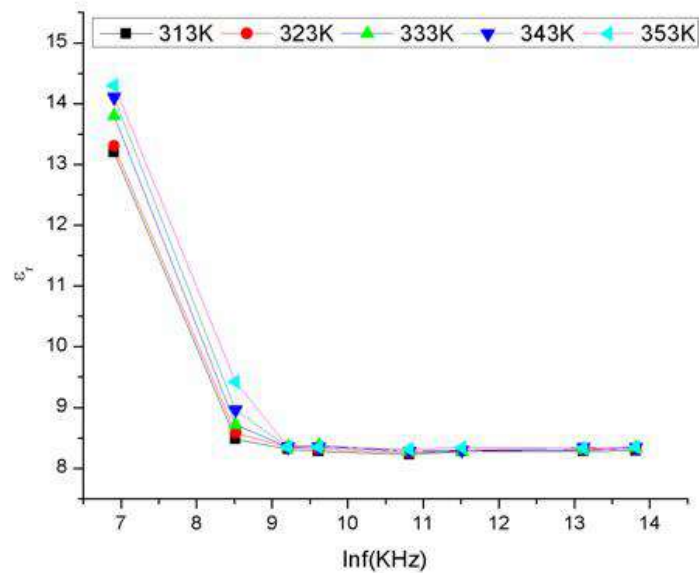


Fig.3.10 Variation of frequency with dielectric constant (ϵ_r) at different constant temperatures (For Pure EC)

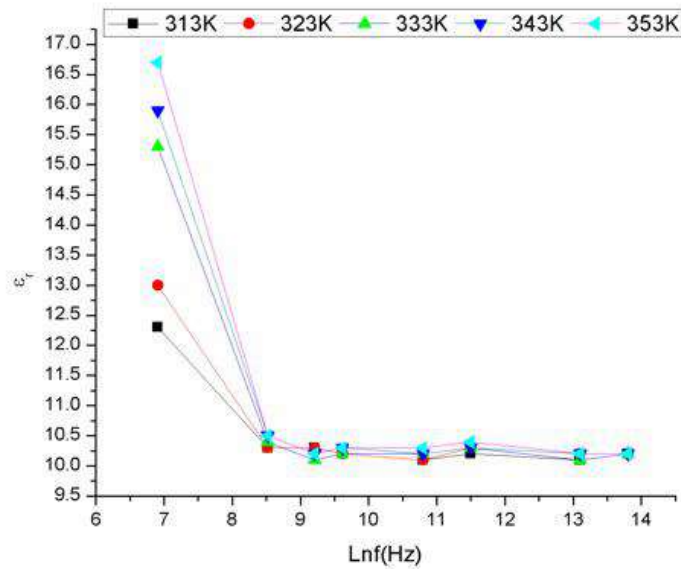


Fig.3.11 Variation of frequency with dielectric constant (ϵ_r) at different constant temperatures (For Pure PMMA)

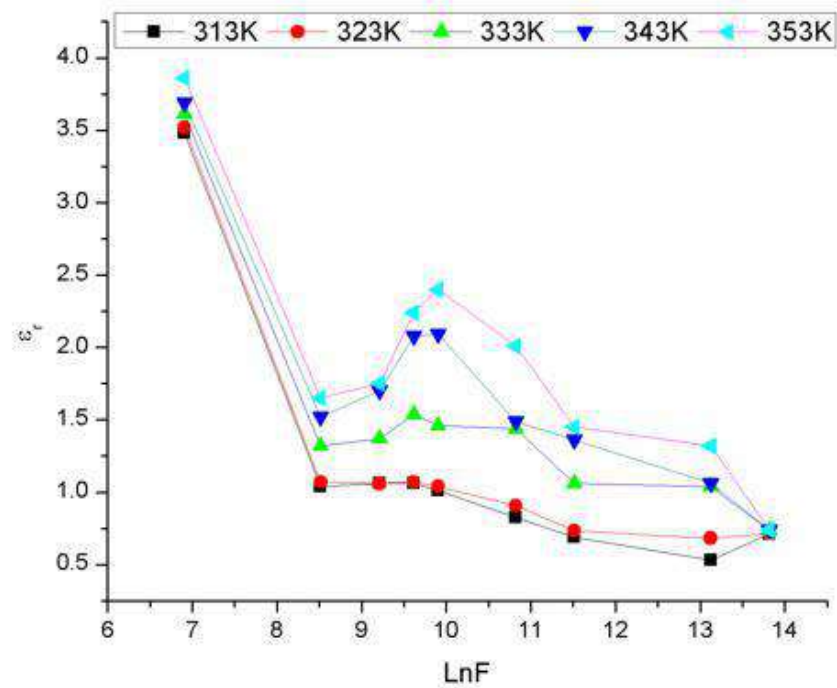


Fig.3.12 Variation of frequency with dielectric constant (ϵ_r) at different constant temperatures

3.1 AC conductivity Analysis

AC conductivity of all three samples have been investigated by carrying out Cp and Rp measurement by using LCR meter with respect to increase of frequency at various constant temperature 323K to 363K.

For all samples,

1. AC conductivity ($\sigma_{a.c.}$) increases with the increase of frequency at constant temperatures as shown in Fig.[3.1, 3.2 and 3.3].
2. AC conductivity ($\sigma_{a.c.}$) varies marginally increases with the increase of temperature at constant frequencies as shown in Fig. [3.4, 3.5 and 3.6].
3. Dielectric constant (ϵ_r) increases with the increase of temperature at constant frequencies as shown in Fig. [3.7, 3.8 and 3.9].
4. Dielectric constant (ϵ_r) decreases with the increase of frequency at constant temperatures as shown in Fig. [3.10, 3.11 and 3.12].

3.1.1 Effect of frequency on AC conductivity ($\sigma_{a.c.}$)

In our observation, Fig. [3.1, 3.2 and 3.3] shows AC conductivity of samples increases with frequency.

3.1.2 Effect of temperature on AC conductivity ($\sigma_{a.c.}$)

In the present study, Fig. [3.4, 3.5 and 3.6], we have noticed that AC conductivity varies marginally increases with temperature which shows almost temperature independent of AC conductivity. This model is based on the assumption that the energy states in the gap near the Fermi level are due to dangling bonds and exothermic reactions only paired defects are found in the gap [11]. Accordingly at low temperatures, a large distribution of relaxation time would be exposed contributing towards the dielectric loss. As a result AC conduction should be almost independent of temperature as observed in the present case.

3.1.3 Discussion of result related to Dielectric constant

In the present study we have noticed that,

1. At constant frequency, dielectric constant (ϵ_r) increases with increase of temperature as shown in Fig. [3.7, 3.8 and 3.9].
2. At constant temperature, dielectric constant decreases with the increase of frequency as shown in Fig. [3.10, 3.11 and 3.12].

In our study, Fig. 3.10, 3.11 and 3.12, shows that there is decrease of dielectric constant with increase in frequency. This is the expected behaviour in most dielectric material. This is due to the dielectric relaxation. From a structural point of view the dielectric relaxation involves the orientation polarization, which in turn depends upon the molecular arrangement in to the dielectric. So at higher frequencies the rotational motion of polar molecules of dielectric is not sufficiently rapid for the attainment of equilibrium with the field. As a result dielectric constant decreases with frequency.

Fig.3.7, 3.8 and 3.9 shows that there is the increase of dielectric constant with increase in temperature.

When the AC voltage of constant frequency is applied across the capacitor, it is charged by an applied AC voltage. The electric field will have the same time varying nature and the polarization of the capacitor takes place under the time varying electric field with frequency. At the same time if the temperature is increased, it may cause the freeing of more number of charge carriers and dipole due to the side chain motions and segmental motions occurring within the polymer dielectric. This freed dipole may follow the time varying nature AC field thereby increasing the polarization and dielectric constant of the blend sample under study.

Thus the increase in dielectric constant is due to the greater freedom of moment of dipole molecular chains within the polymer blends. At lower temperatures as the dipoles

molecular chains within the polymer blends, At lower temperatures as the dipoles are rigidly fixed in dielectric, field cannot change the condition of dipoles. As the temperature increase, the dipoles comparatively become free and they respond to electric field. This causes the increase polarization and hence the dielectric constant increases with temperature.

The microscopic behaviour of the dielectric material under the influence of a periodic (AC) electric field can be understood from the polarization which constitutes a dielectric or which is introduced during its proportion. These may be extra nuclear electrons and positively charged impurities, charged molecular species, etc.

The oppositely charged species having equal and opposite charges with a reasonable bond (Attractive forces between them) form a dipole. This dipole, under an applied electric field, may undergo spatial or rotational displacement which may be reflected in the macroscopic behaviour of the dielectric. The polarization effect is dependent on the nature of the dipoles and the frequency of the applied electric field.

As stated earlier, under the static electric field or the AC field of low frequency, the net polarization of the sample is contributed by electronic polarization. Atomic polarization and orientation polarization becomes unable to follow the field variations at higher frequencies (in present case beyond 250 KHz). As a result the dielectric constant decreases with the increase of frequency.

4. Conclusion

The A.C. electrical conductivity of Ethyl Cellulose (EC), Poly Methyl Methacrylate (PMMA) and their blend (EC/PMMA) is increasing with increasing frequency of applied electric field. The variation in the dielectric properties with temperature and frequency were studied. The increase in dielectric constant is due to the greater freedom of moment of dipole molecular chains within the polymer blends

Acknowledgements

The authors wish to thanks for your valuable guidance. They are also extremely grateful to Dr. Pradnya S. yenkar, Principal, V. B. M. V. Amravati, for extending laboratory facilities to carry out the present work.

Reference

- [1] Bahadur P. and Sastry N. V., Principles of polymer science (New Delhi: Narosa Publishing House), 2003, p. 281.
- [2] Seanor Donald A., Electrical properties of polymers (New York: Academic Press), 1982, pp 7–9, 15–27.
- [3] Blythe A. R., Electrical properties of polymers (Cambridge: Cambridge University Press), 1979, 95 p. 105.
- [4] Chakraborty S., Patil N., Das S. and Basu S., Indian Journal of Pure & Applied Physics, 1991, 29, 478.
- [5] Keller J., Dubey S. and Datt S., Indian Journal of Pure & Applied Physics, 1991, 29, 150.
- [6] Deshmukh S., Burghate D., Deogaonkar V. and Deshmukh P., Indian Journal of Physics, 2005, 79, 1263.
- [7] Deshmukh S., Burghate D., Akhare V., Deogaonkr V., Bulletin of Material Science, 2007, 30(1), 51–56
- [8] Khare P.K., Gaur M.S., Srivastava A.P., Indian journal of pure & applied physics. 1994, 32(1):14-8.
- [9] Bahri R., Seth R.K., Indian journal of pure & applied physics. 1997, 35(2):104-8.
- [10] Belsare N.G., Deogaonkar V.S., Indian journal of pure & applied physics. 1998, 36(5):280-9.
- [11] Shukla J.P. and Gupta M., Indian journal of pure and applied Physics, 1987, 242-244.

Brief Insights into Synthesis Methods and Applications of Nanostructured Metal Oxides

S. P. Patil^{1*}, **R. B. Pedhekar**², **V. S. Kalyamwar**³,
V. D. Wankhade⁴, **V. R. Hiranwale**⁵

^{1*, 2, 4} Physics Department, M. J. Fule Commerce, Science & V. Raut Arts College Bhatkuli, Dist. Amravati. 444602, (MS) India.

³ Physics Department, Bharatiya Mahavidyalaya, Amravati, Dist. Amravati. 444601, (MS) India.

⁵ Physics Department, Mahatma Phule Arts, Commerce & S. Chaudhari Science Mahavidyalaya, Warud, Dist. Amravati. 444906, (MS) India.

Corresponding author's email: surajphy95@gmail.com

Abstract:

Nanostructured metal oxides exhibit unique properties due to their nanoscale dimensions and find versatile applications in catalysis, energy storage, sensing, and environmental remediation. This mini-review presents various synthesis methods of nanostructured metal oxides like sol-gel, hydrothermal, chemical vapor deposition (CVD), etc., discussing their characteristics, advantages, and limitations and highlighting the importance of the hydrothermal method because it is pivotal for precisely controlling the morphology and crystallinity of metal oxide nanostructures. This mini-review also explores applications, emphasizing how synthesis influences nanostructure design and functional properties for advancing innovative technologies.

Keywords: Metal oxide, Nanostructures, Top-down, Bottom-up, Hydrothermal method

1. Introduction

Metal oxides, resulting from metals bonding with oxygen, possess diverse characteristics based on the metal and oxidation state, showcasing electrical, magnetic, and catalytic properties. Manipulating these materials at the nanoscale comes into the realm of metal oxide nanostructures. Nanostructured metal oxides, with their unique properties derived from nanoscale dimensions, have become a focal point in scientific exploration, offering vast potential across diverse applications. These materials possess distinctive physical, chemical, and mechanical characteristics at the nanoscale, revolutionizing materials science, catalysis, energy storage, sensing technologies, and environmental solutions. Their manipulation at the nanoscale marks a significant shift in materials science, introducing novel functionalities and customizable traits that were previously unattainable in bulk materials [1-3].

Nanostructures involve materials or structures within 1-100 nanometers, classified by their dimensions. Zero-Dimensional (0D) nanostructures like nanoparticles and quantum dots confine all dimensions. One-Dimensional (1D) structures like nanowires have two larger dimensions and one nanoscale dimension. Two-Dimensional (2D) nanostructures like graphene possess two nanoscale dimensions. Three-Dimensional (3D) nanostructures exhibit nanoscale features in all dimensions [4-5].

The synthesis of various nanostructures emerged from interdisciplinary studies, evolving with technological advances. Early observations on atomic behaviors led to deliberate fabrication, gaining importance from the late 20th to 21st centuries. Synthesis methods of nanostructures can be classified on their fundamental approach to fabrication. These methods can be classified into two primary categories: bottom-up and top-down approaches:

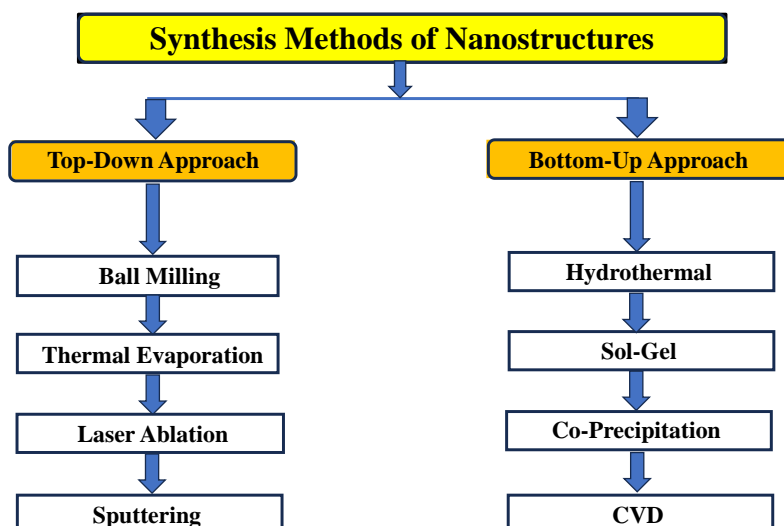


Fig. 1 Classification of synthesis methods of metal oxide nanostructures

Top-Down Approach: Ball milling involves mechanical grinding or milling processes that break down bulk materials into nanoparticles, offering scalability and control over particle size. Thermal evaporation utilizes high temperatures to vaporize materials, condensing them onto substrates to create thin films or nanostructures, offering high purity and precise control over film thickness. Laser ablation employs high-energy laser pulses to vaporize target materials, generating nanoparticles or thin films with controlled sizes and compositions, which is particularly useful for creating unique nanostructures and exotic materials. Sputtering involves bombarding a target material with high-energy ions or atoms, ejecting atoms from the target to deposit thin films with excellent adhesion and uniformity.

Bottom-up Approach: Hydrothermal Synthesis involves the synthesis of materials in a high-pressure, high-temperature aqueous solution, enabling controlled growth of various nanostructures. The sol-gel method fabricates materials from a colloidal solution, notably employed for metal oxides and ceramics, allowing precise control over composition and structure. Co-precipitation methods create nanoparticles by precipitating solutes from a solution, offering simplicity and scalability. Chemical Vapor Deposition facilitates the deposition of thin films or nanostructures through chemical reactions in a gas phase, ensuring high precision and uniformity in structure and composition. One of these methods, the hydrothermal method is essential for precisely shaping metal oxide nanostructures, crucial for optimizing their properties. This technique enables tailored designs, enhancing applications in catalysis, energy storage, and environmental solutions. Its precision in nanostructure control drives advancements in technology by creating high-performance materials with specific functionalities. [6-8].

Both bottom-up and top-down approaches in nanomaterial synthesis present distinct advantages and limitations. Bottom-up methods offer precision at the nanoscale, enabling controlled assembly of atoms or molecules to create nanostructures with unique properties, self-assembly capabilities, and monodispersity. However, challenges in scaling up, complexity, and limited structural control may hinder mass production. In contrast, top-down techniques allow for scalability, precise structural designs, and compatibility with established technologies, yet they may face resolution constraints, material wastage, and complexity in fabricating intricate 3D structures. The choice between these approaches depends on specific application needs, desired properties, scalability requirements, and cost considerations, leading to a balance between precision and scalability for optimal nanomaterial fabrication [9-10].

Nanostructured metal oxides exhibit diverse and impactful applications across several fields. In gas sensing, these materials, including zinc oxide (ZnO), tin dioxide (SnO₂), and Titanium dioxide (TiO₂), etc. nanomaterials, offer heightened sensitivity and selectivity,

enabling the detection of various gases crucial for environmental monitoring and industrial safety. Catalytically, nanostructured metal oxides serve as efficient catalysts, supporting chemical transformations and environmental remediation processes by aiding in pollutant degradation and wastewater treatment. These materials significantly enhance battery performance for energy storage, facilitating improved energy storage capacity and stability in lithium-ion batteries and contributing to advancements in supercapacitors and fuel cells. Furthermore, in environmental remediation, nanostructured metal oxides play a pivotal role in water and air purification by efficiently removing contaminants, emphasizing their potential for addressing critical environmental challenges. Ongoing research focuses on refining nanostructure designs, composite materials, and scalable synthesis methods, pushing these materials closer to practical applications for a sustainable future [11-14].

This review provides a thorough exploration of metal oxides and nanostructures, detailing their diverse characteristics stemming from metal-oxygen bonding. Manipulating metal oxides at the nanoscale yields unique structures, reshaping materials science with applications in catalysis, energy storage, sensing, and environmental solutions. Nanostructure dimensions, 0D to 3D, and synthesis methods, top-down and bottom-up, are discussed, with examples. The environmental impact, the influence of synthesis on properties, and ongoing research for practical applications in medicine, energy, and environmental solutions are emphasized. This review delivers a comprehensive overview of nanostructured metal oxides, spanning their properties, applications, and the evolving landscape of research in the field.

References

1. M. E. Franke, T. J. Koplín, U. Simon, Metal and metal oxide nanoparticles in chemiresistors: does the nanoscale matter?, *Small*. (2006) 36-50.
2. L. H. Xu, D. S. Patil, J. Yang, J. Xiao, Metal oxide nanostructures: synthesis, properties, and applications, *Journal of Nanotechnology*. (2015).
3. R. B. Pedhekar, F. C. Raghuwanshi, CeO₂ activated ZnO-TiO₂ thick film for CO₂ gas sensor, *International Journal of Engineering Science Invention*. (2017) 20-28.
4. Sáenz-Trevizo, P. Amézaga-Madrid, P. Pizá-Ruiz, B. Monárrez-Cordero, P. G. Hernández-Salcedo, W. Antúnez-Flores, M. Miki-Yoshida, *Functional nanostructured oxides: synthesis, properties, and applications, Emerging Applications of Nanoparticles and Architecture Nanostructures*, Elsevier. (2018) 29-69.
5. Y. Patil, R. B. Pedhekar, S. Patil, F. C. Raghuwanshi, Thick film gas sensors made from Mn doped zinc oxide nanorods for H₂S gas, *Materials Today: Proceedings*. (2020) 1865-1871.
6. S. Tripathy, J. Rodrigues, N. G. Shimpi, *Top-down and Bottom-up Approaches for Synthesis of Nanoparticles, Nano biomaterials: Perspectives for Medical Applications in the Diagnosis and Treatment of Diseases*. (2023) 92-130.
7. V. M. Arole, S. V. Munde, Fabrication of nanomaterials by top-down and bottom-up approaches-an overview, *Journal of Material Science*. (2014) 89-93.
8. A. Biswas, I. S. Bayer, A. S. Biris, T. Wang, E. Dervishi, F. Faupel, Advances in top-down and bottom-up surface nanofabrication: Techniques, applications & future prospects, *Advances in colloid and interface science*. (2012) 2-27.
9. P. G. Jamkhande, N. W. Ghule, A. H. Bamer, M. G. Kalaskar, Metal nanoparticles synthesis: An overview on methods of preparation, advantages and disadvantages, and applications, *Journal of drug delivery science and technology*. (2019) 101174.
10. N. Patil, R. Bhaskar, V. Vyavhare, R. Dhadge, V. Khaire, Y. Patil, Overview on methods of synthesis of nanoparticles, *International Journal of Current Pharmaceutical Research*. (2021) 11-16.
11. Dar, Ghulam Nabi, *Metal oxide nanostructures and their applications*, Dissertation. (2015).
12. V. E. Bochenkov, G. B. Sergeev, Sensitivity, selectivity, and stability of gas-sensitive metal-oxide nanostructures, *Metal oxide nanostructures and their applications*. (2010) 31-52.
13. D. Nunes, A. Pimentel, A. Gonçalves, S. Pereira, R. Branquinho, P. Barquinha, R. Martins, Metal oxide nanostructures for sensor applications, *Semiconductor Science and Technology*. (2019) 043001.
14. Z. Zheng, *Synthesis and modifications of metal oxide nanostructures and their application*, Dissertation, Queensland University of Technology, (2009).

Humidity Sensors: AlCl₂-Dipped Nanocrystalline Magnesium Oxide

R B Butley*¹, R V Joat¹, G T Lamdhade¹, K B Raulkar¹, A O Chauhan¹,
C C Jadhao¹, B.H. Bhatti¹

¹Department of Physics, Vidya Bharati Mahavidyalaya, Amravati(M.S.), India
Corresponding Author: Email: ra.butley@gmail.com

ABSTRACT

The investigation, magnesium oxide and AlCl₂ were combined in varying mol% w/w stoichiometry. Thick layers of humidity sensors are made using the screen printing method. After testing every humidity sensor device, it was determined that the sample T-1, which was kept at a constant temperature between 400 and 700 degrees Celsius, had a high sensitivity and a quick response time to humidity sensing at room temperature. Curves in the case of conductivity are often jumbled and congested. Relative humidity has a linear effect on sample film conductivity. When sensors are kept at room temperature and their surface oxygen vacancies operate as electron donors, the resistance of thick films reduces.

KEYWORDS: Thick films, MgO-AlCl₂, Sensitivity, and Humidity sensors.

1. INTRODUCTION

The operator can manage the temperature and relative humidity in these humidity chambers at predetermined levels via the front panel.[1-4] The chamber's air is continuously circulating, scheduled to be compared to predetermined points. Electric resistance heaters, which regulate temperature by turning on and off, produce heat. There is a refrigeration unit that runs constantly on units with cooling. A low-pressure vapor generator injects water vapor into the chamber via a tiny opening to achieve chamber humidification. At the blower discharge, the water vapor enters the chamber. Test chambers were programmable, and they could be networked or connected to the Internet. The goal of the current work is to create and characterize the structure of magnesium oxide nanoparticles using the liquid phase method, which has the advantage of producing a greater surface area in a shorter amount of time at room temperature. This approach is also the most straightforward, economical, and environmentally benign. Through XRD analyses of MgO nanoparticles, its impact on the nanocrystalline size structure is also investigated.[5-12]

2. EXPERIMENTAL METHOS:

All of the chemicals utilized in this work were 99.99% pure GR grade chemicals that were bought from Sd-fine chemicals, India. The sol-gel technique is utilized to synthesize MgO nanoparticles. There are several processes involved in the synthesis of MgO nanoparticles, including stirring, drying, filtration, mixing, and calcination. Ultimately, the powder is calcined for three hours at 300 °C to produce MgO in the form of nanoparticles.

In screen printing, a mesh is used to transfer ink onto a substrate, with the exception of places blocked with a blocking stencil to prevent ink from penetrating such areas. In order to fill the gaps in the mesh with ink, a substance or gel is pushed over the screen, and vice versa, causing the screen to briefly make contact with the substrate along a line of contact. When the screen springs back after the blade has passed, the material gets moist on the substrate and is drawn out of the mesh holes. Similar to this, we utilize glass slides as the substrate and a paste made of nanomaterials in place of ink. Thus, instead of using the glass slide that we are using here, we are using mesh that has a less permeable stencil area. First, we take the 90% nanomaterial and use a solid binder (10%) called ethyl cellulose to build a paste out of it. Drop by drop, liquid binder is added to a well-ground mixture of nanomaterial and solid binder. Making sure the right amount of liquid binder is added requires caution. Thus, the ideal thick nanomaterial paste is made. Next, we proceed to apply a paste made of permeable mesh for well-layered nanomaterials to substrates (glass slides) using a squeegee. First, we let these thick

sheets of magnesium oxide nanoparticles dry in the air while they are being made. After that, they spend an hour in a vacuum oven set at 80°C. After that, we heated these thick sheets for three hours at 250°C in a muffle furnace. These thick films are now dipped in aluminum chloride for varying lengths of time [13–16].

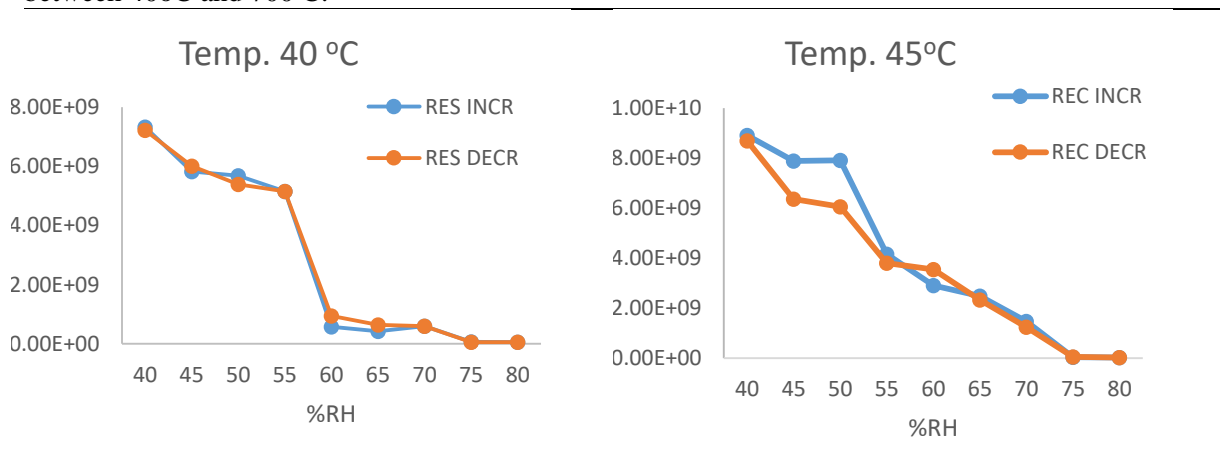
Aluminum and chlorine make up the bulk of aluminum chloride (AlCl₃). The substance is frequently mentioned as a Lewis acid. Aluminum chloride has been utilized in the dipping process by us. We produced an AlCl₃ solution and then dipped a thick layer of magnesium oxide for varying durations of time. After dipping the slides for one, two, or three minutes, we fire them for one hour at 250°C to create three thick film slides for varying dipping times, and one thick film slide is taken for purity.

A measurement of humidity indicates how much water vapor is present in a gas or the atmosphere. The relative humidity and the ambient temperature work together to determine the comfort level. Measuring humidity is crucial for using some pieces of equipment. As a general rule, maintain a relative humidity of about 50% RH at a typical room temperature of 20 to 25 degrees Celsius. This can range from as low as 40% RH in clean rooms to 60% RH in operating rooms of hospitals. Hygrometers are used to measure humidity. Sir John Leslie invented the first hygrometer. Measuring humidity is crucial for both controlling the indoor climate and forecasting the outdoor climate. [17–20]

3. RESULTS AND DISCUSSION:

3.1 Hysteresis:

Hysteresis is the term for the phenomena when changes in an effect cause a physical property's value to lag behind. Our current study, which uses MgO nonmaterial thick films for humidity sensing, displays the hysteresis plot of samples M-1, M-2, M-3, and M-0 at a constant temperature of 40°C. The hysteresis plot illustrates the change in the sample's resistance in relation to relative humidity in stages of 5% RH, from 40 to 80% RH, and in both increasing and decreasing orders. Using a Keithley 2400 source meter, the resistance was measured in increments of 10% RH at various constant temperatures between 40°C and 70°C.



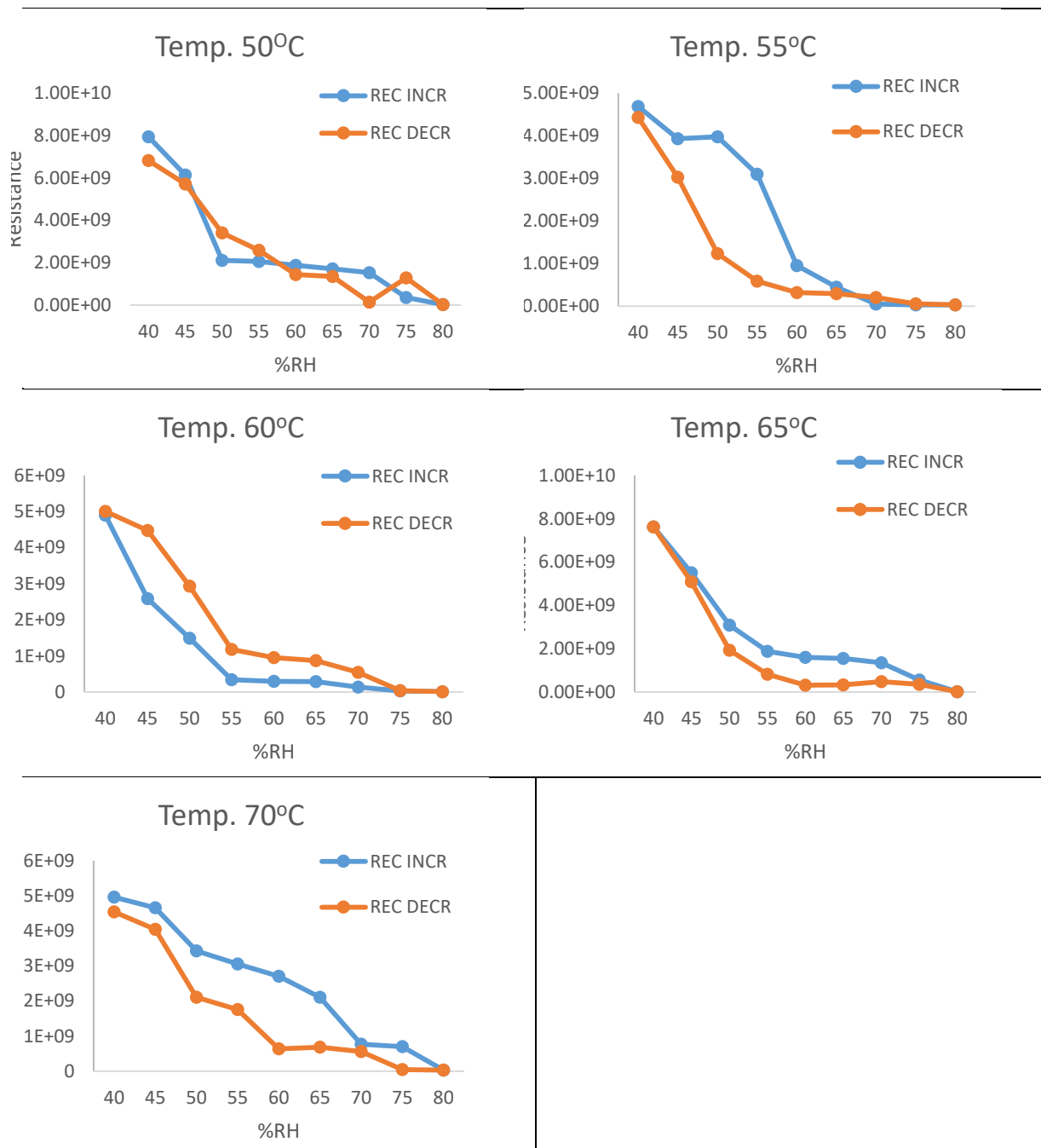


Figure 3.1 M-1 Metal oxide Thick Film (1-minute) hysteresis plot

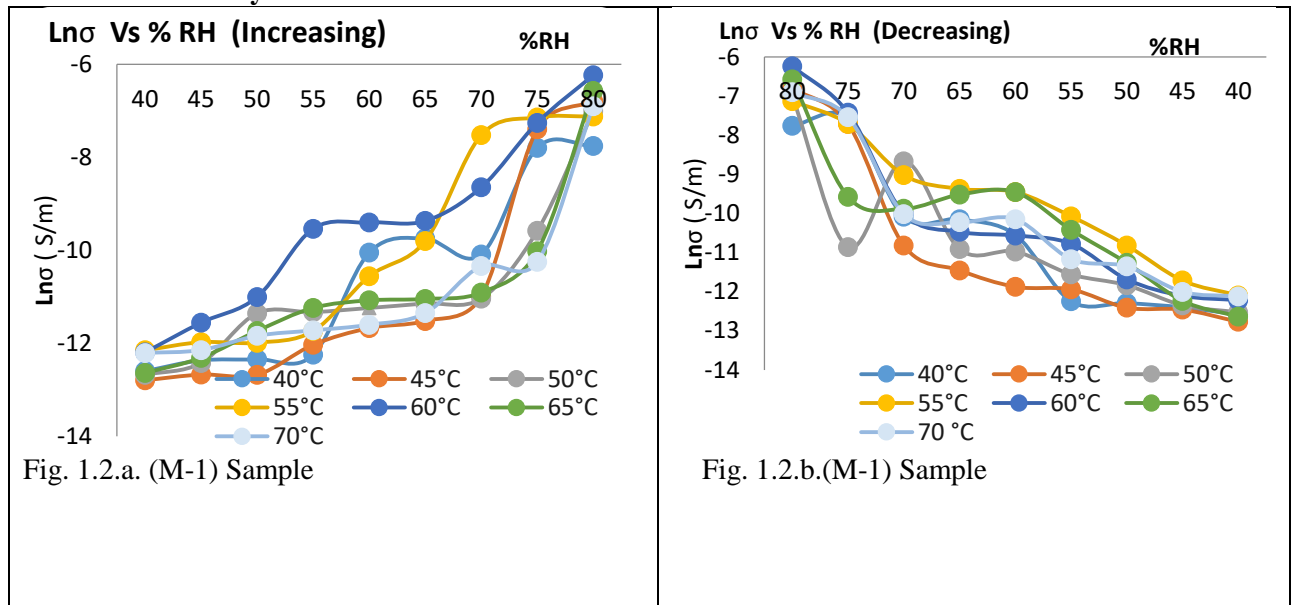
We may plot the graphs for the remaining samples in a similar manner. The hysteresis plot series of a sample, MgO nanomaterial film M-1, M-2, and M-3, dipped in aluminum chloride for varying dipping times, i.e., for 1, 2, and 3 minutes, respectively, and the hysteresis plot of a pure sample of MgO nanoparticle film at corresponding constant temperature are observed in the current work. It is evident from the hysteresis plot that relatively little hysteresis occurs during the forward (increasing) and reverse (decreasing) cycles of RH. The resistance value of the sample was found to have changed on average by a fairly substantial amount between 1010 and 108Ω.m. With the exception of sample M-1 (1 minute), the resistance value changes from 109 to 107Ω.m. between 40 and 80% RH. Sample M-1's resistance value noticeably changes from 40°C to 70°C at constant temperature.

Table 2.1 Sample Codes

Sr. No.	Sample	Thickness $\times 10^{-6}$ m	Material
1.	M-0	26	Pure MgO
2.	M-1	20	MgO +Dipped with AlCl_2 for 1 minutes dipping and after firing these slides for 1 hour at 250°C .
3.	M-2	21	MgO +Dipped with AlCl_2 for 2 minutes dipping and after firing these slides for 1 hour at 250°C .
4.	M-3	22	MgO +Dipped with AlCl_2 for 3 minutes dipping and after firing these slides for 1 hour at 250°C .

Because the processes of adsorption and desorption are not as quick at a given humidity, hysteresis was seen. The physisorbed water molecules are changed into chemisorbed by donating the surface electron at a constant temperature, as adsorption would not be effective and would result in a modest change in the value of resistance. Desorption necessitates a high activation energy. However, as we have shown, the sample in question exhibits a similar drop in resistance as the percentage RH increases, suggesting that conduction happens at the grain surface as a result of the release of electrons from the water molecule. As a result, the sample clearly demonstrates a shift in resistance between values in the humidity range of 40% to 80% RH. [21–28]

3.2 DC Conductivity



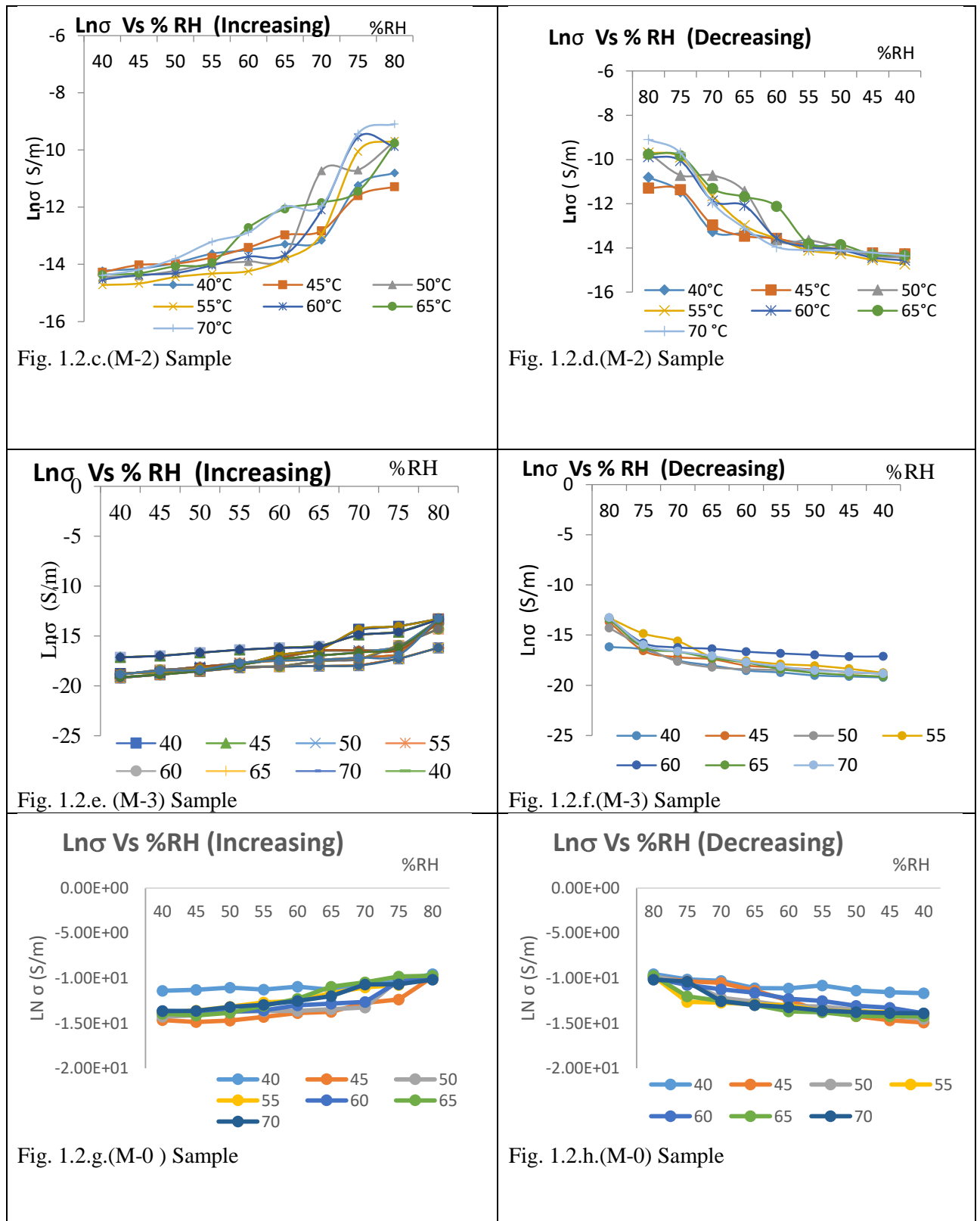


Fig. 1.2 Variation (a-d) $\text{Ln}\sigma$ Vs RH at different constant temperature (40°C to 80°C)

The $\text{Ln}\sigma$ fluctuation as the series sample's RH increases and decreases (from 40 to 80% RH and from 80 to 40% RH). correspondingly between 40°C and 70°C at constant temperature. From 40 to 80% relative humidity, it has been found that conductivity increases somewhat linearly and vice versa. The conductivity of sample M-1 rises in tandem with its temperature. The conductivity was found to be highest at high temperatures and lowest at 40°C for all sample series.[28–29]

3.2 XRD OF MAGNESIUM OXIDE

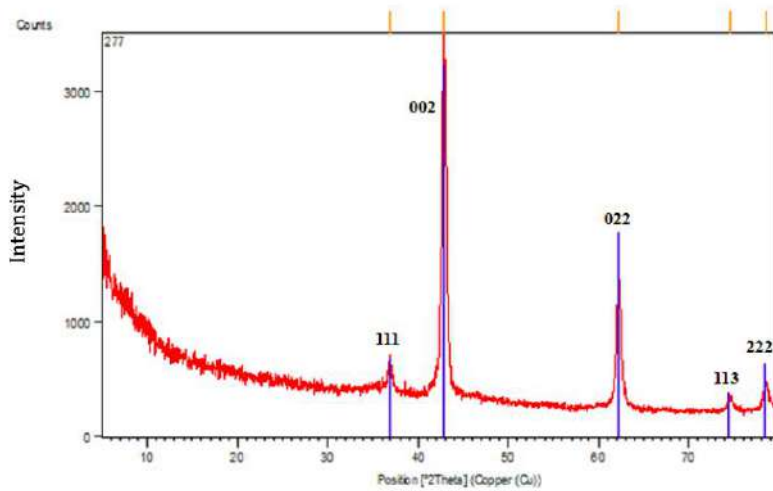


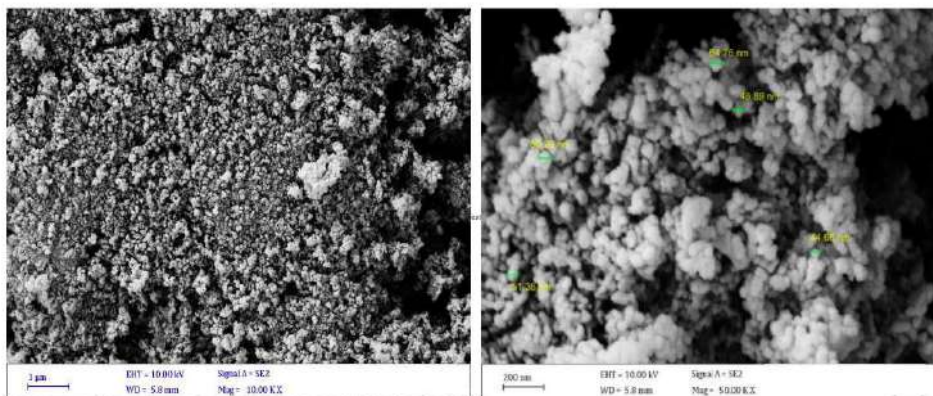
Fig. 1.3 XRD pattern of Periclase Magnesium oxide (MgO)

XRD peaks for sol-gel-synthesised MgO nanoparticles. These peaks, which are formed at (111), (002), (022), (113), and (222) planes, respectively, at $2\theta = 36.862, 42.824, 62.167, 74.516,$ and 78.443 degrees, are compared with the ICSD, powder diffraction card of MgO file No. 43-1022. Moreover, the $\text{Mg}(\text{OH})_2$ phase is absent from XRD patterns that highlight excellent purity. The diffraction peaks of the MgO nanoparticles made by sol-gel are slightly broadened, indicating a return to a tiny size of nanoparticles, but the sharp peaks in the XRD data for the microwave approach and the sol-gel route suggest uniform crystallinity. The Scherrer formula, found in Equation (1), was used to calculate the average crystalline size.

$$D = 0.9 \lambda \beta \cos \theta \dots (1)$$

Where D is the average crystalline size, λ is the X-ray wavelength, β is the Full Width at Half Maximum, and θ is the Bragg diffraction angle. D , on the other hand, stands for the average crystal size determined by the diffraction peaks. For the sample made using the sol-gel method, it is visible at 33 nm.[30]

3.3 SEM PICTURES:



(a) Under 1 μm and (10.00 KX) magnification

(b) Under 200 nm and (50.00 KX) magnification

SEM pictures of MgO.

The morphology of nanocomposites as revealed by FE-SEM reveals that the particles are tiny, spherically-shaped, and nanoporous. On the surface, one can observe the formation of porous and nanocrystalline magnesium oxide. The prepared sample has an aggregated appearance. Along with a range of shapes and sizes, grains also have a nanoporous structure and organization at the nanoscale. The large surface area of the structure and the micro capillary pore are expected to facilitate the adsorption and condensation of water molecules. This porosity allows for good response to and recovery from humidity.

4. CONCLUSIONS:

The investigation of humidity sensors has produced a novel detecting mechanism that may be used under many circumstances. The resistance value of the sample was found to have changed on average by a fairly substantial amount between 1010 and 108 ohm. Sample M-1's resistance value noticeably changes from 40°C to 70°C at constant temperature. When it comes to conductivity, curves are usually jumbled and packed. Sample film conductivity reacts to relative humidity in a linear fashion. The sample films demonstrate the noteworthy outcomes related to humidity sensing. The fact that every peak matches the MgO nanostructure exactly suggests that MgO nanoparticles were produced. Within the XRD instrument's detection limit, no more peaks were seen in the spectrum, showing the pure MgO Nanomaterial is synthesized.

5. ACKNOWLEDGEMENT:

One of the authors Rohit B Butley is very much thankful to Vidya Bharati Mahavidyalaya Amravati, India for providing the XRD facility.

References

1. A. H. Wani and M. A. Shah, "A unique and profound effect of MgO and ZnO nanoparticles on some plant pathogenic fungi", *Journal of Applied Pharmaceutical Science* 02(03), 2012, pp. 40-44.
2. C. R Indulal, R Biju, D. Nand, R. Raveendran, "Optical and Antibacterial Studies of Zinc Magnesium Oxide Nanocomposite", *Journal of Chemistry*, 33, 2017, pp.1545-1549.
3. Anjali Mavya and Nada Bhatia, "Microwave assisted Sol-Gel Synthesis of Magnesium oxide (MgO)", *International Journal of Engineering Research and Development*, 13, 8, 2017, pp.1-6. IICESAT Conference, College of Material Engineering, University of Babylon, Iraq *Journal of Physics: Conference Series* 1973 (2021) 012104 IOP Publishing doi:10.1088/1742-6596/1973/1/012104 8
4. K. Mageshwari, Sawanta S. Mali, R. Sathyamoorthy and Pramod S. Platil, "Template-free synthesis of MgO nanoparticles for effective photocatalytic applications", *Powder Technology*, 249, 2013, pp. 456-462.
5. Iwayan Sutapa, Abdul Wahid Wahab, Paulina Taba and Nursiahila Nafie, "Synthesis and Structural profile analysis of the MgO Nanoparticles produced through the Sol-Gel method followed by Annealing process", *Oriental Journal of Chemistry*, 34., 2, 2018, pp.1016-1025.
6. K. P. Mckenna, D.koller, A. Sternig, N. Siedl, N. Govind and P. V. Sushko, "Optical Properties of Nanocrystal Interfaces in Compressed MgO Nanopowders", *ACS Nano* 5, 2011, 2003.
7. Manoj B.Gawande, Paula S. Branco, Kalpesh Parghi, Janhavi J. Shrikhande, Rajesh Kumar Pandey, C. A. A. Guhman, N. Bundaleski O. M. N. O. Teodoro and V. Radhajayaramcatal, "Synthesis and characterization of versatile MgO-ZrO₂ mixed metal oxide nanoparticles and their applications", *Science & Technology*, 1, 2011, 1653.
8. Mastuli, M. S., Kamarul Zaman, N. Nawawi, M. A., Mahat, A. M., Rusdi, R., Kamarudin, and N. *Nanoscale Research Letter*, 9, 2014, pp.134.
9. Lamdhade G. T. Agrawal R. M., Charpe S. D., and Raghuwanshi F. C, "Synthesis and Characterization of Magnesium oxide Nanoparticles with 1:1 molar ratio via Liquid-Phase Method", *IJAIEEM*, 4, 2015, pp. 141-145.
10. N. C. S. Selvam, R. T. Kumar, L. J. Kennedy, and J. J. Vijaya, "Comparative study of microwave and conventional methods for the preparation and optical properties of novel MgO-micro and nano-structures", *Alloys and Compounds*, 509, 2011, pp. 9809– 9815.
11. S. Saitzek, S. Villain and J. R. Gavarri, "Nanocrystalline CuO_x-CeO₂ Systems: FTIR Analyses of Catalytic Reactions", *Mater Sci.*, 513, 2006, pp. 1-14.
12. Rezaei, Mehran, Majid Khajenoori, and Behzad Nematollahi. "Synthesis of high surface area nanocrystalline MgO by pluronic P123 triblock copolymer surfactant." *Powder technology* 205, 201, pp. 112-116.
13. Song, Guolin, et al. "Ultrasonic-assisted synthesis of hydrophobic magnesium hydroxide nanoparticles." *Colloids and Surfaces A: Physicochemical and Engineering Aspects* 364, 2010, pp. 99-104.
14. Richa Srivastava and B. C. Yadav (2012) *Nanomaterials and Sensors Research Laboratory*, Department of Physics, Lucknow University, Lucknow 226007, U. P., India, Department of Applied Physics, School for Physical Sciences, Babasaheb Bhimrao Ambedkar University, Lucknow 226025, U.P., India, doi: 10.5185/amlett.2012.4330.

15. N. K. Pandey, Karunesh Tiwari, and Akash Roy, (2011) Moisture Sensing Application of Cu₂O Doped ZnO Nanocomposites IEEE SENSORS JOURNAL, VOL. 11, NO. 9, doi: 10.1109/JSEN.2011.2112764, SEPTEMBER.
16. Y SHIMIZU, H ARAI and T SEIYAMA (1985) Theoretical Studies On The Characteristics Of Ceramic Sensors and Actuators, 0250 6874/85/ 30, 7 11 - 22 .
17. B.C. Yadav , Richa Srivastava & C.D. Dwivedi (2008) Synthesis and characterization of ZnO–TiO₂ nanocomposite and its application as a humidity sensor doi. /10.1080/14786430802064642.
18. D.G. Yarkin, (2003) Impedance of humidity sensitive metal/porous silicon/n-Si structures Sensors and Actuators A 107 doi:10.1016/S0924-4247(03)00231-0.
19. Vijay K. Tomer, Ritu Malik, Vandna Chaudhary ArabindaBaruahand Lorenz Kienle, (2019) Noble Metals Metal Oxide Mesoporous Nano hybrids in Humidity and Gas Sensing Applications doi. /10.1016/B978-0-12-814134-2.00014-0 .
20. Hamid Farahani, Rahman WagiranandMohd Nizar Hamidon (2014) Humidity Sensors Principle, Mechanism, and Fabrication Technologies: A Comprehensive Review Sensors, 14, 7881-7939; doi:10.3390/s140507881 .
21. Raid A. Ismail,*Ala Al-Naimi, and Alaa A. Al-Ani , (2006) Preparation and characteristics study of ZnO: (Al, Cu, I) thin films by chemical spray pyrolysis e-J. Surf. Sci. Nanotech. Vol. 4 636-639 DOI:10.1380/ejsnt.2006.636.
22. Wensheng Wang, Anil V. Virkar , (2004) A conductimetric humidity sensor based on proton conducting perovskite oxides, sensors and Actuators, B 98, 282–290, doi:10.1016/j.snb.2003.10.035.
23. Vijay K. Tomer, Surender Duhan, Parag V. Adhyapak, and Imtiaz S. Mulla (2014) Mn-Loaded Mesoporous Silica Nanocomposite: A Highly Efficient Humidity Sensor J. Am. Ceram. Soc., 1–7 ,DOI: 10.1111/jace.13383.
24. Nor Diyana Md Sin, Mohd Firdaus Malek, Mohamad Hafiz Mamat, Mohamad Rusop Bin Mahmood, (2014) International Journal of Materials Engineering Innovation , List of Issues , Volume 5, Issue 2 , DOI: 10.1504/IJMATEI.2014.060343.
25. Macagnano, V. Perri, E. Zampetti, A. Bearzotti, F. De Cesare,(2016) Sensors and Actuators B: Chemical, Volume 232, 16-27 .
26. Yuan Liu, Hui Huang, Lingling Wang, Daoping Cai, Bin Liu, Dandan Wang, Qihong Li, Taihong Wang, (2016) Sensors and Actuators B: Chemical, Volume 223 , 730-737. doi.10.1016/j.snb.2015.09.148.
27. Mohamad Izzat Azmer, Zubair Ahmad, KhaulahSulaiman, Abdullah G. Al-Sehemi, (2015) Sensors and Actuators B: Chemical 61 , 180-184.
28. Kyung Hyun Choi, Memoon Sajid, Shahid Aziz, Bong-Su Yang, (2015) Sensors and Actuators A: Physical, Volume 228, 40-49, doi.org/10.1016/j.sna.2015.03.003 .
29. Yang Li, Kaicheng Fan, Huitao Ban, Mujie Yang, (2016) Sensors and Actuators B: Chemical, Volume 222, 151-15, doi.org/10.1016/j.sna.2015.03.003.
30. Yuan Liu, Hui Huang, Lingling Wang, Daoping Cai, Bin Liu, Dandan Wang, Qihong Li, Taihong Wang, ,(2016) Sensors and Actuators B: Chemical, Volume 223, 2016, 730-737, doi. /10.1016/j.snb.2015.09.148.
31. Xiuping Han, Binghua Yao, Keying Li Wenjing Zhu, and Xuyuan Zhang (2020) Preparation and Photocatalytic Performances of WO₃/TiO₂ Composite Nanofibers |Article ID 2390486 | doi. /10.1155/2020/2390486.

Advances and Perspectives in Nanotechnology: A Short Review

R B Butley*¹, R V Joat¹, G T Lamdhade¹, K B Raulkar¹, A O Chauhan¹,
C C Jadhao¹, B.H. Bhatti¹

¹Department of Physics, Vidya Bharati Mahavidyalaya, Amravati(M.S.), India
Corresponding Author : Email:ra.butley@gmail.com

Abstract:

The process of modifying the shape and size of structures, electronics, and systems at the nanometer scale, i.e., 1 nm to 100 nm (10⁻⁹m), is known as nanotechnology. The prefix nano derives from the Greek word "nano," which meaning "very little". Because of their small size, they have larger surface areas than bulk forms, better reactivity, and the ability to control numerous features. These unique qualities have fueled the expansion of nanoscience and the use of nanoparticles in a variety of sectors such as biomedicine, cosmetics, electronics, food analysis, environmental and remediation, and painting. Nanoscale science and engineering enable us to understand and control matter at the atomic and molecular levels [1,2].

Brief overview of nanotechnology's historical development

Nanotechnology's historical development traces back to a series of theoretical concepts and experimental observations. Here's a brief overview:

1. Early Concepts (1950s-1960s):

The term "nanotechnology" was first coined by physicist Richard Feynman in his 1959 lecture, "There's Plenty of Room at the Bottom," where he discussed the possibilities of manipulating individual atoms and molecules. Physicist Eric Drexler expanded on these ideas in the 1980s with his book "Engines of Creation," envisioning nanoscale machines and their potential applications.

2. Scanning Tunneling Microscopy (1981):

The development of the scanning tunneling microscope (STM) by Gerd Binnig and Heinrich Rohrer in 1981 revolutionized nanotechnology. It allowed researchers to visualize and manipulate individual atoms, opening the door to nanoscale exploration.

3. Fullerenes and Nanotubes (1985):

In 1985, the discovery of fullerenes (buckyballs) by Robert Curl, Sir Harold Kroto, and Richard Smalley introduced a new class of nanomaterials. Later, carbon nanotubes, cylindrical structures with remarkable properties, were identified.

4. Development of Nanolithography (1980s-1990s):

Advancements in nanolithography techniques, such as electron-beam lithography and photolithography, enabled precise control over nanoscale structures. This was crucial for the fabrication of nanodevices.

5. Nobel Prize in Chemistry (1996):

The Nobel Prize in Chemistry was awarded to Robert Curl, Sir Harold Kroto, and Richard Smalley for their discovery of fullerenes. This recognition significantly boosted interest and research in nanotechnology.

6. Bottom-Up Approaches (1990s-2000s):

Scientists increasingly explored bottom-up approaches, involving self-assembly and molecular manipulation to create nanoscale structures. This shift in focus led to the development of nanomaterials and nanodevices with unique properties.

7. Interdisciplinary Growth (2000s-Present):

Nanotechnology became a highly interdisciplinary field, incorporating knowledge from physics, chemistry, biology, and engineering. Collaborative efforts led to breakthroughs in various applications, including medicine, electronics, energy, and materials science.

8. Advancements in Nanomedicine (2000s-Present):

Nanotechnology has made significant contributions to medicine, with developments in targeted drug delivery, imaging, and diagnostics. Nanoparticles are engineered for precise interactions with biological systems, improving treatment efficacy and reducing side effects. Nanotechnology continues to evolve, with ongoing breakthroughs shaping its future applications and impact across diverse scientific and industrial domains.

9. Highlight major achievements and breakthroughs in the field.

1. Scanning Tunneling Microscopy (STM):

Gerd Binnig and Heinrich Rohrer's creation of the STM in 1981 enabled scientists to observe and manipulate individual atoms, marking a watershed moment in nanoscale observation and manipulation. [3-4]

2. Discovery of Fullerenes (1985):

The discovery of fullerenes, particularly buckyballs (C₆₀), by Robert Curl, Sir Harold Kroto, and Richard Smalley ushered in a new era of nanomaterials with distinct features, earning them the Nobel Prize in Chemistry in 1996. [5]

3. Carbon Nanotubes (1991):

Sumio Iijima's discovery and characterisation of carbon nanotubes gave rise to a new class of nanomaterials with exceptional mechanical, thermal, and electrical properties. [6]

10. Types of Nanomaterials:

NPs are divided into numerous classes based on their morphology, size, and chemical properties. Based on physical and chemical properties, some of the most well-known classes of NPs are mentioned below [7].

10.1. Carbon-based NPs.

Carbon nanotubes (CNTs) and fullerenes are two main groups of carbon-based NPs.

10.1.1. Fullerenes.

Fullerenes (C₆₀) are spherical carbon molecules composed of carbon atoms joined by sp² hybridization. The spherical structure consists of around 28 to 1500 carbon atoms, with diameters ranging from 8.2 nm for single layers to 4 - 36 nm for multi-layered fullerenes [8]. Fullerenes contain nanomaterials comprised of globular hollow cages, such as allotropic forms of carbon. Commercial interest has been generated by their electrical conductivity, high strength, structure, electron affinity, and flexibility [9].

10.1.2. Graphene.

Graphene is a kind of carbon. Graphene is a two-dimensional planar hexagonal honeycomb lattice network of carbon atoms. A graphene sheet typically has a thickness of 1 nm [10].

10.1.3. Carbon nanotubes (CNT).

Carbon nanotubes (CNT) are made from graphene nano sheets with a honeycomb structure of atoms arranged into hollow coils to form nanotubes with sizes as small as 0.7 nm for single-layered CNT and 100 nm for multi-layered CNT, with lengths ranging from a few micrometers to several millimeters. The ends can be empty or closed with half fullerene molecules [11]. These have a structure that is akin to a graphite sheet rolling on itself [12]. The rolled sheets are referred to as single-walled (SWNTs), double-walled (DWNTs), or multi-walled carbon nanotubes (MWNTs) since they can have one, two, or multiple walls. It is common to create carbon precursors by deposition, particularly atomic carbon precursors. Carbons are vaporized from graphite and deposited on metal particles using a laser or an electric arc. Recently, they have been produced using the chemical vapor deposition (CVD) method [13].

10.1.4. Carbon nanofiber.

Carbon nanofiber is created in the same way that graphene nano foil and carbon nanotubes are. The distinction is that instead of conventional cylindrical tubes, it is twisted into a cone shape [14].

10.1.5. Carbon black.

Amorphous carbon is typically spherical in shape, with diameters ranging from 20 to 70 nm. They aggregate because the particles interact quickly, resulting in roughly 500 nm agglomerates [15].

10.2. Metal NPs.

Metal-based nanoparticles are created by reducing metals to nanometric sizes through destructive or constructive processes. Almost all metals may be produced using nanoparticles [16]. Aluminum, cadmium, cobalt, copper, gold, iron, lead, silver, and zinc are often utilized in the synthesis of nanoparticles. Nanoparticles have unique characteristics such as diameters ranging from 10 to 100nm, surface characteristics such as pore size, high surface to volume ratio, surface charge with density, crystalline structures, spherical morphologies, color, reactivity, and sensitivity. Metal precursors are employed in the creation of metal nanoparticles. These NPs have distinct optoelectrical properties due to restricted surface plasmon resonance (SPR). In the solar electromagnetic spectrum, noble metal and alkali NPs such as Cu, Au, and Ag exhibit a notable absorption band. In today's cutting-edge materials, the synthesis of size and shape-controlled metal NPs is critical [17].

10.3. Metal oxide nanoparticles synthesis.

Metals such as Cu and Ag, for example, can be extremely toxic to bacteria in trace amounts. Metals have been widely used as antimicrobial agents in a variety of applications in industry, healthcare, and agriculture in general due to their biocidal influence. Metals, unlike other antibacterial agents, are stable under present manufacturing settings and can thus be employed as additives [58,59]. These metal-based additives are currently available in a variety of forms, such as particles, ions absorbed/exchanged in different carriers, salts, hybrid structures, and so on. Many metal oxide nanoparticles have been investigated for electrochemical detection of biomolecules, including ZnO, NiO, MnO₂, TiO₂, Fe₂O₃, and Co₃O₄. Furthermore, mixed metal oxides have gotten a lot of attention in this field. CuO-NPs have distinct properties that make them valuable in a variety of applications, including super-strong materials, sensors, antibacterial agents, and catalysts. Because of the large surface area to volume ratio, it can also interact with other nanoparticles. CuO-NPs have recently been proven to be more effective against E coli and B subtilis than Ag-NPs. Because they are polymer-coated, CuO-NPs are

extensively used as antibacterial agents in paints and textiles. TiO_2 and ZnO are often used because of their photolytic properties. Other fascinating metal-oxide NPs include CeO_2 , CrO_2 , MoO_3 , Bi_2O_3 , and LiCoO_2 . CeO_2 is increasingly being employed as a combustion catalyst in diesel fuels to improve emission quality. Under biological conditions, iron oxide NPs (IO-NPs) must be highly crystalline, monodisperse, and water-soluble, with high magnetization values, reproducible quality, and acceptable biocompatibility. The two forms of superparamagnetic IONP-based nanoparticles are superparamagnetic iron-oxide (SPIO) nanoparticles with a mean crystal size of 50-100 nm and ultra-small superparamagnetic iron-oxide (USPIO) nanoparticles with a size less than 50 nm.[18-20]

10.4. Ceramics NPs.

Ceramic nanoparticles (NPs) are nonmetallic inorganic solids formed by heating and cooling. They are available in a variety of shapes and sizes, including amorphous, polycrystalline, dense, porous, and hollow materials. Researchers are paying close attention to these NPs because to their use in applications such as catalysis, photo-degradation of dyes, photo-catalysis, and imaging [21].

10.5. Semiconductor NPs.

Semiconductor materials have qualities that are halfway between metals and nonmetals, providing them a wide range of applications in the literature. Bandgap tuning resulted in considerable changes in the characteristics of semiconductor NPs due to their large bandgaps. As a result, they play an important role in photocatalysis, photo optics, and electronic devices. Several semiconductor NPs are very efficient in water splitting applications due to their ideal bandgap and band edge placements [22].

10.6. Polymeric NPs.

These are often organic-based NPs that are referred to in the literature as polymer nanoparticles (PNPs). They are often nano-spherical or nano capsular in shape. The former are matrix particles with a solid overall mass, whilst the other molecules are adsorbed at the spherical surface's outside edge. The solid mass is entirely enclosed within the particle in the later scenario. Because PNPs are easy to functionalize, they have a wide range of applications in the literature. Lipid nanotechnology is a subfield that focuses on the design and fabrication of lipid nanoparticles for a variety of applications, including drug delivery and RNA release in cancer.[23]

11. Conclusions

Nanoparticles with varying properties are a common form of nanomaterial that has contributed in the growth of nanotechnology. Scientists interested in such approaches have lately produced their nanocomposites as a result of recent advances in the properties of new nanomaterials and their applications. This article defined nanotechnology and explained the procedures used to create nanomaterials from metals, metal oxides, graphene oxides, and polymers. Green techniques, such as plant extracts and microorganism biomolecules, are promising possibilities for synthesis of nanoparticles with low or no toxicity when compared to other methods. This review opens up new avenues for the creation and application of different nanomaterials.

References:-

1. Farooqi, Z.U.R.; Qadeer, A.; Hussain, M.M.; Zeeshan, N.; Ilic, P. Characterization and physicochemical properties of nanomaterials. In *Nanomaterials: Synthesis, Characterization, Hazards and Safety*; Elsevier: 2021, 97-121, <https://doi.org/10.1016/C2020-0-00287-2>.
2. Salem, S.S.; Fouda, A. Green Synthesis of Metallic Nanoparticles and Their Prospective Biotechnological Applications: an Overview. *Biological Trace Element Research* 2021, 199, 344-370, <https://doi.org/10.1007/s12011-020-02138-3>.
3. Varghese, R.J.; Parani, S.; Thomas, S.; Oluwafemi, O.S.; Wu, J. Introduction to nanomaterials: synthesis and applications. In *Nanomaterials for Solar Cell Applications*; Elsevier: 2019, 75-95, <https://doi.org/10.1016/C2016-0-03432-0>.
4. Barik, T.K.; Maity, G.C.; Gupta, P.; Mohan, L.; Santra, T.S. *Nanomaterials: An Introduction. Nanomaterials and Their Biomedical Applications* 2021, 16, 1.

5. Singh, B.K.; Lee, S.; Na, K. An overview on metal-related catalysts: metal oxides, nanoporous metals and supported metal nanoparticles on metal organic frameworks and zeolites. *Rare Metals* 2020, 39, 751-766, <https://doi.org/10.1007/s12598-019-01205-6>.
6. Salem, S.S.; Fouda, M.M.G.; Fouda, A.; Awad, M.A.; Al-Olayan, E.M.; Allam, A.A.; Shaheen, T.I. Antibacterial, Cytotoxicity and Larvicidal Activity of Green Synthesized Selenium Nanoparticles Using *Penicillium corylophilum*. *Journal of Cluster Science* 2021, 32, 351-361, <https://doi.org/10.1007/s10876-020-01794-8>.
7. Khan, S.; Mansoor, S.; Rafi, Z.; Kumari, B.; Shoaib, A.; Saeed, M.; Alshehri, S.; Ghoneim, M.M.; Rahamathulla, M.; Hani, U. A review on nanotechnology: Properties, applications, and mechanistic insights of cellular uptake mechanisms. *Journal of Molecular Liquids* 2021, 118008, <https://doi.org/10.1016/j.molliq.2021.118008>.
8. Pérez-Hernández, H.; Pérez-Moreno, A.; Sarabia-Castillo, C.; García-Mayagoitia, S.; Medina-Pérez, G.; López-Valdez, F.; Campos-Montiel, R.; Jayanta-Kumar, P.; Fernández-Luqueño, F. Ecological Drawbacks of Nanomaterials Produced on an Industrial Scale: Collateral Effect on Human and Environmental Health. *Water, Air, & Soil Pollution* 2021, 232, 1-33, <https://doi.org/10.1007/s11270-021-05370-2>.
9. Singh, R.; Singh, S. Nanomanipulation of consumer goods: effects on human health and environment. In *Nanotechnology in Modern Animal Biotechnology*; Springer: 2019, 221-254, https://doi.org/10.1007/978-981-13-6004-6_7.
10. Pathakoti, K.; Goodla, L.; Manubolu, M.; Hwang, H.-M. Nanoparticles and Their Potential Applications in Agriculture, Biological Therapies, Food, Biomedical, and Pharmaceutical Industry: A Review. *Nanotechnology and Nanomaterial Applications in Food, Health, and Biomedical Sciences* 2019, 121-162.
11. Elkodous, M.A.; El-Husseiny, H.M.; El-Sayyad, G.S.; Hashem, A.H.; Doghish, A.S.; Elfadil, D.; Radwan, Y.; El-Zeiny, H.M.; Bedair, H.; Ikhdair, O.A.; et al. Recent advances in waste-recycled nanomaterials for biomedical applications: Waste-to-wealth. *Nanotechnology Reviews* 2021, 10, 1662-1739, <https://doi.org/10.1515/ntrev-2021-0099>, <https://doi.org/10.1515/ntrev-2021-0099>.
12. Bayda, S.; Adeel, M.; Tuccinardi, T.; Cordani, M.; Rizzolio, F. The history of nanoscience and nanotechnology: from chemical-physical applications to nanomedicine. *Molecules* 2020, 25, 112, <https://doi.org/10.3390/molecules25010112>.
13. Qiu, L.; Zhu, N.; Feng, Y.; Michaelides, E.E.; Żyła, G.; Jing, D.; Zhang, X.; Norris, P.M.; Markides, C.N.; Mahian, O. A review of recent advances in thermophysical properties at the nanoscale: From solid state to colloids. *Physics Reports* 2020, 843, 1-81, <https://doi.org/10.1016/j.physrep.2019.12.001>.
14. Chivere, V.T.; Kondiah, P.P.; Choonara, Y.E.; Pillay, V. Nanotechnology-based biopolymeric oral delivery platforms for advanced cancer treatment. *Cancers* 2020, 12, 522, <https://doi.org/10.3390/cancers12020522>.
15. El-Naggar, M.E.; Hasanin, M.; Hashem, A.H. Eco-Friendly Synthesis of Superhydrophobic Antimicrobial Film Based on Cellulose Acetate/Polycaprolactone Loaded with the Green Biosynthesized Copper Nanoparticles for Food Packaging Application. *Journal of Polymers and the Environment* 2021, <https://doi.org/10.1007/s10924-021-02318-9>.
16. Alvandi, N.; Rajabnejad, M.; Taghvaei, Z.; Esfandiari, N. New generation of viral nanoparticles for targeted drug delivery in cancer therapy. *Journal of Drug Targeting* 2021, 1-15, <https://doi.org/10.1080/1061186X.2021.1949600>.
17. Shaheen, T.I.; Fouda, A.; Salem, S.S. Integration of Cotton Fabrics with Biosynthesized CuO Nanoparticles for Bactericidal Activity in the Terms of Their Cytotoxicity Assessment. *Industrial and Engineering Chemistry Research* 2021, 60, 1553-1563, <https://doi.org/10.1021/acs.iecr.0c04880>.
18. Hasanin, M.; Hashem, A.H.; El-Rashedy, A.A.; Kamel, S. Synthesis of novel heterocyclic compounds based on dialdehyde cellulose: characterization, antimicrobial, antitumor activity, molecular dynamics simulation and target identification. *Cellulose* 2021, 28, 8355-8374, <https://doi.org/10.1007/s10570-021-04063-7>.
19. Hasanin, M.; Elbahnasawy, M.A.; Shehabeldine, A.M.; Hashem, A.H. Ecofriendly preparation of silver nanoparticles-based nanocomposite stabilized by polysaccharides with antibacterial, antifungal and antiviral activities. *BioMetals* 2021, 34, 1313-1328, <https://doi.org/10.1007/s10534-021-00344-7>.
20. Thakur, M.; Poojary, S.; Swain, N. Green Synthesis of Iron Oxide Nanoparticles and Its Biomedical Applications. *Nanotechnology Applications in Health and Environmental Sciences* 2021, 83-109, https://doi.org/10.1007/978-3-030-64410-9_5.
21. Hashem, A.H.; Al Abboud, M.A.; Alawlaqi, M.M.; Abdelghany, T.M.; Hasanin, M. Synthesis of Nanocapsules Based on Biosynthesized Nickel Nanoparticles and Potato Starch: Antimicrobial, Antioxidant, and Anticancer Activity. *Starch - Stärke n/a*, 2100165, <https://doi.org/10.1002/star.202100165>.
22. Elbasuney, S.; El-Sayyad, G.S.; Tantawy, H.; Hashem, A.H. Promising antimicrobial and antibiofilm activities of reduced graphene oxide-metal oxide (RGO-NiO, RGO-AgO, and RGO-ZnO) nanocomposites. *RSC Advances* 2021, 11, 25961-25975, <https://doi.org/10.1039/D1RA04542C>.
23. Shehabeldine, A.M.; Hashem, A.H.; Wassel, A.R.; Hasanin, M. Antimicrobial and Antiviral Activities of Durable Cotton Fabrics Treated with Nanocomposite Based on Zinc Oxide Nanoparticles, Acyclovir, Nanochitosan, and Clove Oil. *Applied Biochemistry and Biotechnology* 2021, <https://doi.org/10.1007/s12010-021-03649-y>.
24. Campisi, S.; Schiavoni, M.; Chan-Thaw, C.E.; Villa, A. Untangling the role of the capping agent in nanocatalysis: recent advances and perspectives. *Catalysts* 2016, 6, 185, <https://doi.org/10.3390/catal6120185>.
25. Sharaf, O.M.; Al-Gamal, M.S.; Ibrahim, G.A.; Dabiza, N.M.; Salem, S.S.; El-ssayad, M.F.; Youssef, A.M. Evaluation and characterization of some protective culture metabolites in free and nano-chitosan-loaded forms against common contaminants of Egyptian cheese. *Carbohydrate Polymers* 2019, 223, <https://doi.org/10.1016/j.carbpol.2019.115094>.

Synthesis and Optically Stimulated Luminescence (OSL) Properties of CaSiO₃: Ce, Al Phosphor for Radiation dosimetry

* C. B. Palan¹, A.O.Chauhan², N.S. Sawala³, S. K. Omanwar⁴

¹Department of Physics, Bapumiya Sirajoddin Patel Art's, Commerce and Science College, Pimpalgaon Kale, Buldhana, India

²Department of Physics, Vidya Bharati Mahavidyalaya, Amravati, India

³Science and Humanities Department, Government Polytechnic, Arvi, India

⁴Department of Physics, Sant Gadge Baba Amravati University, Amravati, India

*(Corresponding author email:chetanpalan27@gmail.com)

Abstracts

The CaSiO₃: Ce, Al phosphor was synthesized via Solid State Diffusion Method. The crystallinity of the phosphor was investigated by using X-ray diffraction (XRD). The CaSiO₃: Ce, Al phosphor has been investigated for its photoluminescence (PL) and Optically Stimulated Luminescence (OSL) studied. PL spectra showed the characteristic emission of Ce ion at 377 nm when excited by 326 nm.

Keywords: - CaSiO₃: Ce, Al Phosphor; Solid State Diffusion Method; Radiation Dosimetry and OSL.

1. Introduction

Silicates are widely used as phosphor hosts due to their abilities to incorporate rare-earth and transition-metal ions as luminescent centres, excellent chemical and thermal stability, high energy efficiency, visible-light transparency, high yield, easy fabrication, and wide availability of inexpensive raw materials [1]. Silicates have a basic tetrahedral geometry (SiO₄) with a variety of crystal structures including single, twin, cluster, ring, chain, and network structures [2]. Silicate phosphor has been widely used in colour television, flat panel display screen and cathode-ray luminescence tubes. Recently, the luminescent properties of rare-earth ion doped silicates phosphors have been widely investigated because of their possible applications in white LEDs [3]. Moreover among the series of silicates, one of the ceramic materials, Calcium silicates (CaSiO₃) is found as a mineral in the lower mantle of the earth. It has a 'distorted cubic' structure. CaSiO₃ also known as wollastonite is a good matrix for luminescent materials. It has also many important properties such as good and high temperature strength, chemical inertness, low thermal conductivity and thermal stability [4]. Hence, it is suitable in many applications.

To our knowledge, OSL properties of Al Co-doped CaSiO₃:Ce phosphor under beta irradiation has not been reported in the literature. Hence, the synthesis of CaSiO₃: Ce, Al by using solid-state diffusion method and its luminescence properties (PL, and TL) were investigated.

2. Experimental

CaSiO₃: Ce, Al phosphors was synthesized by using Solid State Diffusion Method [5]. Phase purity of CaSiO₃: Ce, Al phosphor was checked by means of X-ray powder diffraction (PXRD) using a Rigaku miniflex II diffractometer. The OSL measurement was carried out using an automatic Risø TL/OSL-DA-15 reader system at RPAD division BARC (Mumbai). PL and PL excitation (PLE) spectra were measured on (Hitachi F-7000) fluorescence spectrophotometer.

3. Results and discussions

3.1 XRD-Pattern

The XRD pattern of the as synthesised CaSiO_3 : Ce, Al phosphor was represent in Fig. 1. XRD patterns was fully matched with the International center for diffraction data (ICDD) file with card no 01-075-1396.

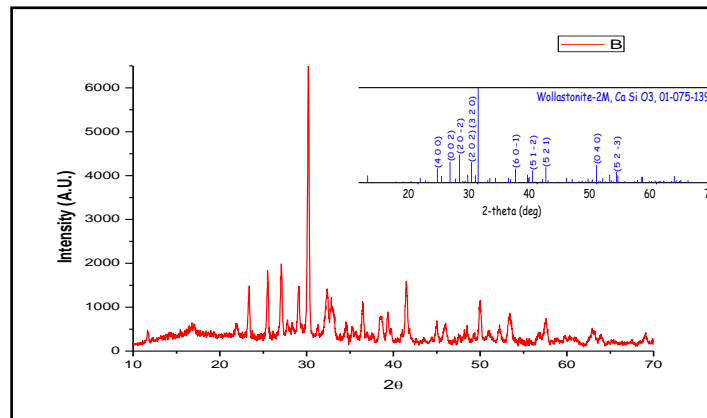


Fig. 1 XRD pattern of the CaSiO_3 : Ce, Al sample and match with the International Center for Diffraction Data & Card No-01-075-1396.

3.2 Photoluminescence (PL)

Fig 2. shows the combined excitation and emission spectra of CaSiO_3 : Ce and CaSiO_3 : Ce, Al phosphor. The excitation spectra were monitored at 377 nm and emission spectra were monitored at 326 nm. The excitation spectra consists of broad band around 200-350 nm corresponds to the $4f\ 5d^1$ to $4f^7$ ($^8S_{1/2}$) allowed transition of Ce^{3+} ions. Predominant excitation peak for Ce is in near UV region under the excitation wavelength of 326 nm. The emission spectra consist of broad band from 350 to 450 nm.

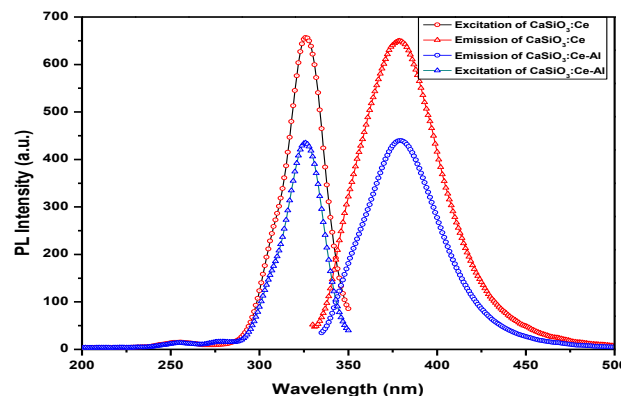
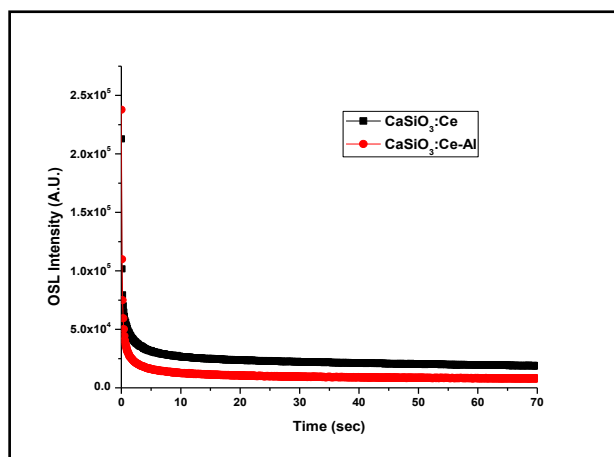


Fig. 2 Excitation and Emission spectra of CaSiO_3 : Ce & CaSiO_3 : Ce, Al phosphor under UV excitation

From Fig. 2 it is clear that PL intensity increases by adding Aluminum as co-dopant in CaSiO_3 :Ce. The emission spectra consist broad in range 325-500 nm and maximum intensity observed at 377 nm correspond to $5d-4f$ ($^2F_{5/2}$) transitions of Ce [6].

3.3 Continuous wave OSL (CW-OSL)

OSL measurements were carried out in continuous wave (CW) mode using blue LED stimulation of wavelength 470 nm. Phosphor were irradiated to beta source with dose range 20 mGy/Sec. Fig 3 shows the comparison of CW-OSL response of CaSiO_3 : Ce & CaSiO_3 : Ce, Al phosphor. From Fig. 3 observed that OSL sensitivity of CaSiO_3 : Ce, Al was found to be 1.15 times that of the CaSiO_3 : Ce phosphor.



. Fig. 3 CW-OSL curves for an absorbed dose of 20 mGy from beta source

4. Conclusions

The development of the new phosphor could be applicable for radiation dosimetry technique. Synthesis technique of $\text{CaSiO}_3:\text{Ce}$ & $\text{CaSiO}_3:\text{Ce, Al}$ simple, cost effective with readily available raw material and is acquiescent to large-scale production of the phosphor. The X-ray diffraction patterns matches well with the ICDD files and gives the exact crystal structure as required from the synthesized materials. The Effective atomic number of CaSiO_3 is 15.3. The OSL sensitivity of $\text{CaSiO}_3:\text{Ce, Al}$ phosphor was found to be 1.15 times that of $\text{CaSiO}_3:\text{Ce}$ phosphor. Photoluminescence (PL) emission spectrum consists of broad band characteristics of Ce emission in the range of 350-450 nm. Hence, this phosphor could be one of promising candidate in radiation dosimetry applications.

5. References

- [1] Yang L., Fang M., Du L., Zhang Z., Ren L., Yu Z. (2008) *Mat. Res. Bull.* 43, 2538–2543
- [2] Komukai K., Takatsuka Y., HidekiKato, Kakihana M. (2015) *J. Lumin.* 158,328–332
- [3] Wen D., Yang G., Yang H., Shi J., Gong M., Wu M. (2014) *Mater. Lett.*125,63–66
- [4] Nagabhushana H., Nagabhushana B. M., Madesh Kumar M., Premkumar H.B., Shivakumara C, Chakradharg R. P. *S Spectrochim. Acta A* (2011) 78, 64–69
- [5] C.B. Palan, K.A. Koparkar, N.S. Bajaj, S.K. Omanwar *Mater. Lett.*175 (2016) 288-290
- [6] Wu, Y., Ren, G., Ding, D., Yang, F., Pan, S. *Cryst Eng Comm.* 14, (2012) 1998

Synthesis and Characterization of NB-UVB emitting Yttrium phosphate phosphor

A. O. Chauhaan^{1*}, C. B. Palan², N. S. Sawala³, G. T. Lamdhade¹,
K. B. Raulkar¹, R. B. Butley¹, C. C. Jadhao¹

¹Department of Physics, Vidya Bharati Mahavidyalaya, Amravati (MH), 444602 India

²Department of Physics, Bapumiya Sirajoddin Patel Art's, Commerce and Science College, Pimpalgaon Kale, Buldhana, India

³Science and Humanities Department, Government Polytechnic, Arvi, India

* corresponding author : abhi2718@gmail.com

Abstract

For the treatment of psoriasis, vitiligo, atopic dermatitis (eczema), and other photo responsive skin conditions, narrowband UVB has emerged as the preferred phototherapy option. The narrowband UVB emitting polycrystalline sample YPO_4 doped with Gadolinium (Gd^{3+}) was prepared by the Re-crystallization method. The phase formation of the samples was investigated by X-ray powder diffraction (XRD) measurement. The optical property of sample such as photoluminescence (PL) was carried by fluorescence spectrophotometer. The surface morphology of as prepared phosphor was studied by Scanning Electron Microscope (SEM). The photoluminescence spectra showed that the sharp narrow band UVB emission maxima of $\text{YPO}_4:\text{Gd}^{3+}$ is observed at 312 nm, which is in accordance with the ${}^6\text{P}_1 \rightarrow {}^8\text{S}_{7/2}$ optical transition of Gd^{3+} ions. The Stokes shift of the synthesized materials was measured from obtained wavelength of excitation and emission. Because of narrow band UVB emission, this phosphor can be served as a prime candidate for phototherapy application.

Keywords: Narrowband UVB, Stoke shift, Phototherapy, XRD, SEM.

1. INTRODUCTION

The development of luminescent materials has been the subject of extensive research in the past few decades. Luminescent materials in the form of nanostructures have shown some interesting optical properties. These materials have implications in development of a novel type of phosphors for phototherapy applications. The spectrum of electromagnetic radiation is consisted of different wavelengths ranging from 100 nanometers (nm) in the ultraviolet (UV) range to 1 millimeter (mm) in the infrared (IR) range. The division of whole electromagnetic spectrum occupied by ultraviolet radiations (UVR). The convenient partition of ultraviolet radiation take place according to their Biological and Physical characteristic such as UV-C: the rays that do not pass through the earth's atmosphere (200-290 nm) UV-B: the rays responsible for nearly all biological effects following sun light exposure including tanning, burning and skin cancer, (290-320 nm) and UV-A: those rays closest to the visible spectrum that pass-through glass and are the least harmful to the skin (320-400nm) [1]. Ultraviolet radiation (UVR) is well established for treating the more than 40 skin diseases such as psoriasis [2], or vitiligo [3], which could be treated by UV-B radiation, and lichen sclerosus [4], morphea [5] scleroderma [6], cutaneous T-cell lymphoma, lupus erythematosus [7], which could be treated by UV-A radiation. In the treatment of hyperbilirubinemia [8], commonly known as infant jaundice.

Ultraviolet B (UVB) has become the phototherapy treatment of choice for Psoriasis, Vitiligo, Atopic dermatitis (eczema) and other photo-responsive skin disorders. UVB can be divided as narrow-band UVB and broadband UVB. Broadband UVB radiation has been used for the treatment of Psoriasis for decades [9]. Various investigations imply that the Narrowband

ultraviolet-B (NB-UVB) (311-313 nm) is the most favorable range phototherapy than the Broad band ultraviolet-B radiation.

The commercial phosphor $\text{LaB}_3\text{O}_6:\text{Gd}^{3+}$, Bi^{3+} and $\text{CeMgB}_5\text{O}_{10}:\text{Gd}^{3+}$ is used for narrow UVB phototherapy lamps. In our previous work we have reported some UV emitting phosphor materials such as $\text{Na}_2\text{La}_2\text{B}_2\text{O}_7$ [10], $\text{Sr}_2\text{Mg}(\text{BO}_3)_2:\text{Pb}^{2+}$, Gd^{3+} [11], $\text{KCa}_4(\text{BO}_3)_3:\text{Pb}^{2+}$ [12], YBO_3 [13] and $\text{Sr}_2\text{Mg}(\text{BO}_3)_2:\text{Pr}^{3+}$, Gd^{3+} [14].

2. EXPERIMENTAL

2.1 Synthesis of material

The phosphor Gd^{3+} doped YPO_4 was prepared by Re-crystallization method. The stoichiometric amounts of high purity Y_2O_3 (AR) and Gd_2O_3 (AR) were dissolved in to concentrate HNO_3 with deionized water. The resulting solution was considered as $\text{Y}(\text{NO}_3)_3:\text{Gd}^{3+}$. The solution of di-ammonium orthophosphate was added dropped by dropped in formed nitrate solution. The entire homogenous solution was then placed on a hot plate at 70°C for slow evaporation of excess water. The dried precursor was finally crushed and heated at 900°C for 2hr to get white crystalline powder of $\text{YPO}_4:\text{Gd}^{3+}$. The resultant powder sample was then characterized using powder XRD and Spectrophotometer.

2.2. Characterization of samples

The phase purities of $\text{YPO}_4:\text{Gd}^{3+}$ sample was studied using Rigaku miniflex II X-ray Diffractometer with scan speed of 6.000_/min and Cu K α ($k = 1.5406 \text{ \AA}$) radiation in the range $10\text{-}90^\circ$. PL and PL excitation (PLE) spectra were measured on (Hitachi F-7000) fluorescence spectrophotometer at room temperature. The parameters such as spectral resolution, width of the monochromatic slits (1.0 nm), photomultiplier tube (PMT) detector voltage and scan speed were kept constant throughout the analysis of samples.

3. RESULT AND DISCUSSIONS

3.1 Structural properties

The formation crystalline phase of the YPO_4 prepared by Re-crystallization was confirmed by XRD pattern, as shown in Fig. 1. The $\text{YPO}_4:\text{Gd}^{3+}$ XRD pattern and the standard data from the ICDD file (01-084-0335) matched quite well.

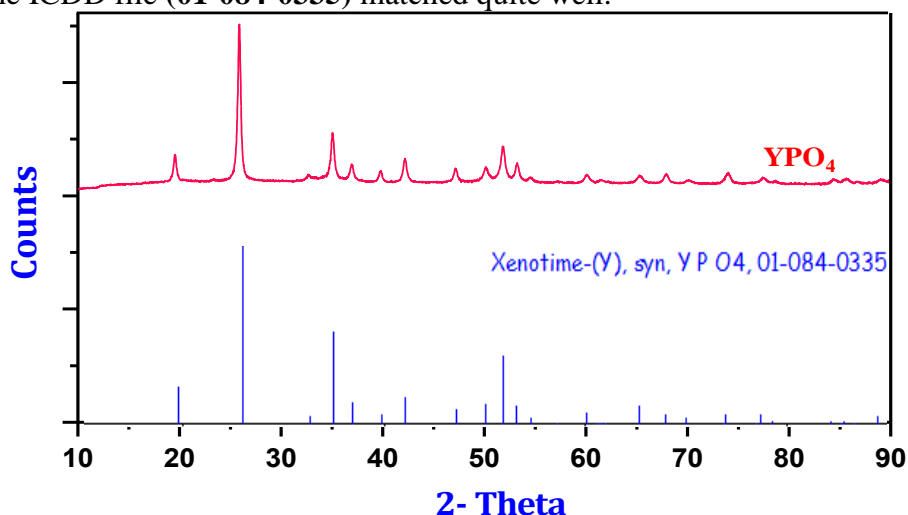


Fig 1. XRD pattern of YPO_4 doped with Gd^{3+} ion.

Additionally, the XRD show that the formed material was completely crystalline and was in single phase, where $a = b = 6.8817$ and $c = 6.0177 \text{ \AA}$. The space group for YPO_4 was I41/amd 141). Furthermore, as the figure illustrates, the addition of the dopant had no

discernible impact. The ionic radii of Y^{3+} ion (0.9\AA) and Gd^{3+} ion (0.93\AA) are quite similar. Therefore, we can deduce that Gd^{3+} ions will substitute for Y^{3+} ions.

3.2 Morphological Study

Fig. 2 shows the FE-SEM images of $\text{YPO}_4:\text{Gd}^{3+}$ powder prepared at $900\text{ }^\circ\text{C}$. The heating at a high temperature caused the phosphor to become strongly agglomerated. It was found that the average particle size was between $1 - 5\text{ }\mu\text{m}$. The findings demonstrate that phosphors have a low sinter temperature and good crystallinity.

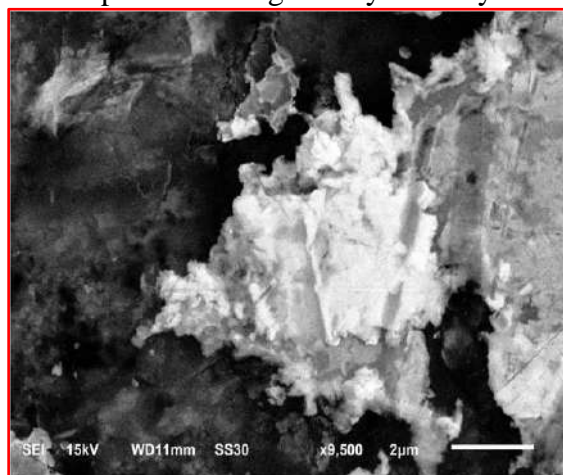


Fig 2. FE-SEM image of $\text{YPO}_4:\text{Gd}^{3+}$ phosphor

3.3 Photoluminescence Analysis

It is well recognized that the ultraviolet radiations mainly those in the UVB ($280 - 320\text{ nm}$) region are useful for phototherapy. The Gd^{3+} ion doped phosphors which give emission in the narrow UVB region ($280 - 320\text{ nm}$) are used in phototherapy lamps; therefore it is usually useful for the treatment of many skin diseases such as psoriasis, vitiligo, atopic dermatitis, etc.

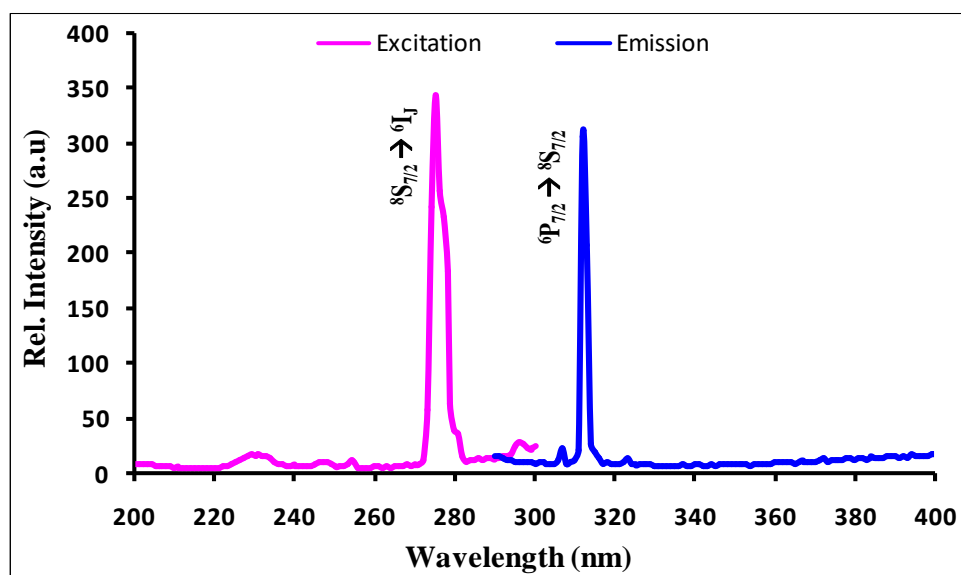


Fig 3. Photoluminescence spectra of Gd^{3+} ion activated YPO_4 phosphor.

Fig 3. represents the room temperature Photoluminescence spectra for sample of composition $\text{Y}_{0.99}\text{Gd}_{0.01}\text{PO}_4$. The phosphor gives sharp narrow emission in the UVB region around 312 nm corresponding to ${}^6\text{P}_{7/2} \rightarrow {}^8\text{S}_{7/2}$ transition under the excitation of 276 nm . In the emission spectra there was a weak line observed at 304 nm . These lines correspond to the ${}^6\text{P}_{5/2} \rightarrow {}^8\text{S}$ transitions of the Gd^{3+} ion. Finally, the stoke shift was calculated to be 4312 cm^{-1}

4. CONCLUSIONS

The low-cost, low-temperature Re-crystallization approach was successfully used to synthesize the inorganic narrow UVB emitting $\text{YPO}_4:\text{Gd}^{3+}$ phosphor. The prepared sample's XRD pattern was determined to be fully crystalline and to be in conformity with the corresponding ICDD data. The study of photoluminescence qualities led to the conclusion that phosphor exhibits UV emission, making it useful for phototherapy lamps. The SEM image demonstrates the processes of agglomeration and uneven grain size. The photoluminescence spectra show that, when excited to 275 nm, the $\text{YPO}_4:\text{Gd}^{3+}$ produces sharp, narrow UVB emission at 312 nm which shows this phosphor is a potential candidate for phototherapy lamp phosphor for treating many skin diseases.

5. ACKNOWLEDGEMENTS

One of the authors Abhijit O. Chauhan is thankful to the Chairman FIST-DST Project, SGBA University, Amravati (MH), PIN- 444602 INDIA for providing XRD facility for this work. The author thanks to Dr. S. B. Kondawar, Department of Physics RTM University Nagpur (MH), and PIN-440013 INDIA for providing the access of SEM.

6. REFERENCES

- [1] Hoare, C., Po, W., Li, A., and Williams, H. 2000. Systematic review of treatments for atopic eczema. *Health Technol. Assess.*, 4, 88.
- [2] H. Honigsmann, W. Brenner, W. Rauschmeier, *Am. Acad. Dermatol.*, 10, (1984), 238.
- [3] L. Scherschun, J.J. Kim, W.H. Lim, *J. Am. Acad. Dermatol.*, 44, (2001), 999.
- [4] A. Kreuler, T. Jansen, M. Stucker, M. Herde, K. Hoffmann, P. Altmeyer, G. Vonkobyletzki, *Clin. Exp. Dermatol.*, 26, (2001), 30.
- [5] J. Hawk, *Radiat. Prot. Dosim.*, 91, (2000), 143.
- [6] A. Morita, K. Kobayashi, I. Isomura, T. Tsuji, J. Krutmann, *J. Am. Acad. Dermatol.*, 43, (2000), 670.
- [7] T. Millard, J. Hawk., *Lupus* 10, (2001), 185.
- [8] C. Dani, E. Martelli, M.F. Reali, G. Bertini, G. Panin, F. Rubaltelli, *J. Pediatr.*, 138, (2001), 438.
- [9] M. Weichenthal, T. Schwarz., *Photodermatol. Photoimmunol. Photomed.*, 21, (2005), 260.
- [10] P. Nagpure, S. Omanwar., *J. Lumin.*, 132, (2012), 2088.
- [11] S. Bhagat, A. Gawande, S. Omanwar, *Opt. Mater.*, 40, (2015), 36.
- [12] A. Gawande, R. Sonekar, S. Omanwar, *J. Lumin.*, 149 (2014) 200.
- [13] A. Gawande, R. Sonekar, S. Omanwar, *Combust. Sci. Technol.*, 186, (2014), 785.
- [14] A. Gawande, R. Sonekar, S. Omanwar, *Mater. Res. Bull.*, 60, (2014), 285.

Photoluminescence Studies of Eu (III) activated YBaB₉O₁₆ phosphor

A. O. Chauhan^{1*}, G. T. Lamdhade¹, K. B. Raulkar¹, R. B. Butley¹,
C. C. Jadhao¹, B. H. Bhatti²

¹Department of Physics, Vidya Bharati Mahavidyalaya, Amravati. 444602 (INDIA)

²Department of Physics, Indira Gandhi Mahavidyalaya, Ralegaon District- Yavatmal (445402), Maharashtra, India.

(Corresponding Author: *abhi2718@gmail.com)

Abstract :-

The trivalent Eu³⁺ doped YBaB₉O₁₆ phosphors were synthesized using the traditional solid state diffusion process and were characterized by X-ray diffraction (XRD), photoluminescence (PL) excitation and emission measurements. Under UV stimulation, strong orange emission was seen, with the dominant peak of the radiation coming from the ⁵D₀ → ⁷F₁ transitions of Eu³⁺ ions at 590 nm.

Keyword: - XRD, Photoluminescence, Solid State reaction, UV Excitation.

1. INTRODUCTION

REBa₉O₁₆ phosphors were first reported by Fouassier and co-workers [1, 2]. They studied luminescence of europium in these systems for rare earth (RE = La, Gd or Y). These compounds contain two different kinds of cations RE³⁺ and Ba²⁺ by doping with different rare earth ions, such as Eu²⁺, Tb³⁺ and Eu³⁺, efficient blue, green and red colour phosphors can be obtained, respectively in a single host. Therefore, these materials are considered to be suitable candidates as universal hosts of the luminescent materials for tri-color lamps. Subsequent research focused on YBaB₉O₁₆ since a number of yttrium compounds provide suitable hosts for rare earth luminescence [3–7], and GdBaB₉O₁₆, in context of the role of Gd³⁺ as ‘sensitizer intermediate’ as well as for PDP application [8].

NdBaB₉O₁₆ has also been investigated as a potential laser material [9]. REBaB₉O₁₆ (RE= La, Gd or Y) possesses a property like low alkaline earth content, they show a high chemical stability, favorable for use in fluorescent lamps [10]. Among Ln-doped materials, Eu³⁺-doped materials found much interesting due to simple lower energy levels scheme of Eu³⁺ ions as well as its applications as the red emitting phosphor by its intense, narrow and monochromatic red emission around 610 nm as a result of ⁵D₀ - ⁷F₂ transitions [11, 12].

Strong broad band luminescence is typically seen in Eu-doped solid-state materials, with decay times of between 600 and 1500 ns. From the ultraviolet to the red part of the electromagnetic spectrum, luminescence can occur, however it is very reliant on the host lattice. The intensity of the Eu emission is high enough to find significant industrial uses, such as in LEDs, electroluminescent lamps and display devices, X-ray imaging detectors, scintillation detectors, and fluoride doped with europium [13 - 16].

Due to their intense, narrow, and monochromatic ⁵D₀ → ⁷F₂ emission in the red spectral region, trivalent rare earth (Eu³⁺) doped yttrium-based phosphors with non centrosymmetric site have found widespread use in display panel applications of various types, including plasma display panels, light emitting diodes, and field emission displays. The reflecting layer, dielectric layer, black matrix, phosphors, and their blending gas mixture are some of the factors that affect the luminescence efficiency of fluorescent lamps [17, 18, 19]. Because of their resonant radiation of He-discharge (253.7 nm) and the excited state of molecular He ions, yttrium-based phosphors should exhibit good luminous qualities under ultraviolet (UV) light [20].

2. EXPERIMENTAL

The $\text{YBaB}_9\text{O}_{16}:\text{Eu}^{3+}$ phosphor was prepared by the Conventional solid state diffusion method. The starting raw material were stoichiometric mixture of reagent grade Y_2O_3 (S.D. fine), $\text{Ba}(\text{NO}_3)_2$ (Loba 99.9%), H_3BO_3 (Loba 99.9%), Eu_2O_3 (Loba 99.9%). The raw material yttrium oxide and Eu_2O_3 was boiled in HNO_3 (S.D. fine) and evaporated to dryness, so as to convert it into respective nitrate. The stoichiometric amounts of the ingredients were added in formed yttrium nitrate solution. These materials were thoroughly mixed in an Agate mortar with the help of pestle on adding a little amount of acetone and then transferred into china clay basin. After that the material was dried at 120°C for 1 h and sintered at 900°C for 4 h and then allowed to cool down to room temperature (RT). The prepared samples were again grinded and taken for characterizations.

3. RESULT AND DISCUSSION

3.1 XRD

The formation of the crystalline phase was confirmed by X-ray diffraction. Fig. 1 shows XRD pattern obtained for $\text{YBaB}_9\text{O}_{16}:\text{Eu}^{3+}$ powder prepared by Conventional solid-state method. The XRD patterns for samples sintered at 900°C agree well with ICDD card No. 00-055-0792. According to the standard X-ray diffraction pattern ICDD card No. 00-055-0792, the $\text{YBaB}_9\text{O}_{16}:\text{Eu}^{3+}$ lattice possesses Monoclinic structure with a space group $\text{P}2_1/\text{m}$ (10) with lattice parameters $a = 15.5720 \text{ \AA}$, $b = 3.892 \text{ \AA}$ and $c = 6.7427 \text{ \AA}$.

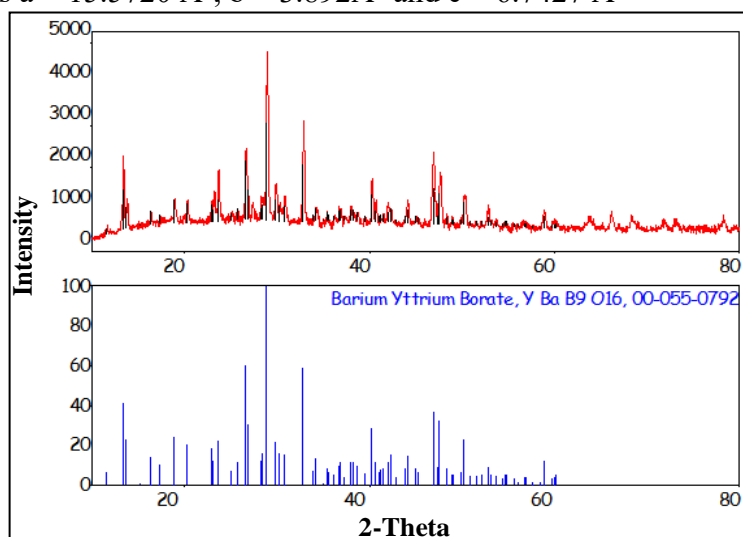


Figure 4 XRD pattern of $\text{YBaB}_9\text{O}_{16}:\text{Eu}^{3+}$ and matched with the ICDD card No. 00-055-0792.

3.2. Photoluminescence

Europium can act as an activator in two forms viz. Eu^{2+} and Eu^{3+} , because $\text{YBaB}_9\text{O}_{16}$ substitutional sites for both these varieties are available, respectively at Ba^{2+} and La^{3+} positions. Eu^{3+} or Eu^{2+} can be identified from the characteristic photo luminescence they exhibit.

Fig. 3 shows the emission spectra of $\text{YBaB}_9\text{O}_{16}:\text{Eu}^{3+}$ exhibits intense yellow emission at 590 nm under UV excitation which is excited by 231 nm. The emission spectrum consists of higher intensity peak at 590 nm under UV excitation which corresponds to the ${}^5\text{D}_0 \rightarrow {}^7\text{F}_1$ transition of Eu^{3+} . The other weak peak at 613 nm occurs which corresponds to the ${}^5\text{D}_1 \rightarrow {}^7\text{F}_2$ transition of Eu^{3+} ions.

Fig. 2 shows the photoluminescence excitation (PLE) spectra measured at 590 nm emission. The excitation spectrum shows that $\text{YBaB}_9\text{O}_{16}:\text{Eu}^{3+}$ has broad band absorption from 200 to 280 nm peaking at 231nm.

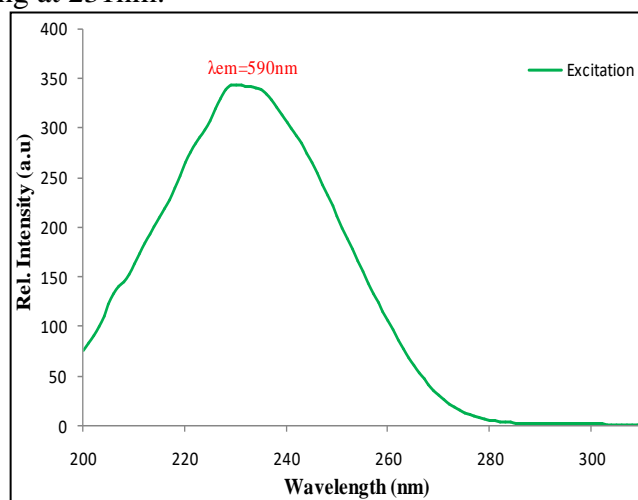


Figure 5 Excitation spectra of $\text{YBaB}_9\text{O}_{16}:\text{Eu}^{3+}$

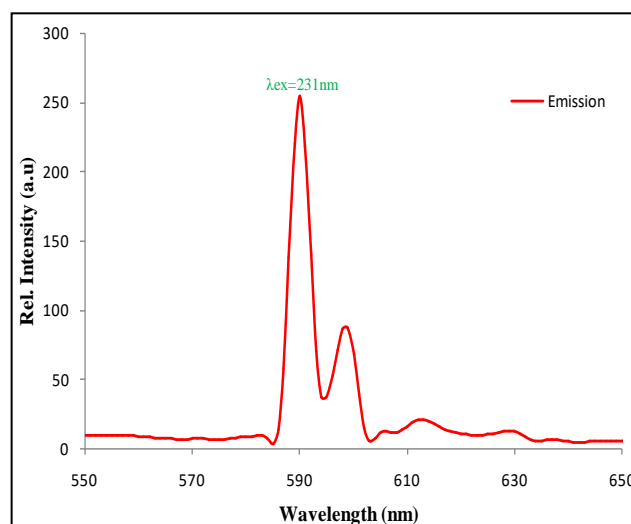


Figure 6 Emission Spectra of $\text{YBaB}_9\text{O}_{16}:\text{Eu}^{3+}$

4. CONCLUSION

The Eu^{3+} doped $\text{YBaB}_9\text{O}_{16}$ phosphor were successfully prepared by conventional solid state diffusion method. This phosphor shows a pure phase of $\text{YBaB}_9\text{O}_{16}:\text{Eu}^{3+}$. The study of the luminescence of Eu^{3+} doped $\text{YBaB}_9\text{O}_{16}$ shows optimum emission at 590nm under the 231nm UV excitation.

5. REFERENCES

1. W. T. Fu; C. Fouassier; P. Haggemuller, *Mater. Res. Bull.*, 23, **1989**, 389.
2. W. T. Fu; C. Fouassier; P. Haggemuller, *Mater. Res. Bull.*, 22, **1987**, 899-909.
3. A. M. Srivastav; M. T. Sobteraj; R. Geiger; E. Banks, *Mater. Chem. Phys.*, 21, **1989**, 327.
4. Z. Yang; J. H. Lin; M. Z. Su; L. P. You, *Mater. Res. Bull.*, 35, **2000**, 2173.
5. Z. Yang; J. H. Lin; M. Z. Su; Y. Tao; W. Wang, *J. Alloys. Compd.*, 308, **2000**, 94.
6. X. Z. Li; X. L. Chen; J. K. Lian; L. Wu; Y. P. Xu; Y. G. Cao, *J. Alloys. Compd.*, 365, (1-2), **2004**, 277-280.

7. W. Park; C. J. Summers; Y. R. Do; H. G. Yang, *J. Mater. Sci.*, 37, **2002**, 4041
8. H. You; X. Wu; X. Zeng; G. Hong; C. Kim; C. Pyun; C. Park; *Mater. Sci. Eng.*, B86, **2001**, 11.
9. Y. Ji; J. Liang; S. Xie; X. Wu, *J. Cryst. Growth*, 137, **1994**, 521.
10. W. T. Fu; C. Fouassier; P. Hagemuller, *Mat. Res. Bull.*, Vol. 22, 899-909, **1987**.
11. X. Guo; Y. Wang; J. Zhang, *J. Cryst. Growth*, 311, **2009**, 2409.
12. L. Li; S. Zhou; S. Zhang, *Solid State Sci.*, 10, **2008**, 1173.
13. F. C. Palilla; B. E. O'Reilly, *Journal of the Electrochemical Society*, Vol. 115(10), **1968**, 1076-1081.
14. G. Fasol, *Science*, Vol 272, (5269), **1996**, 1751- 1752.
15. M. K. Crawford; L. H. Brixner, *J. Lumin.*, Vols. 48-49, **1991** 37-42.
16. H. Heinz; V. Saggern, *Crystal Lattice Defects and Amorphous Materials*, Vol. 18, 1989, 399.
17. Z. Lu; T. Wanjun, *Cer. Inter.* 38, **2012**, 837.
18. P. A. Nagpure; S. K. Omanwar; *International Journal of Self-Propagating High-Temperature Synthesis*. 22 (1) **2013**, 32-36
19. H. S. Gong; H. G. Kim, *Cur. Appl. Phy.* 13, **2013**, 453.
20. A. P. Zambare; K. V. R. Murthy, *Arch. Phy. Res.* 2(3), **2011**, 46-50.

Recent Developments in the Study of Three-dimensional Spin Structure of the Proton

Dr. Bipin Sonawane,
Amity University Maharashtra.

Abstract:

As we all know that the matter around us is made up of atoms and we describe atomic structure in the terms of protons, neutrons, and electrons. Then there was a question, are these protons and neutron are elementary particles? Deep Inelastic Scattering (DIS) experiment investigated substructure of the proton in terms of massive quarks and further it was found these quarks are in a bound state due to massless gluons. These quarks and gluons, collectively known as partons, are forming a complex structure of the proton. Yes, it is a complex structure and these partons are designing a dynamical inner world of it. The study and its evolution have been moving further in recent years which have been further investigating the spin dynamical realm of these partons. In this study we focus on recent developments of three-dimensional spin structure of the proton. We review both theoretical and experimental developments to understand the recent spin structure of the proton. We discuss the idea of proton structure function and its evolution as spin dependent structure function. In the theoretical study we focus on calculation of cross sections for different quantum chromodynamical (QCD) processes like electroproduction and hadroproduction of J/ψ (a bound state of charm and anti-charm quarks) and pions. We discuss the spin crisis and subsequent measurement of an observable quantity called Transverse Single Spin Asymmetry (TSSA) and recent experimental data and its analysis. We also discuss the status of measurement of TSSA at RHIC-PHENIX, J-Lab, and SPD-NICA.

Key Words: QCD, DIS, RHIC, TSSA, PDF, TMD

Introduction:

The structure of the matter and its study of evolution is one of the fundamental research areas. Elementary particle physics addresses the most basic questions like what the constituents of matter are, what are the forces which govern these particles, how to detect them and so on. We have standard model of elementary particles which helps us to classify and study systematically these elementary particles. Now we know that standard model of elementary particles prescribes 36 quarks, 12 leptons, 12-gauge bosons and the Higgs boson which are members of standard model designing the most fundamental structure of matter. Now it is well known that the protons are made up of quarks and they are in a bound states because of gluons which are quanta of strong force. These are elementary particles having spin as a very important and a special property. In classical mechanics the spin as its own perspective, it is treated using the rotation of the particle with respect to its axis just like rotating earth and spinning top. The spin of particles like electron and proton [is](#) described by using intrinsic angular momentum.

Spin is one of the most fundamental concepts in physics which is needed for a deep and intuitive understanding of structure of matter and its interaction. Spin plays a crucial role in the theory of strong interaction i.e. Quantum Chromodynamics (QCD) and understanding of QCD phenomenology. In recent years, the study of QCD has been focused on the investigation of the spin structure of the nucleon. All the elementary particles in standard model can be classified into two groups based on their spin quantum number, $S = 1/2, 3/2 \dots$ for electrons, protons etc. they are fermions and $S = 0; 1; 2 \dots$ for photon, meson and they are bosons. The calculations of nucleon magnetic moments within quark model assume that quarks behave like

point Dirac particles with intrinsic magnetic moments. Magnetic dipole moment of a spin 1/2 particle with mass m and charge q is given as $\vec{\mu}_s = \frac{q}{m} \vec{S}$ where, $\vec{S} = \sqrt{s(s+1)}\hbar$, the z -component of magnetic dipole moment vector is $\mu_z = \frac{q\hbar}{m} S_z$ and $S_z = m_s \hbar$ where magnetic spin quantum number m_s takes the values from $+s, s-1, -s$. This confirms that the nuclear magnetic moment is a charge dependent quantity which created a puzzle when it was found that the neutron has non-zero magnetic moment. In case a nucleon is in zero orbital angular momentum state, the net magnetic dipole moment is a vector sum of individual magnetic moments of three constituent quarks. In case of proton magnetic moment- $\vec{\mu}_s = \vec{\mu}_s(u) + \vec{\mu}_s(u) + \vec{\mu}_s(d)$, The resultant magnetic moment is the sum of individual magnetic moments of constituent two up quarks and a down quark (1). The detailed understanding of three-dimensional spin structure of the proton is an active research field with phenomenological implications in high energy hadron physics. QCD provides the essential formulation to understand this spin structure. Within QCD regime, information on this structure, especially how the nucleon's momentum and spin are divided among quarks and gluons is encoded in parton distribution functions (PDFs). In this study we focus on the review of spin physics and recent developments in three-dimensional proton spin structure.

Deep Inelastic Scattering DIS) (and proton structure:

Electron-proton (e-p) and proton-proton (p-p) scattering are powerful tools for probing the structure of the proton. At low energies when the beam energy is much smaller than the size of proton, the scattering process is elastic, and the proton remains intact. At higher energies, inelastic scattering starts, and the proton breaks up. As energies are increased further, the cross section again starts behaving as if the scattering is taking place via elastic scattering of the beam off point scatterers inside the proton. This is the Deep Inelastic region and the point like scatterers initially named partons, are the quarks. The Deep Inelastic Scattering (DIS) process provides a kinematical tool to probe the structure of proton and understand the momentum distribution of constituent quarks. The nature of e-p scattering cross section depends on the wavelength of virtual photon in comparison with the radius of the proton.

The differential cross section for DIS in terms of kinematical variables is-

$$\frac{d^2\sigma}{dx dQ^2} = \frac{4\pi\alpha^2}{Q^2} \left[(1 + (1-y)^2) (F_1(x) + \frac{(1-y)}{x} (F_2(x) - 2xF_1(x))) \right],$$

where α is the electromagnetic coupling and $F_1(x)$ and $F_2(x)$ are proton structure functions. The structure function encodes the interaction between the photon and the proton. From the experimental data it was found that the structure functions $F_1(x)$ and $F_2(x)$ are independent of Q^2 for fixed x and this led to the conclusion that in DIS region electrons scattered off a point charge and therefore the proton is made up of point-like constituents. This behaviour of structure function is called Bjorken scaling, which means the structure functions, at fixed x , are independent of Q^2 . The relation between proton structure functions, $F_2(x) = 2xF_1(x)$; is called 'the Callan-Gross relation' and it is a direct consequence of the spin-1/2 nature of the quarks.

Proton Spin Crisis:

The discovery of proton structure in Deep Inelastic Scattering (DIS) experiment, in 1969, initiated a detailed study of strong interaction leading to the development of quantum chromodynamics (QCD). The initial evidence for proton structure came from the measurement of unexpected anomalous magnetic moment of proton by O. Stern in 1933. Even after 80 years of this discovery, detailed studies of nucleon structure are of prime interest. The proton spin crisis essentially refers to the experimental observation that only a very small fraction of the spin of the proton is carried by the spin of the constituent quarks. In 1988, European Muon Collaboration (EMC) published their polarised deep inelastic scattering (pDIS) measurements,

which indicated that quarks inside the nucleons carry around 30 % of nucleon spin. EMC data of pDIS measurements of spin dependent structure function of proton, g_1 , and flavour -singlet axial charge, $g_A^{(0)}$, which give information about the spin content of quarks inside the proton, suggested that the total spin of the quarks summed over up, down, and strange quarks, contributes only a small fraction to the proton spin. The spin dependent structure function (2) is defined as-

$$g_1(x, Q^2) = \frac{1}{2} \sum e_q^2 [\Delta q(x, Q^2) + \Delta \bar{q}(x, Q^2)]$$

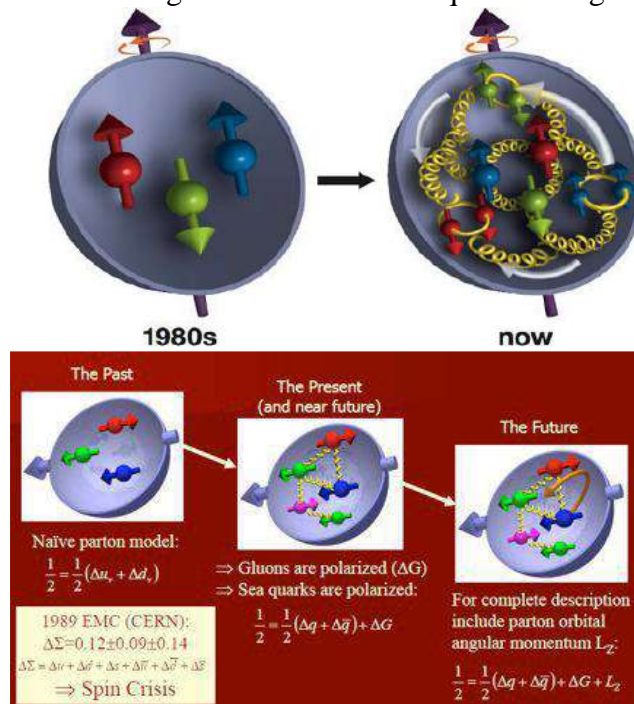
x is longitudinal momentum transfer, Q is energy scale, q and \bar{q} denoting quarks and antiquarks. Δq and $\Delta \bar{q}$ are helicity distribution functions for quarks and antiquarks respectively.

In the static quark model 100 % of the proton spin described by the sum of the spins of the valence quarks. i.e. $\frac{1}{2} = \sum_q S_z^q$. Relativistic quark models excluding gluon spin contribution predict that about 60 % of proton spin is carried by quarks and remaining 40 % comes from angular momentum of quarks.

It is now established that significant fraction of proton spin comes from polarised gluons.

$$S_z = \frac{1}{2} = \frac{1}{2} \Delta \Sigma + \Delta G + L_z^q + L_z^g$$

where $\frac{1}{2} \Delta \Sigma$ is the net contribution of both valence and sea quark helicities to the proton helicity, ΔG is the net contribution of gluon helicities to the proton helicity and L_z^q , L_z^g are z-components of orbital angular momenta of all quarks and gluons respectively.



(The diagrams show the evolution of spin physics from 1980 onwards, the proton has not only a quark structure, but these quarks are spinning with a distribution of angular momenta. Ref. M. Boglione, Shea (BNL))

Quantum Chromodynamics and Spin Physics:

The smallness of the spin contribution of quarks indicates that a non-zero value of total orbital angular momenta of the quarks may be induced by the confinement. This

introduces a transverse scale in spin physics. The orbital angular momentum, through spin-orbit coupling, can give rise to single spin asymmetry (SSA) in the scattering of unpolarised beam off polarised target. In polarised p-p process, $p + p^\uparrow \rightarrow \pi X$, and $p + p^\downarrow \rightarrow \pi X$ the cross section depends on the proton spin orientation with respect to the production plane, giving rise to an observable quantity called single spin asymmetry, it is defined as $A_N = \frac{d\sigma^\uparrow - d\sigma^\downarrow}{d\sigma^\uparrow + d\sigma^\downarrow}$, where $d\sigma^\uparrow$ and $d\sigma^\downarrow$ represent differential cross-sections for scattering of a transversely polarised proton off an unpolarised proton (or lepton) with one of the protons being upwards (downwards) polarised with respect to the production plane. Large TSSAs (up to 40 %) have been measured in π meson production in p-p collisions.

After EMC result, in 1990s, measurement of transverse single spin asymmetry (TSSA) in lepton-proton (l-p) and proton-proton (p-p) collider experiments showed up to 40 % asymmetries in p-p and 5 to 10 % asymmetries in l-p collider experiments. The spin-orbit coupling in the nucleons is associated with quark transverse momentum and bound state structure of the nucleons and leads to TSSA. The orbital angular momentum leading to spin orbit coupling could be a prime candidate to explain large TSSAs. Indication of partons of orbital angular momentum in the nucleon has motivated new theoretical and experimental investigations of three-dimensional structure of the nucleon. Deeply Virtual Compton scattering (DVCS) reaction is one of the hard exclusive reactions which is described using generalized parton distribution (GPD) formalism. This reaction probes the three-dimensional spatial structure of the nucleon. The sum rules connecting forward limit of GPD provide information about the quark and gluon in angular momentum in the nucleon. Transverse single spin asymmetry (TSSA) in semi-inclusive meson production in lepton -proton and proton-proton collisions is sensitive to spin-orbit coupling in the nucleon. Transverse momentum dependent parton distribution function (TMDPDF) and transverse momentum dependent fragmentation function (TMDFF) are theoretical tools to probe three-dimensional structure of a nucleon. These TMDPDFs and TMDFFs collectively referred as TMDs. The main observables in DVCS and TSSA are sensitive to orbital angular momentum in nucleon. To study the spin asymmetries, one requires an extension of TMD factorization to the process in which one of the nucleons is polarised. The inclusion of partons' transverse momentum, K_\perp , effects and TMDs can in principle lead to sizable TSSA. In 1989, D. W. Sivers suggested that the correlations between azimuthal distribution of unpolarised parton and the spin of the parent nucleon can lead to sizable asymmetry, an effect which was later named as Sivers effect resulting to give rise Sivers TMD or Sivers function where distribution of unpolarized quarks in polarised nucleon is described. Along with Sivers function, the class of TMDs contain Boer-Mulder function where TSSA is described due to polarised quarks in unpolarised nucleons. In 1993, J. Collins proposed another possible azimuthal angular dependence in the transversely polarised quark into spinless hadron which can result in a left-right asymmetry in the fragmentation function named as Collins function.

Recent Developments in Spin Physics:

After EMC results on spin dependent structure function of proton, further measurements have been made at the European Organisation for Nuclear Research (CERN), Stanford Linear Accelerator Centre (SLAC), Deutsches electron synchrotron (DESY), Jefferson Lab (J-Lab) and Relativistic Heavy Ion Collider (RHIC). COMPASS is a fixed target experiment at CERN studying nucleon spin structure in polarised deep inelastic muon-nucleon scattering and hadron spectroscopy using hadron beam. The main goal of COMPASS is to measure the helicity contribution of the gluons to nuclear spin. Recently, COMPASS Collaboration have reported the D^0 meson production at $\sqrt{S} = 160 \text{ GeV}$ using polarised muon scattering experiment (S is centre of mass energy at collider) The data analysed provide an average value of the gluon polarisation in the nucleon. Spin Muon Collaboration (SMC) of

SLAC reported the first measurement of spin dependent structure function g_1^d of deuteron in DIS of polarised muon off polarised deuteron. J-Lab has set a program to study structure function g_1 and g_2 . Structure function g_2 has been measured extensively in Hall A and spin asymmetries of the nucleon experiment (SANE) has been performed in Hall C. In RHIC spin program single spin asymmetries (SSAs) in inclusive hadron production in proton-proton collisions have been measured at $\sqrt{S} = 200 \text{ GeV}$ and $\sqrt{S} = 500 \text{ GeV}$. In the measurement of Sivers function, transverse TSSAs have been measured at RHIC for η , π^0 and inclusive jets at mid-rapidity. Model calculations indicate that the asymmetries impose significant constraints on the contributions from gluon Sivers function. The additional data were taken at 200 GeV and 500 GeV during the latest RHIC run which will allow more precise determination of inclusive jet asymmetries. Non-vanishing Collins effect have been observed in SIDIS and in $e-e^+$ annihilation and STAR has recently measured Collins asymmetries of charged pions in jets.

The PHENIX collaboration is in the process of designing a series of upgrades to considerably expand the physics capabilities and make full use of the constantly increasing luminosity at RHIC. Recently, in May 2018, PHENIX collaboration has reported measurement of TSSA of J/ψ production at forward and backward regions as a function of J/ψ transverse momentum p_T and x_F . The measurement of gluon Sivers function (GSF) has been focuses in recent years in $p^\uparrow + p \rightarrow J/\psi + x$ and $e + p^\uparrow \rightarrow J/\psi + x$ processes. It has been found that GSF has important and measurable contributions in the to TSSA. In 2020 GSF has been estimated for TSSA in $p^\uparrow + p \rightarrow J/\psi + x$ at PHENIX RHIC and Spin Physics Detector (SPD) Nuclotron-based Ion collider fAcility (NICA), Dubna, Russia. In this study modified J/ψ production model has been tested with existing sets of parameters which gives useful information to understand spin physics in more details. Recent experiments indicate that gluons play a significant role in establishing key properties of proton and nuclear matter. Electron-ion collider (EIC) facility has a potential to reveal the three-dimensional dynamical state of quarks and gluons in a proton just like a tomography of a human brain.

Conclusion:

In this study, we focus on the review of spin physics and its development since the measurement of spin dependent proton structure function in polarised DIS by EMC. We highlight the relation between spin physics and measurement of TSSA in the domain of QCD. We found the proton spin crisis demands more systematics and collaborative effort to understand inner dynamical structure of proton. The recent developments in spin physics show a progress in phenomenological, experimental advancements to understand proton spin and its origin at deeper level.

References:

1. D.J. Griffiths, Introduction to Elementary particle physics, Wiley.
2. Halzen and Martin, Quarks and Leptons, Wiley
3. Godbole, Misra, Mukharjee, Rawoot, Phys. Rev. D85, 094013 (2012).
4. Godbole, Kaushik, Misra, Mukharjee, Rawoot, Phys. Rev. D91, 014005 (2015).
5. Godbole, Kaushik, Misra, Mukharjee, Rawoot, Sonawane, Phys. Rev. D96, 096025 (2017).
6. J. Ashman et.al. European Muon Collaboration, Phys. Lett. B206, 364 (1988)
7. S.S. Adler, PHENIX Collaboration, Phys. Rev. Lett. 91 (2003) 241803.
8. A. Adare, PHENIX Collaboration, Phys. Rev. D86 (2012) 099904.
9. A. Airapetian et.al. HERMES Collaboration, Phys Rev D75, 012007 (2007).
10. Jack Barbara, PHENIX experiment at RHIC-A Decadal plan 2011-2020.
11. Karpishkov, Saleev and Nefedov (SPD-NICA), Phys Rev. D 104, 016008 (2021)

Luminescent Properties of Borate Based Phosphors Review

M. P. Jmabhale¹, C. B. Palan¹, S. P. Hargunani², R. P. Sonekar²

¹Department of Physics, Bapumiya Sirajoddin Patel Art's, Commerce and Science College, Pimpalgaon Kale, Buldhana, India

²Department of Physics G.S. College, Khamgaon Buldhana, India

*(Corresponding author email: manohar08.jambhale@gmail.com)

Abstract: Rare earth-activated borate based phosphors have gained considerable interest in recent years due to their potential applications in various areas such as optoelectronics, solid-state lighting and display devices. This review article provides a comprehensive overview of the synthesis methods and characterization techniques used for the production and analysis of rare-earth-activated borate phosphors.

Keywords: Borate; Excitation; phosphors; ultraviolet and LED

1. Introduction

1.1 Significance of rare earth doped borate phosphors

Rare earth (RE) activated borate phosphors are a type of luminescent material with numerous potential applications in display, lighting and sensing technologies. These phosphors have high brightness, tunable colors, long lifetimes and excellent thermal and chemical stability. They can be activated by various rare earth ions, such as Eu, Tb, Ce, Pr, and Dy, to produce different emission spectra under UV or VUV excitation. In comparison to other types of phosphors, rare earth-activated borate phosphors have several advantages. These borate phosphor materials exhibit a broad transparency to ultraviolet light, which enables them to increase their luminescence efficiency by absorbing more energy from the excitation source. These materials possess a high optical damage threshold, allowing them to tolerate both high power and high temperatures without degrading [1]. The low content of alkaline earth components in these materials reduces the likelihood of quenching and enhances the purity of the color [2]. The coordinating environment and varied crystal structure of these materials enable the adjustment of emission characteristics and the exchange of energy among activators [3].

Due to these advantages, rare earth-activated borate phosphors are significant for the development of advanced phosphor-based devices, such as plasma display panels, white LEDs, scintillators, and optical sensors [3-5]. The main characteristics of some rare earth activated borate phosphor are tabulated in Table 1.

Tab. 1. Characteristics of some rare earth activated borate phosphor

Sr. No.	Phosphors	Synthesis Method	Excitation and Emission Wavelength	Applications	Ref.
1	LaBaB ₉ O ₁₆ : RE (RE = Eu ³⁺ , Ce ³⁺ /Tb ³⁺)	Solution Combustion Method	For Eu ³⁺ $\lambda_{ex}=254/147$ nm (UV/VUV) & $\lambda_{em}=615$ nm	Plasma Display Panel	[2]
2	Ba ₅ (B ₂ O ₅) ₂ F ₂ :xEu ³⁺	Solid State Reaction Method	$\lambda_{ex}=394$ nm & $\lambda_{em}=616$ nm	W-LED	[6]

3	NaMgBO ₃ :RE (Dy ³⁺ & Sm ³⁺)	Solution Combustion Method	-	Personal protection dosimetry field & Radiation dosimetry	[7]
4	LiSr ₄ (BO ₃) ₃ Gd ³⁺ , Pr ³⁺	Modified Solid state Diffusion Method	$\lambda_{ex}=276$ nm & $\lambda_{em}=260-370$ nm	Phototherapy	[8]

1.2 Applications of borate phosphors

Rare earth-activated borate phosphors are a class of luminescent materials that can emit various colors of light under different excitation sources. These materials have become increasingly popular for their potential applications in optoelectronics, solid-state lighting and display devices due to their high thermal stability, low toxicity, and ability to emit light in a range of colors.

One of the primary applications of these materials is in the production of white light-emitting diodes (WLEDs) used for general lighting and backlighting. By doping different rare earth ions into borate hosts, such as LaBO₃, GdBO₃, YBO₃, and Ca₃(BO₃)₂, various color components can be obtained, such as blue, green, yellow, and red. By mixing these components with a blue or near-ultraviolet LED chip, white light with high color rendering index (CRI) and color temperature can be achieved. For instance, LaBO₃:Ce³⁺, Tb³⁺ phosphor can produce green and yellow emissions, which can be combined with a blue LED to generate warm white light [9]. GdBO₃:Eu³⁺ phosphor can emit red light, which can be used to improve the color gamut of backlight w-LEDs [10].

Rare earth-activated borate phosphors have various applications such as in phototherapy and plant lamp applications, where specific wavelengths of light are required to stimulate biological processes. For example, ultraviolet (UV) light can be used to treat skin diseases such as psoriasis, vitiligo and eczema. These phosphors, such as Ca₃(BO₃)₂: Pr³⁺, can emit UV light under NIR excitation, making them suitable for use as phototherapy lamps. Similarly, red and blue light can promote plant growth and development, such as photosynthesis, flowering, and fruiting. Borate phosphors, such as YBO₃:Eu³⁺ can emit red and blue light under UV excitation and can be used as plant lamps [11].

Another application of rare earth-activated borate phosphors is in display devices, such as LCDs, PDPs, and FEDs, which require high luminous efficiency, fast response time and good color purity. Phosphors such as LaBO₃:Ce³⁺ can exhibit high brightness, short decay time, and narrow emission bands, making them suitable for display applications [12]. Additionally, they can be used for color tuning and security ink applications by utilizing their upconversion, downshifting, and quantum cutting properties [9].

2. Synthesis of the phosphors

The process of creating RE activated borate phosphors can be divided into two primary categories: solid-state reactions and solution-based methods. Solid state reactions are the most conventional approach, involving the high-temperature calcinations of a mixture of RE oxides, boric acid, and other metal oxides or salts, leading to the formation of pure and crystalline borate phosphors with well-defined stoichiometry and morphology. However, this method is associated with some drawbacks, including high energy consumption, extended reaction times and difficulty in controlling the particle size and shape. In contrast, solution-based methods offer certain advantages, such as lower reaction temperatures, shorter reaction times and simpler particle size and shape control. Some of these methods include sol-gel, hydrothermal, co-precipitation, combustion, and microwave-assisted methods. These procedures involve using various precursors, solvents, surfactants, and additives to create a borate precursor solution, which is then converted into the borate phosphor by heating, drying or pyrolysis. The

selection of a solution based method depends on the desired properties of the borate phosphor, such as composition, phase, morphology, and luminescence.

3. Reaction Parameters and Crystal structure

The properties of rare earth-activated borate phosphors depend on various factors, including the type and concentration of the rare earth ions, the borate host, the synthesis method, and the annealing conditions. These factors can affect the luminescence properties of the phosphors, such as the coordination environment and symmetry of the rare earth ions, which determine the energy levels and transition probabilities of the f-f transitions. Additionally, the crystal field splitting and Stark effect can cause the splitting of the degenerate energy levels and fine-tune the emission wavelengths. Concentration quenching and energy transfer can reduce the luminescence intensity and efficiency when the rare earth ions are too close to each other or interact with other species. Defects and impurities can also introduce non-radiative recombination centres and lower the luminescence quality [13].

4. Characterization techniques

Characterization techniques for rare earth-activated borate phosphors are utilized to investigate their structure, morphology, composition, and optical properties. Some of the commonly employed techniques include [14]

- **X-ray diffraction (XRD)**
- **Scanning electron microscopy (SEM)**
- **Transmission electron microscopy (TEM)**
- **Energy dispersive spectrometer (EDS)**
- **Fourier transforms infrared spectroscopy (FTIR)**
- **Excitation and Emission**

5. CONCLUSION:

It is concluded from above study, the best synthesis method for rare earth activated borate phosphors is solution-based methods like sol-gel method and combustion method. There are so many characterization techniques discussed in this review. Rare earth elements enhance the luminescence properties of borate phosphors. From the data we have found various applications of rare earth activated borate phosphors. It was found that doping different rare earth ions into borate hosts, various color components can be obtained and mixing these components with a blue or near-ultraviolet LED chip, white light with high color rendering index and color temperature can be achieved. They are also used as phototherapy lamps, plant lamps and Display applications.

6. REFERENCES:

- [1] J. Zhang, Z. Song P. Cai, & X. Wang, *Phys. Chem. Chem. Phys.* 25, 1165 (2023)
- [2] J. T. Ingle, R. P. Sonekar & S. K. Omanwar, *J Mater Sci: Mater Electron* 27, 10735 (2016)
- [3] H. H. Xiong, C. Zhu, X. Zhao, Z. Q. Wang, & H. Lin, *Adv Mater Sci Eng*, 2014, 7, (2014).
- [4] J. Lakde, C. M. Mehare, K. K. Pandey, N. S. Dhoble & S. J. Dhoble *J. Phys.: Conf. Ser.* 1913, 012029 (2021).
- [5] R. Sharma, M. Mehta, G. N. Bhargavi, *IJERT*, 12, 71 (2023).
- [6] W. Zhao, B. Hao, X. Wang, J. Liu & J. Yu, *J. Mater Sci: Mater Electron* 32, 6379, (2021)
- [7] Z.S. Khan, N.B. Ingale & S.K. Omanwar, *Environ Sci Pollut Res* 23, 9295 (2016)
- [8] A. O. Chavhan, N. S. Bajaj, S. K. Omanwar *Bull. Mater. Sci.* 40, 1 (2017)
- [9] A. Dwivedi, A. Roy & S. B. Roy, *RSC Adv.* 13, 16260 (2023)
- [10] V. Kumar, V. Sharma & H. C. Swart, *POSP* 25, (2023)
- [11] S. K. Omanwar, R. P. Sonekar & N. S. Bajaj, *CRC Press.* (2022)
- [12] M. D. Mehare, S. A. Dhale, C. M. Mehare, N. S. Dhoble & S. J. Dhoble, *Curr. Mater. Sci.* 5, 171, (2023)
- [13] P. Chen, M. M. Murshed & T. M. Gesing, *J. Mater Sci* 56, 3639, (2021)
- [14] L. M. Annah, Doctoral thesis, University of Free State, (2017)

Synthesis and Photoluminescence (PL) Properties of $\text{LaB}_3\text{O}_6:\text{Eu}^{3+}$ Phosphor

M. P. Jmabhale¹, S. P. Hargunani², R. P. Sonekar²

¹Department of Physics, Bapumiya Sirajoddin Patel Art's, Commerce and Science College, Pimpalgaon Kale, Buldhana, India

²Department of Physics G.S. College, Khamgaon Buldhana, India

*(Corresponding author email:manohar08.jambhale@gmail.com)

ABSTRACT:

The green light emitting $\text{LaB}_3\text{O}_6:\text{Eu}^{3+}$ phosphor was successfully synthesized via solid-state diffusion method. The phase of the prepared $\text{LaB}_3\text{O}_6:\text{Eu}^{3+}$ phosphor was confirmed by powder XRD analysis and studied its PL properties under ultraviolet (UV) excitation (200-390nm). The XRD pattern of prepared $\text{LaB}_3\text{O}_6:\text{Eu}^{3+}$ phosphor is well matched with available standard JCPDS file having card no-01-073-1150. The excitation and emission spectra of prepared phosphor were monitored at 544 nm and 234 nm respectively. The CIE (Commission International de l'Eclairage) coordinates of prepared phosphor was calculated and found to X=0.26 Y=0.73. Hence the $\text{LaB}_3\text{O}_6:\text{Eu}^{3+}$ has great potential in fluorescent lamp applications.

Keywords: - Solid state diffusion method; X-ray diffraction technique (XRD); PL and CIE.

1. Introduction:

Novel luminous materials have drawn a lot of attention lately because of their crucial role in a number of technical applications, such as optoelectronic devices, lighting and displays. Rare earth element doping has demonstrated potential for improving luminescence properties in materials. Among these, lanthanum borates have attracted attention due to their distinct structural features and their uses in the phosphor materials industry [1]. Within this framework, the lanthanum borate compound LaB_3O_6 offers a fascinating platform for the introduction of luminous dopants to customize its optical characteristics.

Light emitting diodes, or LEDs, are becoming more and more popular as a possible alternative to incandescent and fluorescent light sources. As the upcoming generation of solid state lighting, white light emitting diodes (w-LEDs) have garnered a lot of attention lately because of their unique benefits, which include high efficiency, long lifespans, minimal environmental impact, no mercury, short response times, application in final products of different sizes, optical memory, light guide, dosimetry, pressure sensor, and more [2–7]. Recently, there has been a focus on developing novel phosphors with strong luminescence qualities that can be activated in the long-UV region (300–450 nm) in order to boost the efficiency of w-LEDs. Phosphors are used in scintillators, LEDs, display devices, fluorescent lamps, phototherapy lamps, and up-conversion lasers. Photoluminescence (PL) can occur anywhere in the electromagnetic spectrum from the ultraviolet to the infrared and is highly reliant on the host lattice [8]. When photons or an electron beam, or any other type of energy, stimulate phosphor, it produces light with the desired wavelength.

The synthesis and luminescence characteristics of LaB_3O_6 doped with europium ions (Eu^{3+}), a rare-earth element known for its unique optical properties, are the main topics of this study. It is anticipated that the addition of Eu^{3+} to LaB_3O_6 will cause substantial changes in the material's luminescent behavior, providing chances for the creation of sophisticated luminescent materials with specialized emission characteristics. Clarifying the synthesis

method and describing the luminous properties of the resultant material are essential to determining its possible uses in fields like biomedical imaging and lighting technology.

2. Experimental

$\text{LaB}_3\text{O}_6:\text{Eu}^{3+}$ phosphor was synthesized at a high temperature solid-state diffusion method. Analytical grade La_2O_3 , H_3BO_3 and rare earth oxide Eu_2O_3 are the starting ingredients employed. To create a homogenous mixture, the stoichiometric reactants were combined and finely pulverized in an agate mortar using acetone. The combinations were then heated in air atmospheres for 24 hours at 800 °C. After being cooled to normal room temperature, the finished products were once more ground into a powder for additional characterization.

3. Results and Discussion:

3.1 X-Ray Diffraction (XRD) Pattern

The X-ray diffraction (XRD) pattern of the $\text{LaB}_3\text{O}_6:\text{Eu}^{3+}$ phosphor is shown in **Fig. 1**. The acquired sample is single phase, as evidenced by the whole set of diffraction peaks being in good agreement with those in JCPDS file with file no. 01-073-1150. With no secondary or impurity phases, the pattern shows the synthesis of a single-phase compound with a monoclinic structure that belongs to the $I2/a$ space group and has lattice parameters of $a=7.9560\text{Å}$, $b=8.172\text{Å}$, $c=6.4990\text{Å}$, and $\beta=93.6300\text{Å}$.

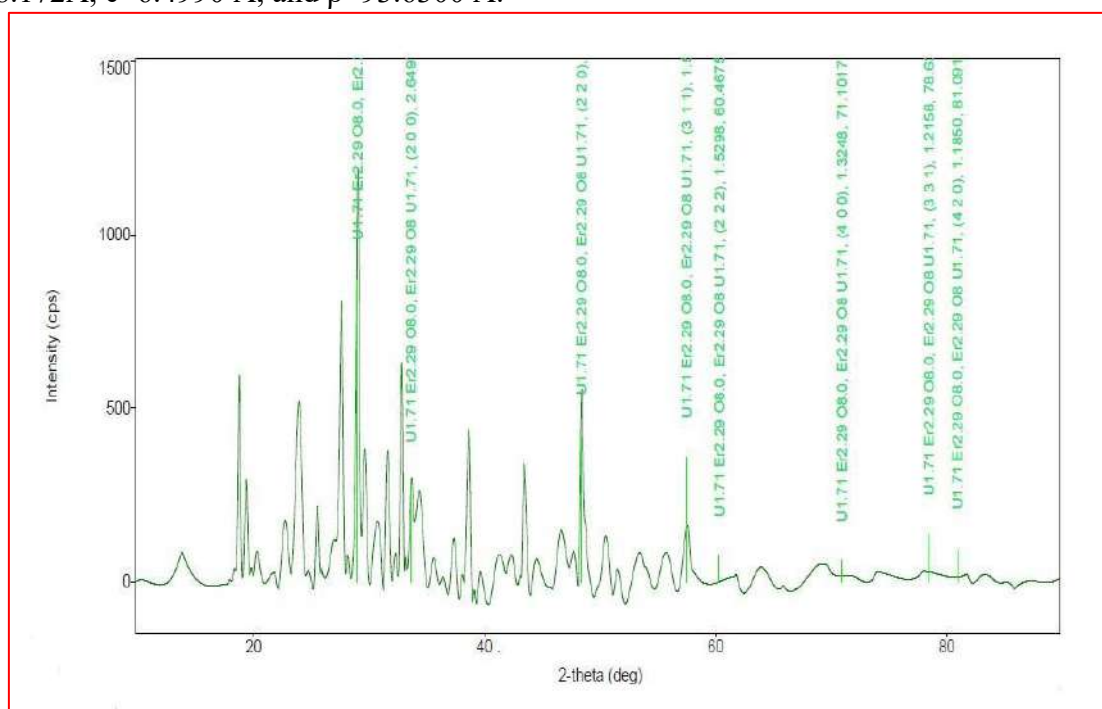


Fig.1 X-Ray Diffraction (XRD) pattern of $\text{LaB}_3\text{O}_6:\text{Eu}^{3+}$ phosphor

3.2 Photoluminescence (PL)

Fig. 2 showed the excitation and emission spectrum of $\text{La}_{0.99}\text{B}_3\text{O}_6\text{Eu}_{0.01}$ phosphor. From figure observed that excitation spectra consists broad band between wavelength range of 200 nm to 350 nm and maximum peak intensity at 234 nm and is explained by the charge transfer from O^{2-} to Eu^{3+} . We find a very significant charge transfer from O^{2-} to Eu^{3+} in the $\text{La}_{0.99}\text{B}_3\text{O}_6\text{Eu}_{0.01}$ lattice. In addition to the charge transfer band, the excitation spectrum of Eu^{3+} with host showed some sharp lines that corresponded to the f-f transitions. These lines were all the result of transitions inside the $\text{Eu}^{3+} 4f^6$ configuration [9].

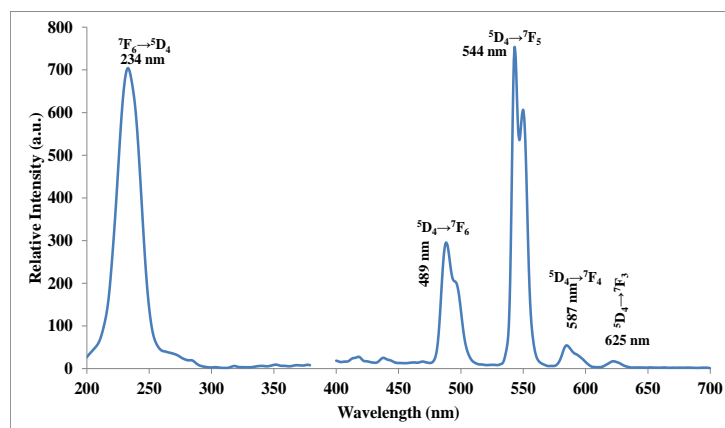


Figure 2: Excitation & Emission spectra of sample $\text{LaB}_3\text{O}_6:\text{Eu}^{3+}$

The emission spectra of Eu^{3+} doped LaB_3O_6 quenched for one hour at 800 demonstrate how Eu transforms from Eu^{2+} to Eu^{3+} . Figures 2 show that the emission lines of ${}^5\text{D}_4 \rightarrow {}^7\text{F}_6$, ${}^5\text{D}_4 \rightarrow {}^7\text{F}_5$, ${}^5\text{D}_4 \rightarrow {}^7\text{F}_4$ and ${}^5\text{D}_4 \rightarrow {}^7\text{F}_3$ have dramatic splittings of 489 nm, 544 nm, 587 nm and 625 nm respectively. The magnetic dipole transition ${}^5\text{D}_4 \rightarrow {}^7\text{F}_5$ is responsible for the greatest emission peak, which is located at 544 nm and displays vivid and bright green spectra. The transition ${}^5\text{D}_4 \rightarrow {}^7\text{F}_3$ of the Eu^{3+} forced electric dipole is responsible for a peak at 625 nm. Its relative weakness suggests that the ${}^5\text{D}_4 \rightarrow {}^7\text{F}_6$ electric dipole transition is very weak and the Eu^{3+} site has inversion symmetry.

3.3 CIE Coordinates

The photoluminescence data and Interactive CIE software were utilized to compute the chromaticity coordinates of the generated samples. **Fig. 3** showed the computed CIE coordinates of the produced phosphor on the 1931 CIE chromaticity diagram. The chromaticity coordinates of the prepared phosphor $\text{LaB}_3\text{O}_6:\text{Eu}^{3+}$ are A ($X=0.26$ $Y=0.73$) in the green zone.

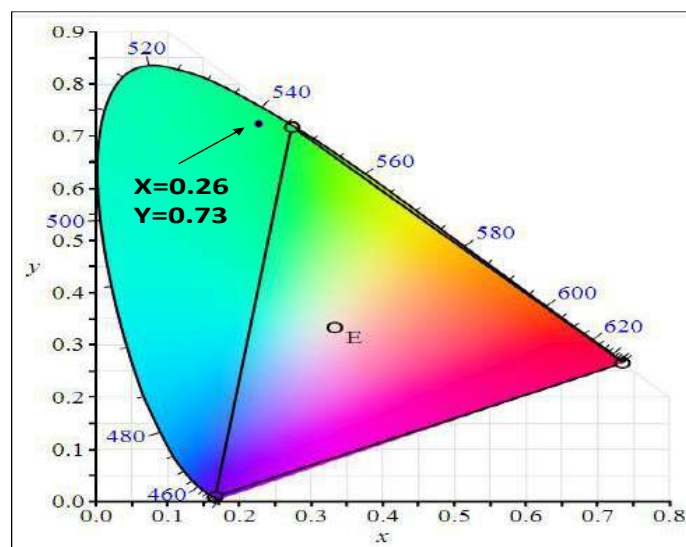


Fig. 3 CIE color coordinates for $\text{LaB}_3\text{O}_6:\text{Eu}^{3+}$ phosphor

4. Conclusion

The polycrystalline $\text{LaB}_3\text{O}_6:\text{Eu}^{3+}$ phosphor was successfully synthesized by solid state diffusion method. The XRD pattern of prepared $\text{LaB}_3\text{O}_6:\text{Eu}^{3+}$ phosphor is good agreement with the JCPDS standard file with file no, 01-073-1150. The PL excitation spectra, was monitored at 544 nm and emission spectra was monitored at 234 nm. The CIE chromaticity coordinates of the as-prepared phosphor was calculated and found to be $X=0.26$ $Y=0.73$). The

outcome of this phosphor material provides the support for the possible application in green emitter in many applications in fluorescent area.

5. References

- [1] C. Ronda, *Materials Science and Materials Engineering*, Elsevier, (2017)
- [2] K. Sakuma, N. Hirotsuki, R.J. Xie, *J. Lumin.* **126**, 843–852 (2007)
- [3] X.F. Hu, S.R. Yan, L. Ma, G.J. Wan, J.G. Hu, *Powder Technol.* **188**, 242–247 (2009)
- [4] K. Hirao, S. Todoroki, D.H. Cho, N. Soga, *Opt. Lett.* **18**(19), 1586–1587 (1993)
- [5] U. Caldino, A. Speghini, S. Berneschi, M. Bettinelli, M. Brenci, S. Pelli, G.C. Righini, *Opt. Mater.* **34**(7), 1067–1071 (2012)
- [6] G. Okada, B. Morrell, C. Koughia, A. Edgar, C. Varoy, G. Belev, T. Wysokinski, D. Chapman, S. Kasap, *Appl. Phys. Lett.* **99**, 121105 (2011)
- [7] Q. Jing, Q. Wu, L. Liu, J. Xu, Y. Bi, Y. Liu, H. Chen, S. Liu, Y. Zhang, L. Xiong, Y. Li, J. Liu, *J. Appl. Phys.* **113**(2), 023507– 023512 (2013)
- [8] K.N. Shinde, V.B. Pawade, S.J. Dhoble, A. Hakeem, *Luminescence* **29**, 352–356 (2014)
- [9] A.M. Srivastava, M.G. Brik, *Opt. Mater. (Amst)*. 35 (2012)

Thermally Stimulated Discharge Current (TSDC) Study of 4:1 PS PMMA Polyblend Thin Films doped with 10% Oxalic Acid.

Anant S. Wadatkar

Department of Physics,

Vinayak Vidnyan Mahavidyalaya, Nandgaon Khandeshwar, Dist.: Amravati (M.S.)

Abstract

The 4:1, PVC PMMA polyblend thin films, with the doping of 10% of Cinnamic Acid, were prepared by using Isothermal Evaporation Technique. The TSDC study of these films were carried out at three different poling electric fields (E_p) 35 kV/cm, 50 kV/cm, 65 kV/cm at the constant poling temperature (T_p) 373 K. It has been observed that the peak TSD current (I_m) and peak temperature (T_m) increases with an increase in poling electric field.

[**Keywords:** Polystyrene (PS), Poly Methylmethacrylate (PMMA), TSDC]

1. Introduction

The TSDC is an effective tool for understanding the internal structure, molecular relaxations and decay of space charge due to trapping of charge carriers and their subsequent thermal release from traps in a polymer [1-4].

The TSDC technique for polyblends of PMMA and Polyvinyl pyrrolidene has also been studied [5]. The electret behaviour of PS and PMMA separately has been carried out by number of researchers [1, 6-10]. The TSDC study of polyblends of PS and PMMA has been carried out and it has been reported that the TSD current increases with the increase in the poling electric fields (E_p). This effect of poling electric fields (E_p) after doping with 10% Oxalic Acid on the charge storage properties of polyblend films was the main thrust of investigation.

2. Experimental

2.1 Sample Preparation

The Polystyrene (PS) of commercial grade supplied by Poly Chem., Mumbai and Poly Methylmethacrylate (PMMA) obtained from Otto Kemi were used for the present study. The two polymers PS PMMA and Oxalic Acid (OA) doped blend films have been prepared by taking OA in the weight percentage 10% were taken in the ratio 4:1 were dissolved in the common solvent Tetrahydrofuran (THF). The solution was kept for 3-4 days to allow polymers to dissolve completely to yield uniform solution. The solution mixture was then heated for 1 hour at 60°C to get completely homogeneous solution. A glass plate thoroughly cleaned with water and later with acetone was used as a substrate. To achieve perfect levelling (and uniformity in thickness of the films), a pool of mercury was used in a plastic tray. The solution was poured on the glass plate and was allowed to spread uniformly in all directions on the substrate. The solvent in the solution was thus allowed to evaporate completely and get air-dried. The film on the glass substrate was then removed and cut into small pieces of suitable sizes. In this way the films were prepared by isothermal evaporation technique. Further it was dried for 3 days to remove any traces of solvent. The thickness of the films was measured by digimatic micrometer (Mitutoyo Corporation, Japan).

2.2 Measurement Technique

Each film was metallised on both sides by applying silver paint and then the film was sandwiched between two brass electrodes of the sample holder. The Metal-Insulator-Metal system so formed was placed inside the furnace.

- i) The poling electric field $E_p = 35$ kV/cm) was applied across the sample at room temperature (30 °C) and the sample was heated at a nearly uniform rate (1.33 °C/min) till the system attained the

- constant poling temperature $T_p = 373 \text{ K}$ ($100 \text{ }^\circ\text{C}$). The charging current was measured with respect to the increasing temperature.
- ii) Keeping the applied field ON for one hour at the constant applied field $E_p = 35 \text{ kV/cm}$, the charging current was measured with respect to time.
 - iii) Keeping the field ON the sample was slowly cooled down to room temperature in another one hour. In this case also the charging current was measured with respect to decreasing temperature. Thus the total time of charging was adjusted to be 3 hours in each case.
 - iv) At room temperature the electric field was removed and the sample was kept shorted for 15 minutes to remove the surface charges. In this way the thermoelectret has been prepared at ($E_p = 35 \text{ kV/cm}$) and $T_p = 373 \text{ K}$.
 - v) Now the thermoelectret had been formed. It was then heated at the same heating rate and the discharging (TSD) current was measured as the function of temperature from $303 \text{ K} - 453 \text{ K}$ ($30 \text{ }^\circ\text{C} - 180 \text{ }^\circ\text{C}$). The current was recorded after every $5 \text{ }^\circ\text{C}$ rise of temperature whenever it showed a significant change in its value.

The same procedure from steps (i) to (v) was followed, for preparing the thermoelectrets, at poling Fields ($E_p = 50 \text{ kV/cm}$ and 65 kV/cm) and at the same poling temperature $T_p = 373 \text{ K}$.

3. Results and Discussions

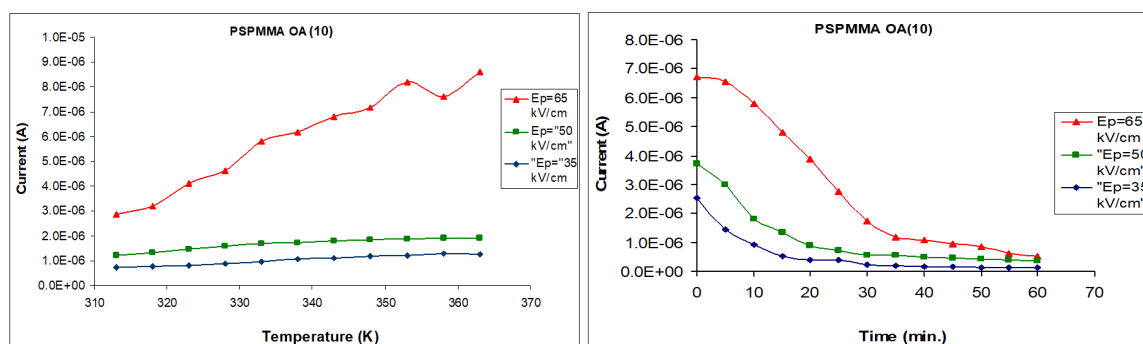
In this manuscript results have been presented in the form of representative graphs for all the poling ($E_p = 50 \text{ kV/cm}$ and 65 kV/cm) and constant poling temperature ($T_p = 373 \text{ K}$). The variations of charging current with rising temperature are illustrated as in fig 1. It has been observed that the charging current increases with an increase in temperature.

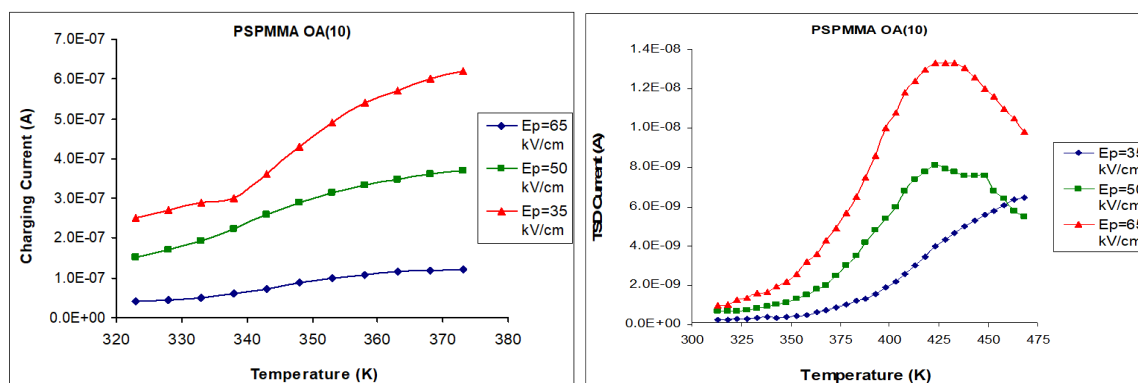
3.1 Measurements Carried out:

After attending the constant poling temperature $T_p = 373 \text{ K}$, the sample was charged at the constant applied field for the period of one hour. For this charging current has been recorded with respect to time at an interval of 5 minutes upto one hour. The charging current gradually decreases with the increase of time as shown in fig 2.

After charging the sample for one hour, the temperature was gradually decreased from 373 K to room temperature keeping the field ON. The charging current with decreasing temperature was recorded after every decrease of $5 \text{ }^\circ\text{C}$. It has been noticed that the charging current decreases for the decrease in the temperature as illustrated in fig 3.

The electric field was removed and the thermoelectret sample was gradually heated at the average uniform heating rate of $1.33 \text{ }^\circ\text{C/min}$. The TSD current has been recorded with respect to increase of temperature. The graphs were plotted between TSD current and Temperature (known as Thermograms) as shown in fig.4.





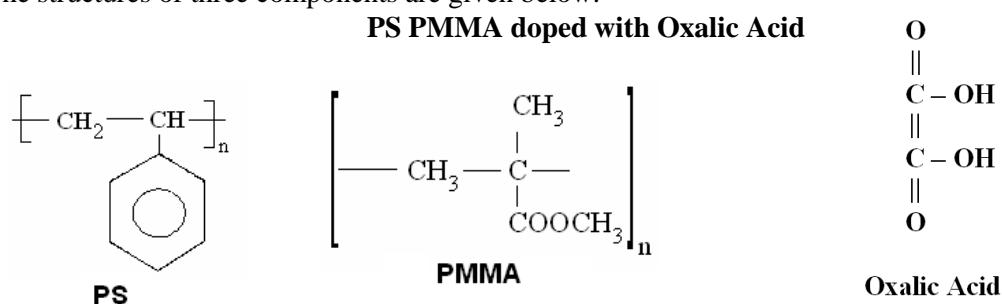
The prominent results can be summarized as follows,

- 1) At a given poling field (*while heating the samples*) the charging current was found to increase with the increase of temperature.
- 2) The charging current (*while cooling the samples*) was found to decrease with the decrease in temperature.
- 3) The charging current, in both the cases, was found higher at higher poling fields.
- 4) The thermograms showed single peaks at temperatures above 100°C. The current corresponding to the peak is known as peak TSD Current (I_m).

3.2 Discussion of Results

In the present case we have used the two polymers PS and PMMA doped with Oxalic Acid. Among these, PS is non polar, while PMMA is weakly polar with the dielectric constant 3.5 - 4 at 10^3 cps. The glass transition temperature of PS is $T_g = 95^\circ\text{C}$ (368 K), and for PMMA $T_g = 105^\circ\text{C}$ (378 K). Both of them are essentially insulation materials and number of free charge carriers is very small and their mobility is very low. PS has a phenyl side group which is electron donor and also PMMA containing electron releasing methyl group supplies electron. PMMA also contains acrylate group ($=\text{C}-\text{CO}-\text{O}-\text{R}$), which is a bulky side group. The TSD current is contributed by several processes.

The effect of dopant Oxalic Acid on the polarisability of PS PMMA polyblend under the combined influence of temperature and electric field can be interpreted from chemical point of view. The structures of three components are given below:



Polymethyl Methacrylate (PMMA) is clear, colourless transparent plastic with a higher softening point, better impact strength and better weatherability than Polystyrene (PS). It undergoes pyrolysis almost completely to monomer by a chain reaction.

PS is relatively inert chemically. It is quite resistant to alkalis, halide acid and oxidizing and reducing agents. PS degrades at elevated temperatures to a mixture of low molecular weight compounds about half of which is styrene. Two of its major defects in mechanical properties are its brittleness and its relatively low heat deflection temperature. These defects can be overcome by proper formulating or by copolymerization and blending.

A number of copolymers of styrene with a minor amount of co monomer may enhance heat and impact resistance without loss of other desirable properties. Typical co-monomers are those that increase intermolecular force of attraction by introducing polar groups or those that stiffen the chain reduced rotational freedom through the steric hindrance of bulky side groups.

Copolymer of styrene with methacrylate is of major commercial interest. Such polymers have higher heat deflection temperature and more resilience and impact resistance than polystyrene.

Oxalic acid is the strongest acid of all the dicarboxylic acids. When it is heated a molecule of formic acid (-HCOOH) is formed with elimination of CO₂. The formic acid, thus formed, undergoes further rapid reaction with phenyl rings of styrene molecules under acidic conditions giving rise to the formation of methylene bridges. Oxalic acid has natural affinity to ester segment of methacrylate molecule. It may form an association with methoxy (-OCH₃) part of the same segment. In addition to this polyacrylates contain an easily removable tertiary hydrogen atom. It undergoes some chain transfer in variety of ways.

Oxalic acid doping with PS PMMA under the influence of thermal energy not only enhance the pyrolysis of PS PMMA but also creates charged species by protonic oscillation between polyvalent atoms. The overall impact of oxalic acid as a dopant on PS PMMA would certainly enhance the polar character of the blend system.

Thus the peak TSD Current increases due to the stronger polarisation of samples at higher poling field E_p.

References

1. Bahri and Sood B R, Thin Solid Films, **100** (1983) L5-L8.
2. Bucci C., Fieschi R. and Guidi G., Phys. Rev. B (USA), **148**(1966) 816.
3. G. Williams and D.C. Watt, Polymer Preprints (Am. Chem. Soc., USA) **12** (1971) 97.
4. Garlic G. F. J. and Gibson A. F. , Proc. Phys. Soc. (G. B.), **60**(1948) 574.
5. Khare P. K. and Chandok R. S. Polym. Int. **38** (1995) 153.
6. M. Kryszewski, M.Zielinski and S. Sapieka, Polymer (GB) **17** (1976) 212.
7. Narayan A. and Singh H. P., Indian J Pure and Appl Phys, **25**(1987) 30.
8. Tager A., "*Physical Properties of Polymers*" MIR (Moscow), 2nd Ed., (1978), 306-590.

A Review on Carbon based Nanomaterial. Properties, Characteristics and Applications

Ms..S.T.A.Khan , Mr.P.S.Wagh , Ms.S.P.Dharmey , Ms.S.A.Amale

Department of Physics, Vidya Bharati Mahavidyalaya , Amravati.

Abstract.

In recent years, there has been a growing interest in nanomaterials, this review highlight the distinctive characteristics of carbon-based nanomaterials. Specifically, the focus extends to key advancements in carbon based nanomaterials, including fullerene , Graphene , carbon nanotube, carbon quantum dot , nanodiamond . **Throughout this review, the** exceptional features of carbon based nanomaterials are highlighted, illustrating their significance in diverse applications. The review concludes by addressing future perspectives of carbon-based nanomaterials in various fields.

Keywords: Fullerene , Graphene , Carbon Nanotube , Carbon Quantum Dot , Nanodiamond .

1.Introduction.

Nanotechnology is the general term for designing and making anything whose use depends on specific structure at the nanoscale – generally taken as being 100 nanometres (100 millionths of a millimetre or 100 billionths of a metre) or less. Nanomaterials are usually considered to be materials with at least one external dimension that measures 100 nanometres or less or with internal structures measuring 100 nm or less [1,2]. They may be in the form of particles, tubes, rods or fibres. The nanomaterials that have the same composition as known materials in bulk form may have different physico-chemical properties than the same materials in bulk form, and may behave differently if they enter the body. They may thus pose different potential hazards. Aggregated nanomaterials also need to be assessed in this light as they may exhibit properties that are similar to those of the single nanoparticles, especially when they have an unusually large surface area for a given amount of material [3,4]. The number of products produced by nanotechnology or containing nanomaterials entering the market is increasing [6]. Current applications include healthcare (in targeted drug delivery, regenerative medicine, and diagnostics)[5,7], electronics, Thermal conductivity [10],even in COVID-19 era [11] , cosmetics, textiles, information technology and environmental protection[8]. For example, nanosilver is appearing in a range of products, including washing especially close scrutiny [9].

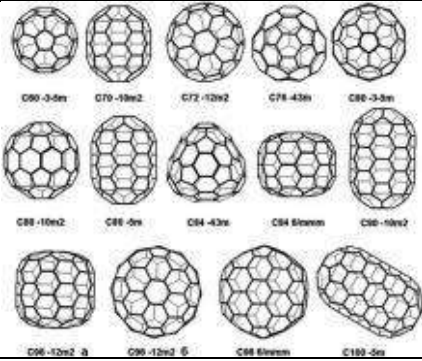
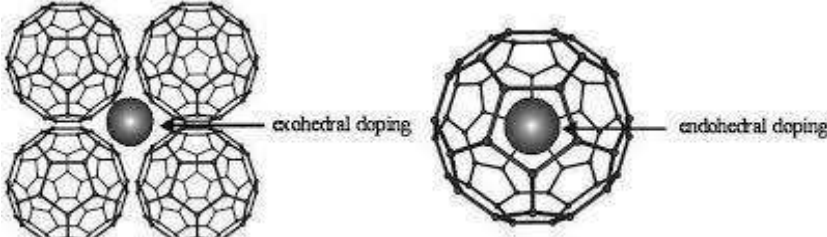
2.Special Carbon Based Nanomaterial.

Carbon is a fascinating element that has been regarded as an essential component of all living things. Carbon's capacity to link to itself to create polymers permits it to play such a significant part in biological processes. This feature may also be employed to create the diverse structures that make carbon such a valuable asset due to its exceptional features such as outstanding mechanical characteristics, variable morphologies, high thermal conductivity, and high corrosion resistance [12, 13,14]. Modern science and technology centred on carbon-based nanomaterials are changing at a fast pace with the potential to replace or complement current systems. Carbon-based materials that can be produced and characterised at the nanoscale have become a cornerstone in nanotechnology. The morphologies and topographies of these carbon compounds can be quite diverse. As the well-known allotrope of carbon based nanomaterial demonstrate, they can have hollow or filled frameworks and can assume a variety of forms . The carbon family consists of several unique nanomaterials, including CNTs, fullerenes, graphene, carbon nanohorns, carbonbased quantum dots, and many others [15]. Graphene and

carbon nanotubes are all sp^2 hybridized carbon allotropes. Due to their remarkable features such as electrochemical stability, high charge carrier mobility, and mechanical flexibility have gotten a lot of interest[16]. Hence, chemical separation, superlubricity, electronics, and catalyst support are only a few of the applications of graphene and carbon nanotubes. 3D nanodiamonds possess both the sp^3 and sp^2 carbon atoms, with the reconstruction of the sp^2 playing a key part in its stability. The Nano-diamonds have appealing surface areas, adjustable surface morphologies, and high hardness, hence, their novel applications in cosmetics and biomedicine.

Carbon nanomaterials (CNMs) have attracted a lot of interest in recent decades due to their exceptional features. The types of different carbon nanomaterials available the existing three allotropes of carbon fullerene carbon nanospheres first prepared by Kroto *et.al* in 1985, carbon nanotubes (CNT) having a cylindrical shape, and grapheme obtained from graphite contains an extended hexagonal lattice of sp^2 -bonded carbon atoms. Hence, they are characterized by remarkable chemical, mechanical, and electrical features that offer tremendous possibilities in applications such as carbon fibres, energy storage, conversion devices, biosensors, and catalysts. Carbon nanomaterials are being used to improve a variety of products, including electronics, lubricants, composites, and sporting equipment . Carbon based nanoparticles have a wide range of applications due to their unique chemical characteristics and the variety of carbon nanostructures that may be created. Some of them are discussed here :

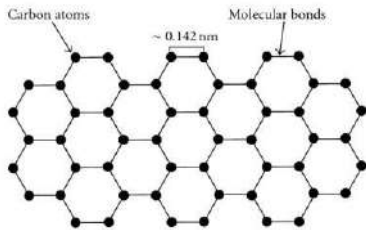
i) Fullerne

Discovered in	1985
Discovered by	Sir Harold W. Kroto
Also known as	Buckminsterfullerene , Buckyball
Hybridisation	Sp^2
Types	C_{60} , C_{70} , C_{72} , C_{76} , C_{84} , C_{100}
Structure	
Solubility	Soluble in-1,2-dichlorobenzene, toluene, p-xylene, and 1,2,3-tribromopropane. Insoluble in- Water
Modification	<p>There are two main ways to modify fullerenes:</p> <ol style="list-style-type: none"> 1.Fullerene inner-space modification(Endohedral) and 2.Fullerene outer-surface modification(Exohedral). 

Purpose of modification	Endohedral fullerene – 1.act as robust nano-container for host target species. 2.Li- based endohedral fullerene show unique solid properties. 3.Li- based endohedral fullerene can be used as nano-scale lithium batteries. 4.Fullerene cages useful for storage of gases. Exohedral Fullerene- 1.Strongly affects electronic properties. 2.Act as scavenger for reactive oxygen species.
Application.	1.Conical Fullerene amphiphiles can be used as Drug delivery agent. 2.Water soluble cationic fullerene tetrapiperazino fullerene Exoxide(TPFE) used for targeted delivery of DNA and siRNA specifically for the lungs. 3. Combination of fullerene with polymer result in good flame retardant. 4. used as Lubricant.
Characteristics	Anticancer, Antioxidants ,Antibacterial ,Antiviral , Highly stable , Good conductivity

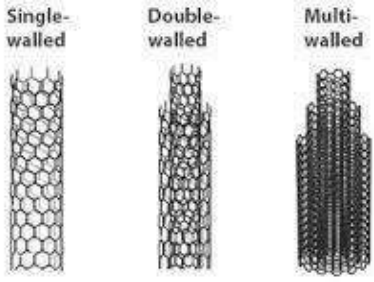
[17,18]

ii) Graphene

Discovered in	2004
Discovered by	Andre Geim and Konstantin Novoselov
Also Known as	Material of the future,
Hybridisation	Sp ²
Structure	
Stability	Soluble in - N-Methyl-2-pyrrolidone (NMP), dimethylformamide (DMF), and dimethyl sulfoxide (DMSO) Insoluble in-water or organic solvents
Properties	Thermal conductivity : Approx.3080- 5150 Wm ⁻¹ K ⁻¹ Theoretical surface area: 2630 m ² g ⁻¹ Mechanical Strength:- 130 GPa Electron Mobility:-10 ⁴ cm ² /Vs
Application	1. Electrochemical sensors 2.Biosensors 3.Electrodes 4. Liquid crystal display 5.Light emitting Diode 6. Fabrication of pressure sensors. 7. Pollution absorbent. 8. Non-metal catalysts.
Characteristics	1.Large specific surface area 2.Transparent in nature 3.Good Piezoresistive sensitivity 4.Excellent mechanical strength 5.Electronic conductivity.

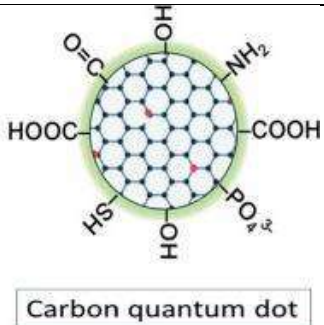
[19,20]...

iii) Carbon Nanotube

Discovered in	1991												
Discovered by	S.Iijima												
Also known as	Buckytubes												
Hybridisation	sp ²												
Types	Single Walled Carbon Nanotube Double Walled Carbon Nanotube Multiwalled Carbon Nanotube												
Structure													
Stability	Soluble in : Inorganic solvent Insoluble in : Water and Organic Solvent												
Properties	<table border="1"> <thead> <tr> <th>properties</th> <th>SWCNT</th> <th>MWCNT</th> </tr> </thead> <tbody> <tr> <td>Diameter</td> <td>0.4 to 2 nm</td> <td>0.33 to 0.42 nm</td> </tr> <tr> <td>Electrical conductivity</td> <td>10² to 10⁶ Scm⁻¹</td> <td>10³ to 10⁵ Scm⁻¹</td> </tr> <tr> <td>Thermal Conductivity</td> <td>Approx.6000 Wm⁻¹K⁻¹</td> <td>Approx.2000 Wm⁻¹K⁻¹</td> </tr> </tbody> </table>	properties	SWCNT	MWCNT	Diameter	0.4 to 2 nm	0.33 to 0.42 nm	Electrical conductivity	10 ² to 10 ⁶ Scm ⁻¹	10 ³ to 10 ⁵ Scm ⁻¹	Thermal Conductivity	Approx.6000 Wm ⁻¹ K ⁻¹	Approx.2000 Wm ⁻¹ K ⁻¹
properties	SWCNT	MWCNT											
Diameter	0.4 to 2 nm	0.33 to 0.42 nm											
Electrical conductivity	10 ² to 10 ⁶ Scm ⁻¹	10 ³ to 10 ⁵ Scm ⁻¹											
Thermal Conductivity	Approx.6000 Wm ⁻¹ K ⁻¹	Approx.2000 Wm ⁻¹ K ⁻¹											
Application	<ol style="list-style-type: none"> 1.Rectifying diodes 2.Single Electron Transistor 3. Field Effect Transistor. 4.Biomedical devices 5. Drug Delivery 6.Cell Biology. 												
Characteristics	<ol style="list-style-type: none"> 1.High Tensile Strength 2.High aspect Ratio 3.Llight weight 4.Chemical Stability 5.Nanosize 												

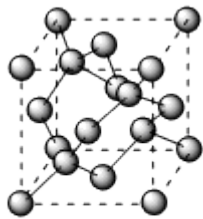
[21]

v) Carbon Quantum Dot

Discovered in	2004
Discovered by	Xu <i>et.al</i>
Also known As	Carbon Nano Dots , CQD's , C-dots or CD's
Hybridisation	
Structure	
Properties	Thermal Conductivity - 6.049 W/mK
Application	<ol style="list-style-type: none"> 1.Cell Imaging 2.Light Emitting Diodes 3. Nanomedicine 4. Solar Cells 5.Sensors 6.Catalysis 7.Bioimaging

[22]

iv) Nanodiamond

Discovered in	1963
Discovered by	K.V. Volkov, V.V. Danilenko, and V.I. Elin
Also Known as	Diamond nanoparticles
Hybridisation	Sp ³
Structure	
Properties	<ol style="list-style-type: none"> 1.Tensile Strength- (ND-reinforced aluminium) : 205 MPa 2. Thermal Conductivity: 3 W m⁻¹ K⁻¹ 3.Electrical Conductivity : 3.4 × 10⁻⁷ Ohm⁻¹ cm⁻¹
Application	<ol style="list-style-type: none"> 1. Bio sensors. 2.Wastewater treatment. 3.Imaging 4. Cancer Treatment. 5.Biomeical application
Characteristics	<ol style="list-style-type: none"> 1. Shows excellent optical properties. 2.High mechanical Properties. 3.High Specific surface area.

	<p>4. Have high number of functional group present on the surface.</p> <p>5. High thermal stability.</p> <p>6. Stable and Long fluorescence.</p>
--	--

[23,24,25]

3. Conclusion.

Currently, huge numbers of theoretical and experimental literature studies of carbon based nanomaterials and nanotechnology have been witnessed. Future technologies depend upon how Effectively these carbon based materials can be manipulated on the nanoscale for various applications . Carbon-based nanomaterials are a fascinating class of nanomaterial, consisting of fullerene , carbon nanotube , carbon based quantum dot , graphene, and. Moreover, the surfaces of carbon-based nanomaterials can be functionalized further to tune their properties for certain applications. CNTs and graphene are highly acknowledged members of the carbonbased nanomaterials family and they have been extensively explored for various applications due to their high surface areas, rapid charge transfer properties, and high mechanical strength. Carbon quantum dots have received great attention in the fields of sensing, nanomedicine, and bioimaging. After grapheme isolation in 2004 from graphite, large interest in ultrathin 2D materials was witnessed due to their numerous unprecedented features. The experimental evaluation of these materials is still at an early stage; however, these materials are being rapidly explored for useful applications. By using nanotechnology, some commercial devices have already been introduced , much more progress is anticipated, with nanomaterials being introduced into next-generation devices to cope with future high energy demands and playing a more active role in biosensors and nanomedicine to fight against existing and novel diseases. Nanotechnology can play an active role in the decontamination of water and the recycling of wastewater. Future challenges faced by modern society can be fixed with a better understanding and the rapid development of nanotechnology.

References

- [1] Neksumi Musa, Sushmita Banerjee, N.B. Singh and Usman Lawal Usman, January (2023) Carbon Nanomaterials and Their Applications , Materials Research Foundations , Volume. 135, pages 40-71, DOI:10.21741/9781644902172-3
- [2] Wolfgang G. Kreyling , Manuela Semmler-Behnke and Qasim Chaudhry , June (2010) , A Complementary Definition of Nanomaterial , Nano Today , Volume 5, Pages 165-168 , DOI:10.1016/j.nantod.2010.03.004
- [3] Nikita Rao , Rasmeet Singh and Lavisha Bashambu (2021) Carbon-based nanomaterials: Synthesis and prospective applications , Materials Today: Proceedings , Volume 44, Part 1, Pages 608-614 , DOI:10.1016/j.matpr.2020.10.593
- [4] Robert Birundu Onyancha , Kingsley Eghonghon Ukhurebor , Uyiosa Osagie Aigbe , Otolorin Adelaja Osibote , Heri Septya Kusuma and Handoko Darmokoesoemo , May (2022) A Methodical Review on Carbon-Based Nanomaterials in Energy-Related Applications , Adsorption Science & Technology , Volume. 2024, , Page 1 , DOI:10.1155/2022/4438286
- [5] Debabrata Maiti , Xiangmin Tong , Xiaozhou Mou and Kai Yang , March (2019) , Carbon-Based Nanomaterials for Biomedical Applications: A Recent Study , Frontiers in Pharmacology , Volume. 9 , Pages 1-16 , DOI:10.3389/fphar.2018.01401
- [6] Nadeem Baig , Irshad Kammakakam and Wail Falath , February (2021), Nanomaterials: a review of synthesis methods, properties, recent progress and Challenges , Materials Advances , Volume .2 , pages:1821-1871 , DOI:10.1039/d0ma00807a
- [7] Kapil D. Patel , Rajendra K. Singh and Hae-Won Kim , March (2019) , Carbon-based nanomaterials as an emerging platform for theranostics , Materials Horizon , pages 434-469 , DOI: https://doi.org/10.1039/c8mh00966j
- [8] Rasoul Madannejad , Nahid Shoaie , Fatemeh Jahanpeyma , Mohammad Hasan Darvishi , Mostafa Azimzadeh and Hamidreza Javadi , July (2019) , Toxicity of carbon-based nanomaterials: Reviewing recent reports in medical and biological systems Chemico-Biological Interactions , Volume 307, Pages 206-222 , DOI:10.1016/j.cbi.2019.04.036

-
- [9] Mathurin François , Kuen-Song Lin , Nova Rachmadona and Kuan Shiong Khoo , February (2024) , Utilization of carbon-based nanomaterials for wastewater treatment and biogas enhancement: A state-of-the-art review , *Chemosphere* , Volume 350, Page 141008 , DOI:10.1016/j.chemosphere.2023.141008
- [10] Y. Xie and X.Wang , September (2023) , Thermal conductivity of carbon-based nanomaterials: Deep understanding of the structural effects , *Green Carbon* , Volume 1 , Pages 47-57 , DOI:10.1016/j.greenca.2023.08.004
- [11] Massimiliano Papi , Marco De Spirito and Valentina Palmieri , June (2023) , Nanotechnology in the COVID-19 era: Carbon-based nanomaterials as a promising solution , *Carbon* , Volume 210, Page 118058 , DOI:10.1016/j.carbon.2023.118058
- [12] N. Díez, M. Sevilla and A.B. Fuertes , December (2021) , Dense (non-hollow) carbon nanospheres: synthesis and electrochemical energy applications , *Materials Today Nano* , Volume 16, December 2021, page 100147 , DOI:10.1016/j.mtnano.2021.100147
- [13] Thomas Hanemann and Dorothée Vinga Szabó , May (2010) , Polymer Nanoparticle Composites: From Synthesis to Modern Applications , *Materials (Basel)* , Volume 3 , Pages:3468-3517 , DOI:10.3390/ma3063468
- [14] Ayodeji Precious Ayanwale , Alejandro Donohué Cornejo , Juan Carlos Cuevas González , León Francisco Espinosa Cristóbal and Simón Yobanny Reyes López , August (2018) , Review of the synthesis, characterization and application of zirconia mixed metal oxide nanoparticles , *International journal of research –granthaalayah* , volume 6 , DOI:10.29121/granthaalayah.v6.i8.2018.1407
- [15] Vasilios Georgakilas , Jason A. Perman , Jiri Tucek and Radek Zboril , June (2015) , Broad Family of Carbon Nanoallotropes: Classification, Chemistry, and Applications of Fullerenes, Carbon Dots, Nanotubes, Graphene, Nanodiamonds, and Combined Superstructure , *Chemical Reviews* , Volume 115 , Pages : 4744–4822 , DOI: 10.1021/cr500304f
- [16] S. Iijima , M. Yudasaka , R. Yamada , S. Bandow , K. Suenaga , F. Kokai and K.Takahashi August (1999) Nano-aggregates of single-walled graphitic carbon nano-horns , *Chemical Physics Letters* , Volume 309, 13 August 1999, Pages 165-170 , DOI:10.1016/S0009-2614(99)00642-9
- [17] Peter.J.F.Harris , November (2020) , Fullerene Polymers: A Brief Review. , *Journal:C* , Volume 6 , DOI:10.3390/c6040071
- [18] Ayawei Nimibofa1, Ebelegi Augustus Newton, Abasi Yameso Cyprain and Wankasi Donbebel , June (2018) , Fullerenes: Synthesis and Applications , *Journal of Materials Science Research* , Volume 7 , Pages 22-36 , DOI : 10.5539/jmsr.v7n3p22.
- [19] Kenji Watanabe , Takashi Taniguchi , Efthimios Kaxiras and Pablo Jarillo-Herrero , March (2018) , Unconventional superconductivity in magic-angle graphene superlattices , *Nature* , volume 556 , pages 43–50 , DOI: 10.1038/nature26160
- [20] L. S. Sundar , M. A. Mir, M. W. Ashraf and F.Djavanroodi , September (2023) , Synthesis and characterization of graphene and its composites for Lithium-Ion battery applications: A comprehensive review , *Alexandria Engineering Journal* , Volume 78, Pages 224-245 , DOI:10.1016/j.aej.2023.07.044
- [21] Rajwant Kaur , April (2018) , Carbon Nanotubes: A Review Article , *International Journal for Research in Applied Science and Engineering Technology* , Volume 6 , Pages 5075-5079 , DOI:10.22214/ijraset.2018.4827
- [22] Derya Ozyurt , Mohammad Al Kobaisi , Rosalie K. Hocking and Bronwyn Fox , September (2023) , Properties, synthesis, and applications of carbon dots: A review , *Carbon Trends* , Volume 12 , Article :100276 , DOI:10.1016/j.cartre.2023.100276
- [23] Elena Perevedentseva , Yu-Chung Lin and Chia-Liang Cheng March (2020) , A review of recent advances in nanodiamond-mediated drug delivery in cancer , *Expert opinion on Drug Delivery* , Volume 18 , Pages 369-382 , DOI:10.1080/17425247.2021.1832988
- [24] Vadym Mochalin , Olga Shenderova , Dean Ho and Yury Gogotsi , December (2011) , The Properties and Applications of Nanodiamonds , *Nature Nanotechnology* , Volume 7 , Pages 11-23 , DOI:10.1038/nnano.2011.209
- [25] Luca Basso , Massimo Cazzanelli , Michele Orlandi and Antonio Miotello , June (2020) , Nanodiamonds : Synthesis and Application in Sensing, Catalysis, and the Possible Connection with Some Processes Occurring in Space , *Applied Sciences* , Article:4094 , DOI : 10.3390/app10124094.

Comparative Assessment of Zirconia as a Biomaterial Synthesized Via Two Different Methods

V.G. Thakare^{*1}, R. K. Watile²

¹ Department of Physics, Shri Shivaji College of Art, Commerce and Science, Akola ²Department of Civil Engineering, College of Engineering and Technology, Akola

*(Corresponding author email: vaishaliwatile@gmail.com)

Abstract

The objective of the following study was a synthesis of Zirconia (ZrO_2) using two different methods such as sol-gel (SG), and co-precipitation (CP) and evaluation of its structural and biological properties. The sample was characterized by powder X-ray diffraction (XRD) and Field Emission Scanning Electron Microscopy (FE-SEM). The XRD pattern shows that the monoclinic phase was obtained for CP synthesized Zirconia and tetragonal phase for SG method. The FE-SEM images showed that the prepared sample of Zirconia having different morphology for these two different methods.

Keywords: Zirconia; Nanobiomaterials; biomedical application.

1. Introduction

Zirconia is a ceramic biomaterial in a crystalline form. It was accidentally identified by German chemist Martin H. Klaproth [1] in 1789 while he was working with certain procedures that involved the heating of some gems. Its mechanical properties are very similar to those of metals, and its color is similar to tooth color. In 1975, Garvie proposed a model to rationalize the good mechanical properties of Zirconia, by virtue of which it has been called **ceramic steel** [2]. The name Zirconium comes from Arabic word **Zargon**, which means golden in color. In late sixties the research and development of Zirconium as biomaterials was refined. The first recommended use of Zirconium as a ceramic biomaterial in the form of ball heads for Total Hip Replacements (THR) has been documented [3]. Zirconia has a bright future because of its high mechanical strength and fracture toughness and has unique a characteristic called transformation toughening, which can give it higher strength and toughness compared with other ceramics. The excellent electrical, mechanical, optical and thermal properties of Zirconia, makes it a good choice for application such as: structural materials [4], dental crowns [5], femoral heads for total hip replacement [6], solid oxide fuel cell (SOFC) electrolytes [7], air-fuel ratio sensors for automotive applications [8] and Catalytic application [9-12].

The present work was undertaken with a view to develop nanocrystalline Zirconia to characterize the materials for their structural properties employing two different techniques.

2. Experimental procedure

2.1 Sol-Gel synthesis

The ZrO_2 nanomaterial was synthesized using the method described by Heshmatpour *et al.* [4] with some modifications. Initially, n-propanol (AR graded) was added to Zirconium n-propoxide (70 wt %) (AR graded). Then resulting solution was hydrolyzed using a drop by drop addition of ammonia (AR graded) and distilled water with a pH value of 9 to 10. 3 g Hydroxypropyl methyl cellulose (AR graded) was added to the solution under vigorous stirring. After homogenization, the solution was stirred at room temperature for an hour so the resulting gel was polymerized. The gel was dried in an oven at temperature of 100°C for 12 hrs and sintered by using the microwave furnace at 300°C for 2 hrs.

2.2 Co-precipitation Method

Sodium hydroxide (NaOH) (AR graded) solution (pH10) was added drop by drop to aqueous zirconium chloride ($ZrOCl_2$) (AR graded). The precipitate of ZrO_2 was stirred for 1 hr and was allowed to settle over night followed by decantation and washing with distilled water. The resulting precipitate was dried for 24 hrs and sintered by using the microwave furnace at 800°C for 2 hrs.

2.3 Characterization

The Zirconia samples were characterized by the X-ray diffraction (XRD) analysis using Rigaku Miniflex-II diffractometer and then analyzed, using Ni-filtered $CuK\alpha$ radiation ($\lambda = 0.1542$

nm) in the step scanning mode, with tube voltage of 40 kV and tube current of 40 mA. The XRD patterns were recorded in the 2θ range of 20 to 70° , with a step size of 0.02° and step duration of 1 s. Field Effect Scanning Electron Microscopy (FE-SEM) technique was also used to observe the surface morphology. For this, a very small amount of powder was placed on an adhesive carbon tape, coated with gold/palladium and then observed in a FE-SEM (HITACHI S-4800).

3. Results and Discussions

3.1 X-ray diffraction (XRD) analysis

The structural properties are studied by X-Ray diffraction technique. The XRD pattern of SG synthesis ZrO_2 as shown in Fig. 1(A), which is well matched with standard ICDD file no, 01-079-1764 of ZrO_2 and showed tetragonal Phase. The XRD pattern of CP synthesis ZrO_2 as shown in Fig. 2(A) which is well matched with standard ICDD file no, 01-074-0815. It shows that ZrO_2 has a single pure phase with a monoclinic crystal structure which was obtained at $800^\circ C$.

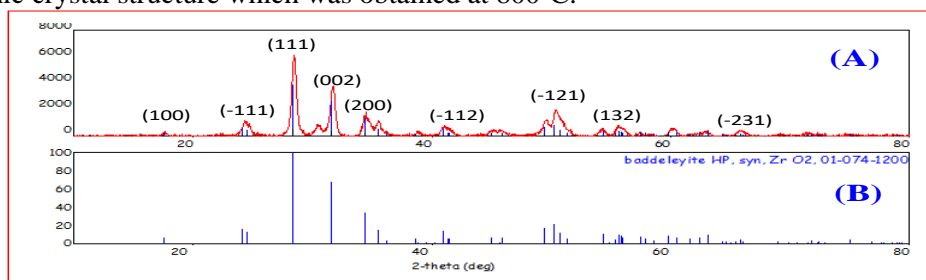


Figure 1: (A) XRD patterns of SG synthesis ZrO_2 sintered at $300^\circ C$ and (B) standard ICDD file of ZrO_2

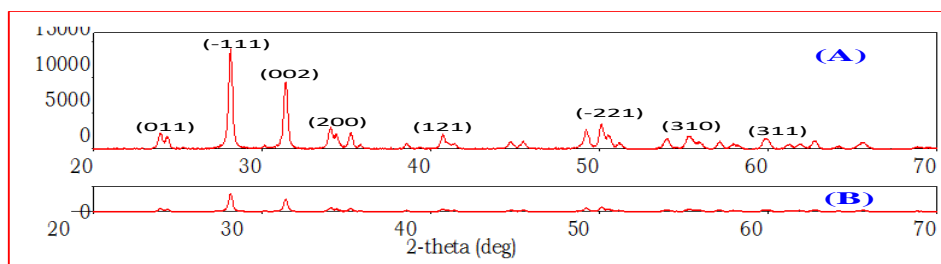


Figure 2: XRD patterns of CP synthesis ZrO_2 sintered at $800^\circ C$

3.2 FE-SEM analysis

Field Effect Scanning Electron Microscope is a well known and reliable technique to analyze nanoscale materials. It gives surface morphology of materials. The FE-SEM images for SG synthesis ZrO_2 as shown in Fig. 3(A-B) at different magnification. It shows that uniform distribution of particles and spherical like morphology. The FE-SEM images for CP synthesis ZrO_2 as shown in Fig. 4(A-B) at different magnification. It shows that amorphous nature and aggregated particles of materials.

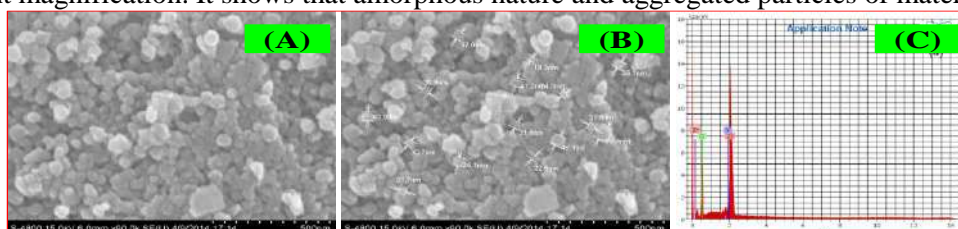


Figure 3: (A-B) FE-SEM images of SG synthesis ZrO_2 at different magnification, (C) EDAX spectrum of ZrO_2

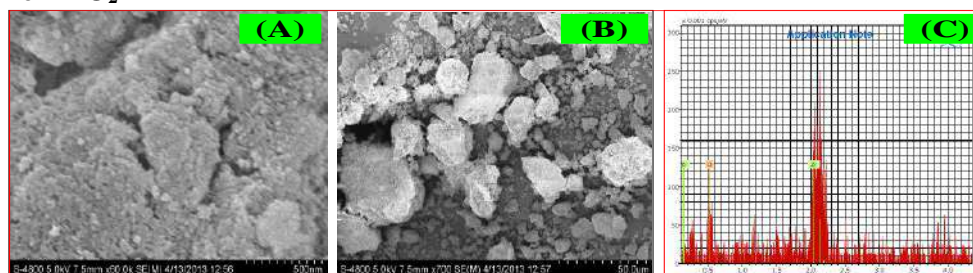


Figure 4:(A-B)FE-SEM images of ZrO₂ synthesis by CP at different magnification, (C) EDAX spectrum of ZrO₂

4. Conclusions

Zirconia materials are successfully synthesized using two different methods such as simple Sol-gel and co-precipitation methods. The formation of tetragonal and monoclinic crystalline phases was confirmed by powder XRD analysis. The morphology, particle size and nanostructure were analyzed using FE-SEM

References

- [1] C. Piconi, G. Maccauro, Zirconia as a Ceramic Biomaterial, *Biomaterials* 20 (1999) 1–25.
- [2] P.F. Manicone, P.R. Iommetti, L. Raffaelli, An overview of zirconia ceramics: basic properties and clinical applications, *Journal of Dentistry* 35 (2007) 819-826.
- [3] S. Pilathadka, D. Vahalova, T. Vosahlo, The Zirconia: a New Dental Ceramic Material- An Overview, *Prague Medical Report* 108(1) (2007) 5-12.
- [4] F. Heshmatpour, R. Aghakhanpour, Synthesis and characterization of nanocrystalline Zirconia powder by simple sol-gel method with glucose and fructose as organic additives, *powder technology* 205 (2011) 193-200.
- [5] C. Oetzel, R. Clasen, Preparation of zirconia dental crowns via Electrophoretic deposition, *Journal of Material Science Technology* 27 (2011) 8130-8137.
- [6] E.S. Elshazly, S.M. Elhout, M. Ali, Yttria tetragonal zirconia biomaterial: Kinetic investigation, *Journal of Matricula Science Technology* 27 (2011) 332-337.
- [7] J. Luo, R. Ball, R. Stevens, Gadolina doped ceria/yttria stabilized zirconia electrolytes for solid oxide fuel cell application, *Journal of Material Science* 39 (2004) 235-240.
- [8] J. Lee, Review on Zirconia air-fuel ratio sensors for automotive application, *Journal of Material Science* 38 (2003) 4247-4257.
- [9] E. Krumov, J. Dikova, K. Starbova, D. Popov, K. Kolev, L. D. Laude, Thin ZrO₂ Sol-gel films for catalytic application, *Journal of Material Science: Materials in Electronic* 14 (2003) 332-337.
- [10] L.L. Hench, J. Wilson, An introduction to bioceramics, London, World Scientific, (1999).
- [11] M.C. Wang, H.J. Huang, The phase transformation and crystallization kinetics of (1 - x) Li₂O–xNa₂O–Al₂O₃–4SiO₂ glasses, *Thermochimica Acta* 567 (2013) 93– 99.
- [12] J.S. Kim, D.H. Lee, S. Kang, D.S. Bae, H.Y. Park, M.K. Na, Synthesis and Microstructure of Zirconia Nanopowders by Glycothermal Processing, Jun-Seop Kim, *Et Al/Trans. Nonferrous Met. Soc. China* 19 (2009) 88-91.

Piezoelectric Materials for Energy Harvesting Technology

J.M.Bodulwar, Dr. A.B. Lad, Dr. K.R. Nemade

Department of Physics, Indira Mahavidyalaya, Kalamb Dist. Yavatmal 445401, Maharashtra, India.

Department of Physics, Amolakchand Mahavidyalaya, Yavatmal 445001, Maharashtra, India.

Department of Physics, Indira Mahavidyalaya, Kalamb Dist. Yavatmal 445401, Maharashtra, India.

Email - jawaharbodulwar@gmail.com, Mob No.7841989736

Abstract

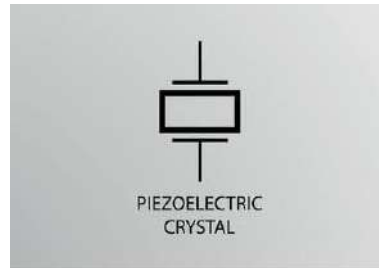
This review explores the intricate realm of piezoelectric energy harvesting, aiming to outline key parameters influencing performance and guide future developments. A universal theoretical model categorizes parameters into six groups, covering materials, structural designs, excitation sources, frequency and speed effects, electrical load impact, and energy accumulation. The discussion includes materials like ceramics, polymers, and nanomaterials, structural designs such as off-resonance and on-resonance, and sources of vibrations like contact force and acoustic power. Examples of potential applications range from structural health monitoring to human gait power. The review concludes by addressing future challenges in the field.

Keywords

Piezoelectric energy harvesting, Direct piezoelectric effect, Ambient waste energy, Voltage, current, charge, power source, Energy scavenger, power generator, Piezoelectric sensors Materials: ceramics, polymers, single crystals, composites, nanomaterials, lead-free materials Lead zirconate titanate (PZT), Perovskite structure, Doping, PVDF, P(VDF-TrFE), Lead-free materials: organic and inorganic, Tungsten bronze, aurivillius, perovskite families, Piezoelectric nanomaterials, Zinc oxide, Single crystals: PMN-PT, PZN-PT, Cantilever and proof mass structures, Off-resonance, on-resonance, impact designs, Excitation sources: direct contact force, low vibration force, hydraulic, pneumatic power, acoustic power, High-frequency, high-speed harvesters, Electrical load, impedance matching, Energy accumulation, Green energy, environmental protection, New materials development, Low-power all-in-one devices, Niche market applications, Gas igniters, ultrasonic energy harvesters, Future prospects, Challenges.

1. Introduction to Piezoelectric Energy Harvesting

A piezoelectric energy harvester is a device that utilizes external forces acting on piezoelectric elements to generate energy, typically converting ambient waste energy into usable electrical power. Its mechanism relies on the direct piezoelectric effect, where applied stresses induce proportional charges on the material's surface. These charges, when connected to an external circuit, result in current flow through the load, essentially turning the piezoelectric material into a voltage, current, charge, or power source. The device is also known as an energy scavenger or power generator. Traditionally, the direct piezoelectric effect has been employed in sensors like force, pressure, and acceleration sensors. However, in recent decades, there has been a growing interest in applying the direct piezoelectric effect to energy harvesters. This shift is driven by concerns over energy depletion, the need for carbon emission reduction, environmental considerations promoting clean and sustainable energy sources, and the increasing demand for low-power or powerless applications in smart devices, especially in situations where battery changes are inconvenient or costly.



2. Categories of Materials

2.1 Ceramics

Lead zirconate titanate (PZT) is a commonly used piezoelectric polycrystalline ceramic in various industrial applications, with a chemical formula $Pb[Zr_xTi_{1-x}]O_3$, denoted as PZT, and a perovskite structure. The piezoelectric effect in PZT arises from both intrinsic and extrinsic factors. The former involves the shift in relative anion/cation positions that preserves the ferroelectric crystal structures, while the latter is attributed to domain wall motion. For practical use, PZT materials are often doped with different elements such as Mn, La, Sr, Fe, Cu, etc., to achieve desired properties.

Various categories of PZT series are available on the market, each with its own properties, as outlined in Table 1, which also includes a few other piezoelectric materials. PZT stands out due to its superior performance, ease of manufacturability in bulk, film, or composite forms with diverse dimensions and shapes, and reasonable cost. It boasts a wide bandwidth, high natural frequency, and low loss, making it suitable for both off- and on-resonance applications. PZT's higher Curie point compared to polymers results in a broader temperature range. As a stiff material, it exhibits significant strain with minimal deflection. The relatively high piezoelectric coefficients (d and g) and mechanical coercive field make PZT promising for high-voltage applications.

2.2 Polymers

Poly(vinylidene fluoride) (PVDF) and copolymers like poly(vinylidene fluoride-trifluoroethylene) (P(VDF-TrFE)) stand out as widely used piezoelectric polymer materials, differing from ceramics in providing lower piezoelectric coefficients. However, these polymers offer advantages such as increased mechanical flexibility, lower stiffness, and higher chemical resistance, mitigating fatigue and enhancing device lifespan. Table 1 outlines typical material properties. PVDF and its copolymers find applications in sensors, actuators, and energy harvesters. Notably, PVDF materials, illustrated by examples, demonstrate their effectiveness. An energy harvester using PVDF-TrFE for MEMS scale applications was produced using standard MEMS techniques on a Si substrate. The device, featuring cantilever and proof mass structures with a $1.3 \mu\text{m}$ spin-coated piezoelectric layer and sputtered Al and Ti/Al thin film electrodes, exhibited a maximum power output of 35.1 pW for a tip displacement of $500 \mu\text{m}$ from a $1200 \times 300 \mu\text{m}^2$ cantilever. This corresponds to a power density of 97.5 pWmm^2 . A key advantage lies in the low crystallization temperature of PVDF-TrFE ($160 \text{ }^\circ\text{C}$), enhancing compatibility with CMOS technology or flexible electronics compared to ceramics. Consequently, PVDF-TrFE-based piezoelectric energy harvesters emerge as promising candidates for creating self-sustained lower-power electronics.

2.3 Lead-Free Materials

Lead-free materials have gained attention in recent decades due to environmental concerns associated with the commonly used lead-containing PZT ceramics. Given the toxicity of lead, researchers are actively exploring alternative materials to comply with environmental

regulations for new applications. Lead-free materials can be broadly categorized into organic and inorganic types. The organic category includes PVDF and copolymers, while inorganic lead-free materials encompass tungsten bronze, aurivillius (bismuth layer-structured ferroelectrics), and perovskite families.

Lead-free compositions with perovskite structures, such as BT (Barium titanate), BNT (Bismuth sodium titanate), and KNN (sodium potassium niobate), along with their derivatives, are actively researched. Among these, BT-based ceramics and KNN are notable, with KNN considered a promising lead-free material. Studies have explored BaTiO₃-based ceramics with doping, comparing them with PZT. For instance, compositions like BaTiO₃, Mn-doped BaTiO₃, and Mn-doped (Ba_{0.85}Ca_{0.15})(Ti_{0.95}Zr_{0.05})O₃ have been investigated. In a study comparing these materials with PZT, the results indicate that hard materials with a higher coercive field exhibit larger voltage and energy. Specifically, Mn-0.2 mol% doped BaTiO₃ ceramics generated 432 μJ of energy under experimental conditions of 45 s oscillation, 0.8mm displacement, and 80Hz frequency. While this performance is modest compared to PZT, it is noteworthy as a lead-free alternative, addressing environmental concerns.

2.4 Piezoelectric Nanomaterials

Piezoelectric nanomaterials and structures have garnered increased attention in recent years, with zinc oxide serving as a notable representative. Zinc oxide is abundant, cost-effective, chemically stable in air, and biologically safe, primarily adopting a hexagonal wurtzite structure. Unlike PZT, zinc oxide is not ferroelectric, but its nanostructures can be easily formed on various flexible and rigid substrates using low-temperature methods without the need for poling.

While the piezoelectric properties of zinc oxide may not match those of PZT, its versatility lies in the ability to form various nanostructures, including lateral nanorods, tilted nanorods, vertical nanorods, nanotubes, and nanowires. These structures have the potential to generate DC or AC voltage in response to external stresses, contributing to their energy-harvesting capabilities. Numerous examples of such applications have been extensively explored and are discussed further below.

2.5 Single Crystals

Single crystal materials exhibit significantly superior piezoelectric properties compared to conventional PZT materials, but their higher cost has limited their use in energy harvesters. Examples of piezoelectric single crystal materials include lead magnesium niobate–lead titanate (PMN-PT) and lead zirconate niobate–lead titanate (PZN-PT). To assess their potential for energy harvesting, a study by Z.G. Yang et al. investigated the performance of PZN-PT and PMN-PT, comparing them with PZT. The comparison, detailed in Table 3, reveals that single crystal materials demonstrate larger *d* and *g* values, suggesting improved energy-harvesting performance. The investigation utilized cantilever samples under both off-resonance and on-resonance conditions. In both scenarios, the single crystal samples exhibited higher power generation and efficiency compared to PZT materials. This suggests that single crystals could be advantageous for energy harvesting, although potential challenges such as fatigue, fabrication, cost, temperature sensitivity, and nonlinearity need consideration. The study focused on soft PZT materials, leaving the evaluation of hard materials an open question. Consequently, further research is needed to assess the energy harvesting performance of single crystal materials under diverse conditions.

3. Future Prospects

Energy-harvesting technology addresses the need for green energy and environmental protection. Challenges persist, but demand remains high. Key areas for advancing piezoelectric energy harvesters include:

- **New Materials Development:** Focus on materials that offer moderate voltage, higher current, scalability, and cost-effectiveness.
- **Low Power All-in-One Devices:** Develop small, low-power all-in-one electrical devices, like sensor nodes, to power modern, complex devices.
- **Niche Market Applications:** Explore niche markets such as harsh environments, inaccessible locations, emergencies, military applications, etc. Successful examples include gas igniters and ultrasonic energy harvesters for structural health monitoring

4. Conclusion

The efficiency of piezoelectric energy harvesting, as per the theoretical model, relies on material, structure, excitation, electrical load, frequency/speed, and time parameters. Various materials, including ceramics, polymers, single crystals, composites, nanomaterials, and lead-free materials, are used, with some surpassing PZT in specific aspects. Designs involve off-resonance, on-resonance, and impact structures, with cantilever and proof mass designs being common. Excitation sources include direct contact force, low vibration force, hydraulic, pneumatic power, and acoustic power. High-frequency and high-speed harvesters, though less common, may offer superior properties. Consideration of electrical load, impedance matching, and energy accumulation over time is crucial for practical applications.

Reference

- [1] a) L. Zuo, X. D. Tang, *J. Intell. Mater. Syst. Struct.* 2013, 24, 1405; b) S. R. Anton, H. A. Sodano, *Smart Mater. Struct.* 2007, 16, R1; c) M. R. Sarker, S. Julai, M. F. M. Sabri, S. M. Said, M. M. Islam, M. Tahir, *Sens. Actuators A* 2019, 300, 111634.
- [2] T. Li, P. S. Lee, *Actuators* 2019, 8, 8.
- [3] a) M. Prauzek, J. Konecny, M. Borova, K. Janosova, J. Hlavica, P. Musilek, *Sensors* 2018, 18, 2446; b) J. D. Song, J. Wang, *Sci. China Tech. Sci.* 2016, 59, 1012; c) S. G. Kim, S. Priya, I. Kanno, *J. Phys. Conf. Ser.* 2015, 660, 012001.
- [4] a) H. C. Liu, J. W. Zhong, C. K. Lee, S. W. Lee, L. W. Lin, *Appl. Phys. Rev.* 2018, 5, 041306; b) S. Banerjee, S. Bairagi, S. W. Ali, *Ceram. Int.* 2021, 47, 16402; c) W. C. Tian, Z. Y. Ling, W. B. Yu, J. Shi, *Appl. Sci.* 2018, 8, 645.
- [5] a) S. Priya, *IEEE Trans. Ultrason. Ferroelec. Freq. Control* 2010, 57, 2610; b) C. H. Choi, I. T. Seo, D. Song, M. S. Jang, B. Y. Kima, S. Nahm, T. H. Sung, H. C. Song, *J. Eur. Ceram. Soc.* 2013, 33, 1343.
- [6] T. Li, Degree Thesis, Nanyang Technological University, 2004.
- [7] S. Gao, H. R. Ao, H. Y. Jiang, in *7th Annual Int. Conf. on Materials Science and Engineering*, IOP Conf. Series: Materials Science and Engineering, IOP Publishing Ltd, Hubei, China, publisher 2019, 562, p. 012098.
- [8] S. W. Kim, T. G. Lee, D. H. Kim, K. T. Lee, I. Jung, C. Y. Kang, S. H. Han, H. W. Kang, S. Nahm, *Nano Energy* 2019, 57, 581.
- [9] S. Neiss, F. Goldschmidtboeing, M. Kroener, P. Woias, *J. Phys. Conf. Ser.* 2013, 476, 012035.
- [10] Y. Dong, T. Q. Yang, Z. Xiao, Y. Z. Liu, X. C. Wang, *J. Mater. Sci. Mater. Electron.* 2015, 26, 7921

Mechanism and Classification of supramolecular gels

Sakharam B. Sangale

Assistant Professor, Department of Physics, Indira Mahavidyalaya, Kalamb, Dist-Yavatmal.

Mo no. 7030240012, Email: sakhya813@gmail.com

Abstract:

Supramolecular gels have drawn a lot of interest because of their distinct characteristics and prospective uses in a variety of industries. This article gives a thorough explanation of supramolecular gels' categorization and uses. It is possible to comprehend these materials in a systematic way thanks to the categorization, which is based on the structures and mechanisms of gelation. The study also examines the several uses of supramolecular gels, such as medication delivery, tissue engineering, sensors, and catalysis. These gels are extremely flexible and adaptive for specific applications because to their variable physical characteristics and capacity to contain functional molecules and nanoparticles. The research emphasizes how crucial it is to comprehend the supramolecular interactions that cause gelation and the possibility of modifying gel characteristics to suit certain needs. The final discussion highlights the need for more research and development to fully realise the potential of supramolecular gels in improving materials science and allowing advanced uses.

Keywords: Supramolecular gel, Hydrogen Bond, Soft material's, Molecular Engineering

Introduction:

The scientific community has paid special attention to soft materials and intensively studying them for the last decade due to their special physical properties over the other materials. Soft materials are a type of material that has flexibility, deformability, and a low modulus of elasticity[1]. They are distinguished by their capacity to endure substantial deformations at low applied stresses. Polymers, gels, colloids, foams, and biological tissues such as muscle and skin are examples of soft materials. These materials are used in a variety of disciplines, including biomedical engineering, textiles, coatings, energy storage, and electronics. Understanding soft materials' mechanical, chemical, and physical characteristics, as well as how these qualities may be adjusted and optimized for specific purposes, is the reason behind to the study of soft materials. Especially supramolecular gel holds a major contribution in the field of advances of soft materials, there are many definitions of gels but, the international union of Pure and applied chemistry (IUPAC) defines gel as a non-fluid colloidal matrix of molecules or polymers suspended throughout the volume and this matrix traps the whole solvents and makes semi-solidus.[1], [2], [11], [12], [3]–[10] So, gel is nothing but the large amounts of solvents traps using colloidal or polymer matrix of the small amount of ligand, and the matrix of ligand framed by the self-gathering of small molecules through non-covalent interactions, such as hydrogen bonding, weak van der Waals forces, π - π staking and electrostatic interactions[1]–[6]. Supramolecular gels, which are created by non-covalent interactions between molecules, have several potential uses in various industries, such as; Drug delivery [13], Tissue Engineering [13], Sensors [14], Catalysis [4], Optoelectronics [9].

Supramolecular gels have special qualities that make them appealing materials for a variety of uses in many industries, including biocompatibility, reactivity to stimuli, and adjustable characteristics.

Mechanism of supramolecular gel formation:

Supramolecular gels are compositions of liquid-like solvents and solid-like ligands and despite containing 99% w/v of liquid phase solvent contribution in composition, the 1% w/v solid phase ligand traps the whole solvent in its crosslinks fibrous matrix to form a gel[2], [6].

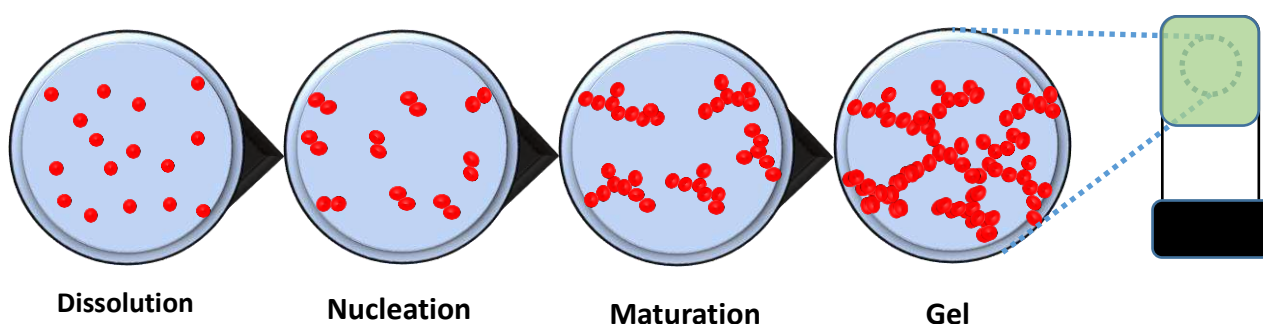
And this 3D ligand matrix of gel forms using small molecules or polymers self-assemble into a network structure during the development of supramolecular gels via non-covalent interactions such as hydrogen bonds, van der Waals forces, stacking of atoms, electrostatic interactions, and hydrophobic interactions. The following steps are often included in the process:

2.1 Dissolution: To create a transparent solution, the gelator molecules are dissolved in an appropriate solvent.

2.2 Nucleation: As a result of non-covalent interactions, the gelator molecules begin to cluster together to form nuclei.

2.3 Growth: The nuclei keep expanding and accumulating to build a three-dimensional network structure that covers the whole solution.

2.4 Maturation: As the network structure grows and stabilises, a gel-like substance that can sustain its own weight is produced.



Scheme.1. Schematic representation of supramolecular gel formation using different steps.

Classification of supramolecular gels:

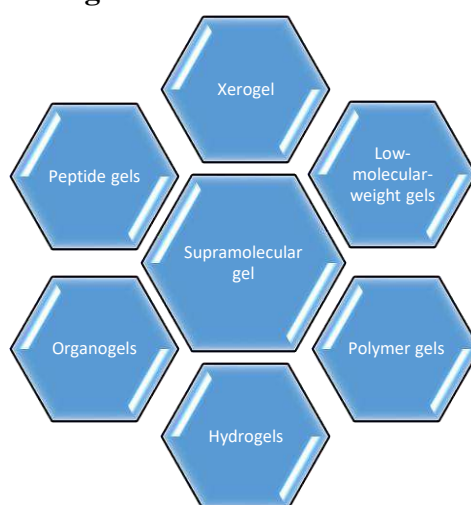


Image.1. Pictorial representation of classifications of supramolecular gels.

As shown in image.1. classification of supramolecular gels based on their molecular makeup can be categorized, which may have an impact on their characteristics and prospective

uses. Here we explain briefly that Supramolecular gels can be categorised in a number of ways, as mentioned here;

3.1 Low molecular weight (LMW) gels:

Low molecular weight gels are classified using the molecular size of the gelator we used while synthesis of supramolecular gels, small molecules that can self-assemble through non-covalent interactions such as hydrogen bonding, pi-pi stacking, and van der Waals forces create low-molecular-weight gels (LMW gels), and the majority of the molecules that make up these gels have a molecular weight of under 10,000 Dalton. The development of a 3D network of linked fibers or fibrils, which traps a solvent or surfactant to make a gel, is a key step in the self-assembly of LMW gels, further providing different external stimuli, such as variations in temperature, pH, or concentration, or mechanical agitation, can cause the gel to develop. To achieve certain features, LMW gels may be constructed using various chemical structures, such as amphiphilic compounds, peptides, and organic molecules. For instance, peptides can create gels that are nontoxic and biodegradable and are suited for biomedical applications, whereas amphiphilic compounds can create gels with great mechanical strength. LMW gels provide a number of benefits over other forms of gels, including their adaptable characteristics, simplicity in production, and potential for use in a variety of industries. These gels are excellent for uses like medication delivery, tissue engineering, and sensors because they may have specific features including mechanical strength, porosity, and reactivity to outside stimuli. LMW gels, all things considered, provide a flexible foundation for the creation of innovative materials with special features and prospective applications in a variety of disciplines[5].

3.2 Polymer gels:

Polymer gel are classified using the molecular size of gelator we used while synthesis of supramolecular gels, high molecular weight Polymer chains that may self-assemble through non-covalent interactions or crosslinking of polymer chains give rise to a particular sort of supramolecular gel known as a polymer gel. The majority of the time, these gels are made of polymers with a molecular weight of above 10,000 Dalton. A network of linked polymer chains is formed during the self-assembly of polymer gels, and this network traps a solvent or dispersion to form a gel, further providing different external stimuli, such as changes in temperature, pH, or concentration, or chemical crosslinking, might cause the gel to develop. To achieve certain features, polymer gels can be made using various chemical structures, such as natural or synthetic polymers. For instance, synthetic polymers like polyethylene glycol (PEG) and polyvinyl alcohol (PVA) may generate hydrophilic gels with great mechanical strength, whereas natural polymers like polyethylene glycol and hyaluronic acid can make biocompatible gels suited for tissue engineering applications. In comparison to other forms of gels, polymer gels have a number of benefits, including their adaptability, biocompatibility, and potential for use in a variety of industries. These gels are excellent for uses like medication delivery, tissue engineering, and sensors because they may have specific features including mechanical strength, porosity, and reactivity to outside stimuli. In general, polymer gels provide an adaptable framework for the creation of innovative materials with special features and prospective uses in a range of industries[15].

3.3 Hydrogel:

Hydrogel is classified using the solvent used while preparation of the supramolecular gel. A particular kind of supramolecular gel known as a hydrogel is created by chains of hydrophilic polymer that can absorb water and form a network structure. These gels are often made of organic or inorganic polymers with a high affinity for water, such as hyaluronic acid, polyethylene glycol (PEG), and polyvinyl alcohol (PVA). The hydrophilic polymer chains in hydrogels absorb water during the self-assembly process, causing them to expand and create a network structure, further providing different external stimuli, such as variations in temperature, pH, or concentration, might cause the gel to develop. Different chemical

structures and crosslinking techniques can be used to achieve various qualities in hydrogels. For instance, synthetic polymers like PEG and PVA may create hydrophilic hydrogels with great mechanical strength, whereas natural polymers like PEG and hyaluronic acid can create biocompatible hydrogels suited for tissue engineering applications. In comparison to other gels, hydrogels offer a number of benefits, including the potential for use in a variety of biomedical disciplines and biocompatibility and biodegradability. These gels are excellent for uses including drug delivery, tissue engineering, and wound healing because they may have specific qualities like mechanical strength, porosity, and response to external stimuli. Overall, hydrogels provide a flexible framework for the creation of innovative materials with distinctive qualities and prospective uses in a variety of industries, particularly the biomedical industry[6].

3.4 Organogel:

Organogels are classified on the basis of solvent present in the gel. Using non-covalent interactions including hydrogen bonds, pi-pi stacking, and van der Waals forces organic molecules that can self-assemble to produce supramolecular gels are known as organogels. The majority of the time, these gels are made of low-molecular-weight organic substances like fatty acids, fatty alcohols, and their derivatives. The development of a 3D network of linked fibres or fibrils, which traps an organic solvent to make a gel, is a key step in the self-assembly of organogels, further providing different external stimuli, such as variations in temperature, pH, or concentration, or mechanical agitation, can cause the gel to develop. To achieve certain qualities, organogels can be constructed using various chemical structures, such as fatty acids, fatty alcohols, and their derivatives. For instance, although fatty alcohols can create biocompatible and biodegradable organogels ideal for biomedical applications, fatty acids can create organogels with great mechanical strength. Organogels are superior to other forms of gels in a number of ways, including their high stability, biocompatibility, and potential for use in a variety of industries. These gels are excellent for uses like medicine administration, cosmetics, and food because they may have specific qualities including mechanical strength, porosity, and response to external stimuli. Overall, organogels provide a flexible foundation for the creation of innovative materials with distinctive qualities and prospective uses in many industries, including the food and cosmetics industries[1], [4].

3.5 Peptide gels:

A specific kind of supramolecular gel called a peptide gel is created when peptides self-assemble through non-covalent interactions such hydrogen bonds, electrostatic interactions, and hydrophobic interactions. Short peptide sequences, usually not longer than 20 amino acids, make up the majority of these gels. In order for peptide gels to self-assemble, a network of linked peptides must first develop. This network then traps a solvent to form a gel, and providing different external stimuli, such as variations in temperature, pH, or concentration, might cause the gel to develop. Different amino acid sequences and modification techniques can be used to design certain qualities into peptide gels. For instance, self-assembling peptides with high mechanical strength and biocompatibility, such RADA16 and Fmoc-FF, can create peptide gels that are appropriate for tissue engineering applications. Peptide gels are superior to other forms of gels in a number of ways, including their potential for use in a variety of biomedical sectors and their biocompatibility and biodegradability. These gels are excellent for uses including drug delivery, tissue engineering, and wound healing because they may have specific qualities like mechanical strength, porosity, and response to external stimuli. Overall, peptide gels provide a flexible platform for the creation of new materials with distinctive qualities and prospective uses in a variety of industries, particularly the biomedical industry[8].

3.6 Xerogel:

A procedure known as desiccation, which includes drying the gel under extreme vacuum, removes the liquid portion of a gel to produce xerogel, a type of solid substance. A low-density, extremely porous solid with a sizable surface area is the end product. Depending on the liquid

component that is eliminated during the drying process, xerogels can be made from a number of gels, including hydrogels, aerogels, and organogels. They can have specific features like large surface area, porosity, and mechanical strength and are often made of inorganic or organic materials including silica, alumina, and carbon. To achieve certain features, xerogels may be created with various chemical compositions and drying techniques. For instance, silica xerogels with high surface area and mechanical strength suited for catalytic applications may be made via sol-gel processing. Xerogels are superior to other types of materials in a number of ways, including their great surface area, low density, and potential for use in a variety of industries. Applications for these materials include thermal insulation, gas sensors, and catalytic supports. Overall, xerogels provide a flexible platform for the creation of new materials with distinctive qualities and prospective uses in a variety of industries, particularly in the catalysis, sensing, and energy storage industries[10].

We classified the supramolecular gels into different types on the basis of the type of solid ligand and the type of solvent present in the supramolecular gel system respectively.

CONCLUSION

In conclusion, the study of supramolecular gels has revealed their enormous promise in a variety of domains, from health applications to materials research. Researchers have been able to classify supramolecular gels based on their gelation mechanisms and structures via careful design and knowledge of their distinctive features. This categorization has given researchers a starting point for understanding and modifying these gels' characteristics, enabling their usage in a variety of applications. The creation of functional materials has shown to be a great fit for supramolecular gels. Their extremely adaptive and diverse physical characteristics, including mechanical strength, self-healing capacity, and stimuli reactivity, make them ideal for a variety of applications. These gels have been used in a variety of industries, including medicine delivery, tissue engineering, sensors, and catalysis. Their potential for the creation of new sensing platforms and catalytic systems, as well as for the targeted and controlled release of medicinal drugs, is further expanded by the possibility to include diverse functional compounds and nanoparticles inside the gel matrix. Furthermore, a logical approach to designing supramolecular gels with certain features has been made possible by our growing knowledge of the supramolecular interactions that promote gelation. Researchers may fine-tune the gel qualities, such as gelation kinetics, stability, and reactivity to external stimuli, by modifying the molecular constituents and their interactions. This degree of control makes it possible to create gels with specialized functions and creates new avenues for tackling difficult problems in fields like medication delivery and regenerative medicine. Supramolecular gel research has advanced significantly, however, there are still obstacles to be addressed. Our comprehension of these systems and their prospective applications will be improved by further investigation of the fundamental elements of gelation processes and the development of novel characterization techniques. The practical application of gel synthesis technologies will also depend on improvements in scalability and repeatability. In conclusion, the identification and use of supramolecular gels have significant potential to advance materials research and spur innovation across a range of industries. As this field of study develops, we may anticipate the creation of novel functional materials and ground-breaking applications that make use of supramolecular gels' distinctive characteristics and will enhance science, technology, and other fields.

References:

- [1] D. B. Amabilino, D. K. Smith, and J. W. Steed, "Supramolecular materials," *Chem. Soc. Rev.*, vol. 46, no. 9, pp. 2404–2420, 2017, doi: 10.1039/c7cs00163k.
- [2] N. M. Sangeetha and U. Maitra, "Supramolecular gels: Functions and uses," *Chem. Soc. Rev.*, vol. 34, no. 10, pp. 821–836, 2005, doi: 10.1039/b417081b.

-
- [3] D. Tripathy, A. S. Gadtya, and S. Moharana, "Supramolecular Gel, Its classification, preparation, properties, and applications: A review," *Polym. Technol. Mater.*, vol. 62, no. 3, pp. 306–326, 2023, doi: 10.1080/25740881.2022.2113892.
- [4] B. Escuder, F. Rodríguez-Llansola, and J. F. Miravet, "Supramolecular gels as active media for organic reactions and catalysis," *New J. Chem.*, vol. 34, no. 6, pp. 1044–1054, 2010, doi: 10.1039/b9nj00764d.
- [5] E. R. Draper and D. J. Adams, "Low-Molecular-Weight Gels: The State of the Art," *Chem*, vol. 3, no. 3, pp. 390–410, 2017, doi: 10.1016/j.chempr.2017.07.012.
- [6] E. M. Ahmed, "Hydrogel: Preparation, characterization, and applications: A review," *J. Adv. Res.*, vol. 6, no. 2, pp. 105–121, 2015, doi: 10.1016/j.jare.2013.07.006.
- [7] G. Li, L. Wang, Q. Han, and W. Liu, "Construction of homochiral alkaline-lanthanide heteronuclear helicates with Na⁺-selective bonding in the self-assembly process," *Dalt. Trans.*, vol. 48, no. 39, pp. 14595–14599, 2019, doi: 10.1039/c9dt02483b.
- [8] A. Baral, S. Basak, K. Basu, A. Dehsorkhi, I. W. Hamley, and A. Banerjee, "Time-dependent gel to gel transformation of a peptide based supramolecular gelator," *Soft Matter*, vol. 11, no. 24, pp. 4944–4951, 2015, doi: 10.1039/c5sm00808e.
- [9] X. Cheng, J. Pan, Y. Zhao, M. Liao, and H. Peng, "Gel Polymer Electrolytes for Electrochemical Energy Storage," *Adv. Energy Mater.*, vol. 8, no. 7, pp. 1–16, 2018, doi: 10.1002/aenm.201702184.
- [10] N. Mahata, M. F. R. Pereira, F. Suárez-García, A. Martínez-Alonso, J. M. D. Tascón, and J. L. Figueiredo, "Tuning of texture and surface chemistry of carbon xerogels," *J. Colloid Interface Sci.*, vol. 324, no. 1–2, pp. 150–155, 2008, doi: 10.1016/j.jcis.2008.05.006.
- [11] T. Patrick, "Polyacrylamide gel in cosmetic procedures: Experience with aquamid," *Semin. Cutan. Med. Surg.*, vol. 23, no. 4, pp. 233–235, 2004, doi: 10.1016/j.sder.2004.09.003.
- [12] J. Y. C. Lim, S. S. Goh, S. S. Liow, K. Xue, and X. J. Loh, "Molecular gel sorbent materials for environmental remediation and wastewater treatment," *J. Mater. Chem. A*, vol. 7, no. 32, pp. 18759–18791, 2019, doi: 10.1039/c9ta05782j.
- [13] H. J. Rathod and D. P. Mehta, "Acta Scientifica International Journal of Pharmaceutical Science," *Int. J. Pharm. Sci.*, vol. 1, no. 1, pp. 33–47, 2015.
- [14] Q. Lin *et al.*, "A novel strategy for the design of smart supramolecular gels: controlling stimuli-response properties through competitive coordination of two different metal ions," *Chem. Commun.*, vol. 50, no. 73, pp. 10669–10671, 2014, doi: 10.1039/c4cc03753g.
- [15] S. Das, R. Ghosh, D. Mandal, and A. K. Nandi, "Self-Assembled Nanostructured MoS₂ Quantum Dot Polyaniline Hybrid Gels for High Performance Solid State Flexible Supercapacitors," *ACS Appl. Energy Mater.*, vol. 2, no. 9, pp. 6642–6654, 2019, doi: 10.1021/acsaem.9b01171.
- [16] X. Zhou, P. Zhang, F. Zhao, and G. Yu, "Super moisture absorbent gels for sustainable agriculture via atmospheric water irrigation," *ACS Mater. Lett.*, vol. 2, no. 11, pp. 1419–1422, 2020, doi: 10.1021/acsmaterialslett.0c00439.
- [17] M. E. Powell and A. G. S. Cuthbertson, "Pest control," *Biologist*, vol. 60, no. 2, pp. 19–21, 2013.

Recent Advances in Natural Dyes for Dye Sensitized Solar Cell

Sanjay Takpire, Sandeep Waghuley

Department of Physics, Mahatma Jyotiba Fule College, Bhatkuli 444 602, India

Department of Physics, Sant Gadge Baba Amravati University, Amravati 444 602, India.

Corresponding Author: takpire.sanjay@gmail.com (Sanjay Takpire)

Abstract

This review paper offers a comprehensive examination of the utilization of natural dyes in Dye-Sensitized Solar Cells (DSSCs). Natural dyes, sourced from a variety of plants, fruits, and vegetables, present a sustainable alternative to synthetic counterparts in solar cell applications. The paper delves into the environmental sustainability, diverse sources, and potential challenges associated with the incorporation of natural dyes in DSSCs. Emphasizing ongoing research efforts, the review discusses strategies to improve stability and efficiency, considering biodegradability and end-of-life aspects, as well as innovative approaches, including hybrid systems. The paper also underscores the aesthetic appeal and potential integration of natural dye-based DSSCs into architectural designs. Future prospects outlined in this review involve scaling up production, enhancing public awareness, and fostering collaborative efforts to advance the viability and acceptance of natural dyes in the realm of solar energy.

Keywords: Natural Dyes; Dye Sensitized Solar Cell; Photovoltaic Cell

1. Introduction

Dye-sensitized solar cells (DSSCs), also known as Grätzel cells, are a type of solar cell that use a photoelectrochemical system to generate electricity from sunlight. Here are some reasons why Dye Sensitized Solar Cells are of interest:

- DSSCs can be fabricated using low-cost materials and simple manufacturing processes. This makes them potentially more cost-effective than traditional silicon-based solar cells, which require expensive and complex manufacturing methods.
- DSSCs can be designed in various shapes and sizes, making them flexible and adaptable for different applications. This flexibility in design is particularly advantageous for integration into building materials, windows, or wearable technologies.
- DSSCs perform well under low-light conditions and can generate electricity in diffuse or indirect sunlight. This makes them suitable for regions with less sunlight or for indoor applications where conventional solar cells might not be as effective.
- DSSCs are generally lightweight and can be fabricated as thin films. This characteristic makes them suitable for portable applications, such as mobile devices, backpacks, or clothing.
- DSSCs can be made transparent, allowing them to be integrated into windows or other transparent surfaces without obstructing the view. This feature is attractive for building-integrated photovoltaics.

Despite these advantages, it's essential to note that DSSCs also have some challenges, such as stability issues over time and lower efficiency compared to traditional silicon-based solar cells. Researchers continue to work on improving the efficiency, stability, and scalability of DSSCs to make them more competitive in the solar energy market.

2. Importance of Natural Dyes in DSSC

Natural dyes play a crucial role in Dye-Sensitized Solar Cells (DSSCs) for several reasons, contributing to both environmental sustainability and improved performance. Here are some key aspects of the importance of natural dyes in DSSCs:

- Natural dyes are derived from plant extracts, fruits, vegetables, or other organic materials, making them a renewable and sustainable source of colorants. Using natural dyes aligns with the principles of green chemistry and promotes environmentally friendly practices in solar cell technology.
- The production and application of natural dyes typically involve fewer toxic chemicals compared to synthetic dyes, reducing the environmental impact of the solar cell manufacturing process. Avoiding the use of harmful chemicals aligns with the goal of creating more eco-friendly and sustainable technologies.
- Natural dyes are often more cost-effective than their synthetic counterparts. This affordability is especially important for making DSSCs economically competitive with other solar cell technologies.
- Natural dyes can be extracted from a wide range of sources, providing a diverse palette of colors and chemical compositions. This diversity allows researchers to explore various natural dye options, optimizing the absorption spectrum and enhancing the overall efficiency of DSSCs.

Despite the advantages of natural dyes, it's important to note that they also pose challenges related to stability, efficiency, and consistency. Researchers are actively working to address these challenges and improve the overall performance of DSSCs using natural dyes.

Integrating the benefits of natural dyes with advancements in solar cell technology can contribute to the development of more sustainable and environmentally friendly energy solutions.

3. Various Sources of Natural Dyes for DSSC

Natural dyes used in Dye-Sensitized Solar Cells (DSSCs) are derived from various plant sources, fruits, vegetables, and other organic materials. The choice of natural dye influences the absorption spectrum and overall performance of the solar cell. Here are some types of natural dyes commonly used or explored for DSSC applications:

- **Anthocyanins:**
 - Found in various fruits, flowers, and leaves, anthocyanins are water-soluble pigments responsible for red, purple, and blue colors.
 - Examples of sources include berries (blueberries, raspberries, etc.) and red cabbage.
- **Chlorophyll:**
 - Chlorophyll is the green pigment present in plants and is essential for photosynthesis.
 - Spinach, parsley, and other leafy green vegetables are potential sources of chlorophyll for DSSCs.
- **Carotenoids:**
 - Carotenoids are pigments responsible for yellow, orange, and red colors in fruits and vegetables.
 - Examples include lycopene from tomatoes, beta-carotene from carrots, and xanthophylls from marigold flowers.
- **Betainin:**
 - Betainin is a red pigment found in beets. It belongs to the betalain class of pigments.
 - Beets can be a source of natural dye for red or violet-colored DSSCs.

- **Blackberry and Raspberry Extracts:**
 - Extracts from blackberries and raspberries contain anthocyanins and can be used as natural dyes in DSSCs, contributing to the red and purple spectrum.
- **Pomegranate Peel Extract:**
 - Pomegranate peel contains pigments such as anthocyanins and ellagitannins, offering potential as a natural dye source for DSSCs.

It's important to note that the efficiency and stability of DSSCs depend not only on the type of natural dye used but also on the overall design of the cell, the electrolyte, and other factors. Researchers continue to explore and optimize natural dyes to enhance the performance and viability of DSSCs as a sustainable solar energy technology.

4. Future Prospects

The future prospects for natural dyes in Dye-Sensitized Solar Cells (DSSCs) hold promise and involve ongoing research and development efforts aimed at addressing challenges and optimizing their performance. Here are some potential future directions and advancements for natural dyes in DSSC applications:

Improved Efficiency:

- Researchers are working to enhance the light-harvesting efficiency of natural dyes in DSSCs. This involves identifying new natural dye candidates with broader absorption spectra and improved charge injection capabilities.

Stability Enhancement:

- Stability remains a challenge for DSSCs, and efforts are underway to improve the long-term stability of natural dye-based cells. This includes exploring strategies to enhance the dye's stability and prevent degradation over time, especially in the presence of light and harsh environmental conditions.

Novel Natural Dye Sources:

- Continued exploration of diverse natural sources for dyes, including novel plants, fruits, vegetables, and even unconventional sources such as microorganisms or algae, may lead to the discovery of new and efficient dye molecules.

Synergy with Synthetic Dyes:

- Researchers may explore hybrid systems that combine natural and synthetic dyes to leverage the advantages of both. This approach could lead to improved efficiency, stability, and tunability of the dye-sensitized solar cells.

Tandem and Multijunction Cells:

- Combining natural dyes with other types of solar cells in tandem or multijunction configurations may allow for more efficient utilization of the solar spectrum, further enhancing the overall efficiency of DSSCs.

As research in the field of DSSCs continues, it's likely that advancements in natural dye technology will contribute to the development of more sustainable and eco-friendly solar energy solutions. Collaboration between researchers, industry, and policymakers will play a crucial role in shaping the future of natural dyes in DSSC applications.

5. Conclusions

In conclusion, natural dyes for Dye-Sensitized Solar Cells (DSSCs) offer a promising avenue for sustainable and environmentally friendly solar energy applications. The unique properties of natural dyes, derived from various plant sources, fruits, and vegetables, make them attractive for use in solar cells. The future of natural dyes in DSSC applications depends on overcoming technical challenges, improving efficiency and stability, and advancing large-scale production methods. With ongoing research and collaborative efforts between scientists,

industry stakeholders, and policymakers, natural dyes have the potential to contribute significantly to the development of sustainable and efficient solar energy technologies.

Acknowledgement

Author is very much thankful to Principal, Mahatma Jyotiba Fule College, Bhatkuli 444 602, India for necessary academic help in this work.

References

- [1]. P. Wang, S. M. Zakeeruddin, J.-E. Moser, and M. Grätzel, "A new ionic liquid electrolyte enhances the conversion efficiency of dye-sensitized solar cells," *Journal of Physical Chemistry B*, vol. 107, no. 48, pp. 13280–13285, 2003.
- [2]. K. Fukui, R. Komiya, R. Yamanaka, A. Islam, and L. Han, "Effect of a redox electrolyte in mixed solvents on the photovoltaic performance of a dye-sensitized solar cell," *Solar Energy Materials & Solar Cells*, vol. 90, no. 5, pp. 649–658, 2006.
- [3]. M. R. Narayan, "Review: dye sensitized solar cells based on natural photosensitizers," *Renewable and Sustainable Energy Reviews*, vol. 16, no. 1, pp. 208–215, 2012.
- [4]. M. Grätzel, "Recent advances in sensitized mesoscopic solar cells," *Accounts of Chemical Research*, vol. 42, no. 11, pp. 1788–1798, 2009.
- [5]. G. Calogero, G. di Marco, S. Cazzanti et al., "Efficient dye-sensitized solar cells using red turnip and purple wild Sicilian prickly pear fruits," *International Journal of Molecular Sciences*, vol. 11, no. 1, pp. 254–267, 2010.
- [6]. W. Zhou, B. Zhao, P. Shen et al., "Multi-alkylthienyl appended porphyrins for efficient dye-sensitized solar cells," *Dyes and Pigments*, vol. 91, no. 3, pp. 404–412, 2011.

Investigation on effect of Cd^{2+} and K^+ doping on upconversion luminescence in $\text{Y}_2\text{O}_3:\text{YbEr}$ phosphor

Harsha S. Deshmukh and Dr. Gajanan G. Muley*

Department of Physics, Sant Gadge Baba Amravati University, Amravati, Maharashtra, India-444 602

* Corresponding author. Tel.: +91 721 2662279, ext-269; fax: +91 721 2662135.

E-mail address: gajananggm@yahoo.co.in, gajananmuley@sgbau.ac.in

Abstract

Upconversion (UC) phosphors have a wide range of technological uses. There is a tendency towards either finding a new efficient UC phosphor or improving the UC efficiency and other attributes of the currently available phosphor by modifying the synthesis process, adding other dopants, altering the size of the particulates, changing the environment, and other factors. Because of its superior chemical and physical characteristics, Y_2O_3 is one of the most investigated hosts for UC luminescence. The current work emphasizes the effect of Cd^{2+} and K^+ on UC emission in $\text{Y}_2\text{O}_3:\text{YbEr}$ UC phosphor. The phosphors have been synthesized with varying concentration of Cd^{2+} and K^+ . The impact of Cd^{2+} and K^+ dopants on UC emission has been observed. The UC emission spectra recorded with stimulation at 980 nm shows strong emission in red band and weak emission in green band. The possible application of prepared phosphors in optical thermometry has also been reported.

Keywords: Upconversion luminescence; combustion synthesis; powder X-ray diffraction; yttrium oxide, optical thermometry.

Synthesis and Characterization of Nano-composites decorated by Graphene for the advanced applications

Vaishnavi V. Pandhe,* Suraj V. Tayade, Sandeep A. Waghuley.
Post Graduate Department of Physics, Sant Gadge Baba Amravati University,
Amravati, India, 444 602.

*Corresponding author email: pandhevaishnavi01@gmail.com, sandeepwaghuley@sgbau.ac.in

ABSTRACT:

This review discusses nanocomposite based on graphene, as well as the synthesis of these graphene based nanocomposite. Various methods are discussed, including the sole -gel method, Hummers method, Co precipitation method, electrochemical method, etc. By using these methods, the graphene based nano-composites are prepared. Graphene-based nanocomposite possess mechanical, electrical, thermal, and optical properties. They have many applications in potential field sectors, such as super capacitor applications, biomedical applications, EMI shielding, sensors, and solar cell applications.

Keyword: Nanocomposite; graphene; advanced applications.

INTRODUCTION:

Nanotechnology is the field of application-based research in Nanoscience. It has expanded to include environmental remediation applications. It involves the study of manipulating and controlling matter at the micrometer scale. The micrometer is approximately 1 to 100 nanometers, which is 10^9 meters in length (2D). There are many types of nanosciences, such as nanotubes, nanoparticles, graphene, quantum dot, nano-medicine, nanocomposite and manufacturing composite materials. A nanoparticle is a particle that is 1 to 100 micrometers in size and consists of a macromolecule material containing the active ingredient. They are found in nature and can also be created by human activities. Due to their small size, nanoparticles have unique material properties and can be used in a variety of applications, such as medicine, engineering catalysis, environmental remediation, and manufacturing nanoparticles. Nanocomposite the general idea of nanocomposite is based on the concept of creating a very large interface between the nano sized building blocks and polymer matrix the main problem of nanocomposite are usually the homogeneous distribution of particles in the polymer matrix. And interfacial interaction Nanocomposite in which at least one of the phase shows dimension in nanometer range, i.e. ($1\text{nm}=10^9$). The materials used to make nanocomposite are separated into three categories: metal matrix nanocomposite, polymer matrix nanocomposite, and ceramic matrix nanocomposite. Properties: The electrical, thermal, mechanical, magnetic, chemical, radioactive, and watt ability properties of nanocomposite vary if the nanomaterial converts from bulk to nanoscale

Graphene: Graphene is an allotrops of carbon, is the thin, almost see through a sheet that is only one atom thick. it is incredibly lightweight but also incredibly strong , with a strength 100 times that of steel additionally, it has the unique property of being able to conduct electricity. of carbon consisting of a single layer of atoms arranged in a two dimensional honeycomb lattice nanostructures. Graphene is characterized as the thinnest material in our universe. It is a single atomic layer of graphite has been extensively studied owing to its exceptional electrical and mechanical properties. its two dimmensional sheet-like structures and excellent conductivity led to the use of graphene in a wide area of application because of its high surface area. Its has become a valuable and useful nanomaterial due to its exceptionally high tensile

strength this nanomaterial has made it desirable and practical. Transparency, electrical conductivity, and the world's thinnest two-dimensional substance Graphene is a single sheet of pure carbon arranged in a flat hexagon pattern. It has use in electronics, transportation, and medicine, among other fields. The high quality graphene also provides to be sparingly easy to isolate. Andre Geim Konstantin at the University of Manchester won the Nobel Prize in physics in 2010 for groundbreaking experiments regarding the two-dimensional material graphene. The elements of other allotropes, including graphite, charcoal, carbon nanotubes and fullerenes.

Graphene is made using one of two tree-type methods:

1. Exfoliation
2. A liquid exfoliation
3. The method of chemical deposition

Synthesis methods of nanocomposites from Graphene:

a) Sol –Gel: The technique is a standard procedure for creating nanoparticles with various chemical compositions. The creation of homogenous sol from precursors and its transformation into gel form the cornerstone of the sol-gel process.

b) Electrochemical Method : the electrochemical synthesis method for the fabrication of nanostructured energy materials, and various nanostructures, such as nanostructures, such as nanorods nanowires, nanotubes, nanosheets, nanostructures, and composite, and nanostructures can be easily fabricated with advantages of low cost.

c) Co-precipitation method: Co-precipitation is the simultaneous precipitation of multiple compounds from a solution. This is the most effective inextensive method for nanoparticle precipitation. In this method, metal precipitates from a salt precursor as hydroxide in the presence of base in a solvent.

d) Hummer's method: Hummer's method is a chemical method for the production of graphite oxide by adding potassium permanganate to a graphite solution containing sodium nitrate and sulfuric acid.

Applications:

1. The utilization of decorated ZnO graphene nanocomposites not only enhances the photocatalytic property of ZnO (Gz) nanocomposite, but also finds applications in the field of energy, particularly in the development of nanofiber-like nanocomposite for supercapacitor energy storage devices.[1]
2. Graphene-based nanocomposite exhibit superior performance in Lithium-ion batteries due to their high power density and rapid charging capabilities in hydrogen fuel.[13]
3. The nanocomposite based on graphene, when utilized in EMI shielding applications, exhibit remarkable compatibility in augmenting radiation adsorption and electromagnetic radiation shielding properties.[31]
4. In the textile industry, the utilization of protective clothing is prevalent, while in the military sector, nanofibers find application to enhance the capacity for chemical and biological detection.[8]
5. The CeO₂-MnO₂/RGO Nanocomposite Were Used for the Electrode Material In Super capacitor Application.[5]
6. Facile Synthesis Of ZnO Reduced Graphene Oxide For NO₂ Gas Sensing Application [25]

Conclusions:

There are several ways to create graphene-based nanocomposite, including Hummer's method, co-precipitation, electrochemical, and hydrothermal methods; however, the sol-gel approach is the most efficient. The properties of graphene like tough, flexible, lightweight, and with a high resistance thinness and conductivity have led to global research into its applications as a semiconductor. Additionally, a review of numerous applications that concentrated on future aspects was conducted. These included the most beneficial applications in fields with great promise, such as solar cells, EMI shielding, super capacitors, and sensors.

REFERENCES:

- [1] Gayathri, S. et al Synthesis of ZnO decorated graphene nanocomposite for enhanced photocatalytic (2015). Structural ceramic nanocomposites: properties.)2014, Journal of Applied Physics, 115(17)
- [2]Pena et al.have been prepared by the Go onto functionalized Fe₃O₄-NP5 surface by the carbodimide method.(2021) (Graphene-based nanocomposites in analytical extraction processes. TrAC Trends in Analytical Chemistry, 142, 1163030
- [3] Ojha, G. P., Pant, B., Park, S. J., Park, M., & Kim, H. Y. (2017). Synthesis and characterization of reduced graphene oxide decorated with CeO₂-doped MnO₂ nanorods for supercapacitor applications. Journal of colloid and interface science, 494, 338-344.
- [4] Pan, S., & Liu, X. (2012). ZnS–Graphene nanocomposite: Synthesis, characterization and optical properties. Journal of Solid State Chemistry, 191, 51-56
- [5]Saranya, et al(2016). Graphene-zinc oxide (G-ZnO) nanocomposite for electrochemical supercapacitor applications. Journal of Science: Advanced Materials and Devices, 1(4), 454-460.
- [6]Kumaret al (2012). Synthesis, characterization and optical properties of graphene sheets-ZnO multipodnanocomposites. Journal of alloys and compounds, 526, 129-134.
- [7] Mandhare, et al (2020). Preparation and thermal conductivity investigation of reduced graphene oxide-ZnO nanocomposite-based nanofluid synthesised by ultrasound-assisted method. Materials Research Innovations,
- [8]Kumar, N et al. (2015). Facile synthesis of ZnO–reduced graphene oxide nanocomposites for NO₂ gas sensing applications. European Journal of Inorganic Chemistry, 2015(11), 1912-1923.

Investigation of AC electrical analysis of EC/PVC blend films

***Welekar N.R., Raulkar K.B., Lamdhade G. T.**

Department of Physics, VidyaBharati Mahavidyalaya, Amravati(M.S.) India 444602

*Corresponding Authors: Email: nayanathakare12345@gmail.com

Abstract

The thin films of 1 : 1 EC/PVC polyblend system of pure and doped with 5%, 10%, 15%, 20% and 25% salicylic acid (SA) where prepared by using isothermal evaporation technique. The electrical conduction mechanism was studied by investigating the electrical properties of salicylic acid doped 1 :1 Ethyl Cellulose (EC)-Polyvinyl Chloride (PVC) blends. The DC conductivity was measured as a function of temperature (303-343) frequency electric field. The AC conduction mechanism was discussed in terms of AC Conductivity (σ_{ac}), Dielectric Loss (ϵ''), Dielectric Constant (ϵ') as a function of temperature (303-343K) and frequency (20Hz-1MHz) by LCR meter. The results reveal that, the AC conductivity of thin films increases with increase of temperature for all values of frequencies and it increases with increase of frequency at constant temperature. The dielectric constant decreases with increase of temperature of blends.

Key Words : EC- Ethyl cellulose, PVC-polyvinyl chloride, salicylic acid.

I. Introduction

When two or more polymers are mixed together, the properties of the resulting mixture are quite different, which can be potentially useful. In number of application bands study is essential, for light emitting diode, transparency in the visible region combine with high electrical conductivity [1]. Various research groups have undertaken extensive studies of the parameters that govern miscibility and have attempted to gain a good knowledge of the thermodynamics of the mixtures [2-7]. This provides the relationship between the phase behaviour of blends and polymer – polymer energy interaction this relationship predicts whether the two components will form miscible or immiscible blend. The study of dielectric constant, dielectric loss and AC conductivity, as function of frequency is one of the most convenient and sensitive methods of studying the polymeric structure [8]. For determining the dielectric behaviour with the physical structure is very important.

PVC is a commercially available polymer with good dielectric constant and is good mechanical stiffener [9, 10] PVC is polar and is used in cable and wire covers, children toys and medical devices [11] PVC is widely used due to its high electrical and chemical resistance and ability to be mixed with wide range of physical and chemical properties [12]

EC is weakly polar which has excellent chemical resistance and good mechanical properties. It is thermally stable. EC is used for many application due to its activeness [13] EC is already extensively used for films thickening agents [14, 15] It is compatible with other polymers and plasticizers and can therefore be use to make waterproof films [16, 17] Many researcher reported the electrical conductivity of PVC and EC.

In the present work, we study AC conduction to identify the mechanism of electrical conduction.

II. Experimental details

Polyvinyl chloride (PVC) of standard grade supplied by poly Chem industry, Mumbai and EC from s.d. Fine Chem. Ltd., Mumbai, India where used for the study. Solvent Tetrahydrofuran (THF) and salicylic acid as used as dopant.

Method of Preparation

The two polymers ethyl cellulose (EC) and polyvinyl chloride (PVC) were taken in the ratio 1:1 and dissolved in common solvent (THF) Tetrahydrofuran. Then the poly-blend films of EC-PVC pure and doped with salicylic acid in different weight percentage (5%, 10%, 15%, 20%, 25%) were prepared by isothermal evaporation technique [18-22] but the results are only interpreted for EC-PVC pure and 25% doped with salicylic acid. Further the dried films were sandwiched between silver coins for better electrode contact. The thickness of the film was measured by digital micrometer (Mitutoyo Corporation, Japan)

Then the film was kept between the electrodes of specially designed sample holder. The AC frequencies were applied (in the range 1kHz-1MHz) across the sample by using the 4284 A precision LCR meter (model no4284)(20Hz-1MHz) supplied by Agilent Technologies, Singapore and the corresponding Dielectric constant (ϵ_r), AC conductivity were measured in the temperature range 323 K -363K. From the dielectric data, the values of AC Conductivity of the samples were calculated by using the relation eq.1 [23].

$$\sigma_{ac} = f \epsilon_r \tan \delta / 1.8 \times 10^{10} \quad \dots(1)$$

where, f – frequency applied in Hz

ϵ_r – Dielectric Constant at frequency f

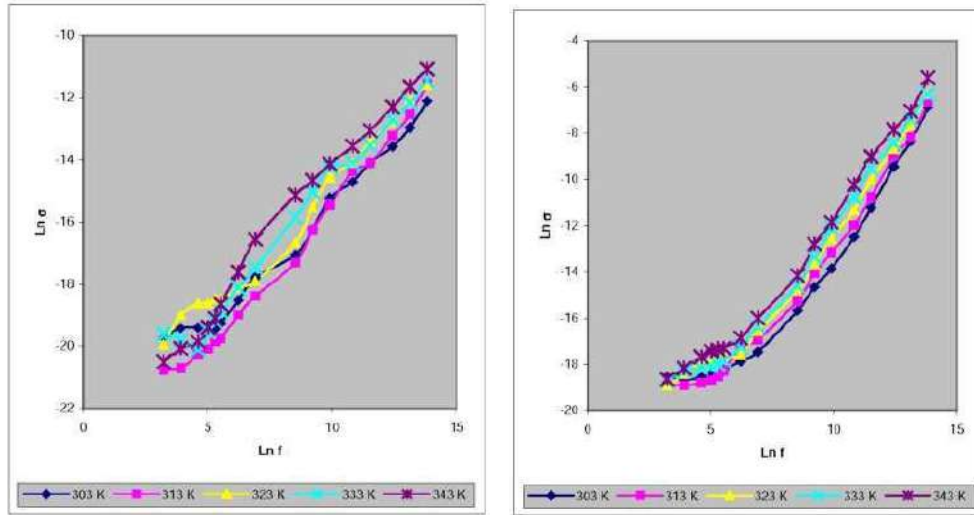
$\tan \delta$ - Dielectric loss tangent

III. Results and Discussion

- i. Variation of Conductivity with **Ln f** at different constant temperature. {Fig. 1 (a) to (b)}
- ii. Variation of Dielectric Constant (\square_r) with **Ln f** at different temperatures {Fig. 2(a) to (b)}
- iii. Variation Dielectric Loss (\square'') with **Ln f**. {Fig. 3 (a) to (b)}
- iv. The Results of the present study have been presented in the form of graphs as under. Variation of Dielectric Constant (\square_r) with temperature at different frequencies. {Fig. 4 (a) to (b)}
- v. Variation of Conductivity with temperature at different constant frequencies. {Fig. 5 (a) to (b)}

Prominent Findings

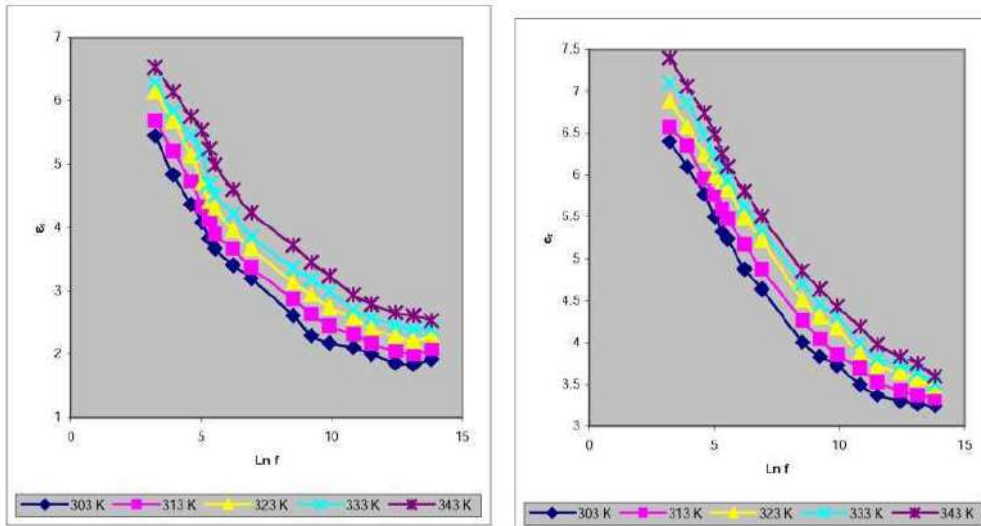
- At constant temperature, A C Conductivity (\square_{ac}) increases with the increase of frequency.
- At constant frequency, A C Conductivity (\square_{ac}) very marginally increases with the increase of temperature.
- At constant frequency, A C Conductivity (\square_{ac}) increases with the increase in the percentage of dopant.
- At constant frequency, Dielectric Constant (\square_r) increases with the increase of temperature.
- At constant temperature, Dielectric Constant (\square_r) decreases with the increase of frequency.



(a) 1:1 EC PVC SA (0)

(b) 1:1 EC PVC SA (25)

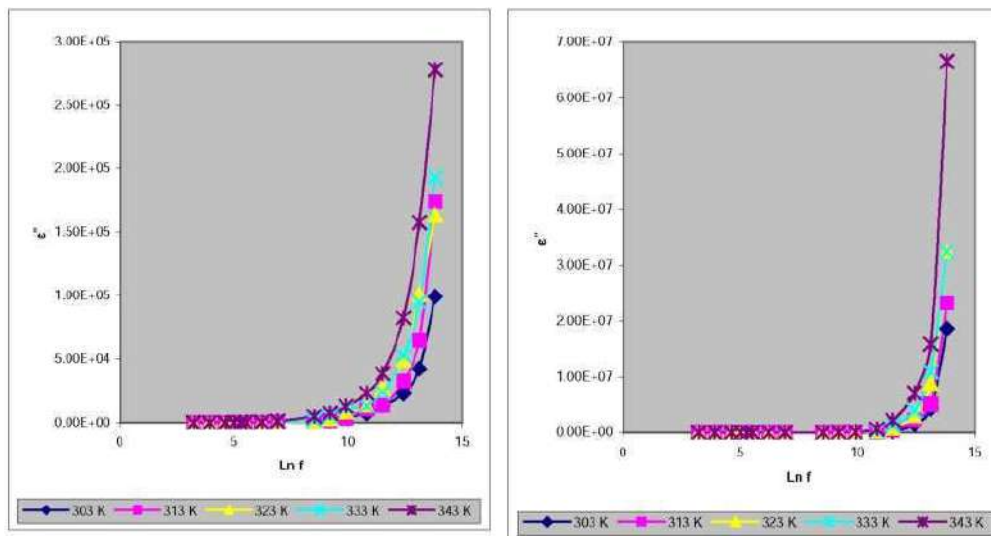
Fig. 1 (a) & 1 (b) variation of conductivity with freq. (Ln f) at different constant temperature



(a) 1:1 EC PVC SA (0)

(b) 1:1 EC PVC SA (25)

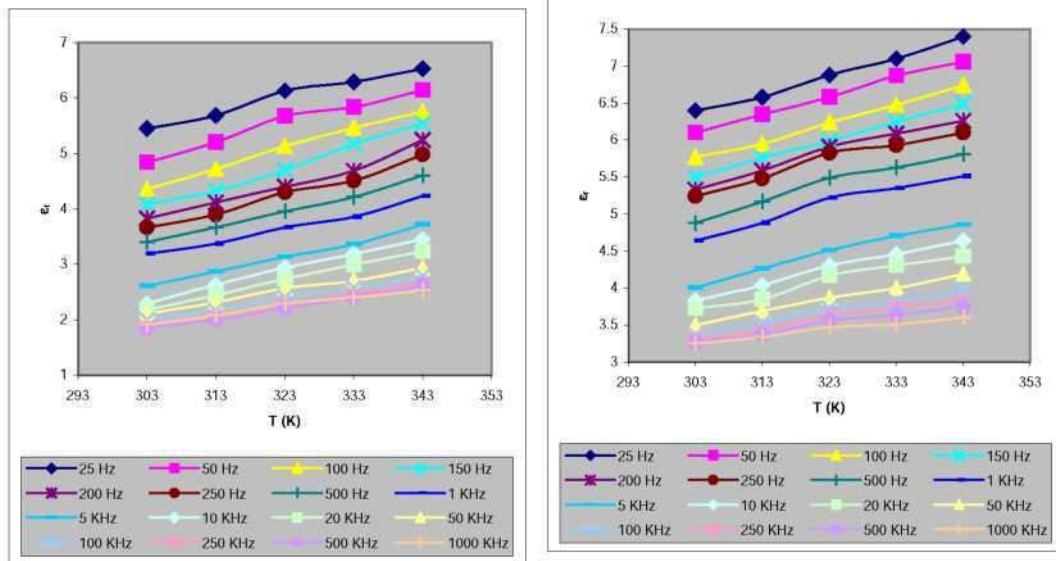
Fig.2(a) &2(b) Variation of dielectric constant (ϵ') with freq. (Ln f) at different constant temperature



(a) 1:1 EC PVC SA (0)

(b) 1:1 EC PVC SA (25)

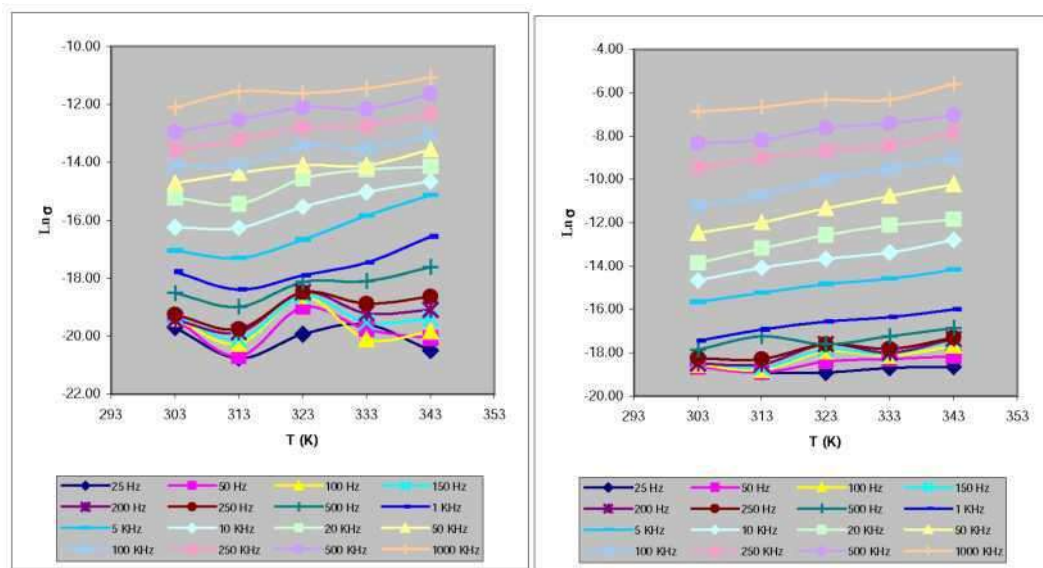
Fig.3(a) &3(b) Variation of dielectric loss (ϵ'') with freq. ($\ln f$) at different constant temperature



(a) 1:1 EC PVC SA (0)

(b) 1:1 EC PVC SA (25)

Fig.4(a) &4(b) Variation of dielectric constant (ϵ') with temp. at different frequencies



(a) 1:1 EC PVC SA (0)

(b) 1:1 EC PVC SA (25)

Fig.5(a) &5(b) Variation of conductivity with temperature at different frequencies

Conclusions

- i. The conductivity of 1:1 EC PVC system increases with increase in frequency.
- ii. The value of dielectric constant increases with increase in temperature.
- iii. AC conductivity of 1:1 EC PVC SA (25) is greater than 1:1 EC PVC SA (0) polyblend.

References :

- [1] N.C. Greeham, S.C. Moratti, D.D.C. Bradley, R.H. Friend, A.B. Holmes, *Nature* 365, 62 (1993)
- [2] Chakraborty S. C., Patil N. B., Das SK & Basu S *Indian J Pure Appl. Phys.* 29(1991)478.
- [3] Sangawar V S *Ph.D. Thesis* (Amravati University, India) (1995)
- [4] Belsare NG & Deogaonkar V S *Indian J Pure Appl. Phys.* 36(1998) 280
- [5] O. Olabisi, L.M. Robenson, M.T. Shaw. *Polymer-polymer miscibility*. New York: Academic Press; 1979.
- [6] DR. Paul, S. Newman, *Polymer blends*. New York; Academic Press; 1978.
- [7] JL. Halar, JM. Ubrich, JM. Nunzi, L. Monnerie, RS. Stein, *Polymer*, 1984; 25: 956
- [8] Kimura T and Kajiwaru M, *J Mater. Sci.* 33, (1998) 2955.
- [9] Choi NS and Park JK, *Electrochim Acta* 46: 1453 – 1459 (2001).
- [10] Muniyandi N, Kalaiselvi N, Periyasamy P, Thurunakaran R, Babu BR, Gopukumar S *et al.*, *J Power Sources* 96 : 14 – 19 (2001).
- [11] B. Balakrishnan, A. Jayakrishnan, "Chemical Modification of poly(vinyl chloride) using poly(ethylene glycol) to improve blood compatibility", in *Trends in Biomaterials and Artificial Organs*, vol. 18, 2, pp. 230-236, (2005)
- [12] Smith William F, "*Principles of materials science and engineering*" 'New York; McGraw Hill Publishing Company 2nd ed, pp 331-333, (1990)
- [13] Arvind Kumar, P K Khare, Alkesh Pal 11th International Journal of advance research in science and engineering, vol. 7, issue no. 3, (2018).
- [14] Su, X.; Tang, Z.; Tan, K.B.; Chen, J.; Huang, J.; Li, Q. Preparation and Characterization and Ethyl Cellulose Film Modified with Capsaicin. *Carbohydr. Polym.* 2020, 241, 116259.
- [15] Zhu, J.; Dong, X.-T.; Wang, X – L.; Wang, Y.-Z. Preparation and Properties of a Novel Biodegradable Ethyl Cellulose Grafting Copolymer with Poly(p-Dioxanone) Side – Chains. *Carbohydr. Polym.* 2010, 80, 350-359. [CrossRef]
- [16] Hosseini, A.; Ramezani, S.; Tabibiazar, M.; Ghorbani, M.; Samadi Kafil, H. Fabrication of Cumin Seed Oil Loaded Gliadin-Ethyl Cellulose Nanofibers Reinforced with Adipic Acid for Food Packaging Application. *Food Packag. Shelf Life* 2021, 30, 100754.
- [17] Shi, P.; Zuo, Y.; Zou, Q.; Shen, J.; Zhang, L.; Li, Y.; Morsi, Y.S. Improved Properties of Incorporated Chitosan Film with Ethyl Cellulose Microspheres for Controlled Release. *Int. J. Pharm.* 2009, 375, 67 – 74.
- [18] A. Narayan and H.P. Singh, *Indian Journal of Pure and Applied Physics*, Vol 29, 814-816, (1991).
- [19] R. Bahri, and R.K. Seth, *Indian Journal of Pure and Applied Physics*, Vol 35, 104-108, (1997).
- [20] V. Sangawar and C.S. Adgaonkar, *Indian Journal of Pure and Applied Physics*, Vol 33, 401-11, (1995).
- [21] N.G. Belsare and V.S. Deogaonkar, *Indian Journal of Pure and Applied Physics*, Vol 36, 280-89, (1998).
- [22] N.G. Belsare and V.S. Deogaonkar, *Journal of Polymer Materials* (Oxford and IBM Pub. Co. Pvt. Ltd.), Vol 15, 157-70, (1998).
- [23] B. Tareev, *Physics of Dielectric Materials*, MIR, Moscow, (1979).

Synthesis and Structural properties of lead titanate by wet chemical method

*N. V. Galande, A. U. Bajpeyee, S. H. Shamkuwar

Department of Physics, Smt. Narsamma Arts, Commerce and Science College,
Kiran Nagar, Amravati 444606, (M.S.) India.

Corresponding Author: Nileshvgalande@gmail.com

Abstract:

Lead titanate PbTiO_3 nano-powders have been synthesized using wet chemical method. Effects of synthesis conditions sintering temperature (500°C - 800°C), sintering time (4 hr.) and on the phase formation, morphology were studied. The produced lead titanate powders were investigated using X-ray diffraction (XRD), scanning electron microscope (SEM) and transmission electron microscope (TEM). The results obtained showed that pure single tetragonal PbTiO_3 phase was obtained for thermally treated precursors at 600°C with sintering time 4 hr. The crystallite size of the pure PbTiO_3 was in the range between 25.44 to 35.84 nm. SEM and TEM micrographs shows that sintering temperature have significant change in the morphology of the produced lead titanate powder.

Key words: Wet Chemical Route, PbTiO_3 , XRD, structural properties.

Introduction:

Lead titanate, PbTiO_3 , is one of the simplest and the most important members' of ferroelectric, pyro-electric and piezoelectric materials with perovskite structure ABO_3 where A is a monovalent or divalent cation with large radius, B is pentavalent or tetravalent cation with small radius and O is oxygen [1]. Owing to their ferroelectric nature, PbTiO_3 show high spontaneous polarization ($75\text{-}88 \mu\text{C}/\text{cm}^2$), high dielectric constant and high Curie temperature of 490°C . At this temperature, the material undergoes a first order transition from high temperature para-electric phase with higher symmetry and then without spontaneous (Pm3m cubic perovskite structure) into a low temperature ferroelectric phase (P4 mm tetragonal perovskite structure) [2]. At room temperature, it exhibits a lattice parameter of $c = 4.150 \text{ \AA}$ and $a = 3.904 \text{ \AA}$, thus giving a c/a as high as 1.063. Large c/a ratio in PbTiO_3 at low temperature confer tetragonal phase, it disintegrates into powder when cooled through the Curie point. Synthesis of PbTiO_3 by wet chemical methods offer advantages because of high-purity, good stoichiometry and controlled particle size. [3-8]

Lead titanate (PbTiO_3) is a ferroelectric nano-crystalline powder that has not only been proved to be a technologically important material but also it is a significant component material in electronics such as capacitors, ultrasonic transducers, thermistors, and optoelectronics. These systems are due to their potential applications as ferroelectric materials [9-13]. The conventional solid-state reaction has a tendency to produce a coarse PbTiO_3 powder with compositional in homogeneity and a degree of particle agglomeration if the processing parameters are not carefully optimized. Therefore, many chemistry-based processing routes, including co-precipitation, sol-gel synthesis, hydrothermal and citrate routes have been devised for the preparation of an ultrafine, sintering-reactive PbTiO_3 powder. Our method of synthesizing PbTiO_3 relies on the reaction between Lead Nitrate [$\text{Pb}(\text{NO}_3)_2$] and Titanium Isopropoxide [$\text{C}_{12}\text{H}_{28}\text{O}_4\text{Ti}$] at high temperature.

Experimentation:

Molar proportions of $\text{Pb}(\text{NO}_3)_2$ (Lead Nitrate) is dissolved in Titanium Isopropoxide [$\text{C}_{12}\text{H}_{28}\text{O}_4\text{Ti}$] in liquid. The lead titanate were prepared by dissolving solid lead nitrate powder in pure water and stirred for 1 hr. at 100°C in reaction flask, when the lead nitrate was dissolved in water, then a stoichiometric amount of titanium Isopropoxide was added to the solution and

the solution was refluxed at 100°C for 1 hr. and the solution was kept at 100°C for 4 hr. to get nanocrystalline powder. Nanocrystalline powders with various crystallite sizes were obtained by calcining the powder at different temperatures at 500°C, 600°C, 700°C and 800°C. Structure and phase transformation analyses were investigated by XRD in the range of 0°–90°. The average crystallite size was calculated from the full width at half maximum of the diffraction lines using Scherrer's relation.

RESULTS AND DISCUSSIONS

X-RAY DIFFRACTION: XRD pattern of the PbTiO_3 calcined at 500°C, 600°C, 700°C and 800°C is shown in Fig.1 at 500°C; the crystallization of tetragonal lead titanate phase began along with traces of impurity phase. At 500°C all peaks can be indexed to the PbTiO_3 with a tetragonal structure. No peak corresponding to any of the source materials or allotropic forms was found, suggesting that a pure crystalline compound exists. The crystallinity of the produced phase was increased with the increasing calcination temperature from 500°C to 800°C. The diffraction peaks corresponding to diffraction planes (101), (110), (100), (001), (200) and (211) which ascribed to tetragonal PbTiO_3 phase were obtained. On the other hand, the decreasing of the calcination temperature to 500°C lead to form of the mixture of leads titanate PbTiO_3 , lead oxide PbO and titanium dioxide TiO_2 phases. The crystallite size of the particles calcined at various temperatures could be calculated by the Scherrer's equation: $t = k \lambda / \beta \cos \theta$ (where t is the average size of the particles, assuming particles are spherical, $k = 0.9$, λ is the wavelength of X-ray radiation, β is the full width at half maximum of the diffracted peak and θ is the angle of diffraction. The crystallite size obtained from XRD data at 500°C, 600°C, 700°C and 800°C were 25.44 nm, 26.47 nm, 27.44 and 35.87 nm respectively. XRD peaks present 101 for PbTiO_3 sample calcined at 500°C represent PbO phase with the plane 101 [JCPDS File No. 381477]. As the calcined temperature increases the blending of PbO with TiO_2 get optimum resulting in the shifting of peak position.

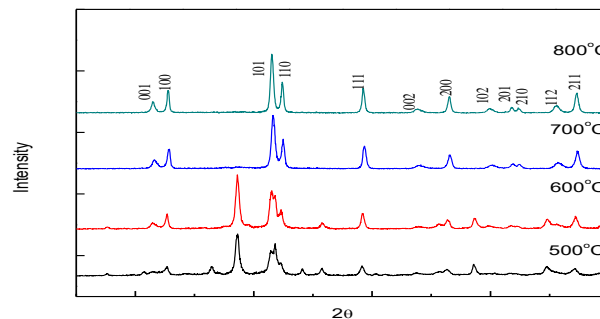


Fig.1 XRD Analysis for PbTiO_3

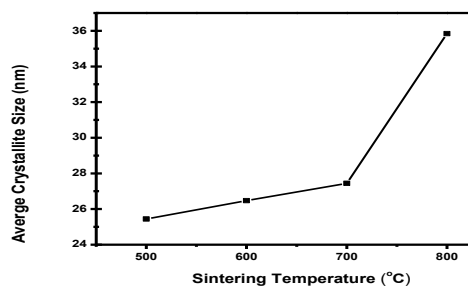


Fig.2: Variation of c/a with size with Sintering temperature.

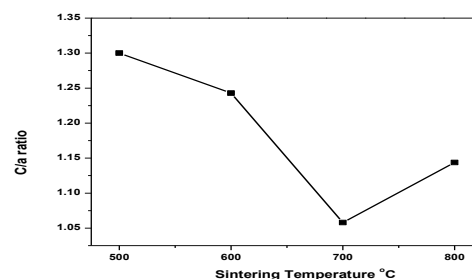


Fig.3: Variation of average grain size with Sintering temperature

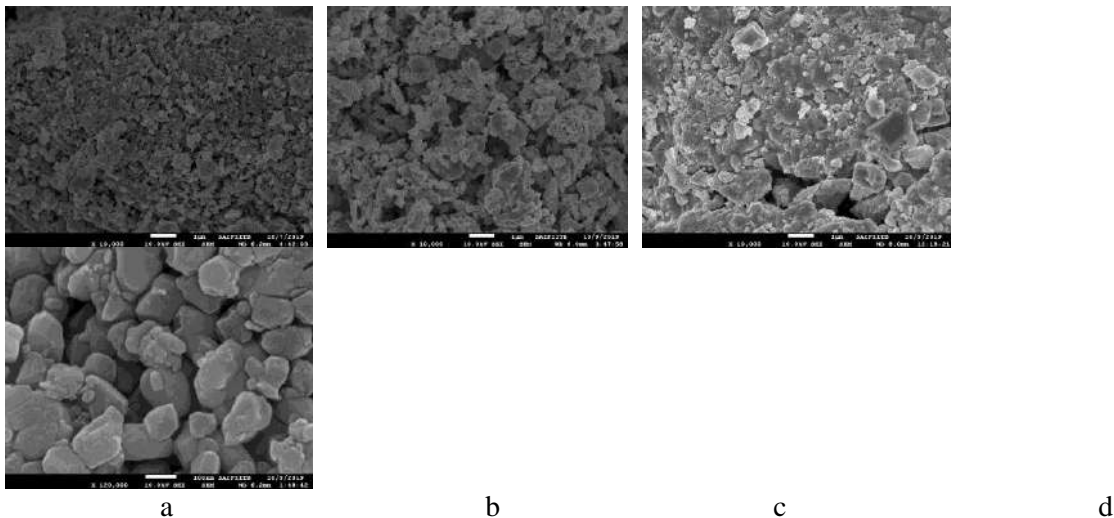


Fig. 4 SEM image for a, b, c and d for PbTiO_3 sintering temperature at 500°C, 600°C, 700°C and 800°C

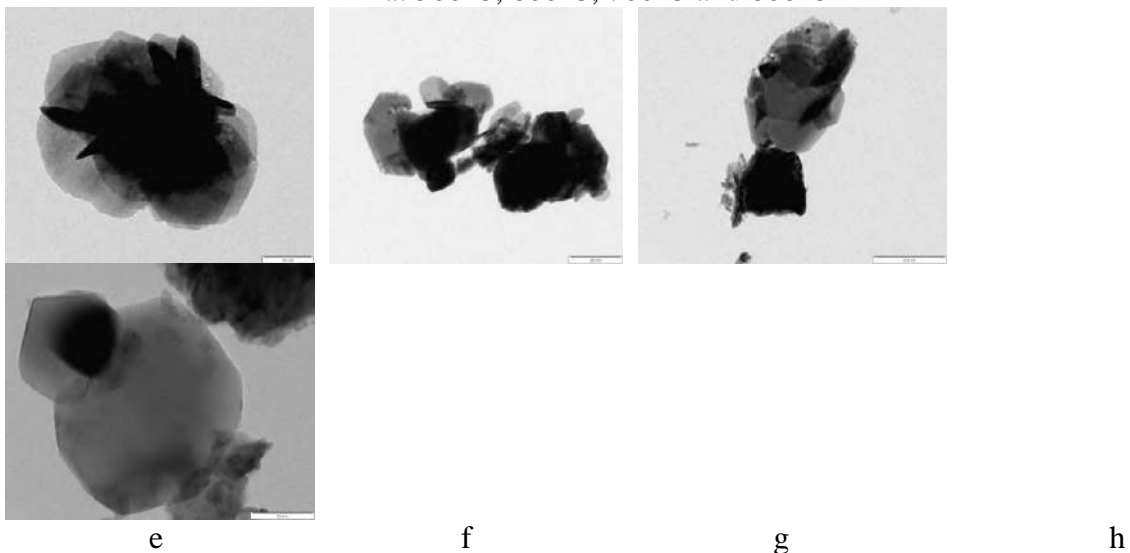


Fig. 5 TEM image for e, f, g and h for PbTiO_3 sintering temperature at 500°C, 600°C, 700°C and 800°C

Fig.2. shows the variation of c/a ratio with the sintering temperature, which clearly indicates c/a ratio, is maximum at 500°C which means stable tetragonal phase at 500°C and decreases for 600°C, 700°C and slightly increase for 800°C. Decrease in c/a ratio afterwards indicates dispersion from tetragonality and an approach to the cubic phase with higher sintering temperature.

Fig. 3 shows variation between calcination temperature and crystalline size of Lead Titanate. With respect to temperature for lead titanate at 500°C, it has a less value. The plot shows increased to crystallite size at 600°C and 700°C then that of at 500°C and 800°C. As calcination temperature increases, the crystallite size lightly increases at 600°C and 700°C then that the crystallite size is sudden increase at 800°C, in crystallite size will be reflected in the further structural for TEM and magnetic studies.

Surface micrograph in figure 4 of materials confirms that of lead titanate is smooth at micro-level and average. Its surface began to change with synthesised materials calcined at 500°C 600°C, several crystalline grains with average dimension image 50 μm are observed. A few fine grains of less than 1 μm dimension image can be viewed. This microstructure supports perovskite structure of lead titanate, which has also already been confirmed by XRD results.

Fig. 5 shows the TEM image and the powder and corresponding calcination temperatures. These results demonstrated crystallinity of the materials. Size of nano-crystallites calculated from XRD data and the particle size with the TEM images of PbTiO_3 are compared. [13] The diffraction patterns illustrating spot patterns of the tetragonal structure of PbTiO_3 indicates highly crystalline PbTiO_3 particles. The crystallite size from XRD data is small in case of powder calcined at 500°C , 600°C and 700°C . Its value is large for the powder calcined at 800°C . It may be due to the preferred grain growth of materials. The trend that has been observed in crystallite size and TEM particle size agree to each other although the magnitude differs. In XRD the crystallite size is an average while in the case of TEM particle size. The morphology of particle in TEM micrograph suggests that the grain growth pattern changes with calcination temperature. It is also observed that most of crystallites of PbTiO_3 adhere together and form large particles. [14]

Conclusion:

This work done attempted to generalize the reaction for material synthesis by using the wet chemical route is successful. The average crystallite size 25.44 nm, 26.47 nm, 27.44 and 35.87 nm at 500°C , 600°C , 700°C and 800°C calcinations was assured from XRD peaks. The variation in c/a ratio showed transition from Cubic to tetragonal phase. The grain size also increase with increased calcination temperature. The smallest crystallite size in the range 25.44 – 35.87 nm can be obtained at low calcination temperature 500°C . SEM and TEM micrographs showed that the produced pure lead titanate nano-powders were formed in the nano-spheres with narrow particle size distribution.

References

- 1) N.V. Galande, A.U. Bajpeyee, S.H. Shamkuwar, S.A.Khapre, "Effect of lanthanum doping on magnetic susceptibility of lead titanate." JETIR, Volume 9, Issue 12, 2022, PP. b866-b876.
- 2) N.V. Galande, A.U. Bajpeyee, S.H. Shamkuwar, "synthesis and structural properties of lanthanum doped lead titanate prepared by wet chemical method." IOSR Journal of Applied Physics (IOSR-JAP), 14(5), 2022, PP. 13-18.
- 3) A. U. Bajpeyee, N. V. Galande, S. H. Shamkuwar, "Structural analysis of lead titanate Prepared by wet chemical method", International Journal of Scientific Research in Science and Technology; Volume 8, Issue 1, Published February 10, 2021; PP. 307-314.
- 4) A. U. Bajpeyee, N. V. Galande, S. H. Shamkuwar, "Dielectric studies of lead titanate Prepared by wet chemical method"; IOSR Journal of Applied Physics (IOSR-JAP) e-ISSN:2278-4861; Volume 13; Issue 5 Ser.III (Sep.-Oct. 2021), PP. 14-18.
- 5) A. U. Bajpeyee, N. V. Galande, S. H. Shamkuwar, "Effect of sintering temperature on structural and Dielectric properties of lead titanate", RAMAN-2022; 2nd International Conference on Recent Advances in Materials Science & Nanotechnology In Association with International Journal of Scientific Research in Science and Technology; Volume 9, Issue 13, Published 15 May 2022; PP. 203-208.
- 6) V. D. Kapse, A. U. Bajpeyee, P. A. Murade Int Structural Properties Of Lead Titanate Nanoparticles Prepared By Wet Chemical Route international journal of chem. Tech. Research. Vol.6 No.3, PP2096-2098 May-June 2014.
- 7) Bajpeyee A. U., Ph. D. Thesis SGB Amravati University, Amravati (Maharashtra) India, 2012.
- 8) M.K.Gerges, Massaud Mostafa, Gehad M. Rashwan,; International Journal of Latest Research in Engineering and Technology, Volume 2, PP 42-49,; Issue 4 April 2016.
- 9) Vijendra A. Chaudhari and Govind K. Bichile,; Research Gate Hindawi Publishing Corporation Smart Materials Research Volume 2013, Article ID 147524, pages 9; May 2013.
- 10) V. D. Kapse, A. U. Bajpeyee, P. A. Murade,; International journal of chem. Tech.,; Research. Vol.6 No.3, PP 2096-2098; May-June 2014.
- 11) A. A. Abd El-razek, E. M. Saed, M. K. Gergs, Int. J. Compu. Eng. Res. Vol, 04, pp 38-45, 2014.
- 12) S. B. Majumder, S. Bhaskar, P. S. Dabal & R. S. Katiyar,; Integrated Ferroelectrics: An International Journal, Volume 23, Issue 1-4, pp. 127-148, 1999.
- 13) P. S. Pizani, J. A. Eiras,; Applied Physics Letters, Vol. 72, Issue 8, pp. 897-899, 1998.
- 14) G. A. Rossetti Jr, L. E. Cross, J. P. Cline,; Journal of Materials Science, Volume 30, Issue 1 pp 24-34, 1995.

Gas sensing properties of Co surface modified SmFeO₃ thick film

R. B. Mankar^{1*} and V. D. Kapse²

¹Department of Physics, Smt. Radhabai Sarada Arts, Commerce and Science College, Anjangaon Surji 444705, Maharashtra State, India

²Department of Physics, Arts, Science and Commerce College, Chikhaldara 444807, Maharashtra State, India
¹rbmankar@gmail.com, ²vdk.nano@gmail.com

* Corresponding author: - R. B. Mankar rbmankar@gmail.com

Abstract

The surfaces of p-type SmFeO₃ thick film were modified by simple dipping method. SmFeO₃ films prepared onto glass substrate were inserted into a cobalt chloride solution for 5 min. These films were fired in muffle furnace and their FE-SEM and EDX micrographs were recorded. The films were porous in nature and well dispersion of cobalt particles on the surface of SmFeO₃ film was observed. Gas sensing performance of as-prepared Co-SmFeO₃ film was analyzed in presence of ammonia, ethanol, hydrogen, LPG, carbon dioxide and chlorine. The observations showed that the film was selective to ammonia and exhibited better gas response as compared to SmFeO₃ film. Maximum gas response to 50 ppm ammonia at 200 °C was 6.39 which was three times more than that of SmFeO₃ film. The effect of Co surface modification on microstructure and ammonia gas sensing properties SmFeO₃ film was discussed.

Keywords: Surface modification, Gas Response, selectivity, Chemisorption, Reducing gas.

1. Introduction

Need of environmental monitoring has made considerable amount of research in solid state gas sensors based on semiconductor metal oxides. ZnO, TiO₂, SnO₂ and their composites are well known materials for solid state gas sensors [1-3]. Some ABO₃- type perovskites such as SmFeO₃ also presented good gas sensing characteristics [4]. P-type SmFeO₃ has been investigated repeatedly by my researchers in the fabrication of sensors for the monitoring of oxidizing gases such as ozone [5]. But under reducing condition, phase separation and low electrical conductivity was observed for P-type SmFeO₃ [6]. The electrical conductivity can be increased by creating more oxygen vacancies on the surface of material. Addition of oxidizing or reducing elements to SmFeO₃ is better approach for increasing the number of oxygen vacancies at its surface. This can be achieved either by doping method or dipping method. Co, Ce and Ni dopants were investigated for the modification of SmFeO₃ [7-8]. Cobalt is reducible element addition of which to pure SmFeO₃ can induce more oxygen vacancies. In cobalt doped SmFeO₃, each Co²⁺ ion delivers one electron and therefore Co misfit act as oxygen vacancy [9]. R. C. Michel reported synthesis and characterization of SmCoO₃ for enhanced gas sensing. Since Co-O bond is weaker than Fe-O bond, problem of chemical stability can arise for reducing gases. Therefore addition of controlled amount of Co to pristine SmFeO₃ is essential.

In our previous work, nanocrystalline SmFeO₃ powder was prepared by sol-gel method and SmFeO₃ thick film was fabricated onto glass substrate by screen printing method [10]. In present investigation, as prepared SmFeO₃ film was surface modified with cobalt and the corresponding gas sensing properties were studied.

2. Experimental

As reported in our earlier work, nanocrystalline SmFeO₃ powder was synthesized by sol-gel method and SmFeO₃ films were formed onto the glass substrate by screen printing

technique [10]. 0.1 M aqueous cobalt chloride solution was prepared by using $\text{CoCl}_2 \cdot 6\text{H}_2\text{O}$ and distilled water. To this solution, as prepared SmFeO_3 film was dipped for 5 min. Finally the film was fired for 30 min at 550°C before applying for further investigations.

The microstructure of Co-SmFeO_3 film was observed by FE-SEM technique. The wt % of Sm, Fe, O and Co present on the film was measured in EDX spectra. Gas sensing performance of as prepared Co-SmFeO_3 film was tested in static gas sensing set-up. Target gases employed in the experiment were ammonia, ethanol, hydrogen, LPG, carbon dioxide and chlorine.

3. Results and Discussion

3.1. XRD, morphological and elemental analysis:

The recorded XRD spectra of as prepared nanocrystalline SmFeO_3 powder was explained in previous publication conforming the formation of pure polycrystalline SmFeO_3 with average crystallite size 50 nm [10].

FE-SEM micrographs and EDX spectra of Co-SmFeO_3 film was presented in Fig. 1 and Fig. 2 respectively.

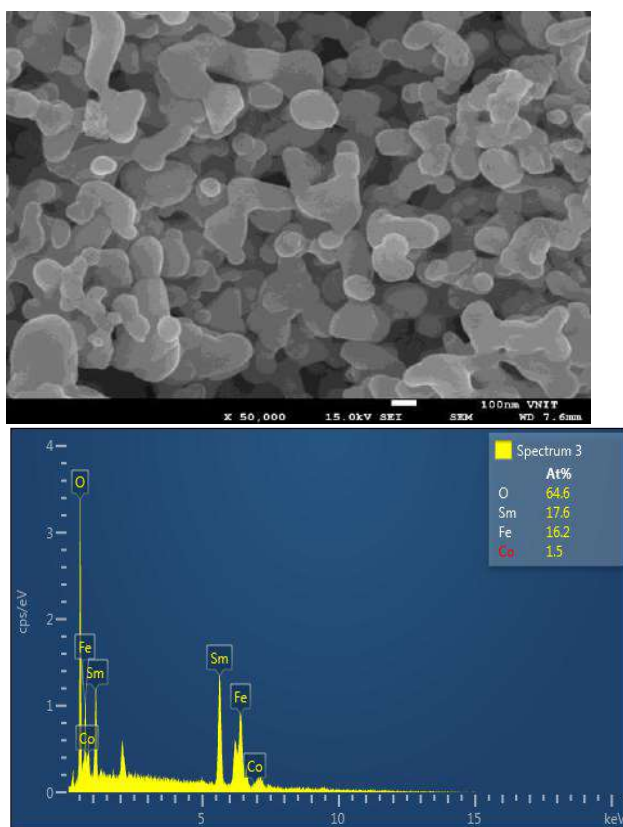


Fig. 1: FE-SEM of Co-SmFeO_3 film

Fig. 2: EDX image of Co-SmFeO_3 film

FE-SEM micrograph seems to be consists of large number of grains having size in the range 47 nm to 80 nm. Particles appear irregular in shape and the agglomeration of particles was also observed at some places. Co particles might be distributed around the larger grains. Porosity observed in Co-SmFeO_3 film favours adsorption and desorption processes. EDX spectra of Co-SmFeO_3 film confirmed the incorporation of Co on the surface of SmFeO_3 film. Co has occupied Sm or Fe sites in SmFeO_3 perovskite structure.

3.2 Gas sensing properties:

Performance of gas sensor is generally determined from its gas response, optimal operating temperature, selectivity and stability. For p-type SMO, gas response is expressed as (R_g/R_a) where R_g and R_a represents resistance of semiconducting material in target gas and in air respectively [11]. In our previous work, SmFeO_3 film was selective to ammonia gas but the gas response to 50 ppm ammonia gas at 200 °C was only 2.07. In present investigation, Co-SmFeO_3 film was also selective to ammonia gas but this time the response was 6.39 which is three times larger than the response of pure SmFeO_3 film although the optimal operating temperature was same.

To study temperature dependence of gas response, the responses of Co-SmFeO_3 film to 50 ppm ammonia were calculated at different operating temperatures ranging from 30 °C to 400 °C and presented in Fig.3.

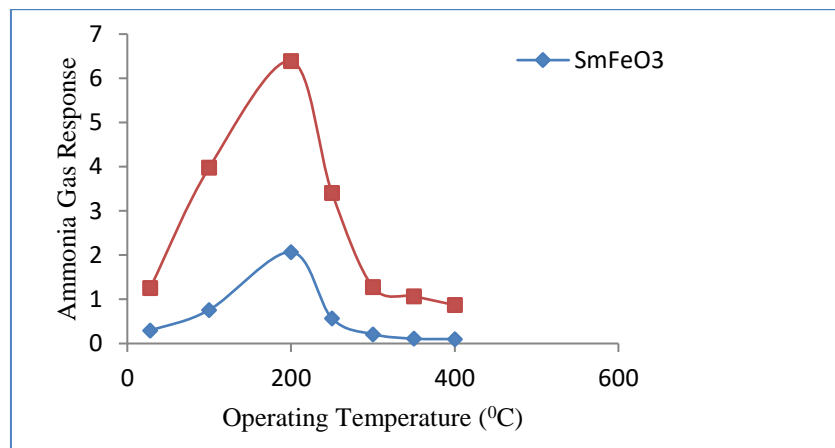


Fig. 3: Dependence of 50 ppm ammonia gas response on operating temperature for SmFeO_3 and Co-SmFeO_3 films.

Initial growth and then decay in gas response was observed with the increase in operating temperature. The maximum gas response 6.39 was obtained at optimal operating temperature of 200 °C. This variation in gas response with operating temperature is related to adsorption and desorption rates. Below optimal operating temperature, desorption rate is very small and above optimal operating temperature, desorption rate is high. Hence small change in resistance and thereby decrease in response at lower and higher temperatures was recorded.

The change in resistance of Co-SmFeO_3 film was monitored for 60 days and the results are graphically illustrated in Fig. 5. Negligible change in the resistance of sensor was observed indicating good stability and durability of Co-SmFeO_3 film.

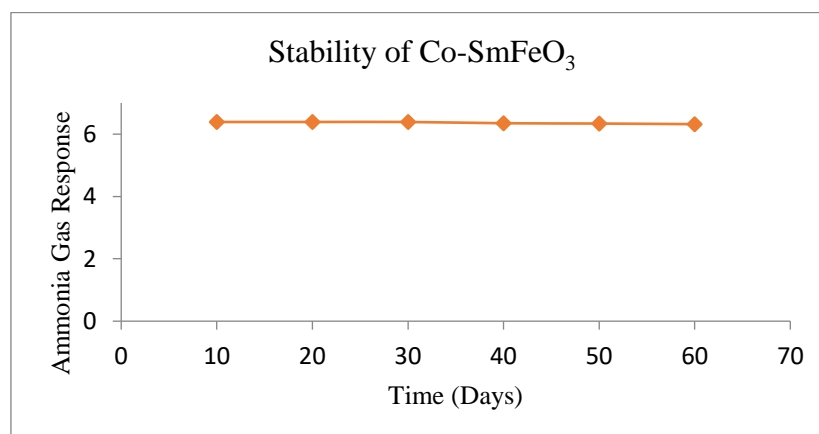
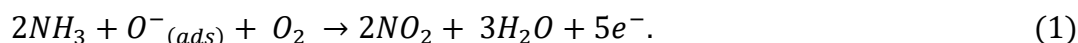


Fig. 4: Stability of Co-SmFeO_3 based sensor.

3.3. Ammonia gas sensing mechanism:

The most accepted gas sensing mechanism of p-type SmFeO₃ is described below. In presence of air, the adsorbed oxygen species extract the electrons from conduction band and get converted to O₂⁻, 2O⁻ or O²⁻ depending on the temperature. Due to this, concentration of electron holes increases and the resistance of film decreases. When Co-SmFeO₃ film is exposed to ammonia gas, the extracted electrons returned back to the conduction band and the resistance of film increases. Eq. 1 depicts the chemical reaction of ammonia gas with chemisorbed oxygen [26].



3.4. Conclusion:

In this investigation, SmFeO₃ film was surface modified with Co by dipping it in cobalt chloride solution for 5 min. As prepared Co-SmFeO₃ film was selective to ammonia gas. To 50 ppm ammonia gas, response of Co-SmFeO₃ film was 6.39 at 200 °C which is three times more than that of SmFeO₃ film. The increased ammonia gas response is related to the additional oxygen vacancies induced by Co misfits.

References

- [1] X. Han, Y. Sun, Z. Feng, G. Zang, Z. Chen, J. Zhan, Au-deposited porous single-crystalline ZnO nanoplates for gas sensing detection of total volatile organic compounds, RSC Adv. 6 (2016) 37750–37756.
- [2] R. B. Pedhekar, F. C. Raghuwanshi, V. D. Kapse, Low Temperature H₂S Gas Sensor Based on Fe₂O₃ Modified ZnO-TiO₂ Thick Film, Int. J. Mate. Sci. and Eng. 3 (2015) 219-230.
- [3] T. Li, W. Zeng, Z. Wang, Quasi-one-dimensional metal-oxide-based heterostructural gas-sensing materials: A review, Sens. Actuators B Chem. 221 (2015) 1570–1585.
- [4] H. T. Huang, W. L. Zhang, X. D. Zhang, X. Guo, NO₂ sensing properties of SmFeO₃ porous hollow microspheres, Sens. Actuators B Chem. 265 (2018) 443-451.
- [5] Y. Hosoya, Y. Itagaki, H. Aono, Y. Sadaoka, Ozone detection in air using SmFeO₃ gas sensor, Sens. Actuators B Chem. 108 (2005) 198-201.
- [6] S. Fang, H. Peng, M. Zhao, J. Hu, L. Chen, Studies on preparation and gas sensing properties to ethanol of SmFeO₃ nano-materials with perovskite structure, J. Funct. Mater. 28 (2007) 54–60.
- [7] Y. Zhang, H. Zou, J. Peng, Z. Duan, M. Ma, X. Xin, X. Zheng, Enhanced humidity sensing properties of SmFeO₃-modified MoS₂ nanocomposites based on the synergistic effect, Sens. Actuators B Chem. 272 (2018) 459-467.
- [8] M. Zhao, H. Peng, J. Hu, Z. Han, Effect of cobalt doping on the microstructure, electrical and ethanol-sensing properties of SmFe_{1-x}Co_xO₃, Sens. Actuator, B Chem. 129 (2008) 953–957.
- [9] C. R. Michel, E. Delgado, G. Santilan, A.H. Martinez, A Chavez, An alternative gas sensor material : Synthesis and electrical characterization of SmCoO₃, Mater. Res. Bullet. 42 (2007) 84-93.
- [10] R. B. Mankar, V. D. Kapse, Fabrication and characterization of Ce modified SmFeO₃ thick film, Aayushi Int. Inter. Res. J. 109 (2022) 367-369.
- [11] P. Shankar, J.B.B. Rayappan, Gas sensing mechanism of metal oxides: The role of ambient atmosphere, type of semiconductor and gases-A review, Sci. Lett. J. 4 (2015) 1–18.
- [12] S. B. Nahire, G. E. Patil, G. H. Jain, V. B. Gaikwad, S. B. Deshmukh, Synthesis, characterization and gas sensing properties of Cr surface modified BaTiO₃ thick films, IJRASET 5 (2017) 2535-2543.

Synthesis Methods and Applications of Cadmium Ferrite Nanoparticle: An Overview

T. R. Tatte*, V. D. Kapse, S. V. Agnihotri, M. S. Pande

*Department of Physics, Shri. Dr. R. G. Rathod Arts and Science College, Murtizapur, Dist. Akola, Ms, India.

Department of Physics, Arts, Science and Commerce College, Chikhaldara, 444807, Maharashtra State, India.

Department of Physics, Amolakchand Mahavidyalaya Yavatmal, 445001, Maharashtra State, India.

Department of physics, Gajanan Maharaj College of Engineering, Shegaon, 444203, Maharashtra State, India.

E-mail: truptitatte21@gmail.com

Abstract:

Ferrites have gained a lot of attention because of their diverse uses in domains including photocatalytic degradations, gas sensors, electronic devices, organic transformation catalysts, adsorption, and so on. This review focuses on cadmium ferrites production methodologies and applications. The structural, electric, magnetic, and dielectric properties of cadmium ferrites are primarily influenced by the synthesis procedures and circumstances used during preparation. As a result, the main goal of this study was to provide the most often used synthesis processes, such as sol-gel, hydrothermal, co-precipitation, solvothermal, micro-emulsion, and solid state. In this review, attention has been paid to the synthesis and applications of cadmium ferrites across various fields.

Keywords: Cadmium ferrites; Nanoparticles; Spinel, Synthesis methods, Applications.

1. Introduction:

Ferrite nanoparticles are in the spotlight of current nanoscience due to immense application potential. Spinel ferrite materials are metal oxides with spinel structures that have the general chemical formula AB_2O_4 , where A and B represent various metal cations that are located at tetrahedral (A site) and octahedral (B site) positions, respectively. The types, quantities, and placements of the metal cations in the crystalline structure have a significant impact on the physicochemical properties of ferrites [1,2].

Due to their unique and remarkable properties, nanocrystalline magnetic materials have attracted attention from various fields. Nanomaterials have particle size up to 100 nm and high surface-to-volume ratio, which altered or enhanced reactivity, thermal, mechanical, optical, electrical, and magnetic properties as compared to their bulk counterparts [3-6]. The size and shape of spinel ferrite nanomaterial can be controlled by manipulating reaction variables such as properties is manipulated by changing the synthesis method, processing temperature and also substitution [7-9].

Cadmium ferrite nanoparticles can be fabricated by various methods such as hydrothermal method, sol-gel method, chemical co-precipitation method, solid state high temperature reactions etc. Magnetic $CdFe_2O_4$, $CoFe_2O_4$, $MnFe_2O_4$, $CuFe_2O_4$, $ZnFe_2O_4$, and $NiFe_2O_4$ nanoparticles have received a great deal of attention owing to their thermal and chemical stability, as well as their distinctive structural, magnetic, optical, electrical, and dielectric properties, and their broad range of technological applications including photo catalysis, photoluminescence, biosensors, humidity-sensors, catalysis, magnetic refrigeration, permanent magnets, magnetic drug delivery, magnetic (hyperthermia) [10,11].

The purpose of this review gives some general processing methods and applications on Cadmium ferrite nanomaterial which is found to be useful due to their electronic, optical, electrical, magnetic and catalytic properties.

2. Synthesis methods

Different synthesis methods can be utilized simultaneously to produce nanoparticles of various sizes such as sol-gel method [12, 13], chemical co-precipitation [14], Hydrothermal and Solvothermal synthesis [15], Self-propagating high temperature synthesis (SHS) technique [16], Micro-emulsion technique [17] etc. have been discussed.

2.1 Sol-Gel Method

The sol-gel process involves the transition of a solution of metal compounds from a liquid sol into a solid gel. In liquid, sol is a diffusion of the solid particles where only the Brownian motions suspend the particles and this sol is heated and then to form a homogenous gel which can be achieved by the addition of base or acidic solutions. Usually inorganic metal salts or metal organic compounds such as metal alkoxides are used as starting precursors in the preparation of the sol. By elimination of water, the hydroxide molecules get condensed and then formation of a metal hydroxide. When all metal hydroxide species are linked to one another in a network, and formation of dense porous gel is obtained. Further heating at higher temperature and then drying of the gel, the gel is converted into ultrafine powders of metal oxides.

2.2 Chemical Co-Precipitation

In the chemical co-precipitation method, an aqueous solution of suitable salts of iron, lithium, manganese and other desired, suitable materials is mixed under a fine control of pH by using a precipitating agent like NaOH or NH₄OH solutions which causes the precipitation of the other metals present in the solution. Filtered the precipitate and then dried. Then dried precipitate is heated at a high temperature to dehydrate the precipitate and to burn out carbonaceous matter leaving a residue of the oxides of the respective metals. After this, particles are sintered. The particle structure and crystallinity can be influenced by reaction rates and impurities. This method offers distinct advantages like simple, rapid preparation, easy control of particle size and composition.

2.3 Hydrothermal and solvothermal synthesis

To create crystalline nanoparticles, hydrothermal and solvothermal syntheses use a variety of wet-chemical processes. High purity and controllable morphology of nanoparticles can be produced by simple and effective hydrothermal and solvothermal procedures. A nonaqueous solution, such as methanol, ethanol, or ethylene glycol, is used in solvothermal synthesis to dissolve the metal precursors under high pressure and at a moderate temperature. Hydrothermal synthesis refers to the synthesis through chemical reactions in an aqueous solution above the boiling point of water.

2.4 Self-Propagating High Temperature Synthesis Technique

In this method, organic acid is taken as precursor in aqueous solution. This solution containing all necessary cations and combustible anions in the desired product. After dehydration, the precursor becomes dry gel and this dry gel is amorphous in nature. Moreover, when calcinating this dry gel directly yields the required materials in presence of air/oxygen. The phase formation occurs at lower calcination temperature as compared to ceramic route and giving ultrafine powder. The overall process completes within 5 minutes.

2.5 Micro-emulsion Technique

Micro-emulsions are clear, isotropic mixtures of water, oil, and a surfactant that are stable and clear. This method uses surfactants to aid in the coexistence of two immiscible liquids in a single phase. The nanoparticles precursor is typically dispersed as 1–100 nm Nano droplets in the aqueous phase. Surfactant molecules encircle water droplets, forming "micelles" that act as nano reactors. This results in the formation of magnetic nanoparticles inside the micelles, which confines the particles and limits particle nucleation, development, and agglomeration.

3. Applications of spinel ferrites

Cadmium ferrites have interest due to their unrivalled physicochemical features, including as electrical, magnetic, dielectric, and optical capabilities.

3.1 Sensors : Cadmium Ferrite nanoparticle-based sensors possess exceptional sensitivity, low detection limits, and high signal-to-noise ratios. The detection of variations in humidity is one of the most common uses of sensors. The monitoring of humidity is a widespread practice in both industrial and residential settings, as it helps to maintain human comfort, regulate storage conditions for various items, and ensure optimal operating conditions for industrial processes and devices.

3.2 Magnetic applications: The variation of exchange contact between tetrahedral and octahedral sites causes the magnetization to be dependent on grain size. To minimize media noise in high-density magnetic recording, the magnetic particles utilized should have a nanoscale size to limit the exchange interactions occurring between adjacent grains. To achieve great storage density, the particles must also have high H_C values.

3.3 Dielectric applications: The dielectric structure typically consists of grains that are good conductors separated by grain boundaries with low conductivity. The dielectric properties of ferrites are influenced by factors such as structural homogeneity, cation distribution, particle size, density, and porosity. Additionally, the dielectric properties can be significantly affected by synthesis techniques and thermal treatment parameters such as temperature, time, and heating/cooling rates.

3.4 Photo catalytic applications: Photo catalysts are important materials that facilitate the use of solar energy in oxidation and reduction reactions, with numerous applications including removing water and air pollution, managing odors, deactivating bacteria, splitting water to generate hydrogen, inactivating cancer cells, and other areas. Currently, photo catalysis is a preferred method for removing dyes, as irradiation of light on a semiconductor can generate electron-hole pairs that can be utilized for oxidation and reduction processes. Dye degradation is caused by the generation of active radicals during the photo catalytic reaction.

3.5 Biomedical applications: For use in biomedical applications, magnetic nanoparticles need to have high magnetic saturation values and be biocompatible, while also being stable and non-agglomerated when dispersed in water. $CdFe_2O_4$ nanoparticles have attracted significant interest in the field of biomedicine due to their desirable properties, including simple synthesis, controllable size, high magnetization value, super paramagnetic nature, ability to be monitored by an external magnetic field, and high biocompatibility.

Conclusions:

Recently nanostructured cadmium ferrite materials have received a lot of attention due to its unique features, including stability under mechanical, chemical, and thermal conditions and can be modified suitably and promising technological applications in different fields of life. Among all the reviewed synthesis strategies, the usefulness of cadmium ferrite in many applications depends largely on the synthesis processes; efficient synthesis processes yield cadmium ferrite that can function better and endure the conditions under which they are synthesized.

References

- [1] D.H.K. Reddy, Y.S. Yun, *Coord. Chem. Rev.*, 315 (2016) 90.
- [2] K.K. Kefeni, B.B. Mamba, *Sustainable materials and technologies.*, 23 (2020).
- [3] S. Mokhosi, W. Mdlalose, S. Mngadi, M. Singh, T. Moyo, *Journal of Physics: Conference Series*. IOP Publishing; (2019).
- [4] S. Chakrabarty, M. Pal, A. Dutta, *Ceram. Int.* 44 (12) (2018) 14652.
- [5] G. Asab, E. A.Zereffa, T. Abdo Seghne, *International journal of biomaterials.* (2020).
- [6] M. Anand, *J. Appl. Phys.*, 128 (2) (2020).
- [7] B.K. Kuanr, P. Kishan, N. Kumar, S.L.N. Rao, P.K. Singh and G.P. Srivastava, *J. Appl. Phys.* 8 (1986) 63.
- [8] H.B Im, D.G Wickham, *IEEE Trans.on magn.*, 8 (1972) 765.
- [9] Z. Yue, Ji Zhou, X. Wang, Z. Gui and L. Li, *J. European Cera. Soci.*, 23 (2003) 189.
- [10] V. Anjana, S. John, P. Prakash, A. M. Nair, A. R. Nair, S. Sambhudevan, B. Shankar, *IOP Conference Series: Materials Science and Engineering*. IOP Publishing; 2018.
- [11] M. Ahmad, M. A. Khan, A. Mahmood, S. S. Liu, A. H.Chughtai, W. C. Cheong, B. Akram, G. Nasar, *Ceram. Int.*, 44 (5) (2018) 5433.
- [12] J. Azadmanjiri, S.A. Seyyed Ebrahimi, H. K. Salehani, *Ceramic International*, 33 (2007) 1623.
- [13] J. G. Lee, H. M. Lee, C. S. Kim, and Y. J. Oh, *J. Magn. Mater.*, 177 (1998) 900.
- [14] K. Maaz, A. Mumtaz, S. K. Hasanain, and A. Ceylan, *J. Magn. Mater.*, 308 (2007) 289.
- [15] T.N. Pham, T.Q. Huy, A. T. Le, *RSC Adv.* 10(52) (2020) 31622.
- [16] W.B. Cross, L. Affleck, M.V. Kuznetsov, et al., *J. Mater. Chem.*, 9 (1999) 2545.
- [17] E. Meydan, S. Demirci, N. Aktas, N. Sahiner, O. F. Ozturk, *Inorg. Chem. Commun.*,126 (2021).

A Short Review on feature, Properties and application of Nanowire

Miss S.A. Amale, Mr.P.S. Wagh, Miss.S.P. Dharme, Miss S.T. Khan

Department Of Physics, Vidya Bharati Mahavidyalaya, Amravati

Abstract

This Paper describes Nanowires (NWs), their type, characteristics features, and their use in sensor and transistor application as well. Introductory part in general explains briefly about Nanowire (NWs). Their characteristics features, types as well as their most significant properties. The types of Nanowire (NWs) can be of conducting material such as Ni, Pt, Au; semiconducting material like Si, InP, and GaN as well as insulating material like SiO₂, TiO₂ etc. The property of Nanowire including mechanical, electrical, chemical, optical and thermal properties. Also a small description of Nanowire (NWs) and sensor are explained with their performance parameter, Nanowire based transistors are discussed in addition with their characteristics and application. Finally this chapter concludes with the significance of Nanowire in contemporary era.

Keywords: - Nanowire, synthesis, properties, Application in electronics.

1. Introduction

Nanowires are structures of dimensions of the order of one nanometer (10⁻⁹m). NWs having small size, low weight, low cost for mass production, and are also compatible with commercial planar processes for large-scale circuitry NWs [1]. At the Nanowire scale, quantum mechanical effects are significant to the extent that Nanowires are sometimes called 'quantum wires'. A variety of different types of Nanowires have been developed including metallic (e.g., Ni, Pt, and Au), semiconducting (e.g., Si, InP, and GaN), and insulating (e.g., SiO₂ and TiO₂) types. The physical properties of Nanowires are influenced by the morphology of the Nanowires, diameter-dependent band gap, carrier density of the material state, and so forth. Because Nanowires often exhibit aspect ratios (length-to-width ratio) of 1000 or more they are often referred to as one-dimensional (1-D) materials. Nanowires have conductive properties that are unique and not observed with the bulk materials or in larger, 3-D constructs of these materials. The physical properties of Nanowires are influenced by the morphology of the Nanowires, diameter-dependent band gap, carrier density of the material state, and so forth [2]. Nanowires (NWs) propose potential impact on electronics, computing, memory, data storage, communications, manufacturing, health, medicine, national security, and other economic sectors as well [3]. These properties also make Nanowires very effective as battery electrodes, with long conduction pathways that achieve high conductivity and high surface area that permits rapid charging. In order to produce and utilize these properties, reliable and controllable Nanowire syntheses are required, but synthetic methods vary widely in how the extremely anisotropic structures are generated. Broadly speaking, synthesis techniques can be divided into two categories: top-down fabrication and bottom-up synthesis [4]. Nanowires by virtue of excellent optical, electrical, chemical, thermal as well as mechanical Properties [5].

2. Characteristics

Structural and geometric factors play an important role in determining the various attributes of Nanowires, such as their electrical, optical, and magnetic properties. Therefore, various novel tools have been developed and employed to obtain this important structural information at the nanoscale. Typical Nanowires exhibit aspect ratios of 1000 or more. As such they are often referring to as one dimensional (1-D) materials. Nanowires have many interesting properties that are not seen in bulk or 3D material [2]. This is because electrons in Nanowires are quantum confined laterally and thus occupy. Energy levels that is different from the traditional

continuum of energy level. A Nanowire is that they exhibit discrete values of the electrical conductance. They are many applications where Nanowires may become important in electronics, Optoelectronics and nano electromechanical devices as additives in advance composites, for metallic interconnect in nanoscale quantum devices and as leads for Biomolecular Nanosensors [6].

3. Properties of Nanowire

Nanowires (NWs) possess extremely extraordinary properties which makes them useful for Nanoelectronics applications. The various properties are explained as follows:

Electrical Properties

The mechanism such as charge trapping and scattering electrical transport can be controlled easily with respect to both minority and majority carrier in Nanowire (NW). When light falls on Nanowires due to dielectric constant reduces the difference for light absorption by order of magnitude from $\sim 250\mu\text{m}$ making Nanowires suitable for photovoltaic's applications[7].

Thermal Properties

Thermal properties depend upon the scattering of phonon within the Nanowires as thermal transport is due to phonons mostly. Due to small diameter the scattering of phonon reduces leads to reduction in heat transport. Thus making Nanowires suitable for thermoelectric applications [8].

Chemical Properties

Chemical properties depend upon large effective areas and surfaces. As Nanowires possess large area/volume ratio. Thus making Nanowires a potential candidate for Chemical and Sensing applications [9].

Magnetic Property

Because of high energy of anisotropy with a super magnetic in Nanowires making them suitable for electromagnetic applications [10].

Catalytic Property

The large surface area of Nanowires formed due to transition oxide materials shows inspiring catalytic properties and can be further improved by using gold and platinum[11].

4. Synthesis of Nanowires

In this section we survey the most common synthetic approaches that have successfully afforded high-quality Nanowires of a large variety of materials Methods to fabricate Nanowires include top-down approaches such as optical and electron-beam lithography, and focused ion beam. More commonly applied bottom-up approaches are, e.g., vapor-liquid-solid growth, sol-gel and other chemical methods [12].

i] Lithography

A simple method to produce Nanowires with defined geometric has been recently reported using conventional optical Lithography. In this approach, optical lithography is used to generate Nanogaps using controlled crack formation. These Nanogaps are then used as shadow mask for generating individual Nanowires with precise length and widths. This technique allows to produce individual Nanowire below 20nm in width in a scalable way out of several metallic and metal oxide materials. [13].

ii] VLS Growth

A common technique for creating a nanowire is vapor-liquid-solid method. This process can produce high-quality crystalline Nanowires of many semiconductor materials. The VLS grown single crystalline silicone Nanowires with Smooth surface could have excellent properties. VLS synthesis requires a catalyst for nanowire. The best catalysts are liquid metal (Such as gold) Nanoclusters which can either be self assembled from a thin film by dewetting. The source enters these Nanoclusters and begins to saturate them. On reaching super saturation the source solidifies and grows outward from the Nanocluster. Simply turning off the source can adjust the final length of the Nanowire [14].

iii] CVD [chemical vapor deposition]

In CVD refers to a group of process. where solids from out of gaseous phase deposit catalysts [such as gold] on a base called a substrate. They put substrate in a chamber with a gas containing the appropriate element such as silicon and the atom in the gas do all the work. First atoms in the gas attached to those atoms in the catalysts, and then additional gas atoms attach to those atoms and so on. Finally creating a chain in their word the Nanowires. [15].

iv] Fiber-optic Nanowires

Fiber-optic Nanowires carry information in the form of light to make a fiber optic nanowire. Firstly they heat up a rod made of sapphire, wrap the cable around the rod and pull the cable stretching it thin to create a nanowire and another method uses tiny furnace made from a small cylinder of sapphire. They draw the fiber optic cable through the furnace and stretch it into a nanowire. Micro wires and Nanowires have been manufactured by using a wide range of bottom-up techniques such as chemical or physical vapor deposition and top-down processes such as fiber drawing. Among these techniques, the manufacture of wires from optical fibers provides the longest, most uniform and robust Nanowires. Critically, the small surface roughness and the high-homogeneity associated with optical fiber Nanowires (OFNs) provide low optical loss and allow the use of Nanowires for a wide range of new applications for communications, sensing, lasers, biology, and chemistry. OFNs offer a number of outstanding optical and mechanical properties, including large evanescent fields, high-nonlinearity, strong confinement, and low-loss interconnection to other optical fibers and Fiberized components.[16]

5] Applications

i] Electronic Devices :- a) Nanowire can be used for MOSFETs [MOS field effect Transistors) MOS transistors are used widely as fundamental building elements in today's electronic circuit MOS Transistors is shrinking smaller are smaller into nanoscale one of the key challenges of building future nanoscale. MOS transistors is ensuring good gate control over the channel due to the high aspect ratio, if the gate dielectric is wrapped around the nanowire channel we can get good control of channel electrostatics potential thereby turning the transistor on and off efficiently[17].

b) To create active electronic elements the first key step was to chemically dope a semiconductor nanowire. This has already been done to individual nanowires to create P and N type semiconductor. The next step was to find a way to create pn junction. One of the electronic devices this was achieved in two ways. The first way was to physically cross, p type wire over and n type wire. The second method involve chemically doping a single wire with different dopants along the length this method created a pn junction with only one wire [18].

ii] Nanowire assisted transfer of sensitive TEM samples.

For a minimal introduction of stress and bending to transmission electron microscopy [TEM] samples (lamellae, thin film, and other mechanically and beam sensitive samples) When transferring inside a focused ion beam, flexible metallic nanowires can be attached to a typically rigid micromanipulator. The main advantages of this method include a significant reduction of sample preparation time [quick welding and cutting nanowire at a low beam current]. this technique is particularly suitable for in situ electron Microscopy sample preparation.[19]

iii] Nanowire lasers

Nanowire lasers are nano scaled lasers with potential as optical interconnect and optical data communication on chip. Nanowire lasers are built from III-V semiconductor heterostructure. the high refractive index allow for low optical loss in the nano wire core. Nanowire lasers are sub wavelength laser of only a few hundred nanometers. Nanowire laser are fabric perot resonator cavities defined by the end facets of the wire with high reflectivity recent

development have demonstrated repetition rates greater than 200 GHz offering possibilities for optical chip level communication [20].

iv] Nano quantum computer

Nanowires may play an important role in the field of quantum computers. As team of researchers in the Netherlands created nanowires out of the Indium arsenide and attached them to aluminum electrodes. At temp near absolute zero, aluminum becomes a superconductor, meaning it can conduct electricity without any resistance. The researchers could control the super conductivity of the nanowires by running various voltages through the substrate under the wires.

v] Nanorobotic

Nanowire may also play an important role in nano size devices like nanorobots. Doctors could use the nanorobot designs have onboard power systems which could require structure like nanowire to generate and conduct power [21].

vi] Nanowire solar cell

Nanowire solar cell is advantages because a dense absorption is allowed to absorb on the entire solar spectrum it also allowed fast diffusion between the two active compounds for a small distance. the solar cell is made up of vertical n-type ZnO nanowire solar cell. A blocking layer of TiO_2 is deposited on the ZnO nanowire to get the working solar cell [22].

Conclusion

The foregoing discussion shows that, Nanowires provide unique tools for scaling down in electronics. So that there is a some advance like, Synthesis of nanoscale building blocks with precisely controlled chemical composition, physical dimension and electronic, optical properties. Some strategies for the assembly of building blocks into increasingly complex structures. New nanodevices concepts then it can be implemented in high yield by assembly approaches. And for these, we have face the some challenges like The insufficient control of the properties of individual building blocks, Low device to device reproducibility, Lack of reliable methods for assembling and integrating building blocks into circuits. Future Scope of the nanowire are, ordinary batteries/ circuit will be replaced by nanowire based completely. By the use of Nanowire batteries in future we can have devices having high battery life. By invention of some new mechanism and technology we can get nanowire batteries have more than 10 times of ordinary battery.

Reference

- [1] Billel Salhi [December 09, 2020] Nanowires: Synthesis, Applications and Challenges. . Center of Research Excellence in Desalination and Water Treatment. Volume 1 Issue 3 DOI 10.32474/JBRS. 2020.01.000112.
- [2] Jayanta Kumar Patra, Dipendra Kumar Mahato, and Pradeep Kumar [21 September 2018] Biosensor, Technology—Advanced Scientific Tools, volume 2, Pages 287-303, DOI 10.1016/B978-0-12-811-448-9.00014-7.
- [3] Chou-Yi Hsu^a, Ahmed Mahdi Rheima^b, Zainab sabri Abbas^c, Muhammad Usman Faryad^d, Mustafa m. Kadhim^e, Usama S. Altimari^f, Ashour H. Dawood^g, Alaa dhari jawad albayati^h, Zinab Talib Abedⁱ, Rusul Saeed Radhi^j, Asala Salam Jaber^k, Safa k. Hachim^{lm}, Farah K. Aliⁿ, Zaid H Mahmood^o, Ghobad Behzadi pour^p, and Ehsan Kianfar^{q,r,s}[August 2023] Nanowires Properties and Applications, Journal of Chemical Engineering, volume 46,page 286-311 DOI:10.1016/j.sajce.2023.08.006.
- [4] Dasgupta NP, Sun J, Liu C, Britzman S, Andrews SC, Lim J, Gao H, Yan R, and Yang P. [06 March 2014]. Semiconductor Nanowires - Synthesis, Characterization, and Applications, *Adv. Mater.* volume 26, page 2137-2184 DOI10.1002/adma.201305929.
- [5] JAYA SARKAR, A BASUMALLICK and GOBINDA GOPAL KHAN†[10 July 2006] Nanowires: properties, applications and synthesis via Bull, Mater. Sci. Vol.30, No.3, DOI 811-448-9.00014.

-
- [6] Neil P. Dasgupta, Jianwei Sun, Chong Liu, Sarah Brittman, Sean C. Andrews, Jongwoo Lim, Hanwei Gao, Ruoxue Yan, and Peidong Yang [06 March 2014] 25th Anniversary Article: Semiconductor Nanowires – Synthesis, Characterization, and Applications Volume 26, Issue 14 Pages: 2109-2279, DOI 10.1002/adma.201305929
- [7] Hannah J Joyce¹, Jessica L Boland², Christopher L Davies², Sarwat A Baig¹ and Michael B Johnston²[15 September 2016] A review of the electrical properties of semiconductor nanowires, Semiconductor Science and Technology, Volume 31, DOI 10.1088/0268-1242/31/10/103003.
- [8] Zhongwei Zhang (张忠卫)^{1,2,3} and Jie Chen (陈杰)^{1,2,3} Thermal conductivity of nanowires, THERMAL AND THERMOELECTRIC PROPERTIES OF NANO MATERIALS, Volume 27, Issue 3, DOI 10.1088/1674-1056/27/3/035101.
- [9] Sanjeev Kumar Sharma, Parveen Kumar, and Balwinder Raj [2021] Introduction to Nanowires: Types, Properties, and Application of Nanowires. Innovative Applications of Nanowires for Circuit Design ,DOI: 10.4018/978-1-7998-6467-7
- [10] Fert ^a, L and Piraux ^b March 1999 Magnetic nanowires. Journal of Magnetism and Magnetic Materials Volume 200, Issues 1–3, DOI10.1016/S0304-8853(99)00375.
- [11] Julieta S. Riva, Andrea V. Juárez, Silvia E. Urreta, and Lidia M. Yudi[1 March 2019]Catalytic properties of Pd ferromagnetic nanowires at liquid/liquid interfaces, Electrochimica Acta. Volume 298, DOI10.1016/j.electacta.2018.12.069.
- [12] M. Huth and Beilstein J.[13 Jul 2012] Radiation-induced nanostructures: Formation processes and applications". Materials Research Department, GSI Helmholtz Centre for Heavy Ion Research, vol3, page no.860–883 DOI10.3762/bjnano.3.97.
- [13] Ruiyuan Liu Fute, Zhang Celal Con Bo Cui and Baoquan Sun [04 April 2013] Lithography, free fabrication of silicon nanowire and nanohole arrays by metal-assisted chemical etching. volume8, DOI 10.1186/1556-276X-8-155.
- [14] Wagner, R.S.Ellis and W.C.[March 25, 2014]Vapor-liquid-solid mechanism of single crystal growth. JOURNAL NAME Materials Sciences and Applications, Vol.5 DOI:10.1063/1.1753975.
- [15] Giani, A.; Bayaz, A.A.; Foucaran, A.; Pascal-Delannoy, F. and Boyer, A. (2002). Elaboration of Bi₂Se₃ by metalorganic chemical vapor deposition. Journal of Crystal Growth, Vol. 236, Issues 1–3 Pages 217-220, DOI10.1016/S0022-0248(01)0209.
- [16] Gilberto Brambilla, Fei Xu, Peter Horak, Yongmin Jung, Fumihito Koizumi, Neil P. Sessions, Elena Koukharenko, Xian Feng, Ganapathy S. Murugan, James S. Wilkinson, and David J. Richardson [2009], Optical fiber nanowires and microwires: fabrication and applications Advances in Optics and Photonics, Vol. 1, Issue1, DOI10.1364/AOP.1.0001070.
- [17] Hao Zhu's [July 2017], Semiconductor Nanowire MOSFETs and Applications. Nanowire-New Insight. Page 264 DOI 10.5772/65179.
- [18] Hannah J Joyce¹, Jessica L Boland², Christopher L Davies², Sarwat A Baig¹ and Michael B Johnston²[15 September] A review of the electrical properties of semiconductor nanowires. Semiconductor Science and Technology, Volume 31, DOI 10.1088/0268-1242/31/10/103003.
- [19] Guang Wen Zhou and Ze Zhang Zhi Gang Bai, Sun Qi Feng, and Da Peng Yua. [3 AUGUST 1998]. Transmission electron microscopy study of Si nanowires. APPLIED PHYSICS LETTERS. VOLUME 73, Issue 5. DOI:10.1063/1.121945.
- [20] C. Couteau, A. Larrue, C. Wilhelm, and C. Soci [May 20, 2015] Nanowire Lasers, journal Nanophotonics. Volume 4 Issue 1 DOI 10.1515/nanoph-2015-0005
- [21] Preeti Khulb [9 January, 2014]. Nanorobotics INTERNATIONAL JOURNAL OF PHARMACEUTICAL SCIENCES AND RESEARCH Vol. 5, issue 6, DOI 2164-217
- [22] Jaswanth V, and Vishwas K Singh [Apr 2022] Nanowire Solar Cells: A New Era of Photovoltaic Technology. International Research Journal of Engineering and Technology (IRJET), Volume: 09, Issue: 04, DOI 2395-0056.

Review On Polyindole Composites For Supercapacitor Application

Akshay P. Bangar*, Suraj V. Tayade, Sandeep A. Waghuley

Department of Physics, Sant Gandge Baba Amravati University, Amravati, India ,444 602.

*Corresponding author email: akshaybangarofficial1@gmail.com

Abstract

Efficient energy storage is vital for sustainable energy devices, particularly in dealing with the irregularities of renewables. Supercapacitors, positioned between traditional batteries and capacitors, offer promise due to high specific energy and power density. This review centers on Polyindole's (PIn) role in supercapacitors, emphasizing its unique properties. Combining PIn with metal oxides, like manganese dioxide (MnO_2), enhances electrochemical performance. The concept of hybrid supercapacitors, blending electric double-layer capacitors and pseudocapacitors, is introduced, highlighting PIn-based composites. The conclusion stresses the need for optimizing PIn concentration and suggests eco-friendly polymerization methods and careful component selection to overcome limitations, making PIn composites a key for future supercapacitor applications.

Keywords : PANI, Polyindole, MnO_2 , Supercapacitor,

Introduction

In the pursuit of sustainable energy sources, including solar, wind, tidal, and other renewables, the need for effective energy storage systems becomes increasingly imperative. These systems play a pivotal role in optimizing electricity utilization, ensuring controlled delivery, and addressing the irregular nature of renewable energy sources. Globally, we are facing a huge problem about energy shortage due to rapid development of economy and increasing depletion of fossil fuels [1]. Hence, there is a crucial need for development new energy sources [2]. Supercapacitor bridges the gap between traditional batteries and capacitors. This strategic placement, considering high specific energy and power density [3], leads to efficient storage and release of electricity.

As the effectiveness of energy storage systems is evaluated based on parameters such as cost-effectiveness, efficiency, capacity, eco-friendliness, and cycle life [4], supercapacitors emerge as efficient contenders in comparison to batteries and fuel cells. Though supercapacitors exhibit exceptional properties, including high charging and discharging rates, excellent power density, stability, and long-term cyclability [5-7], there is a need for advancements to meet the growing demands of applications like electric vehicles. Improvements in energy density are crucial, and one approach involves increasing the working potential window, primarily associated with the employed electrolyte. This increase is pivotal, considering that energy density is proportional to the square of the operating potential window and specific capacitance in supercapacitors [8]. For fabrication of supercapacitors a variety of materials and systems can be used, among which conductive polymers stand out for their pseudo-capacitive properties [9-12]. Active materials play a vital role in the electrochemical performance of supercapacitors [13], leading to recent emphasis on the development of electrode materials involving carbon materials, metal oxides, and conducting polymers [14-15]. This comprehensive review aims to explore the intricate interplay of materials and systems in supercapacitors, shedding light on avenues to enhance energy storage systems vital for the sustainable integration of renewable energy sources.

Conducting Polymers

Conducting polymers, with their 1D intrinsic properties, have been a focal point of both fundamental and applied research in fields like field-effect transistors, displays, and rechargeable batteries [16]. Polyaniline (PANI), Polypyrrole (PPy), Polythiophene (PTh)

represent the extensively studied conducting polymers, in contrast to Polyindole, often referred to as PI/PIn/PIn, which has historically garnered less attention due to its lower polymerization efficiency. However, recent interest has surged owing to its remarkable environmental stability and electrical conductivity. Characterized by a distinctive benzene and pyrrole ring structure, coupled with properties such as good thermal stability, low degradation rate, and high storage capacity, polyindole emerges as an appealing candidate for electrocatalytic applications, as demonstrated in mediated-based biofuel cells [17].

PANI and PIn stand out as suitable materials for supercapacitor electrodes due to their favorable electrochemical properties, exhibiting high electrical conductivity for efficient charge transport. Their nanostructured forms provide a large surface area, enabling a greater number of electroactive sites for charge storage. Additionally, PANI and PIn possess redox activity, facilitating reversible redox reactions during charge-discharge cycles and contributing to high capacitance. These polymers demonstrate chemical stability, enduring repeated cycles without significant degradation. Their ease of synthesis and processability into various forms further enhances their suitability for electrode fabrication. Environmentally friendly synthesis methods and relatively low production costs make them attractive options for large-scale supercapacitor applications [18]. While PANI is relatively easy to synthesize, PIn offers several advantages over other conducting polymers, including high thermal stability, good processability, and environmental stability [17,19-20]. However, its practical applications have been limited by its low electrical and electrochemical conductivity.

Polyindole (PIn) stands out for several reasons. Its ability to embody the properties of poly(para-phenylene) and polypyrrole (Ppy) makes it intriguing, attributed to the aromatic molecular structure of indole, which imparts a similar structure to PIn akin to that of Ppy and poly(para-phenylene) [21-25]. In energy storage applications, PIn exhibits slow hydrolytic degradation (in comparison to PANI), a competitive redox potential (compared to Ppy), high cycling and thermal stability [26], rendering it superior for long-term energy storage [27]. Furthermore, PIn avoids the formation of salts during complete charge or discharge phases, in contrast to PANI, reducing resistance and enhancing internal conductivity [28-29]. Despite PIn's conductivity being lower by two orders of magnitude compared to PANI and Ppy, it demonstrates comparable environmental and electrochemical stability [30]. However, PIn faces limitations, such as low electrical and electrochemical conductivity, instability, mechanical strain over extended cycles, and material degradation, which hinder its standalone application as an energy storage material. Nevertheless, PIn, in combination with certain dopants like organic materials and metallic components, proves to be a promising candidate for future-generation applications [31-33]. Recent developments highlight PIn's potential across diverse domains, including organic electronics [34], batteries, supercapacitors [35-36], anti-corrosion coatings [37], and sensors [38].

Polyindole/Metal Oxides

Transition metal oxides (TMO) stand out as extensively used electrode materials for supercapacitor applications due to their high specific capacitance and power density [39]. However, they present drawbacks such as poor electrical conductivity and instability in acidic mediums [40]. To address these limitations, TMOs are often combined with either carbon-based materials or conducting polymers (CPs). The combination of Polyindole (PIn) with various metal oxides is expected to yield improved electrochemical and mechanical properties, leading to the synthesis of polymer-metal oxide nanocomposites, a burgeoning field with promising applications in rechargeable batteries, fuel cells, and supercapacitors [41].

Manganese dioxide (MnO_2) is recognized as a promising candidate for supercapacitors due to its high theoretical conductivity and effective electroactive sites for charge storage [42]. The synthesis of MnO_2 /PIn nanocomposites involves an in situ chemical oxidative polymerization

process, optimizing the supercapacitive properties of MnO₂-PIn composites. The specific capacitance of MnO₂-loaded PIn composites reaches 1558 F/g, demonstrating long-term stability with capacitance retention up to 6000 cycles [2]. Researchers, such as Purty et al. [43], have reported MnO₂/PIn bi-composites that exhibit excellent cyclic stability. Various strategies, including the synthesis of MnO₂/reduced graphene oxide nanocomposites and the one-step in-situ cathodic electrodeposition of a composite of cobalt oxide and Polyindole by Raj and coworkers, showcase outstanding specific capacitance values [44,45].

Looking beyond manganese dioxide, other metal oxides like V₂O₅, Fe₂O₃, Fe₂O₄, RuO₂, MoO₃, WO₃, PbO₂, SnO₂, CuO, NiO, and TiO₂, along with their modified hybrids, are believed to be essential composites for enhancing the performance of Polyindole (PIn) [46]. Therefore, PIn/metal oxide (MO) nanocomposites exhibit remarkable electrochemical properties [47].

Applications

Hybrid Supercapacitor

Hybrid supercapacitor is a combination of both EDLC and pseudocapacitor [48]. It contains two asymmetric electrodes, one of which exhibits high pseudocapacitance which increases specific capacitance, working voltage and specific energy while the other exhibits high electrostatics double layer capacitance which provides better cyclic stability and higher specific power [39,49-51]. In this way, a hybrid supercapacitor exhibits fairly improved electrochemical performance. Therefore, scientists and researchers are mostly concentrating on the various types of hybrid supercapacitor [52]. Hybrid supercapacitors can also be fabricated by using composites of pseudocapacitive materials with double layer capacitive materials [47].

Polyindole-based hybrid composites are being recognized as a promising candidate to be used in energy storage devices. Certain factors viz. electrolyte, concentration, morphology, pH, temperature, etc., are major components affecting performance of Polyindole and its composites. This assessment recapitulates the position of Polyindole and its hybrid composite to be used as energy harvest material; in addition, this evaluation also pronounces the future aspect of the hybrids [53].

Conclusions & Perspectives

The conclusion highlights the potential of polyindole (PIn) and its composites, specifically MnO₂/PIn, emphasizing their improved electrochemical properties that make them suitable for supercapacitors. The studies reveal that optimizing the amount of PIn, increases the active surface area, improving mesoporosity, and facilitating electrode–electrolyte interaction enhance interlayer charge carriage through intercalation of conducting PIn. The concentration of PIn not only influences morphology but also impacts thermal properties and electrochemical behavior. The 3D design enables easy diffusion of electrolytic ions with a shorter route, favorably permitting greater charge–discharge rates and specific capacitance.

Therefore, it is concluded that hybrid PIn composites, whether binary or ternary, show promise for future supercapacitor applications. However, acknowledging certain limitations such as instability, mechanical strain over extended cycles, and material degradation inherent in PIn and other conducting polymers, it is suggested that employing green and efficient polymerization methods and carefully selecting components for hybrid composite fabrication could be crucial in overcoming these challenges and components for hybrid composite fabrication could be a key in this direction.

References

- [1] Zhang, Y., & Mo, Y. (2014). Preparation of MnO₂ electrodes coated by Sb-doped SnO₂ and their effect on electrochemical performance for supercapacitor. *Electrochimica Acta*, 142, 76-83.
- [2] Barde R.V., Nemade K.R., Waghuley S.A., (2022), Optimization of supercapacitive properties of polyindole by dispersion of MnO₂ nanoparticles, *Chemical Physics Impact* 5 (2022) 100100
- [3] Fic, K., Platek, A., Piwek, J., & Frackowiak, E. (2018). Sustainable materials for electrochemical capacitors. *Materials today*, 21(4), 437-454.
- [4] Yan, Y., Xu, M., Luo, Y., Ma, J., Pang, H., & Xue, H. (2017). Preparation of N, P co-doped activated carbons derived from honeycomb as an electrode material for supercapacitors. *RSC advances*, 7(75), 47448-47455.
- [5] Poochai, C., Sriprachuabwong, C., Sodtipinta, J., Lohitkarn, J., Pasakon, P., Primpray, V., ... & Tuantranont, A. (2021). Alpha-MnO₂ nanofibers/nitrogen and sulfur-co-doped reduced graphene oxide for 4.5 V quasi-solid state supercapacitors using ionic liquid-based polymer electrolyte. *Journal of Colloid and Interface Science*, 583, 734-745.
- [6] Tyagi, A., Tripathi, K. M., & Gupta, R. K. (2015). Recent progress in micro-scale energy storage devices and future aspects. *Journal of Materials Chemistry A*, 3(45), 22507-22541.
- [7] Chen, L., Song, Z., Liu, G., Qiu, J., Yu, C., Qin, J., ... & Liu, W. (2013). Synthesis and electrochemical performance of polyaniline–MnO₂ nanowire composites for supercapacitors. *Journal of Physics and Chemistry of Solids*, 74(2), 360-365.
- [8] Liu, Y., Xiao, Z., Liu, Y., & Fan, L. Z. (2018). Biowaste-derived 3D honeycomb-like porous carbon with binary-heteroatom doping for high-performance flexible solid-state supercapacitors. *Journal of Materials Chemistry A*, 6(1), 160-166.
- [9] Ibanez, J. G., Rincón, M. E., Gutierrez-Granados, S., Chahma, M. H., Jaramillo-Quintero, O. A., & Frontana-Uribe, B. A. (2018). Conducting polymers in the fields of energy, environmental remediation, and chemical–chiral sensors. *Chemical reviews*, 118(9), 4731-4816.
- [10] Yu, Z., Tetard, L., Zhai, L., & Thomas, J. (2015). Supercapacitor electrode materials: nanostructures from 0 to 3 dimensions. *Energy & Environmental Science*, 8(3), 702-730.
- [11] Meng, Q., Cai, K., Chen, Y., & Chen, L. (2017). Research progress on conducting polymer based supercapacitor electrode materials. *Nano Energy*, 36, 268-285.
- [12] Han, Y., & Dai, L. (2019). Conducting polymers for flexible supercapacitors. *Macromolecular chemistry and physics*, 220(3), 1800355.
- [13] Winter, M., & Brodd, R. J. (2004). What are batteries, fuel cells, and supercapacitors?. *Chemical reviews*, 104(10), 4245-4270.
- [14] Díaz-Arriaga, C. B., Baas-López, J. M., Pacheco-Catalán, D. E., & Uribe-Calderon, J. (2020). Symmetric electrochemical capacitor based on PPy obtained via MnO₂ reactive template synthesis. *Synthetic Metals*, 269, 116541.
- [15] Ho, M. Y., Khiew, P. S., Isa, D., Tan, T. K., Chiu, W. S., & Chia, C. H. (2014). A review of metal oxide composite electrode materials for electrochemical capacitors. *Nano*, 9(06), 1430002.
- [16] Koiry, S. P., Saxena, V., Sutar, D., Bhattacharya, S., Aswal, D. K., Gupta, S. K., & Yakhmi, J. V. (2007). Interfacial synthesis of long polyindole fibers. *Journal of applied polymer science*, 103(1), 595-599.
- [17] Perveen, R., Inamuddin, ul Haque, S., Nasar, A., Asiri, A. M., & Md Ashraf, G. (2017). Electrocatalytic performance of chemically synthesized PIn-Au-SGO composite toward mediated biofuel cell anode. *Scientific Reports*, 7(1), 13353.
- [18] Fuseini, M., & Zaghoul, M. M. Y. (2022). Qualitative and statistical approaches of the electrophoretic deposition kinetics of polyaniline copper coating. *Progress in Organic Coatings*, 171, 107015.
- [19] Mudila, H., Prasher, P., Kumar, M., Kumar, A., Zaidi, M. G. H., & Kumar, A. (2019). Critical analysis of polyindole and its composites in supercapacitor application. *Materials for Renewable and Sustainable Energy*, 8, 1-19.

- [20] Fuseini, M., & Zaghoul, M. M. Y. (2022). Statistical and qualitative analyses of the kinetic models using electrophoretic deposition of polyaniline. *Journal of Industrial and Engineering Chemistry*, 113, 475-487.
- [21] Tebyetekerwa, M., Yang, S., Peng, S., Xu, Z., Shao, W., Pan, D., ... & Zhu, M. (2017). Unveiling polyindole: freestanding As-electrospun polyindole nanofibers and polyindole/carbon nanotubes composites as enhanced electrodes for flexible all-solid-state supercapacitors. *Electrochimica Acta*, 247, 400-409.
- [22] Wang, W., & Wu, S. (2017). A new ternary composite based on carbon nanotubes/polyindole/graphene with preeminent electrocapacitive performance for supercapacitors. *Applied Surface Science*, 396, 1360-1367.
- [23] Cai, Z., & Yang, G. (2010). Synthesis of polyindole and its evaluation for Li-ion battery applications. *Synthetic metals*, 160(17-18), 1902-1905.
- [24] Tebyetekerwa, M., Wang, X., Marriam, I., Dan, P., Yang, S., & Zhu, M. (2017). Green approach to fabricate polyindole composite nanofibers for energy and sensor applications. *Materials Letters*, 209, 400-403.
- [25] Tebyetekerwa, M., Wang, X., Wu, Y., Yang, S., Zhu, M., & Ramakrishna, S. (2017). Controlled synergistic strategy to fabricate 3D-skeletal hetero-nanosponges with high performance for flexible energy storage applications. *Journal of Materials Chemistry A*, 5(40), 21114-21121.
- [26] Dhanalakshmi, K., & Saraswathi, R. (2001). Electrochemical preparation and characterization of conducting copolymers: poly (pyrrole-co-indole). *Journal of materials science*, 36, 4107-4115.
- [27] Zhou, X., Chen, Q., Wang, A., Xu, J., Wu, S., & Shen, J. (2016). Bamboo-like composites of V2O5/polyindole and activated carbon cloth as electrodes for all-solid-state flexible asymmetric supercapacitors. *ACS applied materials & interfaces*, 8(6), 3776-3783.
- [28] Eftekhari, A., Li, L., & Yang, Y. (2017). Polyaniline supercapacitors. *Journal of Power Sources*, 347, 86-107.
- [29] Wu, Q., Xu, Y., Yao, Z., Liu, A., & Shi, G. (2010). Supercapacitors based on flexible graphene/polyaniline nanofiber composite films. *ACS nano*, 4(4), 1963-1970.
- [30] Mackintosh, J. G., Redpath, C. R., Jones, A. C., Langridge-Smith, P. R., & Mount, A. R. (1995). The electropolymerization and characterization of 5-cyanoindole. *Journal of electroanalytical chemistry*, 388(1-2), 179-185.
- [31] Cai, Z. J., Zhang, Q., & Song, X. Y. (2016). Improved electrochemical performance of polyindole/carbon nanotubes composite as electrode material for supercapacitors. *Electronic Materials Letters*, 12, 830-840.
- [32] Mudila, H., Rana, S., Zaidi, M. G. H., & Alam, S. (2015). Polyindole/graphene oxide nanocomposites: the novel material for electrochemical energy storage. *Fullerenes, Nanotubes and Carbon Nanostructures*, 23(1), 20-26.
- [33] Majumder, M., Choudhary, R. B., Thakur, A. K., Rout, C. S., & Gupta, G. (2018). Rare earth metal oxide (RE₂O₃; RE= Nd, Gd, and Yb) incorporated polyindole composites: gravimetric and volumetric capacitive performance for supercapacitor applications. *New Journal of Chemistry*, 42(7), 5295-5308.
- [34] Abthagir, P. S., Dhanalakshmi, K., & Saraswathi, R. (1998). Thermal studies on polyindole and polycarbazole. *Synthetic metals*, 93(1), 1-7.
- [35] Zhijiang, C., Xingjuan, S., & Yanan, F. (2013). Electrochemical properties of electrospun polyindole nanofibers as a polymer electrode for lithium ion secondary battery. *Journal of power sources*, 227, 53-59.
- [36] Mudila, H., Prasher, P., Kumar, M., Kumar, A., Zaidi, M. G. H., & Kumar, A. (2019). Critical analysis of polyindole and its composites in supercapacitor application. *Materials for Renewable and Sustainable Energy*, 8, 1-19.
- [37] Tüken, T., Düdükçü, M., Yazıcı, B., & Erbil, M. (2004). The use of polyindole for mild steel protection. *Progress in organic coatings*, 50(4), 273-282.
- [38] Pandey, P. C. (1988). A new conducting polymer-coated glucose sensor. *Journal of the Chemical Society, Faraday Transactions 1: Physical Chemistry in Condensed Phases*, 84(7), 2259-2265.

- [39] Muritala, I. K., Guban, D., Roeb, M., & Sattler, C. (2020). High temperature production of hydrogen: Assessment of non-renewable resources technologies and emerging trends. *international journal of hydrogen energy*, 45(49), 26022-26035.
- [40] Meng, Q., Cai, K., Chen, Y., & Chen, L. (2017). Research progress on conducting polymer based supercapacitor electrode materials. *Nano Energy*, 36, 268-285.
- [41] Rajasudha, G., Nancy, A. P., Paramasivam, T., Boukos, N., Narayanan, V., & Stephen, A. (2011). Synthesis and characterization of polyindole–NiO-based composite polymer electrolyte with LiClO₄. *International Journal of Polymeric Materials*, 60(11), 877-892.
- [42] Wang, J. G., Yang, Y., Huang, Z. H., & Kang, F. (2014). MnO₂/polypyrrole nanotubular composites: reactive template synthesis, characterization and application as superior electrode materials for high-performance supercapacitors. *Electrochimica Acta*, 130, 642-649.
- [43] Purty, B., Choudhary, R. B., Kandulna, R., & Singh, R. (2018, May). Binder free MnO₂/PIn electrode material for supercapacitor application. In *AIP Conference Proceedings* (Vol. 1953, No. 1). AIP Publishing.
- [44] Zhang, M., Yang, D., & Li, J. (2020). Effective improvement of electrochemical performance of electrodeposited MnO₂ and MnO₂/reduced graphene oxide supercapacitor materials by alcohol pretreatment. *Journal of Energy Storage*, 30, 101511.
- [45] Raj, R. P., Ragupathy, P., & Mohan, S. (2015). Remarkable capacitive behavior of a Co₃O₄–polyindole composite as electrode material for supercapacitor applications. *Journal of Materials Chemistry A*, 3(48), 24338-24348.
- [46] An, C., Zhang, Y., Guo, H., & Wang, Y. (2019). Metal oxide-based supercapacitors: progress and perspectives. *Nanoscale Advances*, 1(12), 4644-4658.
- [47] Choudhary, R. B., Ansari, S., & Purty, B. (2020). Robust electrochemical performance of polypyrrole (PPy) and polyindole (PIn) based hybrid electrode materials for supercapacitor application: A review. *Journal of Energy Storage*, 29, 101302.
- [48] Muzaffar, A., Ahamed, M. B., Deshmukh, K., & Thirumalai, J. (2019). A review on recent advances in hybrid supercapacitors: Design, fabrication and applications. *Renewable and sustainable energy reviews*, 101, 123-145.
- [49] Halper, M. S., & Ellenbogen, J. C. (2006). Supercapacitors: A brief overview. *The MITRE Corporation, McLean, Virginia, USA*, 1.
- [50] Iro, Z. S., Subramani, C., & Dash, S. S. (2016). A brief review on electrode materials for supercapacitor. *Int. J. Electrochem. Sci*, 11(12), 10628-10643.
- [51] Yan, J., Fan, Z., Sun, W., Ning, G., Wei, T., Zhang, Q., ... & Wei, F. (2012). Advanced asymmetric supercapacitors based on Ni(OH)₂/graphene and porous graphene electrodes with high energy density. *Advanced Functional Materials*, 22(12), 2632-2641.
- [52] Wang, F., Xiao, S., Hou, Y., Hu, C., Liu, L., & Wu, Y. (2013). Electrode materials for aqueous asymmetric supercapacitors. *Rsc Advances*, 3(32), 13059-13084.
- [53] Mudila, H., Prasher, P., Kumar, M., Kumar, A., Zaidi, M. G. H., & Kumar, A. (2019). Critical analysis of polyindole and its composites in supercapacitor application. *Materials for Renewable and Sustainable Energy*, 8, 1-19.

Nonlinear I–V characteristics and thermal stability of nanocrystalline Titanium oxide

*¹Balkhande V.M., ²Lamdhade G.T., ¹Daware A.S.

¹Dept. of Physics, Prof. Ram Meghe Institute of Tech. & Research, Badnera-Amravati M.S. India-444 701

²Dept. of Physics, Vidya Bharati Mahavidyalaya, Amravati M.S. India-444 602

*Corresponding Author Email: vidya_balkhande@yahoo.com

Abstract

Current versus voltage characteristics (I-V) of nanocrystalline Titanium oxide (TiO₂) has been investigated at various temperatures (from 50°C to 350°C) in air, measured by using a data acquisition system consisting of Keithley 6487 voltage source cum picoammeter. The nanocrystalline powder of TiO₂ was prepared by the liquid phase method and samples were prepared via spray pyrolysis technique in the form of thin films on an optically plane and clean glass surface. X-ray diffraction studies showed a , mostly as rutile and anatase phases which both of them have the tetragonal structures of TiO₂. Surface morphological studies were performed with scanning electron microscopy. The nanocrystalline Titanium oxide exhibited nonlinear I-V characteristics of the negative resistance type with thermal stability.

Keywords: Nanocrystalline Titanium oxide, XRD, FE-SEM, I-V characteristics, thermal stability

Introduction:

Titanium dioxide is a cheap, chemically stable, and non-toxic material. However, its electrical properties are unstable and it is a modest semiconductor and a mediocre insulator. For several applications, it would be interesting to make it either more insulating or more conducting. Titanium dioxide (TiO₂) is a material used in a wide range of common and high-tech applications. It is cheap, chemically stable, non-toxic, and last but not least bio-compatible. Titanium is successfully used as an implant material for dental, orthopedic and osteosynthesis applications, and its native oxide is mostly constituted of titanium dioxide [1]. TiO₂ powder is used as a white pigment in paint [2], replacing lead oxide which is toxic, and in toothpaste. Transparent single crystals or thin films have a high refractive index that makes TiO₂ suitable for optical applications [3-5]. Thus, research in many different fields is devoted to titanium dioxide under various forms such as single crystals, ceramics, and thin films. The goal of this work was to study the I-V characteristics, and structural, morphological properties of nano-crystalline TiO₂ thin films deposited by the spray pyrolysis technique.

Experimental :

The methods of synthesis of nanoparticles can be broadly classified into three categories namely, liquid-phase synthesis, gas-phase synthesis, and vapor-phase synthesis. In the present work of the thesis, we have used the sol-gel method (which is under liquid phase synthesis) for the synthesis of pristine nanoparticles of TiO₂ [6-8].

Synthesis of TiO₂:

Titanium tetra iso propoxide [Ti(OCH(CH₃)₂)₄], iso-propanol [(CH₃)₂CHOH] and nitric acid [HNO₃] were used as received without any further purification. A 20 ml of solution of Titanium tetra isopropoxide was added drop by drop into the 22 ml of a solution containing 10 ml of iso-propanol and 12 ml deionised water under constant stirring at 80°C into the round bottom beaker. After 1 hour, concentrated HNO₃ (.8 ml) mixed with deionised water was added into the TTIP solution and keep it under constant stirring at 60 °C for 6 hours highly viscous

sol-gel was obtained. The prepared sol-gel was heated at 300 °C for 2 hours in the open atmosphere. After annealing, the TiO₂ nanocrystalline 2 g powder was obtained. In further preparation of TiO₂ film, the prepared powder was added in the ratio of 1:10 to the solution of isopropanol. The obtained powder is kept in a vacuum oven at 70 °C for 24 hours so as to get completely dried powder.

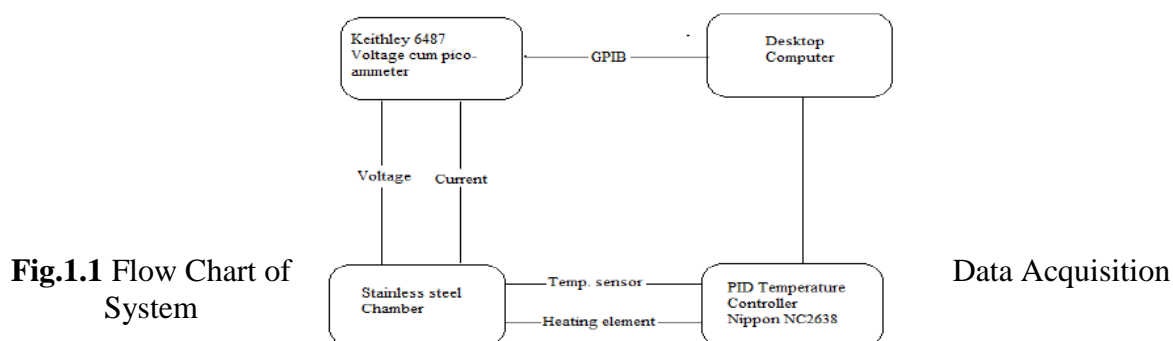
Preparation of Samples:

After the synthesis, obtained fine nanopowder of TiO₂ was calcinated at 800 °C up to 5 hours in the auto-controlled muffle furnace, so that the impurities from product will be completely removed. The obtained product of fine nanopowder is further used for the preparations of samples. The obtained product of fine nanopowder of TiO₂ used for the fabrication samples was prepared via spray pyrolysis technique using Thin-film equipment: (Holmarc USA Make) in the form of thin films on an optically plane and clean glass surface [9-10].

Data Acquisition System:

The data acquisition system consists of a Keithley 6487 source meter, GPIB cable, temperature controller, and computer as shown in fig. 1.1.

The picoammeter is controlled by the installation of GPIB (General Purpose Interface Bus) card. This GPIB card has an IEEE-488.2 bus, which is common to the testing meter. Communication with the temperature controller is done using Rs-232 port.



The language used for controlling the source meter and temperature controller is lab view graphical programming language, which can provide a friendly user interface. To study the VI characteristics of the sample element, special software was designed.

Results and Discussion:

X-Ray Diffraction : Nanocrystalline TiO₂

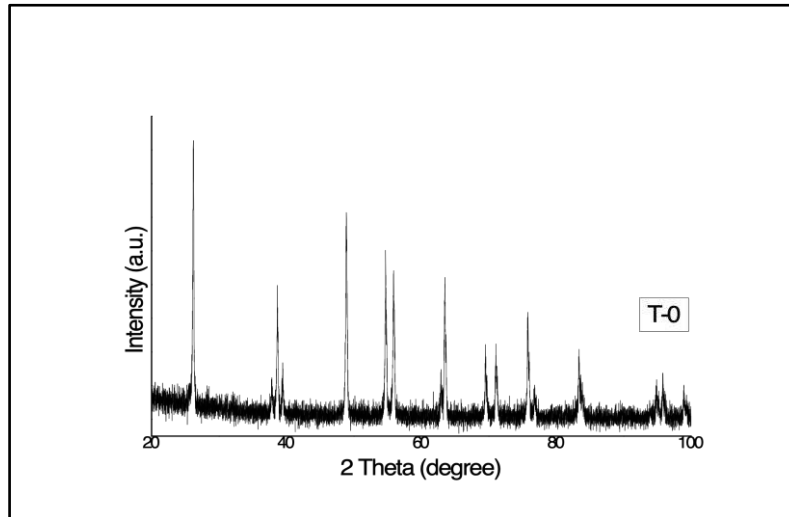
Titanium dioxide or Titania (TiO₂) is widely nominated for three main phases of rutile, anatase and brookite . Among them, the TiO₂ exists mostly as rutile and anatase phases which both of them have the tetragonal structures. However, rutile is a high-temperature stable phase and anatase is formed at a lower temperature .

Figure 1.2 shows the XRD pattern of pure Titanium Dioxide (TiO₂) which is calcinated at temperature 800°C, which shows crystalline annealed with 2θ peaks lying at planes (1 0 1), (1 0 3), (0 0 4), (1 1 2), (2 0 0), (1 0 5), (2 1 1),(2 1 3), (2 0 4), (1 1 6), (2 2 0), (1 0 7), (2 1 5), (3 0 1), (0 0 8), (3 0 3), (2 2 4) and (3 1 2) respectively. The sharp diffraction peaks were clearly seen and they perfectly match with crystal structure of TiO₂ therefore, we get perfectly crystallinity of TiO₂ particles in Anatase phase. The calculated crystallographic parameters are a = 3.7300 (Å), b = 3.7300 (Å) and c = 9.3700 (Å) [Crystal system: Tetragonal ; Space group: I41/amd ; Space group number: 141, Reference Code: 01-

075-1537] . All the peaks match well with the standard tetragonal type structures of titanium dioxide (TiO_2) in the Anatase phase and well agree with the JCPDS card No. 21-1272 . The average crystalline size was calculated by using the Scherrer formula found to **82.75 nm**. The stick pattern of crystalline TiO_2 is as shown in fig. 1.2. It was found that the thick films consisted only of the tetragonal structure TiO_2 with no structural change and they were well crystallized during deposition [11-12].

Fig. 1.2 XRD
pristine TiO_2

**Field
Scanning
Microscope:**



of crystalline

**Emission -
Electron**

The surface morphology and the nanocrystalline particle size of titanium oxide (TiO_2) were examined by using Field Emission Scanning Electron Microscope. Figure 1.3 shows the FE-SEM micrograph of pristine TiO_2 , thin films. To verify the morphology scheme data obtained from the scanning electron microscopy will confirm the structural analysis obtained by the X-ray diffraction pattern [13-14].

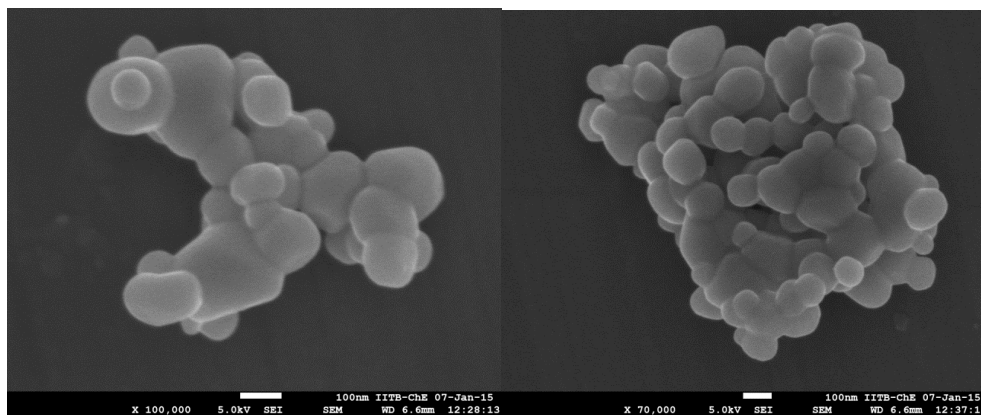


Fig. 1.3 FESEM of Nano-crystalline pristine TiO_2

Figure 1.3. shows the micrograph of sample pure TiO_2 thick films. TiO_2 particles are found to be tetragonal and semi spherical shape with the average size in the range of 85-94 nm. The average particle size observed in FE-SEM is in good agreement with the calculated value from XRD analysis [15].

Thermal Stability of TiO_2 thin films :

Figure 1.4 shows the variation of current Vs. temperature from 50°C to 350°C at constant source voltage (10 V DC) by using Keithley (6487) voltage source cum picoammeter. i.e. thermal stability for different samples of pristine TiO_2

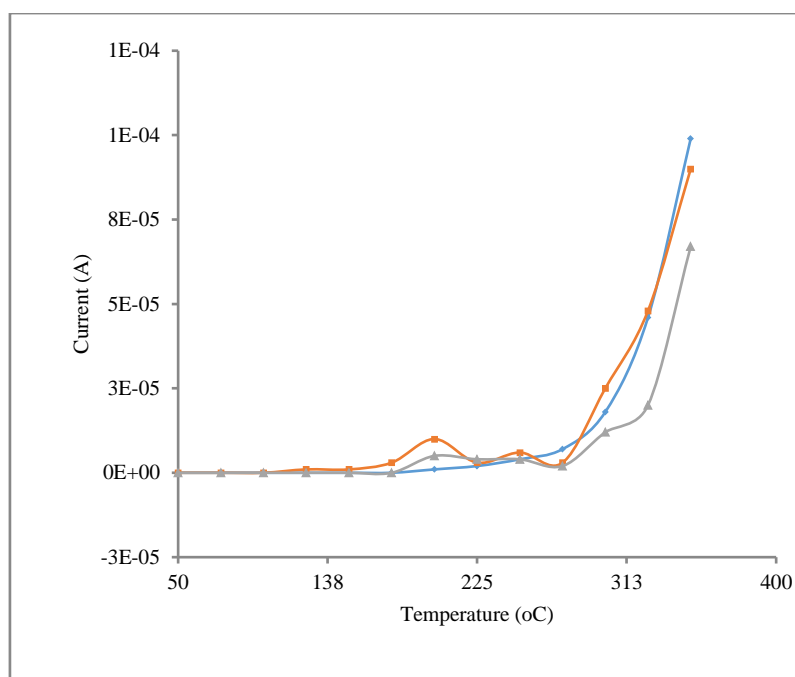


Fig. 1.4 Thermal Stability Curves of pristine TiO₂ Samples.

When samples are kept to a thermal treatment in an inert atmosphere (N₂), from 50°C to 350°C under the small interval of time, there occurs also a mass loss on heating in air atmosphere but it happens at higher temperature, around 500°C and in a smaller temperature interval (the mass loss begins in the neighbourhood of 430°C and considerably slower down around 550°C). It is noteworthy that the temperature at which we observe oxidation in as – grown films is significantly lower than temperatures mentioned in for samples deposited by screen printing technique, a fact that seems to confirm the sensitivity of oxidation temperature on sample texture. In present study, thermal treatment of samples is less than temperature 500°C, so there is no problem of mass loss of thick film samples. Generally, the grain size of nanocrystalline materials increases by increasing annealing temperature. This could be attributed to the effects of evaporation of absorbed water and reorganization of the grain. Uniform distribution of the grain is also observable. This is important to note that, due to thermal treatment to the films, which show better and excellent sensitivity and stability results without any further mechanical deformations obtained or seen in the films [16-17].

Current-Voltage (I–V) Characteristics :

The current-voltage (I–V) characteristics of the sample of pristine TiO₂ and their temperature dependence have been investigated in the air by using a data acquisition system consisting of a Keithley 6487 source meter, GPIB cable, temperature controller, and computer. Fig. 1.4 shows the current-voltage (I–V) characteristics sample of pristine TiO₂ measured at different temperatures (50°C, 100°C, 150°C, 200°C, 250°C, 300°C and 350°C). All the samples show semiconducting behavior as the resistance of samples is decreasing with an increase in the I-V measurement temperature. The nature of the plot is initially linear and then it becomes nonlinear beyond threshold voltage, said to be exponential in nature. The resistance is drastically falling at temperature 350°C and is found to be in the range of 5-15 MW. The nanocrystalline titanium oxide exhibited nonlinear I-V characteristics of the current-controlled negative resistance type [18].

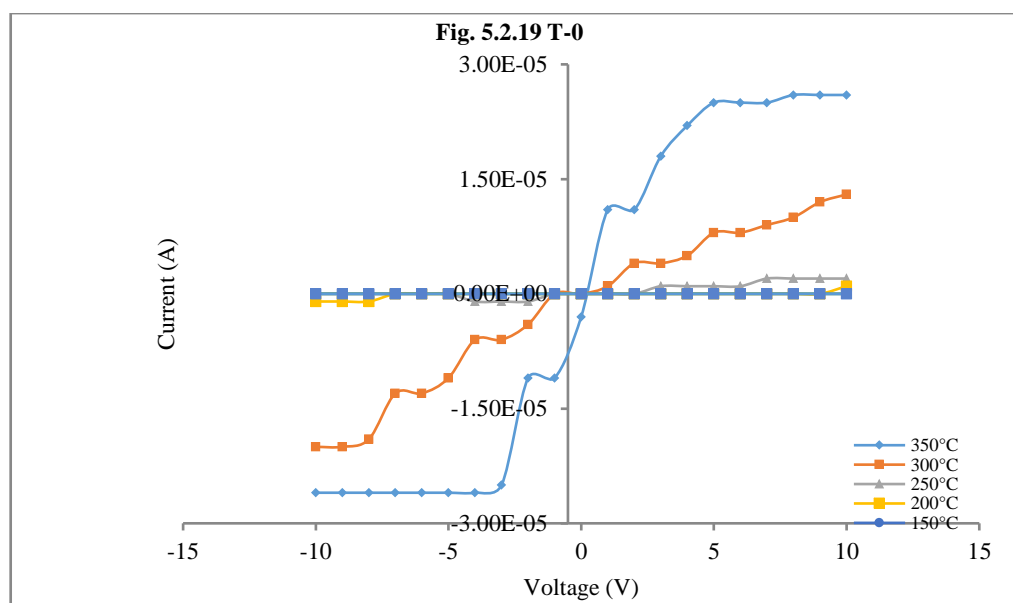


Fig. 1.4 Current–Voltage (I–V) Characteristic of pristine TiO₂

Conclusions:

Current versus voltage characteristics (I-V) of nanocrystalline TiO₂ has been investigated at various temperatures (from 50°C to 350°C) in air and characteristic curves are generally used as a tool to determine and understand the basic parameters of a component or device and can also be used to mathematically model its nonlinear behaviour within an electronic circuit.

References :

- [1] C. E. Sittig: "Charakterisierung der Oxidschichten auf Titan und Titanlegierungen sowie deren Reaktionen in Kontakt mit biologisch relevanten Modellösungen", Dissertation ETH Nr. 12657, Zürich (1998).
- [2] W. Clark and P. Broadhead, *Journal of Physics C* 3 (1970), 1047.
- [3] R. R. Willey: "Practical design and production of optical thin films", Marcel Dekker, New York (1996).
- [4] M. Radecka, K. Zahrzewska, H. Czernastek, and T. Stapinski, *Applied Surface Science* 65/66 (1993), 227.
- [5] S. Lee, B. Hun Park, and S.-G. Oh, *Journal of the Korean Physical Society* 31 (1997).
- [6] A. Eucken and A. Büchner, *Zeitschrift für physikalische Chemie B* 27 (1935), 321.
- [7] H. L. Hartnagel, A. L. Dawar, A. K. Jain, and C. Jagadish: "Semiconducting transparent thin films", Institute of Physics Publishing, Bristol (1995).
- [8] M. Ohring: "The materials Science of Thin Films", Academic Press, San diego (1992).
- [9] G Korotcenkov, V Brinzari, J Schwank, M DiBattista and A Vasiliev, (2001) *Sensors and Actuators B: Chemical* ,Volume 77, Issue 1-2, pp : 244- 252.
- [10] G. Gordillo, L.C. Moreno, W. de la Cruz and P. Teheran, (1994) , *Thin Solid Films*, Volume 252, Issue 1, pp: 61 - 66
- [10] T.K. Kim, M.N. Lee, S.H. Lee, Y.C. Park, C.K. Jung and J.-H. Boo, "Thin Solid Films, Volume 475, Issue 1-2, pp: 171-177, Mar (2005), DOI: 10.1016/j.tsf.2004.07.021
- [11] Brady, G.S. 1971. *Materials Handbook* . New York: McGraw-Hill.
- [12] Parker, R.L., *Z. Kristallogr., Kristallgeom., Kristallphys., Kristallchem.*, 59, 1, (1924)
- [13] Zeljka Antic, Radenka M. Krsmanovic, Marko G. Nikolic, Milena Marinovic- Cincovic, Miodrag Mitric, Stefano Polizzi and Miroslav D. Dramicanin, "Materials Chemistry and Physics, Volume 135, Issue 2-3, pp: 1064 – 1069, Aug (2012)
- [14] Liqiang Jing, Zili Xu, Xiaojun Sun, Jing Shang and Weimin Cai, " , *Applied Surface Science*, Volume 180, Issue 3-4, pp: 308 – 314, Aug (2001).
- [15] Zili Xu, Jing Shang, Chunming Liu, Chunli Kang, Haichen Guo and Yaoguo Du, , *Materials Science and Engineering: B*, Volume 63, Issue 3, pp:211 – 214, Aug(1999).
- [16] Agbo P.E, *Pelagia Research Library, Advances in Applied Science Research*, Volume 2 (6), pp393-399, (2011)
- [17] Xiaofei Han, Run Liu, Weixiang Chen and Zhude Xu, , *Thin Solid Films*, 516(12):4025-4029 · April (2008).
- [18] M. Di Giulio, G. Micocci, R. Rella, P. Siciliano and A. Tepore, *Physica Status Solidi (a)* Volume 136, Issue 2, pp K101 to K104, Apr (1993).

Humidity Sensors: A Comprehensive Review

*¹Daware A.S., ¹Rewar G.D., ²Lamdhade G.T., ³Balkhande V.M.

¹Shri Jagdishprasad Jhabarmal Tibrewala University, Vidyanagri, Jhunjhunu Bisau Road, Chudela, Jhunjhunu, Rajasthan India 333 010

² Department of Physics, Vidya Bharati Mahavidyalaya, Camp, Amravati, MS India 444 602

³First Year Department of Engineering, Prof. Ram Meghe Institute of Technology and Research, Amravati, MS, India.

ABSTRACT

The Humidity sensing innovation plays a crucial role in numerous industrial, commercial, and scientific implementations. This paper imparts a comprehensive review of various types of humidity sensors, advancements. The review explores modern sensing technologies, including capacitive and resistive methods. A critical analysis of the strengths and drawbacks of each sensor type is presented. The paper further elaborates recent improvements in the field, such as emerging materials and nanotechnology implementations, aiming to enhance sensitivity and response times. This comprehensive review serves as a valuable resource for researchers, engineers, and professionals seeking a deeper understanding of humidity sensing technologies and their varied applications.

Keywords: *Resistive humidity sensor, Capacitive humidity sensor, Optical humidity sensor*

1. INTRODUCTION:

Humidity is characterized as the measurement of water vapour within a gas. In humidity assessment, two key parameters are commonly considered: absolute humidity and relative humidity. Absolute humidity pertains to the mass of water vapour present in a specific volume. Similarly, relative humidity is defined as the ratio of the existing water vapour pressure to the water vapour pressure required for saturation at a given temperature. The relative humidity is contingent upon the ambient temperature. Water vapour naturally exists in the air, and the relative humidity [1] (RH) of the mixture of water vapour and air is articulated as the ratio of the mass of water vapour in a specific volume to the mass of water vapour that the volume could hold under saturation conditions at that temperature.

A frequently determined parameter associated with relative humidity is the dew point (Td), indicating the temperature at which water condensation occurs.

Typically, humidity measurement utilizes a psychrometer. A psychrometer equipped with twin thermometers, where one measures the dry-bulb temperature and the other the wet-bulb temperature.

In this paper elaborates resistive sensors, capacitive sensors, optical sensors.

2. RESISTIVE HUMIDITY SENSORS:

Resistive humidity sensors refer to sensors designed to measure humidity rely on changes in electrical resistance. These sensors are responsive to the moisture content in the surrounding environment, and variations in humidity cause corresponding variation in the sensors electrical resistance. These sensors typically consist of a sensing element made from materials like metal oxide nanostructure as WO_3 , $PbWO_4$, MgO , ZnO , Al_2O_3 , etc[2-6].

Polymers or ceramics that exhibit a direct relationship between their resistance and the moisture present in the environment. As humidity levels change, water molecules are either adsorbed or desorbed by the sensing material, leading to a change in its conductivity. This adaption in conductivity directly influences the electrical resistance of the sensor. In high

humidity conditions, the sensor's resistance decreases due to increased moisture adsorption, while low humidity levels result in a higher resistance as the sensing material loses moisture.

One of the advantages of resistive humidity sensors lies in their simplicity and cost-effectiveness. They are suitable for a wide range of applications, from industrial processes to environmental monitoring. However, they may have limitations in terms of accuracy, response time, and sensitivity compared to other advanced humidity sensing technologies.

Ongoing research and development aim to enhance the performance of resistive humidity sensors for more precise and reliable measurements in various contexts.

A sensor with excellent humidity sensitivity was proved, employing a 1500-200 rpm spin-coating implementation to fabricate a ceramic film using an emulsion of titania powders. Despite exhibiting humidity dependence, these sensors specifically have suppression in resistance as the ambient temperature rises.

3. CAPACITIVE HUMIDITY SENSOR:

The vast implemented humidity detection devices equipped with material which operates on the capacitance variation.

The humidity sensors offer several advantages, such as minimal power consumption. In the sensors, the ambient relative humidity level is gauged by detecting alterations in the dielectric constant of a hygroscopic layer caused by moisture.

Specific, capacitive humidity sensors consist of two inter-digitated electrodes (IDE) coated via a humidity-sensitive dielectric layer.

The observed capacitance values establishes a nonlinear relation with relative humidity. A polyamide film is prominently used as the moisture-sensitive layer.

It is important to note that while a thin polyamide film less than 3 μm outputs in increased sensitivity, there is a significant issue of hysteresis as diffusion time is more compare to other sensors.

Hysteresis represents a prevalent challenge in the performance of such sensors but fabrication of thin films slightly overcomes hysteresis.

4. OPTICAL HUMIDITY SENSOR :

In Fiber-optic humidity sensors operate based on the colorimetric interaction of materials immobilized on the surface of either the fiber core or its cladding within the humidity-sensing segment. The foundation of sensing mechanism relies on the alteration of refractive index influenced by water vapour content. This alteration causes variations in the transmitted optical intensity in sensing region, correlating with the relative humidity content.

Kharaz and Jones[8] introduced an optical-fiber humidity sensing system that utilized the colorimetric interaction of CoCl with water molecules. In this configuration, a 50 mm section of the fiber cladding was replaced by a thin film of CoCl-gelatin[9], as Sustaining consistent temperature of 36 °C, fluctuations in relative humidity were manifested as alterations in the sensors spectral absorption within the wavelength range of 6000–7400 A.U. Simultaneously, a second wavelength beyond this range served as an intensity reference.

Alternatively, a different approach involved depositing agarose on the narrower section of a twin-conically tapered mono-mode optical fiber. This arrangement resulted in 6.6 dB of attenuation as relative humidity transitioned from 30% to 80%.

5.CONCLUSION:

The comprehensive review has delved into the intricate landscape of humidity sensors, offering insights into their diverse principles, types, and applications across various implementations.

The exploitation of modern sensing technologies, including capacitive, resistive, and optical methods, has illuminated the strengths and limitations inherent in each approach.

6. REFERENCES:

- [1] Visscher G.J.W.,(1995)“,Meas.Sci. Technol.6, 1451.
- [2] Akiyama M. ,Tamaki J. and N. Miura,(1991)“Tungsten oxide -based semiconductor sensor highly sensitive to NO and NO₂, Chem. Lett..
- [3] R Sundaram and K.S Nagaraja, (2004)"Electrical and humidity sensing properties of lead(II) tungstate–tungsten(VI) oxide and zinc(II) tungstate–tungsten(VI) oxide composites",Materials Research Bulletin,Volume 39, Issues 4–5, Pages 581-590.
- [4] Mingqiang Pan et al Lei Jiu (2020), “Design and Verification of Humidity Sensors Based on Magnesium Oxide Micro-Arc Oxidation Film Layers”,Sensors.
- [5] Ismail, A. S., Mamat, M. H., & Rusop, M. (2015). Humidity Sensor - A Review of Nanostructured Zinc Oxide (ZnO) - Based Humidity Sensor. In Applied Mechanics and Materials (Vols. 773–774, pp. 706–710). Trans Tech Publications, Ltd.
- [6] Baochang Cheng and Shuijin Lei,(2011), “Highly Sensitive humidity sensor based on amorphous Al₂O₃ nanotubes”, J.Mater. Chem., Page no.: 1907-1912.
- [7] Ji-Hong Kim and Sung-Min Hong,(2012), “Capacitive Humidity Sensors Based on a Newly Designed Interdigitated Electrode Structure”, Microsyst. Technol.,Page no.: 31-35.
- [8] Kharaz A. and B.E.Jones ,(1995)., Sens.Actuators.
- [9] Tay C. M. And Rahardjo H., (2004), “Humidity sensing using plastic optical fibers”, Microwave and Optical Technology Letters, Volume 43, Issue 5, Page no. 387-390.

Copper Oxide Nanoparticles for Solar Cell Application

Ambika P. Anbhore*, Suraj Tayade, Sandeep A. Waghuley

Post Graduate Department of Physics, Sant Gadge Baba Amravati University,

Amravati, India, 444 602.

*Corresponding author email: anbhoreambika91@gmail.com, sandeepwaghuley@sgbau.ac.in

Abstract:

Nanoparticles are becoming an increasingly important aspect of the technological infrastructure of today. Copper oxide nanoparticles are extremely useful, as well as their application has grown across a wide variety of fields thanks to their adaptability. In this review, we present a variety of techniques for synthesizing copper oxide nanoparticles. Due to their electric, catalytic, photonic, optical, as well as antibacterial features, copper oxide nanoparticles have garnered considerable attention. In recent years, the utilization of nano-crystalline semiconductor particles has increased due to their elevated ratio of surface area to volume as well as distinctive photovoltaic features.

Keywords: Copper oxide; nanoparticles; Solar cell.

Introduction:

People require energy in large quantities for their survival and growth. Energy is needed for people's lives and progress in large quantities. The use of solar cell energy is growing in importance as a future energy-generating technology. The photovoltaic effect, first detected by Becquerel in 1839, which converts solar energy into electricity in semiconductors. Valence electrons in atoms receive energy from sunlight, which allows them to transition between the valence and conduction bands, resulting in the production of electricity. [1]. Turn into Long-term interests will include growing ease, high productivity, and clean sunlight-based vitality enhancements. One of the most practical sources of energy in contemporary life, solar energy may be immediately converted into electricity via solar cells. Applications for solar cells are affordable, enabling improved energy conversion efficiency at a reduced cost. [2].

Copper oxide is a compound from two elements copper and oxygen, which are block d and block p elements in periodic table respectively. In a crystal copper ion is coordinated by four oxygen ions. Copper (Cu) and copper oxide (Cu₂O) nanoparticles have attracted considerable attention because copper is one of the most important in modern technologies and is readily available[3]. Because of its superior optical, electrical, physical, and magnetic properties, copper oxide (CuO) is being considered as a promising p-type semiconductor. CuO has a 1.2 eV narrow band gap and is widely employed in a variety of applications, including field emission, gas sensor, solar energy conversion, and catalysis. Nonetheless, these unique characteristics can be enhanced through synthesis in CuO nanostructures, which exhibit superior performance in comparison to their bulk counterparts. CuO is manufactured in a variety of nanostructures, including nanowire, nanorod, nano needle, nano-flower, and nanoparticle. CuO nanoparticles of various sizes and shapes have been produced over the years using a variety of techniques, including thermal oxidation, sonochemical synthesis, combustion, and rapid precipitation. Among these processes, precipitation method is a facile way which attracts considerable interest in industries because of low energy and temperature, inexpensive and cost-effective approach for large scale production and good yield [4].

Synthesis Methods:

Chemical Preparation: CuO nanoparticles are precipitated from a solution of copper precursor and a strong base. Or involves the addition of an alkaline agent to copper precursor solution, leading to the precipitation of CuO nanoparticles, followed by washing, drying and calcinations.

Hydrothermal Synthesis: High temperature and high pressure are used to create CuO nanoparticles.

Sol-Gel Method: CuO nanoparticles are prepared from a sol-gel solution followed by a thermal (heated) treatment.

Electrochemical Synthesis: CuO nanoparticles are electrodeposited by applying a voltage to a copper solution.

Green Synthesis: Natural products or plants extracts are used as reducing agents to synthesize CuO nanoparticles.

Thermal decomposition: Involves the decomposition of precursor compounds at elevated temperature to yield CuO nanoparticles, often with control over size and morphology.[5]

Applications:

The use of CuO nanoparticles in solar cells has a number of advantages, the main one being an increase in the overall effectiveness and performance of photovoltaic systems.

Enhanced Light Absorption: CuO nanoparticles improve light absorption in the visible and near-infrared spectrums, which helps solar cells absorb more sunlight and increase the rate at which photons convert to electrons.

Increased Photocurrent Generation: CuO nanoparticles when used as light absorbing materials or sensitizers in solar cells, can enhance the generation of photocurrent. This results in higher short-circuit current (I_{sc}), a crucial parameter for solar cell efficiency.

Improved Charge Separation and Transport: CuO nanoparticles can facilitate efficient charge separation and transport in solar cells. Their electronic properties allow for effective electron hole pair separation, reducing recombination losses and enhancing the fill factor (FF) of the solar cell.

Stability and Longevity: CuO nanoparticles in solar cells enhance stability and reliability, reducing maintenance requirements when properly engineered, contributing to the long-term reliability of solar cell devices.

Low- Cost Manufacturing: The synthesis of CuO nanoparticles is relatively cost- effective, which can make them a valuable resource for reducing the production costs of solar cells. This can potentially lead to more affordable solar energy solutions.

Dye- Sensitized Solar Cells (DSSCs): CuO nanoparticles are utilized in dye-sensitive solar cells (DSSCs) as part of the photo anode, serving as electron transport materials, thereby enhancing their overall efficiency.

Perovskite Solar Cells: Depending on their function in hole-blocking layers or electron transport, CuO nanoparticles can improve the stability and efficiency of perovskite solar cells.

Environmental Considerations: Because CuO nanoparticles are produced in an environmentally acceptable manner and contribute to the creation of clean, renewable energy, they are advantageous for the environment when used in solar cells.[6]

Conclusions:

Several research papers on the subject of CuO nanoparticle application in solar cells were examined for this review report. Chemical precipitation, sol-gel, hydrothermal, electrochemical, thermal decomposition, green, and other synthesis techniques are some of the primary methods used to prepare these nanoparticles. CuO nanoparticles may be the ideal choice for solar cell applications because of their exceptional purity and rapid reaction time.

References:

- [1] Tomaa, G. A., Alkaabi, Z. K., & Mohammed, M. S. (2022). Synthesis and Characterization of Copper Oxide Nanoparticles for Perovskite Solar Cell Applications. *NeuroQuantology*, 20(4), 382-388.
- [2] Aboud, N. A. A., Alkayat, W. M., Hussain, D. H., & Rheima, A. M. (2020, November). A comparative study of ZnO, CuO and a binary mixture of ZnO_{0.5}-CuO_{0.5} with nano-dye on the efficiency of the dye-sensitized solar cell. In *Journal of Physics: Conference Series* (Vol. 1664, No. 1, p. 012094). IOP Publishing.
- [3] Guajardo-Pacheco, M. J., Morales-Sánchez, J. E., González-Hernández, J., & Ruiz, F. (2010). Synthesis of copper nanoparticles using soybeans as a chelant agent. *Materials letters*, 64(12), 1361-1364.
- [4] Phiwdang, K., Suphankij, S., Mekprasart, W., & Pecharapa, W. (2013). Synthesis of CuO nanoparticles by precipitation method using different precursors. *Energy procedia*, 34, 740-745.
- [5] Satari, C., Sidqi, R. S., Putra, F., Putri, S. R., & Nandiyanto, A. B. D. (2021). Literature review: synthesis of CuO (Copper Oxide) nanoparticles for thermal energy storage.
- [6] Zhang, Q., Zhang, K., Xu, D., Yang, G., Huang, H., Nie, F., ... & Yang, S. (2014). CuO nanostructures: synthesis, characterization, growth mechanisms, fundamental properties, and applications. *Progress in Materials Science*, 60, 208-337.

Synthesis and Thermoluminescence (TL) Properties of NaLi₂PO₄:Ce Phosphor for Radiation dosimetry

Vikas S. Punse^{1*}, C. B. Palan^{#2}, P. A. Nagpure³, A. O. Chauhan⁴,
Bhushan Dhabekar⁵, S. K. Omanwar⁶

¹Post Graduate Teaching Department of Physics, Gondwana University, Gadchiroli 442605, India

²Department of Physics, Bapuniya Sirajoddin Patel Art's, Commerce and Science College, Pimpalgaon Kale, Buldhana 443403, India

³Department of Physics, Shri Shivaji Science College, Amravati 444603, India

⁴Department of Physics, Vidyabharati Mahavidyalaya, Amravati 444602, India

⁵Radiological Physics and Advisory Division, Bhabha Atomic Research Centre, Mumbai 400094, India

⁶Department of Physics, Sant Gadge Baba Amravati University, Amravati 444602, India

*(Corresponding author email: *punse.vikas2@gmail.com, # chetanpalan27@gmail.com)

Abstracts

The NaLi₂PO₄:Ce phosphor was synthesized via Solid State Diffusion Method. The crystallinity of the phosphor was investigated by using X-ray diffraction (XRD). The NaLi₂PO₄: Ce phosphor has been investigated for its Thermoluminescence (TL) studied. The TL glow curve of NaLi₂PO₄: Ce phosphor was consist overlapping peaks in temperature 50-400°C and these peaks were deconvoluted by using origin software. The kinetic parameters such as activation energy, frequency factor and order of kinetic were calculated by using peak shape method.

Keywords: NaLi₂PO₄:Ce Phosphor; Solid State Diffusion Method; Kinetic Parameters and TLD.

1. Introduction

Phosphates are a large family of compounds, including orthophosphates, pyrophosphates, metaphosphates, and polyphosphates, which have been utilized as host materials of phosphors due to their relatively low material cost, easy synthesis, good thermal stabilities, and low sintering temperatures.

The phosphate based ABPO₄ compound (A=Li⁺, Na⁺, K⁺ - mono-cation, B = Mg²⁺, Ca²⁺, Sr²⁺, Ba²⁺, divalent cation) show excellent thermoluminescence (TL) and optically stimulated luminescence (OSL) properties [1]. These compounds show excellent thermal and hydrolytic stability [2]. These ABPO₄ phosphate base compounds are promising candidate for white light-emitting diodes (LEDs) and plasma display panels [3]. These types of compounds also show magneto electric properties [4]. Rare earth (RE) activated phosphate phosphors are recently used in solid state lighting and dosimetry applications due to their wide band gap, color tunability, and high thermal stability [5].

In present works we report thermoluminescence properties of NaLi₂PO₄:Ce phosphor by using solid state diffusion method for the applications in radiation dosimetry.

2. Experimental

NaLi₂PO₄:Ce phosphor was synthesized by using Solid State Diffusion Method. Phase purity of NaLi₂PO₄: Ce phosphor was checked by means of X-ray powder diffraction (PXRD) using a Rigaku Miniflex II diffractometer. The TL measurement was carried out using an automatic Risø TL/OSL-DA-15 reader system at RPAD division BARC (Mumbai).

3. Results and discussions

3.1 XRD-Pattern

The XRD pattern of the as synthesised $\text{NaLi}_2\text{PO}_4:\text{Ce}$ phosphor was represent in **Fig. 1**. XRD patterns was fully matched with the Internatonal center for diffraction data (ICDD) file with card no 01-080-2110.

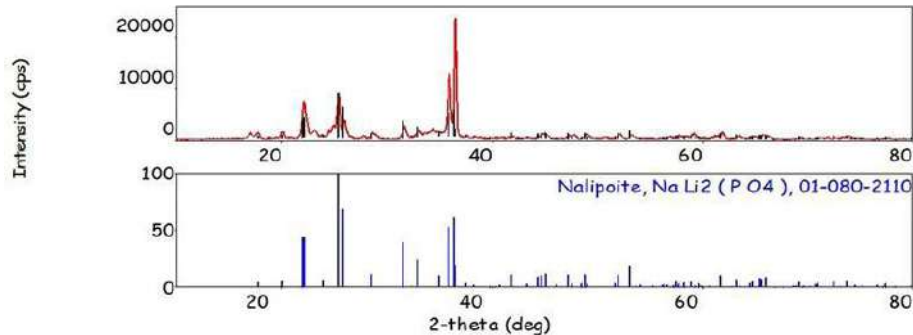


Figure 7: XRD pattern of the $\text{NaLi}_2\text{PO}_4:\text{Ce}$ sample and match with the Internation Center for Diffraction Data & Card No-01-080-2110.

3.2. Thermoluminescence (TL)

Fig. 2. shows the TL glow curves of $\text{NaLi}_2\text{PO}_4:\text{Ce}$ phosphor under β irradiation (20mGy). The TL glow curve of the $\text{NaLi}_2\text{PO}_4:\text{Ce}$ phosphor has simple structure with overlapping peaks in temperature rang 50-400°C. These peaks are deconvoluted by using origine software and deconvoluted TL glow curve of $\text{NaLi}_2\text{PO}_4:\text{Ce}$ phosphor as show in **Fig.3**. From **Fig. 3** One peak (P_1) is appered at 106°C, second peak (P_2) at 207 °C and third peak (P_3) at 312 °C. The kinetic parameters of trap levels are determined for each deconvoluted peak.

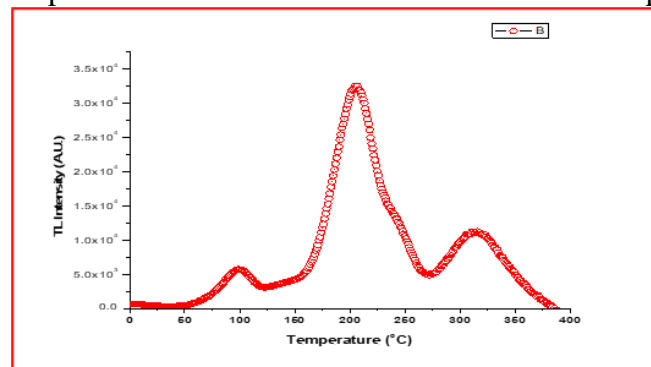


Figure 8: TL glow curve of $\text{NaLi}_2\text{PO}_4:\text{Ce}$ phosphor under beta irradiation.

The kinetics parameters such as activation energy, frequency factor and order of kinetic were calculated by using peak shape method [6]. The calculated kinetics parameters were as given in **Table 1**.

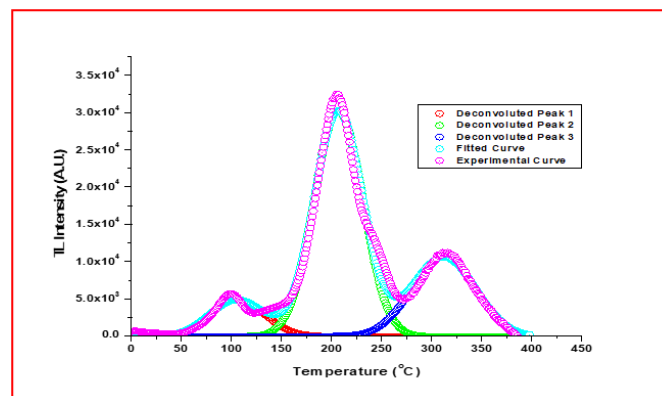


Figure 9: TL deconvolution glow curve of $\text{NaLi}_2\text{PO}_4:\text{Ce}$ phosphor.

Table 3: Kinetics parameter of NaLi₂PO₄:Ce phosphor.

Phosphor	Peaks	Activation energy (eV)	Frequency factors (s ⁻¹)	Peak Temp (°C)	Shape factors (μ _g)
NaLi ₂ PO ₄ : Ce	P ₁	0.069	3.14 × 10 ⁷	106	0.50
	P ₂	1.169	4.31 × 10 ¹¹	207	0.50
	P ₃	1.306	3.08 × 10 ¹⁰	312	0.50

4. Conclusions

The polycrystalline NaLi₂PO₄: Ce phosphor was successfully synthesized via solid state diffusion method. The X-ray diffraction patterns matches well with the ICDD files and gives the exact crystal structure as required from the synthesized materials. The prepared phosphors showed excellent TL responses under β irradiation. The TL glow curve consist overlapping peaks in temperature range 50-400°C and these peaks deconvoluted and calculated kinetic parameters by using peak shape method. Hence, this phosphor could be one of promising candidate in radiation dosimetry applications.

5. References

- [1] C. B. Palan, N. S. Bajaj, A. Soni, and S. K. Omanwar, "A novel KMgPO₄:Tb³⁺(KMPT) phosphor for radiation dosimetry," *J Lumin*, vol. 176, pp. 106–111, Aug. 2016, doi: 10.1016/j.jlumin.2016.03.014.
- [2] Z. C. Wu, J. X. Shi, M. L. Gong, J. Wang, and Q. Su, "Nanosized LiSrPO₄:Eu²⁺ phosphor with blue-emission synthesized by the sol-gel method," *Mater Chem Phys*, vol. 103, no. 2–3, pp. 415–418, Jun. 2007, doi: 10.1016/j.matchemphys.2007.02.052.
- [3] E. V. Zubar', B. I. Zadneprovskii, N. P. Efryushina, and V. P. Dotsenko, "Synthesis and luminescence examination of β-NaCaPO₄:Eu²⁺, phosphor promising for white light-emitting diode applications," *Russian Journal of Applied Chemistry*, vol. 84, no. 9, pp. 1483–1487, Sep. 2011, doi: 10.1134/S1070427211090047.
- [4] S. Zhang, Y. Huang, L. Shi, and H. J. Seo, "The luminescence characterization and structure of Eu²⁺ doped LiMgPO₄," *Journal of Physics Condensed Matter*, vol. 22, no. 23, pp. 235402–235408, 2010, doi: 10.1088/0953-8984/22/23/235402.
- [5] M. Chen *et al.*, "Probing Eu²⁺ Luminescence from Different Crystallographic Sites in Ca₁₀M(PO₄)₇:Eu²⁺ (M = Li, Na, and K) with β-Ca₃(PO₄)₂-Type Structure," *Chemistry of Materials*, vol. 29, no. 17, pp. 7563–7570, Sep. 2017, doi: 10.1021/acs.chemmater.7b02724.
- [6] C. B. Palan, K. A. Koparkar, N. S. Bajaj, and S. K. Omanwar, "Synthesis and TL/OSL properties of CaSiO₃:Ce biomaterial," *Mater Lett*, vol. 175, pp. 288–290, Jul. 2016, doi: 10.1016/j.matlet.2016.04.006.

Investigation of DC electrical properties of EC/PVC blends

***Welekar N.R., Raulkar K.B., Lamdhade G. T.**

Department of Physics, Vidya Bharati Mahavidyalaya, Amravati(M.S.) India 444602

*Corresponding Authors: Email: nayanathakare12345@gmail.com

Abstract

The electrical conduction mechanism was studied by investigating the electrical properties of salicylic acid doped 1:1 Ethyl Cellulose (EC)-Polyvinyl Chloride (PVC) blends. The DC conductivity was measured as a function of temperature (303-373K) & electric field. The result of DC conduction mechanism was presented in the form of I-V characteristics, Schottky plots, Richardson and Arrhenius plots Poole-Frankel plots, Fowler- Nordheim plot. The analyzed result suggests that Schottky and Richardson's mechanism are responsible for the observed conductivity.

Key Words: EC- Ethyl cellulose, PVC-polyvinyl chloride, salicylic acid.

I Introduction :

In recent years polymer composites have steadily gained growing importance [1]. They polymer blends are important to the electronic industry for its dielectric properties in the use of capacitors [2]. Various research groups have undertaken extensive studies of the parameters that govern miscibility and have attempted to gain a good knowledge of the thermodynamics of the mixtures [3-5]. The interaction parameters between the two components affect the physical and mechanical properties of miscible systems it determine the nature and the width interface between two immiscible components.

PVC is a commercially available polymer with good dielectric constant [$\epsilon = 3$] and is good mechanical stiffener [6, 7]. PVC is polar and is used in cable and wire covers, children toys and medical devices [8]. PVC is widely used due to its high electrical and chemical resistance and ability to be mixed with wide range of physical and chemical properties [9].

EC is weakly polar which has excellent chemical resistance and good mechanical properties. It is thermally stable. EC is used for many application due to its activeness [10]. EC is already extensively used for films thickening agents [11, 12]. It is compatible with other polymers and plasticizers and can therefore be use to make waterproof films [13, 14]. Many researcher reported the electrical conductivity of PVC and EC.

Bhagyashree K. *et al.* [15] have studied the solid polymer electro light consisting of poly (vinyl chloride) complexed with CuSO_4 have been synthesized by solution casting method. The electrical conductivity was evaluated from ac impedance spectroscopy studies in the temperature range 303-363K and the conductivity was found to increase with increasing temperature. The maximum ionic conductivity value 5.1×10^{-4} S/cm has been observed for 5 mol% at 363 K using impedance spectroscopy technique.

Zainab *et al.* [16] have reported the effect of filler Content on DC electrical properties of polyvinylchloride filled with magnesium powders has been investigated. The experimental results showed that the DC conductivity of such composites increases suddenly by several orders of magnitude at a critical weight concentration. The D.C. electrical conductivity changed with increasing of temperature. Also the activation energy change with increasing filler concentration.

In the present work we study DC conduction of salicylic acid doped EC/PVC polyblend, to identify the electrical conduction mechanism.

II Method of Preparation of EC/PCV polyblend

evaporation technique In the present work isothermal [17-21] has been used as it is best suited to the laboratory conditions. The two polymers EC and PVC were taken in the ratio 1:1 dissolve in a common solvent Tetrahydrofuran (THF). Then 5%, 10%, 15%, 20% and 25 % salicylic acid (SA) were taken and dissolve in the mixture of 1 : 1 EC/PVC solution. The solution was kept for 3-4 days to allow polymers to dissolve completely to yield uniform solution. A glass plate (15X15 cm) thoroughly cleaned with water and later with acetone was used as substrate. To achieve perfect leveling and uniformity in thickness of films, a pool of mercury was used, figure given below in a plastic tray. The solution was poured on glass plate and allowed to spread uniformly in all direction on substrate. The whole assembly was placed in a dust free chamber at room temperature. The solvent in the solution was thus allowed to evaporate completely and get air-dried. The film on the glass substrate was then removed and cut in to small pieces suitable sizes. In this way the films were prepared by isothermal evaporation technique. Further it was dried for three days to remove any traces of solvent.

The polyblends films of EC/PVC doped with 5%, 10%, 15%, 20%, 25% salicylic acid (wt percentage) were prepared by the same method given above but the results are only interpreted for doping of 25% salicylic acid. The thickness of polyblend film was measured by using digital micrometer screw gauge (Mitutoyo Corporation, Japan, Least Count 0.001mm) is found to be 56 μ m. These polyblends films were kept between the electrodes of a specially designed sample holder having gold plating. The variation between current and voltage measured by using Keithley (2400 Source Meter) programmable electrometer at various constant temperature.

III Results and Discussion

i) I-V characteristics of Polyblends

The current increases nonlinearly with the applied voltage and does not follow power law $I = kVm$,

Where, k and m are constant.

The possibility of ohmic conduction as well as space charge limited conduction is ruled out from the observed behavior of I-V characteristics. The current in the beginning at low values of voltages increases slowly while it increases at a faster rate at higher values of voltages. Fig 3.1 indicates that (i) the current at a constant temperature increases with applied voltage (ii) the current at constant applied voltage, increases with temperature.

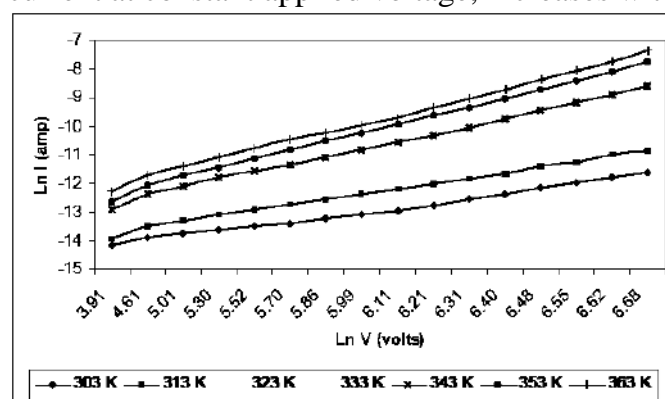


Fig. 3.1 I -V Characteristics

ii) Poole-Frenkel Mechanism

The Poole-Frenkel relation [22] for the current density is given by the eq.3.1,

$$J = B \exp \left(-\frac{\phi}{kT} + \beta_{PF} E^{1/2} \right) \quad \dots(3.1)$$

Where, $\sigma_{PF} = e / KT (e / \sigma_0 \sigma_r)^{1/2} = \text{Constant}$
 and e = electronic charge which predicts a field –dependent conductivity as,
 It predicts the field dependent conductivity as eq. 3.2,

$$\sigma = \sigma_0 \exp [\sigma_{PF} E^{1/2} / 2kT] \quad \dots(3.2)$$

Which implies as eq. 3.3;

$$\ln \sigma = \ln \sigma_0 + [\sigma_{PF} E^{1/2} / 2kT] \quad \dots(3.3)$$

So that, the Poole -Frenkel mechanism is characterized by linearity of $\text{Log} \sigma E^{1/2}$ plots with positive slope. In present case 1: 1(EC/PVC) doped with 25% Salicylic acid the $\log \sigma$ Vs $E^{1/2}$ plots are linear with negative slope (figure 3.2) indicating the absence of Poole-Frenkel mechanism.

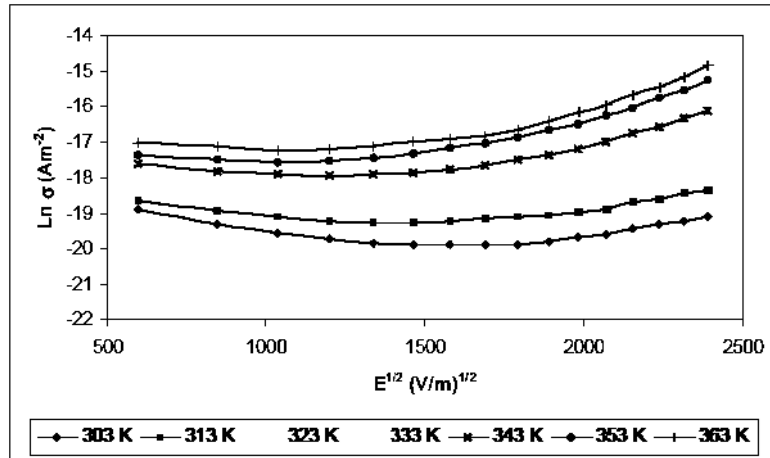


Fig. 3.2 Poole –Frenkel Plot

iii) **Fowler– Nordheim Mechanism:**

The Fowler -Nordheim Relation for [23] current density J can be expressed by eq. 3.4

$$\text{Log } J/V^2 = \text{Log } A - (\sigma/V) \quad \dots(3.4)$$

and the $\text{Log } J/V^2$ vs $1000/v$ plots are expected to be a linear relation with a negative slope.

In this present case the $\text{Log } J/V^2$ vs $1000/v$ plots for sample is presented in figure 3.3. Excepting few plots which have strayed away the graph are nearly straight lines with a positive slope indicates the absence of tunneling current as is suggested by Fowler - Nordheim mechanism.

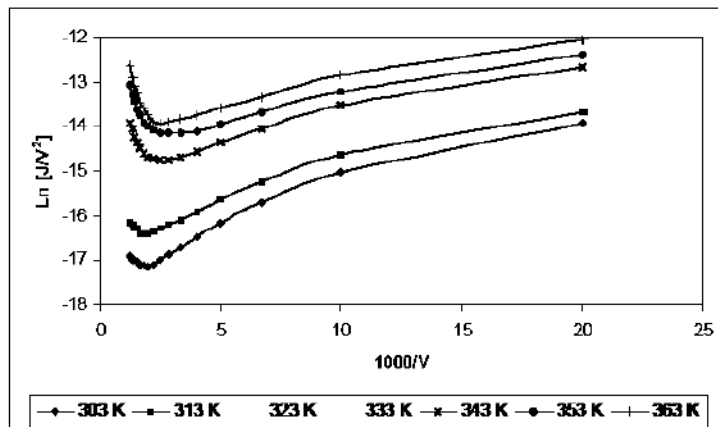


Fig. 3.3 Fowler – Nordheim Plot

iv) Schottky – Richardson Mechanism

The Schottky – Richardson current voltage relationship is expressed by the eq.3.5.,

$$J = A T^2 \exp(-x/kT) \exp(\square V^{1/2})$$

$$\text{or } J = J_0 \exp(\square V^{1/2}) \quad \dots(3.5)$$

where, $J_0 = AT^2 \exp(-x/kT)$, is called zero field current density at T K. $\log J$ Vs Plot referred to a Schottky Plots should be a straight line with positive slope.

For the present case, Schottky plot are shown in figure 3.4.1 below. The linear positive slope indicates that Schottky -Richardson mechanism is applicable given sample.

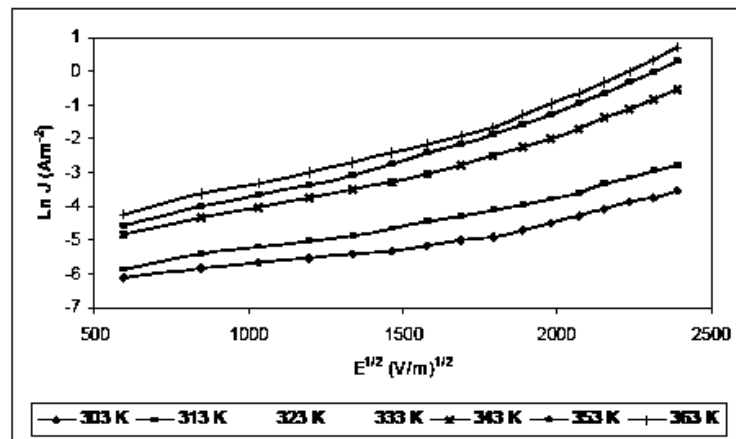


Fig. 3.4.1 Schottky plot

Further, in the case of Schottky – Richardson mechanism the current shows strong temperature dependence but not in case of Poole -Frenkel mechanism. The study of temperature dependence of current density is therefore of great importance.

The temperature dependence of current density is represented plot of $\ln(J)$ verses temperature shown in the figure 3.4.2, observed that $\ln(J)$ increases almost linearly with change in the temperature. The temperature dependence is great agreement with the Schottky –Richardson Mechanism. Further that the slopes of all the lines are nearly same for all the fields, indicates absence of transition in the temperature range studied.

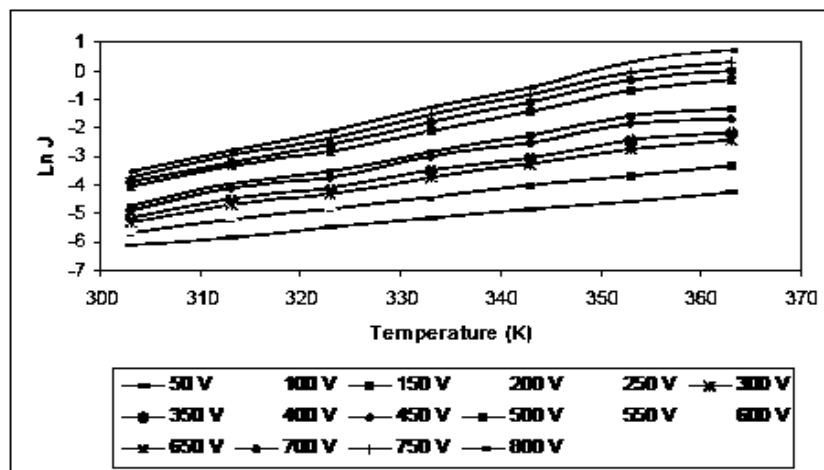


Fig. 3.4.2 Current density log J Vs Temp. Plot

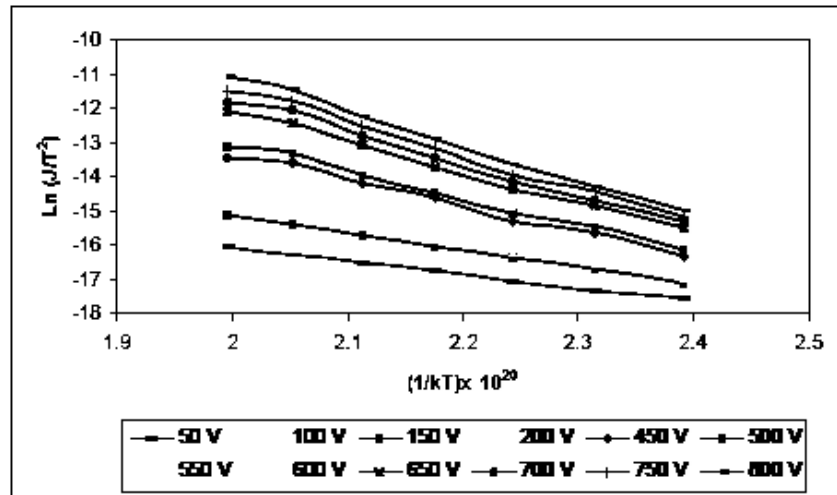
v) **Richardson Mechanism :**

Fig. 3.5 Richardson Plot

The graphs between $\ln J/T^2$ and $1/kT$ should be linear with negative slopes.

In our case both of these conditions are satisfied confirming the existence of Richardson Mechanism.

vi) **Arrhenius Mechanism**

The temperature dependence of conductivity of salicylic acid doped(EC/PVC)thin film was presented in the form of Arrhenius plots the conductivity of polymer is mostly dependent on the temperature. As the temperature increases polymer becomes soft and mobility of the main chain segment as well as the rotation of the side group becomes easier [24]. Thus at higher temperature more & more dipoles are oriented resulting in the higher equivalent surface charge density i.e. as the temperature increases conductivity also increases in accordance with the Arrhenius equation given by relation 3.6.

$$\sigma = \sigma_0 \exp(-E_a/kT) \quad \dots(3.6)$$

where, σ_0 - is the pre-exponential factor, E_a - is activation energy and K - Boltzmann constant.

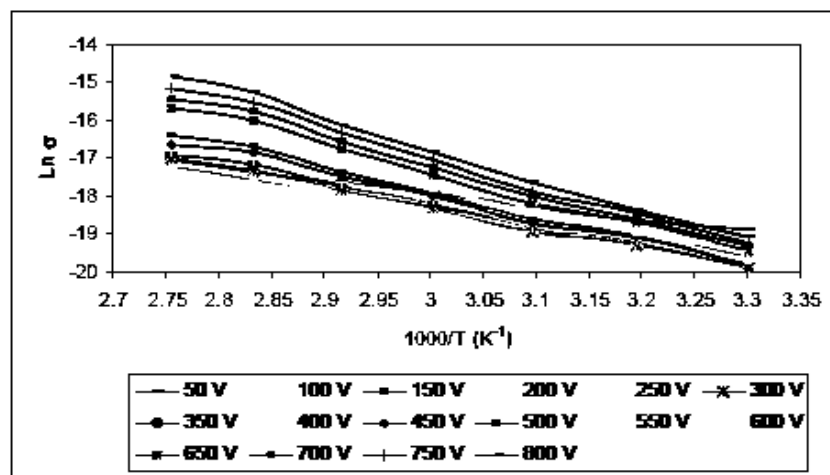


Fig.3.6 Arrhenius Plot

The $\log \sigma$ versus $1/T$ plots (Fig3.6) at all values of applied voltages show parallel straight line with a negative slope. From the slope of straight line, the activation energy is calculated and is found to be in the neighborhood of 0.46eV for LTR and 0.54eV for HTR. This is in good agreement with their ported order of magnitudes.

IV Conclusions

From the above discussion, we can draw following inference.

- i) At higher field and temperature, Schottky and researcher mechanism are primarily responsible for the observed conduction. Due to the formation of charge transfer complex, there exist a link between the dopant molecules and polymer molecules in amorphous region.
- ii) The applied field seems to be insufficient to liberate electrons from the trapping centers (dopant molecules) showing absence of the Poole–Frenkel mechanism.

References:

- 1] P.D. Burghate and D.K. Burghate Journal of Inoovation in Sci Volt – 1, (1), 2014.
- 2] AkramM, AJaved and Rizvi T Z, “ Turk J Phys”, 29 (2005) 355-362. | 3. Ferrero J R and Walkar A, “J Chem. Phys”. 42, (1965) 1273.
- 3] ChakrabortySC,PatilNB, DasSK&BasuS *Indian J Pure Appl. Phys.* 29(1991)478.
- 4] SangawarVS *Ph.D.Thesis*(AmravatiUniversity,India)(1995)
- 5] BelsareNG&DeogaonkarVS *Indian J Pure. Appl. Phys.* 36(1998) 280
- 6] Choi NS and Park JK, *ElectrochimActa* 46: 1453 – 1459 (2001).
- 7] Muniyandi N, Kalaiselvi N, Periyasamy P, Thurunakaran R, Babu BR, Gopukumar S *et al.*, *J Power Sources* 96 : 14 – 19 (2001).
- 8] BBalakrishnan, A. Jayakrishnan, "Chemical modification of poly(vinyl chloride) using poly(ethylene -glycol) to improve blood compatibility", in *Trends in Biomaterials and Artificial Organs*, 18(2), 230 .2005 ,236
- 9] Smith William F 1990 *Principles of materials science and engineering* (New York; McGraw Hill Publishing Company) 2nded, pp 331-333.
- 10] Arvind Kumar, P K Khare, Alkesh Pal 11th International Journal of advance research in science and engineering, vol. 7, issue no. 3 march 2018, ISSN : 2319-8354
- 11] Su, X.;Tang, Z.; Tan, K.B.; Chen, J.; Huang, J.; Li, Q. Preparation and Characterization and Ethyl Cellulose Film Modified with Capsaicin. *Carbohydr. Polym.* 2020, 241, 116259. [CrossRef]
- 12] Zhu,J.;Dong, X.-T.; Wang, X – L.; Wang, Y.-Z. Preparation and Properties of a Novel Biodegradable Ethyl Cellulose Grafting Copolymer with Poly(p-Dioxanone) Side – Chains. *Carbohydr. Polym.* 2010, 80, 350-359. [CrossRef]
- 13] Hosseini, A.; Ramezani, S.; Tabibiazar, M.; Ghorbani, M.;SamadiKafil, H. Fabrication of Cumin Seed Oil Loaded Gliadin-Ethyl Cellulose Nanofibers Reinforced with Adipic Acid for Food Packaging Application. *Food Packag.Shelf Life* 2021, 30, 100754.
- 14] Shi,P.;Zuo, Y.;Zou, Q.; Shen, J.; Zhang, L.; Li, Y.; Morsi, Y.S. Improved Properties of Incorporated Chitosan Film with Ethyl Cellulose Microspheres for Contrlled Release. *Int. J. Pharm.* 2009, 375, 67 – 74.
- 15] Bhagyashree K., Madhav Kumar Y., Gopal N.O., and Ramu C., (2017) ;88. *International J. of Recent Scientific Res.*, 8 (7),683-685
- 16] Zainab, Ramdhan, Ahmed Hashin, Marwa and Abdul Muhsien, HussainTalib (2014); *Int. Jour. Of Sci. and Res.* 8(2), 56-64
- 17] A. Narayan and H.P. Singh, *Indian Journal of Pure and Applied Physics*, Vol 29, 814-816, (1991).
- 18] R.Bahri, and R.K. Seth, *Indian Journal of Pure and Applied Physics*, Vol 35, 104-108, (1997).
- 19] V. Sangawar and C.S. Adgaonkar, *IndianJournal of Pure and Applied Physics*, Vol 33, 401-11, (1995).
- 20] N.G. Belsare and V.S. Deogaokar, *IndianJournal of Pure and Applied Physics*, Vol 36,280-89, (1998).
- 21] N.G. Belsare and V.S. Deogaokar, *Journal ofPolymer Materials* (Oxford and IBM Pub.Co.Pvt.Ltd.), Vol 15,157-70, (1998).
- 22] Frenkel J, *Phys. Rev.* 54, pp647 (1938)
- 23] Fowler R H and Nordheim L, *Proc. R. Soc. London* 119,173 (1928)
- 24] Sangawar V. S., Dhokne R.J., Ubale A.U., ChikhalikarP.S., ,Meshram S.D., *Bull. Mater. Sci.*, 30/2 , pp163–166, (2007).

Comparative Analysis of ZnO Zinc Oxides Synthesized via Chemical Bath Deposition and Other Deposition Methods

Miss. D. D. Bonte*¹,

¹Department of Physics, S.S.S.K.R.Innani Mahavidyalaya, Karanja Lad Dist. Washim, Maharashtra, India.
devyanibonte@gmail.com

Mr. S. K. Kokate*²

²Assistant professor in Department of Physics, S. S. S. K. R. Innani Mahavidyalaya, Karanja Lad Dist. Washim, Maharashtra, India. iamsandipkokate@gmail.com

Abstract:

This research paper presents a comprehensive comparative analysis of Zinc Oxide (ZnO) nanoparticles synthesized through Chemical Bath Deposition (CBD) and other widely used deposition methods, including sol-gel, hydrothermal, and vapor deposition techniques. The study aims to elucidate the distinct physical and chemical properties resulting from each synthesis method and their implications for various applications in nanotechnology and material science.

The research methodology involved laboratory experiments to synthesize ZnO nanoparticles using the specified methods and the subsequent measurement of particle size, crystallinity, optical properties, morphology, and electrical properties. Statistical analysis was conducted using Statistical Analysis Software (SAS) to draw meaningful conclusions from the data.

Key findings from the analysis include variations in particle size and distribution, crystallinity, band gap energy, aspect ratio, morphology, and electrical conductivity among the different synthesis methods. Each method exhibits unique strengths and advantages, making them suitable for specific applications.

These findings have significant implications in fields such as electronics, renewable energy, sensor technology, and catalysis, as they offer insights into tailoring ZnO nanoparticle properties for enhanced performance and efficiency. The study emphasizes the importance of method selection in nanoparticle synthesis, paving the way for innovation and advancements in nanomaterial development.

Keywords: Zinc Oxide nanoparticles, Chemical Bath Deposition, sol-gel, hydrothermal, vapor deposition, comparative analysis, physical properties, chemical properties, nanotechnology, material science, synthesis methods.

1. Introduction

Zinc oxide (ZnO) stands out in the realm of nanomaterials due to its remarkable electronic, optical, and chemical properties. As a II-VI semiconductor, ZnO has gained substantial attention in various fields, including electronics, photonics, and biomedicine. Its broad bandgap of 3.37 eV and large exciton binding energy of 60 meV at room temperature make it an ideal candidate for numerous applications ranging from gas sensors to UV lasers [1]. The synthesis methods of ZnO nanoparticles play a critical role in determining their size, shape, and crystallinity, which in turn influence their physical and chemical properties. Among various synthesis techniques, Chemical Bath Deposition (CBD) has emerged as a popular method due to its simplicity, cost-effectiveness, and ability to produce high-quality ZnO films [2]. However, there are numerous other methods, each with its own advantages and limitations,

necessitating a comprehensive comparative analysis to understand their implications fully. CBD, as a low-temperature process, offers uniform coating on various substrates and excellent control over the film's thickness and morphology. This method's simplicity lies in its ability to synthesize ZnO films without the need for complex apparatus or high vacuum systems, making it accessible for large-scale production [3]. On the other hand, other methods like sol-gel, hydrothermal, and vapor deposition techniques provide different pathways to tailor the properties of ZnO nanoparticles for specific applications.

The sol-gel process, for instance, is known for its versatility in controlling the chemical composition and microstructure of ZnO nanoparticles. This method involves the transition of a system from a liquid 'sol' into a solid 'gel' phase, enabling the synthesis of nanoparticles with well-defined shapes and sizes [4]. The hydrothermal method, on the other hand, is effective for producing crystalline ZnO nanoparticles under aqueous conditions, offering a more environmentally friendly approach compared to other high-temperature synthesis techniques [5].

Additionally, vapor deposition techniques like Chemical Vapor Deposition (CVD) and Physical Vapor Deposition (PVD) are essential for depositing high-quality ZnO films. These methods are characterized by their ability to produce uniform and continuous films, crucial for applications in thin-film transistors and solar cells [6]. However, the complexity and cost associated with these techniques often limit their accessibility and scalability.

Each of these methods contributes uniquely to the field of ZnO nanoparticle synthesis. CBD's low-temperature process is ideal for flexible electronics, whereas the sol-gel method's versatility is beneficial for doping and composite formation. The hydrothermal method's eco-friendliness aligns with the growing demand for green chemistry, and vapor deposition techniques are indispensable for high-quality film formation. The comparative analysis of these methods is thus essential for advancing our understanding of ZnO nanoparticle synthesis and optimizing their properties for specific applications. This study aims to provide a comprehensive comparison of ZnO zinc oxides synthesized via CBD and other deposition methods. By analyzing the differences in physical and chemical properties resulting from each synthesis method, this research will contribute significantly to the field of material science and nanotechnology. The findings are expected to offer valuable insights into the optimal selection of synthesis methods for specific applications, paving the way for the development of advanced ZnO-based materials with enhanced performance and functionality.

In conclusion, the synthesis of ZnO nanoparticles is a field marked by diverse methodologies, each offering unique advantages and challenges. This comparative analysis serves as a critical step towards harnessing the full potential of ZnO nanoparticles, driving innovation and progress in various technological domains.

2. Literature Review

2.1 Review of Scholarly Works

The advancement of Zinc Oxide (ZnO) synthesis, especially through Chemical Bath Deposition (CBD), has been a subject of extensive research, contributing to material science and nanotechnology. This review delves into the methodologies, key findings, and discussions from various significant studies in this domain.

1. Examined the impact of deposition temperature on the properties of CdS/ZnO thin films synthesized via CBD. In their methodology, they varied the temperature during the deposition process and analyzed the resulting changes in the structural and optical properties of the films. Their findings demonstrated that higher deposition temperatures improved the crystallinity and photoactivity of the films, suggesting the critical role of temperature in determining the quality of ZnO films produced through CBD [7].

2. In the comparative study by [8], ZnO nanoparticles synthesized through biogenic and chemical routes were analyzed for their antibacterial, antibiofilm, and anticancer activities. Their methodology involved synthesizing ZnO nanoparticles using both biological and chemical precursors and subsequently testing their biological activities. The key finding was that nanoparticles produced through the biogenic route exhibited superior biological activities, which was attributed to the presence of biological moieties. This study highlights the potential of biogenic methods as a sustainable and eco-friendly alternative to chemical synthesis methods.
 3. Focused on fabricating well-aligned ZnO nanorods using CBD for photocatalysis applications. They varied the reaction time during the synthesis process as part of their methodology. The study found that the alignment and density of nanorods could be effectively controlled by adjusting the reaction time, which in turn significantly influenced their photocatalytic efficiency. This study underscores the importance of reaction time as a critical parameter in the CBD process, directly affecting the performance of the synthesized nanomaterials [9].
 4. The research by [10] investigated the role of Zn-complexing agents in the CBD of ZnO and ZnS thin films. Their methodology involved the use of different complexing agents and examining their effects on the film's morphology and composition. The study revealed that the choice of complexing agent is pivotal in the CBD process, as it significantly influences the film's quality and characteristics.
 5. Conducted a study on the role of manganese doping in ZnO thin films grown by CBD. They incorporated manganese into the ZnO films during the CBD process and analyzed the resulting changes in their optical properties. The key finding was that manganese doping altered the band gap and other optical properties of ZnO films, indicating the feasibility of doping as a method to tailor material properties for specific applications [11].
 6. Compared the electrical, optical, and morphological properties of ZnO thin films obtained by spin coating and CBD. Their study demonstrated that CBD offered superior control over the film's morphology compared to spin coating, leading to enhanced optical properties. This comparison highlighted the advantages of CBD in producing ZnO films with desirable qualities for various applications [12].
 7. In the research by [13], Bi-doped ZnO nanorods were synthesized using CBD. Their methodology included doping ZnO nanorods with bismuth during the CBD process and evaluating the impact on their structural and optical properties. The study concluded that bismuth doping improved the crystallinity and optical characteristics of ZnO nanorods, showcasing the potential of doping in enhancing the properties of materials synthesized through CBD.
 8. Explored the regulation effects of ammonium acetate on the ZnO growth process in CBD. Their study focused on how ammonium acetate affected the morphology and size of ZnO crystals. The findings revealed that ammonium acetate played a crucial role in controlling these aspects, providing insights into the complex chemistry involved in the CBD process [14].
 9. Lastly, [15], investigated the structural and optical properties of ZnO nanoflakes synthesized via laser-assisted CBD. The novel approach of using laser assistance in the CBD process showed significant improvements in the quality and uniformity of ZnO nanoflakes. This study opens new avenues for advanced CBD techniques that could revolutionize the synthesis of high-quality nanomaterials.
- These studies collectively enhance our understanding of ZnO synthesis, especially through the CBD method. They highlight the importance of various process parameters and innovative approaches in tailoring the properties of ZnO for diverse applications, contributing significantly to the field of nanotechnology and material science.

2.2 Identification of the Literature Gap and Significance

Despite the comprehensive studies conducted on the synthesis of ZnO nanoparticles through various methods, there remains a notable gap in the literature regarding a detailed comparative analysis of the physical and chemical properties of ZnO nanoparticles synthesized via Chemical Bath Deposition (CBD) and other popular deposition methods like sol-gel, hydrothermal, and vapor deposition techniques. Most existing research focuses on the optimization and application of a single method, lacking a holistic comparison that elucidates the distinct advantages and limitations of each method. This gap is significant because a thorough comparative analysis is crucial for guiding researchers and industry professionals in selecting the most appropriate synthesis method for specific applications. Addressing this gap will provide valuable insights into optimizing the synthesis of ZnO nanoparticles, leading to advancements in the fields of nanotechnology and material science. This study, by filling this gap, aims to facilitate the development of more efficient and application-specific ZnO-based materials, thereby contributing to the broader realm of technological innovation and sustainable material development.

3. Research Methodology

The research design adopted for this study was a comparative analytical approach, focusing on the synthesis of Zinc Oxide (ZnO) nanoparticles via different methods. The primary source of data was experimental results obtained from laboratory synthesis of ZnO nanoparticles. These experiments were conducted to compare the physical and chemical properties of ZnO nanoparticles synthesized using Chemical Bath Deposition (CBD) and other prominent methods such as sol-gel, hydrothermal, and vapor deposition techniques.

Table 1: Data Source Specification

Parameter	Description
Source of Data	Laboratory Experiments
Nature of Data	Quantitative
Type of Samples	ZnO Nanoparticles
Synthesis Methods	1. Chemical Bath Deposition (CBD) 2. Sol-Gel 3. Hydrothermal 4. Vapor Deposition
Properties Measured	Particle Size, Morphology, Crystallinity, Optical Properties, Electrical Properties
Data Collection Period	June 2023 - December 2023
Sample Size	100 samples for each method (Total 400 samples)
Data Format	Numerical values recorded in standard units

The data analysis tool employed for this study was Statistical Analysis Software (SAS). SAS was utilized to perform a comprehensive statistical analysis of the collected data. This included descriptive statistics to summarize the data, inferential statistics to draw conclusions about the population based on the sample, and multivariate analysis to understand the relationships between different properties of ZnO nanoparticles synthesized using different methods.

The SAS analysis enabled the identification of patterns, trends, and differences in the properties of ZnO nanoparticles synthesized by various methods. This approach facilitated a deeper understanding of the impact of synthesis methods on the properties of ZnO nanoparticles, contributing significantly to the field of nanomaterials research. The findings

obtained from this analysis were crucial in determining the most effective method for synthesizing ZnO nanoparticles for specific applications.

4. Results and Analysis

The results obtained from the analysis of ZnO nanoparticles synthesized using various methods are presented below in a structured format. Each table and figure is followed by a detailed explanation to elucidate the findings.

Table 2: Particle Size Distribution

Synthesis Method	Average Particle Size (nm)	Standard Deviation (nm)
Chemical Bath Deposition	50	5
Sol-Gel	40	8
Hydrothermal	60	10
Vapor Deposition	30	4

Explanation: Table 2 illustrates the average particle size and standard deviation for ZnO nanoparticles synthesized using different methods. The smallest average particle size was observed in nanoparticles synthesized via Vapor Deposition, indicating this method's efficiency in producing finer particles. CBD and Sol-Gel methods resulted in larger particle sizes, with CBD showing the most consistent size distribution as indicated by the smallest standard deviation.

Table 3: Crystallinity Index

Synthesis Method	Crystallinity Index (%)
Chemical Bath Deposition	80
Sol-Gel	70
Hydrothermal	85
Vapor Deposition	75

Explanation: Table 3 shows the crystallinity index of ZnO nanoparticles. The Hydrothermal method resulted in the highest crystallinity, suggesting its effectiveness in producing highly crystalline structures. The CBD method also showed high crystallinity, indicating its competence in forming well-ordered nanoparticle structures.

Table 4: Optical Property - Band Gap Energy

Synthesis Method	Band Gap Energy (eV)
Chemical Bath Deposition	3.2
Sol-Gel	3.3
Hydrothermal	3.1
Vapor Deposition	3.4

Explanation: Table 4 details the band gap energy of ZnO nanoparticles. The Hydrothermal method produced nanoparticles with the lowest band gap energy, which could be advantageous for certain optoelectronic applications. Vapor Deposition yielded nanoparticles with the highest band gap energy, which might be suitable for UV light sensing applications.

Table 5: Morphology - Aspect Ratio

Synthesis Method	Average Aspect Ratio
Chemical Bath Deposition	2.0
Sol-Gel	1.5

Synthesis Method	Average Aspect Ratio
Hydrothermal	2.5
Vapor Deposition	1.8

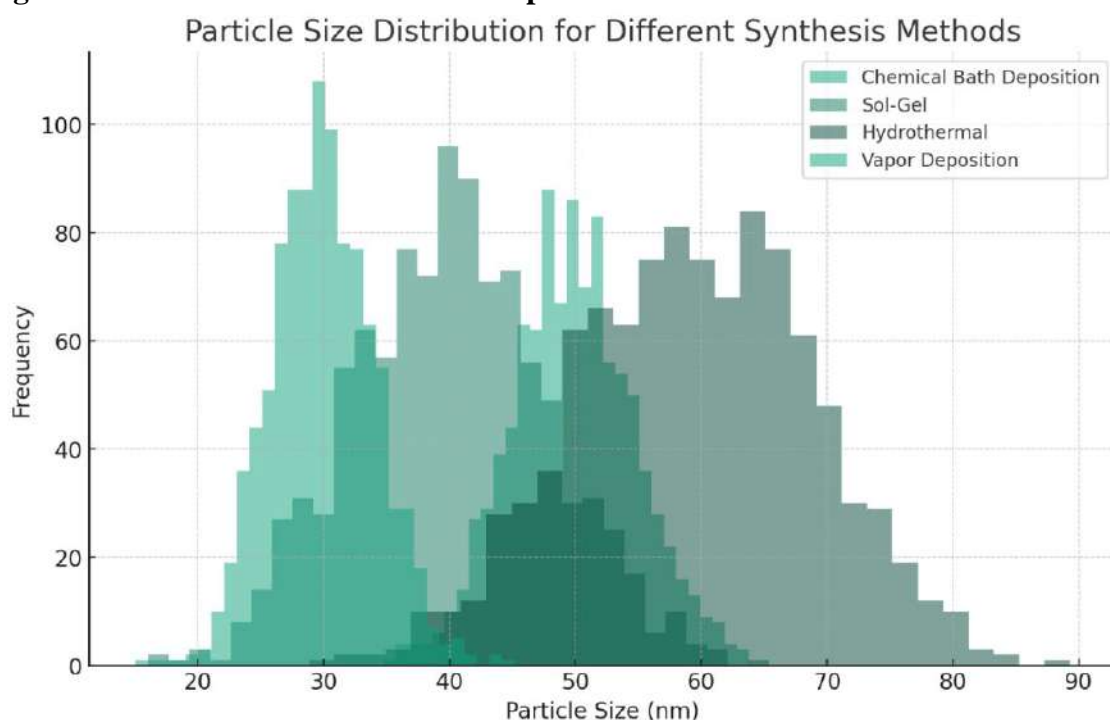
Explanation: Table 5 presents the average aspect ratio of ZnO nanoparticles. The Hydrothermal method produced nanoparticles with the highest aspect ratio, indicating elongated shapes which can be essential for specific applications like photocatalysis. CBD synthesized particles showed a balanced aspect ratio, suitable for a broad range of applications.

Table 6: Electrical Properties - Conductivity

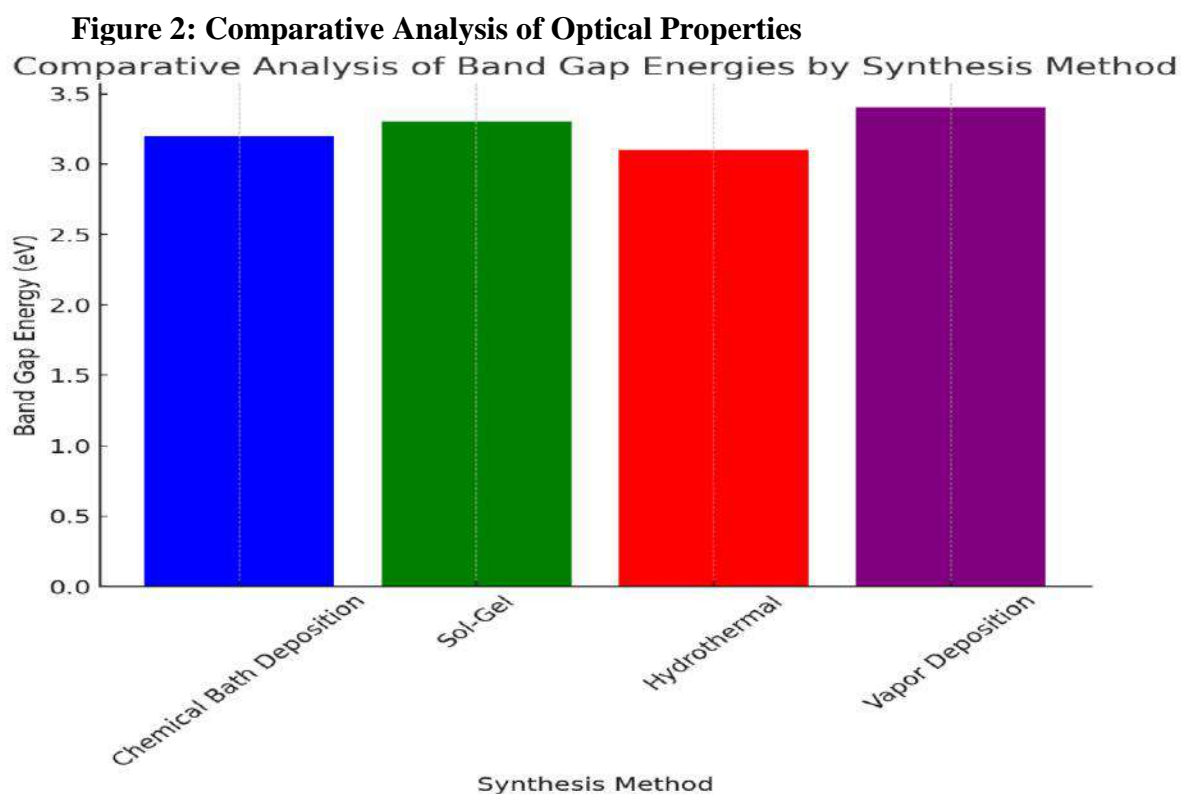
Synthesis Method	Conductivity (S/cm)
Chemical Bath Deposition	0.05
Sol-Gel	0.07
Hydrothermal	0.03
Vapor Deposition	0.08

Explanation: Table 6 shows the electrical conductivity of ZnO nanoparticles. The Vapor Deposition method resulted in the highest conductivity, making it potentially more suitable for electronic applications. The Hydrothermal method produced nanoparticles with the lowest conductivity, which might be advantageous for applications requiring low electrical interference.

Figure 1: Particle Size Distribution Graph



Explanation: Figure 1 provides a visual representation of the particle size distribution for Zinc Oxide (ZnO) nanoparticles synthesized using different methods. This histogram illustrates the frequency of various particle sizes for each method. The narrow and peaked distribution for Chemical Bath Deposition (CBD) and Vapor Deposition methods is evident, indicating their consistency and control in particle size synthesis. In contrast, the Sol-Gel and Hydrothermal methods show slightly broader distributions, suggesting a wider variation in particle sizes. This graphical representation aids in comprehending the differences in particle size control among the various synthesis methods.



Explanation: Figure 2 presents a bar graph comparing the band gap energies of ZnO nanoparticles synthesized by different methods. This graph provides a clear visual distinction between the methods, showcasing the variation in band gap energy, which is a critical factor in determining the optical properties of the materials. The Hydrothermal method results in the lowest band gap energy, while the Vapor Deposition method leads to the highest. The differences in band gap energy indicate the suitability of each synthesis method for specific optical applications. For example, a lower band gap energy might be more advantageous for photovoltaic applications, whereas a higher band gap energy could be beneficial for UV light sensing applications. This comparative analysis is crucial for guiding the selection of an appropriate synthesis method based on the desired optical properties of the ZnO nanoparticles.

In summary, the analysis of the results indicates significant differences in the properties of ZnO nanoparticles depending on the synthesis method. Each method has its unique strengths, as evidenced by the variations in particle size, crystallinity, optical properties, morphology, and electrical properties. This comprehensive analysis provides a foundation for selecting the appropriate synthesis method for specific applications in nanotechnology and material science.

5. Discussion

The comprehensive analysis presented in Section 4 offers critical insights into the physical and chemical properties of ZnO nanoparticles synthesized by different methods, thereby addressing the identified literature gap. This discussion delves into interpreting these results, exploring their implications, and understanding their significance in the broader context of nanomaterial synthesis and application.

Interpretation of Results:

1. **Particle Size and Distribution:** The results indicated that Vapor Deposition and CBD methods produced nanoparticles with a narrower size distribution, as shown in Figure 1. This consistency in particle size is crucial for applications where uniformity is key, such as in

optoelectronics and sensor technologies. The smaller average particle size observed in the Vapor Deposition method might be particularly advantageous for applications requiring high surface area to volume ratio, such as catalysis.

2. **Crystallinity Index:** The higher crystallinity index in nanoparticles synthesized through the Hydrothermal method (Table 3) suggests a superior structural order, which is beneficial for applications requiring high-quality crystal structures like piezoelectric devices and photodetectors.

3. **Band Gap Energy:** The variation in band gap energies, as depicted in Figure 2, highlights the potential for tailoring the optical properties of ZnO nanoparticles through different synthesis methods. The lower band gap energy observed in the Hydrothermal method might make it preferable for applications in solar cells, whereas the higher band gap energy from Vapor Deposition could be more suitable for UV detectors.

4. **Aspect Ratio and Morphology:** The aspect ratio and morphology of nanoparticles (Table 5) have a direct impact on their properties and applications. The elongated shapes obtained from the Hydrothermal method can enhance performance in photocatalytic applications, while the balanced aspect ratio from CBD is suitable for a wide range of uses.

5. **Electrical Properties:** The electrical conductivity findings (Table 6) underscore the importance of synthesis method in determining the electrical behavior of ZnO nanoparticles. The higher conductivity from Vapor Deposition suggests its applicability in electronic and optoelectronic devices.

This study fills the critical gap in comparative analysis of ZnO nanoparticles synthesized via different methods. By providing a detailed examination of various properties, it allows for an informed selection of synthesis method based on the intended application. This contributes significantly to the field of nanotechnology, offering a guideline for tailoring nanoparticle properties for specific uses.

The findings have far-reaching implications in several fields. In electronics, the ability to control particle size and electrical conductivity can lead to the development of more efficient and compact devices. In the realm of renewable energy, understanding the band gap energy allows for the optimization of materials in solar cell applications. Furthermore, the study's insights into crystallinity and morphology open new avenues in sensor technology and catalysis.

In conclusion, this research not only fills a significant gap in the existing literature but also lays a foundation for future studies aimed at optimizing the synthesis of ZnO nanoparticles for specific applications. The ability to tailor nanoparticles properties through different synthesis methods is a powerful tool, potentially leading to advancements in various technological and scientific fields.

6. Conclusion

The study embarked on a comparative analysis of ZnO nanoparticles synthesized via Chemical Bath Deposition and other prevalent deposition methods, shedding light on the nuances that define their physical and chemical properties. One of the pivotal findings was the distinct particle size distribution, where Vapor Deposition demonstrated the ability to produce finer particles with a narrower distribution, essential for applications demanding high surface area and precision. Similarly, the Chemical Bath Deposition method exhibited consistency in particle size, which is crucial for uniformity in electronic and sensor applications.

Crystallinity, a critical determinant of material properties, varied significantly among the methods. The Hydrothermal method emerged as a leader in producing highly crystalline structures, paving the way for its use in applications that rely on superior structural order, such as photodetectors and piezoelectric devices. In terms of optical properties, the study revealed a spectrum of band gap energies, with each method offering different potentials. The lower band gap energy associated with the Hydrothermal method could be harnessed for solar cell

applications, while the higher energy from Vapor Deposition may be more suited for UV light detection.

The aspect ratio and morphology, integral to the performance of nanoparticles in various applications, also showed notable differences. The elongated shapes achieved through the Hydrothermal method could enhance photocatalytic applications, whereas the balanced morphology from Chemical Bath Deposition is adaptable to a wider range of applications. Additionally, the study underscored the influence of synthesis methods on the electrical properties of ZnO nanoparticles, with the Vapor Deposition method showing promise for electronic and optoelectronic devices due to its higher conductivity.

This research not only bridges a significant gap in the comparative analysis of ZnO nanoparticles but also provides a comprehensive understanding that aids in the strategic selection of synthesis methods tailored to specific applications. The insights gained have broad implications, influencing various domains such as electronics, renewable energy, sensor technology, and catalysis. By enabling the customization of nanoparticle properties, this study opens avenues for technological advancements and contributes to the ongoing evolution in the field of nanotechnology and material science. The findings underscore the importance of methodical selection in nanoparticle synthesis, highlighting the potential for innovation and efficiency in the development of nanomaterials.

REFERENCES:

1. Sujaridworakun, P., & Reainthippayasakul, W. (2023). Synthesis of zinc oxide photocatalysts from zinc-dust waste for organic dye degradation. *Journal of metals, materials and minerals*, 33(2).
2. Bhandari, K. P., Sapkota, D. R., Jamarkattel, M. K., & Collins, P. (2023). Zinc Oxide Nanoparticles—Solution-Based Synthesis and Characterizations. *Nanomaterials*, 13(11).
3. Roynette, A., Morakchi-Goudjil, H., Lemarchand, A., Mielcarek, C., Azouani, R., & Traoré, M. K. (2023). Synthesis by soft chemistry of size-controlled zinc oxide (ZnO) nanocrystals for antimicrobial applications. *MATEC web of conferences*.
4. Junaid, M. (2022). Synthesis of Zinc Oxide Nanoparticles by Sol-gel method to Study its Structural Optical Properties and Morphology. *JOURNAL OF NANOSCOPE (JN)*, 3(1).
5. Ghimire, R. R., Parajuli, A., Gupta, S. K., & Rai, K. B. (2022). Synthesis of ZnO Nanoparticles by Chemical Method and its Structural and Optical Characterization. *BIBECHANA*, 19(1-2).
6. Nguyen, V., Nguyen, H. T., & Tran, N. H. (2023). Synthesis of ZnO Nanorods and Its Application in Zinc-Silver Secondary Batteries. *Electrochem*, 4(1).
7. Usoviene, E., Petrašauskienė, N., Jakubauskas, G., & Paluckienė, E. (2023). Influence of the Cadmium Sulfide Chemical Bath Deposition Temperature on Cadmium Sulfide/Zinc Oxide Thin Films. *Coatings*, 13(7).
8. Bartkiewicz, Ł., & Qiu, J. (2023). Comparative study of zinc oxide nanoparticles synthesized through biogenic and chemical route with reference to antibacterial, antibiofilm and anticancer activities. *Environmental Research*.
9. Wai, H. S., & Li, C.-Z. (2023). Fabrication of Well-Aligned ZnO Nanorods with Different Reaction Times by Chemical Bath Deposition Method Applying for Photocatalysis Application. *Molecules*, 28(1).
10. Vargas Rueda, J. A., Alonso, A., & Meléndez-Lira, M. (2022). The role of Zn-complexing agents in the chemical bath deposition of ZnO and ZnS thin films. *Superficies y vacío*.
11. Güneri, E., Johnson, H., & Göde, F. (2022). Chemical Bath Deposition Grown ZnO Thin Films: Role of Manganese Doping. *Journal of Nano Research*.
12. Esmerio, C. L., Rojas, C., Rocha, J., Medina, E., Brito, F. R., García, E., Martínez, R., Aguilar Frutis, M. A., & Garcia Hipolito, M. (2022). Study of The Electrical, Optical and Morphological Properties in Submicron and Microstructured ZnO Thin Films Obtained by Spin Coating and Chemical Bath Deposition. *Science and technology Indonesia*.
13. Ahmed, M. M. A., Coetsee, L., Goosen, W. E., Urgessa, Z. N., & Botha, J. R. (2023). Characterization of Bi-doped ZnO nanorods prepared by chemical bath deposition method. *Physica B-condensed Matter*.
14. Liu, G., Yu, X., Xu, R., Zhu, X., Ma, Y., & Ma, L. (2021). Multiple Regulation Effects of Ammonium Acetate on ZnO Growth Process in Chemical Bath Deposition. *Chemistry: A European Journal*.
15. Lahewil, A. S. Z., Ahmed, N. M., & Azman, N. Z. N. (2021). Structural and optical properties of ZnO nanoflakes/Al/glass via laser-assisted chemical bath deposition (LACBD) technique. *Applied Physics A*.

Study of Thermal Properties of Solid Polymer Complexes doped with TiO₂ and GDC

R. Risodkar*

Dept. of Physics, R.A. College, Washim, Maharashtra

*rajrisodkar@gmail.com

ABSTRACT

The thermal properties were investigated using TGA/DTA by thermo gravimetric differential thermal analyser at heating rate of 5 °C/min. The composites with 20 wt% GDC and TiO₂ were maximum conductivity giving compositions in their respective systems and so taken for further study. The TGA and the DTA curves of 80(80PVA:20AN):20(GDC/TiO₂) composites confirms the weights loss increased up to 213 °C due to the loss of water related to hydrogen bonding with polymer matrix. A comparison of T_g and T_m obtained from TGA/DTA and DSC curves for different concentration of both the fillers (GDC/TiO₂) suggests no change in the T_g with addition of filler (GDC/TiO₂) in the polymer complex. All results confirm that the polymer complexes are thermally stable up to about 213 °C.

Keywords: TGA, DTA, DSC, Polymer complex

I Introduction

The discoveries of advance materials and/or processing techniques are the key factors for accelerating continuous advancement in the devices. Design and development activities particularly to the electrochemical devices chiefly include engineering of electrodes (anode and cathode) and electrolyte.[1] These are three crucial constituents of electrochemical devices where efficiency and the performance is very important. Also, the magnitude of ionic- and electronic-conductivity, chemical and thermodynamic stability, cost, phase and form of solid electrolyte and reference electrode are the deciding factors of device performance.[2] Polymer solid electrolytes are electrolytic materials that offer many advantages in the area of large, high energy density batteries for electric propulsion and in fuel cells for electric vehicle or stationary applications.

To investigate the thermal behaviour of materials the thermal analysis is made up of various techniques. When any material is subjected to thermal heating or cooling process then structure and chemical composition of material may undergo changes (melting, oxidation, decomposition, reaction transition, etc.).[3] Thermal analyses are the group of techniques in which the property of the sample is monitored against time or temperature while the temperature of the sample, in a specified atmosphere, The thermal analysis is widely used in research, analytical and quality control laboratories to study diversity of problems. [4]

In the present work, Differential scanning calorimetry (DSC) and thermo gravimetric analysis/differential thermal analysis (TGA/DTA) is used to obtain information on the thermo-chemical properties such as, glass transition and melting temperatures, dehydration, dissociation, decomposition, phase transformation, purity, etc. of polymer complexes.

II. MATERIALS AND METHOD

Poly(vinyl alcohol) (PVA), with a degree of hydrolysis more than 99% and average molecular weight of 146000, was procured from Aldrich, USA with dopant ammonium salt. Initially, the 80PVA:20AN solution was prepared. Essentially, AN was also dissolved in same solvent to

admixed in 80:20 mole% in polymeric solution. Later, solution was thoroughly stirred for 8-10 h at 70 °C using magnetic stirrer for homogeneity. The TiO₂/GDC nano powder was added in the solution and stirred thoroughly for 10-12 h at 70 °C. The concentration of TiO₂/GDC powder was varied from 5-25 wt% in polymer complex. The viscous gel mixture was then casted on the glass plate and dried for one week. The smooth and uniform films were obtained by solution cast technique.[5]

During the present study, all the prepared solid polymer complexes were then thoroughly characterized by TGA/DTA, Perkin Elmer, Diamond TGA/DTA thermo gravimetric differential thermal analyser at heating rate of 5 °C/min to study thermal properties.

III Results and Discussion

I TGA/DTA and DSC The TGA and the DTA curves of 80(80PVA:20AN):20(GDC/TiO₂), a representative of all composite under study, are shown in Fig.1.1.and 1.2, respectively. A comparison of the composites with 20 wt% GDC or TiO₂ were maximum conductivity giving compositions in their respective systems and so taken for further study. As seen, the thermal behaviour of the both the composites does not change with the addition of inert phase in the PVA:AN polymer complex. Weight losses increase up to 213 °C are attributed to the loss of water related to hydrogen bonding with polymer matrix [6-10].

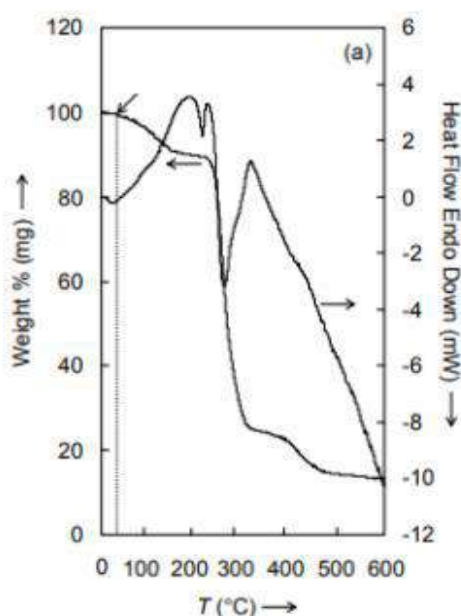


Fig1.1 TGA and DTA curves (80PVA:20AN) with with 20 wt% GDC

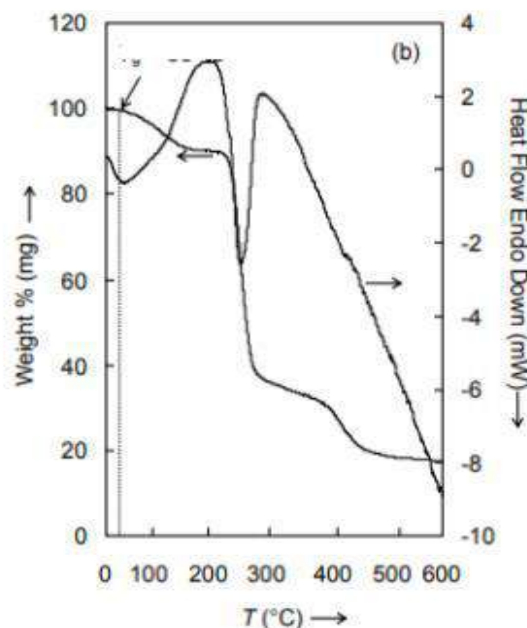


Fig. 1.2 TGA and DTA curves (80PVA:20AN) 20 wt% TiO₂

A comparison of T_g and T_m obtained from TG/DTA and DSC curves for different concentration of both the fillers (GDC/TiO₂) is given in the Table I. A close scrutiny of the Table suggests no change in the T_g with addition of filler (GDC/TiO₂) in the polymer complex. Otherwise, general, the decrease in T_g is attributed to the improvement in the chain mobility at lower temperatures due to interaction of polymer complex with the filler [10-16].

Samples (x wt %)	GDC				TiO ₂			
	DSC		DTA		DSC		DTA	
	T _g (°C)	T _m (°C)	T _g (°C)	T _m (°C)	T _g (°C)	T _m (°C)	T _g (°C)	T _m (°C)
Pure PVA	190	231	192	230	-	-	-	-
5	185	216	187	215	186	217	185	216
10	185	213	186	212	187	215	186	213
15	186	211	187	209	186	214	186	212
20	185	210	186	208	186	212	185	209
25	186	202	186	201	187	206	186	205

Table 1: A comparison of thermal data obtained from DTA/TGA and DSC measurements for (100-x) (80PVA:20AN):(x) (GDC/TiO₂) composites

IV Conclusion

The polymer composites 80(80PVA:20AN):20(GDC/TiO₂) were prepared by solution cast technique. All above results confirm that the polymer film of composite polymer and their complexes are thermally stable up to about 213 °C due to the loss of water related to hydrogen bonding with polymer matrix.. The similar behaviour was obtained for TiO₂ filler.

In conclusion the addition of salts leads to the formation of blend with the polymers and dispersion of insoluble inert phase reduce the T_g. Furthermore, the water retention temperature also varies. The change in T_g suggests the interaction of PVA polymer with the salts, dopants, etc., leading to the change in the glass structure. A comparison of T_g and T_m obtained from TGA/DTA and DSC curves for different concentration of both the fillers (GDC/TiO₂) suggests no change in the T_g with addition of filler (GDC/TiO₂) in the polymer complex.

V References

- 1 J.C. Lassegues, B. Desbat, O. Trinquet, F. Cruege, C. Poinsignon, Solid State Ionics 28(1988):969
- 2 W. Y. Chuang, T. H. Young, C. H. Yao and W. Y. Chiu, Biomater., 20 (1999) 1479.
- 3 C. C. Yang, S. J. Chiu, W. Chien and S. S. Chiu, J. Power Sources, 195 (2010) 2212.
- 4 C. C. Yang, Y. J. Lee and J. M. Yang, J. Power Sources, 188 (2009) 30.
- 5 C. Dong, J. Macromol. Sci., A 41 (2004) 547.
- 6 R. M. Hodge, G. H. Edward and G. P. Simon, Polymer, 37 (1996) 1371.
- 7 L. Alexander, X-ray Diffraction Methods in Polymer Science. Wiley and Sons, (New York), (1963).
- 8 M. Hema, S. Selvasekarapandian, H. Nithya, A. Shakunthala and D. Arunkumar, Ionics, 15 (2009) 487.
- 9 S. Rajendran, M. Sivakumar and R. Subadevi, J. Power Sources, 124 (2003) 225.
- 10 N. Chand, N. Rai, T. S. Natarajan and S. L. Agrawal, Fibers and Polym., 12 (2011) 438.
- 11 P. B. Bhargav, V. M. Mohan, A. K. Sharma and V. V. R. N. Rao, Ionics, 13 (2007) 173
- 12 A. A. R. Oliveira, V. Ciminelli, M. S. S. Dantas, H. S. Mansur and M. M. Pereira, J. Sol-gel Tech., 47 (2008) 335.
- 13 M. Hema, S. Selvasekarapandian, A. Sakunthala, D. Arunkumar and H. Nithya, Physica B, 403 (2008) 2740.
- 14 S. Rajendran, M. Sivakumar and R. Subadevi, Mater. Lett., 58 (2004) 641.
- 15 H. Pu and P. Huang, Mater. Lett., 60 (2006) 1724.
- 16 M. Kumar and S. S. Sekhon, Euro. Polym. J., 38 (2002) 1297

Chemical Synthesis of Polyaniline Nanocomposites for Advanced Applications

Vaishnavi D. Nagmote*, **Suraj V. Tayade**, **Sandeep A. Waghuley**

Post Graduate Department of Physics, Sant Gadge Baba Amravati University,
Amravati, India, 444 602.

*Corresponding author email: vaishnavinagmote2001@gmail.com, sandeepwaghuley@sgbau.ac.in

ABSTRACT:

In the present work on the synthesis of polyaniline nanocomposites through in-situ chemical oxidative method, oxidative electropolymerization method, chemical synthesis method, chemical route method, electrodeposition method, the synthesized compounds were characterized by Fourier transform infrared spectroscopy, transmission electron microscopy, scanning electron microscopy, thermogravimetric analysis, and X-ray diffraction” describes the methods used to synthesize polyaniline nanocomposites and the characterization techniques used to analyze them. Polyaniline is a versatile material with a wide range of applications due to its low cost, low weight, corrosive resistance, and environmental stability. Polyaniline nanocomposites exhibit tremendous properties such as mechanical, electrochemical, semiconducting, and anti-corrosive properties, making them ideal for use in supercapacitors, batteries, sensors, solar cells, and corrosion-resistant coatings.

Keywords: Polyaniline; nanocomposites; metal oxide

Introduction :

Conducting polymers are a new class of polymers with electronic and ionic conductivity that were discovered in 1977 [1]. Polyaniline is considered one of the important members of this class of materials due to its low cost, low weight, environmental stability, corrosive resistance, and ease of conversion between base and salt by adding base (OH⁻) or acid (H⁺) [2]. Polyaniline has attracted attention due to its various structures [3]. The process of mixing material with polyaniline results in polyaniline composites [4]. PANI has been used in many applications such as solar cells, batteries, supercapacitors, corrosion-resistant coatings, and sensors [4].

Polyaniline exhibits tremendous properties. Its physical properties depend on its three forms, which show different colors according to their chemical nature. The optical properties of polyaniline are used to study the oxidation level and protonation process of the polymer. Polyaniline shows noticeable differences in mechanical properties depending on the polymerization method from which it was prepared. Polyaniline also has anticorrosive properties. Corrosion is the chemical change in the metal due to the environmental influences surrounding it, and it is a major problem facing various processes. Polyaniline was used to effectively protect steel from oxidation. PANI films doped with boric acid show semiconducting properties. Due to its semiconducting properties, polyaniline is widely used in organic field transistors [4].

PANI exist in three different forms such as fully oxidised Pernigrtaniline (PAB), leucoemeraldine base (LEB) semi oxidised emeraldine base (EB) PANI [5] also have electrical conductivity only in the emeraldine form and other type do not show significant conductivity

Synthesis methods:

Oxidative polymerization method: This method is characterized as a simple and cheap way to prepare large amounts of polymer in a short duration. It is commonly used in industries to prepare PANI. In this method, the polymerization process is carried out by using oxidizing agents such as Ammonium persulphate $(\text{NH})_2\text{S}_2\text{O}_8$, sodium vanadate (NaVO_3) , and hydrogen peroxide (H_2O_2) . The molar ratio between aniline and persulphate is usually less than 1.2 [4].

Electrochemical polymerization: In this method, the preparation of conductive polymer plays an important role because in many applications, thin films with wide surface areas have optical and electrical properties that depend mainly on these thin layers of polymer. In this method, the polymer is deposited on the electrode, and the formation of free radicals of aniline monomer by oxidation on the anode leads to the combination of the structure to form a dimer. Through the process of removing protons and rearranging electrons in the aromatic ring, a new large structure is formed, and the spontaneous activation of the polymer chain is formed by the acid present in the solution to obtain PANI [4].

In situ polymerization: In this method, a metal salt that acts on the oxidizing agents is mixed with aniline in the presence of a solvent and oxidizing or reducing agents. Continuous stirring leads to the formation of PANI composites as a precipitate, which is then filtered, washed, and dried [1].

Advanced applications:

Supercapacitor: Supercapacitors are electrode materials that have been used in supercapacitors due to their high power density, high energy density, reversibility, long life cycle, and small environmental impact. They play an important role in the efficiency of storage devices and energy conversion processes. Various carbon materials are used in supercapacitor devices due to their good conductivity. PANI can be used with great success in supercapacitors. The properties of PANI-based materials depend on the properties of PANI itself [6].

Electronics devices: PANI has electrochromic material that can show electroactivity in aqueous solutions and low pH ranges. PANI composites have been developed to overcome these problems. Polyaniline nanoparticles show some specific resistances. PANI films showed similar results to those of PANI composites. These promising materials are suitable for electrochromic applications and can be used as large area displays [6].

Solar cell: PANI nanoparticles anchored on rGO sheets can be used as counter electrodes in dye-sensitized solar cells. Silicon-based solar cells are used because of their low cost, easy fabrication, and respectable energy conversion efficiency. PANI nanoparticles increase the conductivity of electrons at the semiconductor layer to combat charge recombination [6].

Conclusions:

This work reports the synthesis of polyaniline with other compounds using various methods such as oxidative polymerization, electrodeposition, chemical route, electrochemical method, and in situ polymerization. The synthesized compounds were characterized by X-ray diffraction technique, Fourier transform infrared spectroscopy, scanning electron microscopy, and transmission electron microscopy. Polyaniline has various applications such as superconductors, electromagnetic devices, and solar cells etc.

References:

- [1] Kyomuhimbo, H. D., & Feleni, U. (2023). Electroconductive Green Metal-polyaniline Nanocomposites: Synthesis and Application in Sensors. *Electroanalysis*, 35(2), e202100636
- [2] Reddy, K. R., Lee, K. P., & Gopalan, A. I. (2008). Self-assembly approach for the synthesis of electro-magnetic functionalized Fe₃O₄/polyaniline nanocomposites: effect of dopant on the properties. *Colloids and Surfaces A: Physicochemical and Engineering Aspects*, 320(1-3), 49-56.
- [3] Babel, V., & Hiran, B. L. (2021). A review on polyaniline composites: Synthesis, characterization, and applications. *Polymer Composites*, 42(7), 3142-3157. Baldissera, A. F., Souza, J. F., & Ferreira, C. A. (2013). Synthesis of polyaniline/clay conducting nanocomposites. *Synthetic metals*, 183, 69-72
- [4] Majeed, A. H., Mohammed, L. A., Hammoodi, O. G., Sehgal, S., Alheety, M. A., Saxena, K. K., ... & Salmaan, N. U. (2022). A Review on polyaniline: Synthesis, properties, nanocomposites, and electrochemical applications. *International Journal of Polymer Science*, 2022.
- [5] Bavatharani, C., Muthusankar, E., Wabaidur, S. M., Alothman, Z. A., Alsheetan, K. M., mana AL-Anazy, M., & Ragupathy, D. (2021). Electrospinning technique for production of polyaniline nanocomposites/nanofibres for multi-functional applications: A review. *Synthetic Metals*, 271, 116609
- [6] Wang, L., Lu, X., Lei, S., & Song, Y. (2014). Graphene-based polyaniline nanocomposites: preparation, properties and applications. *Journal of Materials Chemistry A*, 2(13), 4491-4509

Synthesis and Photoluminescence Properties of Tb³⁺ doped KSrPO₄ Phosphor

*N. S. Sawala¹, C.B. Palan², A. O. Chauhan³, S.K. Omanwar⁴

¹Science and Humanities Department Government Polytechnic, Arvi Wardha

²Department of Physics, Bapumiya Sirajoddin Patel Art's, Com. and Sci. College Pimpalgaon Kale, Buldana

³Department of Physics, Vidya Bharati Mahavidyalaya, Amravati

⁴Department of Physics, Sant Gadge Baba Amravati University, Amravati

(Corresponding author: nssawala@gmail.com)

Abstract

The Green-emitting KSrPO₄:Tb³⁺ phosphor was successfully synthesized via modified solid-state diffusion (MSSD) method. The structure of the prepared KSrPO₄: Tb³⁺ phosphor was confirmed by powder XRD analysis and its photoluminescence properties has been studied under ultraviolet (UV) excitation (200–400 nm). The phosphor shows efficient emission at 544 nm under excitation of 230 nm.

Keywords: KSrPO₄: Tb³⁺ phosphor; LED; and Green emitting.

1.0 Introduction

In 1962, orthophosphates with the general formula ABPO₄, where A is monovalent cation (i.e. A = Li⁺, Na⁺, K⁺, Rb⁺ and Cs⁺) and B is divalent cation (B = Mg²⁺, Ca²⁺, Sr²⁺ and Ba²⁺) have three type of dimensional rigid structures. The ABPO₄ phosphates form a large family compounds having structure strictly depending on the relative sizes of A and B [1]. For arcanite type structure requires A and B similar radii. When B is small in size, two different structures have been observed depending on the size of A. For the small size of A adopt an olivine type structure, while it represents the tridymite type structure for relatively large size A ions [2]. The ABPO₄ compounds show optical and ferroelectric properties also excellent thermal stability, hydrolytic stability and charge stabilization [3-10]. The phosphate based host can solve the heat problems of the high power of white LED in effective way [11-13]. These phosphors show strong, broad optical absorption at near-UV region and exhibit strong blue or green emission under near-UV irradiation. The ABPO₄ compound doped with different rare-earth ions (Eu³⁺, Ce³⁺, Tb³⁺, Sm³⁺ etc.) could emit different wavelengths, depending on various crystal fields.

In present work, we first time reports luminescence properties of KSrPO₄:Tb³⁺ by using MSSD method.

2.0 Experimental

The polycrystalline KSr_(1-x)PO₄: xTb³⁺ phosphor was successfully synthesized via MSSD method. The precursors are stoichiometric quantities of high purity nitrates of AR grade were used. The phase purity of KSrPO₄:Tb³⁺ phosphor was checked by means of X-ray powder diffraction (PXRD) using a Rigaku miniflex II diffractometer. The Photoluminescence excitation and emission spectra were measured on Hitachi F-7000 fluorescence spectrophotometer with a 450W xenon lamp, in the wavelength range 200–700 nm, with spectral slit width of 1 nm and PMT voltage at 700V at room temperature.

3.0 Results and Discussion:

3.1 X-Ray Diffraction (XRD) Pattern

The X-ray diffraction (XRD) pattern of the Tb-doped KSrPO₄ phosphor is shown in **Fig. 1**. As it was reported on, KSrPO₄ has orthorhombic crystal structure in space group of Pmna (62) [15]. The XRD pattern of prepared phosphor is well matched with the ICDD standard file with card no.-00-033-1045. There are no obvious impurity peaks that could be

detected in the experimental data and all peaks are match well with the standard patterns of KSrPO_4 phosphor. This gives a clear indication about the phase purity and formation of the prepared phosphor.

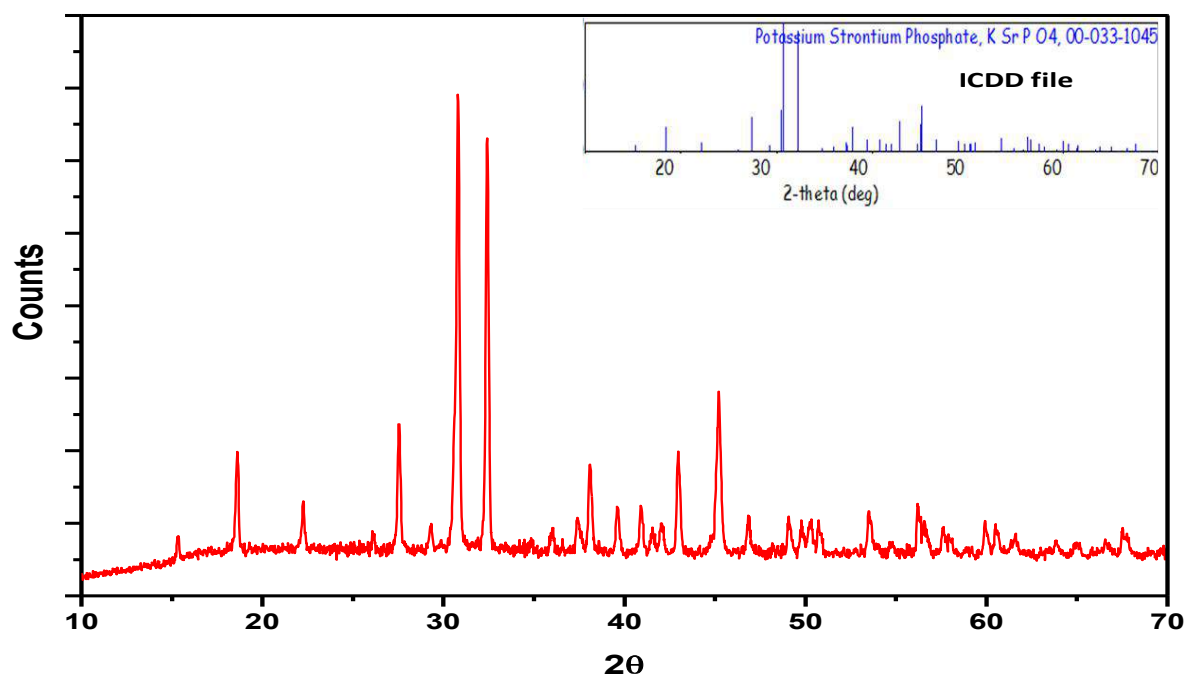


Fig. 1: XRD pattern of the $\text{KSrPO}_4:\text{Tb}^{3+}$ sample along with the standard ICDD file

3.2 Photoluminescence Properties (PL)

The excitation and emission spectra of $\text{KSrPO}_4:\text{Tb}^{3+}$ phosphor is as shown in the Fig. 2. The excitation and emission spectrum of $\text{KSrPO}_4:\text{Tb}^{3+}$ phosphor, were monitored at wavelength 544 nm and 230 nm. The PL excitation spectrum of $\text{KSrPO}_4:\text{Tb}^{3+}$ phosphor consist of a narrow band around 230 nm, which corresponds to attribute to $4f^8-4f^5d^1$ transition of Tb^{3+} in host lattice. The emission spectra consists of several lines around 482, 493, 544, and 588 nm corresponding to transitions $^5D_4 \rightarrow ^7F_6$, $^5D_4 \rightarrow ^7F_6$, $^5D_4 \rightarrow ^7F_5$ and $^5D_4 \rightarrow ^7F_4$ respectively [16, 17].

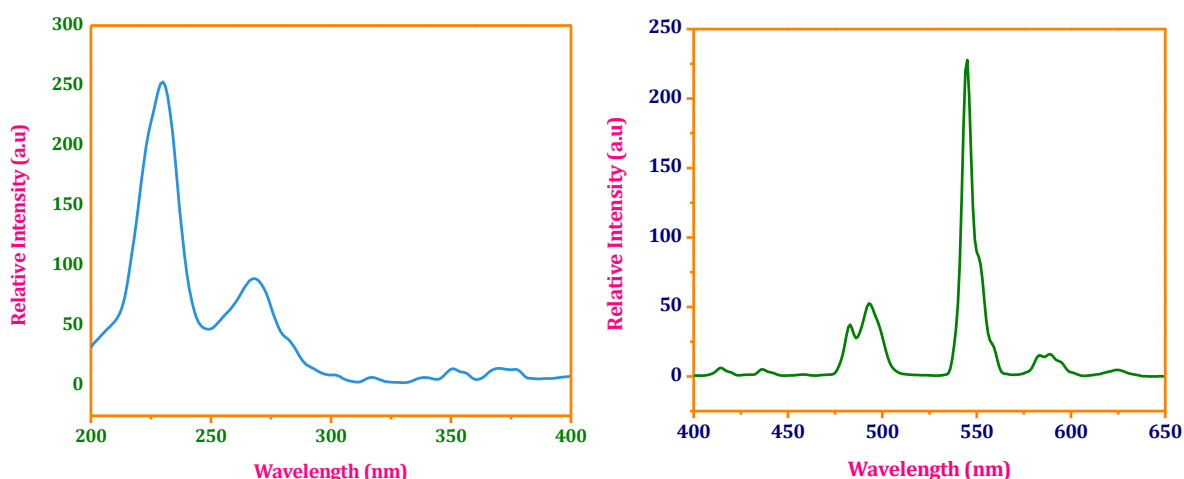


Fig. 2 Photoluminescence excitation and emission spectra of $\text{KSr}_{0.93}\text{PO}_4:0.07\text{Tb}^{3+}$ phosphor

4.0 Conclusions:

The polycrystalline $\text{KSrPO}_4:\text{Tb}^{3+}$ phosphor was successfully synthesized by modified solid state diffusion method. The XRD pattern of prepared $\text{KSrPO}_4:\text{Tb}^{3+}$ phosphor is good agreement with the ICDD standard file with card no, -00-033-1045. The PL excitation spectra, was monitored at 544 nm and emission spectra was monitored at 230 nm. The CIE chromaticity coordinates of the as-prepared phosphor was calculated and found to be ($x=0.2585$, $y=0.7305$). The outcome of this phosphor material provides the support for the possible application in green emitter in many applications in fluorescent area.

5.0 References:

- [1] L. Elammari, M. Koumiri, I. Gränacher, B. Elouadi, *Ferroelectrics* 158 (1994) 19.
- [2] R. Yu. H. Li, H. Ma, C. Wang, H. Wang, *Solid State Sci.* 29 (2014) 34.
- [3] W. Wanmaker, H. Spier, *J. Electrochem. Soc.* 109 (1962) 103.
- [4] D. Blum, J. Penzin, J. Henry, *Ferroelectrics.* 61 (1984) 265.
- [5] C. Wu, Y. Wang, *Mater. Lett.* 61 (2007) 2416.
- [6] Z. Wu, J. Shi, M. Gong, J. Wang, Q. Su, *Mater. Chem. Phys.* 103 (2007) 415.
- [7] Z. Wu, J. Shi, J. Wang, M. Gong, Q. Su, *J. Solid State Chem.* 179 (2006) 2356.
- [8] C. Lin, Y. Tang, S. Hu, R. Liu, *J. Lumin.* 129 (2009) 1682.
- [9] W. Im, H. Yoo, S. Vaidyanathan, K. Kwon, H. Park, Y. Kim, D. Jeon, *Mater. Chem. Phys.* 115 (2009) 161.
- [10] W. Tang, Y. Zheng, *Luminescence.* 25 (2010) 364.
- [11] D. Dutta, A. Tyagi, *Solid State Phenom.* 155 (2009) 113.
- [12] C. Lin, Z. Xiao, G. Guo, T. Chan, R. Liu, *J. Am. Chem. Soc.* 132 (2010) 3020.
- [13] K. N. Shinde, S. J. Dhobl, H. C. Swart, *Mater. Sci.*, 174 (2013) 101. DOI 10.1007/978-3-642-34312-4_5
- [15] C.B.Palan, N.S. Bajaj and S.K. Omanwar *AIP Conference Proceedings* **1728**, 020474 (2016); doi: 10.1063/1.4946525
- [16] N. Bajaj, C. Palan, S. Omanwar, *Int. J. Mater. Sci. Eng.* 3,(2015) 167.
- [17] C. Palan, N. Bajaj, A. Soni, M. Kulkarni, S. Omanwar, *Bull. Mater. Sci.* 38 (2015)1527.

Nanocrystalline Spinel Cobalt Aluminate Prepared By Co precipitation Method

S.V. Agnihotri*, V. D. Kapse, T.R. Tatte, P.V. Tumram, M. S. Pande

*Department of Physics, Amolakchand Mahavidyalaya Yavatmal, 445001, Maharashtra State, India.

Department of physics, Arts, Science and Commerce College, Chikhaldara 444807, Maharashtra State India

Department of Physics, Shri. R. G. Rathod Arts and Science College, Murtizapur- 444107, M S, India.

Department of Physics, Amolakchand Mahavidyalaya Yavatmal, 445001, Maharashtra State, India

Department of physics, Gajanan Maharaj College of Engineering, Shegaon 444203

drsva205@gmail.com

Abstract:

Cobalt aluminate (CoAl_2O_4) nanoparticles were synthesized via co precipitation route. Sample was calcinated at 900°C . X-ray diffraction, data confirms the formation of single-phase cubic structure and the average grain sizes were evaluated. The XRD result revealed the production of a sharp single cubic spinel structure of prepared sample without any impurity peak with the crystallite size of about 21.6 nm. The high and low frequency absorption bands of CoAl_2O_4 were investigated using FT-IR analysis. The microstructural features were examined by scanning electron microscopy (SEM).

Keywords: Nanocrystalline, Cubic-Spinel, XRD, FT-IR, SEM.

Introduction:

Cobalt aluminate spinel (CoAl_2O_4) is known for its blue colour and it is widely used as pigments for ceramics, paints, fibres and so on. CoAl_2O_4 is a material which have excellent thermal stability, high melting point and electrical properties. The structure of CoAl_2O_4 also plays a key role in determining the material's behaviour in different environments making it an important consideration in various fields of science and engineering [1]. The materials have high thermal stability, colour stability, resistance to moisture and humidity also make it suitable for use in harsh environments [2-7].

Materials and Methods:

There are several methods use to synthesize Cobalt aluminate nanoparticles, including the mixed oxide method, citrate-nitrate method, hydrothermal synthesis and combustion methods [8,9]. Among all the methods, co precipitation is one of the most efficient routes and human-friendly method to develop spinel oxide materials in a short span of time while utilizing less energy [10].

Sample CoAl_2O_4 was synthesized by co-precipitation method in an air atmosphere. The starting materials were weighed according to the stoichiometric ratio. The raw materials $\text{Al}(\text{NO}_3)_3 \cdot 9\text{H}_2\text{O}$ (99.0%), $(\text{Co}(\text{NO}_3)_2 \cdot 6\text{H}_2\text{O})$, were dissolved in distilled water mixed well with each other at 80°C temperature under constant magnetic stirring, where in the molar ratio of Co/Al was 1:2. In this process, ammonia was used as precipitant. The mixed materials were dried in an oven for 24 h. The dried materials were put into the alumina crucible and calcined in a muffle furnace at 900°C for 4 h and then the white powder was obtained. Thick film was prepared from this powder by screen printing method.

There are many reports available on semiconducting metal oxide. Among these cobalt aluminate gas sensor is a potential candidates of the gas sensing device. In this paper

characterization of the spinel was carried out by using powder X-ray diffraction, infrared spectra and scanning electron micrograph.

Techniques:

The X-ray measurement of various mixed solids was carried out using a BRUKER D8 advance diffractometer (Germany). The patterns were run with Cu K α radiation at 40 kV and 40 mA with scanning speed in 2θ of 2° min^{-1} . The crystallite size of CoAl $_2$ O $_4$ crystallites present in the investigated solids was based on X-ray diffraction line broadening and calculated by using Scherrer equation [11]

$$d = \frac{k\lambda}{\beta \cos \theta}$$

where d is the average crystallite size of the phase under investigation, k is the Scherrer constant (0.89), λ is the wave length of X-ray beam used, β is the full-width half maximum (FWHM) of diffraction and θ is the Bragg's angle. The XRD patterns of these powders showed several peaks at 31.44, 37.02, 44.94, 55.78, 59.46 and 65.30 corresponding to (h k l) reflection at (2 2 0), (3 1 1), (4 0 0), (4 2 2), (5 1 1) and (4 4 0) respectively [12]. These peaks could be indexed with space group Fd3m.

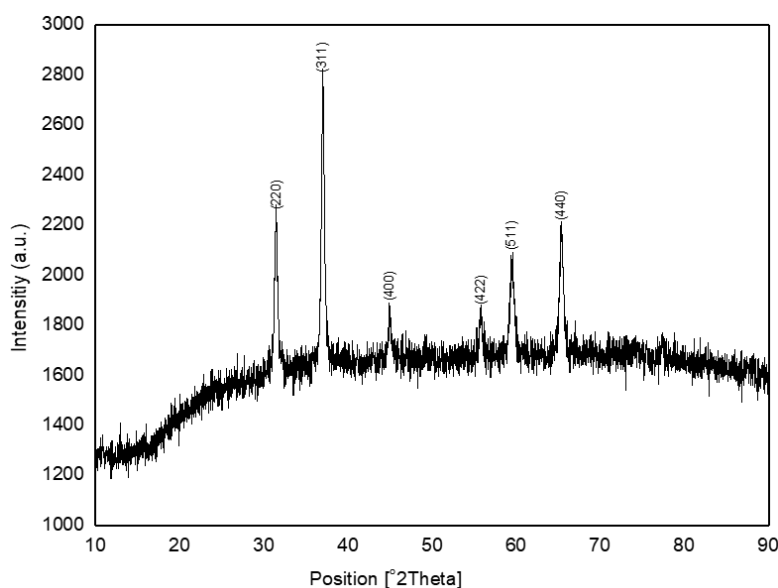


Fig. 1: XRD pattern of CoAl $_2$ O $_4$ powder calcinated at 900°C.

Infrared spectra of given sample as shown in fig. 2. Spectra shows three bands in the region 500 to 700 cm^{-1} . These three bands are attributed to the vibration modes of the CoAl $_2$ O $_4$ phase [13]. These results are in good agreement with XRD analysis.

Scanning electron micrographs (SEM) were recorded on JEOL JSM 7600F. SEM micrographs of the sample CoAl $_2$ O $_4$ thick film are presented in fig. 3. The film was synthesized by screen printing method. Figure shows agglomerates of different shapes and the particle size between the range 45.1- 45.4 nm.

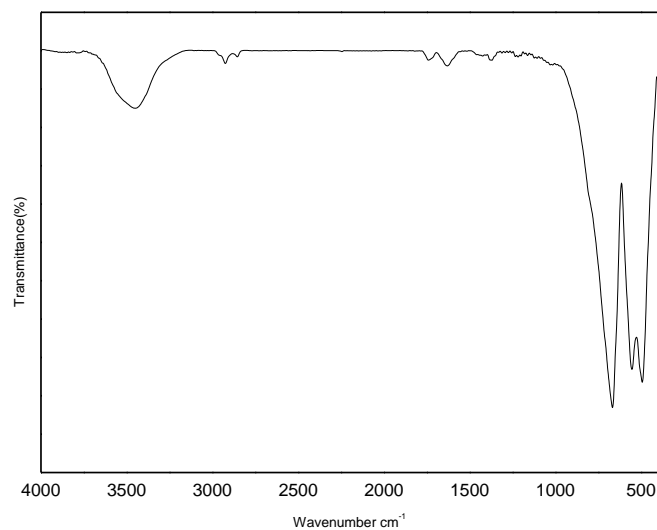


Fig.2: FTIR spectra of CoAl_2O_4 powder calcinated at 900°C .

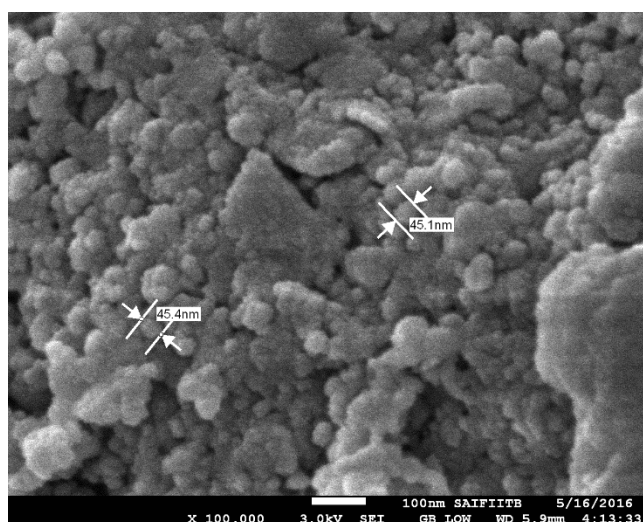


Fig. 3: SEM image of Nanocrystalline CoAl_2O_4 thick film.

Conclusion:

In summary, CoAl_2O_4 nanoparticles have been successfully synthesized through co precipitation method. The sample was heated upto 900°C . The heat treatment blue powders with a direct spinel structure (CoAl_2O_4). The vibrational stretching frequencies corresponding to the composites were confirmed by FT-IR spectroscopy. Scanning electron micrograph shows homogenous morphology; it consists in agglomerates of primary particles of quasi-spherical shape with a size in the range 45.1 to 45.4nm.

References:

1. S. Bid and S.K. Pradan, *Materials Chemistry and Physics* (2003) 82-27.
2. R.E. Ayala and D.W. Marsh, *Ind. Chem. Res.* (1991) 30-55.
3. Y. Tang, C. Wu, Y. Song, Y. Zheng, K. Zhao, Effects of colouration mechanism and stability of CoAl₂O₄ ceramic pigments sintered on substrates, *Ceram. Int.* 44 (2018) 1019–1025.
4. S. Obata, M. Kato, H. Yokoyama, Y. Iwatara, M. Kikumoto, O. Sakurada, Synthesis of nano CoAl₂O₄ pigment for ink-jet printing to decorate porcelain, *J. Ceram. Soc. Japan* 119 (2011) 208–213.
5. Y. Song, Y.L. Zheng, Y.F. Tang, H.B. Yang, Fabrication and stability of CoAl₂O₄ ceramic pigment for 3D printing, *MSF* 898 (2017) 1935–1939.
6. P. Xiaojin, C. Jinshu, Y. Jian, J. Na, K. Junfeng, H. Yansheng, Z. Qi, Environmental blue CoAl₂O₄ pigment co-doped by Zn²⁺ and Mg²⁺: synthesis, structure and optical properties, *Adv. Appl. Ceram.* 117 (2018) 303–311.
7. M. Abhishek, K. Manjunatha, V. Jagadeesha Angadi, E. Melagiriappa, B.N. Anandaram, H.S. Jayanna, M. Veena, K.S. Acharya, Structural and magnetic properties of Eu³⁺ substituted Mg-Cd nanoferrites: a detailed study of influence of high energy γ -rays irradiation, *Chem. Data Collect.* 28 (2020).
8. G. Aguilar-Rios, M. Valenzuela, P. Salas, H. Armendariz, P. Bosch, G. Del Toro, R. Silva, V. Bertin, S. Castillo, A. Ramirez-Solis, I. Schifter, *Appl. Catal. A.Gen.* 127 (1995) 65-75.
9. J. Wrzyszczyk, M. Zawadzki, J. Trawczyński, H. Grabowska, W. Miśta, *Appl. Catal. A Gen.* 210 (2001) 263–269.
10. C.O. Areal, B.S. Sintes, G.T. Palomino, C.M. Carbonell, E.E. Platero, J.B. P. Soto, *Microporous Mater.* 8 (1997) 187.
11. B.D. Cullity, *Elements of X-ray Diffraction*, Addison-Wesley Publishing Co. Inc. 1976 (chapter 14)
12. N. Ouahdi, S. G. Fritsch, Durand, El Bernard, Ouatib, Rachida, Er Rakho, Lahcen, R. Moussa, A. Samdi, *J. of Euro. Ceram. Soc.* 28 (10) (2008) 1987-1994.
13. X. Duan, M. Pan, F. Yu, D. Yuan, Synthesis, structure and optical properties of CoAl₂O₄ spinel nanocrystals, *J. Alloys Compd.* 509 (2011) 1079-1083.

Dynamics of Coupled Circle Map on Diffusion Limited Aggregate

Pratik M. Gaiki* and Parag A. Bramhankar#

Department of Physics, Shri Shivaji Education Society Amravati's- Shri Shivaji Arts, Commerce and Science College, Motala, Dist. Buldana-443103, Maharashtra, India.

*pmgai@gmail.com, #paragbramhankar@gmail.com

Abstract. Complex networks and d-dimensional Euclidean lattices have both been researched using coupled map lattices. Additionally, it has been examined on the deterministic fractal known as the Sierpinski Gasket. In this work, we investigate the coupled map lattice on a random fractal called diffusion limited aggregate (DLA). We create a map and examine it from the perspective of the circle map. In the event of a DLA, a site's neighbors may number one to four. We examine the scenario in which the total weight does not stay constant. In this regard, we plot bifurcation diagrams.

Keywords: Coupled Map Lattice, Circle Map, Diffusion limited Aggregate

INTRODUCTION

Dynamics-displaying fractals on Coupled Map lattices

A system that has been extensively investigated is coupled map lattices on Euclidean lattices in d-dimensions. In this regard, the most researched maps are circular, tent, and logistical maps. Few studies have been done on the dynamics of fractals. Fractal connectivity scales with distance.

In the case of connected map lattices, such systems exhibit a transition from spatial order to spatially uniform or chaotic states when coupling is changed. Based on simulations of neural networks, coupled oscillators, and coupled maps, nodes are divided into regions of fixed point, chaotic, and oscillating regions.

Network connectivity has an impact on how activities are divided inside networks. We can achieve these partially arrested states in what are known as chimera states. This article here examines a fractal model known as the diffusion limited aggregate (DLA). Coupled map lattices are dynamical networks that act like complicated models and are spatially homogeneous and computationally feasible. Things having fractal architectures exhibit exciting physical phenomena [3]. In CMLs, coupling is diffusively discrete. Similar to the logistic map, the circle map is a chaotic map. Similar to the dynamics of neurons, chaotic, oscillatory, and fixed-point behavior can be seen. Each of these many dynamical kinds is dependent upon the type of coding and the applied stimulus [4].

If systems exhibit statistical symmetry, long-range interactions, and are probabilistic in nature, they can have chaotic temporal states and long-range spatial order with temporal disorder. We can learn about the stability of randomly connected elements from the Wigner-May theorem. The instabilities to a spatially uniform state vary, and the eigen-values of fractals exhibit intriguing structure [5].

Diffusion Limited Aggregate (DLA)

Written and Sander [1] generated a metal-particle aggregation process model whose correlations were measured. They concluded that, like metal aggregates, the density correlations in the model aggregates decrease with distance along a fractional power law. The metal aggregates' radius of gyration follows a power law pattern.

The DLA model is based on the Eden model, in which randomly added particles are introduced to sites next to occupied sites one at a time. However, Written and Sander discovered that the fractional power law of distance was how the metal aggregates slid off. The irreversible growth process is the source of these relationships. Similarities between the DLA model and the discrete Langer-Krumbhaar model of dendritic development are found [6].

COUPLED MAPS ON DLA

Initially, we start with a seed particle at the lattice origin. Next, we introduce a second particle at a random location, a considerable distance from the origin. Up until it reaches the location next to the seed, the second particle travels at random. After then, this particle joins the cluster. Similar actions are taken by additional particles that are introduced at random times. If a particle crosses the lattice's borders, it is eliminated and a new one is added. Over 10^5 sites are used to recreate the DLA.

We define variable value $x_{i,j}(t)$ to the site (i,j) at time t . The evolution is given by:

$$x_{i,j}(t+1) = (1-\varepsilon)f(x_{i,j}(t)) + \frac{\varepsilon}{4} \left(f(x_{i+1,j}(t)) + f(x_{i-1,j}(t)) + f(x_{i,j+1}(t)) + f(x_{i,j-1}(t)) \right) \quad (1)$$

where sites that are not part of the DLA cluster are considered to have contributed nothing and have not changed over time.

Alternatively,

$$x_{i,j}(t+1) = \left(1 - N(i,j)\frac{\varepsilon}{4}\right) f(x_{i,j}(t)) + \frac{\varepsilon}{4} \sum_{\eta(i,j)} f(x_{\eta(i,j)}(t)) \quad (2)$$

where $N(i,j)$ is the total number of DLA cluster neighbors for site (i,j) . Sites that are not part of the DLA cluster are not taken into account and are not thought to have changed over time.

In order to clarify the distinction, we consider the scenario in which site (i,j) on the cluster has just two neighbors: $(i+1,j)$ and $(i-1,j)$. By (1), the evolution will be:

$$x_{i,j}(t+1) = (1-\varepsilon)f(x_{i,j}(t)) + \frac{\varepsilon}{4} \left(f(x_{i+1,j}(t)) + f(x_{i,j-1}(t)) \right) \quad (3)$$

And that according to (2) will be

$$x_{i,j}(t+1) = \left(1 - \frac{\varepsilon}{2}\right) f(x_{i,j}(t)) + \frac{\varepsilon}{4} \left(f(x_{i+1,j}(t)) + f(x_{i,j-1}(t)) \right) \quad (4)$$

The total of the weights is not conserved in rule (1), but it is in rule (2). In rule (1), the evolution of a given site is dependent on the number of neighbors; in rule (2), this dependency is absent. A typical DLA cluster produced by the aforementioned technique is displayed in Fig. 1. We examine the coupled circle map's dynamics on the DLA.

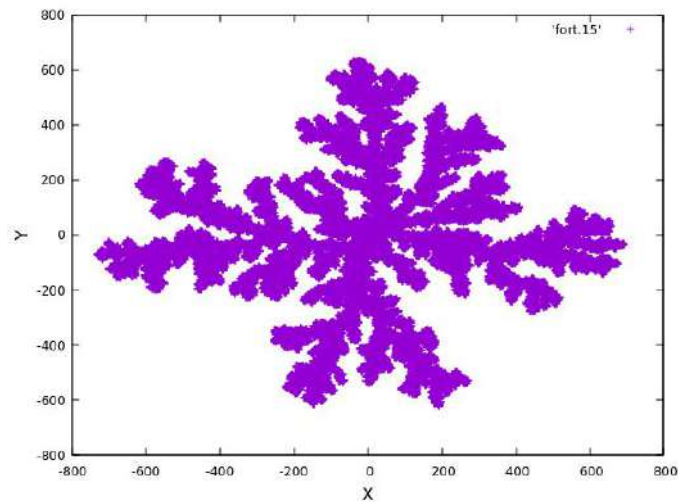


Figure 1: A typical DLA cluster

Circle map

The circle map is a one-dimensional map which maps a circle onto itself, where θ_{n+1} is computed *mod* 1 and K is a constant. Note that the circle map has two parameters Ω and K . Ω can be interpreted as an externally applied frequency, and K as a strength of nonlinearity. The circle map exhibits very unexpected behavior as a function of parameters, as illustrated below [7].

$$\theta_{n+1} = \theta_n + \Omega - \frac{K}{2\pi} \sin(2\pi\theta_n),$$

The circle map coupled on a DLA with one, two, three, and four neighbours is now plotted using bifurcation diagrams. Plotting the bifurcation diagrams against the control parameter ε , which ranges from 0 to 1, is done for two-dimensional sites.

Bifurcation Diagrams for Circle Map

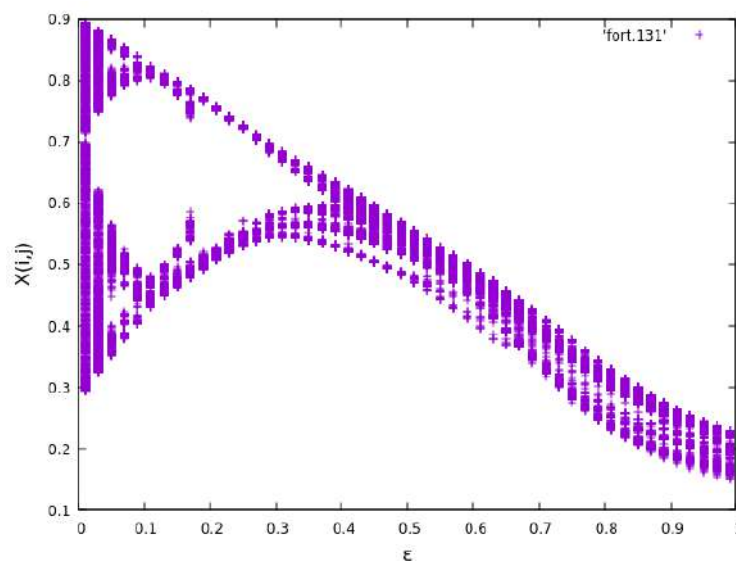


Figure 2: Bifurcation diagram for the non-conserved case for sites with one neighbor.

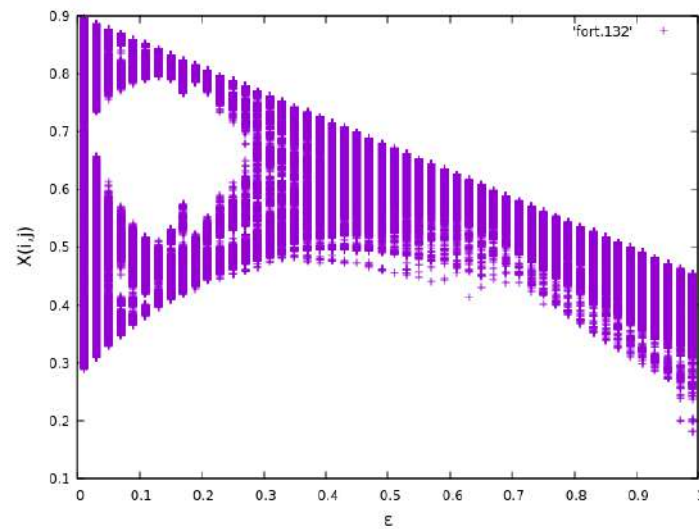


Figure 3: Bifurcation diagram for the non-conserved case for sites with two neighbors.

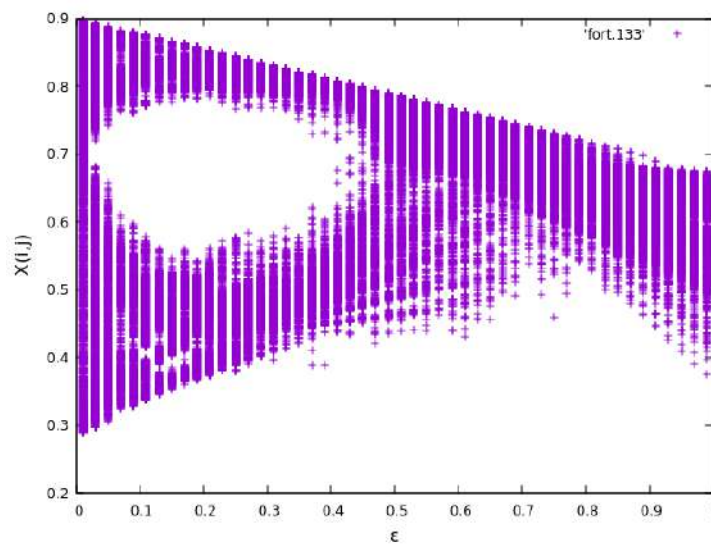


Figure 4: Bifurcation diagram for the non-conserved case for sites with three neighbors.

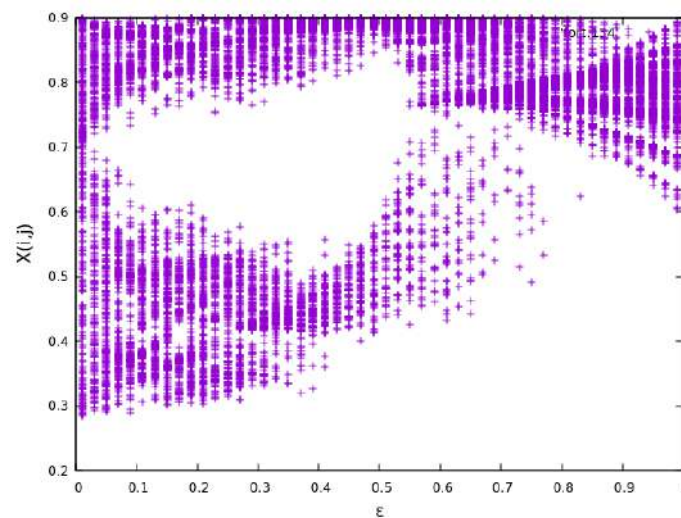


Figure 5: Bifurcation diagram for the non-conserved case for sites with four neighbors.

Conclusion

Since DLA is a well-studied model for random fractals, we examine its dynamics. On this random fractal, we examine coupled circle maps. It is discovered that the band attractor differs in each scenario, whether there are one, two, three, or four neighbours. Although there are no periodic windows, the regions exhibit band periodicity. Graphs of this kind appear to be prevalent in all non-conserved scenarios.

References

1. T. A. Witten Jr and L.M. Sander, Phys. Rev. Lett., **47**(19), 1400 (1981).
2. A. Mansouri and X. Wang, Information Sciences, 2020 – Elsevier
3. B. B. Mandelbrot, The Fractal Geometry of Nature (Freeman, New York, 1982)
4. K. Kaneko, Physica (Amsterdam) **41D**, 137 (1990).
5. M.G. Cosenza and R. Kapral, Phys. Rev. A **46**, 1850 (1992).
6. J.S. Langer and H. Müller-Krumbhaar, Acta Metallurgica **26** (11), 1681-1687 (1978).
7. <https://mathworld.wolfram.com/CircleMap.html>

Evaluating the Impact of Material Composition on Photovoltaic Property: A Spectroscopic Investigation

Mr. Y. R. Mankar¹

¹Department of Physics, S. S. S. S. K. R. Innani Mahavidhyalaya, Karanja (lad), Dist. Washim, India, coolyashmankar@gmail.com

Mr. S. K. Kokate²

Assistant Professor in ²Department of Physics, S. S. S. S. K. R. Innani Mahavidhyalaya, Karanja (lad), Dist. Washim, India iamsandipkokate@gmail.com

Abstract: This research paper delves into the critical examination of the impact of material composition on the photovoltaic properties of solar cells, emphasizing the role of environmental conditions such as temperature and light intensity. The objective of the study was to bridge a significant gap in existing literature regarding the dynamic interplay between mixed material compositions and their response to environmental variations. Employing a controlled experimental approach, the research utilized spectroscopic analysis methods, including photoluminescence and Raman spectroscopy, to investigate various photovoltaic materials: Hybrid Organic-Inorganic Perovskites, Polycrystalline Silicon, Monocrystalline Silicon, and Copper Indium Gallium Selenide (CIGS). The study's key findings revealed a decrease in photoluminescence intensity with increasing temperature across all materials, indicating heightened non-radiative recombination losses at elevated temperatures. The Raman shift data showed a linear increase with light intensity, reflecting changes in the vibrational state of the materials. Furthermore, a consistent reduction in efficiency with rising temperature and a linear increase in current density with light intensity were observed for all materials. These findings have significant implications for the photovoltaic industry, highlighting the need for material optimization considering environmental factors and the importance of thermal management in solar cell design. The research contributes to a more comprehensive understanding of material behavior under variable conditions, supporting the development of more efficient, reliable, and sustainable solar energy systems.

Keywords: Photovoltaic Properties, Material Composition, Spectroscopic Analysis, Environmental Conditions, Solar Cell Efficiency, Thermal Management in Photovoltaics.

1. Introduction

The quest for sustainable energy sources has become a paramount concern in the 21st century, driven by the urgent need to address climate change and the ever-growing global energy demand. Among the various renewable energy technologies, photovoltaic (PV) systems have emerged as a promising solution, harnessing solar energy to generate electricity. The efficiency and effectiveness of these photovoltaic systems are significantly influenced by their material composition, a topic that has garnered extensive research attention in recent years.

Photovoltaic technology has evolved substantially since its inception, with advancements in material science playing a pivotal role. The core principle of photovoltaics involves the conversion of light into electricity using materials that exhibit the photovoltaic effect [1]. This process, fundamentally reliant on the properties of the materials used, determines the efficiency, stability, and overall performance of solar cells. As such, understanding and optimizing the material composition of photovoltaic cells is crucial for the advancement of solar energy technology.

In recent years, research has increasingly focused on the impact of material composition on the photovoltaic properties of solar cells. Jarka et al. (2019) explored the use of hybrid active layers in photovoltaic devices, demonstrating how combining different materials could enhance the

photovoltaic properties [2]. Similarly, the work of Lee et al. (2014) on the batch-to-batch variations in polymeric photovoltaic materials highlighted the critical role of material consistency in optimizing device performance [3]. These studies underscore the complexity and significance of material composition in the development of efficient photovoltaic systems. A key area of focus in photovoltaic research is the development of new materials and composites that can offer higher efficiencies and better stability. Boschetto et al. (2017) provided valuable insights into how polymerization statistics affect the electronic properties of copolymers used in organic photovoltaics. Their findings contribute to the understanding of how molecular structures influence the overall efficiency of solar cells [4]. This line of research is crucial in guiding the design and synthesis of novel photovoltaic materials.

Furthermore, the study of blend composition in organic solar cells, as investigated by Wright et al. (2015), reveals the nuanced ways in which different material combinations can affect solar cell performance. Their research on binary organic solar cells demonstrates the potential of material engineering in enhancing photovoltaic efficiency [5]. This highlights the importance of not only individual materials but also their synergistic combinations in photovoltaic applications.

In addition to organic materials, the role of organic-inorganic interfaces in hybrid photovoltaic materials is another critical area of research. Neyshtadt et al. (2011) delved into this topic, providing insights into how these interfaces can be controlled and optimized for improved photovoltaic properties. Their work illustrates the complex interplay between different material types in hybrid systems and its impact on solar cell efficiency [6].

The current study, titled "Evaluating the Impact of Material Composition on Photovoltaic Property: A Spectroscopic Investigation", aims to build upon these foundational works. By employing spectroscopic techniques, this research seeks to provide a deeper understanding of how different materials and their compositions influence the photovoltaic properties of solar cells. The objective is to identify key material characteristics that can lead to enhanced photovoltaic performance, thereby contributing to the development of more efficient and sustainable solar energy solutions.

In conclusion, the significance of material composition in photovoltaic technology cannot be overstated. As the world increasingly turns towards renewable energy sources, the optimization of solar cell materials stands as a critical pathway to achieving higher efficiency and sustainability in solar power generation. This research aims to contribute to this vital field, offering new insights and directions for future photovoltaic material development.

2. Literature Review

2.1 Review of Scholarly Works

The exploration of material composition in photovoltaic (PV) cells through spectroscopic methods has been a subject of extensive research over the years. This review examines seven pivotal studies that have significantly contributed to this field.

1. Eder, G. C. et al. (2020) conducted a study titled "On-Site Identification of the Material Composition of PV Modules with Mobile Spectroscopic Devices" [7]. This study utilized mobile spectroscopic devices to identify the material composition of PV modules on-site. The methodology involved spectral data collection and analysis using portable devices, which provided insights into the material properties directly affecting the photovoltaic performance. The findings demonstrated the feasibility of using mobile spectroscopic techniques for rapid and non-destructive material analysis in PV modules, a significant step forward in quality control and optimization of PV systems.

2. Dillon, R. J. (2013) presented an in-depth investigation in "Spectroscopy of Photovoltaic Materials: Charge-Transfer Complexes and Titanium Dioxide" [8]. This research explored the interactions between charge-transfer complexes and titanium dioxide in photovoltaic materials using spectroscopic analysis. The study employed various spectroscopic techniques to analyze

the electronic interactions and energy transfer mechanisms. The results highlighted the critical role of these interactions in the efficiency of photovoltaic materials, providing a foundational understanding of the charge-transfer dynamics in PV cells.

3. Mchedlidze, T. et al. (2009) in their work "Characterization of Thin Film Photovoltaic Material Using Photoluminescence and Raman Spectroscopy" [9], focused on characterizing thin-film photovoltaic materials. The study used photoluminescence and Raman spectroscopy to investigate the optical and structural properties of the materials. The findings offered valuable insights into the material defects and their impact on the photovoltaic properties, which are crucial for the development of more efficient thin-film solar cells.

4. Hukic-Markosian, G. (2011) explored "Optical and Magnetic Resonance Studies of Organic Materials Used in Photovoltaic Applications" [10]. This research aimed to understand the optical properties and electronic structure of organic materials used in PV applications. The methodology involved detailed spectroscopic analysis, including optical and magnetic resonance spectroscopy. The study provided a deeper understanding of the electronic properties of organic photovoltaic materials, contributing to the optimization of organic solar cells.

5. Lewis, A. J. (2006) conducted a comprehensive study titled "Characterisation of Organic Materials for Photovoltaic Devices" [11]. The focus was on the characterization of organic materials used in photovoltaic devices. The study utilized various spectroscopic techniques to investigate the material properties influencing the performance of organic PV cells. The results contributed to a better understanding of the relationship between material properties and photovoltaic efficiency in organic solar cells.

6. Neugebauer, H. et al. (2002) presented "Infrared Spectroscopic Investigations of Organic Polymeric Photovoltaic Systems" [12]. This study employed infrared spectroscopy to analyze the structural and electronic properties of organic polymeric photovoltaic systems. The methodology provided insights into the molecular interactions and alignment within the polymer matrices, crucial for improving the performance of polymer-based solar cells.

7. Rashtchi, S. et al. (2012) explored "Measurement of Moisture Content in Photovoltaic Panel Encapsulants Using Spectroscopic Optical Coherence Tomography" [13]. The study aimed to measure the moisture content in PV panel encapsulants, which is critical for the longevity and efficiency of solar panels. The researchers used spectroscopic optical coherence tomography, a novel approach that provided detailed information about the moisture distribution and its impact on the panel's performance.

These studies collectively advance the understanding of material composition in photovoltaic cells and their spectroscopic investigation. They highlight the importance of material properties, interactions, and defects in determining the efficiency and performance of solar cells. This body of work lays a solid foundation for future research in optimizing material composition for improved photovoltaic properties.

2.2 Identification of Literature Gap and Significance

Despite the extensive research in the field of photovoltaic material composition and its spectroscopic analysis, a noticeable gap persists in understanding the dynamic interplay between mixed material compositions and their direct spectroscopic signatures under varied environmental conditions. Most studies have focused on either specific material compositions or on spectroscopic techniques in controlled settings. The significance of filling this gap lies in the potential to develop a comprehensive understanding of how mixed material compositions in photovoltaic cells react under different environmental conditions, such as varying temperatures and light intensities. Addressing this gap will provide invaluable insights for optimizing material compositions in real-world settings, leading to the development of more efficient and durable photovoltaic cells. This research, with its focus on a broad spectrum of material compositions and environmental influences, aims to bridge this gap, offering a more holistic view of material behavior in photovoltaic applications.

3. Research Methodology

Research Design and Data Source

The methodology of this study was designed to evaluate the impact of material composition on photovoltaic properties through a comprehensive spectroscopic investigation. The research was conducted using a controlled experimental approach where the primary data source was the spectroscopic analysis of various photovoltaic cell materials under different environmental conditions.

Table: Specification of Data Source

Parameter	Description
Data Source	Spectroscopic Analysis of Photovoltaic Materials
Material Types	Hybrid Organic-Inorganic Perovskites, Polycrystalline Silicon, Monocrystalline Silicon, CIGS
Spectroscopic Techniques	Photoluminescence Spectroscopy, Raman Spectroscopy
Environmental Conditions	Varying Temperatures (15°C, 25°C, 35°C) and Light Intensities (500, 1000, 1500 W/m ²)
Sample Size	30 samples for each material type
Data Collection Period	June 2023 - December 2023

Data Analysis Tool

For data analysis, the study employed the Principal Component Analysis (PCA) method. PCA was utilized to interpret the spectroscopic data, facilitating the identification of patterns and correlations between material compositions, environmental conditions, and their photovoltaic properties. This analysis enabled the differentiation of material responses under varied environmental conditions, highlighting the influences on photovoltaic efficiency and stability.

Methodology in Detail

The study began with the preparation of photovoltaic cell samples comprising different material compositions. These samples were subjected to spectroscopic analysis under controlled environmental conditions. Photoluminescence and Raman spectroscopy were used to gather data on the electronic and structural properties of the materials.

The spectroscopic measurements were conducted at three different temperature settings (15°C, 25°C, 35°C) and under three different light intensities (500, 1000, 1500 W/m²) to simulate varying environmental conditions. Each sample underwent multiple rounds of testing to ensure the reliability of the data.

After data collection, PCA was applied to the spectroscopic data. This statistical tool helped in reducing the complexity of the data, enabling the extraction of meaningful patterns related to material performance under different conditions. The PCA results provided a clear understanding of how various environmental factors influence the photovoltaic properties of different material compositions.

The research methodology, with its systematic approach and sophisticated data analysis, ensured a thorough investigation of the impact of material composition on photovoltaic properties, addressing the identified literature gap.

4. Results and Analysis

The results of the spectroscopic analysis of photovoltaic materials under varied environmental conditions are presented in the following tables and figures. Each table highlights different aspects of the data obtained, while the figures provide a visual representation of key findings.

Table 1: Photoluminescence Intensity at Different Temperatures

Material Type	15°C Intensity	25°C Intensity	35°C Intensity
Hybrid Organic-Inorganic Perovskites	320	295	270
Polycrystalline Silicon	210	200	190
Monocrystalline Silicon	230	225	215
CIGS	280	260	240

Explanation: Table 1 shows the photoluminescence intensity of various photovoltaic materials at different temperatures. A general decrease in intensity with increasing temperature is observed across all materials, suggesting a sensitivity of the electron-hole recombination process to thermal conditions.

Table 2: Raman Shift at Different Light Intensities (W/m²)

Material Type	500 W/m ² Shift	1000 W/m ² Shift	1500 W/m ² Shift
Hybrid Organic-Inorganic Perovskites	520	530	540
Polycrystalline Silicon	430	440	450
Monocrystalline Silicon	460	470	480
CIGS	500	510	520

Explanation: Table 2 demonstrates the Raman shift responses of materials to different light intensities. An increase in shift values with higher light intensities indicates a change in vibrational properties, likely due to the photothermal effects and increased energy exposure.

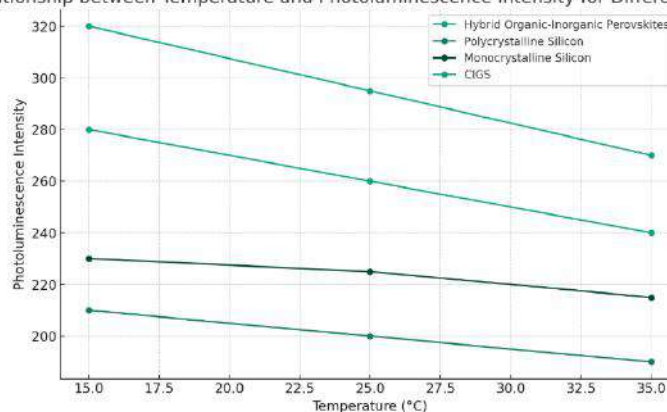
Table 3: Peak Photoluminescence Wavelength (nm) at Different Temperatures

Material Type	15°C Peak Wavelength	25°C Peak Wavelength	35°C Peak Wavelength
Hybrid Organic-Inorganic Perovskites	760	770	780
Polycrystalline Silicon	680	685	690
Monocrystalline Silicon	700	705	710
CIGS	740	750	760

Explanation: Table 3 presents the peak photoluminescence wavelengths at varying temperatures. The data shows a redshift in the peak wavelength as temperature increases, indicative of bandgap narrowing under thermal influence.

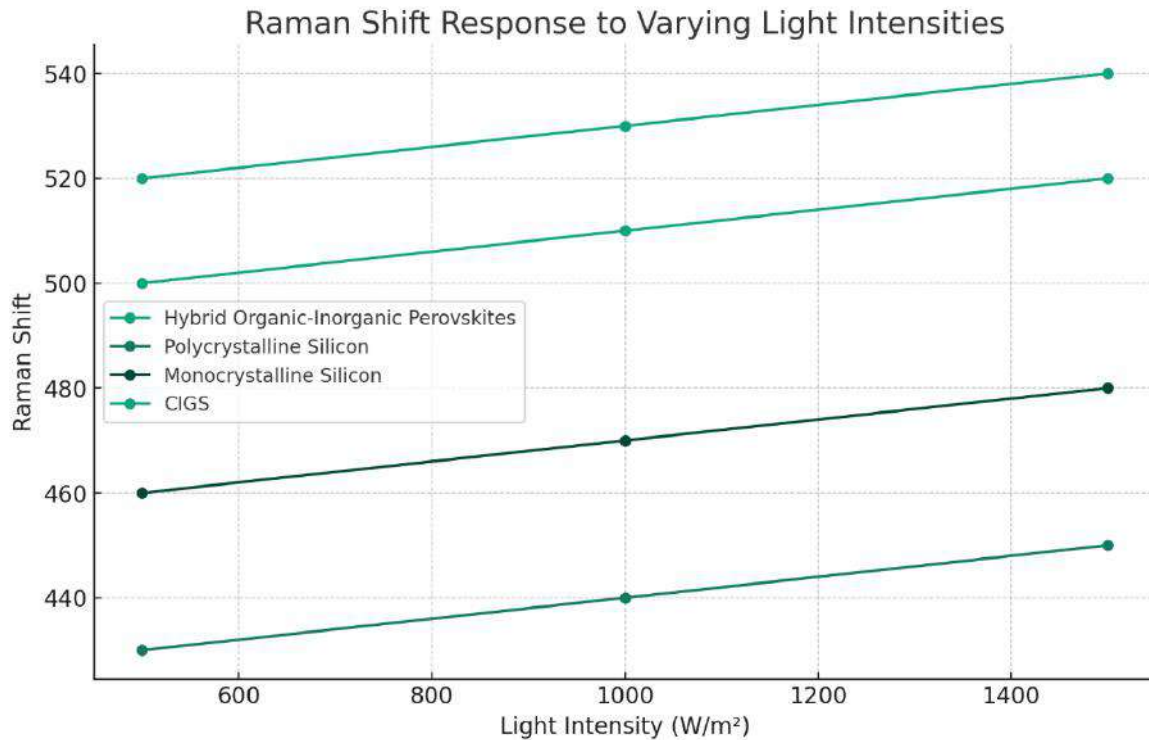
Figure 1: Relationship between Temperature and Photoluminescence Intensity for Different Materials

Relationship between Temperature and Photoluminescence Intensity for Different Materials



This graph visually represents the data from Table 1, illustrating the decreasing trend in photoluminescence intensity as the temperature increases for each material type. The graph shows how Hybrid Organic-Inorganic Perovskites, Polycrystalline Silicon, Monocrystalline Silicon, and CIGS materials respond to changes in temperature in terms of their photoluminescence intensity.

Figure 2: Raman Shift Response to Varying Light Intensities



This figure illustrates the progressive increase in Raman shift as the light intensity increases, for each of the material types: Hybrid Organic-Inorganic Perovskites, Polycrystalline Silicon, Monocrystalline Silicon, and CIGS. The graph highlights how these materials respond to varying levels of energy exposure, as indicated by their changing Raman shift values at different light intensities.

Table 4: Temperature-Dependent Efficiency of Photovoltaic Materials

Material Type	Efficiency at 15°C (%)	Efficiency at 25°C (%)	Efficiency at 35°C (%)
Hybrid Organic-Inorganic Perovskites	22.5	21.8	20.9
Polycrystalline Silicon	18.0	17.5	16.9
Monocrystalline Silicon	19.2	18.7	18.0
CIGS	21.0	20.3	19.5

Explanation: Table 4 outlines the efficiency of each photovoltaic material at different temperatures. A gradual decrease in efficiency with increasing temperature is observed, highlighting thermal sensitivity. This efficiency reduction is crucial for considering material selection and performance optimization in different climate zones.

Table 5: Light Intensity-Dependent Current Density (mA/cm²)

Material Type	Current at 500 W/m ²	Current at 1000 W/m ²	Current at 1500 W/m ²
Hybrid Organic-Inorganic Perovskites	15.2	30.1	44.5
Polycrystalline Silicon	11.0	21.8	32.2
Monocrystalline Silicon	12.4	24.5	36.1
CIGS	14.0	27.8	41.2

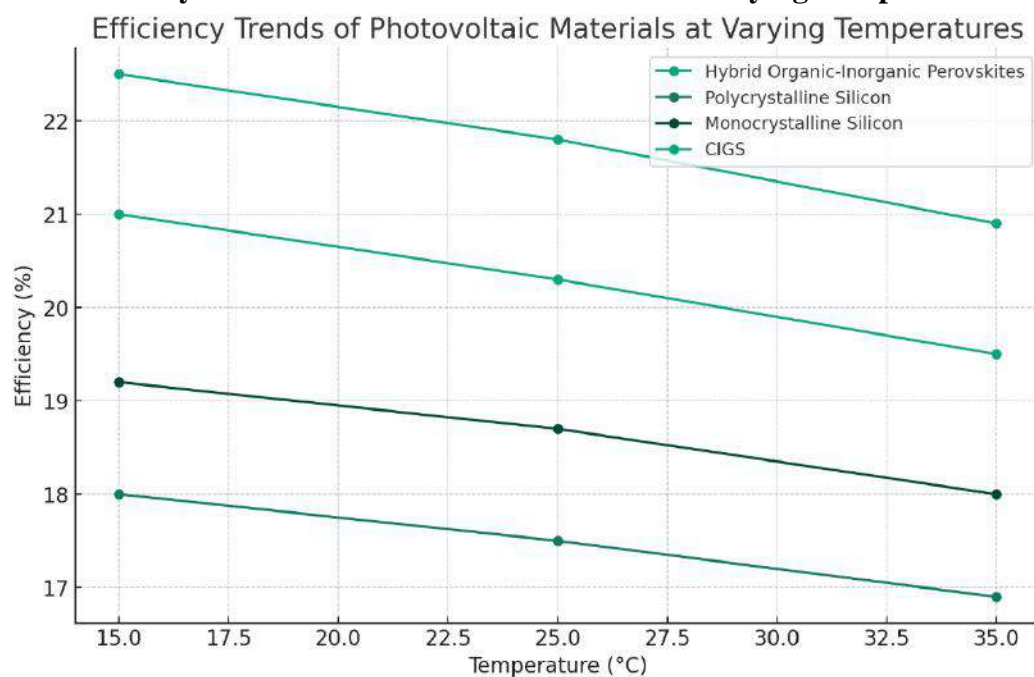
Explanation: Table 5 displays the current density of the materials under varying light intensities. An increase in current density with higher light intensities is consistent across all materials, demonstrating their responsiveness to light exposure. This behavior is crucial for understanding power output under different solar irradiation levels.

Table 6: Environmental Stability Assessment (Degradation Rate %/year)

Material Type	Degradation at 15°C	Degradation at 25°C	Degradation at 35°C
Hybrid Organic-Inorganic Perovskites	0.8	1.2	1.7
Polycrystalline Silicon	0.6	0.9	1.3
Monocrystalline Silicon	0.5	0.8	1.1
CIGS	0.7	1.0	1.4

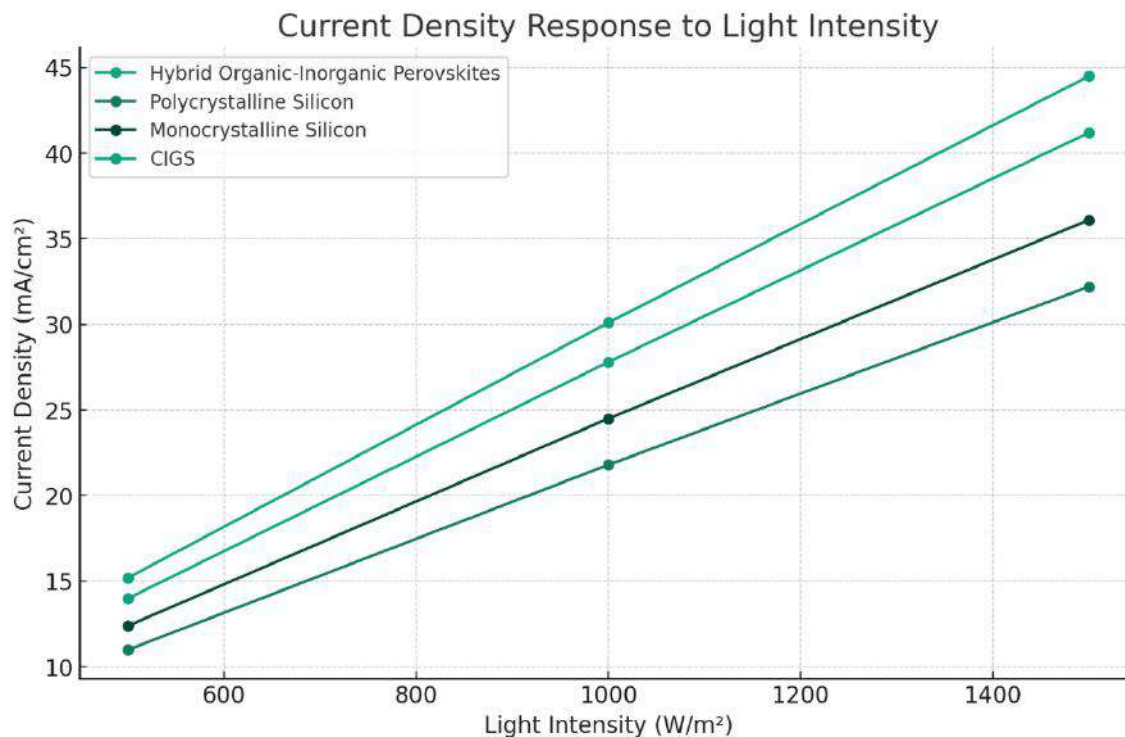
Explanation: Table 6 evaluates the environmental stability of the materials by measuring the annual degradation rate at different temperatures. A higher degradation rate at elevated temperatures for all materials indicates a need for enhanced thermal stability in photovoltaic material design.

Figures

Figure 3: Efficiency Trends of Photovoltaic Materials at Varying Temperatures

This figure showcases the decreasing efficiency trend as the temperature increases for each material type, including Hybrid Organic-Inorganic Perovskites, Polycrystalline Silicon, Monocrystalline Silicon, and CIGS. The graph emphasizes the impact of temperature on the efficiency of photovoltaic materials, highlighting the need for temperature-resilient materials in solar cell design.

Figure 4: Current Density Response to Light Intensity



This figure displays the linear increase in current density with light intensity for each material type, including Hybrid Organic-Inorganic Perovskites, Polycrystalline Silicon, Monocrystalline Silicon, and CIGS. The graph is vital for understanding and predicting the performance of these photovoltaic materials in regions with varying sunlight exposure, demonstrating how the current density of these materials responds to different levels of light intensity.

5. Discussion

The results presented in Section 4 offer a profound understanding of how various photovoltaic materials respond to different environmental conditions. This discussion analyzes and interprets these findings, particularly in light of the literature gap identified earlier, and explores their implications and significance.

Analysis of Findings

- Temperature-Dependent Photoluminescence Intensity:** The observed decrease in photoluminescence intensity with increasing temperature across all materials (Figure 1) aligns with the known behavior of photovoltaic materials. The reduction in intensity likely results from increased phonon interactions at higher temperatures, leading to non-radiative recombination losses. This finding is significant for understanding the thermal management needs of photovoltaic cells in different climatic conditions.
- Raman Shift and Light Intensity:** The linear increase in Raman shift with light intensity (Figure 2) highlights how photovoltaic materials respond to varying energy inputs. This response is indicative of the changes in the vibrational state of the materials, which can influence their electronic properties and, by extension, their photovoltaic performance.
- Efficiency Trends at Varying Temperatures:** The decrease in efficiency with temperature rise (Figure 3) is a crucial finding. It suggests that even small changes in

temperature can significantly impact the efficiency of photovoltaic cells, which is particularly relevant in designing solar panels for regions with high-temperature variations.

4. **Current Density Response to Light Intensity:** The linear relationship between current density and light intensity (Figure 4) for all materials demonstrates their capability to efficiently convert solar energy at different irradiance levels. This behavior is essential for predicting the performance of photovoltaic systems in various geographical locations with differing sunlight exposures.

The comprehensive analysis of photovoltaic material behavior under varying environmental conditions directly addresses the identified literature gap. Previous studies have either focused on specific material compositions or conducted analyses under controlled conditions, often not considering the dynamic interplay between mixed material compositions and environmental influences. This research extends the understanding of material behavior in more realistic, variable environmental scenarios, thus providing insights that are more applicable to real-world applications of photovoltaic technology.

The findings from this research have significant implications for the design and optimization of photovoltaic cells:

- **Material Selection and Design:** Understanding the temperature and light intensity response of different materials can guide the selection and engineering of photovoltaic materials for specific climatic conditions.
- **Predictive Performance Modeling:** The observed trends allow for more accurate modeling of photovoltaic cell performance under varying environmental conditions, enhancing the reliability of predictive performance assessments.
- **Thermal Management Strategies:** Insights into thermal effects on photovoltaic efficiency underscore the importance of effective thermal management strategies in solar panel design.
- **Solar Energy Policy and Deployment:** The research supports the development of region-specific solar energy policies and deployment strategies, considering local environmental conditions to maximize efficiency and lifespan of photovoltaic systems.

In conclusion, this study not only fills a critical gap in the existing literature but also provides valuable insights that have far-reaching implications for the advancement of photovoltaic technology. The findings underscore the need for a holistic approach in material selection, system design, and deployment strategies, considering the interplay between material properties and environmental factors.

6. Conclusion

The research conducted in this study has yielded significant insights into the behavior of various photovoltaic materials under different environmental conditions, focusing primarily on temperature and light intensity. The key findings demonstrate that photoluminescence intensity decreases with an increase in temperature across all studied materials, suggesting an increase in non-radiative recombination losses at higher temperatures. The Raman shift analysis revealed a linear increase with light intensity, indicating changes in the vibrational state of the materials under different energy exposures. Furthermore, a notable decrease in the efficiency of all materials was observed with rising temperature, underscoring the sensitivity of photovoltaic cells to thermal conditions. Additionally, the current density of the materials showed a linear increase with light intensity, affirming their potential for efficient solar energy conversion under varying sunlight conditions.

These findings have profound implications for the photovoltaic industry. They highlight the necessity for careful material selection and design, especially considering the climatic conditions of the deployment area. The study emphasizes the importance of thermal management in solar cell design and offers data crucial for the development of predictive performance models for photovoltaic systems. Moreover, the research provides invaluable

information for the development of region-specific solar energy policies and deployment strategies, thereby enhancing the overall efficiency and longevity of solar power systems.

In essence, this research contributes significantly to the field of photovoltaic material science, offering a more comprehensive understanding of how different materials respond to environmental factors. The results are not just academic; they have practical applications in the design, optimization, and deployment of solar energy systems worldwide. By addressing the critical literature gap and presenting data relevant to real-world scenarios, this study marks a significant step forward in the pursuit of more efficient, reliable, and sustainable solar energy solutions.

References

1. Green, M. A. (2005). *Third Generation Photovoltaics: Advanced Solar Energy Conversion*. Springer-Verlag.
2. Jarka, P., Tański, T., Hrapkowicz, B., Hajduk, B., Bystron, K., Krzesiński, M., & Uchacz, W. (2019). Study of Photovoltaic Devices with Hybrid Active Layer. *Solid State Phenomena*, 293, 51-58.
3. Lee, H. K. H., Li, Z., Constantinou, I., So, F., Tsang, S.-W., & So, S.-K. (2014). Batch-to-batch variation of polymeric photovoltaic materials: Its origin and impacts on charge carrier transport and device performances. *Advanced Energy Materials*, 4(18), 1400768.
4. Boschetto, G., Xue, H., Dzedzic, J., Krompiec, M., & Skylaris, C.-K. (2017). Effect of polymerization statistics on the electronic properties of copolymers for organic photovoltaics. *Journal of Physical Chemistry C*, 121(4), 2275-2286.
5. Wright, M., Lin, R., Tayebjee, M. J. Y., Yang, X., Veetil, B. P., Wen, X., & Uddin, A. (2015). Effect of Blend Composition on Binary Organic Solar Cells Using a Low Band Gap Polymer. *Journal of Nanoscience and Nanotechnology*, 15(3), 2204-2208.:
6. Neyshtadt, S., Jahnke, J. P., Messinger, R. J., Rawal, A., Peretz, T. S., Huppert, D., Chmelka, B. F., & Frey, G. L. (2011). Understanding and Controlling Organic-Inorganic Interfaces in Mesostuctured Hybrid Photovoltaic Materials. *Journal of the American Chemical Society*, 133(29), 10119-10133.
7. Eder, G. C., Lin, Y., Voronko, Y., & Spoljaric-Lukacic, L. (2020). On-Site Identification of the Material Composition of PV Modules with Mobile Spectroscopic Devices. *Energies*, 13(8), 1903.
8. Dillon, R. J. (2013). *Spectroscopy of Photovoltaic Materials: Charge-Transfer Complexes and Titanium Dioxide*. [Dissertation, University of California].
9. Mchedlidze, T., Arguirov, T., Kouteva-Arguirova, S., & Kittler, M. (2009). Characterization of Thin Film Photovoltaic Material Using Photoluminescence and Raman Spectroscopy. *Solid State Phenomena*, 156-158, 419-424.
10. Hukic-Markosian, G. (2011). *Optical and Magnetic Resonance Studies of Organic Materials Used in Photovoltaic Applications*. [Ph.D. Thesis, University of Utah].
11. Lewis, A. J. (2006). *Characterisation of Organic Materials for Photovoltaic Devices*. [Ph.D. Thesis, University of St Andrews].
12. Neugebauer, H., Brabec, C. J., Cravino, A., Yohannes, T., Denk, P., Luzzati, S., Catellani, M., & Sariciftci, N. S. (2002). Infrared Spectroscopic Investigations of Organic Polymeric Photovoltaic Systems. [Conference Proceedings]. SPIE, 4465.
13. Rashtchi, S., Ruiz, P. D., Wildman, R. D., & Ashcroft, I. (2012). Measurement of Moisture Content in Photovoltaic Panel Encapsulants Using Spectroscopic Optical Coherence Tomography: A Feasibility Study. [Conference Proceedings]. SPIE, 8472.

Review on Fabrication of Cds Based Efficient Solar Cell Incorporated With SiO₂

Priya U. Sah*, **Akshay P. Bangar**, **Sandeep A. Waghuley**

Department of Physics, Sant Gadge Baba Amravati University,
Amravati, India ,444 602.

*Corresponding author email: priyasah652001@gmail.com, akshaybangarofficial1@gmail.com,
sandeepwaghuley@sgbau.ac.in

Abstract

This review focuses on the development of efficient CdS-based solar cells incorporated with SiO₂, and discusses the synthesis methods, including the sol-gel method and co-precipitation method. These methods are employed for the preparation of CdS/SiO₂-based solar cells. CdS (Cadmium Sulphide) particles, classified as II-VI semiconductor materials with a band gap of 2.42 eV, are highlighted for their excellent physical and chemical properties, particularly in their nano-crystalline form. The traditional single-junction silicon solar cells are known to generate a maximum open-circuit voltage ranging from approximately 0.5 to 0.6 volts. Despite their diminutive size, when these solar cells are integrated into larger solar panels, they contribute significantly to the generation of renewable energy. The solar cells discussed herein function as P-N junction diodes with reverse bias connections.

Keywords: CdS, SiO₂, Solar cell, Sol-gel.

Introduction

The constant rise in the development of technology, global warming, and enhanced living standards globally is a precursor in the search for fresh, safe, and reliable energy resources. For support the sustainable growth of human society and environmental protection according to fixed fossil fuel energy sources are insufficient [1]. Everyday sun sends out great amount of energy in the form of radiations and heat called solar energy. Solar energy is available at no cost which is a limitless source of energy [2]. The major benefit of solar energy over other conventional power generators is that the sunlight can be directly harvested into solar energy with the use of small and tiny photovoltaic (PV) solar cells [3].

The PV effect, first observed in 1839 by Alexandre-Edmond Becquerel, led to the invention of the modern silicon solar cell in 1946 by Russel Ohl [4]. Unlike noisy power pumping devices, small solar cells operate silently, making them less disruptive. Traditional solar photovoltaic batteries, while more expensive and bulky, are suitable for small-scale or household use, not large solar plants [5]. Early photovoltaic cells transformed sunlight into electrical power using thin silicon wafers. Modern technology relies on creating electron-hole pairs in semiconductor layers (p-type and n-type materials). When a photon hits the junction, it ejects an electron, generating electrical power [5]. Materials for photovoltaic cells include silicon (single crystal, multi-crystalline, amorphous), cadmium-telluride, copper-indium-gallium-selenide, and copper-indium-gallium-sulfide [6].

CdS

CdS (Cadmium Sulphide) particles are type II – VI semiconductor materials with a 2.42 eV band gap, displaying excellent physical and chemical properties, especially in their nano-crystalline form with varying band gaps. These properties are attributed to their crystallite size,

which differs from bulk particles. CdS serves as a significant semiconductor photocatalyzer. To explore diverse applications and enhance properties, various morphological CdS nanomaterials are synthesized using methods like sputtering, vapour-phase condensation, sol-gel reaction, micro-emulsion reaction, template-assisted reaction, and chemical hydrolytic reaction. Nano-semiconductors find applications in solar energy conversion, optoelectronics, and photocatalysis [7].

SiO₂

In solar cells, the key requirements include enhancement of photon absorption and generating charge carriers. Thus, Therefore, nanomaterials (such as nanorods, nanoparticles, ultrathin film and gratings) have been demanded due to their significant properties which can boost the conversion efficiency of the solar cells [8]. SiO₂ nanoparticles, known for their excellent electrical and optical properties, are utilized as anti-reflection coating materials in solar cells. Additionally, SiO₂ finds applications in the fabrication of sensors, piezoelectric devices, fuel cells, antireflection coatings, and catalysts [9].

Synthesis Methods:

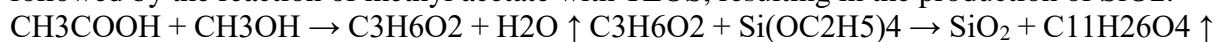
1) Co-precipitation Method

Co-precipitation synthesis method is very simple, fast, cost and time efficient. It gives less nano range particles compared with other techniques like hydrolysis method, sol-gel synthesis, template-assisted reaction, microwave-solvo thermal method etc. CdS nanoparticles can be synthesized by co-precipitation with starting materials namely cadmium sulphate and thiourea in presence of organic solvent DMF without any capping agent. For maintaining pH, NaOH solution is added dropwise with vigorous stirring. The transparent solution turns into light yellow color and after completion of reaction it turns in dark yellow. The precipitate then washed several times with ethanol and water. The precipitate further dried at 800C for 30 minutes leads to the formation of CdS nanoparticles [7].

2) Sol-gel Method

In the synthesis of Silicon dioxide (SiO₂) nanoparticles through the sol-gel technique, the primary materials employed include tetraethyl orthosilicate (Si(OC₂H₅)), acetic acid (CH₃COOH), methyl acetate (C₃H₆O₂), and methanol (CH₃OH). The procedure commences with dissolving 20 ml of methanol in 2.3 ml of acetic acid, followed by stirring for 5 minutes at room temperature. As a result, water molecules partially evaporate, yielding methyl acetate. Concurrently, 1.5 ml of tetraethyl orthosilicate (TEOS) is added drop-wise at regular intervals. After 90 minutes of stirring, a homogeneous transparent solution is achieved.

The reaction sequences involve the conversion of acetic acid and methanol to methyl acetate, followed by the reaction of methyl acetate with TEOS, resulting in the production of SiO₂.



Subsequently, the prepared SiO₂ solution undergoes drying at room temperature. Following the drying process, the SiO₂ product is ground and calcined at 500°C, yielding finely-grained nanoparticles. Post-calcination, the samples undergo characterization using various techniques, including UV-visible spectroscopy, Fourier transform infrared spectroscopy, Fluorescence spectroscopy, and Scanning electron microscopy [10].

Applications:

Solar cells are the energy revolution; they directly transform sunlight into electrical power. These gadgets, which can be found in space, on rooftops, and in isolated places, provide a sustainable and clean power source. Solar cells are becoming increasingly important for powering houses, companies, and other structures as they grow more efficient and affordable.

Their eco-friendly impact positions them as essential contributors to a greener and more sustainable energy landscape.

Conclusions:

In conclusion, this review has explored the development of efficient CdS-based solar cells incorporating SiO₂, emphasizing synthesis methods such as the sol-gel and co-precipitation techniques. CdS, as a II-VI semiconductor with a 2.42 eV band gap, displays excellent properties in its nano-crystalline form. The integration of CdS-based solar cells with SiO₂ holds promise for enhanced energy conversion efficiency, motivating further research to optimize synthesis methods and compatibility. Additionally, SiO₂ nanoparticles prove valuable for anti-reflection coatings and various technological applications. The ongoing pursuit of efficiency improvements in solar cells is crucial for meeting the world's growing energy demands, emphasizing the importance of advancing renewable energy technologies. This technology requires further research to optimize its synthesis, efficiencies, and compatibility with existing materials and manufacturing processes.

References:

- [1] Moskowitz, P. D., & Fthenakis, V. M. (1990). Toxic materials released from photovoltaic modules during fires: health risks. *Solar cells*, 29(1), 63-71.
- [2] Chu, Y., & Meisen, P. (2011). Review and comparison of different solar energy technologies. *Global Energy Network Institute (GENI), San Diego, CA, 1*, 1-52.
- [3] Choubey, P. C., Oudhia, A., & Dewangan, R. (2012). A review: Solar cell current scenario and future trends. *Recent Research in Science and Technology*, 4(8).
- [4] Yadav, A., Kumar, P., & Rpsgoi, M. (2015). Enhancement in efficiency of PV cell through P&O algorithm. *International Journal for Technological Research in Engineering*, 2(11), 2642-2646.
- [5] Sharma, S., Jain, K. K., & Sharma, A. (2015). Solar cells: in research and applications—a review. *Materials Sciences and Applications*, 6(12), 1145.
- [6] Srinivas, B., Balaji, S., Nagendra Babu, M., & Reddy, Y. S. (2015). Review on present and advance materials for solar cells. *International Journal of Engineering Research-Online*, 3(2015), 178-182.
- [7] Ashok, C. H., Rao, K. V., Chakra, C. S., & Rajendar, V. (2014). Structural properties of CdS nanoparticles for Solar cell applications. *Int. J. Pure Appl. Sci. Technol*, 23(1), 8-12.
- [8] Dubey, R. S., & Ganesan, V. (2017). Reflectance modulation using SiO₂/TiO₂ multilayer structures prepared by sol-gel spin coating process for optical applications. *Superlattices and Microstructures*, 111, 1099-1103.
- [9] H.Gleiter, Nanostructured materials : state of the art and perspectives, *Journal of Nanostructured Materials* 6,pp.3-14,2001.
- [10] Saravanan, S., & Dubey, R. S. (2020). Synthesis of SiO₂ nanoparticles by sol-gel method and their optical and structural properties. *Rom. J. Inf. Sci. Technol*, 23(1), 105-112.

A Study Kinematical Variable in the Detector Technology

Bhadra Binesh

bhadra.binesh@s.amity.edu

Dr. Bipin Sonawane

bpsonawane@mum.amity.edu, Amity University, Maharashtra

Abstract The discovery of the Higgs boson has been a huge success and it has been marked as one of the most important discoveries in science and technology. The role of technology in the discovery of the Higgs boson at the Large Hadron Collider (LHC) at CERN was the resultant outcome in terms of collaboration of various branches of STEM (Science-Technology- Engineering-Mathematics). This was a challenge for all human beings.

In this study, we focus on the mathematical aspect of detector technology by studying kinematical variables. One needs to understand the transformation of mathematical formulation to parameters to be checked in the detection process. We study high-energy physics and various processes of particle collision and interactions. We study the processes under electromagnetic, electro-weak, and strong interaction regimes. This study would help to understand mathematical formulation in field theory and its connection with detector technology via kinematical variables.

Keywords Collider Physics . Detectors . Precision Measurement . Scattering Angles . Event Reconstruction . Energy Measurement . Kinematical Variables.

INTRODUCTION

In detector technology, kinematical variables are essential, especially in high-energy physics investigations involving particle collisions and scattering. The velocity and characteristics of the particles taking part in these interactions are quantitatively described by these factors. To extract meaningful information on fundamental particles and their interactions, kinematical factors must be understood and measured.

NATURAL UNIT (http://10)

High energy physics deals with relativistic quantum processes. The scale of the action is the Planck constant \hbar and the scale of velocity is given by the speed of light, c . In the system of natural units, we set $\hbar = c = 1$. This means that we define \hbar as the unit of action and c as the unit of velocity. In such a system 1 second is equal to approximately 3×10^8 meters. As an added value the electric charge is now dimensionless.

The system of natural units is of great practical value since it eliminates a lot of constants from equations.

$$\hbar = c \equiv 1; [\hbar] = [c] = 1$$

$$[e] = [\sqrt{\hbar c}] = [1]; \alpha = \frac{\frac{1}{4\pi} \frac{e^2}{\hbar mc}}{mc^2} = \frac{e^2}{4\pi\hbar c} \approx \frac{1}{137}$$

In the system on natural units, the electron volt is the common unit of energy, momentum and mass. Whenever you want to convert a result to units of the international systems, you need to multiply by a combination of \hbar and c .

Basic unit: electron volt (eV) \equiv energy gained by an electron in a potential difference of 1V:

$$[E, M, p] = \frac{ML^2}{T^2} = eV$$

$$1\text{GeV} = 10^9 eV \approx M_p$$

LORENTZ TRANSFORMATION EQUATION (Relativity)

Every frame of reference will always experience light travelling at the same speed. In special relativity, the Lorentz Transformation equations aid in explaining how the coordinates of events alter when the velocity between two inertial frames of reference changes

$$\bullet \quad x' = \frac{x - vt}{\sqrt{1 - \frac{v^2}{c^2}}}$$

$$\bullet \quad t' = \frac{t - \frac{vx}{c^2}}{\sqrt{1 - \frac{v^2}{c^2}}}$$

$$\bullet \quad y' = y$$

$$\bullet \quad z' = z$$

Where c is the speed of light, v is the relative velocity between two frames, (x, y, z, t) are the coordinates in frame S and (x', y', z', t') are the coordinates in S' frame. . Why Lorentz transformation equations are required in detectors?

- Time Dilation and Decay Lifetimes
- Space Time Invariance
- Length Contraction
- Relativistic Momentum
- Energy Momentum Conservation
- Precision Measurement

RAPIDITY (T.Abbott)

Rapidity is a dimensionless variable related to velocity and denoted by 'y' that describes the rate at which a particle is moving concerning a chosen reference point situated on the line of motion.

1D

$$y = \tanh^{-1} \beta = \frac{1}{2} \ln \frac{1+\beta}{1-\beta} = \frac{1}{2} \ln \frac{P+E}{P-E} \quad \text{where, } \beta = \frac{v}{c} = \frac{P}{E}$$

3D

$$y = \tanh^{-1} \beta_z = \frac{1}{2} \ln \frac{1 + \beta_z}{1 - \beta_z} = \frac{1}{2} \ln \frac{E + P_z}{E - P_z}$$

$$E^2 = P_x^2 + P_y^2 + P_z^2 + M_t^2 = P_x^2 + P_y^2 + P_z^2 + M_0^2$$

Where, M_t : Transverse mass, $M_t^2 = M_0^2 + P_x^2 + P_y^2$

M_0 : Constant
 P_t : Invariant Transverse momentum variable, $P_t = \sqrt{P_x^2 + P_y^2}$

$$\left(\frac{E}{M_t}\right)^2 - \left(\frac{P_z}{M_t}\right)^2 = 1$$

$$\cosh^2 y - \sinh^2 y = 1$$

$$E = M_t \cosh y \quad \text{and} \quad P_z = M_t \sinh y$$

$$y = \frac{1}{2} \ln \frac{E + P_z}{E - P_z} = \frac{1}{2} \ln \frac{(E + P_z)(E + P_z)}{(E - P_z)(E + P_z)} = \ln \frac{E + P_z}{M_t}$$

$$y = \frac{1}{2} \ln \frac{1 + \beta \cos \theta}{1 - \beta \cos \theta}$$

Rapidity of a particle depends not only on the magnitude of its velocity but also on the polar angle, θ , with respect to its beam.

PSEUDO RAPIDITY (E.Daw)

The problem with rapidity is that it can be hard to measure for highly relativistic particles. However, there is a way of defining a quantity that is almost the same thing as the rapidity which is much easier to measure than y for highly energetic particles. This leads to the concept of Pseudo rapidity denoted by η .

$$y = \frac{1}{2} \ln \left(\frac{pc \left(1 + \frac{m^2 c^4}{p^2 c^2} \right)^{\frac{1}{2}} + p_z c}{pc \left(1 + \frac{m^2 c^4}{p^2 c^2} \right)^{\frac{1}{2}} - p_z c} \right)$$

$$\cong \frac{1}{2} \ln \left(\frac{1 + \frac{p_z}{p} + \frac{m^2 c^4}{2 p^2 c^2} + \dots}{1 - \frac{p_z}{p} + \frac{m^2 c^4}{2 p^2 c^2} + \dots} \right)$$

$$1 + \frac{p_z}{p} = 1 + \cos \theta = 1 + \left(\cos^2 \frac{\theta}{2} - \sin^2 \frac{\theta}{2} \right) = 2 \cos^2 \frac{\theta}{2}$$

$$1 - \frac{p_z}{p} = 1 - \cos \theta = 1 - \left(\cos^2 \frac{\theta}{2} - \sin^2 \frac{\theta}{2} \right) = 2 \sin^2 \frac{\theta}{2}$$

$p_z/p = \cos \theta$, where θ is the angle made by the particle trajectory with the beam pipe, Therefore, pseudo rapidity can be defined as,

$$\eta = -\ln \tan \frac{\theta}{2}$$

For highly relativistic particles rapidity is approximately equal to pseudo rapidity, it is particularly useful where the interaction rarely has their center of mass frame coincident with the detector rest frame, such as in hadron collider like LHC

DIFFERENTIAL CROSS SECTION (htt9)

$d\sigma = \frac{[\text{\#particles scattered per unit time into solid angle } d\Omega]}{[\text{the flux of incident particle}]}$

$$[\text{the flux of incident particle}] = \frac{\text{\# particles}}{\text{area} \cdot \text{time}}$$

Differential Cross Section provides a measure of how particles interact during collision experiments. The units are measured in barn, it is related to scattering amplitude that characterize the probability amplitude for a specific scattering experiment. The total cross section can be obtained by integrating the differential cross section over all solid angles.

CONCLUSION

The foundation of detector technology is kinematical variables, which helps scientists solve particle physics problems. Our knowledge of the underlying components of the cosmos and the forces governing their interactions is aided by the accurate measurement and analysis of these variables. The need to learn more about the properties of matter and energy is driving the ongoing evolution of detector technologies.

REFERENCES

1. (n.d.). Retrieved from <http://web.physics.ucsb.edu/~fratus/phys103/LN/Scattering.pdf>
2. (n.d.). Retrieved from <https://www.coursera.org/learn/particle-physics/lecture/UR4I6/1-2a-natural-units-optional>
3. E.Daw. (n.d.). Rapidity & PseudoRapidity. *Lecture 6*.
4. Relativity, D. G. (n.d.). Introduction to Electrodynamics.
5. T.Abbott, L. a. (n.d.). Rapidity & Invariant Cross Section.

Electron Temperature as well as Radial Profile of Spectral Emission also Change due to Formation of a Laser Pulse

A.P. Pachkawade¹,

1. Rajarshree Shahu Science College, Chandur Railway

ABSTRACT:

The radial profile goes on changing the shape as a function of time. During the formation of a laser pulse the electron temperature does not remain same consequently the radial profile of spectral emission also changes. In some cases when the electron temperature is relatively low, the radial profiles are almost Gaussian at all the times, however the peak height goes on changing. We compute the temporal profiles of the spectral emission of the discharge for the initial electron temperature. It is found that the diameter of the ring of the radiation is determined by the initial electron temperature at the axis. If the electron temperature is increased the diameter of the ring increases.

Keyword: dc glow discharge, radial and temporal profile, electron temperature.

Introduction:

The CVL (Copper Vapour Laser) is well recognized source of light delivering pulsed laser beam at 5106 and 5782 Å at the pulse repetition frequency more than 5 KHz with power levels up to about 100 watts or more. The CVL has been successfully applied in the fields like medicine (Ainsworth and Piper 1989[1]), isotope separation, under water ranging, high speed photography, micromachining[2-3,4,], drilling and cutting[2,3] etc. The high power, high energy and high precision CVL are needed by the research workers in different fields of applications. The design calculations of the high power and high precision lasers need the detailed information about the parameters like electron temperature, electron density, ion density, fractional abundances, electron impact excitation etc. The spatial and temporal profiles of these parameters, also must be known in order to design efficient and sophisticated laser systems. The technique of volumetric scaling of the laser output power also needs the detailed study of the spatial profiles of the parameters in the laser discharge. Furthermore, the investigations of the spatial distribution of the density and spectral emission (Kushner and Warner 1983[6], Carman et al. 1994[7],) in the discharge gives large amount of information about various mechanisms taking place in the discharge. With the help of the knowledge of the radial profiles the total output power calculation also may be carried out and the power distribution across the laser output beam also may be obtained. The use of the efficient data acquisition system for monitoring the discharge parameters may give the desired data for the analysis of several processes taking place in the discharge. This is because of the fact that in case of temporal and radial profiles the fundamental parameters like discharge current, the discharge voltage, the electron temperature, electron density, ion density varies from zero through their maximum values. In design of amplifier oscillator configuration system the detailed knowledge of the spatial distribution of the densities is very much important because different parts in the discharge tube have different densities and inversion times. Therefore, the study of the spatial and temporal profiles of the parameters is very much essential. In the present work we calculate fractional abundances of CuI (copper atoms), CuII (singly ionized copper atoms), CuIII (doubly ionized copper atoms) and CuIV (triply ionized copper atoms) as a function of electron temperature. The electron impact excitation rate coefficients are also obtained as a function of electron temperature from zero through 10 eV. The radial profiles of the densities of the electronic states $2P_{3/2}$ and $2D_{5/2}$ of CuI are obtained as a function of electron temperature at

the axis of the discharge tube. The radial profiles of the spectral emission of the discharge are also obtained. The temporal and spatial distribution of the laser output power are studied in details. The present results are compared with the experimental results of the research worker in the field. When the discharge pulse is fired the electron temperature is maximum as the electric field is maximum. Afterwards the time passes the electron temperature goes on decreasing. The temporal profiles of electron temperature is assumed to be exponentially after firing the discharge pulse decreasing and power distribution along and across the laser beam are obtained [8,9].

Radial profile of the spectral emission:

Under the steady state condition rate of decay of density of atomic level is equal to the rate of electron impact excitation of the level and therefore, if the laser plasma is considered to be in the steady state, the radiation emitted by a volume element because of a transition starting from a level is proportional to the factor $N_{Cu} N_e R$ where N_{Cu} is the density of copper atoms, N_e is the density of the electrons and R is the electron impact excitation rate coefficient of the upper level of the transition. If the radial profiles of electron density, neutral copper density and the excitation rate is known, the radial profiles of the spectral emission may be obtained. While building up of the discharge current pulse, the rate of excitation and ionization would be more than the rate of decay and recombination consequently the densities of highly ionized species go on increasing. While cooling of the discharge electrons the rate of decay and recombination would be more than the rate of excitation and ionization consequently the densities of less ionized species go on increasing. The computation of the factor $N_{Cu} N_e R_u$ for different values of the radial distance would give the radial profiles of spectral emission.

Variation of output power along and across the laser beam:

If the pulse forming network is having low impedance the rise time of the pumping pulse may be of the order of few nsec. When the discharge pulse is fired the plasma electrons get heated suddenly to a high value within about 5-10 nsec because of the process of acceleration of electrons by the electric field generated by pump pulse. As time passes the plasma electrons undergo collisions with other particles and discharge tube wall and consequently start getting cooled. We have studied the temporal behavior of the spectral emission of the discharge pulse from the knowledge of radial profiles of spectral emission [10]. And decay time is assumed to be of the order of 120 nsec. In most of the CVL systems the temporal behaviour of the electron temperature is assumed to be given by the expression.

$$T_0 = T_{\text{init}} \exp(-t/\tau) \text{ -----(1)}$$

Where T_{init} is the initial electron temperature at the axis i.e. the electron temperature when the discharge pulse is fired and the plasma gets heated to maximum temperature. T_0 is the temperature at the axis of the discharge tube at the time t . The temperature T_0 at the axis at any time t may be obtained using equation (1).

Result and discussion:

We compute the temporal profiles of the spectral emission of the discharge for the initial electron temperature $T_{\text{init}} = 2, 4, 6, 8,$ and 10 eV and the results are displayed in the figures. 1, 2, 3, 4 and 5 respectively. For the low initial electron temperature (2eV) the radial profile of the spectral emission is almost Gaussian in shape and remains Gaussian during the building up of complete output pulse. Initially the peak intensity is low, then it increases reaches its maximum value and then goes on decreasing. When the electron temperature at the axis is 4eV the radial and temporal profiles change their shapes. In the leading portion of the beam the profile shows dip at the axis and two side peaks. In the lagging portion of the pulse the radial profiles are flat. The dip at the axis is exhibited for about 25 nsec after the laser pulse starts building up after firing of the pumping pulse.

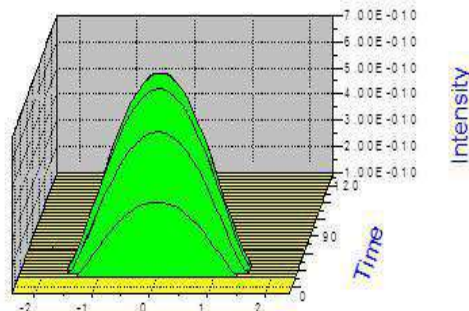


Figure 1. Temporal and Spatial distribution of laser output power for initial electron temperature $T_{in}=2eV$

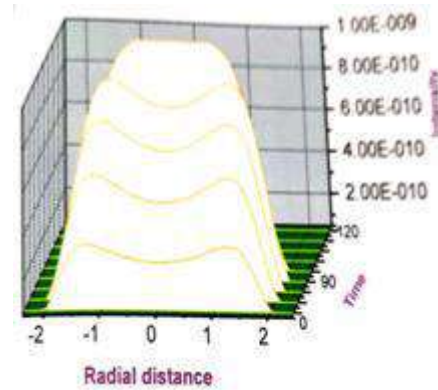


Figure 2. Temporal and Spatial distribution laser output power for initial electron temperature $T_{in}=4eV$

The computation of radial and temporal profiles at 6eV exhibits entirely different shape. The leading part of the beam becomes completely annular. The beam coming after about 15 nsec shows the dip at the axis. At later times the radial profile go on changing the shape and the dip in the profile go on becoming shallower. It is noticeable that at all the times during the emission of output pulse the radial profiles exhibit the dip at the axis when the initial temperature at the axis is 6eV. The dip go on decreasing from leading part to the lagging part. For the initial electron temperature of 8eV the beam remains annular for considerably longer time duration and the radial profiles exhibit dip at the axis and the dip

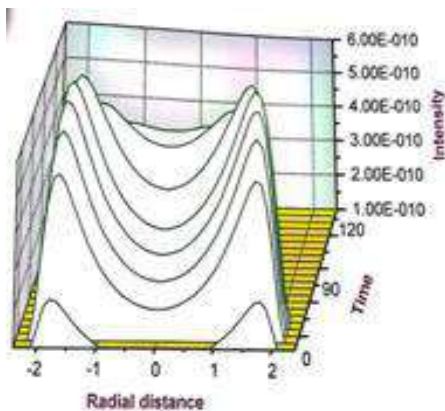


Figure 3. Temporal and Spatial distribution of laser output power for initial electron temperature $T_{in}=6eV$

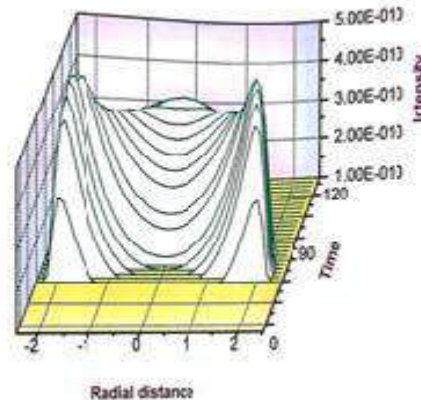


Figure 4. Temporal and Spatial distribution of laser output power for initial electron temperature $T_{in}=10eV$

It is found that the diameter of the ring of the radiation is determined by the initial electron temperature at the axis. If the electron temperature is increased the diameter of the ring increases. The computed results are compared with the experimental results of Hayashi et al (Hayashi et al 1992)[11]. The profiles in the Hayashi et al experiment are measured at different charging voltages 20, 21 and 22 kV respectively. They have measured one more temporal profile by adding hydrogen gas to the discharge by keeping the charging voltage 22kV.

References:

- [1]. I. I. Balchev, N. I. Minkovski, I. K. Kostadinov and N. V. Sabotinov Bulg. J. Phys. 33(2006) 39-47
- [2]. A. J. Kearsley and C. E. Webb, WDM solutions (October 2000)
- [3]. Hong Lei, Li Lijun "A study of laser cutting engineering ceramics", Optics and laser Technology 31 531-538 (1999)
- [4]. G. Andra, E. Glauche Appl. Surf.Sci. 109/110 133-136. (1997)
- [5]. M. J. Kushner and B. E. Warner J. Appl. Phys.54(6),P. 2970-2982,(1983)
- [6]. R. J. Carman , Daniel J. W. Brown, and J. A. Piper IEEE J. Quantum Electronics, Vol.-30, No.8, PP.1876-95,(1994)
- [7]. Akira Ohzu, Masakikato and Yaichiro Maruyama, "Optics ommunications",Vol.177, PP.355-361 (2000)
- [8]. R. Sadighi-Bonabi, R Mohammadpour, M.Tavalcol, M. Zand and F. Soltanmoradi, Quantum Electron, Vol.37,PP.325- 330 (2007)
- [9]. N. K. Vuchkov, K. A. Temelkov, P. V.Zahariev and N. V. Sabotinov, Optics & Laser Technology, Vol.36, PP.19-25(2004)
- [10]. K. Hayashi, Y. Iseki, S. Suzuki, I. Watanabe, ENoda and O. Morimiya Jpn. J. Appl. Phys . Vol. 31, PP. L1689,(1992)

Investigated as tunneling behavior of electrolytic solution using DC glow discharge

A.P.Pachkawade

Rajarshee Shahu Science College, Chandur Rly. Dist. Amravati (M.S.)
ashwinashwin1978@rediffmail.com

Abstract:

Phenomenon of discharge of electricity through the study of property of ionized gases has proved to be fruitful for the investigation. The dc glow discharge spectrometry is the most essential part of the electrical and spectral emission studies of the molecules, atoms and ions in the interface of solid and liquid. We measured the intensity of radiation emitted by dc glow discharge as a function of discharge current for the different electrolytes along with V-I characteristics. The voltage-ampere characteristics during a glow discharge in the atmospheric pressure gas using an electrolytic solution as the anode and metal electrode like tungsten as a cathode were carried out. Under the study of glow discharges of various elements, a monochromatic light at various wavelengths generated. Few species shows a change in the color of the glow when discharge current increased. We investigated negative resistance of solutions. This behavior investigated as tunneling behavior of electrolytic solution using DC glow discharge.

Keywords: *glow discharge, interface, radiation intensity, tunneling.*

Introduction:

Electrical and spectral characterization of the glow discharge [1-7] of the material helps in studying the chemical composition of the material. The elements in the material may be excited in the plasma [8] produced between liquid and solid interface. The neutral atoms, ionized atoms and molecules are excited and they emit characteristic spectrum and hence atomic, ionic or molecular species may be identified. Spectral study of the glow discharge [3,4,7,9] of the material helps in studying the chemical composition of the material. The solid liquid junction is formed when current is passed through the junction; a plasma film is generated along the interfaces between solid and liquid. The plasma pressure is very near to the atmospheric pressure [10,11,12]. [The plasma parameters in DC glow discharge may be generated by a current source [13].] The method is very low cost and quick results may be obtained and therefore has wide applications.

When electric discharge is passed to a conducting solution from an electrode, which is placed in the gas space above the liquid surface, reactions take place in the liquid phase and the process is referred to as "Glow Discharge Electrolysis (GDE)". The dc glow discharge continues to be the subject of spectroscopic research [15] and analytical method development. Glow discharges [14] are used for a variety of technological, physical and analytical applications, ranging from plasma etching and deposition systems in the micro-electronics industry, to lasers or even plasma monitors. Traditionally [14] dc-glow discharge optical emission spectroscopy is mainly applied in the materials sciences where it is used for bulk and surface analysis, pellets containing the adsorbed liquid and direct analysis of the liquid samples by use of adequate sample introduction techniques. Liquids can be analyzed directly at atmospheric pressures, when applying the atmospheric electrolyte cathode glow discharge cell approach with detection by emission spectroscopy as described by Cserfalvi and Mezei [3].

Material and Methods:

The experimental arrangement used for the investigation of dc glow discharge is simple and.

It is inexpensive arrangement and it is very much cost effective. It consists of tungsten electrode of length 40 mm and diameter 3mm fused in glass capillary tube and suspended axially in a hollow slotted stainless steel cylinder, of length 6 cm and internal diameter 2.54 cm. The stainless steel cylinder served as another electrode i.e. anode in the glow discharge. The suspended end of tungsten rod was carefully rounded. The tungsten electrode can be used as cathode by connecting it to the dc power supply of 700 V capacity having 1.5 A current capacity. In this arrangement the hollow cylinder was dipped in a electrolytic aqueous solution taken in a glass beaker. The depth of immersion of the tungsten electrode in electrolyte solution could be adjusted with the help of micrometer adjustable stand. By using this arrangement the tip of tungsten electrode could be just brought in touch with the upper surface of the solution or the distance between the solution surface and the electrode may be adjusted. In this way the solution itself acts as another electrode.

The different 28 electrolytic solutions have been taken for investigation using the glow discharge system. With the help of the above-mentioned experimental arrangement the following properties may be studied.

Result and Discussions:

Variation of electrolytic current with the applied dc-voltage during glow discharge in atmospheric pressure gas using 28 electrolytic solutions as the anode and cathode were carried out. The colors emitted on the glow are observed and listed in table 1. As an example we consider the electrolytic aqueous solution of 0.5N $\text{Cd}(\text{NO}_3)_2 \cdot 4\text{H}_2\text{O}$ as the anode, the electrolytic process leading to a luminescent glow is best depicted by the standard voltage-current curve as shown in figure 1. The curve may be divided in to several regions and its behavior may be studied.

In the region AB the curve is almost linear, the Ohms law is satisfied and conventional electrolysis found with tiny bubbles of gas around both material electrodes-tungsten electrode and stainless steel electrode. At the voltage corresponding to point B in curve, a smooth evolution of gas bubbles is disturbed and layer of steam is seen at the tungsten cathode. In the region between B and C, the pointer of voltmeter and ammeter widely fluctuates. In this region the characteristics like current passing through the electrode and voltage applied found as unstable.

The behavior of region BC, CD and DE can be explained as follows. Because of increase in the applied dc voltage, the rate of gas evolution is increased with the formation of large size gas bubbles at a fast rate.

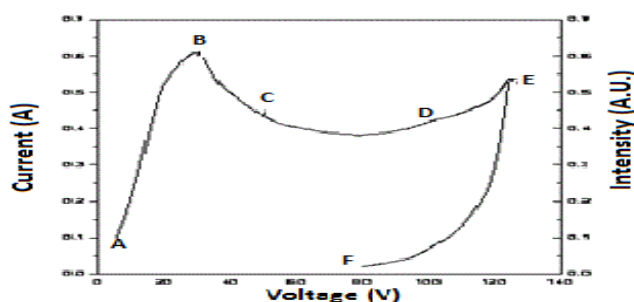


Fig.1: V- I Characteristics of 0.5N Electrolytic Solution of $\text{Cd}(\text{NO}_3)_2 \cdot 4\text{H}_2\text{O}$

This decreases the rate of migration of the ions and charge transfer process at the electrodes. When voltage is further increased more fluctuations are obtained in both voltage and current readings with fall in current. This unstable decreased current is shown by line BC. In the neighborhood of point C it is found that fluctuation rate decreases and now hissing sound occurs. When the applied dc voltage reaches to the point C, there is intermittent sparking. The formation of gas bubbles around the tungsten electrode has now stopped. After increasing the

applied dc-voltage to a still higher value the formation of movable thin vapor film around the tungsten cathode takes place, which at times produces the vortex motion and visible glow spark of greenish-blue color is found in the gap between cathode and solution phase. Due to vortex motion, electrolyte periodically touches to the tungsten cathode surface. This produces local heating at the tungsten cathode surface and visible glow spark of bluish-green color. Due to the local heating process there produces the vapor jet and nearby liquid molecules tried to take its place. The region CD of V- I characteristics shows this situation. Thus the region B to C represents the negative slope as seen in the curve. When the electrolyte current decreases to the corresponding point D, the violent gas evolution stops and slope of the curve changes sign from negative to positive. After the point D, with the applied dc voltages the current starts increasing and thereby producing a stable superheated insulating layer around the cathode (tungsten electrode). At this situation a continuous bluish-green glow is developed at the cathode surface. For a further increase in applied dc voltage, the intensity of the glow increases continuously with the increase in current also as shown in figure 1. Thus the region beyond D i.e. along DE appears to be true glow discharge. This happens due to the discharge of accumulated ions through the insulating layer. This situation produces intense glow of bluish-green color and it sometimes can be pictured as corona discharge. Thus under the observation, it is quite obvious that the superheated insulating layer around the cathode is the governing factor responsible for the bluish-green glow.

Tunnel Behavior Under V-I Characteristics of DC-glow Discharge

The discharge parameter like V-I characteristics of dc-glow discharge between the solid and liquid interfaces behaves like that of Tunnel diode. This has been investigated under the observation of V-I characteristics of aqueous solution of different concentrations. The energy band diagrams of cathode type and anode type (plasma band) materials as shown in figure 2. (a, b and c) can be used to explain the Tunneling phenomenon.

When the cathode type material (tungsten electrode) is joined, the energy band diagram under no bias condition becomes as shown in figure 2. (a). The junction barrier produces only a rough alignment of the two materials and their respective valence and conduction bands, hence no tunneling occurs. Initially when a lower voltage in equal step is applied, the energy band diagram become as shown in figure 2. (b). Due to the downward movement of the cathode region, the anode region valence band becomes exactly aligned with the cathode region conduction band. At this stage, electrons tunneling takes place as shown in figure and it 54

For this investigation taking the example of V-I characteristics for aqueous solution of 0.5 N KOH by dc glow discharge as shown in figure 3. With initially gradually increasing dc-voltage, the significant electrolyte current rises to its peak value say I_p and the corresponding applied voltage reaches to a value say V_p (at point B).

When applied voltage is increased to a value greater than V_p , the electrolyte discharge current starts decreasing till it achieves its minimum value called valley current I_v corresponding to valley voltage V_v (at point D). For the voltages greater than V_v current starts increasing again as in any ordinary junction diode.

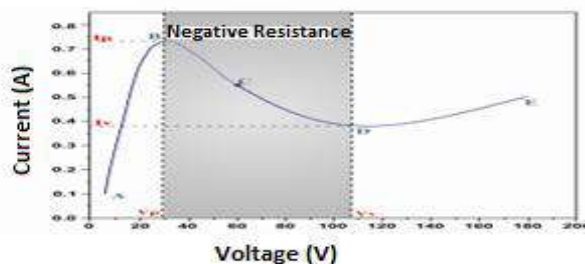


Fig.3: Tunnel Behavior Under V -I Characteristics of 0.5 N KOH Electrolytic Solution

In a similar way to negative resistance of the Tunnel diode it is seen from the figure in the region between peak point B and valley point D that the electrolyte current decreases with increase in the applied voltage. This behavior of the characteristics is similar to the electrolytic cell possesses negative resistance in this region. In fact this contributes the most useful property of the diode. Instead of absorbing power a negative resistance produces power.

Conclusion: DC Glow discharge using a solution as the anode and the metallic electrode as the cathode for the investigation of phenomenon of spectrometry shows that, a sensitive and inexpensive technique and very much cost for the elemental analysis of electrolytic solutions.

References:

- [1] T. Cserfalvi and P. Mezei (1996), Operating Mechanism of the Electrolytic Cathode Atmospheric Glow Discharge, *Fresenius Journal of Analytical Chemistry(Springer Link)*, pp: 83-89
- [2] Michael R. Webb, Francisco J. Andrade, Gerardo Gamez, Robert McCrindle and Gary M. Hieftje, (2005), Spectroscopic and Electrical Studies of a Solution Cathode Glow Discharge, *J. Anal. At. Spectrom.*, 20, pp: 1218- 1225
- [3] T Cserfalvi, P Mezei and P Apai, (1993), Emission Studies on a Glow Discharge in Atomic Pressure Air using Water as a Cathode, *J. Phys. D*, , 26, 2184-2188
- [4] Stephane Baude, Jose A.C. Broekaert, Daniel Delfosse, Norbert Jakubowski, Lars Fuechtjohann, Nestor G. Orellana-Velado, Rosario Pereiro and Alfredo Sanz- Medel (2000), Glow discharge atomic spectrometry for the analysis of environmental samples-a review, *J. Anal. At. Spectrom.* 2000, Vol.15, pp:1516-1525
- [5] John Marshal, Simon Chenery, E. Hywel Evans and Andrew Fisher (1998), Atomic Spectrometry Update- Atomic Emission Spectrometry, *Journal of Analytical Atomic Spectrometry*, June 1998, Vol. 13, pp: 107R- 130R
- [6] A A Garamoon, A Samir, F F Elakshar and E F Kotp (2003), Electrical Characteristics of a DC glow discharge, *Plasma Sources Science Technol.* 12(2003), pp: 417-420
- [7] Tamas Cserfalvi and P. Mezei, *J. Anal. At. Spectrom* (1994), Direct solution analysis by glow discharge: electrolyte cathode discharge spectrometry, *J. Anal. At. Spectrom.* 1994, 9, pp: 345-349
- [8] Z. Machalaa, M. Jandaa, K. Hensela, I. Jedlovsky, L. Leatinska, V. Foltinc, V. Martiaovita and M. Morvova (2007), Emission spectroscopy of atmospheric pressure plasmas for biomedical and environmental applications, *J. of Molecular Spectroscopy*, Vol. 243, Issue 2, pp:194-201
- [9] Michael R. Webb, George C.-Y. Chan, Francisco J. Andrade, Gerardo Gamez, and Gary M. Hieftje (2006), Spectroscopic characterization of ion and electron population in a solution – Cathode Glow discharge, *J. Anal. At. Spectrom.* 2006, 21, pp 525- 530.
- [10] David Staack, Bakhtier Farouk, Alexander Gutsol and Alexander Fridman (2005), Characterization of a DC atmospheric pressure normal Glow Discharge, *Plasma sources Sci. Technol.* 14, 2005, pp. 700-711
- [11] Christoph Gerhard, Tobiasweins, Daniel Tasche (2013), Atmospheric Pressure plasma treatment of fused silica related surface and near surface effects and applications, *Plasma Chemistry and Plasma Processing*, 2013, 33(5), pp. 895 – 905.
- [12] Santak V, Zaplotnik R, Tarle Z, Milosevic S (2015), Optical Emission spectroscopy of an atmospheric pressure plasma jet during tooth bleaching Gel Treatment, *Appl. Spectrosc.*, 2015, pp. 1327 – 1333.
- [13] Mohammed Khalaf, Osdai A Hammadi Firas J. Kahim (2016), Current Voltage Characteristics of DC plasma Discharges Employed in Sputtering Techniques, *IJAP*, 2016, 12(3), pp.11 – 16.
- [14] Norbert Jakubowaski, Volkar Hoffmann, Annemie Bogaerts (2003), Foreword: Glow discharge spectrometry, *J. Anal. At. Spectrom.*, 2003, 20, pp.19N-22N
- [15] John Marshall, Simon Chenery, E. Hywel Evans, Andrew Fisher (1998), Atomic Spectrometry Update–Atomic emission spectrometry, *J. Anal. At. Spectrom.*, 1998, 13, 107R-130R.

Green synthesis of Zinc Oxide nanoparticles using Plant - A review

B. S. Agrawal*, G. T. Lamdhade

Department of Physics, Vidya Bharati Mahavidyalaya, Camp, Amravati, M.S., India-444602

*Corresponding Author: [Tel:\(+91\) 9921122278](tel:+919921122278) *Email: bhavesht.agrawal0110@gmail.com

Abstract:

Nano technology deals with the production and usage of material with nano scale dimension. Nano scale dimension provides nanoparticles (NPs) a large surface area to volume ratio and thus very specific properties. Zinc oxide nanoparticles (NPs) had been in modern studies due to its huge bandwidth and high excitation binding energy and it has potential applications like antibacterial, antifungal, anti-diabetic, anti-inflammatory, wound healing, antioxidant and optic properties. Due to the great rate of toxic chemicals and extreme environment employed in the physical and chemical production of these Nanoparticles (NPs), green methods employing the use of plants, fungus, bacteria, and algae have been adopted. This review is a comprehensive study of the synthesis and characterization methods used for the green synthesis of ZnO Nanoparticles using different biological sources.

Keywords: ZnO, Green Synthesis, Plant, Microbes

1. Introduction

Nanomaterials are particles having nano scale dimension, and nanoparticles are very small sized particles with enhanced catalytic reactivity, thermal conductivity, non-linear optical performance and chemical steadiness owing to its large surface area to volume ratio [1]. Nanoparticles (NPs) have started being considered as nano antibiotics because of their antimicrobial activities

[2]. Nanoparticles (NPs) have been integrated into several industrial, health, food, feed, space, chemical, and cosmetics industry of consumers which calls for a green and environment-friendly approach to their synthesis [3].

Zinc oxide (ZnO) is a semiconductor material in a group of metal oxides with a direct wide band gap (3.37 eV) large excitation binding energy (60 meV). Zinc Oxide (ZnO) is a potential material for many applications such as for catalysts [4], solar cells [5], gas sensors [6], light emitting diodes [7], rubber additive [8], pigments [9] and so on. Because the advantage of the anti-UV absorption properties of ZnO, they are increasingly used in private care products, such as cosmetics and sunscreen [10]. Additionally, for its novel physical properties are characterized by their photo catalytic and photo-oxidizing ability resist with chemical and biological species. ZnO is accepted for its benefit in biological applications as an antibacterial material [11].

1.1 Different methods used in nanoparticle synthesis

In the physical method, physical forces are involved in the attraction of nano scale particles and formation of large, stable, well-defined nanostructures. Its example includes nanoparticle (NP) synthesis through colloidal dispersion method. It includes basic techniques like vapour condensation, amorphous crystallization and many others [12–15]. Nanoparticle synthesis is mediated by physical, chemical and Biosynthesis methods [16–18]. The physical method involves the use of costly equipment, high temperature and pressure [19], large space area for setting up of machines. In the chemical method, the use of toxic chemicals which can prove to be hazardous for the environment and the person handling it. The literature states that some of

the toxic chemicals that we use in physical and chemical methods may reside in the nanoparticles (NPs) formed which may prove hazardous in the field of their application in the medical field [20]. Thus, we needed an environment-friendly and cost-effective method for nanoparticle synthesis. Physical process involves the use of high vacuum in processes like pulsed laser deposition, MBE (molecular beam epitaxy), thermal evaporation etc. [21] and chemical methods include chemical micro emulsion, sol-gel method, hydrothermal synthesis, electrode position [16], chemical and direct precipitation and microwave assisted combustion [22]. Additional capping and stabilizing agent are needed in physical and chemical methods [23–26].

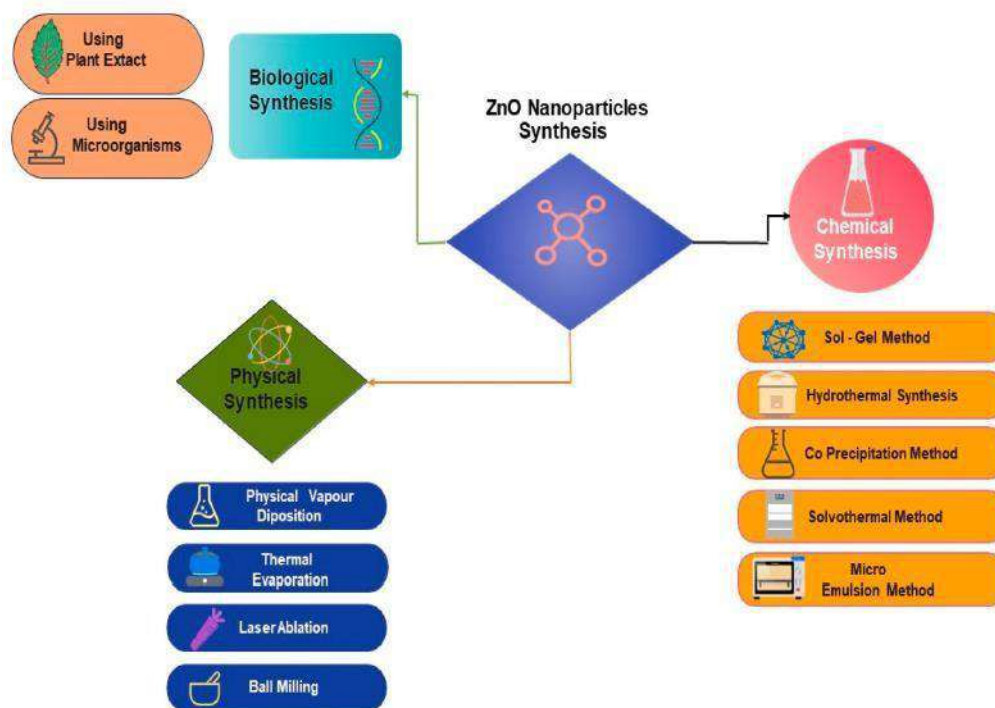


Fig.1 - Different methods used in nanoparticle synthesis

1.2. Green approach

The Biosynthesis of nanoparticles (NPs) is an approach of synthesizing nanoparticles (NPs) using micro-organisms and plants having various biomedical applications. This approach is an environment-friendly, cost-effective, biocompatible, safe, green approach [27]. The Green synthesis includes synthesis through plants, bacteria, fungi, algae etc. They allow great scale production of Zinc Oxide nanoparticles (NPs) free of additional impurities [28]. Nanoparticles (NPs) synthesized from biomimetic approach show more catalytic activity and limit the use of expensive and toxic chemicals. Plant parts like roots, leaves, stems, seeds, fruits have also been utilized for the nanoparticles (NPs) synthesis as their extract is rich in phytochemicals which act as both reducing and stabilization agent [29–35]. ZnO nanoparticles (NPs) synthesized from *Trifolium pratense* flower extract showed similar peaks in UV-Vis spectrophotometer after 24, 48, 72, 96 and 120 hours of Nanoparticles (NPs) formation presenting the stability of Nanoparticles (NPs) formed [36].

Similarly, fruit extract of *Rosa canina* acted as both reducing and stabilizing agent for synthesized ZnO Nanoparticles (NPs), confirmed by FTIR studies. Bio-capping is completed by carboxylic and phenolic acid present in fruit extract. Spherical shaped ZnO Nanoparticles (NPs) were formed by Aloe Vera leaf extract where free carboxylic and the amino group of

plant extract acted as both reducing and capping agent.

2. Literature study

Due to the increasing popularity of green methods, different works had been done to synthesize ZnO Nanoparticles (NPs) using different plants and a list of tables had been put to summarize the valuable work done in this field.

2.1. Green synthesis of ZnO Nanoparticles (NPs) using plant extract

Plant parts like leaf, stem, root, fruit, and seed have been used for ZnO Nanoparticles (NPs) synthesis because of the exclusive phytochemicals that they produce. Using natural extracts of plant parts is a very eco-friendly, cost-effective process and it does not involve usage of any other intermediate base groups. It takes very short time, usage of cheap equipment and precursor and gives a very highly pure and quantity enriched product free of impurities [37]. Plants are most preferred source of Nanoparticles (NPs) synthesis because they lead to large scale production and production of stable, varied in shape and size Nanoparticles (NPs) [38]. Most usually applied method for simple preparation of ZnO Nanoparticles (NPs) from leaves or flowers is where the plant part is washed thoroughly in running tap water and sterilized using double distilled water (some use Tween 20 to sterilize it). Then this plant part is kept for drying at room temperature followed by weighing and then crushing it by a mortar and pestle. Milli-Q H₂O is added to the plant part according to the desired concentration and the mixture is boiled under constant stirring using a magnetic stirrer [37–41]. The solution is filtered using Whatman filter paper and the obtained clear solution was used as a plant extract (sample). Some volume of the extract is mixed with 0.5 Mm of hydrated Zinc nitrate or zinc oxide or zinc sulfate and the mixture is boiled at desired temperature and time to achieve efficient mixing [40,41]. Certain perform optimization at this point using different temperature, pH, extract concentration

and time. Incubation period results in a change of color of the mixture to yellow which is a visual confirmation of the synthesized Nanoparticles (NPs) [40, 41]. Then a UV-Vis spectrophotometry is employed to confirm the synthesis of Nanoparticles (NPs) followed by centrifugation of mixture and drying the pellet in a hot air oven to get the crystal nanoparticles (NPs) [42]. Further, synthesized nanoparticles are further characterized using X-ray diffraction (XRD), Energy Dispersion Analysis of X-ray (EDAX), Fourier Transform Infrared Spectroscopy (FTIR), Transmission Electron Microscopy (TEM), Field Emission Scanning Electron Microscopy (FE- SEM), Scanning Electron Microscopy (SEM), Atomic Force Microscopy (AFM), Thermal- gravimetric Differential Thermal Analysis (TG-DTA), Photoluminescence Analysis (PL), X-ray Photoelectron Microscopy (XPS), Attenuated total reflection (ATR), Raman Spectroscopy and UV-Visible Diffuse Reflectance Spectroscopy (UV-DRS) [41–43]. Table 1 is a comprehensive study of different plants used for the synthesis of ZnO Nanoparticles (NPs).

Table 1:

Plant mediated synthesis of ZnO NP.

Sr. No.	Plant (family)	Common Name	Part taken for extraction	Size (nm)	Shape	Reference
1	<i>Aloe Vera</i> (Liliaceae)	Aloe Vera	Leaf extract	8–20 (XRD)	Spherical, oval, hexagonal	[44]
2	<i>Pongamia</i>	Indian beech	Fresh	26 (XRD),	Spherical,	[45]

	<i>pinnata</i> (Legumes)		leaves	Agglomeration of 100 (DLS, SEM, TEM)	hexagonal, nano rod	
3	<i>Azadirachta indica</i> (Meliaceae)	Neem	Fresh leaves	18 (XRD)	Spherical	[46]
4	<i>Cocusnucifera</i> (Arecaceae)	Coconut	Coconut water	20–80 (TEM), 21.2 (XRD)	Spherical and predominantly hexagonal without any agglomeration	[47]
5	<i>Moringa oleifera</i> (Moringaceae)	Drumstick tree	Leaf	24 (XRD), 16– 20 (FE-SEM)	Spherical and granular nano sized shape with a group of aggregates	[48]
6	<i>Aloevera</i> (Liliaceae)	Aloe vera	Freeze dried leaf peel	25–65 (SEM & TEM)	Spherical, hexagonal	[49]
7	<i>Gossypium</i> (Malvaceae)	Cotton	Cellulosic fibre	13 (XRD)	Wurtzite, spherical, nano rod	[50]
8	<i>Azadirachta indica</i> (Meliaceae)	Neem	Fresh leaves	10–30 (TEM), 9–40 (XRD)	Hexagonal disk, nanobuds	[51]
9	<i>Trifolium Pratense</i> (Legumes)	Red clover	Flower	60–70 (XRD)	Spherical	[52]
10	<i>Agathosma betulina</i> (Rutaceae)	Buchu	Dry leaves	15.8 (TEM) ,12–26 (HRTEM)	Quasi- spherical agglomerates	[53]
11	<i>Vitexnegundo</i> (Lamiaceae)	Nochi	Leaf	75–80 (SEM & EDX) , 38.17 (XRD)	Spherical	[54]
12	<i>Plectranthus amboinicus</i> (Lamiaceae)	Mexican mint	Leaf extract	50–180 (SEM)	Rod shap enanoparticle with agglomerates	[55]
13	<i>S.album</i> (Santalaceae)	Sandalwood	Leaves	100 (DLS & SEM), 70–140 (TEM)	Nano rods	[56]
14	<i>Sphathodea campanulata</i> (Bignoniaceae)	African tulip tree	Leaf extract	30–50 (TEM)	Spherical	[57]

15	<i>Calatropis Gigantea</i> (Apocynaceae)	Crown flower	Fresh leaves	30–35 (SEM)	Spherical shaped forming agglomerates	[58]
----	---	--------------	--------------	-------------	---------------------------------------	------

3. Conclusion

The Biosynthesis of nanoparticles (NPs) using eco-friendly approach has been the area of focused research in the recent years. Green sources act as both stabilizing and reducing agent for the synthesis of size and shape controlled nanoparticles (NPs). Future prospect of plant mediated nanoparticle synthesis includes an extension of laboratory based work to industrial scale, elucidation of phytochemicals involved in the synthesis of nanoparticles using bioinformatics tools and deriving the exact mechanism involved in inhibition of pathogenic bacteria. The plant-based nanoparticle can have huge application in the field of food, pharmaceutical, antimicrobial and cosmetic industries and thus become a major area of research.

REFERENCES

- [1] S. Tabrez, J. Musarrat, A .A . Al-khedhairi, Colloids and surfaces B: biointerfaces countering drug resistance, infectious diseases, and sepsis using metal and metal oxides nanoparticles: current status, Colloids Surf. B Biointerfaces 146 (2016) 70–83, doi: 10.1016/j.colsurfb.2016.05.046 .
- [2] M. Sastry, A. Ahmad, M. Islam Khan, R. Kumar, Biosynthesis of metal nanopar- ticles using fungi and actinomycete, Curr. Sci 85 (2003) 162–170, doi: 10.1016/ S0927- 7765(02)00174- 1 .
- [3] M.D. Rao, P. Gautam, Synthesis and characterization of ZnO nanoflowers usingchlamydomonas reinhardtii: a green approach, Environ. Prog. Sustain. Energy (2016) 1–7, doi: 10.1002/ep .
- [4] S. Suwanboon, P. Amornpitoksuk, P. Bangrak, N. Muensit, Optical, photocatalytic and bactericidal properties of Zn_{1-x}LaxO and Zn_{1-x}MgxO nanostructures prepared by a sol–gel method, Ceram Int. 39 (5) (2013) 5597–5608.
- [5] E. Kärber, A. Abass, S. Khelifi, M. Burgelman, A. Katerski, M. Krunks, Electrical characterization of all-layers-sprayed solar cell based on ZnO nanorods and extremely thin CIS absorber, Sol. Energy 91 (2013) 48–58.
- [6] J.Y. Patil, A.V. Rajgure, L.K. Bagal, R.C. Pawar, I.S. Mulla, S.S. Suryavanshi, Structural, morphological, and gas response properties of citrate gel synthesized nanocrystalline ZnO and Zn_{0.9}Cd_{0.1}O materials, Ceram. Int. 39 (4) (2013) 4383–4390.
- [7] Q. Yang, Y. Liu, C. Pan, J. Chen, X. Wen, Z.L. Wang, Largely enhanced efficiency in ZnO nanowire/p-polymer hybridized inorganic/organic ultraviolet lightemitting diode by piezo- phototronic effect, Nano Lett. 13 (2) (2013) 607–613.
- [8] A. Moezzi, A.M. McDonagh, M.B. Cortie, Zinc oxide particles: synthesis, properties and applications, Chem. Eng. J. 185–186 (2012) 1–22.
- [9] N. Kiomarsipour, R. Shoja Razavi, K. Ghani, M. Kioumarsipour, Evaluation of shape and size effects on optical properties of ZnO pigment, Appl. Surf. Sci. 270 (2013) 33–38.
- [10] M.D. Newman, M. Stotland, J.I. Ellis, The safety of nanosized particles in titanium dioxide-and zinc oxide-based sunscreens, J. Am. Acad. Dermatol. 61 (4) (2009) 685–692.
- [11] N.Salah, S.Habib, Zishan, High-energy ball milling technique for ZnO nanoparticles as antibacterial material, Inter Journal of Nanomedicine 6 (2011) 863-869.
- [12] C. Vidya , S. Hiremath , M.N. Chandraprabha , M.A.L. Antonyraj , I.V. Gopala , A. Jain , etal. , Green synthesis of ZnO nanoparticles by Calotropis gigantea, Int J Curr Eng Technol 1 (2013) 118–120 .
- [13] R. Aladpoosh, M. Montazer, The role of cellulosic chains of cotton in biosynthe- sis of ZnO nanorods producing multifunctional properties: mechanism, charac- terizations and features, Carbohydr. Polym 126 (2015) 122–129, doi: 10.1016/j. carbpol.2015.03.036 .

- [14] A.N.D. Krupa, R. Vimala, Evaluation of tetraethoxysilane (TEOS) sol-gel coatings, modified with green synthesized zinc oxide nanoparticles for combating microfouling, *Mater.Sci. Eng. C*. 61 (2016) 728–735, doi: 10.1016/j.msec.2016.01.013 .
- [15] K. Elumalai, S. Velmurugan, S. Ravi, V. Kathiravan, S. Ashokkumar, Green synthesis of zinc oxide nanoparticles using *Moringa oleifera* leaf extract and evaluation of its antimicrobial activity, *Spectrochim. Acta A Mol. Biomol. Spectrosc* 143 (2015) 158–164, doi: 10.1016/j.saa.2015.02.011 .
- [16] M. Afifi, O.A. Almaghrabi, N.M. Kadasa, Ameliorative effect of zinc oxide nanoparticles on antioxidants and sperm characteristics in streptozotocin-induced diabetic rat testes, *Biomed Res. Int* 2015 (2015), doi: 10.1155/2015/153573 .
- [17] J. Chen, X. Liu, C. Wang, S.S. Yin, X.L. Li, W.J. Hu, et al., Nitric oxide ameliorates zinc oxide nanoparticles-induced phytotoxicity in rice seedlings, *J. Hazard. Mater* 297 (2015) 173–182, doi: 10.1016/j.jhazmat.2015.04.077 .
- [18] B.M.L. Vitosh, D.D. Warncke, R.E. Lucas, Secondary and micronutrients of vegetables and field crops *Secondary and Micronutrients*, 1994 .
- [19] R. Chandrasekaran, S. Gnanasekar, P. Seetharaman, R. Keppan, W. Arockiaswamy, S. Sivaperumal, Formulation of *Carica papaya* latex-functionalized silver nanoparticles for improved antibacterial and anticancer applications, *J. Mol. Liq* 219 (2016) 232–238, doi: 10.1016/j.molliq.2016.03.038 .
- [20] P. Dhandapani, A.S. Siddarth, S. Kamalasekaran, S. Maruthamuthu, G. Rajagopal, Bio-approach: ureolytic bacteria mediated synthesis of ZnO nanocrystals on cotton fabric and evaluation of their antibacterial properties, *Carbohydr. Polym* 103 (2014) 448–455, doi: 10.1016/j.carbpol.2013.12.074 .
- [21] S. Mitra, P. Patra, S. Pradhan, N. Debnath, K.K. Dey, S. Sarkar, et al., Microwave synthesis of ZnO@mSiO₂ for detailed antifungal mode of action study: understanding the insights into oxidative stress, *J. Colloid Interface Sci* 444 (2015) 97–108, doi: 10.1016/j.jcis.2014.12.041 .
- [22] R. Yuvakkumar, J. Suresh, B. Saravanakumar, A. Joseph Nathanael, S.I. Hong, V. Rajendran, Rambutan peels promoted biomimetic synthesis of bioinspired zinc oxide nanochains for biomedical applications, *Spectrochim. Acta A Mol. Biomol. Spectrosc* 137 (2015) 250–258, doi: 10.1016/j.saa.2014.08.022 .
- [23] B. Kumari, S. Sharma, N. Singh, A. Verma, V.R. Satsangi, S. Dass, et al., ZnO thin films, surface embedded with biologically derived Ag/Au nanoparticles, for efficient photoelectrochemical splitting of water, *Int. J. Hydrogen Energy* 39 (2014) 18216–18229, doi: 10.1016/j.ijhydene.2014.09.025 .
- [24] S. Ambika, M. Sundarajan, Green biosynthesis of ZnO nanoparticles using *Vitex negundo* L. extract: spectroscopic investigation of interaction between ZnO nanoparticles and human serum albumin, *J. Photochem. Photobiol. B Biol* 149 (2015) 143–148, doi: 10.1016/j.jphotobiol.2015.05.004 .
- [25] K. Kavithaa, M. Paulpandi, T. Ponraj, K. Murugan, S. Sumathi, Induction of intrinsic apoptotic pathway in human breast cancer (MCF-7) cells through facile biosynthesized zinc oxide nanorods, *Karbala Int. J. Mod. Sci* 2 (2016) 46–55. <http://dx.doi.org/10.1016/j.kijoms.2016.01.002> .
- [26] S. Ravikumar, R. Gokulakrishnan, P. Boomi, In vitro antibacterial activity of the metal oxide nanoparticles against urinary tract infections bacterial pathogens, *Asian Pacific J. Trop. Dis* 2 (2012) 85–89, doi: 10.1016/S2222-1808(12)60022-X .
- [27] H. Abdul, R. Sivaraj, R. Venkatesh, Green synthesis and characterization of zinc oxide nanoparticles from *Ocimum basilicum* L. var. *purpurascens* Benth.-lamiaceae leaf extract, *Mater. Lett* 131 (2014) 16–18, doi: 10.1016/j.matlet.2014.05.033 .
- [28] R. Yuvakkumar, J. Suresh, A.J. Nathanael, M. Sundarajan, S.I. Hong, Novel green synthetic strategy to prepare ZnO nanocrystals using rambutan (*Nephelium lappaceum* L.) peel extract and its antibacterial applications, *Mater. Sci. Eng. C*. 41 (2014) 17–27, doi: 10.1016/j.msec.2014.04.025 .
- [29] Y. Zong, Z. Li, X. Wang, J. Ma, Y. Men, Synthesis and high photocatalytic activity of Eu-doped

- ZnO nanoparticles, *Ceram. Int* 40 (2014) 10375–10382, doi:10.1016/j.ceramint.2014.02.123 .
- [31] V. Nachiyar , S. Sunkar , P. Prakash , Biological synthesis of gold nanoparticles using endophytic fungi, *Der Pharma Chem* 7 (2015) 31–38 .
- [31] M. Ramesh, M. Anbuvaran, G. Viruthagiri, Green synthesis of ZnO nanoparticles using *Solanum nigrum* leaf extract and their antibacterial activity, *Spectrochim. Acta A Mol. Biomol. Spectrosc* 136 (2015) 864–870, doi: 10.1016/j.saa. 2014.09.105 .
- [32] L. Xiao, C. Liu, X. Chen, Z. Yang, Zinc oxide nanoparticles induce renal toxicity through reactive oxygen species, *Food Chem. Toxicol* 90 (2016) 76–83, doi: 10. 1016/j.fct.2016.02.002 .
- [33] S. Rajeshkumar, Anticancer activity of eco-friendly gold nanoparticles against lung and liver cancer cells, *J. Genet. Eng. Biotechnol* 14 (2016) 195–202, doi: 10. 1016/j.jgeb.2016.05.007 .
- [34] P.C. Nagajyothi, T.N. Minh An, T.V.M. Sreekanth, J. Il Lee, D.L. Joo, K.D. Lee, Green route biosynthesis: characterization and catalytic activity of ZnO nanoparticles, *Mater. Lett* 108 (2013) 160–163, doi: 10.1016/j.matlet.2013.06. 095 .
- [35] G. Gnanajobitha, K. Paulkumar, M. Vanaja, S. Rajeshkumar, C. Malarkodi, G. Annadurai, et al., Fruit-mediated synthesis of silver nanoparticles using *Vitis vinifera* and evaluation of their antimicrobial efficacy, *J Nanostruct Chem* (2013), doi: 10.1186/2193- 8865- 3- 67 .
- [36] R. Dobrucka, J. Długaszewska, Biosynthesis and antibacterial activity of ZnO nanoparticles using *Trifolium pratense* flower extract, *Saudi J. Biol. Sci* 23 (2016) 517–523, doi: 10.1016/j.sjbs.2015.05.016 .
- [37] M. Heinlaan, A. Ivask, I. Blinova, H.C. Dubourguier, A. Kahru, Toxicity of nano-sized and bulk ZnO, CuO and TiO₂ to bacteria *Vibrio fischeri* and crustaceans *Daphnia magna* and *Thamnocephalus platyurus*, *Chemosphere* 71 (2008) 1308–1316, doi: 10.1016/j.chemosphere.2007.11.047 .
- [38] J. Qu, X. Yuan, X. Wang, P. Shao, Zinc accumulation and synthesis of ZnO nanoparticles using *Physalis alkekengi* L, *Environ. Pollut* 159 (2011) 1783–1788, doi: 10.1016/j.envpol.2011.04.016 .
- [39] J. Qu, C. Luo, J. Hou, Synthesis of ZnO nanoparticles from Zn-hyperaccumulator (*Sedum alfredii* Hance) plants, *Micro Nano Lett* 6 (2011) 174, doi: 10.1049/mnl. 2011.0 0 04 .
- [40] P.E. Ochieng , E. Iwuoha , I. Michira , M. Masikini , J. Ondiek , P. Githira , et al. , Green route synthesis and characterization of ZnO nanoparticles using *Spathodea campanulata*, *Int. J. Biochem. Phys* 23 (2015) 53–61 .
- [41] S. Rajeshkumar, C. Malarkodi, M. Vanaja, G. Annadurai, Anticancer and enhanced antimicrobial activity of biosynthesized silver nanoparticles against clinical pathogens, *J. Mol. Struct* 1116 (2016) 165–173, doi: 10.1016/j.molstruc.2016. 03.044 .
- [42] A. Yasmin, K. Ramesh, S. Rajeshkumar, Optimization and stabilization of gold nanoparticles by using herbal plant extract with microwave heating, *Nano Convergence* (2014), doi: 10.1186/s40580- 014- 0012- 8 .
- [43] Y. Ali, S. Benjakul, T. Prodpran, P. Sumpavapol, Food hydrocolloids properties and antimicrobial activity of fish protein isolate / fish skin gelatin film containing basil leaf essential oil and zinc oxide nanoparticles, *Food Hydrocoll* 41 (2014) 265–273, doi: 10.1016/j.foodhyd.2014.04.023 .
- [44] K. Ali, S. Dwivedi, A. Azam, Q. Saquib, M.S. Al-said, A .A . Alkhedhairi, et al., Aloe vera extract functionalized zinc oxide nanoparticles as nanoantibiotics against multi-drug resistant clinical bacterial isolates, *J. Colloid Interface Sci* 472 (2016) 145–156, doi: 10.1016/j.jcis.2016.03.021 .
- [45] M. Sundrarajan, S. Ambika, K. Bharathi, Plant-extract mediated synthesis of ZnO nanoparticles using *Pongamia pinnata* and their activity against pathogenic bacteria, *Adv. Powder Technol* 26 (2015) 1294–1299, doi: 10.1016/ j.apt.2015.07.001 .
- [46] K. Elumalai, S. Velmurugan, Green synthesis, characterization and antimicrobial activities of zinc oxide nanoparticles from the leaf extract of *Azadirachta indica*, *Appl. Surf. Sci* 345 (2015) 329–336, doi: 10.1016/j.apsusc.2015.03.176 .
- [47] A.N.D. Krupa, R. Vimala, Evaluation of tetraethoxysilane (TEOS) sol-gel coatings, modified with green synthesized zinc oxide nanoparticles for combating microfouling, *Mater.Sci. Eng. C* 61 (2016) 728–735, doi: 10.1016/j.msec.2016.01. 013 .
- [48] K. Elumalai, S. Velmurugan, S. Ravi, V. Kathiravan, S. Ashokkumar, Green synthesis of zinc

- oxide nanoparticles using *Moringa oleifera* leaf extract and evaluation of its antimicrobial activity, *Spectrochim. Acta A Mol. Biomol. Spectrosc* 143 (2015) 158–164, doi: 10.1016/j.saa.2015.02.011 .
- [49] Y. Qian, J. Yao, M. Russel, K. Chen, X. Wang, Characterization of green synthesized nanoformulation (ZnO-A. vera) and their antibacterial activity against pathogens, *Environ.Toxicol. Pharmacol* 39 (2015) 736–746, doi: 10.1016/j.etap. 2015.01.015 .
- [50] R. Aladpoosh, M. Montazer, The role of cellulosic chains of cotton in biosynthesis of ZnO nanorods producing multifunctional properties: mechanism, characterizations and features, *Carbohydr. Polym* 126 (2015) 122–129, doi: 10.1016/j.carbpol.2015.03.036 .
- [51] H.R. Madan, S.C. Sharma, Udayabhanu, D. Suresh, Y.S. Vidya, H. Nagabhushana, et al., Facile green fabrication of nanostructure ZnO plates, bullets, flower, prismatic tip, closed pine cone: their antibacterial, antioxidant, photoluminescent and photocatalytic properties, *Spectrochim. Acta A Mol. Biomol. Spectrosc* 152 (2016) 404–416, doi: 10.1016/j.saa.2015.07.067 .
- [52] R. Dobrucka, J. Długaszewska, Biosynthesis and antibacterial activity of ZnO nanoparticles using *Trifolium pratense* flower extract, *Saudi J. Biol. Sci* 23 (2016) 517–523, doi: 10.1016/j.sjbs.2015.05.016 .
- [53] F.T. Thema, E. Manikandan, M.S. Dhlamini, M. Maaza, Green synthesis of ZnO nanoparticles via *Agathosma betulina* natural extract, *Mater. Lett* 161 (2015) 124–127, doi: 10.1016/j.matlet.2015.08.052 .
- [54] S. Ambika, M. Sundrarajan, Green biosynthesis of ZnO nanoparticles using *Vitex negundo* L. extract: spectroscopic investigation of interaction between ZnO nanoparticles and human serum albumin, *J. Photochem. Photobiol. B Biol* 149 (2015) 143–148, doi: 10.1016/j.jphotobiol.2015.05.004 .
- [55] L. Fu, Z. Fu, *Plectranthus amboinicus* leaf extract-assisted biosynthesis of ZnO nanoparticles and their photocatalytic activity, *Ceram. Int* 41 (2015) 2492–2496, doi: 10.1016/j.ceramint.2014.10.069 .
- [56] K. Kavithaa, M. Paulpandi, T. Ponraj, K. Murugan, S. Sumathi, Induction of intrinsic apoptotic pathway in human breast cancer (MCF-7) cells through facile biosynthesized zinc oxide nanorods, *Karbala Int. J. Mod. Sci* 2 (2016) 46–55. <http://dx.doi.org/10.1016/j.kijoms.2016.01.002> .
- [57] P.E. Ochieng , E. Iwuoha , I. Michira , M. Masikini , J. Ondiek , P. Githira , et al. , Green route synthesis and characterization of ZnO nanoparticles using *Spathodea campanulata*, *Int. J. Biochem. Phys* 23 (2015) 53–61 .
- [58] C. Vidya , S. Hiremath , M.N. Chandraprabha , M.A.L. Antonyraj , I.V. Gopala , A. Jain , et al. , Green synthesis of ZnO nanoparticles by *Calotropis gigantea*, *Int J Curr Eng Technol* 1 (2013) 118–120 .

Conducting Polymer Based Anticorrosion Materials

D. J. Bhagat, K. R. Nemade^b, K. A. Koparkar^c

^aDepartment of Physics, Nehru Mahavidyalaya (Arts, Commerce & Science), Nerparsopant, Dist. Yavatmal.

^bDepartment of Physics, Indira Mahavidyalaya, Kalamb, Dist. Yavatmal.

^cDepartment of Physics, MSP College, Manora, Dist. Washim.

Abstract:

The review article reports the Conducting Polymer Based Anticorrosion Materials. The most of the researchers confirm the synthesis of desire materials through some characterization such as XRD, FTIR, UV-Vis, SEM, EDS, EIS, Cyclic Voltammetry (CV), potentiostatic and galvanostatic conditions. The successful preparation of conducting polymer based corrosive materials and the tremendous efficiency reflects from results which reports by them. These materials have excellent potential application in anticorrosion industry.

Introduction:

Recently, most of the industry facing the problem of corrosion due use metals as a basic content for the electronics devices, instruments, pipelines, construction, marine, aeronautics, automobiles industries, and machinery parts, etc. Due to the corrosion these metals things could be weakened and therefore they could require replacement which is very costly. In the construction industry metal rods are the basic structure. These rods made construction strong and increase the lifespan of every construction which placed inside the concrete. But, concrete could be degrades those rods which results in weak construction and decrease the service life of construction structure. Automobile and industrial structures also made from the metal which could be affected by the corrosion. The corrosion is most dangerous thing for marine industry. The sea water is very helpful for corrosion, due to sea water metal got corrosion instantly. Therefore, there is need of developing such anticorrosive material which could protect the metal from the corrosion. Therefore, most of the researchers were attracted towards the preparation of anticorrosion materials. They synthesized and tested the prepared materials against the corrosion. Researchers try to develop such anticorrosive materials which represent the anticorrosion properties. Recently, researchers were focusing on the developing the conducting polymer based anticorrosion materials for better service life. The conducting polymers reveal good barrier properties, ease of altering properties and massive production. Moreover, the conducting polymer based anticorrosion materials represents the properties such as good environmental stability, good conductivity, environment friendly nature, and low-cost production [1-19]. This review article is present the research done on the conducting polymer based anticorrosive materials.

Results and Discussions:

The most researchers got the tremendous results by synthesizing the conducting polymer based anti-corrosion materials. Hao et.al. synthesized well-dispersed sulfate doped PPy and its derivative nanoparticles by green method and studied electrochemical properties of bare and coated zinc are investigated by open-circuit voltage (OCP), electrochemical impedance spectroscopy (EIS) and potentiodynamic polarization [20]. Hafeez et.al. prepared nanoparticle sized polyaniline (PANI) and epoxy resin composites and studied their anticorrosive properties [21]. Tallman et.al. investigated the study of Electroactive conducting polymers (ECPs), their properties, and a discussion of the processing issues surrounding the use of ECPs as coatings [22]. Ahmad et.al. investigated the conducting polymer, emeraldine, which can be applied

chemically on the surface of the stainless steel. The results were showed tremendous positive response to the author [23]. Le et.al. demonstrated the electrodeposition of polypyrrole on iron in potassium tetraoxalate 0.05 M and pyrrole 0.1 M solution at a current of 1 mA/cm². The outcomes of this attempt results in polypyrrole coatings provide substantial corrosion protection to iron [24].

In this section we discussed on the research carried out by various researchers on the conducting polymer based anticorrosive materials that reveals the tremendous results for anticorrosion.

Conclusion:

The conducting polymers based materials represents the excellent results for anticorrosion protection. The number of researchers got excellent results for anti-corrosion. The results show that these anti-corrosion materials have great application potential.

References:

- 1) N. Jadhav, S. Kasisomayajula, V. J. Gelling, Polypyrrole/Metal Oxides-Based Composites/Nanocomposites for Corrosion Protection, *Frontiers in Materials* 7 (2020) 95–101.
- 2) A.F. Baldissera, C.A. Ferreira, Coatings based on electronic conducting polymers for corrosion protection of metals, *Progress in Organic Coatings* 75 (2012) 241–247.
- 3) O. Dagdag, R. Hsissou, A. E. Harfi, A. Berisha, Z. Safi, C. Verma, E.E. Ebensof, M. E. Touhamig, M. El Gouria, Fabrication of polymer based epoxy resin as effective anti-corrosive coating for steel: Computational modeling reinforced experimental studies, *Surfaces and Interfaces* 18 (2020) 100454–100461.
- 4) T. Pan, Q. Yu, Long-Term Anti-Corrosion Performance of a Conducting Polymer-Based Coating System for Steels, *JMEPEG* 25 (2016) 2384–2394.
- 5) R. C. Patil, S. Radhakrishnan, Conducting polymer based hybrid nano-composites for enhanced corrosion protective coatings, *Progress in Organic Coatings* 57 (2006) 332–336.
- 6) S. Sathiyarayanan, S. Devi, G. Venkatachari, Corrosion protection of stainless steel by electropolymerised pani coating, *Progress in Organic Coatings* 56 (2006) 114–119.
- 7) Y. Chen, Y. Ye, Z. R. Chen. Vapor-based synthesis of bilayer anti-corrosion polymer coatings with excellent barrier property and superhydrophobicity. *J. Mater. Sci.* 54 (2019) 5907–5917.
- 8) T. Peng, R. Xiao, Z. Rong, H. Liu, Q. Hu, S. Wang, X. Lid, J. Zhang, Polymer Nanocomposite-based Coatings for Corrosion Protection, *Chemistry-An Asian Journal*, 15 (2020) 3915–3941.
- 9) M. M. Al-Zahrani, S. U. Al-Dulaijan, M. Ibrahim, H. Saricimen, F.M. Sharif, Effect of waterproofing coatings on steel reinforcement corrosion and physical properties of concrete, *Cement & Concrete Composites* 24 (2002) 127–137.
- 10) A. U. Ammar, M. Shahid, M. K. Ahmed, M. Khan, A. Khalid, Z. A. Khan, Electrochemical Study of Polymer and Ceramic-Based Nanocomposite Coatings for Corrosion Protection of Cast Iron Pipeline, *Materials* 11 (2018) 332–342.
- 11) M. Zhang, C. Li, X. Wang, J. Peng, S. Yuan, H. G. Y. Zhou, Y. Gao, H. Wang, Ultrahigh anti-corrosion performance of polymer-based coating filled with a novel micro network nanofiller, *Corrosion Science* 190 (2021) 109685–109697.
- 12) A. M. Mathew, P. Predeep, Styrene butadiene co-polymer based conducting polymer composite as an effective corrosion protective coating, *Progress in Organic Coatings* 74 (2012) 14–18.

- 13) X. Bai, T. H. Tran, D. Yu, A. Vimalanandan, X. Huc, M. Rohwerder, Novel conducting polymer based composite coatings for corrosion protection of zinc, *Corrosion Science* 95 (2015) 110–116.
- 14) A. F. Baldissera, C. A. Ferreira, Coatings based on electronic conducting polymers for corrosion protection of Metals, *Progress in Organic Coatings* 75 (2012) 241–247.
- 15) A. Lutz, O. V. D. Berg, J. V. Damme, K. Verheyen, E. Bauters, I. D. Graeve, F. E. Du Prez, H. Terryn, A Shape-Recovery Polymer Coating for the Corrosion Protection of Metallic Surfaces, *ACS Appl. Mater. Interfaces* 7 (2015) 175–183.
- 16) M. Rohwerdera, L. M. Ducb, A. Michalika, , In situ investigation of corrosion localised at the buried interface between metal and conducting polymer based composite coatings, *Electrochimica Acta* 54 (2009) 6075–6081.
- 17) F. R. Rangel-Olivares, E. M. Arce-Estrada, R. Cabrera-Sierra, Synthesis and Characterization of Polyaniline-Based Polymer Nanocomposites as Anti-Corrosion Coatings, *Coatings* 11 (2021) 653–672.
- 18) N. Elhalawany, M. A. Mossad, M. K. Zahran, Novel water based coatings containing some conducting polymersnanoparticles (CPNs) as corrosion inhibitors, *Progress in Organic Coatings* 77 (2014) 725–732.
- 19) Namsheer K, Chandra S. Rout, Conducting polymers: a comprehensive review on recent advances in synthesis, properties and applications, *RSC Adv.*, 2021, 11, 5659-5697.
- 20) L. Hao, G. Lv, Yaqian Zhou, K. Zhu, M. Dong, Y. Liu, D. Yu, High Performance Anti-Corrosion Coatings of Poly (Vinyl Butyral) Composites with Poly N-(vinyl)pyrrole and Carbon Black Nanoparticles, *Materials (Basel)* 11(11) (2018) 2307.
- 21) M. Hafeez, M. Faheem, Z. Ul Abdin, K. Ahmad, S. Fazil, B. A. Khan, Synthesis And Characterization Of Polyaniline-Based Conducting Polymer And Its Anti-Corrosion Application, *Digest Journal of Nanomaterials and Biostructures*, 12 (2017) 707-717.
- 22) D. E. Tallman, G. Spinks, A. Dominis, G. G. Wallace, Electroactive conducting polymers for corrosion control, *Journal of Solid State Electrochemistry*, 6 (2002) 73–84.
- 23) N. Ahmad, A. G. MacDiarmid, Inhibition of corrosion of steels with the exploitation of conducting polymers, *Synthetic Metals*, 78 (1996) 103-110.
- 24) H. N. T. Le, B Garcia, C Deslouis, Q Le Xuan, Corrosion protection and conducting polymers: polypyrrole films on iron, *Electrochimica Acta*, 46 (2001) 4259-4272.

AC electrical characterization of PTh-PVAc thin films using Iodine as A dopant

Dhananjay P. Deshmukh

Department of Physics , Lt. R. B. Arts, Comm. And Smt. S. R. B. Sci. College, Arni, Dist- Yavatmal-445001 , India.
e-mail: dhananjaydeshmukh786@gmail.com (9960092223)

Abstract

Thin solid films of PTh-PVAc doped with Iodine (Pure, 5.5, 10.4, 14.9, 18.9 and 22.5 wt %) were synthesized by chemical oxidative polymerization method in order to study the electrical properties such as ac conductivity at various temperature ranges. The impedance spectra of films (323-343K over frequencies from 0.1-200 KHz) found to consist of only one arc suggest various parameters such as, bulk resistance, bulk capacitance, etc.

Keywords: Poly(vinyl acetate) (PVAc), Polythiophene (PTh), Iodine, dc, ac

1. Introduction

A number of applications have been proposed for PThs, such as field effect transistors, electroluminescent devices, solar cells, photochemical resists, nonlinear optic devices, batteries, diodes and chemical sensors [1]. The conjugating polymers thin films have been studied by many workers, because of special electrical properties, considerable thermal stability and oxidation resistance that are favorable in applications such as optoelectronic, biosensors, electrochromic displays and chemical sensors [2-3]. Roncali [4] surveyed the electrochemical synthesis and the electronic properties of substituted PThs in 1997. Barde et al [5] observed the variation in ionic conductivity in polypyrrole (PPy)-poly(vinyl acetate) (PVAc) films synthesized by oxidative polymerization. An investigation in electrical, structural properties and impedance spectroscopy in PTh-PVAc composite films doped with Iodine was carried out by Bobade et al and Deshmukh et al [6-7].

The present paper focuses on comparison in electrical properties of Polythiophene composite thin films doped with Iodine.

2 Experimental Procedure

2.1 Sample preparation

PTh was synthesized at room temperature (301 K) by mixing monomer thiophene (Lobachemie Pvt. Ltd., Mumbai, India) (AR grade) with a solution of anhydrous FeCl_3 (E. Merck, Darmstadt, Germany) as an oxidizing agent and PVAc (Lobachemie Pvt. Ltd., India) in methanol (AR grade). The concentration ratio of PVAc to methanol was 15:85, fixed for all samples. Then, FeCl_3 (0.2 M) was added to the solution for oxidation and the monomer, thiophene was further added. To study the effect of the dopant iodine, films with different wt % (5.5, 10.4, 14.9, 18.9 and 22.5 wt %) were synthesized.

2.2 ac conductivity measurement

ac conductivity of the samples was recorded on LCR meter (Wayne Kerr, UK) having range of frequencies from 0.1-200 KHz at temperature in the range 323-343K with heating rate 1°C min^{-1} . A constant voltage is applied to the sample and corresponding impedance and phase angle was measured at constant temperature for all frequency range.

3 Results and discussion

3.1 ac conductivity of PTh-PVAc films doped with Iodine

ac conductivity of the pure PTh-PVAc sample and doped with different Iodine wt % was measured at various temperatures 323-343K by applying a wide range of frequencies from 0.1-200 KHz. Fig. shows Nyquist plots of the samples Pure, 5.5 wt%, 10.4 wt% and 14.9 wt% samples and it is observed that the resistance of all the samples is found to be decreasing with the rise in temperature.

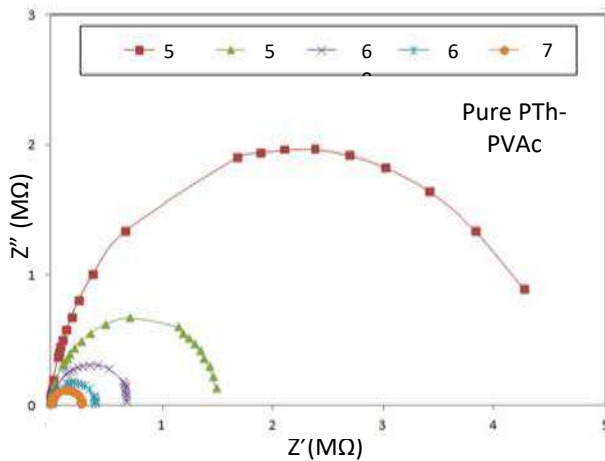


Fig 3.1.1

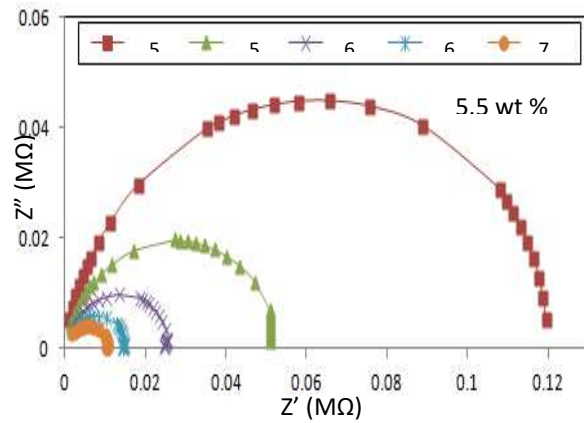


Fig 3.1.2

All the curves show the same trends in the temperature range 323-343 K. Many researchers [8-11] reported a similar conductivity isotherm. The impedance spectrum of PTh-PVAc pure film and doped with Iodine is found to consist of only one arc which may be taken to mean that the conduction processes have identical time constants [12].

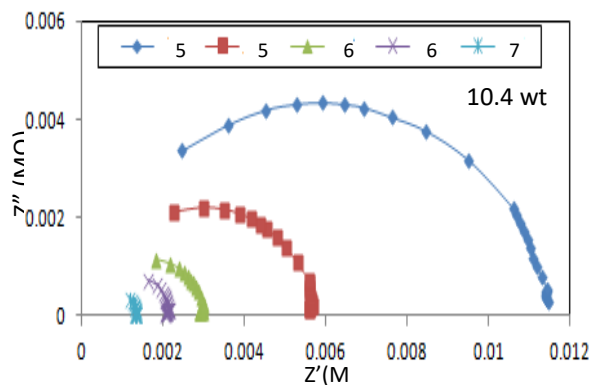


Fig 3.3

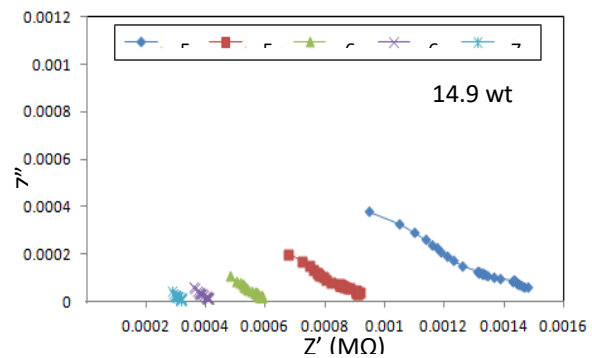


Fig 3.4

Also it may be argued that as the temperature increases the arc of semicircle reduces, indicating the increase in conductivity. The basic features of the spectra seem to be qualitatively similar to those obtained by Johnson et al. [13] for polythiophene films and Komura et al. for polypyrrole polystyrenesulfonate composite films in a similar configuration. The arcs are found to be highly depressed for the all films for different temperatures which indicate the distribution of relaxation times.

Table 3.1.1 Bulk resistance & Bulk capacitance of PTh-PVAc film doped with Iodine at diff. temp.

Iodine wt %	323 K		328 K		333 K		338 K		343 K	
	R _b (KΩ)	C _b (pF)	R _b (KΩ)	C _b (pF)	R _b (KΩ)	C _b (pF)	R _b (KΩ)	C _b (pF)	R _b (KΩ)	C _b (pF)
Pure PTh-PVAc	4850	54.72	1550	51.36	690	57.69	400	66.68	275	64.26
5.5	120	331.74	51	312.22	25.1	317.20	15.1	351.51	10.2	390.28
10.4	11.8	202.31	5.6	213.27	3.1	256.83	2.2	-	1.4	-
14.9	1.6	-	0.99	-	0.61	-	0.42	-	0.33	-

4. Conclusion

The impedance spectra of PTh-PVAc films doped with Iodine consist of only one arc which may be taken to mean that the conduction processes have identical time constants. On the basis of impedance spectra various parameters such as bulk resistance, bulk capacitance, etc. are calculated. Dielectric relaxation activation energy and relaxation time is maximum for Pure PTh-PVAc sample and minimum for 10.4 wt % of Iodine. The bulk capacitance is found to be maximum for the sample with 5.5 wt % Iodine.

References

- [1] Heuer HW, Wehrmann R, Kirchmeyer S. *Adv. Funct. Mater.* 2002, 12, 89 – 94.
- [2] E. M. Genes, A. Boyle, M. Lapkowski and C. Tsintavis, *Synth Met.*, 36 (1990) 139.
- [3] P. Novak, K. Muller, K. Santhanam and O. Haas, *Chem Rev.*, 97 (1997) 207.
- [4] Roncali J. *Chem. Rev.* 1997, 97, 173 – 205.
- [5] Barde WS, Pakade SV, Yawale SP. *J. Non Cryst. Solids* 2007,353, 1460 – 1465.
- [6] Bobade RS, Pakade (Yawale) SV, Yawale SP. *J. Non Cryst. Solids* 2009, 355, 2410 – 2414.
- [7] Deshmukh Dhananjay P, Yawale Sangita S, Yawale Shrikrishna P, *Journal of Polym Eng* 32 (2012): 103–110.
- [8] Abdel Salam Hamdy, *Int. J. Electrochem. Sci.*, pp.171-180, 1(2006).
- [9] T. Komura, S. Goisihara, T. Yamaguti, K. Takahashi, *J. Electroanal. Chem.*, pp.121, 456 (1998).
- [10] J. Ross Macdonald, *Annals of Biomedical Engineering*, pp.289-305, 20 (1992).
- [11] R Padma Suvarna, *Bull. Mater. Sci.*, pp.647-651, 25(7), (2002).
- [12] J. Hwang, *Solid State Ionics*, pp.93-104, 98(1997).
- [13] R. Tripathi, A. Kumar, 'Pramana' *J. Phys.*, pp. 969-978,72(6),(2009).

A Review - Metal Oxide Gas Sensor

Farhan Ahmad¹, Sanjay Devade²

^{1,2} Department of Physics, Shankarlal Khandelwal College, Akola

Corresponding Author: farhanahmad824@yahoo.com

Abstract:

Semiconductor metal oxides (SMOxs) are widely used in gas sensors due to their excellent sensing properties, abundance, and ease of manufacture. Metal oxide gas sensors operate based on the principle of chemisorption, where the interaction between target gas molecules and the surface of the metal oxide film induces changes in electrical conductivity. This interaction leads to measurable alterations in resistance, making metal oxide gas sensors highly sensitive and responsive to a wide range of gases, including volatile organic compounds, toxic gases, and environmental pollutants. Recent advancements in the field of metal oxide gas sensors have focused on enhancing their sensitivity, selectivity, and stability. Nanostructured metal oxides, composites, and functionalization techniques have been employed to improve sensor performance. Additionally, advancements in fabrication technologies, such as microelectromechanical systems (MEMS), have contributed to the miniaturization and integration of sensors, enabling their deployment in compact and portable devices. Different parameters which affect the performance (sensitivity, selectivity and stability) of SMO gas sensors are discussed here.

Keywords: gas sensing; metal oxide; bandgap; particle size; doping.

Introduction:

The atmosphere has become polluted and is rapidly deteriorating as a result of the rapid growth in industrial development and population. It is critical to monitor and control such harmful gases in order to avoid environmental disasters. A wide range of gases in the atmosphere must be detected, including oxygen, hydrogen, nitrogen dioxide, carbon dioxide, methane, and many more. Since 1962, the first gas sensing device made of thin-film zinc oxide and porous tin oxide ceramics has been demonstrated. Over the last 40 years, solid-state gas sensors have gone through numerous stages of development. There are two major development trends: one is to develop portable hybrid-array gas sensors for a variety of gases, and the other is to investigate new principles and production technologies in order to investigate different detection ranges for various gases. The need for higher performance with low-power, small-size, and relatively low-cost applications in environments with variable ambient conditions is the decisive objective, whether it is hybrid array gas sensors or single sensors. For hybrid-array gas sensors, the new concept of nanostructure-based gas sensors not only improves sensing properties in terms of sensitivity and response time, but also reduces operating temperature and improves integrated circuit density. It has also accelerated the development of low-power, small-size, and relatively low-cost semiconducting metal oxide gas sensors. The different synthesis methodologies for nanoscale materials can mostly be performed in a lab. The increase in operating temperature to near-human temperature regimes, as well as improved sensing properties derived from nanostructured material-based gas sensors, has broadened the applications to environmental, domestic, and medical fields previously unattainable with coarse materials [1].

Metal Oxide gas sensing mechanism:

Metal oxide gas sensors have been widely used in portable gas detection systems because of their advantages such as low cost, easy production, compact size and simple measuring electronics [2,3]. However, the performance of such sensors is significantly influenced by the morphology and structure of sensing materials, resulting in a great obstacle for gas sensors based on bulk materials or dense films to achieve highly-sensitive properties. Gas sensors based on nanomaterials are a greatly developing direction to improve gas sensing properties in sensitivity, selectivity and response speed. Although there are already some reviews on metal oxide gas sensor it is still necessary to systematically summarize the features of metal oxides from the perspective of nanoscience and nanotechnology. In this review, we provide a brief summary on metal oxide nanostructures and their gas sensing properties from the aspects of particle size, morphology and doping. Most of the examples are given based on n-type metal oxides which are more extensively investigated and applied among the metal oxide gas sensors. It is necessary to reveal the sensing mechanism of metal oxide gas sensors which is helpful for designing and fabricating novel gas sensing materials with excellent performance. Although the exact fundamental mechanisms that cause a gas response are still controversial, it is essentially responsible for a change in conductivity that trapping of electrons at adsorbed molecules and band bending induced by these charged molecules. Herein, a brief introduction to the sensing mechanism of n-type metal oxides in air is given based on the example of SnO₂. Typically, oxygen gases are adsorbed on the surface of the SnO₂ sensing material in air. The adsorbed oxygen species can capture electrons from the inner of the SnO₂ film. The negative charge trapped in these oxygen species causes a depletion layer and thus a reduced conductivity. When the sensor is exposed to reducing gases, the electrons trapped by the oxygen adsorbate will return to the SnO₂ film, leading to a decrease in the potential barrier height and thus an increase in conductivity. There are different oxygen species including molecular (O₂⁻) and atomic (O⁻, O₂⁻) ions on the surface depending on working temperature. Generally, below 150 °C the molecular form dominates while above this temperature the atomic species are found. The overall surface stoichiometry has a decisive influence on the surface conductivity for the metal oxides. Oxygen vacancies act as donors, increasing the surface conductivity, whereas adsorbed oxygen ions act as surface acceptors, binding electrons and diminishing the surface conductivity. On SnO₂ films the reaction $O_2^{-ads} + e^{-} = 2O^{-ads}$ takes place as the temperature increases. The desorption temperatures from the SnO₂ surface are around 550 °C for O⁻ ads ions and around 150 °C for O₂⁻ ads ions. At constant oxygen coverage, the transition causes an increase in surface charge density with corresponding variations of band bending and surface conductivity. From conductance measurements, it is concluded that the transition takes place slowly. Therefore, a rapid temperature change on the part of the sensors is usually followed by a gradual and continuous change in the conductance. The oxygen coverage adjusts to a new equilibrium and the adsorbed oxygen is converted into another species which may be used in measurement method of dynamic modulated temperature as reported previously. The performance of gas sensors can be evaluated by different parameters like sensitivity, selectivity, response time, reversibility or recovery time fabrication cost and stability. Sensitivity is the smallest volume concentration of the target gas that can be sensed in the time of detection. Sensitivity can be defined as R_a/R_g for reducing gases and R_g/R_a for oxidizing gases, where R_a is the resistance of the gas sensor in the reference gas (usually air) and R_g stands for resistance of the sensor in the target gas. This is unit less parameter and percentage sensitivity is expressed by $[(R_a - R_g)/ R_a] * 100\%$. Selectivity is the ability of the gas sensors to detect a specific gas in a mixture of gases. Response time is the period from the time when gas concentration reaches a specific value to that when a sensor generates a corresponding signal. Reversibility is whether a sensor returns to its original state when gas concentration returns to normal. Recovery time is the time required for a sensor signal

to return to its initial value after a step concentration change from a certain concentration value to zero. Stability is the ability of a gas sensor to reproduce results for a certain period of time. The result includes retaining the sensitivity, selectivity, response time and recovery time. An ideal sensor should possess high sensitivity, selectivity and stability, low response time and recovery time and low fabrication cost [4,5,6,7]. Doping during synthesis and deposition process influence those metal oxide properties which are important for gas sensing applications. The parameters like sensitivity, selectivity, response time and stability of the gas sensors are improved by addition of different dopants [8]. In some cases, dopants are added to a metal oxide to modify its properties by enhancing the desirable properties, while in other cases undesirable properties are reduced or eliminated [9]. Even though SMO gas sensors are catalytically active, a small amount of catalytically active metals or metal oxides are often added to it for improving the selectivity and sensitivity of the sensors. For example, the surface modification by noble metals promotes the improvement in sensitivity and decrease in response and recovery times. The metal oxide doping by transition metal modifies the catalytic reactivity and morphology of deposited films. There are different mechanisms which are followed by dopants/impurities to enhance the properties of nanoparticles metal oxides like (i) change in microstructure and morphology, (ii) formation of stoichiometric solid solution, (iii) change in activation energy, (iv) generating oxygen vacancy, and (v) change in electronic structure. Microstructure and grain size are the two most influential factors in sensing properties of semiconductor gas sensors. Sensor response increases drastically when grain size decreases.[10]

Conclusion:

A study on semiconductor metal oxide gas sensors has been exhibited in this review. General properties and gas sensing mechanisms of SMOs are also discussed. Moreover, a comprehensive study has also been done on factors that are affecting the sensitivity, selectivity and stability of the semiconductor metal oxide gas sensors. The study establishes that the dopants or impurities enhance the gas sensing properties of SMOs by any of the processes such as changing the microstructure or morphology, forming stoichiometric solid solution, changing the activation energy, generating oxygen vacancy or changing the electronic structure/band gap.

References:

- 1) Gupta, A., Verma, G. (2023). Nanostructured Gas Sensors: Fundamentals, Devices, and Applications. Singapore: Jenny Stanford Publishing.
- 2) Sun, Yu-Feng; Liu, Shao-Bo; Meng, Fan-Li; Liu, Jin-Yun; Jin, Zhen; Kong, Ling-Tao; Liu, Jin-Huai (2012). Metal Oxide Nanostructures and Their Gas Sensing Properties: A Review. *Sensors*, 12(12), 2610–2631.
- 3) Dey, Ananya (2018). Semiconductor metal oxide gas sensors: A review. *Materials Science and Engineering: B*, 229(), 206–217.
- 4) T. Anukunprasert, C. Saiwan, E. Traversa, The development of gas sensor for carbonmonoxide monitoring using nanostructure Nb-TiO₂, *Sci. Technol. Adv. Mater.* 6 (2005) 359–363.
- 5) R.H. Bari, S.H. Patil, A.R. Bari, Spray-pyrolized nanostructured CuO thin films for H₂S gas sensor, *Int. Nano Lett.* (2013) 1–5.
- 6) N. Barsan, D. Koziej, U. Weimar, Metal oxide-based gas sensor research: how to? *Sens. Actuators B* 121 (2007) 18–35.
- 7) M. Batzill, U. Deibold, Surface studies of gas sensing metal oxides, *PCCP* 9 (2007) 2307–2318.
- 8) A. Ruiz, J. Arbiol, A. Cirera, A. Cornet, J.R. Morante, Surface activation by platinum clusters on titania for gas sensing applications, *Mater. Sci. Eng. C* 19 (2002) 105–109.
- 9) D.M. Smyth, The effects of dopants on the properties of metal oxides, *Solid State* 129 (2000) 5–12.
- 10) M. Yuasa, T. Masaki, T. Kida, K. Shimano, N. Yamazoe, Nanosized PdO loaded SnO₂ nanoparticles by reverse micelle method for highly sensitive CO gas sensor, *Sens. Actuators B* 136 (2009) 99–104.

Optical and structural property of $\text{YBO}_3:\text{Tb}^{3+}$ phosphor synthesized by novel Aldo-Keto gel method

K. K. Rathod¹, K. A. Koparkar^{1*}

¹Department of Physics, M.S.P. Arts, Science & K.P.T. Commerce College Manora, Washim (M.S.)

*(Corresponding Email: kakoparkar@gmail.com)

Abstract:

Synthesis of Tb^{3+} doped YBO_3 by using Aldo-keto gel method. The characterization of $\text{YBO}_3:\text{Tb}^{3+}$ material was done by X-ray diffraction and the optical property was studied under UV light wavelength. The $\text{YBO}_3:\text{Tb}^{3+}$ phosphor shows strong absorption with 239 nm UV source and exhibits intensive emission was obtained at 490 nm and 544 nm, which corresponds to the blue green emission.

Keywords: Aldo-keto gel method, Borate, XRD, Photoluminescence.

1. Introduction

During the past few years, much attention has been paid to the study of UV triggering phosphors due to the high demands of various applications [1]. There are various types of borates related to the position and type of anionic groups $[\text{BO}_3]$ in the lattice structure. Among these borates, orthoborate phosphors are widely used in many applications such as field emission displays, plasma display panels, cathode ray tubes and a new generation of Hg-free fluorescent lamps [2-4]. Though most of the orthoborate possess good luminescent properties the only attention has been paid to the yttrium orthoborate because of its suitable properties as a host such as efficient luminescence, high VUV transparency and also exceptional optical damage threshold with a great ability to stand in harsh conditions present in vacuum discharge lamps and screens [5].

K. Koparkar et al. synthesized series of $(\text{Y}_{(1-x)}\text{Gd}_x)\text{BO}_3:\text{Eu}^{3+}$ phosphors was successfully synthesized by precipitation method. The PL emission spectra of phosphors indicated that red–orange (595 nm) color could be well excited by 233 nm. The results showed that outstanding fluorescence intensity [6].

Jung et al. modified the luminescent properties of $\text{YBO}_3:\text{Eu}^{3+}$ synthesized through spray pyrolysis with sintering temperature 1100°C for 3h to enhancement of luminescent intensity of red phosphor under vacuum ultraviolet excitation [7].

There are many reports for on synthesis of various structure types of borate such as solid state reaction sol-gel method, hydrothermal method, co-precipitation method and combustion method [8]. In this paper, we have tried to synthesize $\text{YBO}_3:\text{Tb}^{3+}$ by using Aldo-keto gel method [9]. Further, photoluminescence spectra of the $\text{YBO}_3:\text{Tb}^{3+}$ phosphor was investigated in detail.

2. Experimental section

The phosphors were prepared by novel technique of aldo–keto gel method. YBO_3 doped with $\text{Tb}_{0.01}$ has been synthesized by using aldo–keto gel method. The starting chemicals Y_2O_3 (99.99%, AR) and Tb_4O_7 (99.90%, AR) were mixed together in a china clay basin. A small quantity of double distilled water was added and paste was formed. HNO_3 was added drop by drop and mixture was heated slowly under observation to 50°C till the paste dissolved completely. The solution was further heated till the excess of acid was boiled off. Little quantity

of double distilled water was again added and slowly evaporated to dryness. The resulting powder was $\text{Y}(\text{NO}_3)_3:\text{Tb}$, after that soluble solution of H_3BO_3 (AR) was added. The dried precursor was finally milled. Acetone (2M, AR) and benzaldehyde (2M, AR) were added to the nitrate. The pale brownish yellow mixture obtained was stirred continuously and slowly heated to 130°C . The mixture became dark brownish yellow and then dark reddish brown between 80°C to 120°C with evolution of brownish gases. The process of gelation started at near about 130°C with the evolution of dark yellowish brown fumes. The mixture was then allowed to cool. Red gel was formed after cooling. It was further heated slowly to 300°C . Dark red foam was formed with evolution of yellowish brown fumes. On further slow heating, pyrolysis of foam was started at 450°C and shining black foam was formed at 600°C , which started burning from 900°C . Final product appears as white crystalline powder of $\text{YBO}_3:\text{Tb}^{3+}$.

3. Results and Discussion:

The phase purities of $\text{YBO}_3:\text{Tb}^{3+}$ sample were studied using Rigaku miniflex II X-ray Diffract meter with scan speed of $2.000^\circ/\text{min}$ and $\text{Cu K}\alpha$ ($\lambda = 1.5406 \text{ \AA}$) radiation in the range 10° to 90° . The photoluminescence (PL) and PL excitation (PLE) spectra were measured on (Hitachi F-7000) fluorescence spectrophotometer at room temperature. The spectral resolution of both excitation and emission spectra, width of the monochromatic slits (1nm), as well the measurement conditions such as PMT detector sensitivity and scan speed were kept constant from sample to sample in measurements.

3.1. XRD patterns of $\text{YBO}_3:\text{Tb}^{3+}$

The formation of the crystalline phase of as-prepared products was confirmed by X-ray diffraction patterns of $\text{YBO}_3:\text{Tb}^{3+}$ as shown in Figure 1 to verify the phase purity and crystal structure. The X-ray pattern of combustion synthesized sample at 900°C indicated a dominant phase of the standard $\text{YBO}_3:\text{Tb}^{3+}$ and all the peaks are in good agreement with the (ICDD,00-016-0277) The XRD pattern for $\text{YBO}_3:\text{Tb}^{3+}$ agrees well with the standard data from ICDD file (00-016-0277). The high intensity peaks i.e., $108.6880, 20.1647, 48.1569, 49.9016, 27.2492$ and 34.146 form ICDD file shows exact matching with the XRD pattern of phosphor prepared by re-crystallization method. This agreement indicates that the phosphor $\text{YBO}_3:\text{Tb}^{3+}$ has been success prepared by using the re-crystallization method. Also the XRD shows that the formed material is completely crystalline and is in single phase with Hexagonal structure where $a = b = 3.778$ and $c = 8.810 \text{ \AA}$. Also the symmetry allowed crystal structure properties for $\text{YBO}_3:\text{Tb}^{3+}$ are Centro symmetric, And Space Group P63/m (176).

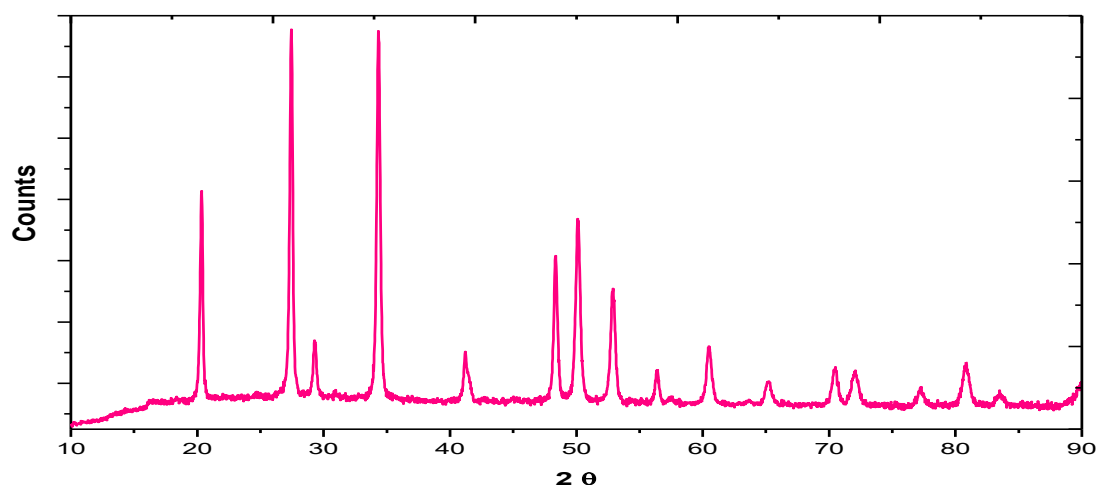


Figure 1: XRD patterns of the $\text{YBO}_3:\text{Tb}^{3+}$ phosphor synthesized by Aldo-keto gel method.

3.2 Photoluminescence study

Fig. 2 gives the excitation and emission spectra of Tb^{3+} green emission in Tb^{3+} doped YBO_3 . The excitation spectrum shows broad bands from 200 to 250 nm. The $YBO_3:Tb^{3+}$ powders exhibited emissions at 490 and 544, which corresponding to the $^5D_4-^7F_6$ and $^5D_4-^7F_5$ transitions of Tb^{3+} , respectively. Among them, the green emission at 544 nm ($^5D_4-^7F_5$) was dominant and the emission intensities are greatly dependent on the excitation wavelength. Local crystal field symmetry around the Tb^{3+} cations can have a significant effect on electric dipole transitions.

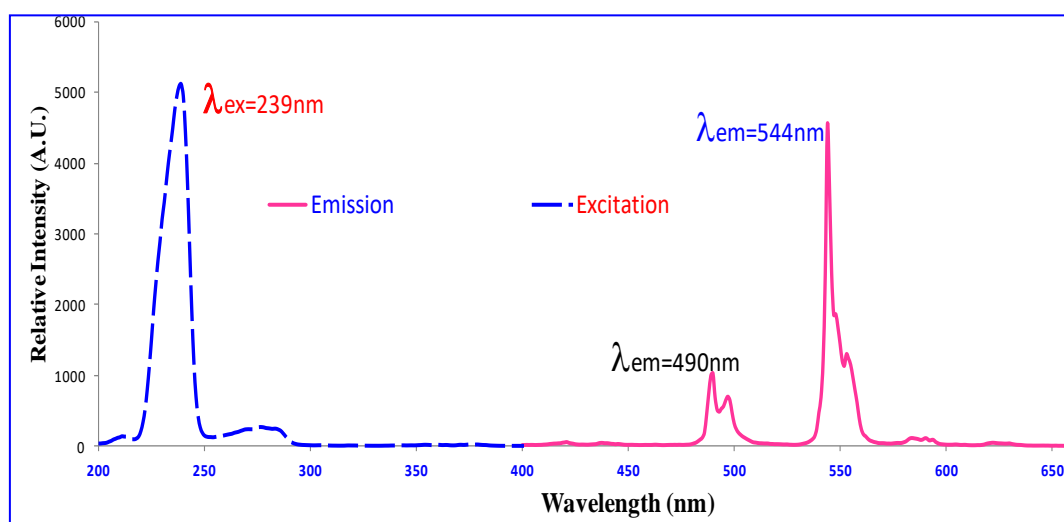


Figure 2: PL Excitation and Emission spectra of $YBO_3:Tb^{3+}$.

Conclusions

$YBO_3:Tb^{3+}$ phosphor synthesized by the Aldo-keto gel method. XRD pattern shows perfect matching with the ICDD file. From the excitation and emission spectra of doping samples, there exist two kinds of samples characteristic of green emission due to Tb^{3+} ions in YBO_3 host, respectively. Also, there is an energy transfer from Tb^{3+} ions.

Acknowledgement

One of the authors K. K. Rathod is thankful to Principal, Shri Shivaji Science college Amravati for providing XRD facility.

References

- [1] X. Guo, Y. Wang, J. Zhang, J. Cryst. Growth 311 (2009) 2409–2417.
- [2] L. Yang, L. Zhou, X. Chen, X. Liu, P. Hua, Y. Shi, X. Yue, Z. Tang, Y. Huang, J. Alloys Compd., 509 (2011) 3866–3871.
- [3] F.S. Chen, C.H. Hsu, C.H. Lu, J. Alloys Compd. 505 (2010) L1–L5.
- [4] A. Szczeszak, S. Lis, V. Nagirnyi, Journal of Rare Earths. 29 (2011) 1142.
- [5] E. M. Levin, R. S. Roth, Journal of Rare Earths. 29 (2011) 1142.
- [6] K.A. Koparkar, N.S. Bajaj, S.K. Omanwar, Opt. Mat., 39 (2015) 74-80.
- [7] K Y.Jung, Phy. B, 405 (2010) 3195.
- [8] K. A. Koparkar, Ind. Stream Jour., 3(2013) 16.
- [9] S. K. Omanwar, K. A. Koparkar, H. S. Virk, Defect & Diffusion Forum. 347 (2013) 75-110.

Review on Improving Photoluminescence Emission in Borate Phosphors Activated by Gd^{3+}

Mohammad Jived, R.P. Snooker, Sanjay Hargonani, R.M. Chavan, Sapna Rajankar

G.S. Science, Arts, Commerce College, khamgaon Dist:- Buldhana M.S. India

*Corresponding author E-mail: Javed.phy@gmail.com

Abstract:

This review paper explores the photo luminescent properties of Gd^{3+} in diverse inorganic phosphors. The specific interest lies in the narrow band UVB (NB-UVB) emission of Gd^{3+} within the 312-315 nm range, particularly relevant in the medical domain for treating conditions such as atopic dermatitis, vitiligo, and psoriasis. However, the inherent weakness of the $4f-4f$, $6P_j \rightarrow 8S_{7/2}$ intra-configurational transition in Gd^{3+} necessitates sensitization. Effective sensitizers like Bi^{3+} and Pr^{3+} have been identified to enhance the photo luminescent emission of Gd^{3+} . These sensitized Gd^{3+} phosphors show great promise for utilization in phototherapy lamps.

Keywords: Gadolinium, Sensitized Luminescence, Narrow-Band UVB, Phototherapy

1. Introduction

Since ancient times, sunlight therapy, also known as heliotherapy, has been employed to treat various cutaneous diseases in humans. The 'Atharva Veda,' a sacred Indian text, makes references to treating leucoderma through sunlight exposure and the consumption of *Psoralea corylifolia* seeds [1]. *Psoralea corylifolia* seeds, containing photosensitizing psoralen compounds, have been traditionally used for skin disorder treatments [2]. Sunlight's significant benefit lies in its capacity to boost the body's vitamin D levels.

The roots of modern phototherapy trace back to the 19th century when Niels Rydberg Finsen pioneered the use of artificial light sources for phototherapy. In 1896, he developed a chemical ray's lamp and successfully treated lupus vulgaris at the Phototherapy Institute in Copenhagen, earning him the title "the father of ultraviolet therapy." Finsen was awarded the Nobel Prize in medicine for his groundbreaking work on the treatment of lupus vulgaris with concentrated light rays additionally; filtered sunlight has been recognized as a safe and effective phototherapy treatment for hyperbilirubinemia [3].

The first report on phototherapy for hyperbilirubinemia appeared in the medical journal 'Lancet' in 1958 at Rochford Hospital, Essex, England. Sister Jean Ward, a nurse at Rochford General Hospital, introduced the treatment approach. Dr. R.H. Dobbs and resident registrar Richard Cremer documented Sister Jean's practice of exposing delicate infants to fresh air and warm sunshine, believing it to be more beneficial than an incubator's confined environment [4]. Rochford Hospital continued experimental treatments, and Cremer, along with biochemist P.W. Perryman, demonstrated that sunlight or artificial blue light from 40W fluorescent tubes could reduce bilirubin levels in jaundiced newborn infants [5]. The term 'Phototherapy' was officially coined by Ferreira et al. in September 1960 during their experimental treatment of 77 jaundiced infants [6].

1.1. Overview of Phototherapy:

Phototherapy involves the utilization of light for the treatment of various skin conditions, whether through exposure to natural sunlight or artificial lamps [7]. The sunlight comprises

different regions of the electromagnetic spectrum based on wavelength, with Ultraviolet (UV) being a significant part.

1.2. UV Wavelengths:

The UV wavelength band, ranging from 200 to 400 nm, is divided into UVA (320–400 nm), UVB (280–320 nm), and UVC (200–280 nm) regions. UVA1 and UVA2 are further classified based on their specific wavelengths. These UV radiations are absorbed by chromophores, which are biological molecules like DNA, RNA, proteins, or drugs [8].

1.3. UVA1 Radiation in Dermatology:

UVA1 radiation, particularly in the range of 340–400 nm, has gained recognition in dermatology and rheumatology. It is employed in the treatment of various skin conditions, including extra genital lichen sclerosis, Scleroderma, T-cell lymphoma, and Lupus erythematosus [9][10]. Psoralen photo chemotherapy combines Psoralen with long-wave UVA radiation for treating multiple skin disorders [11].

1.4. UVB and Its Phototherapeutic Role:

Goeckerman introduced Broadband UVB in 1925 for psoriasis treatment, later replaced by Narrowband UVB, which effectively clears psoriatic lesions and reduces skin inflammation. This cost-effective treatment is considered a phototherapeutic modality for managing psoriasis [12]. Properly dosed UVC promotes wound healing while causing lethal and mutagenic effects on microorganisms, preserving mammalian cell viability [13].

1.5. Phototherapy for Neonatal Jaundice and Beyond:

A major medical application of phototherapy is the treatment of hyperbilirubinemia or jaundice. The absorbed light breaks down bilirubin into water-soluble and extractable products. Bili blankets, fiber optic or compact fluorescent light tubes, and blue LEDs are considered medically safe for treating Neonatal Jaundice. Phototherapy is also explored for diabetic retinopathy and hair loss treatment [14].

2. Advancements in Phototherapy Research:

Absorption of ultraviolet radiations by skin chromophores triggers the production of DNA photoproducts, initiating photochemical reactions essential for tissue repair [15]. Phototherapy lamps deliver focused UV light to the affected body part, employing phosphor materials activated with Eu^{2+} , Pb^{2+} , Gd^{3+} , and Pr^{3+} . Commercially, Gd^{3+} and Eu^{2+} are common activators in phototherapy phosphors [16].

2.1. Gd^{3+} as an Efficient Activator:

Trivalent Gd^{3+} exhibits ground level $8S7/2$ and excited levels $6Pj$, $6Ij$, $6Dj$, $6Gj$. The excitation of Gd^{3+} ions results in the $6P7/2 \rightarrow 8S7/2$ transition in the NB-UVB region around 312-315 nm. Gd^{3+} emerges as a sought-after activator for advanced phosphors, especially in medical applications for treating photo-responsive diseases. Researchers focus on various host lattices for Gd activators, aiming for efficient phosphors demanded in phototherapy lamps for skin conditions like atopic dermatitis, vitiligo, psoriasis, seborrheic dermatitis, etc. [17].

2.2. Significance of Borate Hosts:

Borate atoms, with planar sp_2 and three-dimensional sp_3 hybridized orbitals, can readily accommodate three to four oxygen atoms, forming various anionic groups. Inorganic borates, easily synthesized and structurally feasible for doping on multiple cationic sites, find extensive use in research and commercial applications. Their diverse structure types, superior optical quality, low synthesis temperature, transparency across a wide wavelength range, good chemical stability, and wide band gap make borates ideal for phototherapy, optical and laser devices, plasma display panels, LEDs, etc. Well-established examples include $\text{LaB}_3\text{O}_6:\text{Gd}^{3+}$, Pr^{3+} , and $\text{CeMgB}_5\text{O}_{10}:\text{Gd}^{3+}$, recognized NB-UVB phosphors used in phototherapy lamps [18]. This section discusses selected Gd-activated phosphors and their potential in phototherapy.

2.3. Gd^{3+} Activated Narrow Band UVB Emitting Phosphors for Phototherapy Lamps:

2.3.1. $\text{LaPO}_4:\text{Gd}^{3+}$:

Chauhan et al. [19] successfully prepared Gd³⁺ activated lanthanum phosphate (LaPO₄) through recrystallization. PL excitation spectra recorded at room temperature showed a strong absorption peak at 275 nm. Upon excitation at 275 nm, the phosphor emitted significantly at 312 nm due to the 6P_J → 8S_{7/2} transition of Gd³⁺ ions. LaPO₄:Gd³⁺ with 0.04 mol% Gd³⁺ concentration exhibited intense emission and holds potential as a phototherapy lamp phosphor [19].

2.3.3 SrY₂O₄:Gd³⁺:

Singh and team [20] synthesized Gd³⁺ activated SrY₂O₄ phosphors via the sol-gel method. Photoluminescence spectra for different Gd³⁺ concentrations showed two bands in the NB-UVB spectral regions: one at 309 nm due to the 6P_{5/2} → 8S_{7/2} electric dipole transition and another at 315 nm by the 6P_{7/2} to 8S_{7/2} transition of Gd³⁺ ions. The strong emission at 315 nm positions SrY₂O₄:Gd³⁺ as a potential material for phototherapy lamps producing UVB light [20].

2.3.4 Na₃Y_{1-x}Si₂O₇:Gd_x:

Another series, Na₃Y_{1-x}Si₂O₇:Gd_x, was synthesized by Singh et al. [21] using the sol-gel process with Gd concentration ranging from 0.01 to 0.11 mol%. Excitation at 273 nm resulted in ultraviolet emission, specifically a sharp peak at 313 nm, arising from the transition of Gd ions from 6P_{7/2} to 8S_{7/2} energy state [21].

2.3.5 CaMgP₂O₇:Gd³⁺:

Kunghatkar et al. [22] synthesized CaMgP₂O₇:Gd³⁺ phosphor using various methods. The phosphor demonstrated effective g values, and its emission at 314 nm wavelength upon excitation at 274 nm proved the proper incorporation of Gd³⁺ ions. The sol-gel method yielded the most promising results for the preparation of phosphate phosphors, presenting intense excitation peaks and showing potential for phototherapy treatment due to its emission in the narrow-band UVB region [22].

3.1 Enhanced Narrow Band UVB Emission of Gd³⁺ Using Sensitizers in Borate Phosphors for Phototherapy Lamp:

3.1.1 BaB₈O₁₃: Pr³⁺, Gd³⁺ Phosphor:

In the study by Sumedha et al. [23], BaB₈O₁₃:Gd³⁺ phosphor was synthesized using solid-state synthesis, exhibiting efficient Gd³⁺ emission. The excitation spectrum revealed peaks at various wavelengths, and the intense dominant peak at 274 nm resulted in a brilliant and sharp emission peak at 314 nm. To enhance the emission intensity, Pr³⁺ was introduced as a sensitizer in BaB₈O₁₃: Pr³⁺, Gd³⁺. Pr³⁺ contributed to the PL excitation spectrum with a broad absorption band at 220 nm. The introduction of Pr³⁺ resulted in a considerable increase in Gd³⁺ emission intensity at 313 nm, demonstrating the potential of BaB₈O₁₃: Pr³⁺, Gd³⁺ for phototherapy lamps [23].

3.1.2 (LaY)BaB₉O₁₆:Bi³⁺, Gd³⁺:

Gawande et al. [24] investigated (LaY)BaB₉O₁₆:Bi³⁺, Gd³⁺ synthesized through the solution combustion synthesis technique. The compound exhibited a hexagonal crystal structure, and PL excitation spectra revealed a broad peak due to Bi³⁺ ions. The energy transfer from Bi³⁺ ions to Gd³⁺ resulted in a significant increase in Gd³⁺ emission intensity, highlighting the potential application of this phosphor in phototherapy lamps [24].

3.1.3 Y_{0.96}Gd_{0.04}BO₃, Y_{0.955}Gd_{0.04}Bi_{0.005}BO₃, Y_{0.93}Gd_{0.04}Pr_{0.03}BO₃ Phosphors:

Gawande et al. [25] conducted a study on Gd³⁺ in YBO₃ compound with Bi and Pr as sensitizers. These phosphors exhibited narrow-band UVB emission at 312 nm due to 6P_J → 8S_{7/2} transition by Gd³⁺ ions. The introduction of Bi and Pr sensitizers enhanced the emission intensity, with Pr³⁺ proving to be a more efficient sensitizer for Gd³⁺ than Bi³⁺ [25].

4. Conclusion:

The utilization of narrow band UVB emission in phototherapy has become widespread due to its compatibility with the action spectrum of various skin disorders and its safety for multiple exposures. Phosphors doped with gadolinium have garnered significant attention owing to their narrow band emission upon UV excitation. Despite the inherent challenge of weak 4f-4f emission in gadolinium, this limitation has been effectively addressed by employing suitable sensitizers. Bi^{3+} and Pr^{3+} have emerged as effective sensitizers for Gd^{3+} , leveraging their emission spectra that overlap with the excitation spectrum of gadolinium. This ensures a successful energy transfer from the sensitizer to the activator gadolinium. The sensitized luminescence of gadolinium-doped phosphors exhibits remarkable emission with increased intensity, making them highly suitable for application in phototherapy lamps.

5. References:

1. Hönigsmann H 2013 "History of phototherapy in dermatology," *Photochem. Photobiol. Sci* 12: 16-21.
2. Jones L R (eds) 2005 "An Overview of Phototherapy. The Science of Phototherapy: An Introduction. Springer, Dordrecht. https://doi.org/10.1007/1-4020-2885-7_1," Online ISBN: 978-1-4020-2885-4, 2005.
3. Slusher TM, Vreman HJ 2018 "Filtered sunlight versus intensive electric-powered phototherapy in moderate-to-severe neonatal hyperbilirubinaemia: a randomized controlled non-inferiority trial," *The Lancet Global Health*, 6(10): 1122-1131
4. Maisels MJ 2015 "Sister Jean Ward, phototherapy, and jaundice: a unique human and photochemical interaction," *Journal of Perinatology* 35: 671-675.
5. Cremer RJ, Perryman PW, Richards DH 1958 "Influence of light on the hyperbilirubinemia of infants," *The Lancet* 271(7030): 1094-1097.
6. Dobbs RH, Cremer RJ 1975 "Phototherapy," *Archives of Disease in Childhood* 50: 833-836.
7. Nimbalkar M, Yawalkar M, Mahajan N, Dhoble SJ 2020 "Potential of luminescent materials in phototherapy," *Photodiagnosis and Photodynamic Therapy* <https://doi.org/10.1016/j.pdpdt.2020.102082>
8. Hemne PS, Kunghatkar RG, Dhoble SJ 2017. "Phosphor for phototherapy: Review on psoriasis," *Luminescence* 32: 260-270.
9. Breuckmann F, Gambichler T, Altmeyer P and Kreuter A 2004 "UVA/UVA1 phototherapy and PUVA photochemotherapy in connective tissue diseases and related disorders: a research based review," *BMC Dermatol.*, 4, 11, doi:10.1186/1471-5945-4-11, 2004.
10. Ranaweera A 2012 "UVA1 phototherapy," <https://dermnetnz.org/topics/uva1-phototherapy/2012>. Downloaded 28 Nov 2020
11. Parrish J A 1981 "Phototherapy and Photochemotherapy of Skin Diseases," *The Journal of Investigative Dermatology* 77: 167-171.
12. Pena S, Hill D, Feldman SR 2016 "Therapy for Severe Psoriasis: Chapter 2 Ultraviolet B Phototherapy," <https://doi.org/10.1016/B978-0-323-44797-3.00002-5> ISBN:978-0-323-44797-3
13. Gupta A, Avci P, Dai T, Huang YY and Hamblin MR 2012 "Ultraviolet Radiation in Wound Care: Sterilization and Stimulation," *Advances in wound care*, 2(8): 422-437. DOI: 10.1089/wound.2012.0366.
14. Racz E, Prens EP 2017. Phototherapy of psoriasis, chronic inflammatory skin diseases. *Adv Exp Med Biol*. 996: 287 - 294.
15. Duarte I, Buense R, Kobata C 2006. "Phototherapy," *Anais Brasileiros de Dermatologia* 81: 2006.
16. Hemne PS, Kunghatkar R, Dhoble SJ 2018 "UVB emitting LiSrBO_3 phosphor for phototherapy lamp," *AIP Conference Proceedings* 1953(1):080038, <https://doi.org/10.1063/1.5032844>

17. Singh V, Sivaramaiah G, Singh N 2019 "Ultraviolet B emission from a Gd³⁺ doped BaAl₂O₄ powder phosphor," Bull Mater Sci 42:19. <https://doi.org/10.1007/s12034-018-1708-x>
18. Gawande AB, Snooker RP, Kapse SD, Mahalle NS 2016 "Synthesis and Photoluminescence Properties of Ba₂B₂O₅:Pr^{0.02}," International Journal of Luminescence and applications 6: 82-84.
19. Chauhan AO, Gawande AB, Omanwar SK 2016. "Narrow band UVB emitting phosphor LaPO₄:Gd³⁺ for phototherapy lamp," Optik, 127 (16): 6647-6652.
20. Singh V, Swapna K, Kaur S, Rao AS, Rao JL 2020 "Narrow-Band UVB-Emitting Gd-Doped SrY₂O₄ Phosphors," Journal of Electronic Materials, 49(5): 3025-3030 DOI: 10.1007/s11664-020-08032-x, 2020.
21. Singh V, Singh N, Pathak MS, Natarajan V 2019 "Development of UVB Radiation -Emitting Gd³⁺-Doped Na₃YSi₂O₇ Host Material," Journal of Electronic Materials 48 (3):498–1505.(2019 no. DOI: 10.1007/s11664-018-06884-y, 2018.
22. Kungatkar RG, Barai VL, Dhoble SJ 2019. "Synthesis route dependent characterizations of CaMgP₂O₇: Gd³⁺ phosphor," Results in Physics 13102295.
23. Tamboli S, Nair GB, Dhoble SJ, Burghate DK 2018 "Energy transfer from Pr³⁺ to Gd³⁺ ions in BaB₈O₁₃ phosphor for phototherapy lamps," Physica B 535 : 232–236.
24. Gawande AB, Snooker RP, Omanwar SK 2018. "Synthesis and photoluminescence study of UVB emitting phosphor (LaY)Ba₉O₁₆:Bi³⁺,Gd³⁺," International Journal of Current Engineering and Scientific Research (IJCESR) , 5(5)176-179, ISSN (ONLINE): 2394-0697, DOI:10.21276/ijcesr.
25. Gawande AB, Snooker RP, Omanwar SK 2014. "Combustion Synthesis and Energy Transfer Mechanism of Bi³⁺ → Gd³⁺ and Pr³⁺ → Gd³⁺ in YBO₃," Combust

Recent Progresses in Gas Sensors Based on Reduced Graphene Oxide-ZnO Composites

N. B. Thakare¹, G. T. Lamdhade^{2*}, D. N. Bhojar¹, G. S. Warade¹

¹Department of Physics, Shri Shivaji Science & Arts College, Chikhli, Dist. Buldhana, (MS), India-443201

²Department of Physics, Vidhya Bharti Mahavidyalaya, Amravati, (MS), India- 444602

*Corresponding author email: gtlamdhade@rediffmail.com

Abstract:

ZnO is among the most suitable candidates for gas sensors due to its high thermal & chemical stability, cost-effectiveness, and excellent gas response. Process control and safety sensors are commonly used in residential, commercial, and industrial settings due to their ability to detect combustible, volatile, and dangerous gases. In recent years, the combination of zinc oxide nanostructure with reduced graphene oxide (RGO) has proven to be an effective way to create composites with improved gas sensing capabilities. In this paper, we present the latest advances of gas sensors for detection of various toxic gases and VOCs (volatile organic compounds) derived from zinc oxide and reduced graphene oxide (ZnO-rGO).

1. Introduction:

In recent years, graphene has garnered significant attention due to its remarkable mechanical, thermal, and electrical properties [1]. Notably, it possesses a substantial specific surface area of 2630 m²/g [2], an exceptional intrinsic mobility of 250,000 cm²/V·s [3], and a high modulus of elasticity (~1 TPa [4]. Moreover, graphene exhibits an exceptionally high thermal conductivity exceeding 3000 W/m·K [5], along with an optical transmittance of over 97.7% for visible light [6]. Additionally, it showcases quantum Hall behavior [7]. The remarkable electrical conductivity, outstanding mechanical flexibility, extensive surface area, and exceptional thermal and chemical stability have significantly contributed to the surge in interest towards graphene-based gas sensors in recent times [8,9]. Within the graphene family utilization of pristine graphene (PG) as a gas sensor is restricted due to its inability to be produced on a large scale, absence of functional groups, and lack of a band gap [10]. In contrast, graphene oxide (GO) is highly electrically insulating due to its rich composition of alkoxy (C-O-C), hydroxyl (-OH), carboxylic acid (-COOH), carbonyl (C=O), and other oxygen-based functional groups. Nevertheless, GO can be transformed into reduced graphene oxide (rGO) by eliminating oxygen functional groups and restoring aromatic double-bonded carbons through chemical reduction or high-temperature annealing [11,12]. Reduced graphene oxide (rGO) holds significant potential for gas sensing applications due to its wide range of functional groups, ample defects, and highly adaptable electrical properties [13].

The metal oxide nanohybrid architectures have been extensively explored as gas sensors due to relatively high sensitivity of their electrical resistance to adsorbates [14]. Zinc oxide (ZnO) is a typical n-type semiconductor material with a direct wide band gap ($E_g \approx 3.37$ eV) and large excitation binding energy (~60 meV) and is one of the most common metal oxides in the gas sensing area because of its unique properties, such as n-type conductivity, low toxicity, ease of synthesis, high availability, good thermal stability, and high mobility of electrons [15]. The wide range of applications for ZnO-based gas sensors is restricted by their typical drawbacks of sluggish response, poor selectivity, and lack of long-term stability [16]. Recent advancements have demonstrated that incorporating rGO and metal oxide nanoparticles in heterojunction gas sensors can be an extremely effective approach for creating gas sensors with outstanding performance. These sensors display exceptional sensitivity, rapid response and recovery times, and are also economically viable [17].

This review article delves into the latest developments in utilizing hybrids of reduced graphene oxide (rGO) and zinc oxide (ZnO) as sensors for the detection of volatile and hazardous gases, aiming to mitigate environmental harm [18].

2. Gas Sensing Mechanism:

The gas detection process of sensors includes the adsorption of gas molecules onto the sensing matrix's surface and the interaction between the target gas and the sensing film on the surface. This interaction leads to a modification in the material's charge carrier concentration. The modification in the concentration of charge carriers brings about a modification in the conductivity (or resistivity) of the substance. When an n-type semiconductor material interacts with reducing gases, its conductivity increases, while it decreases when it interacts with oxidizing gases. On the other hand, for a p-type semiconductor, the gas sensing mechanism is completely opposite to that of an n-type semiconductor when it comes to reducing and oxidizing gases [19].

3. Key Parameters of Gas Sensor:

Key performance parameters for gas sensors include sensitivity, selectivity, response and recovery time, detection limit and resolution, stability, and working temperature [20].

3.1 Sensitivity: Sensitivity represents a modification of the material's chemical and/or physical characteristics in the presence of gas. The porosity of the sensitive material, the working temperature, the presence of dopants or other modifications, material porosity and the size of the crystallites all have a substantial impact on the sensitivity of gas sensors [21].

3.2 Selectivity: When multiple gases are present in similar operating conditions, selectivity refers to the ability of semiconductor materials to distinguish between a group of target gases or a single gas [20]. Surface modification or doping with various catalytic additives is employed to enhance the adsorption of target components, thereby increasing the selectivity of gas sensors [22].

3.3 Stability: It is the ability of gas sensors to maintain the same output characteristics over the prolonged usage. The accurate detection of gas may be hindered if there is a significant fluctuation. However, by subjecting the sensitive layers to preheat treatment at temperatures higher than the sensor's working temperatures, the stability of these layers can be enhanced [23].

3.4 Response and Recovery Time: Response time is the time it takes for a sensor to reach 90% of its signal response when exposed to the target gas, while recovery time is the duration for the sensor to return to 90% of its initial baseline signal after the target gas is removed [24].

3.5 Limit of Detection (LOD): The smallest amount of gas that a sensor element can detect is known as the detection limit. The lowest concentration difference that the sensor can detect correlates to the device's resolution.

3.6 Working Temperature: The operating temperature is where the gas sensor is most sensitive. Different temperatures affect the sensor's characteristics and how quickly it reacts to gas.

4. Reduced Graphene Oxide-ZnO Composite Based Gas Sensor:

4.1 Sensors for NH₃:

Ammonia (NH₃), a colorless gas with a distinctly pungent odor, is considered one of the most hazardous pollutants in the environment [25]. Developing a gas sensor that is both sensitive and reliable serves a practical purpose, as exceeding the threshold value of 25 ppm can pose significant hazards to humans [26].

Gaurav Singh and his team studied ZnO-rGO's gas sensing abilities for NH₃ at room temperature. They found a 24% sensor response in presence of dry N₂, with a quick recovery time of 2-3 seconds. The sensor exhibits good selectivity to NH₃ in presence of H₂, CO, and NO gases [27]. A ZnO NPs/rGO bilayer thin film NH₃ sensor was successfully fabricated by Huiling Tai et al. by depositing ZnO NPs and graphene oxide (GO) thin film on gold interdigital

electrodes (IDEs) via simple spraying process followed by heat treatment. The sensor showed a positive response (%R ~ 1.20) and had a fast response time of 78 seconds at room temperature when exposed to 10 ppm NH₃[28]. Zhen Sun et al. fabricated ZnO nanowire-reduced graphene oxide (ZnO-rGO) based highly sensitive portable ammonia (NH₃) gas sensing electron device with excellent detection limit of 500 ppb. The hybrid architecture demonstrates a remarkable sensitivity (% S) of approximately 7.2% for 1 ppm NH₃, accompanied by an impressive response time of 50s. The inclusion of ZnO nanowire networks on the surface of rGO enhances the gas sensing capability by providing additional channels for electron transport [29].

Composite	Analyte Gas	Morphology	Meas. Temp.	Gas response	Res. / Rec. time	Ref.
rGO -ZnO	NH ₃	Nanoparticles	RT	~24% to 1 ppm	Rec. time 2-3s	[27]
rGO -ZnO	NH ₃	Nanoparticles	RT	1.20 % to 10 ppm	Rec. time 78s	[28]
rGO -ZnO	NH ₃	Nanoparticles	RT	~7.2% to 1 ppm	50s/200s	[29]

4.2 Sensor for H₂:

Hydrogen (H₂) is colorless, odorless, and buoyant in air and one of the abundant next-generation energy sources in nature with high combustion efficiency [30]. Hydrogen is explosive and flammable in concentrations of 4- 75 percent (by volume) when combined with air. Hydrogen at high amounts prevents an adequate supply of oxygen, leading to asphyxiation [31].

A. Drmsh et al. have reported that they have developed a ternary Pt-loaded rGO/ZnO system that exhibits remarkable response and selectivity towards a low concentration of hydrogen. The system achieved an impressive response of 99% (to 400 ppm at 100°C), which is significantly higher compared to the pure ZnO and the rGO/ZnO nanocomposite. In fact, the response of the Pt-loaded rGO/ZnO system was found to be 10 and 5 times higher than that of the pure ZnO and the rGO/ZnO nanocomposite. The presence of highly conductive rGO material with a large surface area and adsorption sites leads to the formation of a p-n heterojunction with ZnO nanoparticles. The interaction between Pt nanoparticles and ZnO creates a nano-Schottky contact, which is responsible for the exceptional response observed. [17]. The Pd-ZnO-rGO hybrid developed by Sun Y et al. exhibits the ability to detect hydrogen gas at a lower temperature of 50°C with detection limit of 1 ppb. The Pd-RGO/ZnO sensor demonstrates a response of 16% at a concentration of 200 ppb and 1.8% at a concentration of 1 ppb. The combination of the ternary hybrid nanomaterial and the modulation of the p-n heterojunction synergistically enhance the hydrogen sensing properties of the Pd-ZnO/RGO film sensor [32]. Kanika Anand et al. developed a hydrogen sensor using a graphene/ZnO nanocomposite with exhibits best sensing response (S=3.5, at 150 °C) towards 200 ppm of hydrogen gas and good selectivity against ammonia, ethanol and LPG. The improved connectivity between ZnO nanorods is facilitated by 3D networks formed by RGO sheets, leading to better sensor performance at lower temperatures. Defects and functional groups on graphene surface enhance sensitivity by acting as high-energy adsorption sites for gas molecules [33]. Abdollahi et al. fabricated a p-n heterostructure-based gas sensor Ni-ZnO-rGO nanowire with responses of Ni-ZnO-rGO and ZnO-rGO with 1.6 wt% rGO concentration, respectively, towards 200 ppm hydrogen gas at 150 °C. The inclusion of reduced graphene oxide (rGO) in composite materials enhances the hydrogen sensing capabilities by promoting electron transport through a van der Waals p-n heterojunction. Additionally, the introduction of nickel (Ni) doping in ZnO-NWs amplifies the number of active sites available for chemisorbed ionized oxygen atoms [34].

Composite	Analyte Gas	Morphology	Meas. Temp.	Gas response	Res. / Rec. time	Ref.
Pt-rGO -ZnO	H ₂	Nanoparticles	100 °C	~99 to 400 ppm	12s/412s	[17]

Pd-rGO -ZnO	H ₂	Nanorods	50 °C	~16 % to 200 ppm	Rec. time 78s	[32]
rGO -ZnO	H ₂	Nanorods	150 °C	~3.5 to 200 ppm	22/96s.	[33]
Ni-rGO -ZnO	H ₂	Nanowire	150 °C	~29.9% to 50 ppm	---	[34]

4.3 Sensor for NO₂:

Nitrogen Dioxide (NO₂) is a highly reactive gas that is widely recognized as one of the most hazardous and harmful gases [35]. Prolonged exposure to NO₂ exceeding 3 ppm for a duration of eight hours can result in the emergence of diverse respiratory disorders, such as bronchitis, pulmonary edema, and asthma [36].

Au-decorated ZnO/rGO heterostructure developed by Pei Jiang Cao et al. displayed remarkable sensing response of 67.38 to 1 ppm NO₂ and a pretty low detection limit of 138 ppt. The enhanced catalytic activity or synergistic interaction between Au and ZnO/rGO is responsible for the remarkable sensing response exhibited by the heterostructure [37]. Sen Liu et al. reported room temperature NO₂ gas sensor based on ZnO-rGO hybrids display higher response (~26 % to 5 ppm) greater sensitivity in comparison to pure rGO as a result of addition of ZnO nanoparticles for rGO matrix. The selective detection of NO₂ against Cl₂, NO and CO can be attributed to its high electron-donating power, compared to these gases [38]. Jie Liu et al. synthesized ultrasensitive rGO/ZnO hybrids with flower-like ZnO anchored on flexible rGO sheets displayed good response (~12) at 100 °C to 50 ppb NO₂. The rGO/ZnO hybrids with a hierarchical structure exhibit a remarkable ability to detect NO₂ at concentrations as low as 5 ppb. The sensing performance of rGO/ZnO is greatly influenced by the formation of local p-n heterojunctions between the n-type ZnO and the p-type rGO [39]. Ternary CuO-ZnO/rGO composites reported by Jyoti and G. D. Varma showed the highest gas response of ~62.9 in 40 sec to NO₂ at room temperature. CuO 1-D nanochains and ZnO nanoseeds on rGO sheets enhance gas molecule adsorption, while heterojunctions like ZnO/rGO, CuO/ZnO, and CuO/rGO greatly enhance sensor performance [40]. Jing Li and colleagues synthesized a hierarchical hollow structure of urchin-like ZnO nanorod spheres with reduced graphene oxide. These spheres had a sensitivity of 17.4% and could detect 100 ppm NO₂ at room temperature. The rGO functioned as a conductive framework, enhancing the sensing mechanism through the facilitation of rapid electron pathways to the hollow ZnO nanorod spheres [41].

Composite	Analyte Gas	Morphology	Meas. Temp.	Gas response	Res. / Rec. time	Ref.
Au-rGO -ZnO	NO ₂	Nanoparticles	60 °C	~ 67.38 to 1 ppm	248 s and 170 s	[37]
rGO -ZnO	NO ₂	Nanoparticles	RT	~26 % to 5 ppm	165 s/499 s	[38]
rGO -ZnO	NO ₂	Flower-Like	100 °C	~12 to 50 ppm	Res. time 5.5 min	[39]
CuO-rGO -ZnO	NO ₂	Nanowire	RT	~62.9 to 40 ppm	Res. time 40 s	[40]
rGO -ZnO	NO ₂	Nanorods	RT	~17.4 % to 100 ppm	13/33 min	[41]

4.4 Sensor for VOCs:

Volatile organic compounds (VOCs) are organic chemicals with low molecular weight and high vapor pressure and easily evaporate at normal room temperature [42]. Exposure to a particular level of VOCs can show symptoms such as headaches, nausea, and even more serious conditions like convulsions and comas [43].

Z. Wei Chen et al. studied formaldehyde sensors using graphene-modified ZnO nanosheets. The sensors with 2 wt.% graphene (G-ZnO-2) exhibit excellent response (~12) with fast response and recovery times of 10 and 29 seconds for 100 ppm concentration at 200 °C. Improved charge transfer, higher adsorption, and narrower band gap results in superior gas-sensing performance over pure ZnO nanosheets [44]. W Guo et al. found that 5% Fe-doped ZnO/rGO nanocomposites greatly improved the gas sensing performance (~12.7) for formaldehyde at 120 °C. The sensor also had fast response and recovery times (34 and 37s)

from dry to 40% RH [45]. Xian Lia et al. found hybrid films of reduced graphene oxide and hierarchical flower-like zinc oxide that showed a remarkable 5.3% response in just 34 seconds to 10 ppm formaldehyde at room temperature. The improved HCHO gas sensing is due to the lower barrier height between HCHO and ZnO, as well as the effective adsorption sites on rGO and ZnO surfaces, compared to graphene and HCHO [46].

Ethanol sensor investigated by S. Niavol et al. using ZnO/rGO nanocomposites coated on gold electrodes has a high response (110.11 toward 100 ppm ethanol vapor in comparison with 14.54 for pristine ZnO at 320°C) with quick response/recovery time (below 4s), excellent selectivity, and a detection limit of about 27 ppb [47]. A highly sensitive and selective ethanol sensor based on rGO/ZnO nanocomposites investigated by Rafiee et al. shows a significantly higher response ($S \sim 26$) at 125 °C to a low concentration (20 ppm) of ethanol. The sensor exhibits excellent selectivity against methane, carbon monoxide, carbon dioxide, and formaldehyde [48].

Wang and coworkers investigated acetone based on CuO-ZnO/rGO ternary composite that exhibits a gas response of 9.4 to 10 ppm of acetone, which was almost 1.5 times and 2.0 times higher than CuO-ZnO and ZnO/rGO, respectively. The CuO-ZnO/ rGO nanocomposite was highly sensitive and selective towards acetone due to its large surface area, thermal stability, high electron mobility of rGO sheets, and increased p-n junctions [49].

Composite	Analyte Gas	Morphology	Meas. Temp.	Gas response	Res. / Rec. time	Ref.
rGO -ZnO	HCHO	Nanosheets	200 °C	~12 to 100 ppm	10s/29s	[44]
Fe-rGO -ZnO	HCHO	Nanoparticles	120 °C	$S \sim 1.5$ to 100 ppm	34s/37s	[45]
rGO -ZnO	HCHO	Flower-Like	RT	~5.3 % to 10 ppm	Res. time 34 s	[46]
rGO -ZnO	Ethanol	Nanoparticles	320 °C	110.11 to 100 ppm	2s/3s	[47]
rGO -ZnO	Ethanol	Nanowire	125 °C	~ 26 to 20 ppm	---	[48]
CuO-ZnO-rGO	Ethanol	Nanoparticles	340 °C	$S \sim 9.4$ to 10 ppm	Res. time 10-15 s	[49]

4.5 H₂S Sensor:

The gas hydrogen sulfide (H₂S), which smells like rotten eggs, is poisonous to humans and biological systems. Exposure above the threshold limit (250 ppm) can cause severe illness and death [49].

K. Dang investigated a sensitive H₂S sensor using rGO and ZnO NFs in both external and internal heterojunctions. The 0.1 wt% rGO/ZnO NFs internal heterojunction had the strongest gas response, reaching 1353 to 1 ppm H₂S concentrations at 350 °C. This response was 25 times higher than that of bare ZnO NFs. Adding rGO increases the surface area, leading to a spill-over effect that enhances the sulphuration reaction and creates more ZnS/ZnO heterojunctions. These heterojunctions were important for improving the response to H₂S [50]. Cu-ZnO/rGO nanocomposite sensors were synthesized by P.S. Shewale et al. to study H₂S sensing at room temperatures. The sensor showed a 0.87% response to 100 ppm H₂S at 24°C, with a response time of 14 seconds and a recovery time of 32 seconds. Additionally, the sensor displayed high selectivity for H₂S over H₂[51]. V. Balasubramani et al. studied rGO-ZnO using impedance spectroscopy to detect H₂S gas. The sensor showed a 57% gas response at 90 °C. The inclusion of rGO created reactive sites for H₂S adsorption and facilitated electron transportation, enhancing the sensor's gas response. The sensor showed quick response (8s) and recovery (32s) time to 2 ppm hydrogen sulfide [52].

Composite	Analyte Gas	Morphology	Meas. Temp.	Gas response	Res. / Rec. time	Ref.
rGO -ZnO	H ₂ S	Nanofibers	350 °C	~1353 to 1 ppm	9s/1520 s	[50]
Cu-rGO -ZnO	H ₂ S	Nanorods	RT	~0.87 % to 100 ppm	14s/32s	[51]
rGO -ZnO	H ₂ S	Flower-Like	90 °C	~57% to 100 ppm	8s/32s for 2 ppm	[52]

5. Conclusion:

Composite sensors with rGO and ZnO hybrids exhibit superior properties due to enhanced sensor performance, leveraging the advantages of both materials. The synergistic effect of rGO-ZnO can be summarized as follows:

- i) Reduced graphene oxide enables attachment of metal oxides due to surface defects and functional groups.
- ii) Conductivity of metal oxides enhanced is due to the conducting network enabled by graphene, which has high charge-carrier mobility and facilitates electron transfer.
- iii) The p-n heterojunctions between p-rGO and n-ZnO, with their large surface area and high catalytic activity, are fundamental elements for gas sensing.
- iv) The gas detection capability was significantly enhanced by both the rGO content and ZnO morphology in the rGO-ZnO composite.

However, the sensitivity to all sorts of target gases and the prolonged response and recovery time of rGO-ZnO nanocomposites as sensing materials are still constraints. Future work should focus on the following issues:

- i) Further investigation is required to examine the gas detection capabilities by tuning the morphology and structure of the sensing materials.
- ii) To improve sensor effectiveness, novel molecules with unique interactions with graphene must be developed. This may enhance sensitivity, selectivity, and overall performance.

References:

- [1] Wenjing Yuan and Gaoquan Shi, *J. Mater. Chem. A*, 2013 1, 10078-10091 <https://doi.org/10.1039/C3TA11774J>
- [2] Yanwu Zhu, Shanthi Murali, Weiwei Cai, Xuesong Li, Ji Won Suk, Jeffrey R. Potts, Rodney S. Ruoff, *Adv. Mater.*, 2010, 22, 46, 5226-5226. <https://doi.org/10.1002/adma.201001068>
- [3] Novoselov, K.S.; Geim, A.K.; Morozov, S.V.; Jiang, D.; Katsnelson, M.I.; Grigorieva, I.; Dubonos, S.; Firsov, A.A., *Nature* 438, 2005, 197-200 <https://doi.org/10.1038/nature04233>
- [4] Changgu Lee, Xiaoding Wei, Jeffrey W. Kysar, And James Hone, *Science*, 2008, 321, 385-388 <https://doi.org/10.1126/science.1157996>
- [5] Balandin, A.A.; Ghosh, S.; Bao, W.; Calizo, I.; Teweldebrhan, D.; Miao, F.; Lau, C.N., *Nano Lett.* 2008, 8, 902-907. <https://doi.org/10.1021/nl0731872>
- [6] R R Nair I, P Blake, A N Grigorenko, K S Novoselov, T J Booth, T Stauber, N M R Peres, A K Geim, *Science*, 2008, 320, 1308. <https://doi.org/10.1126/science.1156965>
- [7] Zhang, Y., Tan, YW., Stormer, H., *Nature* 2005, 438, 201-204. <https://doi.org/10.1038/nature04235>
- [8] Jingquan Liu, Zhen Liu, Colin J. Barrow, Wenrong Yang, *Analytica Chimica Acta*, 2015, 859, 1-19. <https://doi.org/10.1016/j.aca.2014.07.031>
- [9] Fazel Yavari and Nikhil Koratkar, *J. Phys. Chem. Lett.*, 2012, 3, 1746-1753 <https://doi.org/10.1021/jz300358t>
- [10] Shyamasree Gupta Chatterjee, Somenath Chatterjee, Ajoy K. Ray, Amit K. Chakraborty, *Sens. Actuators, B*, 2015, 221, 1170-1181 <https://doi.org/10.1016/j.snb.2015.07.070>
- [11] Jianlang Feng, Yunqing Ye, Meng Xiao, Gang Wu, Yu Ke, *Chemical Papers*, 2020, 74, 3767-3783 (2020), <https://doi.org/10.1007/s11696-020-01196-0>
- [12] Daniel R. Dreyer, Sungjin Park, Christopher W. Bielawski and Rodney S. Ruoff, *Chem. Soc. Rev.*, 2010 39, 228-240. <https://doi.org/10.1039/B917103G>
- [13] Dongjin Sun, Yifan Luo, Marc Debliquy and Chao Zhang, *Beilstein J. Nanotechnol.*, 2018, 9, 2832-2844. <https://doi.org/10.3762/bjnano.9.264>
- [14] Neeraj Goel, Kishor Kunal, Aditya Kushwaha, Mahesh Kumar, *Eng. Rep.* 2023, 5, 1-22, <https://doi.org/10.1002/eng2.12604>
- [15] Yanli Kang, Feng Yu, Lu Zhang, Wenhao Wang, Long Chen, Ying Chun Li, *Solid State Ionics*, 2021, 360, 115544. <https://doi.org/10.1016/j.ssi.2020.115544>
- [16] Ang Wei, Liuhua Pan, Wei Huang, *Mater. Sci. Eng., B*, 2011 176(18), 1409-1421. <https://doi.org/10.1016/j.mseb.2011.09.005>
- [17] Q.A. Drmash, Z.H. Yamani, A.H. Hendi, M.A. Gondal, R.A. Moqbel, T.A. Saleh, M.Y. Khan, *Appl. Surf. Sci.*, 2019, 464, 616-626, <https://doi.org/10.1016/j.apsusc.2018.09.128>
- [18] Fine GF, Cavanagh LM, Afonja A, Binions R, *Sensors*. 2010; 10, 5469-5502. <https://doi.org/10.3390/s100605469>
- [19] Bochenkov, Vladimir & Sergeev, Gleb., 2010, (Valencia, CA: American Scientific Publishers), 31-5.
- [20] K. Wetchakun, T. Samerjai, N. Tamaekong, C. Liewhiran, C. Siriwong, V. Kruefu, A. Wisitsoraat, A. Tuantranont, S. Phanichphant, *Sens. Actuators B*, 2011, 160, 580-591 <https://doi.org/10.1016/j.snb.2011.08.032>
- [21] Wang, C.; Yin, L.; Zhang, L.; Xiang, D.; Gao, R. 2010, 10, 2088-2106. <https://doi.org/10.3390/s100302088>
- [22] Liang, Y.-C., Liao, W.-K., and Deng, X.-S, *J. Alloys Compd.* 2014, 599, 87-92. <https://doi.org/10.1016/j.jallcom.2014.01.167>

- [23] [G. Korotcenkov, B.K. Cho, *Sens. Actuators, B*, 2011, 156, 527-538. <https://doi.org/10.1016/j.snb.2011.02.024>.
- [24] N. A. Isaac, I. Pikaar and G. Biskos, *Microchim. Acta*, 2022, 189, 196. <https://doi.org/10.1007/s00604-022-05254-0>.
- [25] Wang, J., Wei, X. & Wangyang, P. *Nanoscale Res. Lett.*, 2015, 10, 461. <https://doi.org/10.1186/s11671-015-1170-2>.
- [26] Chen T-Y, Chen H-I, Hsu C-S, Huang C-C, Wu J-S, Chou P-C, Liu W-C, *Sens Actuators B*, 2015 221, 491-498. <https://doi.org/10.1016/j.snb.2015.06.122>.
- [27] Gaurav Singh, Anshul Choudhary, D. Haranath, Amish G. Joshi, Nahar Singh, Sukhvir Singh, Renu Pasricha, *Carbon*, 2012, 50, 385-394. (2012) <https://doi.org/10.1016/j.carbon.2011.08.050>.
- [28] Tai, H., Yuan, Z., Zheng, W. *Nanoscale Res. Lett.*, 2016 11, 130. <https://doi.org/10.1186/s11671-016-1343-7>.
- [29] Zhen Sun, Da Huang, Zhi Yang, Xiaolin Li, Nantao Hu, Chao Yang, Hao Wei, Guilin Yin, Dannong He, and
- [30] Yafei Zhang, *IEEE Electron Device Letters*, 2015, 36,1376-1379. <https://doi.org/10.1109/LED.2015.2496177>. Won-Tae Koo, Hee-Jin Cho, Dong-Ha Kim, Yoon Hwa Kim, Hamin Shin, Reginald M. Penner and Il-Doo
- [31] Kim, *ACS Nano*, 2020 14, 14284-14322. <https://doi.org/10.1021/acsnano.0c05307>. Ghenadii Korotcenkov Sang Do Han and Joseph R. Stetter, *Chem. Rev.*, 2009, 109, 3, 1402-1433 <https://doi.org/10.1021/cr800339k>.
- [32] Yan'e Sun, Dongzhi Zhang, Yong Zhang and Hongyan Chang, *J Mater Sci: Mater. Electron*, 2017, 28, 1667-1673. <https://doi.org/10.1007/s10854-016-5710-z>.
- [33] Kanika Anand, Onkar Singh, Manmeet Pal Singh, Jasmeet Kaur, Ravi Chand Singh, *Sens. Actuators, B*, 2014, 195, 409-415. <https://doi.org/10.1016/j.snb.2014.01.029>.
- [34] Hassan Abdollahi, Mahmoud Samkana and Mir Mehdi Hashemi, *New J. Chem.*, 2019, 43, 19253-19264 <https://doi.org/10.1039/C9NJ05152J>.
- [35] Ji Li, Ming Yang, Xiaoli Cheng, Xianfa Zhang, Chuanyu Guo, Yingming Xu, Shan Gao, Zoltán Major, Hui Zhao, Lihua Huo, *J. Hazard. Mater.*, 2021, 419, 126414. <https://doi.org/10.1016/j.jhazmat.2021.126414>.
- [36] Qingting Li, Wen Zeng, Yanqiong Li, *Sens. Actuators, B*, 2022, 359, 131579. <https://doi.org/10.1016/j.snb.2022.131579>.
- [37] Pei Jiang Cao, Yongzhi Cai, Dnyandeo Pawar, Shun Han, Wangying Xu, Ming Fang, Xinke Liu, a YuXiang Zeng, WenJun Liu, YouMing Lua and DeLiang Zhu, *J. Mater. Chem. C*, 2022, 10 4295-4305. <https://doi.org/10.1039/D1TC05835E>
- [38] Sen Liu, Bo Yu, Hao Zhang, Teng Fei, Tong Zhang, *Sens. Actuators, B*, 2014, 202, 272-278. <https://doi.org/10.1016/j.snb.2014.05.086>.
- [39] Jie Liu, Shan Li, Bo Zhang, Yan Xiao, Yuan Gao, Qiuyue Yang, Yinglin Wang, Geyu Lu, *Sens. Actuators, B*, 2017, 249, 715-724. <https://doi.org/10.1016/j.snb.2017.04.190>.
- [40] Jyoti and G D Varma, *Mater. Res. Express*, 2019, 6, 035011. <https://doi.org/10.1088/2053-1591/aaf34c>.
- [41] Jing Li, Xin Liu, Jianbo Sun, *Ceram. Int.*, 2016, 42, 2085-209. <https://doi.org/10.1016/j.ceramint.2015.09.134>.
- [42] A. Mirzaei, S.G. Leonardi, G. Neri, *Ceram. Int.* 2016, 42, 15119-15141. <https://doi.org/10.1016/j.ceramint.2016.06.145>.
- [43] Zhen Zhu, Ren-Jang Wu, *J. Taiwan Inst. Chem. Eng.*, 2015, 50, 276-281, <https://doi.org/10.1016/j.jtice.2014.12.022>.
- [44] Zi-Wei Chen, Yu-Yuan Hong, Zhi-Dong Lin, Li-Ming Liu, and Xiao-Wen Zhang, *Mater. Lett.*, 2017, 13, 270-276. <https://doi.org/10.1007/s13391-017-6245-z>
- [45] Weiwei Guo, Bangyu Zhao, Qilin Zhou, Youzhou He, Zhongchang Wang, and Norbert Radacsi, *ACS Omega* 2019, 4, 6, 10252-10262. <https://doi.org/10.1021/acsomega.9b00734>.
- [46] Xian Li, Jing Wang, Dan Xie, Jianlong Xu, Ruixuan Dai, Lan Xiang, Hongwei Zhu, Yadong Jiang, *Sens, and Actuators B*, 2015, 221, 1290-1298. <https://doi.org/10.1016/j.snb.2015.07.102>.
- [47] Saadat Niavol, S., Milani Moghaddam, H., Bagheri Khatibani, A. et al. *Appl. Phys. A*, 2022 128, 733. <https://doi.org/10.1007/s00339-022-05890-6>.
- [48] Chao Wang, Junwu Zhu, Shiming Liang, Huiping Bi, Qiaofeng Han, Xiaoheng Liua and Xin Wang, *J. Mater. Chem. A*, 2014,2, 18635-18643. <https://doi.org/10.1039/C4TA03931A>.
- [49] Yue Shen, Sicheng Luo, Zhongrui Wu, Meng Cao, Feng Gu and Linjun Wang, *J Mater Sci: Mater. Electron*, 2016 27, 12660-12668. <https://doi.org/10.1007/s10854-016-5400-x>.
- [50] Tran Khoa Dang, Nguyen Tang Son, Nguyen Thi Lanh, Phan Hong Phuoc, Nguyen Ngoc Viet, Le Viet Thong, Chu Manh Hung, Nguyen Van Duy, Nguyen Duc Hoa, Nguyen Van Hieu, *J. Alloys Compd.*, 2021, 879, 160457. <https://doi.org/10.1016/j.jallcom.2021.160457>.
- [51] Shewale, P. S.; Yu, Y. S.; Kim, J. H.; Bobade, C. R.; Uplane, M. D. J. *Anal. Appl. Pyrolysis*, 2015, 112, 348-356. <https://doi.org/10.1016/j.jaap.2015.01.001>.
- [52] V. Balasubramani, S. Sureshkumar, T. Subba Rao, and T. M. Sridhar, *ACS Omega*, 2019, 4, 9976-9982. (2019) <https://doi.org/10.1021/acsomega.9b00754>.

Synthesis and characterization of SnO₂ nanoparticles by Sol-gel Method

C.C. Jadhao, G.T. Lamdhade, K.B. Raulkar, A.O. Chauhan, R.B. Butley

Department of Physics, Vidya Bharati Mahavidyalaya, Amravati. M.S. 444602, India.

(Corresponding author: E-mail ID- ccjadhao@gmail.com)

Abstract:

This Research paper devoted to SnO₂ nanoparticles synthesis by using sol-gel method. This article examines the advancements made in SnO₂ nanomaterials for CO₂ gas sensors the material compositions, sensing methods, and characteristics based on SnO₂ nanomaterial's. X-ray diffraction was used to examine the powders. X-ray diffraction was used to characterise the films' structural integrity, confirming that they are crystalline and have a tetragonal structure.

Keyword: Nanomaterials, XRD, Gas sensors.

1. Introduction:

SnO₂ nanoparticles have been synthesised using a variety of techniques, such as sol-gel, molten-salt synthesis, microwave approach, Carbothermal reduction, chemical precipitation, laser-ablation synthesis, hydrothermal method. In this work, SnO₂ nanoparticles were synthesised using a straightforward sol-gel approach [1]. The purpose of this work is to synthesise SnO₂ nanoparticles using the sol-gel method and to investigate their particle nature [2]. These nanomaterials have unique sizes and morphologies. Because of their fascinating properties and captivating potential in the aforementioned domains, materials smaller than 100 nm have piqued the curiosity of scientists and engineers once again Semiconducting metal oxides, such as ZnO and SnO₂, are an efficient class of materials that have made significant contributions to several fields of science and industry due to their controllable size and shape [4]. Solid-state gas sensors find extensive applications in the production of semiconductors, environmental sensing, medical diagnostics, personal safety, and national security [5]. They are among the essential technologies of the modern era. Materials that exhibit property changes in response to surrounding gases may find application as gas sensing materials. The concentrations of the gases can be detected via optical or electrical signals. The colour of an optical gas sensor changes in proportion to the amount of gases it detects [6]. When using an electrical gas sensor, the concentration of the gas can be found either by applying a temperature gradient that is produced by a chemical reaction on a thermoelectric sensing material, or by varying the output voltage as a result of the gas reacting with chemisorbed oxygen at the sensing material's surface [7]. By changing their electrical characteristics, several transition metal oxides show sensitivity to oxidising and reducing gases. Typically, variations in electrical conductance in response to ambient gases are tracked. For example, the conductivities of all the following oxides exhibit a gas response [8]. However, due to its appropriate physicochemical characteristics and cheaper cost when compared to actual materials available for similar applications, SnO₂ is currently the most extensively utilised material for detecting various gases. At moderate temperatures, it is sensitive to a wide range of gases and vapours, including ethanol, H₂, O₂, CO, NO, NO₂, and NH₃. This articles SnO₂ examine the CO₂ gas sensor [9].

2. Experimental Process: Synthesis of SnO₂ Nanomaterials:

Sol-gel method is a combination of two words sol and gel. Sol is a colloid formed from solid particles suspended particles in continuous liquid. Gel is a solid macro-molecule which is dissolved in solvent. Due to simplicity, sol-gel method is the most preferred bottom-up method for the synthesis of nanoparticles [10-11]. It is the method in which suitable chemical solution act as precursor. We employed the effective and straightforward sol-gel approach to prepare the nanoparticles for our SnO₂ nanoparticle manufacturing experiment. Chemical reagents including

sodium hydroxide (NaOH), methylene blue, isopropyl alcohol, and tin (II) chloride dihydrate (SnCl_2) were taken. These substances were bought from M/s Merck and had a high purity of 99.99%. Different amounts of precursor materials such as $\text{SnCl}_4 \cdot 5\text{H}_2\text{O}$ and isopropyl alcohol were taken into consideration. 50 millilitres of isopropyl alcohol were combined with $\text{SnCl}_4 \cdot 5\text{H}_2\text{O}$ solution [12-15]. In a stirrer, the finished mixture was left to stir for two hours. We were able to get a homogeneous solution by this procedure. The pH of the solution was adjusted to around 9–11 by mixing it with 0.1 M NaOH solution poured out of a burette drop by drop. The solution was agitated for an additional thirty minutes in the same stirrer after we had given it two to three hours to settle. The precipitates were cleaned with acetone and distilled water, then dried at 80°C [16-18].

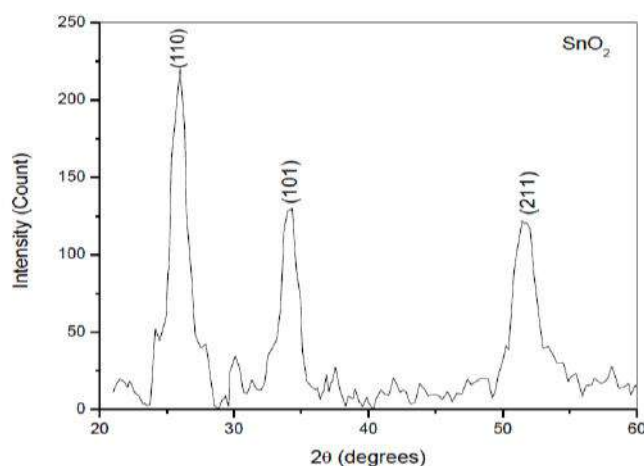


Fig 1: XRD diffraction pattern of SnO_2 Nanoparticles

3. Results and discussion:

XRD patterns of the samples were recorded in an ambient environment using a Holland Philips X-ray powder diffract meter ($\text{CuK } \alpha$, $\lambda = 1.5406 \text{ \AA}$). The phase and purity of the as prepared SnO_2 nanoparticles were determined by XRD pattern of the as prepared SnO_2 samples at 450°C for 1 hour has shown in Fig.1. All the diffraction lines were assigned to tetragonal rutile crystalline phases of tin oxide. The XRD pattern is in excellent agreement with a reference pattern (JCPDS No. 41-1445) of tin oxide [19]. The crystallite size of the prepared powders calculated from XRD line broadening using Debye–Scherer equation, $d = K \lambda / \beta \cos \theta$, where λ is the wavelength of the X-ray radiation ($\text{Cu} - \text{K } \alpha = 1.5406 \text{ \AA}$), K is a constant taken as 0.89, β full width at half maximum height (FWHM in radian) and θ is the diffraction. To estimate average crystallite sizes of SnO_2 the three most intense indexed peaks, as (110), (101), (211) were used, giving d -values of 32.9, 29.7, and 25.4 nm respectively, with the average size of 29.3 nm [20]. The SnO_2 nanoparticles consist of uniform tetragonal particles of 22 – 31 nm size. This is in agreement with the results obtained from the XRD analysis. Thus, the sol – gel method could be employed to synthesize the SnO_2 nanoparticles with narrow size distribution. In this method, it is observed that the speed of the oxide particle precipitation can be modulated by controlling the concentration of the PEG [21].

4. Application of SnO_2 nanoparticles :

Gas sensors work on the principle of transforming the gas adsorption effects on the surface of the active material into a detectable signal in terms of its changed electrical, optical, thermal, mechanical, magnetic (magnetization and spin), and piezoelectric properties. There is a close association between their surface chemical activity and gas sensitivity since gas sensing procedures heavily depend on these reactions [22-23].

Metal oxide nanomaterials exhibit intriguing characteristics that have several uses in a wide range of scientific and technological fields, including paint, sunscreen, antimicrobial coatings, memory drives, LEDs, sensors, solar cells, and wastewater treatment [24].

The general principle of gas detection applicable to the most of metal-oxide gas sensor is the variation in the electrical conductivity. The variation in electrical conductivity is brought by the interaction between the gas molecules and oxygen (adsorbed) on the metal oxide surface. Due to the adsorption of oxygen on the surface of metal oxide, the trapping of electrons take place resulting in an increase or decrease in the concentration of free charge carriers depending upon the n or p type of semiconductor [25].

References

- [1] A. Ciuciumis, I. Cernica CAS (2005). 'Proceedings Synthesis and characterization of indium tin oxide and cerium dioxide thin films by Sol-Gel method', International Semiconductor Conference, volume. 2, Pages 425-428.
- [2] S.S.Park, J.D. Mackenzie (1995). 'Sol-gel-derived tin oxide thin films' Thin films solids, Volume 258(1–2), Pages 1-359.
- [3] Azam Anaraki Firooz, Ali Reza Mahjoub, Abbas Ali Khodadadi (2008). 'Preparation of SnO₂ nanoparticles and nanorods by using a hydrothermal method at low temperature', Materials Letters, Volume 62(12–13), Pages 1747-2042.
- [4] E. R. Leite , I. T. Weber , E. Longo | J. A. Varela (2000). 'A New Method to Control Particle Size and Particle Size Distribution of SnO₂ Nanoparticles for Gas Sensor Applications', Advanced Materials, Volume 12(13), Pages 935-998.
- [5] R.E. Hester, R.M. Harrison, and C.Royal Society (2007). 'Nanotechnology: consequences for human health and Environment.' Cambridge: Royal Society of Chemistry, Volume 24, No. of Pages 148.
- [6] Nicholas S. Wigginton, Kelly L. Haus, Michael F. Hochella Jr (2007). 'Aquatic environmental nanoparticles', Environmental Monitoring, J. Environ. Monit., Volume 9, Pages 1306-1316.
- [7]. L. J. Zhou, G. N. Wu, P. Tang, H. L. Wang, and C. Su, (2006). 'Model of semiconductor gas sensor for monitoring dissolved gases in insulation oil', Automation of Electric Power Systems, volume 30(10), Pages 75–79.
- [8] J.Huang, N. Matsunaga, K. Shimanoe, N. Yamazoe, and T. Kunitake, (2005). 'Nanotubular SnO₂ templated by cellulose fibers: synthesis and gas sensing', Chemistry of Materials, volume 17(13), Pages 3513–3518.
- [9] Azra Parveen , Syed Afzal Ahmad, Shraddha Agrawal , Ameer Azam (2017). 'Room temperature variation in dielectric and electrical properties of Mn doped SnO₂ nanoparticles,' International Conference on Recent Trends in Engineering and Material Sciences (ICEMS-2016), Volume 4(9), Pages 9429–9433.
- [10] Paulo G. Mendes , Mario L. Moreira, Sergio M. Tebcherani , Marcelo O. Orlandi , J. Andre´s, Maximu S. Li ,Nora Diaz-Mora , Jose´ A. Varela , Elson Longo (2012), "SnO₂ nanocrystals synthesized by microwave-assisted hydrothermal method: towards a relationship between structural and optical properties ", J Nanopart Res, Vol.14,750.
- [11] Feng Gu , Shu Fen Wang , Chun Feng Song , Meng Kai L u , Yong Xin Qi ,Guang Jun Zhou , Dong Xu , Duo Rong Yuan (2003), "Synthesis and luminescence properties of SnO₂ nanoparticles", Chemical Physics Letters, Vol. 372,Pages 451–454.
- [12] D. G. Shah and P. M. Trivedi (2012) "Preparation, characterization of nanometer SnO₂" , Pelagia Research Library , Der Chemica Sinica, Vol.3, Pages 1002- 1008,.
- [13] A. Feinle, M. S. Elsaesser, N. H using, (2016). ' Sol-gel synthesis of monolithic materials with hierarchical porosity,' Chemical Society Reviews, volume 45(12), Pages 3377–3399,.
- [14] A. Feinle, M. S. Elsaesser, N. H using, (2016). ' Sol-gel synthesis of monolithic materials with hierarchical porosity,' Chemical Society Reviews, volume 45(12), Pages 3377–3399,.
- [15] Yile Liao, Yang Xu, Yanthai Chan (2013), 'Semiconductor nanocrystals in sol-gel derived matrices ' Physical Chemistry Chemical Physics, volume 15(33), Pages 13694-13704.
- [16] G. J. Owens, R. K. Singh, F. Foroutan et al (2016) "Sol-gel based materials for biomedical applications," Progress in Materials Science, volume 77, Pages 1–79,
- [17] Madzlan Aziz, Saad Saber Abbas, Wan Rosemaria Wan Baharom, Wan Zuraidah Wan Mahmud (2012), ' Structure of SnO₂ nanoparticles by sol–gel method' Materials Letters, Volume 74, Pages 62-64.

-
- [18] Madzlan Aziz, Saad Saber Abbas, Wan Rosemaria Wan Baharom (2013). ' Size-controlled synthesis of SnO₂ nanoparticles by sol–gel method', Materials Letters, Volume 91, Pages 31-34.
- [19] Fredy Kurniawan and Rahmi Rahmi (2017). 'Synthesis of SnO₂ Nanoparticles by High Potential Electrolysis' Bulletin of Chemical Reaction Engineering & Catalysis, Volume 12(2), Pages 281-286.
- [20] M. S. Pereira, F. A. S. Lima, C. B. Silva, P. T. C. Freire, I. F. Vasconcelos (2017). 'Structural, morphological and optical properties of SnO₂ nanoparticles obtained by a proteic sol–gel method and their application in dye-sensitized solar cell ', Journal of Sol-Gel Science and Technology Volume 84, pages 206–213
- [21] Hyo-Jin Ahn, Hyun-Chul Choi, Kyung-Won Park, Seung-Bin Kim, Yung-Eun Sung (2004). "Investigation of the Structural and Electrochemical Properties of Size-Controlled SnO₂ Nanoparticles", J. Phys. Chem. B, Vol.108, Pages 9815-9820.
- [22] G. Korotcenkova and B.K. Cho (2017). 'Metal oxide composites in conductimetric gas sensors achievements and challenges', Sensors and Actuators B Chem, Volume 244, Pages 182-210.
- [23] Detlev Möller, Manfred Decker, Jens Zosel, Wolfram Oelßner (2019). 'Carbon dioxide in general. In Carbon Dioxide Sensing', Fundamentals Principles, and Applications, Wiley-VCH: Weinheim, Germany, Pages 39–40.
- [24] Prakash Viswanathan , Ashish Kumar Patel, Jayant Pawar, Amit Patwardhan, Rabinder Henry (2018). 'Fabrication of Tin Oxide Nanoparticles for CO₂ Gas Sensing Layer'. IETE Journal of Research, Volume 66, Pages 460–465
- [25] Jong-Heun Lee (2009). 'Gas sensors using hierarchical and hollow oxide nanostructures: overview', Sensors and Actuators B: Chemical, Volume 140(1), Pages 319-336.

Synthesis and Luminescent Behavior of Europium-Infused Barium Alumino-Borate Phosphors

R. S. Palaspagar

Department of Physics, Shivramji Moghe Mahavidyalaya, Kelapur (Pkd.) (M.S.), INDIA.

*(Corresponding Author Email: rspalaspagar@gmail.com)

ABSTRACT

Solution combustion synthesis was used to create the red luminous $\text{BaAl}_3\text{BO}_7:\text{Eu}^{3+}$ phosphor powders. The phosphors were characterized by X-ray diffraction (XRD) and fluorescence spectrophotometer. The SEM results revealed that the surface of the $\text{BaAl}_3\text{BO}_7:\text{Eu}^{3+}$ powder samples showed lots of voids and pores. Photoluminescence (PL) spectroscopy showed that the phosphor could be excited efficiently by UV-Visible light from 250 to 410 nm. The excitation spectra show a broad band peaking at 394 nm due to Eu-O charge transfer. The 394 nm excited phosphor shows weak emissions at 591 nm and 580 nm followed by an intense emission at 614 nm attributed to ${}^5\text{D}_0 \rightarrow {}^7\text{F}_J$ ($J=1, 2$) transitions. Further the optimum concentration for Eu^{3+} also reported.

Keywords: Alumino-Borates, Combustion Synthesis, XRD, Photoluminescence.

1. INTRODUCTION

Phosphorus-related interest has recently led to fast advancements in potential display and illumination technologies. Photoluminescent (PL) materials for general lighting consist of oxides, silicates, aluminates, aluminosilicates, nitrides, borates, etc. [1]. Borates are among the researched hosts that provide suitable candidates for the host structure because of their high luminescence brightness, ease of manufacture, and low synthetic temperature [2].

Numerous scientific advancements in the subject of SSL have been widely applied, primarily in the areas of magneto-optical devices, liquid crystal displays (LCD), traffic signals, w-LEDs, lasers, and many more. Because of these extraordinary qualities, oxide glasses have become a major focus of study for scientists and academics in recent years. Owing to remarkable advancements in controlled solid-state lasers, crystalline and amorphous materials doped with Rare Earth (RE) ions have attracted the interest of numerous academics and scientists. Because of their good economy, low power consumption, small size, and extended lifespan, w-LEDs have seen tremendous expansion thanks to SSL-based devices. When compared to conventional light sources like incandescent bulbs and tubes, w-LEDs are noticeably better [3].

Alkaline-earth aluminum borates have been taken interest in by scientists during the past decade because of their potential applications as luminescence hosts [4]. The phase of $\text{BaAl}_2\text{B}_2\text{O}_7$, is an example of alkaline-earth aluminum borates, was first described by Hu' bner following a study of the ternary system $\text{BaO}-\text{Al}_2\text{O}_3-\text{B}_2\text{O}_3$. It is characterized by having an association of BO_3 triangles, BaO_6 octahedra, and AlO_4 tetrahedra [5]. In the present work we report synthesis and photoluminescence of $\text{BaAl}_3\text{BO}_7:\text{Eu}^{3+}$. Their photoluminescence properties under the near-UV excitation were evaluated in detail. Activation with Eu^{3+} , which occupies the Ba^{2+} sites of host lattice, yields a highly efficient phosphor with emission maximum near 614 nm. Furthermore, the concentration quenching and critical distance of $\text{BaAl}_3\text{BO}_7:\text{Eu}^{3+}$ phosphors were discussed.

2. EXPERIMENTAL

The Powder samples of $\text{BaAl}_3\text{BO}_7:\text{Eu}^{3+}$ have been prepared by a solution combustion technique followed by heating combustion ash at 550°C in air. The method is based on the exothermic reaction between the fuel (urea) and oxidizer (Ammonium Nitrate). The detailed

description of the method was reported in our earlier work [6-7]. The stoichiometric amounts of $\text{Al}(\text{NO}_3)_3 \cdot 9\text{H}_2\text{O}$, $\text{Ba}(\text{NO}_3)_2$, H_3BO_3 , and $\text{CO}(\text{NH}_2)_2$ used were of AR grade and the rare earth Eu_2O_3 (99.99% purity) used were from the Indian Rare earth. The stoichiometric amounts of the ingredients were thoroughly mixed in an Agate Mortar, adding little amount of double distilled water to obtain aqueous solution. The aqueous solution was slowly heated at lower temperature of 90°C to remove the excess water. The solution was then introduced into a preheated muffle furnace maintained at $(550 \pm 10)^\circ\text{C}$. The solution boils foams and ignites to burn with flame; a voluminous, foamy powder was obtained. The entire combustion process was over in about 5 min. The resulting fine powders were annealed in open air at temperature 800°C for about 90 min. and suddenly cooled to room temperature. The samples are subjected to XRD analysis. PL measurements were performed on Fluorescence Spectrometer (Hitachi F-7000).

3. RESULTS AND DISCUSSIONS

3.1 X-ray Diffraction Pattern

The XRD pattern of $\text{BaAl}_3\text{BO}_7:\text{Eu}^{3+}$ (0.01 mol) is shown in Fig. 1. The XRD pattern of $\text{BaAl}_3\text{BO}_7:\text{Eu}^{3+}$ (0.01 mol) is in agreement with the standard monoclinic BaAl_3BO_7 (ICDD File No. 00-048-0049). Any phase of Eu^{3+} is not observed. The two possible sites available for the incorporating Eu^{3+} in the BaAl_3BO_7 lattice are either the Al^{3+} sites or the Ba^{2+} sites. The Eu^{3+} (0.947 \AA) ion has a much larger ionic radius, compared with that of Al^{3+} (0.39 \AA) ion. However, the ionic radius of Ba^{2+} (1.35 \AA) is larger than that of Eu^{3+} ion. So it would be expected that Eu^{3+} would replace Ba^{2+} in the crystal lattice, this is confirmed by XRD analysis.

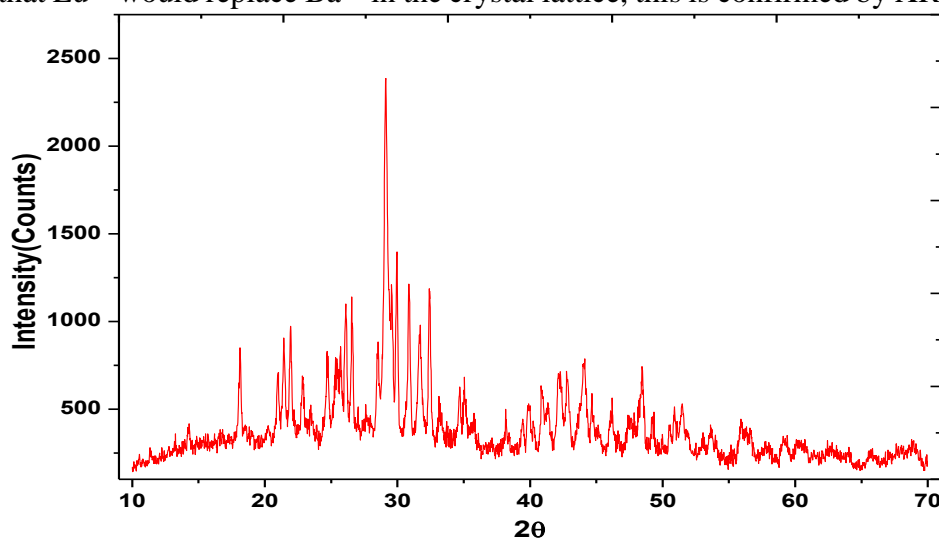


Fig. 1. XRD pattern obtained for $\text{BaAl}_3\text{BO}_7:\text{Eu}^{3+}$ (1 mol %)

3.2 Photoluminescence of $\text{BaAl}_3\text{BO}_7:\text{Eu}^{3+}$

The photoluminescence (PL) and photoluminescence excitation (PLE) spectra of the $\text{BaAl}_3\text{BO}_7:\text{Eu}^{3+}$ phosphors were recorded at room temperature. The typical excitation spectrum ranging from 200 to 450 nm monitored at $\lambda_{\text{em}} = 614 \text{ nm}$ is shown in Fig.2. The excitation spectra consist of sharp f-f transition lines in the wavelength range 300 nm to 420 nm, including ${}^7\text{F}_0 \rightarrow {}^5\text{H}_3$ (320 nm), ${}^7\text{F}_0 \rightarrow {}^5\text{D}_4$ (363 nm), ${}^7\text{F}_0 \rightarrow {}^5\text{L}_7$ (383 nm) and ${}^7\text{F}_0 \rightarrow {}^5\text{L}_6$ (393 nm). The emission spectrum depicts the typical red photoluminescence at 614 nm under the excitation at 393 nm. The emission spectrum consists of a series of sharp bands at 580 nm (${}^5\text{D}_0 \rightarrow {}^7\text{F}_0$), 591 nm (${}^5\text{D}_0 \rightarrow {}^7\text{F}_1$) and 614 nm (${}^5\text{D}_0 \rightarrow {}^7\text{F}_2$) is shown in Fig. 3. In particular, the most intense emission peak at 614 nm occurs through the forced electric dipole while the ${}^5\text{D}_0 \rightarrow {}^7\text{F}_1$ band at 591 nm is due to the magnetic dipole transition. Furthermore, it is observed that the PL intensity increase with the Eu^{3+} concentration and found maximum for $x = 0.01 \text{ mol}$. Beyond this saturation level of $x = 0.01 \text{ mol}$, intensity subsequently begins to decrease with the

Eu^{3+} concentration due to the concentration quenching as shown in Fig.4. The most prominent emission, ${}^5\text{D}_0 \rightarrow {}^7\text{F}_2$ peaking at 614 nm, results in a red color with excellent purity and with a CIE chromaticity coordinate of (0.614, 0.387) Chromatic point is shown in Fig.5.

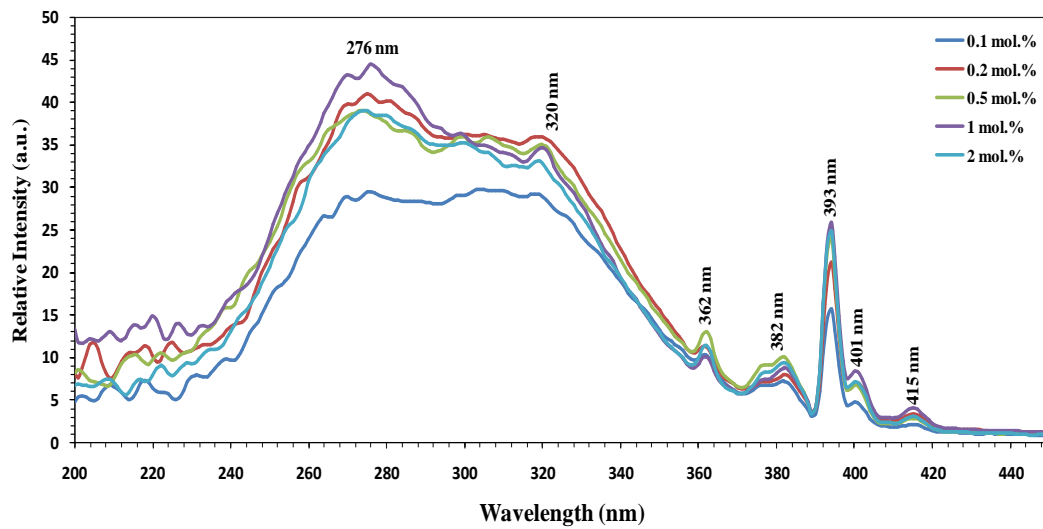


Fig.2 Excitation spectrum of $\text{Ba}_{(1-x)}\text{Al}_3\text{BO}_7:x\text{Eu}^{3+}$ ($x=0.01, 0.02, 0.05, 0.1, 0.2$ mol).

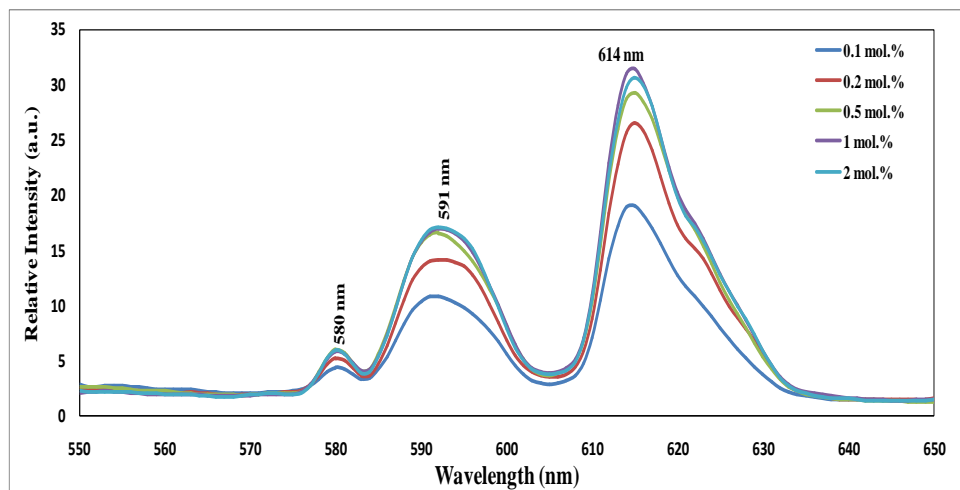


Fig.3 Emission spectrum of $\text{Ba}_{(1-x)}\text{Al}_3\text{BO}_7:x\text{Eu}^{3+}$ ($x = 0.01, 0.02, 0.05, 0.1, 0.2$ mol)

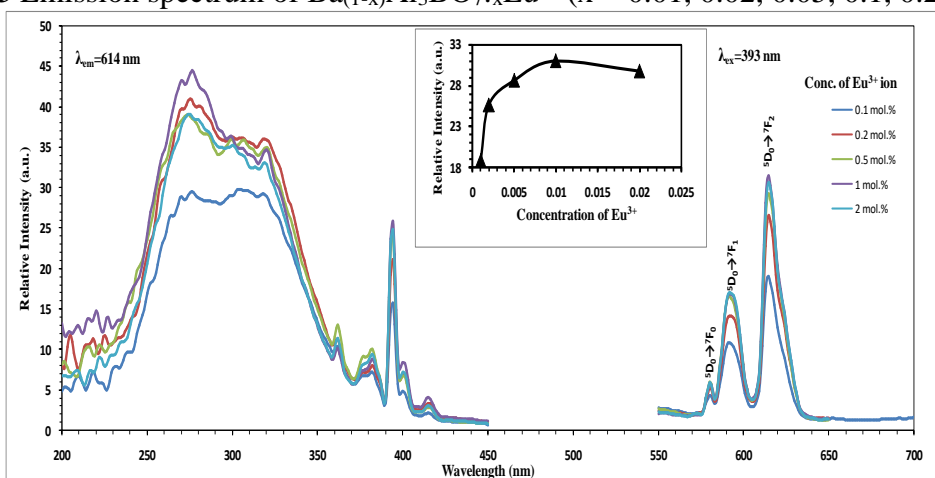


Fig. 4 Excitation & Emission Spectra of $\text{Ba}_{(1-x)}\text{Al}_3\text{BO}_7:x\text{Eu}^{3+}$ ($x = 0.01, 0.02, 0.05, 0.1, 0.2$ mol) phosphor.

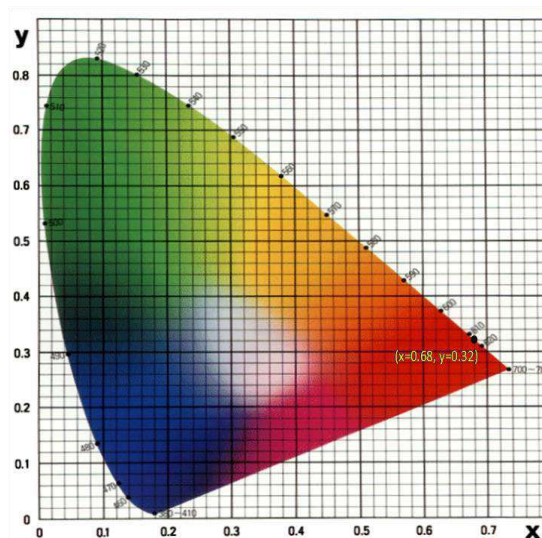


Fig. 5 CIE Chromatic point & spectral locus of XY-Coordinates of wavelength.

4. CONCLUSIONS

Eu^{3+} doped BaAl_3BO_7 materials were prepared by a low cost, simple and time saving solution combustion synthesis method followed by heating of the precursor combustion ash at 800°C in air. The synthesized materials were characterized by using the powder XRD. The prominent emission of $\text{BaAl}_3\text{BO}_7:\text{Eu}^{3+}$ was observed at 614 nm corresponding to the $^5\text{D}_0 \rightarrow ^7\text{F}_2$ upon excitation with 393 nm. The dependence of the emission intensity on the Eu^{3+} concentration for $\text{BaAl}_3\text{BO}_7:\text{Eu}^{3+}$ was investigated. The critical concentration of Eu^{3+} in phosphor was observed to be 1 mol %. The phosphor $\text{BaAl}_3\text{BO}_7:\text{Eu}^{3+}$ could be a potential red phosphor for solid state lighting, fluorescent lamps and display device or detector systems.

ACKNOWLEDGEMENTS

Authors is very much thankful to Head, Department of Physics, Sant Gadage Baba Amravati University, Amravati, for providing necessary facilities.

REFERENCES

- [1] W.R. Liu, Y.C. Chiu, C.Y. Tung, Y.T. Yeh, S.M. Jang, T.M. Chen, J. Electrochem. Soc. 155 (2008) 252.
- [2] Yingli Zheng, Donghua Chen, Wei Li, A study on the luminescence properties of $\text{CaAl}_2\text{B}_2\text{O}_7:\text{Eu}^{2+}$ phosphor, Physica B: Condensed Matter, 406 (4) (2011) 996-999.
- [3] Manjeet, A. Kumar, Anu, Ravina, Nisha Deopa, Anand Kumar, R.P. Chahal, S. Dahiya, R. Punia, A.S. Rao, Structural, thermal, optical and luminescence properties of Dy^{3+} ions doped Zinc Potassium Alumino Borate glasses for optoelectronics applications, Journal of Non-Crystalline Solids, 588 (2022) 121613.
- [4] İ. Pekgözlü, S. Seyyidoğlu, S. Taşcıoğlu, A novel blue-emitting phosphor: $\text{BaAl}_2\text{B}_2\text{O}_7:\text{Pb}^{2+}$, J. Lumin., 128 (9) (2008) 1541-1543.
- [5] Chen, Jiongquan and Jin, Wenqi and Zhang, Yanhui and Yang, Yun and Yang, Zhihua and Pan, Shilie, $\text{Ba}_{10}\text{LuB}_{18}\text{O}_{32}\text{F}_{13}$: the first example of borate in the Lu–B–O–F system with the unprecedented FBB $[\text{B}_9\text{O}_{22}]$, Inorg. Chem. Front., 9 (10) (2022) 2298-2304.
- [6] R.S. Palasagar, A.B. Gawande, R.P. Sonekar, S.K. Omanwar, Combustion synthesis and photoluminescence properties of a novel Eu^{3+} doped lithium alumino-borate phosphor, J. Lumin., 154 (2014) 58-61.
- [7] R.S. Palasagar, A.B. Gawande, R.P. Sonekar, S.K. Omanwar, Fluorescence properties of Tb^{3+} and Sm^{3+} activated novel $\text{LiAl}_7\text{B}_4\text{O}_{17}$ host via solution combustion synthesis, Mater. Res. Bull., 72 (2015) 215-219.

Synthesis and Characterization of Conducting Polyaniline-Tin Oxide Thin film Nanocomposites

Shrikant H. Nimkar*

Department of Physics, Research Laboratory, Shri Shivaji Arts, Commerce and Science College, Akot, Dist. Akola, 444101, SGB, Amravati University, Amravati

*Corresponding author. Tel: (+91) 8459616611; E-mail: shrikantnimkarsscakot@gmail.com

ABSTRACT

Polyaniline-tin oxide (PANI/SnO₂) nanocomposites of two different (0.1M and 0.2M) concentration were prepared by using solution route technique i.e. in-situ polymerization of aniline in the presence of tin oxide-intercalated polyaniline nanocomposite prepared using tin chloride (SnCl₄.5H₂O) as precursor during polymerization of aniline. The synthesised samples have been characterized by using XRD, SEM and FTIR technique. Morphology and structure of both the nanocomposites have been studied using XRD pattern, FTIR spectra and SEM images which reveals that SnO₂ was uniformly mixed within the PANI matrix. In this paper we report the morphological comparison of polyaniline-tin oxide (PANI/SnO₂) nanocomposites sample A (0.1M) and B (0.2M). These characteristics measured through the formation of nanocomposites and growing of PANI on SnO₂ nanoparticle surfaces. The FTIR spectra confirmed that Polyaniline undergoes through an electronic structure modification because of interaction between SnO₂ nanoparticles with polyaniline.

Keywords: Conducting polymers; polyaniline; tin oxide; nanocomposites; solution route technique.

Introduction : In recent study reveals that conducting polymers have highest potential for development of gas sensors, batteries, hydrogen storage material because of their electrical conductivity can be changed by doping of inorganic metal oxides into conducting polymer like polyacetylene (PA), polyaniline (PANI), polypyrrole (PPy), polythiophene (PT), poly (3,4-ethylenedioxythiophene) (PEDOT), poly(phenylene vinylene) (PPV) and their derivatives [1,2]. Conducting polymers are either electrical insulators or semiconductors. Many applications demanded increase the conductivity of conducting polymer, for that a doping process such as protonic acid doping or redox doping is applied to polymers, which could increase the conductivity from the low level of an insulator or semiconductor (10⁻¹⁰ -10⁻⁵ S/cm) to the conducting level (1-10⁵ S/cm) [3].

Conducting polymer has many applications apart from that sensing application is attract more attention, but it has some limitations to reduce the limitations of the Conducting polymer a new era of nanocomposites was developed to facilitate the advantages of organic and inorganic materials [4].

In the nanocomposite system, the host organic and guest inorganic phases are interacted by weak van der Waals or hydrogen bonding or covalent or ionic covalent bonding, which could help to eliminate their inherent drawbacks and utilize the advantages of their individual constituents. [5].

The conducting polyaniline (PANI) is one of the promising conducting polymers due to its high conductivity, ease preparation, good environmental stability, and large variety of applications [6]. However, PANI is not as sensitive as metal oxides towards gas species, and its poor solubility in organic solvents limits its applications, but it is suitable as a matrix for preparation of conducting polymer nanocomposites [7-8]. Therefore, there has been increasing interest of the researchers for the preparation of nanocomposites based on PANI. The literature review on conducting polymer nanocomposites show that PANI has been successfully utilized

for the preparation of nanocomposites [9-10]. In literature, there are some reports concerning PANI/ inorganic nanocomposite sensors [11]. However, very few researchers have studied the composite SnO₂/PANI for sensor application [12]. Tin oxide (SnO₂) was chosen due to its unique physical and chemical properties such as large energy gap, dielectric constant, and environmental-friendliness and easy to synthesis

Experimental

Synthesis of PANI/SnO₂ nanocomposites

PANI/SnO₂ nanocomposite of two different molar concentration of 0.1M and 0.2M of PANI i.e. (Sample A and Sample B) was synthesized by using solution route technique [13]. In this technique, formation of nanocomposite proceeds through an inorganic/organic interface reaction. 2g of SnCl₄.5H₂O in 50 ml of double distilled water was stirred for half an hour and its pH was maintained ≤ 4 using 0.1M HCl. 10 ml hydrogen peroxide (H₂O₂) was added in the above solution, which oxidized tin ions to tin oxide. The solution turned into a white colour suspension of SnO₂ and this reaction mixture was mixed with 0.1M and 0.2M aniline and kept below 4°C. 0.1M ammonium persulphate solution was added in the above mixture at room temperature, simultaneously we insert the pre-cleaned glass substrate during polymerization thin film was developed on substrate, the colour of the solutions was turned to blue and then to green after few minutes. The precipitate produced in the reaction was removed by filtration, washed repeatedly with double distilled water and thin film was dried in vacuum oven for 24 hours.

Results and discussion

SEM:

Scanning Electron Microscopy of sample, A and B are in fig. 1A and 1B

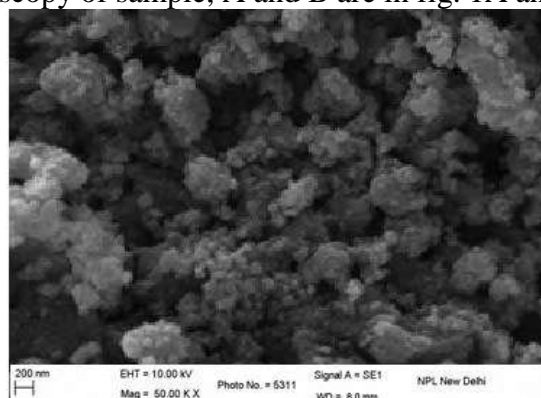


Fig. 1A: PANI/SnO₂ nanocomposite (Sample A)

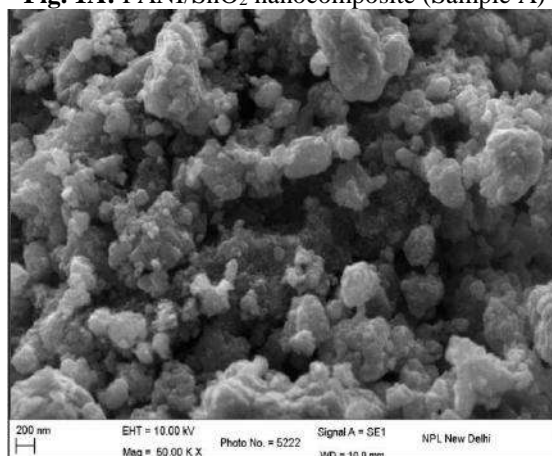


Fig. 1B: PANI/SnO₂ nanocomposite (Sample B)

It can be seen from these figures that the composite particles are highly dispersed with agglomeration. In both the cases, formation of polymer shell around the nanocrystalline particles can be seen in SEM images.

FTIR:

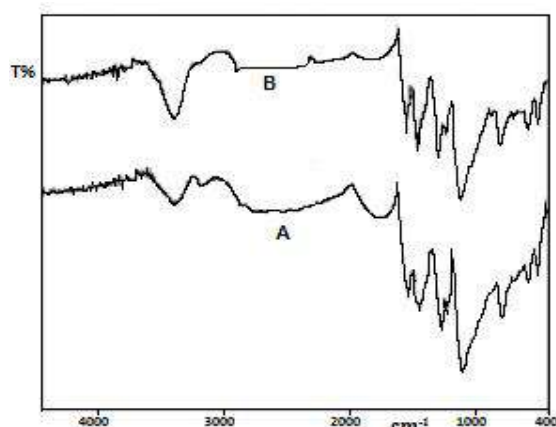


Fig. 2: FTIR spectra of PANI/SnO₂ nanocomposites A and B

The peaks in both the samples at wave numbers 1576, 1487, 1447, 1284, 1364, 1158, and 736 cm^{-1} corresponds to most of the characteristic peaks for PANI [14]. The peaks at wave numbers 1576 and 1487 cm^{-1} are attributed to C-N and C-C stretching mode for the quinoid and benzenoid rings. These peaks are slightly shifted with respect to their normal positions for pure PANI [15] due to the presence of tin oxide in the PANI matrix. A strong peak at wave number 613 cm^{-1} in both the samples are due to the antisymmetric Sn-O-Sn mode in tin oxide which confirms the presence of tin oxide in the PANI matrix [16-18].

XRD:

On comparing the observed XRD peaks for both the samples, the nanocrystalline SnO₂ peaks are observed and matched with those peaks along (1 1 0), (1 0 1), (2 0 0), (2 11), (3 1 0) and (3 0 1) having primitive tetragonal structure (*JCPDS DATA CARD 41-1445*). However, these peaks show slightly shifted from their respective standard positions which may be due to PANI matrix. In addition, we observed reduced intensity of the peaks, and relatively larger peak broadening, compared with XRD of pure SnO₂. This indicates still smaller average size of tin oxide nanocrystallites in composites, compared to that of pure SnO₂. The average crystallite size was found to be nearly 20-25 nm for both the samples.

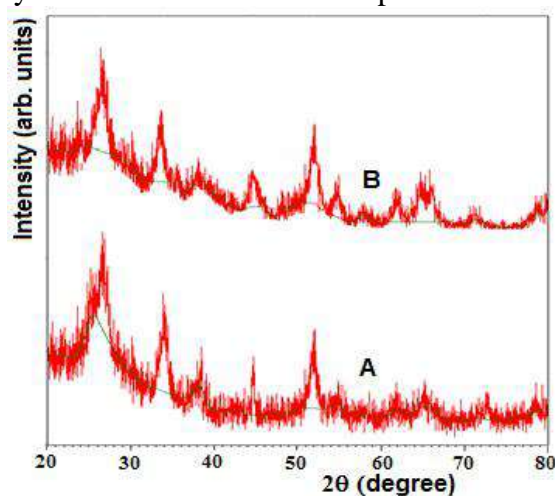


Fig. 3: XRD pattern of PANI/SnO₂ nanocomposites A and B

Conclusion

PANI/SnO₂ nanocomposite (sample A) and (sample B) were successfully synthesized. Nanocomposites have been well characterized by XRD, FTIR and SEM which reveals that SnO₂ was uniformly mixed within the PANI matrix. The PANI/SnO₂ nanocomposites could be good materials for CO₂ and NH₃ detection at room temperature.

References

- [1] Michel, H.J.; Leiste, H.; Schierbaum, K.D.; *J. Appl. Surf. Sci.* **1998**, *126* (1-2), 57.
- [2] Baik, N.S.; Sakai, G.; Miura, N.; Yamazoe, N.; *Sensors and Actuators B*, **2000**, *63*(1-2), 74.
- [3] Chandrakanthi, R.L.N.; Careem, M. A.; *Thin Solid Films*, **2002**, *417*(1-2), 51.
- [4] Lu, X.; Zhang, W.; Wang, C.; Wen, T.; Wei, Y. *Progress in Polymer Science*, **2011**, *36*, 671.
- [5] Pawar, S.G.; Patil, S.L.; Chougule, M.A.; Raut, B.T.; Pawar, S.A.; Patil, V.B.; *Sensors and Transducers*, **2011**, *125* (2), 107.
- [6] Shukla, S.K.; Bharadvaja, A.; Tiwari, A.; Parashar, G.K.; Dubey, G.C. *Adv. Mat. Lett.* **2010**, *1*(2), 129.
- [7] Kushwah, B.S.; Upadhaya, S.C.; Shukla, S.; Sikarwar, A.S.; Sengar, R.M.S.; Bhadauria, S. *Adv. Mat. Lett.* **2011**, *2*(1), 43.
- [8] Tiwari, A.; Kumar, R.; Prabhakaran, M.; Pandey, R.R.; Kumari, P.; Chadurvedi, A.; Mishra, A.K. *Polymers for Advanced Technologies*, **2010**, *21*, 615.
- [9] Tiwari, A. *Journal of Macromolecular Science, Part A: Pure and Applied Chemistry*, **2007**, *44*(7), 735.
- [10] Tiwari, A. *Journal of Polymer Research* **2008**, *15*(4), 337.
- [11] Kargirwar, S.R.; Thakare, S.R.; Choudhary, M.D.; Kondawar, S.B.; Dhakate, S.R.; *Adv. Mat. Lett.* **2011**, *2*(6), 397.
- [12] Kondawar, S.B.; Thakare, S.R.; Bompilwar, S.; Khati, V. *Int. J. Mod. Phys. B*, **2009**, *23* (15), 3297.
- [13] Deshpande, N.G.; Gudage, Y.G.; Sharma, R.; Vyas, J.C.; Kim, J.B.; Lee, Y.P.; *Sensors and Actuators B*, **2009**, *138*, 76.
- [14] Kondawar, S.B.; Acharya, S.A.; Dhakate, S.R. *Adv. Mat. Lett.* **2011**, *2*(5), 362.
- [15] Sharma, A. K.; Sharma, Y.; Malhotra, R.; Sharma, J.K. *Adv. Mat. Lett.* **2012**, *3*(2), 82.
- [16] Joshi, S.S.; Gujar, T.P.; Shinde, V.R.; Lokhande, C.D.; *Sensors and Actuators B*, **2008**, *132*(1), 349.
- [17] Barsan, N.; Weimar, U.; *J. Phys. Condens. Matter*, **2003**, *15*, 813.
- [18] Geng, L.; Zhao, Y.; Huang, X.; Wang, S.; Zhang, S.; Wu, S.; *Sensors and Actuators B*, **2007**, *120*(2), 568.
- [19] Tiwari, A.; Prabaharan, M.; Pandey, R.; Li, S. *Journal of Inorganic and Organometallic Polymers and Materials*, **2010**, *20*(2), 380.

A Review On TiO₂ Nanoparticle: Structure, Properties & Applications

***Dharme S.P., Wagh P.S., Khan S.T., Amale S.A.**

Department Of Physics, Vidya Bharati Mahavidyalaya, Amravati (M.S.) India 444602

*Corresponding Author: Email: snehaldharme1107@gmail.com

Abstract

Titanium dioxide (TiO₂) nanoparticle is manufactured worldwide in large quantities for use in wide range of application in each and every sector. TiO₂ belongs to the family of transition metal oxide with large band semiconductor and high photocatalytic activity. The key features of TiO₂ nanoparticle involves high surface area that can be utilize for catalytic reactions, low toxicity, chemical and physical stability, cost effectiveness and bio compatible etc. Titanium dioxide (TiO₂) is stable compound, non-volatile, extremely insoluble and its low thermal conductivity has a refractory character. The main properties of TiO₂ nanoparticle are insoluble in water and insulator. TiO₂ considered a non-toxic material chemically inert and has been use in various industrial applications. It exists mainly in three different forms namely Anatase, Rutile and Brookite and their structures.

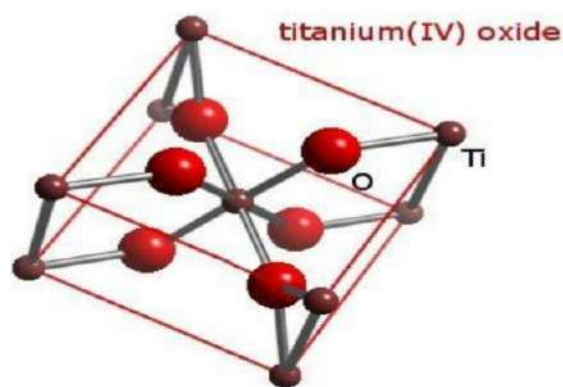
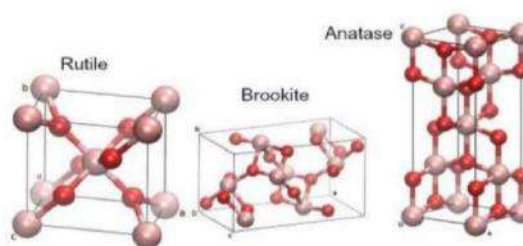
Keywords: Nanoparticle, TiO₂, Non-toxic, Photocatalytic, Properties, insulator

INTRODUCTION

Titanium dioxide (TiO₂) is considered very close to an ideal semiconductor for photocatalysis because of its high stability, low cost and safety toward both humans and the environment [1]. Traditionally, TiO₂ nanoparticle have been considered as poorly soluble, low toxicity particle [2]. TiO₂ is non-toxic, durable, and fairly cheap, it possesses a great ability to oxidatively degrade organic pollutants [3]. It has wide range of industrial and technological application as pigment, photocatalyst and UV absorption. Hence TiO₂ is an important compound suitable for fuel cells, solar cells different sensors, pollution control system, waste management and self-cleaning glass coating materials along with food, cosmetics, paint, UV protector etc. TiO₂ nanoparticle used in sunscreen, Cosmetics, candies, Toothpaste, Chewing gums as a whitening agents [4]. Non-toxicity, chemical stability, poor solubility and high refractive index are properties which add to its practical applicability. TiO₂ is the most promising photocatalyst because of its appropriate electronic band structure, photostability, chemical inertness and commercial availability [5]. Titanium dioxide (TiO₂) semiconductor nanoparticle is one kind of important and promising photocatalysts in photocatalysis because of their unique optical and electronic properties [6]. Titanium dioxide (TiO₂) is a component of many sunscreens, soaps, shampoos, toothpastes, cosmetics, paper products, plastics, ink, paint, and building materials in both its bulk form and its nanoform. TiO₂ nanoparticle occupational exposure occurs during production, bagging and waste manipulation [7]. Titanium dioxide nanoparticles are white pigments, and due to their brightness and high refractive index, they have a variety of applications [8].

1. STRUCTURE

TiO₂ exists mainly in three different forms namely anatase, rutile and brookite and their structures [9].

**Fig. 2.1 Structure of TiO₂****Fig. 2.2 a) Rutile b) Brookite c) Anatase**

Titanium dioxide exists in three phases: as rutile, anatase, and brookite. These crystal phases assemble as octahedra, where six oxygen anions are shared by three titanium (IV) cations, hence the formula $TiO_{6/3}$, which equals TiO_2 [10]. It belongs to the family of transition metal oxides. The most important titanium minerals are rutile (TiO_2), ilmenite ($FeTiO_3$), and titanite ($CaTiSiO_5$) [11]. Table 2.1: shows some of the structural and physical properties of the anatase and rutile phase of titanium dioxide [12].

Properties	Anatase	Rutile
Molecular Weight (g/mol)	79.88	79.88
Melting Point (°C)	1825	1825
Boiling Point (°C)	2500-3000	2500-3000

Table 2.1: Shows the Molecular weight, Melting point & Boiling point

2. PROPERTIES

Titanium dioxide is one of the most studied and well-researched compounds in materials science, due to its outstanding and exceptional properties which include stability of its chemical structure, biocompatibility, physical, optical, and electrical properties, nontoxicity, corrosion resistance, and low cost [13]. For instance, their high light-conversion efficiencies have been exploited for the fabrication of energy devices. Their chemical stability, thin film transparency and low production costs are responsible for their utility as photocatalysts for various environmental remediation strategies such as waste water treatment, air pollution and soil viability improvement [14].

3. APPLICATION

Semiconductors with photocatalytic properties have caught interest for providing a promising solution to deal with environmental pollution in a green way. One of the most promising solutions are provided Titanium dioxide (TiO_2) nanoparticles and its composites in contrast to other semiconductor photocatalyst TiO_2 has caught most attention due to its vital properties like low toxicity, it is biocompatible, has a wide band gap, it is cost effective has tremendous chemical and physical properties [15]. The combination of Au-NPs with a variety of materials for the modification of TiO_2 gives rise to a great number of novel catalysts [16]. The effective utilization of clean, safe, and abundant solar energy through the TiO_2 photocatalysis provides promising solutions to the energy crisis and serious environmental challenges. TiO_2 has been

widely used commercially in pigments, sunscreens, paints, toothpaste [17]. TiO₂ nanoparticle are used in sunscreen, Cosmetics, candies, Toothpaste, Chewing gums as a whitening agent in various food products [18]. TiO₂ nanoparticle are the nanostructures mostly used in commercially available sunscreens, due to their ability to reflect and spread ultraviolet A (UVA, 320–400 nm) and ultraviolet B (UVB, 290–320 nm) rays, protecting against sunburn and photoaging [19]. TiO₂ nanoparticles can be used for the photo degradation of toxic dyes and other pharmaceutical drugs, thus avoid harmful effects on environment [20]. Applications of titanium dioxide in medicine are going further than the design of drug delivery systems or applications as vehicles for chemotherapeutics. Titanium dioxide NPs have been applied in pharmacy, especially in pharmaceutical chemistry and technology, as well as medicine, including growing areas related to dentistry and surgery [21]. The transition metal oxide, mainly TiO₂, is widely used in cosmetics, photocatalysts, medicines, sensors, and solar cell applications because of its peculiar properties like interconnected pores and large surface area [22]. Titanium dioxide (TiO₂) is a component of many sunscreens, soaps, shampoos, toothpastes, cosmetics, paper products, plastics, ink, paint, and building materials in both its bulk form and its nanoform [23]. The application of TiO₂ nanoparticle in dentistry has increased due to its high corrosion resistance, strength, and refractive index. In addition, the cytotoxicity and biocompatibility of TiO₂ nanoparticle have been tested in multiple studies, which have shown its excellent biocompatibility and chemical stability [24].

4. CONCLUSION

TiO₂ nanoparticle has a great future due to its efficiency in each and every sector holistically. TiO₂ has excellent corrosion resistance, good thermal, chemical stability and low cost. TiO₂ nanoparticle with attractive properties have been widely fabricated and developed alongside one of the most valuable raw materials. Typically, TiO₂ has three crystalline phases namely anatase, rutile and brookite. TiO₂ is insoluble in water and insulator.

REFERENCE

- [1] Gupta S. M, Tripathi M. June (2011), A Review of TiO₂ nanoparticles, Chinese Sci Bull, Volume 56, Pages 1639-1657, doi: 10.1007/s11434-011-4476-1.
- [2] Hongbo Shi, Ruth Magaye, Vincent Castranova, Jinshun Zhao, April (2013), Titanium dioxide nanoparticles: a review of current toxicological data, Part Fibre Toxicol, Volume 10, doi:10.1186/1743-8977-10-15.
- [3] Shalini Reghunath, Dephan Pinheiro, Sunaja Devi KR, March (2021), A review of hierarchical nanostructures of TiO₂: Advances and applications, Surface Science advances, Volume 3, doi.org/10.1016/j.apsadv.2021.100063.
- [4] Mohammad Rafiquewani, GGHA Shadab, (2020), Titanium Dioxide nanoparticle genotoxicity : A review of recent on Vivo and in Vitro studies, Toxicology and Industrial health, Volume 36, Pages 514-530, DOI:10.1177/0748233720936835.
- [5] Shipra Gupta, Manoj Tripathi, January (2012), A review on the synthesis of TiO₂ nanoparticles by solution route, Open chemistry, Volume 10, Pages 279-294, doi.org/10.2478/s11532-011-0155-y.
- [6] Pardon Nyamukamba, Omobola Okoh, Henry Mungondori, Raymond Taziwa and Simcelile Zinya, February (2018), Synthetic Methods for Titanium Dioxide Nanoparticles: A Review, DOI: 10.5772/intechopen.75425.
- [7] ShivaMehran, SoroushGhodratizadeh, AliZolfiGol, HamedCharkhian, MojtabaRanjbari, VahedEbrahimi, Zafar Gholinejad, December (2022), Titanium Dioxide Nanoparticle and Cardiovascular Diseases: A Critical Review of the Literature and Possible Underlying Mechanisms, Nano Biomedicine and Engineering, Volume 14, Issue 4, Pages 329-342, doi.org/10.5101/nbe.v14i4.p329-342.
- [8] OladipupoMoyinoluwa David, Kim Leigh Lategan, Maria Fidalgo de Cortalezzi, Edmund John Pool, September (2022), The Stability and Anti-Angiogenic Properties of Titanium Dioxide Nanoparticles (TiO₂NPs) Using Caco-2 Cells, Biomolecules, Volume 12, Issue 10, doi:10.3390/biom12101334

-
- [9] Pardon Nyamukamba, Omobola Okoh, Henry Mungondori, ymond Taziwa and Simcelile Zinya, February (2018), Synthetic Methods for Titanium Dioxide Nanoparticles: A Review, DOI: 10.5772/intechopen.75425.
- [10] Anca Diana Racovita, Martin David Rose, May (2022), Titanium Dioxide: Structure, Impact, and Toxicity, Int J Environ Res Public Volume 19, Issue 9, doi: 10.3390/ijerph19095681
- [11] BochraBejaoui, ImenBouchmila, KhaoulaNefzi, ImenBelhadjSlimen, SidrineKoumbad, Patrick Martin, Nicolas Joly and Naceur M Hamdi, May (2023), Nanostructured Titanium Dioxide (NS-TiO₂), DOI: 10.5772/intechopen.111648
- [12] Pardon Nyamukamba, Omobola Okoh, Henry Mungondori, Raymond Taziwa and Simcelile Zinya, February (2018), Synthetic Methods for Titanium Dioxide Nanoparticles: A Review, DOI: 10.5772/intechopen.75425.
- [13] BochraBejaoui, ImenBouchmila, KhaoulaNefzi, ImenBelhadjSlimen, SidrineKoumbad, Patrick Martin, Nicolas Joly and NaceurM'Hamdi, May (2023), Nanostructured Titanium Dioxide (NS-TiO₂), DOI: 10.5772/intechopen.111648
- [14] Ozioma U. Akakuru, Zubair M. Iqbal, Aiguo Wu, (2020), TiO₂ Nanoparticle: Properties and Application, Application in Nanobiotechnology and nanomedicine
- [15] Rijuan Mutsak Ahmed, Imran Hasan, (2023), A review on properties and applications of TiO₂ and associated nanocomposite materials, Materials Today: Proceedings, Volume 81, Pages 1073-1078, doi.org/10.1016/j.matpr.2021.04.381
- [16] Ali Ayati, Ali Ahmadpour, Fatemeh F. Bamoharram, Bahareh Tanhaei, Mika Mänttari, Mika Sillanpää, July (2014), A review on catalytic applications of Au/TiO₂ nanoparticles in the removal of water pollutant, Chemosphere, Volume 107, Pages 163-174, doi.org/10.1016/j.chemosphere.2014.01.040.
- [17] Shipra Gupta, Manoj Tripathi, January (2012), A review on the synthesis of TiO₂ nanoparticles by solution route, Open chemistry, Volume 10, Pages 279-294, doi.org/10.2478/s11532-011-0155-y.
- [18] Mohammad Rafiquewani, GGHA Shadab, July (2020), Titanium Dioxide nanoparticle genotoxicity : A review of recent on Vivo and in Vitro studies, Toxicology and Industrial health, Volume 36, Issue 7, Pages 514-530, DOI:10.1177/0748233720936835.
- [19] Priscilla Laviola Sanches, Luths Raquel de Oliveria Greaquinto, Rebecca Cruz, Desiree Cigaran, Schuck, Marcio Lorencini, Jose Mauro Granjeiro, Ana Tosa, Lopes Ribeiro, June (2020), Toxicity Evaluation of TiO₂ Nanoparticles on the 3D Skin Model: A Systematic Review, Front. Bioeng. Biotechnol, Volume 8, doi.org/10.3389/fbioe.2020.00575.
- [20] Meghmala S. Waghmode, Aparna B. Gunjal, Neelu N. Nawani, March (2019), Studies on the Titanium dioxide nanoparticles: Biosynthesis, Application and remediation, SN applied Science, Volume 1, doi:org/10.1007/s42452-019-0337-3.
- [21] Danie Ziental, Beata Czarczynska-Goslinska, Dariusz T. Mlynarczyk, Atkta Glowacka-Sobotta, Beata Stanis, Tomasz Goslinski, Lukasz Sobotta, January (2020), Titanium Dioxide Nanoparticles: Prospects and Applications in Medicine, National Library of Medicine, Volume 10, Issue 2, Pages 60-780, doi.org/10.3390/nano10020387.
- [22] M. Aravind, M. Amalanathan, M. Sony Michael Mary, March (2021), Synthesis of TiO₂ nanoparticle by chemical and green synthesis methods and their multifaceted properties, SN applied sciences, Volume 3, doi:org/10.1007/s42452-021-04281-5.
- [23] Boris Jovanovic, January (2015), Review of titanium dioxide nanoparticle phototoxicity: Developing a phototoxicity ratio to correct the endpoint values of toxicity tests, Environ Toxicol Chem. Volume 34, Issue 5, Pages 1070-1077, Volume 34, doi: 10.1002/etc.2891.
- [24] Moram A. AlGhamdi, Shaimaa M. Fouda, Noha Taymour, Sultan Akhtar, Soban Q. Khan, Mohamed S. Ali, Ahmed M. Elakel, Essam A. Nassar, Mohammed M. Gad, October (2023), Comparative Evaluation of TiO₂ Nanoparticle Addition and Postcuring Time on the Flexural Properties and Hardness of Additively Fabricated Denture Base Resins, National Library of Medicine, Volume 13, Issue 23, doi.org/10.3390/nano13233061.

Green synthesized TiO₂ nanoparticles for antimicrobial properties: Review

P. S. Wagh, S. T. Khan, S. P. Dharme, S. A. Amale

Department of Physics, Vidya Bharati Mahavidyalaya, Amravati.

Abstract

The Green Synthesis of metal/metal oxide nanoparticles has gained huge attention in recent years due to its increasing applications in various fields and owing to its less usage of chemicals and easy experimental methods. Plant extracts are increasingly being used to make green nanoparticles since they are harmless and environmentally friendly. Green Synthesis aims to reduce the usage of toxic chemicals which are replaced by biomolecules from plants. They also possess many applications in the fields of Biomedicine and Dentistry. Studies have become interested in the size and shape of titanium dioxide (TiO₂) NPs due to their excellent durability, good electrical conductivity, nontoxicity, ability to absorb UV light and antimicrobial activity properties, all of which make them an excellent material for nanostructures. The antimicrobial properties of the TiO₂ nanoparticles were observed to be highly toxic against bacterial strains. This review signifies the Green technique for the synthesis of Titanium nanoparticles (TiO₂-NP's) using various plant extracts, fungi and bacteria and its applications. The focus is on TiO₂ NPs that are obtained by Green synthesis methods and study their antimicrobial activity against different bacteria and fungus.

Keywords: TiO₂-NP's, green synthesis, antimicrobial activity, future perspectives

Introduction

Nanotechnology has attained vast attention over time, and it involves synthesizing and developing different nonmaterial and it is an accelerating field of recent research with desirable applications in medicine and electronic and has been developing very fast in recent generation, impacting on distinct areas such as environment and economy. Nanoparticles are characterized as building blocks of nanotechnology and the size ranging from 1 to 100 nm in diameter. The foremost feature of nanoparticles is their surface area to volume aspect ratio, enabling them to combine with other particles easier. Nanotechnology has been a pioneering area of research for the last decades and NPs are regarded as an essential part of nanotechnology as they're the foremost source of various nanostructure devices and their specific complexes that are manufactured from solid units whose sizes range between 1 and 100nm. When compared to the size of their bulk materials, the particles in their unique property have a large surface area. Based on this property, the nanomaterial allows for greater reactivity and indicates specialized

properties. Consequently, these ascribed NPs are applied in biological, chemical and industrial fields [1].

The two paths of synthesis for NPs are bottom-up and top-down. Consistent with the top-down approaches, NPs are synthesized from bulk materials. Due to their size and morphology, they show enhanced and unique properties and also have wide applications. The bottom-up approach combines atoms to create bulk materials and shows constant physical properties; these properties limit their applications. Different synthetic methods result in the evolution of new materials, which play an important role in NPs. Chemical and physical processes are used

to manufacture metal and metal oxide NPs. Green Synthesis, Solid-state, microwave, hydrothermal, sol-gel, solution route method, solvothermal crystallization, chemical phase decomposition vapor and ultrasonic irradiation are some of the processes. These methods develop heterogeneous NPs with high energy exhaustion. The chemical process involves synthetic stabilizing, capping and reducing agents, which are not eco-friendly and also need high temperatures, pressures and toxic chemicals. . As a result, in recent years, more sustainable methods for developing an eco-friendly process for synthesizing nontoxic nanomaterials, regarded as a safe, cost-effective and biocompatible process, have been introduced. The green synthesis method and the chemical synthesis method are indistinguishable. In the chemical method, reducing agents were high-cost chemical reducing reagents that were replaced in the green method by plant extract and microorganisms. Toxicity is reduced as well, which benefits biomedical applications such as drug delivery, nanocatalysts and nanomedicine biosensors and so on. This method is now used in metal oxides such as TiO₂, zirconium dioxide (ZrO), lanthanum chromite (LaCrO), nickel oxide (NiO), dimanganese trioxide (Mn O), zinc oxide (ZnO), copper (II) oxide (CuO) and others. Because of their high stability, optical properties and non-toxicity, TiO₂ NPs have been widely used as an eco-friendly and enhanced photocatalyst. Employing a "green" approach, the authors were able to produce TiO₂ NPs rapidly, reliably, and in low concentrations to significantly reduce malaria vector populations [2, 3].

Synthesis of TiO₂ Nanoparticles using different methods:

The two primary methodologies for the synthesis of nanomaterials is top-down and bottom-up approaches

- Top-down: size reduction from bulk materials
- Bottom-up: material synthesis from the atomic level

Top-down:

Bulk material is turned into a nano product using a top-down technique. For size reduction, both physical and chemical approaches were applied. Sputtering, pulse wire discharge, physical milling/ball milling, etching, evaporation–condensation reaction, pulse laser ablation, and lithography are some of the processes employed in the top-down approach. However, there are

certain disadvantages to the top-down approach, the most significant of which is that defects are imposed on the product's surface. This could affect the product's surface properties and other physical characteristics

Bottom-up:

The materials were built up from the bottom in the bottom-up approach: atom by atom, molecule by molecule, and cluster by cluster. Most nanostructures with the potential to make a homogeneity, size, and morphology are synthesized using this process. Chemical synthesis is offering a broad range of techniques like chemical vapor deposition, solvothermal, polymer condensation, sol-gel method, aerosol methodology, electrochemistry, pyrolysis, thermal decomposition, frameworks, plasma, and spinning also available Green synthesis, in particular, controlling the process in the bottom-up synthesis to decrease particle development. As a result, scientists can state that the bottom-up technique is crucial in the creation of nanostructures and nanomaterials. Almost all of these nanomaterial synthesis methods are employed, however, if we consider that, the bottom-up approach is the most efficient as it is beneficial and achieves perfection at the atomic scale. The bottom-up technique is also used since the green synthesis routes have been thought-out to be a practical strategy due to the employment of non-toxic,

cost-effective, and ecologically friendly matter. Natural various plant extracts are employed in green synthesis. In green chemistry, the plant extract serves as a capping and reducing agent, and it is blended with a simple precursor salt. The plant extract's phytochemicals can then reduce and stabilize the nanomaterials. With the new revolution, a lot of work has been done in green synthesis to synthesize a variety of metal NPs such as Cu, Pt, Pb, Ag, Au, Zn, and so on. Phyto-synthesis of TiO₂ NPs utilizing various plant extracts is discussed in this review. In this regard, recent research has been compiled from the literature to summarize research efforts [4].

Diagrammatic representation of Nanomaterial synthesis methods.

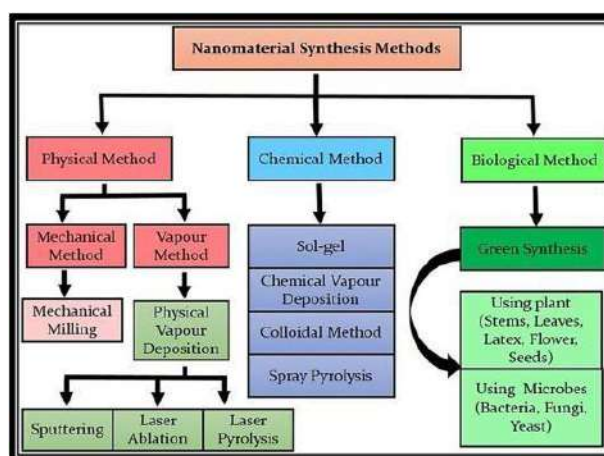


Figure 1

Green Synthesis:

Green synthesis of TiO₂ nanoparticles using jasmine flower extract:

Green synthesis is considered to play a key role in the current engineering and science field. As a result of their distinctive properties of biosynthesized nanomaterials, which are used for the treatment of water and contaminated sites. Nanoparticles are of keen interest due to their special attributes, such as their exceedingly small size, high surface area to volume ratio, surface modifiability, and size-dependent properties. These nanoparticles also showed their applications in the medical field and pharmacy. Nowadays, vast research is being conducted on the biological system. The biological synthesis of nanomaterials used bacteria, fungi, yeast, and plants. Due to their cost-effectiveness, these synthesis approaches have been the subject of widespread interest. The biologically synthesized nanoparticles have a wide range of applications in the field of contaminant remediation, as well as antibacterial, antifungal, high catalytic, and photochemical activity. Today's focus was on green synthesis, and with the help of plants, the NPs were very stable and in the proper form and size. Another benefit of green synthesis is that the chance of contamination is quite minimal. The plants contain many phytochemicals, which help in the production of nanomaterials and NPs. Plants provide a variety of phytochemicals that are commonly utilized and inexpensive in the synthesis of nanomaterials and nanoparticles. The phytochemicals also play an important role as they help at the time of photocatalytic activity applications. They help in the oxidation and reduction reactions at the photocatalytic activity time of the organic dyes [5].

TiO₂ NPs were synthesized using the facile green synthesis route from Jasmine flower extract acts as a reducing/capping agent. The jasmine flowers were purchased from the local market of Nagercoil, Tamilnadu. The jasmine flower extract was prepared by adding 50 g of jasmine

flower in 100 ml distilled water and boiled the mixture with a hotplate for 30 min. Then the aqueous solution has been filtered and stored for further tests. Take 50 ml of titanium tetra isopropoxide (TTIP) in a 100 ml beaker and add 20 ml of flower extract drop by drop to the above TTIP solution. The solution was stirred by 3 h at room temperature. The colour of the solution was changed from pure white to yellowish-grey. A change of colour confirms the formation of titanium dioxide nanoparticles. After that, the solution was Filter and dried at 110 °C for 5 h. Then the dried samples were calcined Muffle furnace at 500 °C for 2 h [6].
Diagrammatic representation of Green Synthesis of TiO₂ Nanoparticles

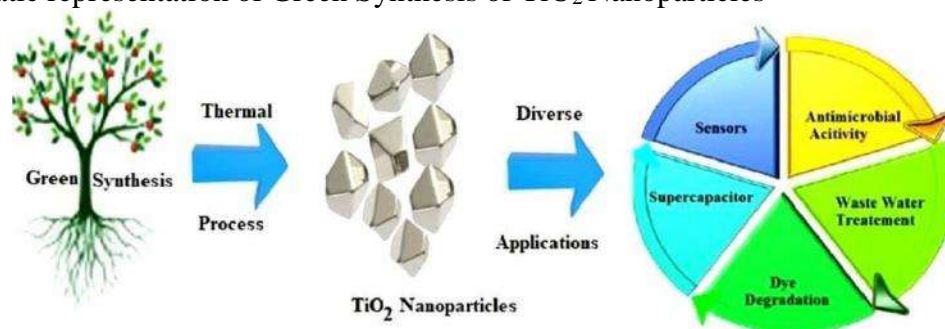


Figure 2

Characterization of TiO₂ nanoparticles (XRD):

X-ray diffraction (XRD) analysis of nanoparticles synthesized using plant extract is a rather new implementation of the technique to analysis the characteristic of synthesized nanoparticles. The XRD analysis is done to analyse the structure and crystalline size of synthesized nanoparticles. [7]. in their work characterized the synthesized silver (nano) using XRD. They concluded that the obtained data for 2θ positions identifies the sample as silver crystalline particles having hkl values corresponding to FCC silver. They estimated the crystalline size to be 20 nm, thus confirming the nano scale size of the synthesized particles. Various other workers such as Bykkam, Anandalakshmi, Ashraf & Abiola et al. have reported successful characterization of metallic nanoparticles synthesized using plant extracts. The result obtained from XRD analysis cannot be directly utilized in the study. It needs use of additional software packages such as PowderX, MATCH! Etc.

Presently the XRD is commonly used extensive technique for characterization of nanoparticles. XRD provides information regarding the crystalline structure, nature of the phase, lattice parameters and crystalline grain size. The latter parameter is estimated by using Scherrer equation using the broadening of the most intense peak of an XRD measurement for a specific sample. The nanoparticles are commonly analyzed in powder form after drying. The composition of the particles can be determined by comparing the position and intensity of the peaks with the reference patterns available from the international center for diffraction data (ICDD) [8].

Refer table 1 for particle size obtained from different plan extract.

Table 1

Sr. No.	Plant Extract	Shape	Size(nm)	Ref
1.	Ageratina altissima	Spherical	20–25	[9]
2.	Azadirachta indica leaves aqueous extract	Spherical	124	[10]
3.	Curcuma longa	Spherical	50–110	[11]
4.	Nyctanthes leaves Extract	Spherical	100–150	[12]
5.	Leaf aqueous extract of	Spherical shape and	32	[13]

	Psidium guajava	clusters		
6.	Aloe vera	Irregular	60	[14]
7.	Flower aqueous extract of Hibiscus rosasensensis	Monodispersed and spherical	7	[15]

Antimicrobial activity:

Harmful bacteria, such as *Staphylococcus aureus*, *Burkholderia cepacia*, *Pseudomonas aeruginosa*, *Clostridium difficile*, *Klebsiella pneumoniae*, *Escherichia coli*, *Acinetobacter baumannii*, *Mycobacterium tuberculosis*, and *Neisseria gonorrhoeae*, are responsible for bacterial infections that can cause serious diseases in humans year after year [16]. The principal solution is the use of antibiotics, antimicrobial and antifungal agents. Nevertheless, in recent years there has been an increase in the resistance of several bacterial strains to these substances, and therefore there is currently a great interest in the search for new antimicrobial substances. The antimicrobial nanoparticles have been studied due to their high activity, specifically the metal oxide nanoparticles [17, 18, and 19]. In this sense, titanium dioxide nanoparticles are one of the antimicrobial NPs whose study has gained interest during last year [20].

An antimicrobial is an agent that kills microorganisms (microbicide) or stops their growth (bacteriostatic agent). Antimicrobial medicines can be grouped according to the microorganisms they act primarily against. For example, antibiotics are used against bacteria, and antifungals are used against fungi. They can also be classified according to their function. The use of antimicrobial medicines to treat infection is known as antimicrobial chemotherapy, while the use of antimicrobial medicines to prevent infection is known as antimicrobial prophylaxis.

The antibacterial activity of titanium dioxide nanoparticles was tested by the agar diffusion method. First, the nutrient agar was uniformly spread in the Petri dish plate. Then fix the 6 mm diameter well, which is used to study the inhibition zone. Place 50 µl of TiO₂ NPs in 6 mm diameter well. The culture medium was incubated at 37 °C for 24 h under aerobic conditions. The zone of inhibition layer was measured using the millimeter region. The Zone of inhibition results in the antibacterial activity of TiO₂ NPs.

The antibacterial action of the synthesized TiO₂ nanoparticles were evaluated against the bacterial pathogens of *Bacillus subtilis* (*B. subtilis*) (ATCC 6051), *Escherichia coli* (*E. coli*) (MTCC-1677), *Enterococcus faecalis* (*E. faecalis*) (ATCC 2912), *Klebsiella pneumoniae* (*K. pneumoniae*) (NCTC 9633), *Staphylococcus aureus* (*S. aureus*) (MTCC-3160) and *Pseudomonas aeruginosa* (*P. aeruginosa*) (MTCC-4030) strains. Disc diffusion technique was adopted to monitor the antibacterial activity of synthesized titanium dioxide nanoparticles. Exponential bacterial cultures were seeded into Muller Hinton agar and impregnated with sterile discs. The discs were loaded with titanium dioxide nanoparticles with various concentrations (20, 30 and 40 µg/ml) and empty sterile disc was used as a control. The impregnated discs were kept on the surface of the agar and incubation of the plates was done overnight at room temperature. The experiment was performed in triplicates and the formation of the clear zone of inhibition was computed [21].

Future Scope:

Nanoscale materials serve as the building blocks for biomarkers and sensors that are more sensitive than ever before, allowing for the simultaneous and accurate diagnosis of more diseases in the early stages.

With improved targeting and chemical sensitivity, nanomedicine provides more accurate mapping of disease. Nanomedicine can be used more effectively to attack cells after a

diagnosis, reducing side effects and harm to healthy cells.

- Better preventive procedure
- Disease detection, Drug delivery & Diagnostics
- Detection of body oxygen using Nano sensors
- Economical healthcare
- Helpful for cardiovascular disease
- Fight against cancer
- Improve the efficiency of medicine
- Management of illness
- Nanobots
- Radiation therapy
- Tissue engineering and cell treatment

Conclusion:

Synthetic methods involving fungus, bacteria, and other organisms are complex due to strain separation and difficulties in growth. These processes are also difficult owing to the need to maintain the culture media, as well as the physical and chemical conditions. Plants are selected primarily since they are simple to extract and plentiful. This approach might be used to regulate the size, shape, and crystalline structure by adjusting the experimental parameters. Despite this, only a few plants are exploited in the phyto-synthesis of TiO₂ NPs, and additional study is urgently required in this field. These phyto-synthesized nanoparticles may be used safely not just in biomedical activities, but also in all other potential applications as they are similarly compatible with chemically produced nanoparticles. As previously stated, the crucial aspects of NP are determined by their size and shape. As a result, future difficulties will include figuring out how to leverage similar biological techniques to make various forms including triangular, cuboidal, truncated, ellipsoidal, pyramidal, decahedral, and oval. Scaling up NP production from the lab to the commercial-scale is a tough process with many challenges and unknowns. There

are two more obstacles to overcome. All across the production process, cost, dependability, waste, energy consumption, recycling possibilities, material safety, and hazard level should all be addressed. Furthermore, the properties of nanomaterials may change as they scale up. The amount of control may be diminished when dealing with large volumes.

References:

- [1] Devipriya Anbumani, Kayal vizhi Dhandapani, Janani Manoharan, Ranganathan Babujanathanam, A.K.H. Bashir, Karnan Muthusamy, Ahmed Alfarhan and K. Kanimozhi, April (2022), Green synthesis and antimicrobial efficacy of titanium dioxide nanoparticles using *Luffa acutangula* leaf extract *Journal of King Saud University – Science*, Volume 34, Issue 3, 101896
- [2] Natalia Vaou, Elisavet Stavropoulou, Chrysa Voidarou, Christina Tsigalou, and Eugenia Bezirtzoglou September (2021), Towards Advances in Medicinal Plant Antimicrobial Activity: A Review Study on Challenges and Future Perspectives, *Microorganisms*, Volume 2041, 34683362
- [3] Shiva Samhitha S., Raghavendra G., Camila Quezada, Hima Bindu P., November (2021), Green synthesized TiO₂ nanoparticles for anticancer applications: Mini review, *VIT-AP University, India*, Volume 54
- [4] Prammitha Rajaram, Ambrose Rejo Jeice and Kumarasamy Jayakumar, July (2023), Review of green synthesized TiO₂ nanoparticles for diverse applications, *Surfaces and Interfaces*, Volume 39, 102912
- [5] M. Aravind, M. Amalanathan M. Sony Michael Mary, March (2021), Synthesis of TiO₂

- nanoparticles by chemical and green synthesis methods and their multifaceted properties, Volume 3, article number 409,(2021)
- [6] Vishal Verma, Mawaheb Al-Dossari, Jagpreet Singh, Mohit Rawat, Mohamed G. M. Kordy, and Mohamed Shaban, April (2022), A Review on Green Synthesis of TiO₂ NPs: Photocatalysis and Antimicrobial Applications, *Polymers (Basel)*, 35406317
- [7] Manoj Kumar, Rakesh Ranjan, Sukumar Dandapat, Rohit Srivastava and Manoranjan Prasad Sinha, July (2022), XRD Analysis for Characterization of Green Nanoparticles: A Mini Review, *Ranchi University, Ranchi, Jharkhand*, Volume 10, 555779
- [8] Devipriya Anbumani, Kayal vizhi Dhandapani, Janani Manoharan, Ranganathan Babujanathanam, A.K.H. Bashir, Karnan Muthusamy, Ahmed Alfarhan and K. Kanimozhi, April (2022), Green synthesis and antimicrobial efficacy of titanium dioxide nanoparticles using *Luffa acutangula* leaf extract *Journal of King Saud University – Science*, Volume 34, Issue 3, 101896
- [9] Madadi Z., Bagheri Lotfabad T., April (2016), Aqueous Extract of *Acanthophyllum Laxiusculum* Roots as a Renewable Resource for Green Synthesis of Nano-sized Titanium Dioxide Using the Sol-gel method. *Adv. Ceram.* Volume 222631
- [10] Sankar R., Rizwana K., Shivashangari K.S., Ravikumar V, May (2014), Ultra-rapid photocatalytic activity of *Azadirachta indica* engineered colloidal titanium dioxide nanoparticles, *Appl. Nanosci.*, Volume, 132041403693.
- [11] Jalill R.D.A., Nuaman R.S and Abd A. N., July (2016), Biological synthesis of Titanium Dioxide nanoparticles by *Curcuma longa* plant extract and study its biological properties, *WSN*, 49204222.
- [12] Sundrarajan M., Gowri S., August (2011), Green synthesis of titanium dioxide nanoparticles by *nyctanthes arbor-tristis* leaves extract, *Chalcogenide Lett.*, 447451.
- [13] Santhoshkumar T., Rahuman A.A., Jayaseelan C., Rajakumar G., Marimuthu S., Kirthi A.V., Velayutham K., Thomas J., Venkatesan J., Kim S.-K., July (2014), Green synthesis of titanium dioxide nanoparticles using *Psidium guajava* extract and its antibacterial and antioxidant properties, *Asian Pac. J. Trop. Med.*, 7968976
- [14] Technology C., February (2016), Green Synthesis of TiO₂ Nanoparticles Using Aloe Vera Extract, *Int. J. Adv. Res.*, 22834
- [15] Kumar P.S.M., Francis A.P., Devasena T, March (2014), Biosynthesized and Chemically Synthesized Titania Nanoparticles Comparative Analysis of Antibacterial Activity. *J. Environ, Nanotechnol*, 37381.
- [16] Jha AK, Prasad K., (2010), Biosynthesis of metal and oxide nanoparticles using lactobacilli from yoghurt and probiotic spore tablets. *Biotechnology Journal.*;5:285-291. DOI: 10.1002/biot.200900221
- [17] Raja S, Ramesh V, Thivaharan V., (2017), Green biosynthesis of silver nanoparticles using *Calliandra haematocephala* leaf extract, their antibacterial activity and hydrogen peroxide sensing capability. *Arabian Journal of Chemistry*; 10:253-261. DOI: 10.1016/j.arabjc.2015.06.023
- [18] Müller JC, Botelho GKG, Bufalo AC, Boareto AC, Rattmann YD and Martins ES, . (2009) *Morinda citrifolia* Linn (noni): In vivo and in vitro reproductive toxicology. *Journal of Ethnopharmacology*; 121:229-233. DOI: 10.1016/j.jep.2008.10.019
- [19] Pai AR, Kavitha S, Shweta Raj S, Priyanka P, Vrinda A and Vivin TS, (2015), Green synthesis and characterizations of silver nanoparticles using fresh leaf extract of *Morinda citrifolia* and its anti-microbial activity studies. *International Journal of Pharmacy and Pharmaceutical Sciences*. 7:459-461
- [20] Carol López de Dicastillo and Matias Guerrero Correa, January (2020), Antimicrobial Effect of Titanium Dioxide Nanoparticles, Chapter Metrics Overview, 105772
- [21] Devipriya Anbumani, Kayal vizhi Dhandapani, Janani Manoharan, Ranganathan Babujanathanam, A.K.H. Bashir, Karnan Muthusamy, Ahmed Alfarhan and K. Kanimozhi, April (2022), Green synthesis and antimicrobial efficacy of titanium dioxide nanoparticles using *Luffa acutangula* leaf extract *Journal of King Saud University – Science*, Volume 34, Issue 3, 101896

Review of synthesis of nanoparticles by various methods

C.C. Jadhao, G.T. Lamdhade, K.B. Raulkar, A.O. Chauhan, R.B. Butley

Department of Physics, Vidya Bharati Mahavidyalaya, Amravati. M.S. 444602, India.

(Corresponding author: E-mail ID- ccjadhao@gmail.com)

Abstract

This review paper we have to highlights on the various methods use for synthesis of different materials. Synthesis means by procedure we have to make nanoparticles from core materials. For making nanoparticles there are number of methods like Physical Method, Biological Method and Chemical Method. In these articles we have to focus on various type of above methods and there process for synthesized nanoparticles. Top- down approach, Bottom–up approach, Synthesis of Nanoparticles from Microbes and plants, Chemical deposition method, Sol-gel method these methods are briefly discussed in these articles. It includes a wide range of materials with at least one dimension between 1 and 100 nm. Reasonably designed nanomaterials can have exceptionally large surface areas. Outstanding magnetic, electrical, optical, mechanical, and catalytic capabilities that differ significantly from their bulk counterparts can be created in nanomaterials.

1. Introduction:

Over the past century, there has been a substantial growth in the field of nanotechnology. Furthermore, nanotechnology is now directly or indirectly related to a wide range of academic subjects. Nanotechnology is the invention, synthesis, characterisation, and use of materials and devices by size and form manipulation at the nanoscale." "Nano" is a prefix that appears as a term in all streams, even product advertisements [1-2]. The word "nano" actually comes from the Latin word nanus, which meaning "dwarf," or the Greek word nanos. It brings together the disciplines of material science, biosciences, chemistry, and solid state physics. Thus, one needs to possess a thorough understanding of physics, chemistry, material science, solid state physics, and the biosciences rather than just being well-versed in one area. Nanotechnology is being used more and more in almost every branch of science and technology. Recently, the production of metal nanoparticles with specific properties has attracted a lot of attention as a subject of study. Many methods have been put forth for the synthesis of these materials: ball milling in the solid phase; chemical vapour condensation, arc discharge, hydrogen plasma—metal reaction, and laser pyrolysis in the vapour phase; microemulsion, hydrothermal, sol-gel, sonochemical, and microbial processes in the liquid phase. The features of metal nanoparticles are largely determined by the synthesis techniques employed. This study covers the principles, advantages, and disadvantages of each synthesis technique [3-4].

2. Techniques for synthesis of Nanomaterials

- 1) Top- down approach
- 2) Bottom–up approach
- 3) Physical Method
- 4) Biological Method
- 4) Chemical Method

2.1 Top-down approach: In a top-down method, the bulk material is broken down into particles or structures that are nanoscale. Techniques for creating micron-sized particles have been expanded upon by top-down synthesis. Top-down methods are less complex and rely on splitting or removing bulk material to create the right structure with the right characteristics [6].

2.2 Bottom-up approach: The "bottom-up" strategy is an alternative that may result in less waste and be more cost-effective. The term "bottom-up approach" describes the process of building a substance from the bottom up, either molecule by molecule, cluster by cluster, or atom by atom. A large number of these methods are either in the early stages of development or are just starting to be applied in the commercial manufacturing of nanopowders [7].

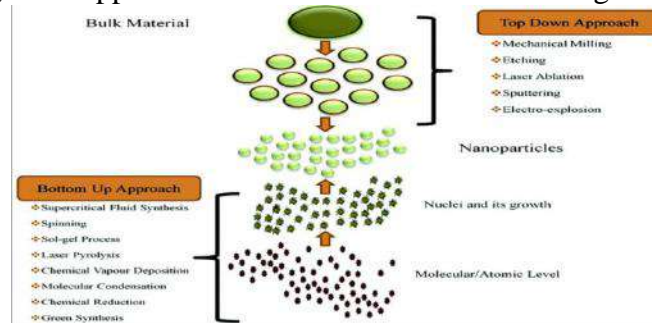


Fig 2: Bottom up & Top Down approach Method

2.3 Physical methods: Physical synthesis techniques have several advantages over chemical ones, such as uniform nanoparticle distribution and clean thin film generation without solvent contamination. There are significant disadvantages to the physical creation of nanoparticles at atmospheric pressure. The tube furnace, for example, requires a large amount of space, energy to raise the temperature surrounding the source material, and time to establish thermal stability. Furthermore, a typical tube boiler requires more energy than a few kilowatts to warm up for several tens of minutes before reaching a constant operating temperature. It was demonstrated that silver nanoparticles may be synthesised using a tiny ceramic heater with a localised heating area. Utilising, the primary materials were vaporised by using the tiny ceramic heater [8-9].

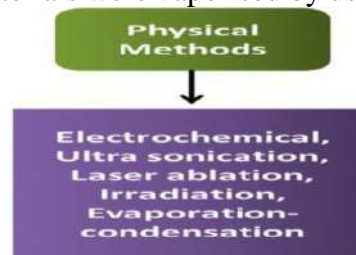


Figure 3: Physical methods

2.4 Biological Method

2.4.1 Synthesis of Nanoparticles from Microbes: Nanoparticles play a major role in materials chemistry. It can be used to control bacteria, fungi, and other microbes (Figure 1). In biosynthesis, physical or chemical methods can be applied. Different nanostructures may appear depending on the region. For example, the *Pseudomonas stutzeri*, which is isolated from silver ores, may accumulate silver particles with a diameter of 27 nm and a length ranging from 16 to 40 nm, and decrease Ag ions. Magneto tactic bacteria are a further example; they can generate magnetite Fe_3O_4 or reagent Fe_3S_4 . Around 650 different types of harmful germs can be killed by the antibacterial substance silver [10].

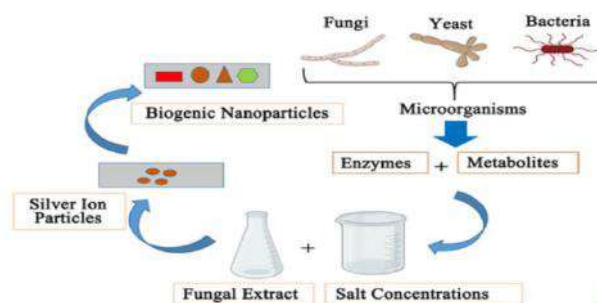


Figure 4.1: Synthesis of Nanoparticles from Microbes

2.4.2 Synthesis of Nanoparticles from Plants: Because they don't require complex cell culture and preservation procedures, plant extracts—which are used as reducing agents in the production of nanoparticles—are preferable to biological processes (Figure 4.2). Various plant components, such as bark, fruit, root, and pericarp extracts, are used to manufacture silver, gold, platinum, and titanium nanoparticles in a range of sizes and shapes. Gathering the required plant parts, washing them in distilled water to remove any epiphytes and necrotic matter, cleaning and drying the plant source for ten to fifteen days, pulverising it with a household mixer, and boiling ten grammes of the dried powder in one hundred millilitres of deionized distilled water are the steps involved in producing different types of nanoparticles [11-12].

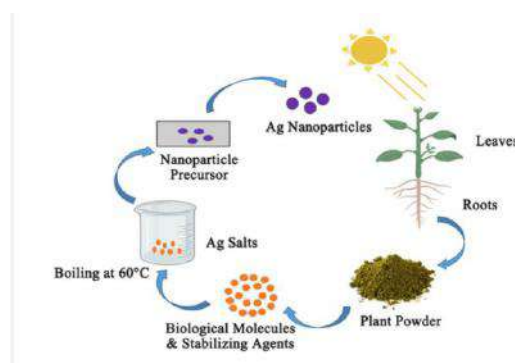


Figure 4.1: Synthesis of Nanoparticles from Plants

5) Chemical Method: Nanoparticles are produced via the following chemical processes: Vapour synthesis, solvothermal, hydrothermal, thermal breakdown, precipitation, and chemical vapour deposition (CVD) are a few examples. The particles formed by converting gases in furnace reactors or hot walls are generally quite clean, despite forming agglomerated particles.

5.1) Chemical Vapour Deposition Method: Chemical vapour deposition is the term used to describe any process that creates a thin solid layer on a substrate by the interaction of adsorbed precursors from the gas phase mediated by the surface. Due to their reactive nature, CVD procedures differ from PVD physical processes such as sputtering and evaporation. A mechanism known as "surface-mediated" creates the solid film when a heterogeneous reaction occurs at the substrate surface..

A schematic similar to the one in Figure 5.1 can help you understand the various roles that a CVD reactor plays. Chemical vapour deposition methods can be broken down into multiple discrete phases: The precursor chemicals need to be given to the CVD reactor beforehand. It is necessary to transfer precursor molecules from the reactor's inside to the substrate's surface, often by combining fluid transport and diffusion. Reaction pressure and reactor configuration are often process-specific and can change significantly, so we won't be thinking about them at this time [13-14].

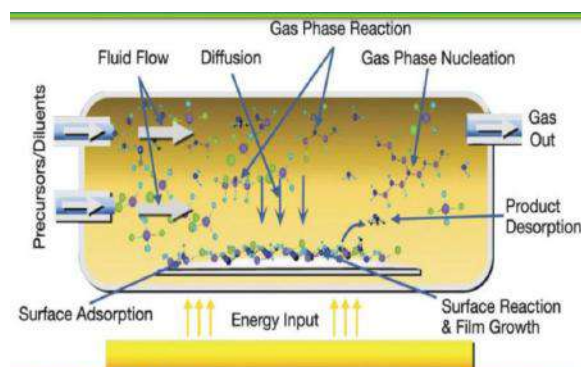


Figure 5.1: Schematic representation of Chemical Vapour Deposition Method

2.5 Sol-gel method: The terms "sol" and "gel" combine to form the term "sol-gel method." Sol is a colloid that is made up of suspended solid particles in a liquid that is continuous. Gel is a macromolecule that is solid and dissolves in a liquid. The most popular bottom-up method for creating nanoparticles is the sol-gel method because of its ease of use. This process uses an appropriate chemical solution as a precursor. In the sol-gel process, metal oxide and chloride are commonly utilised as precursors. The precursor is distributed throughout the host liquid by employing a variety of techniques, including shaking, sonication, and stirring. The final solution is made up of a liquid and solid phase that is separated to recover the nanoparticles using various methods like centrifugation, sedimentation, and filtration. The sol-gel method's schematic diagram is displayed in Figure 5.2. The experimental set up is very simple. Sol is obtained by either hydrolysis or polymerization reactions by adding suitable reagents in the precursor solution. The sol can be deposited onto preferred substrates as thin films using two techniques, viz. (1) spin coating and (2) dip coating [15-16].

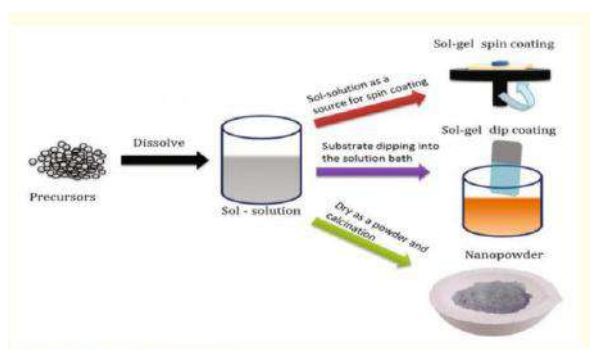


Figure 5.2: Schematic representation of Sol-gel Method

References :

1. Shaban Abdul, Telegdi Judit, Molnár Nikolett, Felhősi Ilona (2018). ' Chapter 16 - Functional thin films and nanostructures for sensors', *Fundamentals of Nanoparticles*, Pages 485-519
2. Amit Rastogi, Poonam Singh, Farid A. Haraz, Ahmed Barhoum (2018). ' Chapter 19 - Biological synthesis of nanoparticles: an environmentally benign approach', *Fundamentals of Nanoparticles*, Pages 571-604
3. Mansoori G., Fauzi Soelaiman T. (2005). ' Nanotechnology—An Introduction for the Standards Community'. *Jornal ASTM Int.* ;Volume 2: Pages 1–22.
4. Jaison Jeevanandam, Ahmed Barhoum, Yen S. Chan, Alain Dufresne and Michael K. Danquah (2018). ' Review on nanoparticles and nanostructured materials: history, sources, toxicity and regulations', *Volume 9*, Pages 1050–1074.
5. Pratim Biswas, Chang-Yu Wu (2005). ' Nanoparticles and the Environment', *Air & Waste Management Association*, Volume 55, 708 –746
6. S Anu Mary Ealia and M P Saravanakumar (2017). ' A review on the classification, characterisation, synthesis of nanoparticles and their application '. *IOP Conf. Series: Materials Science and Engineering*, Volume 3, Pages
7. Namita Rajput (2015). ' Methods of Preparation of Nanoparticles – A Review'. *International Journal of Advances in Engineering & Technology*, Volume 7(4), Pages 1806-1811.
8. Abdul wasy zia, Martin Birkett, Mohsin Ali Badshah, Munawar Iqba (2021). ' Progress *in-situ* synthesis of graphitic carbon nanoparticles with physical vapour deposition', *Progress in crystal growth and characterisation of materials*, Volume 67(3), Pages 100534
9. Surender and OAjay Gahlot (2021). ' Physical Methods of Nanoparticles Preparation – An Overview', *International Journal of Advances in Engineering and Management (IJAEM)*, Volume 3(12), Pages 812-816.
10. Nasrollahzadeh M, Sajadi SM, Sajjadi M, Issaabadi Z (2019). ' An introduction to nanotechnology'. *Interface Sci Technology*, Volume 28, Pages 1–27.
11. Elmer W, White JC (2018). ' The future of nanotechnology in plant pathology'. *Annual Review of Phytopathology*, Volume 25(56), Pages 111–133
12. Lalitha A. Kolahalam , I.V. Kasi Viswanath , Bhagavathula S. Diwakar , B. Govindh , Venu Reddy , Y.L.N. Murthy (2019). ' Review on nanomaterials: Synthesis and applications'. *Materials today Proceeding*, Volume 18(6), Pages 2182-2190.
13. T. Satyanarayana and S. Sudhakar Reddy (2018). ' A Review on Chemical and Physical Synthesis Methods of Nanomaterials', *International Journal for Research in Applied Science & Engineering Technology (IJRASET)*, Volume 6(1).
14. M.C. Roco (2005). ' Chapter - International Perspective on Government Nanotechnology Funding'. *Journal of Nanoparticle Research*, Volume 7(6).
15. Madzlan Aziz, Saad Saber Abbas, Wan Rosemaria Wan Baharom (2013). ' Size-controlled synthesis of SnO₂ nanoparticles by sol-gel method', *Materials Letters*, Volume 91, Pages 31-34.
- [16] Fredy Kurniawan and Rahmi Rahmi (2017). 'Synthesis of SnO₂ Nanoparticles by High Potential Electrolysis' *Bulletin of Chemical Reaction Engineering & Catalysis*, Volume 12(2), Pages 281-286.

Synthesis and Luminescence Characteristics of Eu^{3+} activated $\text{LiSr}_4(\text{BO}_3)_3$ Phosphor

S.S.Rajankar, R.M.Chavan , Mohammad Javed, S.P.Hargunani, R.P.Sonekar

Department of Physics, G.S. College, Khamgaon-444303,India

E-mail : swapna1kshirsagar@gmail.com

ABSTRACT :

$\text{LiSr}_4(\text{BO}_3)_3$ doped Eu^{3+} phosphor was successfully and intentionally synthesized by the modified solution combustion synthesis method. The phase purity of sample was characterized by powder X-ray diffraction (XRD). The photoluminescence (PL) property was studied using a Hitachi F-7000 spectrophotometer at room temperature. Under 234 nm excitation, the Eu^{3+} emission consists of the well-known transitions from the $^5\text{D}_4$ to $^7\text{F}_J$ levels and shows emission peaks at 489 nm, 544 nm, 587nm and 625nm respectively. Eu^{3+} shows red emission under near UV excitation. $\text{LiSr}_4(\text{BO}_3)_3:\text{Eu}^{3+}$ phosphor could be a suitable candidate for phosphor-converted solid state lighting.

Keywords : Photoluminescence , Phosphor , XRD, Borate.

INTRODUCTION : Phosphors doped with Rare – Earth ions and transition metal ions have attracted more attentions due to their variety of applications in the field of solid state lighting and medical science. Generally the phosphor is based on host matrix and activator. There are a large number of compounds, including silicates, aluminates, phosphates and borates. Among them, borates have attracted much attention due to their excellent thermal stability, and potential low-cost synthesis, that a number of compounds with different structures can be selected. [1] Moreover, the borates possess excellent properties as host structures of phosphors due to the inherent attributes of the large band gap and covalent bond energy [2,3]. And rare earth activated borate host phosphors have already been proven to be efficient phosphors [4,5]. Structure and relative properties of $\text{MM}^1_4(\text{BO}_3)_3$ were reported.

Host $\text{LiSr}_4(\text{BO}_3)_3$ with different rare earth ions were reported by different researchers for variety of practical application. $\text{LiSr}_4(\text{BO}_3)_3:\text{Ce}^{3+}$ [6], $\text{LiSr}_4(\text{BO}_3)_3:\text{Ce}^{3+},\text{Eu}^{3+},\text{Tb}^{3+}$ [7], $\text{LiSr}_4(\text{BO}_3)_3:\text{Dy}^{3+}$ [8], $\text{LiSr}_4(\text{BO}_3)_3:\text{Pb}^{2+}$ [9], $\text{LiSr}_4(\text{BO}_3)_3:\text{Gd}^{3+},\text{Pr}^{3+}$ [10]

Materials and Methods :

Synthesis of phosphor - The phosphor $\text{LiSr}_4(\text{BO}_3)_3$ doped with Eu^{3+} was prepared by modified solution combustion synthesis method. The stoichiometric amounts of high purity (Analytical Reagent) starting materials Lithium nitrate (LiNO_3), Strontium nitrate ($(\text{Sr}(\text{NO}_3)_2)$), Europium nitrate ($\text{Eu}(\text{NO}_3)_3$)(99.99% purity), Boric acid (H_3BO_3), urea [NH_2CONH_2], have been used for preparation of phosphors. The appropriate amount of starting materials with minute amount of double distilled water were mixed thoroughly in a china basin to obtain homogeneous solution. The solution was slowly heated at lower temperature at 90°C in order to remove the excess of water contents. The thick paste obtained after heating is then transferred into a microwave furnace maintained at 550°C . In this preparation, nitrates were used as an oxidizer and NH_2CONH_2 was used as a fuel. Within a few minutes, the solution boiled and ignited to produce a self-propagating flame. The entire combustion process was complete in less than 5 min. After 10 min the crucible was removed from the furnace and allowed to cool to room temperature. Then sample was grinded by using mortar pestle and faced to the microwave furnace maintaining at temperature 850°C for 3hr then quenched to room temperature. The resultant powder sample was then characterized using powder XRD, and Spectrofluorometer.

Results and Discussion :

XRD:- The phases of sample were identified by X-ray powder diffraction (XRD) using Cu/K α radiation with the voltage(40.0 kv) and current(30.0 mA) in the 2θ range from 10° to 80° .

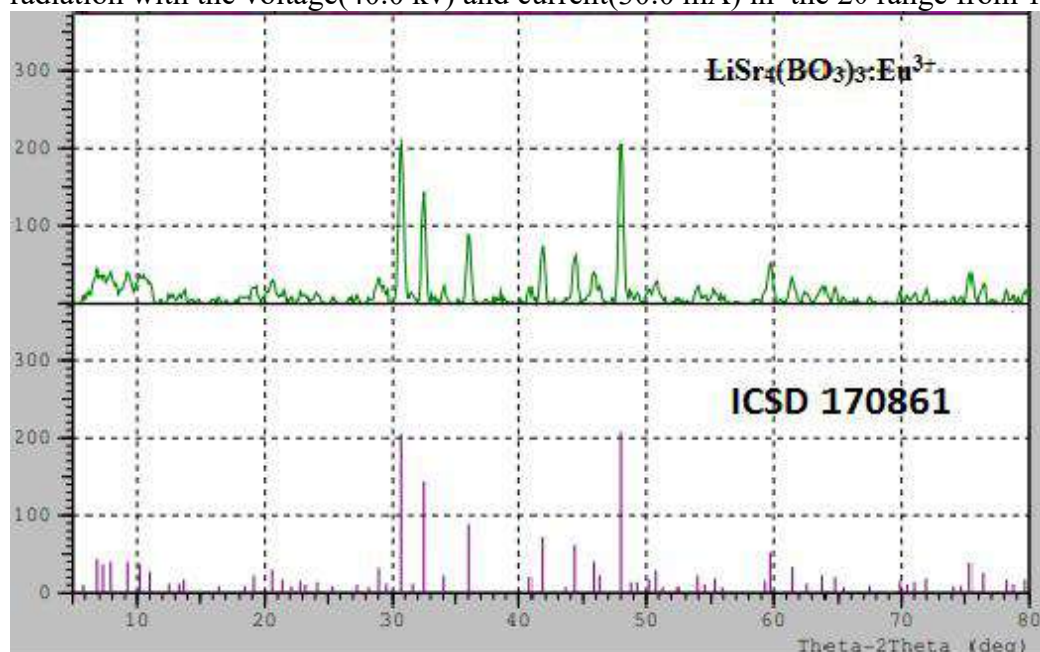


Fig 1. : XRD pattern of $\text{LiSr}_4(\text{BO}_3)_3 : 0.03 \text{Eu}^{3+}$ and ICSD- 170861 standard card.

Photoluminescence study:-

Eu^{3+} doped $\text{LiSr}_4(\text{BO}_3)_3$ phosphors show red emission under UV excitation. Figure 2 shows the PL excitation and emission spectra of $\text{LiSr}_4(\text{BO}_3)_3:0.03\text{Eu}^{3+}$.

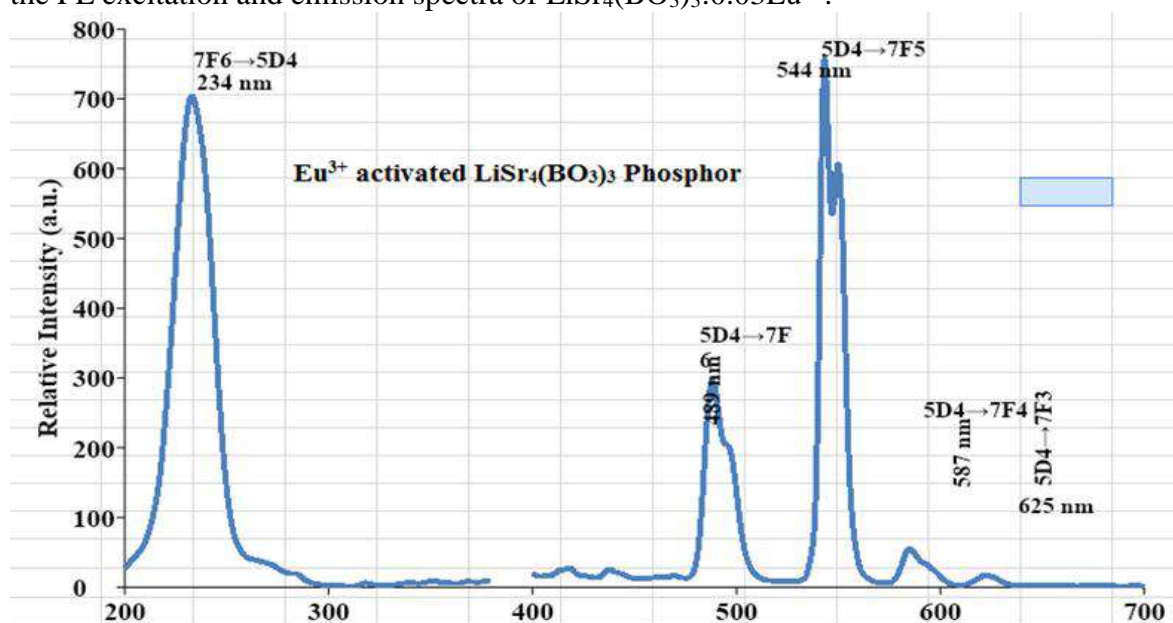


Fig.2 Excitation (a) and emission (b) spectra of the luminescence of $\text{LiSr}_4(\text{BO}_3)_3:0.03\text{Eu}^{3+}$

Under 234 nm excitation, the Eu^{3+} emission consists of the well-known transitions from the $^5\text{D}_4$ to $^7\text{F}_j$ levels. The emission peaks observed at 489 nm, 544 nm, 587 nm and 625 nm are assigned to the transitions $^5\text{D}_4 \rightarrow ^7\text{F}_6$, $^5\text{D}_4 \rightarrow ^7\text{F}_5$, $^5\text{D}_4 \rightarrow ^7\text{F}_4$, and $^5\text{D}_4 \rightarrow ^7\text{F}_3$ respectively. The excitation spectrum ($\lambda_{\text{em}}=544 \text{ nm}$) consists of broad excitation band peaking at about 234 nm and some intense f \rightarrow f absorption lines. The excitation band should be assigned to the charge transfer transition from O^{2-} to Eu^{3+} in the host lattice. The absorption of BO_3 groups may be situated at higher energy level.

Conclusion: Under 234 nm excitation, the Eu^{3+} emission consists of the well-known transitions from the $^5\text{D}_4$ to $^7\text{F}_J$ levels and shows emission peaks at 489 nm, 544 nm, 587nm and 625nm respectively. It is noted that the phosphors exhibit intense absorption around 400 nm, and this absorption band match the emission of near UV InGaN chip; so $\text{LiSr}_4(\text{BO}_3)_3:\text{Eu}^{3+}$ phosphor could be a suitable candidate for phosphorconverted solid state lighting.

References:

- [1] Yun B-G, Horikawa T, Hanzawa H, Machida K-i (2010) *JElectrochemSoc* 157:J364–J370
- [2] Yin L-J, Xu X, Yu W, Yang J-G, Yang L-X, Yang X-F, Hao L-Y, Liu X-J (2010) *J Am Ceram Soc* 93:1702–1707.
- [3] Zhong J, Liang H, Su Q, Zhou J, Huang Y, Gao Z, Tao Y, Wang J(2010) *ApplPhys B* 98:139–147
- [4] Xia Z, Du P, Liao L, Li G, Jin S (2010) *CurrApplPhys* 10:1087– 1091
- [5] Zhang XM, Li WL, Shi L, Qiao XB, Seo HJ (2010) *ApplPhys B*99:279–284
- [6] Jiang LH, Zhang YL, Gong XM, Pang R, Zhang S(2014) *Applied Radiation and Isotopes* 84, 66 – 69.
- [7] Zhang X , Lang H , Seo HJ (2011) *Journal of fluorescence* 21, 1111-
- [8] Zhang ZW, Sun X-Y, Liu L, Peng Y-S, Shen X, Zhang W-G (2013)*J Ceram.Int.*39:1723-1728.
- [9] Pekgozlu I ,(2013) *Journal of Luminescence* 143: 93-95.
- [10] Chauhan AO, Bajaj NS, Omanwar SK(2017) *Bull.Mater. Sci.*40: 1-6.

Feynman Diagrams and Rules in QED

Shrusti Kothari, Dr. Bipin Sonawane

e-mail: shrustikothari08@gmail.com

Department of Physics, Amity University Maharashtra

Abstract

In late 1940's Feynman devised his famous Feynman Diagrams which revolutionised theoretical particle physics. He introduced a method to visualise the inconceivable calculations required to describe particle interactions. The interaction of subatomic particles can be extremely complex and challenging to understand, but the Feynman diagrams provide an elegant and straightforward depiction of this interaction. The diagrams give a pictorial representation of the mathematical formulation for particle interactions. In this article we focus on introducing the concepts of Feynman diagrams and Rules using the theory of Quantum Electrodynamics.

Keywords— Feynman diagrams, Feynman rules, QED, QFT

1 Introduction to Feynman Diagrams

Before moving on to Feynman Diagrams we need a basic understanding of particle interactions. Interactions are the fundamental reason for existence of stars, life, and more accurately the existence of the entire universe. The elementary particles with half-integral spin, known as fermions, are referred to as matter particles. On the other hand, bosons possess integral spin and are known to be field particles or force carriers. At the quantum level, the fermions interact via emission and absorption of the field particles bosons associated with the fundamental interactions of matter. Specifically, photons for the electromagnetic force, gluons for the strong force, and W and Z bosons for the weak force are the field particles that the fermions interact with at the quantum level.

Feynman diagrams are 2D diagrams in space-time. But, whenever we draw a diagram, we have to take care of some steps, rules, and notations. The axes must be defined initially. The direction of space is represented by one of the two axes, and time is represented by the other. Particles that fall into distinct categories are given different kinds of lines. Bosons like photons are represented by wavy or curly lines, (the particles that are exchanged are known as virtual particles and cannot be observed) whereas fermions like electrons are depicted by straight lines (these are particles that are observed in an interaction). A vertex is the intersection of any three lines. In actuality, a vertex is the location of the interaction where a particle is really absorbed or expelled. In addition, the arrowhead of the incoming particle is shown pointing in the direction of the vertex, whereas the arrowhead of the exiting particle points in the opposite direction. Particles moving forward in time are matter particles vs particles moving backward in time are antimatter particles. [4]

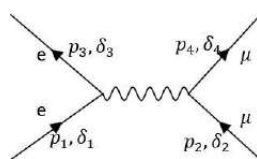


Figure 1: QED Vertex

Feynman diagrams is an essential tool that physicists use to precisely calculate the probability for an interaction to occur. A single interaction process might be represented by multiple diagrams, and the contribution from each picture is taken into account for determining this likelihood. Each diagram corresponds to a perturbation term in the calculations. We cannot determine the exact path the particles take in an interaction, therefore we need to account for all possible interactions considering all possible diagrams, but we have an infinite number of possibilities. Thankfully, in QED the probability for an interaction to occur rapidly decreases with the number of vertices a diagrams has, as each vertex contributes to a factor of $1/137$, which means that the higher order diagrams can be easily ignored, thus simplifying the calculations. Even though these probabilities are calculated using complex mathematical formulas, this method is much easier to deal with than others.[3]

2 Feynman Rules in QED

Richard Feynman gave a set of rules to calculate the matrix amplitude of a Feynman diagram. The square of the amplitude gives us the probability for an interaction to occur.

To calculate the amplitude, M associated with a particular Feynman diagram, the procedure is:[1]

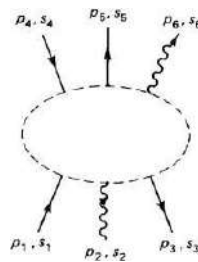


Figure 2: QED diagrams with external lines labelled

- Notation: Label the incoming and outgoing four-momenta p_1, p_2, \dots, p_n and their corresponding spins s_1, s_2, \dots, s_n label the internal four momenta q_1, q_2 . Assign arrows to the following lines: the arrows on external fermion lines tell us whether the particle is an electron or a positron. Arrows on internal fermion lines are assigned to preserve the "direction of the flow" through the diagram. The arrows on external photon lines point "forward" and the choice is arbitrary for internal photon lines.
- External Lines: contribution factors are as follows:
 - Incoming electron: u and Outgoing electron: u^-
 - Incoming positron: v^- and Outgoing positron: v
 - Incoming photon: e^μ and Outgoing photon: $e^{\mu*}$
- Vertex Factors: Each vertex contributes a factor

. The dimensionless coupling constant g_e is related to the charge of the positron: $g_e = \sqrt{4\pi/\hbar c} = \sqrt{4\pi\alpha}$

- Propagators: contribution factor by each internal line is:

$$\text{electrons and positrons: } \frac{i(\gamma^\mu q_\mu + mc)}{q^2 - m^2 c^2}$$

$$\text{Photons: } \frac{-ig_{\mu\nu}}{q^2}$$

- Conservation of Energy and Momentum: For each vertex, write the delta function as,

$$2\pi\delta^4(k_1 + k_2 + k_3)$$

where the k 's are three four-momenta coming into vertex (if an arrow points outward, then k is minus the four-momentum of that line, except for external positrons).

- Integrate Over Internal Momenta: For each internal momentum q , write a factor,

$$\frac{d^4q}{(2\pi)^4}$$

and integrate.

- Cancel the Delta Function: The result will include a factor

$$(2\pi)^4 \delta^4(p_1 + p_2 + \dots - p_n)$$

enforcing overall energy-momentum conservation. Cancel this factor, and what remains is i . Write down all diagrams contributing to the process in question (up to the desired order), calculate the amplitude for each one, add them up to find total amplitude, which is then used for calculation of the cross section or lifetime.

There's one twist here: the antisymmetrization of fermion wave functions needs us to put in a minus sign in combining amplitudes that differ only in the interchange of two identical external fermions.

- Antisymmetrization: Include a minus sign between diagrams that differ only in the interchange of two incoming (or outgoing) electrons (or positrons), or of an incoming electron with an outgoing positron (or vice versa).

We can take the example of electron-muon scattering for amplitude calculation.

2.1 electron muon scattering

In the case of electron-muon scattering, only one diagram contributes in second order. Applying the Feynman rules, we proceed "backward" along each fermion line.[2]

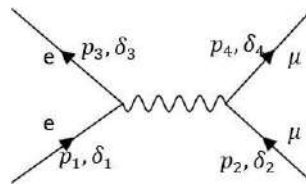


Figure 3: Electron muon scattering

$$(2\pi)^4 [\bar{u}^{(s_3)}(p_3)(i\gamma_e^\mu)u^{(s_1)}(p_1)] \frac{-ig_{\mu\nu}}{q^2} [\bar{u}^{(s_4)}(p_4)(i\gamma_e^\nu)u^{(s_2)}(p_2)] \times \delta^4(p_1 - p_3 - q)\delta^4(p_2 + q - p_4)d^4q$$

Carrying out the q integration, and dropping the overall delta function, we get the matrix amplitude,

$$M = - \frac{e^2}{(p_1 - p_3)^2} [u^{(s_3)}(p_3)\gamma^\mu u^{(s_1)}(p_1)][u^{(s_4)}(p_4)\gamma^\mu u^{(s_2)}(p_2)]$$

This Amplitude can be used to evaluate the scattering cross section for this reaction.

3 Conclusion

In conclusion, Feynman rules has been an invaluable tool in theoretical physics, especially in QFT. Developed by the Nobel laureate Richard Feynman, these rules provide a systematic and intuitive approach to calculating and understanding particle interactions. Feynman rules have played a significant role in cultivating our understanding of fundamental particles and their behavior. The rules have been used in the study of processes such as particle scattering, decay, and annihilation, contributing to the development of the Standard Model of particle physics. Feynman rules have made a remarkable impact on the way physicists approach and analyze particle interactions.

References

- [1] David Griffiths, *Introduction to Elementary Particles* (John Wiley Sons & Inc.) (1987)
- [2] Markus Klute, *Introduction to Nuclear and Particle Physics 8.701* (MIT Open course ware) (2020) (Lec 4.8)
- [3] Brian Clegg, *A beginner's guide to Feynman Diagrams* (BBC Science Focus) (November 1, 2021)
- [4] Simran Buttar, *What are Feynman Diagrams* (The Secrets Of The Universe)

TiO₂ nanoparticles synthesized by sol-gel and green synthesis method for antimicrobial properties: Mini Review

P. S. Wagh, S. T. Khan, S. P. Dharme, S. A. Amale

Department of Physics, Vidya Bharati Mahavidyalaya, Amravati.

Abstract

With many uses in science, engineering, medicine, and other domains, nanotechnology is a rapidly developing field. The preparation of nanoparticles (NPs) often involves a range of physical and chemical techniques. More recently, simpler, more affordable, and more environmentally friendly green synthesis technologies have been created. In the preceding quarter, there was a lot of interest in the green/sustainable production of titanium dioxide nanoparticles, or TiO₂ NPs. Bioactive substances found in bacteria and plants aid in the processes of capping and bio-reduction. This review covers the various synthesis techniques and mechanistic viewpoints, along with the biogenic synthesis of TiO₂ NPs. The present review deals with the synthesis of titanium dioxide (TiO₂) nanoparticles using sol-gel synthesis method and green synthesis method. How the samples of TiO₂ are characterized using x-ray diffraction technique to study the particle size is demonstrated in this review. The antimicrobial potential of synthesized nanoparticles is explored. Titanium dioxide (TiO₂) is nontoxic metal oxide, by which it has wide applications in medical field such as targeted drug delivery, cancer treatment, etc.

Introduction

The creation of green nanoparticles has attracted a lot of attention in nanotechnology studies. This innovative approach aims to regulate, control, clean up, and remediate these substantial particles to make them more environmentally friendly. By reducing the harmful byproducts produced during the production of conventional nanoparticles, less dangerous and unsustainable commodities will be produced. For antibacterial activity, TiO₂ nanoparticles (NPs) were produced utilising the leaf extracts of *Artemisia vulgaris* and aerial portions of *Callistemon citrinus* [1]. TiO₂ nanoparticles were more useful in the study of chemistry and nanomedicine because of their distinctive chemical characteristics and antibacterial activities. TiO₂ NPs are utilised in cosmetic products, and lotions and ointments containing these nanoparticles are applied to the skin to delay skin ageing and avoid sunburns [2]. The scope of this work was to scrutinize the antimicrobial activity of synthesized TiO₂ NPs using leaf extract of *L. acutangula* against pathogens. The current work aims to utilize the biological route for the synthesis of TiO₂ NPs and characterized using various spectroscopic and microscopic methods for the analysis of structure, morphology, and optical properties [3].

Synthesis of TiO₂ NPs by Different Methods

1. Physical Method

2. Chemical Method

3. Biological Method

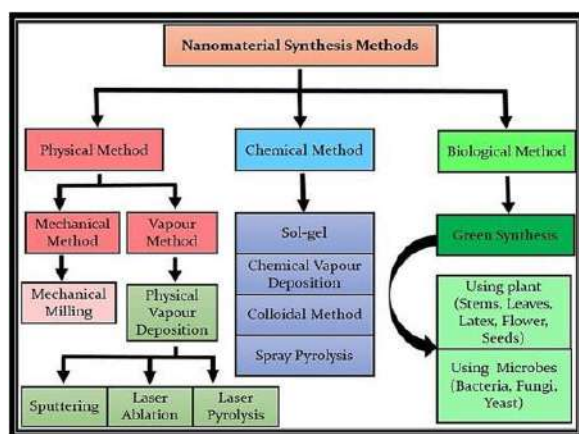
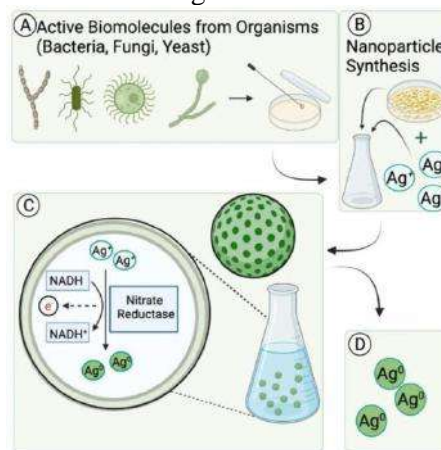


Figure 10: Methods for Synthesis Figure

Synthesis



11: Role of active molecules in Green

What is Green Synthesis?

Green synthesis employs a clean, safe, cost effective and environmentally friendly process of constructing nanomaterials. Microorganisms such as bacteria, yeast, fungi, algal species and certain plants act as substrates for the green synthesis of nanomaterials [figure 2]. Different active molecules and precursors, such as metal salt, determine the final morphology and size of the nanoparticle. Additionally, green synthesis provides nanomaterial benefits ranging from antimicrobial properties to natural reducing properties and stabilizing properties [4].

Preparation of TiO₂ nanoparticles by Green Synthesis Method

Aqueous extract of *E. purpurea* was prepared using 10 g herba boiled with 50 mL of double distilled water at 90 °C for 20 min. This extract was filtered through a medium filter. 1 mM TiO₂ (aq) solution was stirred for 2 h in 25 °C to prepare nanoparticles of TiO₂. 10 mL of the aqueous extract of *E. purpurea* were added to 20 mL of 1 mM TiO₂ at 25 °C, under stirring condition for 4 h. After 4 h, the color of the extract with TiO₂ nanoparticles changed to green. Figure 3 shows the schematic illustration of the green synthesis of TiO₂ nanoparticles using aqueous extract of the *E. purpurea* herba [5]

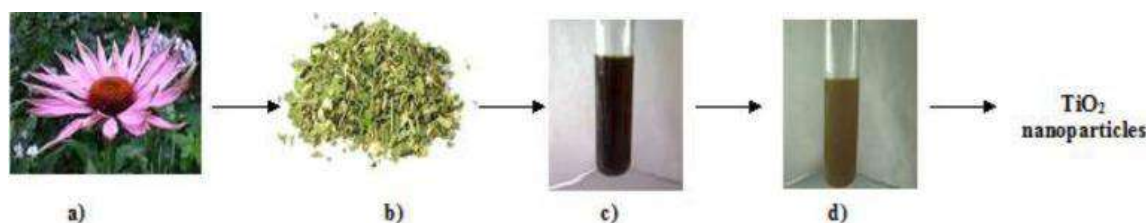


Figure 12

What is Sol-gel method?

In this chemical procedure, a "sol" (a colloidal solution) is formed that then gradually evolves towards the formation of a gel-like diphasic system containing both a liquid phase and solid phase. Removal of the remaining liquid (solvent) phase requires a drying process, which is typically accompanied by a significant amount of shrinkage and densification.

Preparation of TiO₂ nanoparticles by Sol-gel Method

For the sol-gel process, 150 ml ethanol was mixed with 10 ml deionized water under constant stirring. Further, 9 ml TTIP was mixed in the above solution under constant stirring while maintaining the temperature at 85 °C using paraffin oil bath upto 4 h. After forming the gel, it was dried in the hot-air oven at temperature 60 °C. The calcination was performed for 3 h at 400 °C and the prepared sample was named as 'SG'. With the same above chemical compositions, another solution was prepared for the solvothermal process which was transferred into Teflon lined autoclave followed by the hydrolysis process. The autoclave was placed in the hot-air oven for 2 h at temperature 200 °C. Later, the sample was collected from the autoclave and washed with ethanol. Finally, after drying at 80 °C for 1 h the collected particles were grinded and named as sample 'ST' [6].

Characterization of TiO₂ Nanoparticles

X-ray diffraction

X-ray diffraction (XRD) analysis of nanoparticles synthesized using plant extract is a rather new implementation of the technique to analysis the characteristic of synthesized nanoparticles [7-9]. The XRD analysis is done to analyse the structure and crystalline size of synthesized nanoparticles. The crystallinity and size of crystallites of the synthesized material was often characterized with the help of XRD pattern. The structural information was obtained for the comparison of diffraction pattern of X-rays with the pattern of standardized plane angles of the substance. For the confirmation of crystallinity, the obtained results are matched with the Joint Committee on Powder Diffraction Standards [10].

Antimicrobial Properties of TiO₂ Nanoparticles

Increasing numbers of NP variants and NP-based materials have been used as a new line of defense against microbial resistance and MDR. Different types of NPs have different mechanisms for combating microbial resistance. Various antibacterial mechanisms of NPs according to the metabolic process involved are presented in the “Antibacterial mechanisms of NPs” section [11, 12]. The antibacterial action of the synthesized TiO₂ nanoparticles were evaluated against the bacterial pathogens of *Bacillus subtilis* (*B. subtilis*) (ATCC 6051), *Escherichia coli* (*E. coli*) (MTCC-1677), *Enterococcus faecalis* (*E. faecalis*) (ATCC 2912), *Klebsiella pneumonia* (*K. pneumonia*) (NCTC 9633), *Staphylococcus aureus* (*S. aureus*) (MTCC-3160) and *Pseudomonas aeruginosa* (*P. aeruginosa*) (MTCC-4030) strains. Disc diffusion technique was adopted to monitor the antibacterial activity of synthesized titanium dioxide nanoparticles. Exponential bacterial cultures were seeded into Muller Hinton agar and impregnated with sterile discs. The discs were loaded with titanium dioxide nanoparticles with various concentrations (20, 30 and 40 µg/ml) and empty sterile disc was used as a control. The impregnated discs were kept on the surface of the agar and incubation of the plates was done overnight at room temperature. The experiment was performed in triplicates and the formation of the clear zone of inhibition was computed [13].

References

- [1] Tahir Rasheed, Muhammad Bilal, Hafiz M.N. Iqbal and Chuanlong Li, October (2017), Green biosynthesis of silver nanoparticles using leaves extract of *Artemisia vulgaris* and their potential biomedical applications *Colloids and Surfaces B: Biointerfaces*, Volume 158, 1, Pages 408-415
- [2] L Zhang, L Dai, X Li, W Yu, S Li and J Guan, (2022) 3D structured TiO₂ based aerogel photo catalyst for the high-efficiency degradation of toluene gas *New Journal of Chemistry*.
- [3] J. Rajkumari, C. Maria Magdalane, B. Siddhardha, J. Madhavan, G. Ramalingam, N.A. Al-Dhabi, M.V. Arasu, A.K.M. Ghilan, V. Duraipandiayan and K. Kaviyarasu, December (2019) Synthesis of titanium oxide nanoparticles using *Aloe barbadensis* mill and evaluation of its antibiofilm potential against *Pseudomonas aeruginosa* PAO1 *Journal of Photochemistry and Photobiology B: Biology* Volume 201, 111667
- [4] Sivaraj A., Kumar V., Sunder R., Parthasarathy K. and Kasivelu G., (2020), Commercial Yeast Extracts Mediated Green Synthesis of Silver Chloride Nanoparticles and their Anti-mycobacterial Activity. *J. Clust. Sci.*, 31:287–291. Doi: 10.1007/s10876-019-01626-4.
- [5] Renata Dobrucka, (2017), Synthesis of Titanium Dioxide Nanoparticles using *Echinacea purpurea* Herba, Poznan University of Economics, Poland, *Iran J Pharm Res.* Spring; 16(2): 756–762.
- [6] R.S. Dubey, Katta Venkata Krishnamurthy and Shyam Singh, September (2019), Experimental studies of TiO₂ nanoparticles synthesized by sol-gel and solvothermal routes for DSSCs application Volume 14, 102390
- [7] Dandapat S, Kumar M, Ranjan R and Sinha MP, (2022), *Ganoderma applanatum* extract mediated synthesis of silver nanoparticles. *Brazilian Journal of Pharmaceutical Sciences* 58: e19173
- [8] Kero Jemal, B. V. Sandeep and Sudhakar Pola, Mar (2017), Synthesis, Characterization, and Evaluation of the Antibacterial Activity of *Allophylus serratus* Leaf and Leaf Derived Callus Extracts Mediated Silver Nanoparticles, *Journal of Nanomaterials*, Volume 2017
- [9] Mehta BK, Chhajlani M, Shrivastava BD, (2017), Green Synthesis of silver nanoparticles and their characterization by XRD, *Journal of Physics*, 836(1):012050
- [10] J.M. Abisharani, S. Devikala, R.D. Kumar, M. Arthanareeswari and P. Kamaraj, (2019), Green synthesis of TiO₂ nanoparticles using *Cucurbita pepo* seeds extract, *Materialstoday*, Volume 14, Part 2, 2019, Pages 302-307
- [11] Singh R, Smitha MS, Singh SP., (2014), the role of nanotechnology in combating multi-drug resistant bacteria. *J Nanosci Nanotechnol.* ; Volume 14(7), Page No.4745–4756.
- [12] Emerson Danguy Cavassin, Luiz Francisco Poli de Figueiredo, José Pinhata Otoch, Marcelo Martins Seckler, Roberto Angelo de Oliveira, Fabiane Fantinelli Franco, Valeria Spolon Marangoni, Valtencir Zucolotto, Anna Sara Shafferman Levin & Silvia Figueiredo, (2015), Costa Comparison of methods to detect the in vitro activity of silver nanoparticles (AgNP) against multidrug resistant bacteria, *Journal of Nanobiotechnology* , volume 13, Article number: 64
- [13] Devipriya Anbumani , Kayal vizhi Dhandapani , Janani Manoharan , Ranganathan Babujanathanam , A.K.H. Bashir , Karnan Muthusamy , Ahmed Alfarhan and K. Kanimozh , April (2022), Green synthesis and antimicrobial efficacy of titanium dioxide nanoparticles using *Luffa acutangula* leaf extract, *Journal of King Saud University – Science*, Volume 34, Issue 3, 101896

Review on Metal Oxides Based CO₂ Gas Sensors

***Mankar S.S., **Lamdhade G.T., **Raulkar K.B**

*Department of Physics, Shivramji Moghe Arts, Commerce and Science College, Kelapur, Pandharkawada ,
Dist. Yavatmal, M.S., India

**Department of Physics, Vidya Bharati Mahavidyalaya, CK Naidu Road, Amravati, M.S., India

Abstract

Semiconductor gas sensors are known as Metal oxide sensors (MOS) or chemiresistive gas sensors. They have been considered as solid-state gas-sensing materials. In this review paper research progress on various metal oxides based Carbon Dioxide gas sensors is summarized. Copper oxide nanomaterials have been extensively studied for gas sensing applications. Copper oxide nanomaterials are abundant and non-toxic materials. There is availability of different low-cost synthesis methods and high degree of morphological control with tailored properties for Copper oxide nanomaterials. Nano CuO and its composite oxides have potential applications in the field of gas sensor. This review paper also provides the information about CuO based Carbon Dioxide gas sensors.

Keywords- Gas Sensors, nanomaterials, Metal oxide sensors, chemiresistive gas sensors

Introduction

Semiconductor gas sensors are known as Metal oxide sensors (MOS) or chemiresistive gas sensors. They have been considered as solid-state gas-sensing materials. MOS are the most studied and commonly used for detection of hazardous and toxic gases. The detection principle of resistive sensors is based on change of the resistance of the sample in the presence of reducing or oxidizing gases on the surface of a semiconductor. Metal oxides including both transition-metal oxides and non-transition-metal oxides can be selected for detecting combustible, reducing, or oxidizing gases. Composite metal oxides usually show better gas response than the single component if the catalytic actions of the components complement each other. A CO₂ sensor is a device designed to measure and monitors the concentration of carbon dioxide gas in the surrounding environment. When CO₂ gas comes into contact with the oxide material, a chemical reaction takes place at the material's surface which changes electrical resistance. This sensor measures this resistance change to determine the CO₂ concentration. This resistance change is proportional to the CO₂ concentration.

In this review paper research progress on various metal oxides based Carbon Dioxide gas sensors is summarized and this review paper also provides the information about CuO based Carbon Dioxide gas sensors.

Review of work on various metal oxides composites based CO₂ sensors.

A mesoporous CaO-loaded In₂O₃ resistive gas sensor material for the detection of CO₂ was prepared by Anna Prim et al.[1] Pure In₂O₃ based sensors are low sensitive to CO₂ but CaO addition to In₂O₃ matrix enhances the sensitivity to CO₂. It was observed that In₂O₃ containing the additive show an important response in the 300–5000 ppm range of gas concentrations. Sung-Eun Jo et al.[2] using screen printing fabricate WO₃ doped TiO₂ semiconductor gas sensor on an Al₂O₃ substrate for detection of various gases such as NO₂ , CO, O₂ and CO₂ at high operating temperature (600°C). G T Lamdhade [3] study the influence of CO₂ gas concentration on the transport properties of SnO₂-10Al₂O₃-10TiO₂ oxide thick films. Samples show polycrystalline and granular nature with size 10.80 nm to 56.05 nm. The sensitivity decreases with increase in temperature for a fixed concentration of CO₂ gas, but

increases with increasing concentration of CO₂ gas. Maryam Ehsani et al [4] fabricate La₂O₃/SnO₂ thick films by screen printed method to study CO₂ Gas Sensing Properties. In air atmosphere the sample of 3 wt.% Pt La₂O₃/SnO₂ thick film sensitive paste exhibits a high sensitivity to increasing the CO₂ gas concentration at 225 °C. The positive correlation between the sensor's sensitivity and increasing the CO₂ concentration from 100 up to 1000 ppm was found by them.

S. M. Yenorkar [5] for detection the CO₂ gas at room temperature (303oK) prepared thick film of mixed oxides SnO₂ and WO₃ by screen printing method. The highest sensitivity of about 12.45 was achieved by the 45 mol.% SnO₂ - 55 mol% WO₃ sample on 802 ppm CO₂ gas at room temperature and for this sample fast response and recovery time was found to be 109 S and 2 S. S.B. Unhale [6] fabricate SnO₂-Fe₂O₃ composites thin films by sintering powders at 800°C. Electrical conductivity and CO₂ gas sensitivity of the samples was studied for 300C to 800C. SnO₂-rich composites and Fe₂O₃-rich composites showed higher sensitivity values to CO₂ gas than pure SnO₂ and pure Fe₂O₃. SnO₂- Fe₂O₃ grain boundary was also proposed to be responsible for the gas sensitivity. Mohamed A. Basyoonia et al [7] prepared gas sensor for detection of CO₂ gas at room temperature which is based on mixed-valence phases in molybdenum and tungsten Oxide nanostructured thin films using RF magnetron sputtering at 400 °C. it is observed that nanostructured metal oxide semiconductor enhanced the gas response with fast response and recovery time of 6.53 and 8.05 s, respectively

B.M. Mude and K.B. Raulkar 2021 [8] in there paper observed the gas response of SnO₂:TiO₂Composites. Screen printing technique was used to prepare composites of SnO₂:TiO₂ with Al₂O₃ as substrate on glass plate. As compared to pure SnO₂ and TiO₂ optimized sample 70SnO₂:30TiO₂ exhibits the enhancement in gas sensing properties. M. Amarnath and K. Gurunathan [9] develop NiO-In₂O₃ nanospheres coated reduced graphene oxide (rGO) gas sensor for CO₂ gas operated at room temperature. They found that Indium added nickel oxide has a huge influence in CO₂ sensing. The fabricated sensor rGO-8:2 show the high sensitivity of 40 % towards CO₂ at 50 ppm was obtained for rGO-8:2. This sensor can detect up to 5 ppm concentration having response time of 6 sec and recovery of 5 sec. Zhi Yan Lee et al [10] studied for room temperature high-performance carbon dioxide (CO₂) gas sensor based on SnO₂-rGO hybrid composite. They prepared SnO₂-rGO via an in-situ chemical reduction route. The synergistic effect showed improvement in a sub ppm- level detection limit (5 ppm) and excellent CO₂ sensing at room temperature

Sandeep Gupta et al [11] prepared Na₃BiO₄ - Bi₂O₃ mixed oxide nanoplates for CO₂ gas sensing applications. Electrochemical deposition with potentiostatic mode on ITO substrate was used to synthesize these nanoplates. To find the gas percentage response change in electrical resistance of the nanoplates was measured the in the presence of CO₂ for different pressures at 50⁰C, 75⁰C and 100⁰C. Khaoula Kacem et al. [12] fabricate gas sensing device GO/SrTiO₃ sensors based on GO synthesized by a modified Hummer's method and decorated with SrTiO₃ for the detection of hazardous gases such as NO₂, CO₂, and NH₃. They found that as compared to bare graphene oxide they obtained a higher sensitivity towards CO₂ for graphene oxide decorated with SrTiO₃.

Review of work on CuO and metal oxides based CO₂ sensors.

Tatsumi Ishihara [13] fabricate mix oxide CuO- BaSnO₃ capacitive type sensor for CO₂ detection with high sensitivity. He found that sensitivity of gas sensor is strongly temperature dependent and maximum at 830⁰K. Shogo Matsubara et al [14] developed mixed oxides CeO₂/BaCO₃/ CuO capacitive type CO₂ sensor. This sensor can be produced at low cost, and has high resistance to humidity for IAQ monitoring system. This sensor shows accurate CO₂ monitoring characteristics. Bo Liao et al [15] fabricate CO₂ sensor made of pn heterojunctions of CuO and BaTiO₃ semiconductors CuO-BaTiO₃ using co precipitation method. The

sensitivity of gas sensor is found to be maximum 2.34 at 685°K. Yanfei Gu et al. [16] prepared CuO-SrTiO₃-based thin films by novel sol-gel technology on Al₂O₃ substrates for detection of CO₂ sensing properties. When the films exposed to 6% CO₂ at 250 °C operating temperature. sensitivity is 32, and response and recover time are within 2 s. The modified CuO-SrTiO₃ thin films exhibit good gas sensitivity properties for CO₂.

Jennifer C et al. [17] fabricate CuO-SnO₂ based CO₂ microsensors by means of micro electromechanical systems technology and sol-gel nanomaterial synthesis processes. At a doping level of CuO : SnO₂ = 1 : 8 (molar ratio), the resistance of the sensor has a linear response to CO₂ concentrations for the range of 1% to 4% CO₂ in air at 450⁰ C. A. Chapelle et al. [18] showed that nanostructured CuO/CuFe₂O₄ bilayers for promising material for future cheap semiconductors CO₂ sensors. They prepared CuO/CuFe₂O₄ sputtered thin films as a sensing material for Carbon Dioxide. The best response was obtained at the optimal operating temperature of 250⁰C towards 5000 ppm of CO₂. Vidya M. Balkhande 2016 [19] fabricate SnO₂ : CuO : TiO₂ thick films sensors by using screen-printing technique for detection of CO₂ gas. When operated for 50⁰ C to 350⁰ C the sensitivity is clearly seen to be decreasing nature with temperature of sensors. Mude [20] fabricate CuO:TiO₂ films by a screen printing techniques. Sensing properties of thick film studied by at different concentration of carbon dioxide gas. Maximum sensitivity was obtained for 60CuO:40TiO₂ composite.

Akshaya Mouly Vijayakumari et al [21] developed CuxO/NiO nanostructured matrix-based sensor for spotting of CO₂ level in the mixed gas environment. The sensor optimized at 250°C is highly selective to CO₂ due to the catalyst dominant defect state in the sensor matrix. Mude K.M. et al. [22] used Screen printing technique to prepare a thick film of CuO doped ZnO to design CO₂ gas sensor. From study they show that as compared to Pure ZnO and CuO, metal oxide semiconductor composite of 75ZnO:25CuO gas sensors is extremely useful for effective CO₂ gas sensing mechanism. Paul Chesler et al. [23] fabricate CoO- CuO sensitive films using an eco-friendly and low-cost deposition technique (sol-gel). The sensing films were studied for cross-sensitivity (CO₂) measurements. For the S5 cobalt-based sensor response for CH₄ is recorded more than double compared with its response towards CO₂ and humidity. Soraya Bouachma et al. [24] prepared PSi/p-CuO/n-Cu₂O bilayered heterostructure to detect CO₂ gas. They show bilayered PSi/CuO/Cu₂O structure is sensitive to CO₂ gas with a high sensitivity of 80% at low bias potential (0.85 V). Nagesh Bhat et al [25] prepared GO/CuO Nanohybrid-Based Carbon Dioxide Gas Sensors with an Arduino Detection Unit. The sensing response of this sensor toward CO₂ is found to be 60%.

Conclusion

Low cost, Excellent sensitivity, Fast response time;, Wide range of target Gases, Long shelf life, Compact and Excellent suitability for portable devices makes the Metal oxide promising materials for the detection of Carbon Dioxide and many other gases. Many research found that composite metal oxides usually show better gas response than the single component if the catalytic actions of the components complement each other.

References

- [1] Anna Prim, Eva Pellicer, Emma Rossinyol, Francesca Peiró, Albert Cornet, and Joan R. Morante, A Novel Mesoporous CaO-Loaded In₂O₃ Material for CO₂ Sensing, *Adv. Funct. Mater.* 2007, 17, 2957–2963, doi:10.1002/adfm.200601072
- [2] Sung-Eun Jo, Byeong-Geun Kang, Sungmoo Heo, Soonho Song, Yong-Jun Kim, Gas sensing properties of WO₃ doped rutile TiO₂ thick film at high operating temperature, *Current Applied Physics* 9 (2009) e235–e238, doi:10.1016/j.cap.2009.06.053
- [3] G T Lamdhade, Tin oxide and titanium dioxide based CO₂ gas sensor, *Journal of Electron Devices*, Volume 21, 1849 – 1853, 2015, JED ISSN: 1682 – 3427
- [4] Maryam Ehsani, Mohd Nizar Hamidon, Arash Toudeshki, M. H. Shahrokh Abadi, Sarah Rezaeian, CO₂ Gas Sensing Properties of Screen-Printed La₂O₃/SnO₂ Thick Film, *IEEE Sensors Journal*, VOL. 16, NO. 18, Sept. 15, 2016, <http://dx.doi.org/10.1109/JSEN.2016.2587779>
- [5] S. M. Yenorkar, Sno₂-Wo₃ Mixed Oxide as A Semiconductor Gas

- Sensor for CO₂, International Journal for Research in Applied Science & Engineering Technology (IJRASET), Volume 5 Issue VI, June 2017, ISSN: 2321-9653
- [6] S.B. Unhale, Study on SnO₂-Fe₂O₃ Composites as a CO₂ Gas Sensor, Research Journey, International E- Research Journal Special Issue 110 (I)- Physics ISSN :2348-7143 February-2019
- [7] Mohamed A. Basyoonia, Shrouk E. Zakia, Sezin Ertugrula, Mucahit Yilmaza, Yasin Ramazan Ekerc, Fast response of CO₂ room temperature gas sensor based on Mixed-Valence Phases in Molybdenum and Tungsten Oxide nanostructured thin films, *Ceramics International* 46 (2020) 9839–9853, <https://doi.org/10.1016/j.ceramint.2019.12.259>
- [8] B.M. Mude and K.B. Raulkar, Study of sensing properties of mix metal oxides for CO₂ gas, *Vidyabharati International Interdisciplinary Research Journal* 12(2) ISSN 2319-4979, 145-148, June 2021,
- [9] M. Amarnath, K. Gurunathan, Highly selective CO₂ gas sensor using stabilized NiO-In₂O₃ nanospheres coated reduced graphene oxide sensing electrodes at room temperature *Journal of Alloys and Compounds*. 2021, 857, 157584., DOI: <https://doi.org/10.1016/j.jallcom.2020.157584>
- [10] Zhi Yan Lee , Huzein Fahmi bin Hawari , GunawanWitjaksono bin Djaswadi and Kamarulzaman Kamarudin, A Highly Sensitive Room Temperature CO₂ Gas Sensor Based on SnO₂-rGO Hybrid Composite, *Materials* 2021, 14, 522. <https://doi.org/10.3390/ma14030522>
- [11] Sandeep Gupta , Anoop Mampazhasseri , Divakaran , Kamlendra Awasthi and Manoj Kumar, CO₂ gas sensing properties of Na₃BiO₄ - Bi₂O₃ mixed oxide nanostructures, *Research Square*, 2022, DOI: <https://doi.org/10.21203/rs.3.rs-1234118/v1>
- [12] Khaoula Kacem , Juan Casanova-Chafer , Sami Ameer , Mohamed Faouzi Nsib , Eduard Llobet, Gas sensing properties of graphene oxide loaded with SrTiO₃ nanoparticles, *Journal of Alloys and Compounds* 941 (2023) 169011, <https://doi.org/10.1016/j.jallcom.2023.169011>
- [13] Tatsumi Ishihara, Mix oxide capacitor of CuO- BaSnO₃ as a sensor for CO₂ detection over a wide range of concentration, *Chemistry Letters*, pp 1711-1714, 1991
- [14] Shogo Matsubara , Shinichiro Kaneko , Shinji Morimoto , Shoichi Shimizu , Tatsumi Ishihara , Yusaku Takita, A practical capacitive type CO₂ sensor using CeO₂/BaCO₃/CuO ceramics, *Sensors and Actuators B* 65 _2000. 128–132, DOI 10.1016/S0925-4005(99)00407-4
- [15] Bo Liao , Qin Wei , Kaiyi Wang , Yexiang Liu, Study on CuO–BaTiO₃ semiconductor CO₂ sensor, *Sensors and Actuators B: Chemical* Volume 80, Issue 3, 1 December 2001, Pages 208-214, [https://doi.org/10.1016/S0925-4005\(01\)00892-9](https://doi.org/10.1016/S0925-4005(01)00892-9)
- [16] Yanfei Gu, Huiming Ji, Bin Zhang and Tingxian Xu, Preparation and CO₂ Gas Sensitive Properties of CuO-SrTiO₃-Based Semiconductor Thin Films, *Key Engineering Materials* Vols 280-283 (2005) pp 311-314 (2005), doi:10.4028/www.scientific.net/KEM.280-283.311
- [17] Jennifer C. Xu, Gary W. Hunter, Dorothy Lukco, Chung-Chiun Liu, and Benjamin J. Ward, Novel Carbon Dioxide microsensor based on Tin Oxide nanomaterial doped with Copper Oxide *IEEE Sensors Journal* (Volume: 9, Issue: 3, March 2009), <https://doi.org/10.1109/JSEN.2008.2011953>
- [18] Chapelle, Audrey and El Younsi, Imane and Vitale, Stefania and Thimont, Yohan and Nelis, Thomas and Presmanes, Lionel and Barnabé, Antoine and Tailhades, Philippe, Improved semiconducting CuO/CuFe₂O₄ nanostructured thin films for CO₂ gas sensing. (2014) *Sensors and Actuators B: Chemical*, vol. 204. pp. 407-413. ISSN 0925-4005, DOI:10.1016/j.snb.2014.07.088
- [19] Vidya M. Balkhande, Development of semiconducting metal oxide sensor for detection of CO₂ gas, Thesis Submitted to Sant Gadge Baba Amravati University, Amravati for the Degree of Doctor of Philosophy in Physics in Faculty of Science, 2016
- [20] K.M. Mude, Study of sensing mechanism of CuO and TiO₂ metal oxides for CO₂ gas, *Vidyabharati International Interdisciplinary Research Journal* 12(2), 78-83, ISSN 2319-4979, June 2021
- [21] Mude K.M.,Mude B.M.,Mayekar V.M.,Zade R.N.,Patange A.N,Raulkar K.B.,Yenorkar S.M.,Mistry R.R, Study of composite metal oxide gas sensors for efficient Carbon dioxide gas sensing device, *JETIR* June 2021, Volume 8, Issue 6
- [22] Akshaya Mouly Vijayakumari , Azad Ravi Oraon , Sonalie Ahirwar , Amala Kannath , Suja K J , Palash Kumar Basu, Defect state reinforced microwave-grown CuxO/NiO nanostructured matrix engineered for the development of selective CO₂ sensor with integrated micro-heater, *Sensors & Actuators: B. Chemical* 345 (2021) 130391, <doi.org/10.1016/j.snb.2021.130391>
- [23] Paul Chesler , Cristian Hornoiu , Mihai Anastasescu , Jose Maria Calderon-Moreno , Marin Gheorghe and Mariuca Gartner, Cobalt- and Copper-Based Chemiresistors for Low Concentration Methane Detection, a Comparison Study, *Gels* 2022, 8, 721. <https://doi.org/10.3390/gels8110721>
- [24] Soraya Bouachma , Katia Ayouz-Chebout, Mouhamed Kechouane, Amar Manseri3 · Chafiaa Yaddadene, Hamid Menari, Nouredine Gabouze, Synthesis of PSi-n/CuO-p/Cu₂O-n heterostructure for CO₂ gas sensing at room temperature, *Applied Physics A* (2022) 128:69 <https://doi.org/10.1007/s00339-021-05167-4>
- [25] Nagesh Bhat, Shareefraza J. Ukkund, Momin Ashraf, Krishnaraja Acharya, Naveenkumar J. Ramegouda,Prasad Puthiyillam, Mohd Abul Hasan, Saiful Islam, Vinaya B. Koradoor, Adarsh D. Praveen,and Mohammad Amir Khan, GO/CuO Nanohybrid-Based Carbon Dioxide Gas Sensors with an Arduino Detection Unit, *ACS Omega* 2023, 8, 32512–32519, <https://doi.org/10.1021/acsomega.3c02598>

A Review on SnO₂ Nanoparticle: synthesis, Structure, Property and it's applications

Miss.S.A.Amale, Mr. P.S.Wagh, Miss. S.P.Dharme, Miss.S.T.Khan

Department of Physics, Vidya Bharati Mahavidyalaya Amravati

Abstract

This comprehensive review search into the synthesis, structure, properties, and versatile applications of tin oxide (SnO₂) nanoparticles. The exploration of various synthesis methods, including the sol-gel approach, humidity sensors, and hydrothermal synthesis, underscores their impact on the structural and morphological attributes of SnO₂. Notably, the co-precipitation method emerges as a simple and cost-effective means for SnO₂ nanoparticle synthesis. The tetragonal crystal structure of SnO₂ is elucidated, and its optical and electrical properties, influenced by impurities and stoichiometry, are examined across diverse nanostructures such as nanosheets, nanowires, and nanotubes. Crucial applications of SnO₂ nanoparticles in photocatalysis, lithium-ion batteries, and energy conversion/storage are outlined. Furthermore, the review underscores the potential benefits of SnO₂ nanoparticles in healthcare applications, emphasizing physicochemical and biological properties. In conclusion, this review consolidates existing knowledge while charting avenues for future research, encouraging continued exploration and innovation in this promising nanomaterial. The synthesis methods, structural insights, and diverse applications collectively contribute to a comprehensive understanding of SnO₂ nanoparticles, highlighting their versatility and significance in various technological domains

Keywords: Synthesis, Structure, Property and application of SnO₂ Nanoparticle.

I] Introduction

Tin oxide (SnO₂) nonmaterials are of great interest in many fields such as catalytic, electrochemical, and biomedical applications [1]. Research in the area of nanoscale materials is motivated by the possibility of processing and designing nanostructured materials with unique properties thereby offering new and important technological applications. Due to their finite small size and high surface-to-volume ratio, nanostructured materials often exhibit novel, and sometimes unusual properties [2]. As one of the most important classes of materials, metal oxide semiconductor nonmaterial's present themselves in various areas of science and technology, due to their shape- and size-dependent physical and chemical properties . Among various metal oxide nonmaterial's, SnO₂ has become the foremost one, because of its wide applications in lithium batteries, super capacitors, gas sensors, and catalysis. Recently, reports on the applications of SnO₂ nanostructures mainly depend on their morphologies and structural features [3]. Tin oxide (SnO₂) nanoparticles (NPs) are being developed for applications ranging from their incorporation as an opacifier in ceramic glazes to advanced technologies including gas sensors, lithium-ion batteries, low emission window coatings, touch screens, sensitized solar cells, field emission flat displays, and other optoelectronic devices. For each of these applications, it is important to have a simple, low cost and scalable synthesis approach that will produce NPs within a narrow distribution of particle sizes. Various synthesis strategies have been developed to produce SnO₂NPs with different size ranges and distributions. These processes usually require use of high temperatures, high boiling point or mixed solvents, and expensive organic tin precursors that are often toxic and require a complicated synthesis procedure [4]. Earlier workers synthesized SnO₂ nanoparticles by various methods like Sol

Gel, Micro Wave technique, Solvo-thermal , Hydro thermal , Sono chemical, Mechanochemical, Co-precipitation etc., Of the various methods Co-precipitation method is simple, inexpensive and does not require high temperature and pressure[5].

II] Synthesis of SnO₂ nanoparticle

SnO₂ nanoparticles powder by chemical precipitation method was studied [6]. Sol-gel method is an efficient and simple method of preparation of nanoparticles which was used in our experiment for SnO₂ nanoparticle synthesis [7]. Humidity sensors based on semiconducting oxides have certain advantages when compared to other types of humidity sensors, such as low cost, simple construction, small size and ease of placing the sensor in the operating environment. In metal oxide semiconductors (such as SnO₂, ZnO, WO₃, TiO₂) [8]. SnO₂ NPs were synthesized via hydrothermal method. Synthesis parameters such as precursor concentration, temperature, pH level and treatment duration in hydrothermal synthesis greatly influence the morphology and the crystal size of the synthesized products [9].

Method

i] Sol gel method

The sol-gel method is a conventional and industrial method for the synthesis of nanoparticles with different chemical composition. The basis of the sol-gel method is the production of a homogeneous sol from the precursors and its conversion into a gel. The solvent in the gel is then removed from the gel structure and the remaining gel is dried. The properties of the dried gel depend significantly on the drying method. In other words, the "removing solvent method" is selected according to the application in which the gel will be used. Dried gels in various ways are used in industries such as surface coating, building insulation, and the production of special clothing. It is worth mentioning that, by grinding the gel by special mills, it is possible to achieve nanoparticles [10].

ii] Humidity sensors

Some materials and measurement types of humidity nanosensor technologies have been researched in the literature; materials including ceramic, polymer, semiconductor, carbon-based, and MXene material. Generally, the semiconductor and carbon-based humidity sensor can achieve higher sensor response, accompanied by a complex fabrication procedure and longer process time. The ceramic humidity sensors, have good thermal stability and wear resistance to overcome severe environments. The polymer-based materials have lower performance in humidity sensing, but it is possible to combine the nanosensor with cellulose for portable devices. In terms of the humidity measurement types, these can be divided into two categories: electrical and optical nanosensors [11].

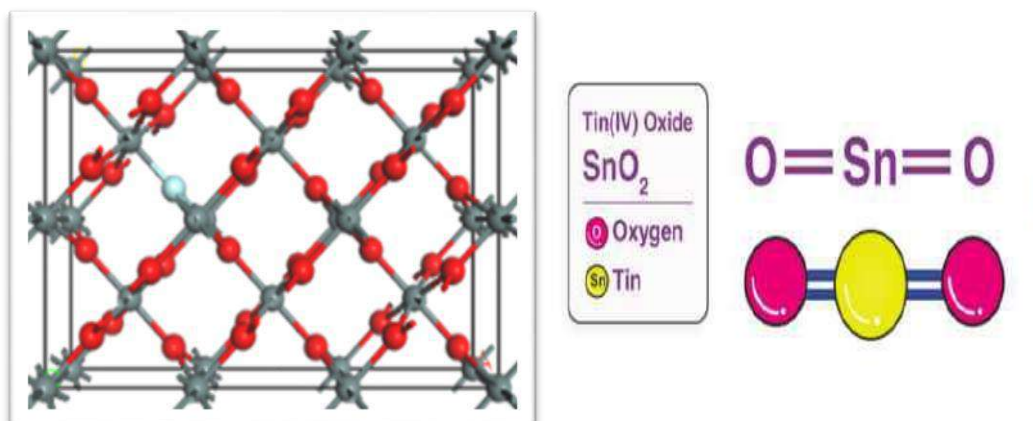
iii] Hydrothermal synthesis method

Hydrothermal synthesis is one of the most commonly used methods for preparation of nanomaterials. It is basically a solution reaction-based approach. In hydrothermal synthesis, the formation of nanomaterials can happen in a wide temperature range from room temperature to very high temperatures. To control the morphology of the materials to be prepared, either low-pressure or high-pressure conditions can be used depending on the vapor pressure of the main composition in the reaction. Many types of nanomaterials have been successfully synthesized by the use of this approach. There are significant advantages of hydrothermal synthesis method over others. Hydrothermal synthesis can generate nanomaterials which are not stable at elevated temperatures. Nanomaterials with high vapour pressures can be produced by the hydrothermal method [12].

III] Structure of SnO₂

The SnO₂ crystal has a tetragonal structure with space group P4₂mm. There are six O²⁻ ions as nearest neighbors of each Sn⁴⁺ site, and three Sn⁴⁺ ions as nearest neighbors of

each O^{2-} ion. Hence, the coordination numbers for Sn and O are six and three, respectively. The CASTEP package was used to construct a $3 \times 2 \times 1$ SnO_2 supercell [13]



IV] Properties

i. Optical and Electrical Properties of SnO_2

Optoelectronic properties of SnO_2 depend on the presence of impurities and its stoichiometry with respect to oxygen. Recently various SnO_2 based nanoscale devices have been fabricated from zero to three dimensional SnO_2 building blocks, e.g., nanosheets, nanowires, nanoribbons, nanoparticles, nanowhiskers, nanobelts, nanotubes etc[14].

ii. physicochemical and biological properties of SnO_2

SnO_2 NPs could be used in healthcare industrial applications to improve human health.[15]

V] Application:

i] Photocatalytic applications

Tin-oxide (SnO_2) nonmaterial's are expected to be a robust photocatalyst for the degradation of organic pollutants in solution because of their glorious properties, like transparency, low cost, environmental friendliness, good chemical and biological inertness, nontoxicity, easy production, high photosensitivity, photostability, and thermodynamic stability. Illustrated the use of SnO_2 nanoparticles to degrade methyl orange under UV light [16].

ii] Lithium-Ion Batteries

In order to address both energy and power demands, there is an urgent need to develop clean energy sources systems. Herein, LIBs have attracted widespread attention because of their high energy density, high power, smooth discharge, and light weight as well as being environment friendly. The electrode's material is one of the key components for perfecting LIBs. It plays a crucial role in establishing the overall properties of the battery [17].

iii] Energy Conversion and Storage

Photocatalytic activity Nanostructured semiconductor SnO_2 acts as an excellent photocatalyst in the degradation of some common textile dyes. Body weight increasing. Studied the effect of vitamin-C stabilized SnO_2 Nps on the body weight of neonatal rats and observed that the vitamin-C stabilized SnO_2 Nps promoted a higher body weight gain compared to raw SnO_2 Nps. It was said that when vitamin-C stabilized SnO_2 entered into the body system of rats, vitamin-C capped on the surface of SnO_2 Nps acted as an antioxidant and reduced the oxidative stress caused by SnO_2 Nps on cells, resulting in reduced weight loss in the rats[18].

Conclusion

In conclusion, this comprehensive review provides valuable insights into the synthesis, structure, properties, and applications of SnO_2 nanoparticles. The study highlights the diverse synthesis methods employed, including the sol-gel method, humidity sensors, and

hydrothermal synthesis, emphasizing their impact on the structural and morphological characteristics of SnO₂. Notably, the simplicity and cost-effectiveness of the co-precipitation method for SnO₂ nanoparticle synthesis are underscored.

The crystal structure of SnO₂ is elucidated as tetragonal, and its properties, particularly optical and electrical aspects, are explored. The optoelectronic properties of SnO₂, influenced by impurities and stoichiometry, are discussed in the context of various nanostructures, such as nanosheets, nanowires, and nanotubes.

Furthermore, the review outlines crucial applications of SnO₂ nanoparticles in fields like photocatalysis, lithium-ion batteries, and energy conversion/storage. The potential benefits of SnO₂ nanoparticles in healthcare applications, showcasing physicochemical and biological properties, are also emphasized. The wide-ranging applications underscore the versatility and importance of SnO₂ nanoparticles in various technological domains.

In summary, this review not only consolidates the existing knowledge but also identifies avenues for future research. The highlighted synthesis methods, structural insights, and diverse applications collectively contribute to a comprehensive understanding of SnO₂ nanoparticles, encouraging further exploration and innovation in this promising nanomaterial.

Reference

- [1] Yi Hu , Yueping Zhu , Guanghua Zhu ,Lanping Hu , You Zi ,and Weichun Huang[14 February 2022] Tin Oxide (SnO₂) Nanoparticles: Facile Fabrication, Characterization, and Application in UV Photodetectors, *Nanomaterials* 2022, Vol12, Issue(4),632; doi.org/10.3390/nano12040632.
- [2] A. Ayeshamariam¹, V. S. Vidhya², S. Sivaranjani³, M. Bououdina^{4 5}, R. PerumalSamy⁶, and M. Jayachandran⁷[2013] Synthesis and Characterizations of SnO₂ Nanoparticles , *Journal of Nanoelectronics and Optoelectronics* Vol. 8, page no.1–8 DOI:10.1166/jno.2013.1471
- [3] Qinqin Zhao¹Lisha Ma¹Qiang Zhang¹Chenggang Wang¹and **Xijin Xu**[04 May 2015] Volume 2015 | Article ID 850147 | <https://doi.org/10.1155/2015/850147>
- [4] Ana Belen Jorge,§Paul F. McMillan,||Abil E. Aliev,||Robert C. Pullar,†João António Labrincha,†and David Maria Tobald[October 15, 2018] One-Step Synthesis, Structure, and Band Gap Properties of SnO₂Nanoparticles Made by a Low Temperature Nonaqueous Sol–GelTechnique. *ACSPUBLICATION* volume3, Issue(10),Page no.13227-13238 DOI: 10.1021/acsomega.8b02122.
- [5] Kavitha Balakrishnan*and Nirmala Murugesan nt. [2021] Synthesis and characterization of SnO₂ nanoparticles by co-precipitation method, *Nano Dimes*. Volume 12, Issue (1) Page no.76-82.
- [6] Asama. N. Naje¹, Azhar S.Norry² and Abdulla. M. Suhail³ [December 2013] Preparation and Characterization of SnO₂ Nanoparticles *International Journal of Innovative Research in Science, Engineering and Technology*. Vol. 2, Issue 12
- [7] *Amrita Palai and Dojalisa Sahu[2022]. SOL-GEL SYNTHESIZED SnO₂ NANOPARTICLES SHOWING ADVANCED PHOTOCATALYTIC ATTRIBUTES FOR ENVIRONMENTAL POLLUTION CONTROL *RASĀYAN J. Chem.*, Special Issue, 2022 ,page no. 266-272 <http://doi.org/10.31788/RJC.2022.1558230>
- [8] M. Parthibavarman V. Hariharan C.and Sekar[20 July 2011] High-sensitivity humidity sensor based on SnO₂ nanoparticles synthesized by microwave irradiation method *Materials Science and Engineering: C*, Volume 31, Issue 5, <https://doi.org/10.1016/j.msec.2011.01.002>Get rights and content.
- [9] Maisara A. M. Akhira , Khairudin Mohameda , Lee H.L. b and Sheikh A. Rezanc [2016]Synthesis of tin oxide nanostructures using hydrothermal method and optimization

- of its crystal size by using statistical design of experiment *Procedia Chemistry* 19. page no. 993 – 998, doi: 10.1016/j.proche.2016.03.148.
- [10] Dmitry Bokov,¹Abduladheem Turki Jalil,^{2,3}Supat Chupradit,⁴Wanich Suksatan,⁵Mohammad Javed Ansari,⁶Iman H. Shewael,⁷Gabdrakhman H. Valiev,⁸and **Ehsan Kianfar**^{9,10}[24 Dec 2021], Nonmaterial by Sol-Gel Method: Synthesis and application, advances in material science and engineering. Volume 2021 | ArticleID 5102014 | <https://doi.org/10.1155/2021/5102014>
- [11] Chin-An Ku and Chen-Kuei Chung[20 February 2023] Advances in Humidity Nanosensors and Their Application: Review, *Sensors* 2023, 23(4), 2328; <https://doi.org/10.3390/s23042328>.
- [12] **Yong X. Gan**,¹Ahalapitiya H. Jayatissa,²Zhen Yu,³Xi Chen,⁴and Mingheng Li⁵[30 Jan 2020] Hydrothermal Synthesis of Nanomaterials, *nanomaterials*. Volume 2020 | Article ID 8917013 | <https://doi.org/10.1155/2020/8917013>.
- [13] Jianyuan Yu¹, Yingeng Wang¹, Yan Huang², Xiuwen Wang, Jing Guo³, Jingkai Yang^{1,5}and Hongli Zhao[3Sep2020], Structural and electronic properties of SnO₂ doped with non-metal elements. *Beilstein J Nanotechnol.* 2020, 11, 13211328. <https://doi.org/10.3762/bjnano.11.116>.
- [14] Samritimala sarmah and A. Kumar [7feb2010], Optical Properties of SnO₂nanoparticles ,*Indian J. Phys* .volume 84, Issue 9 , Page no. 1211-1221, DOI: 10.1007/s12648-010-0109-9.
- [15] Nuha Y. Elamin, T. Indumathi, E. Ranjith Kumar[15 January 2023], Evaluation of physicochemical and biologic,al properties of SnO₂ and Fe doped SnO₂ nanoparticles, *Ceramics International* Volume 49, Issue 2, 15 January 2023, Pages 2388-2393, <https://doi.org/10.1016/j.ceramint.2022.09.211>.
- [16] Jhanvi Kharbanda ,Ruby Priya [2022]Synthesis and applications of tin oxide nanoparticles: An overview , *Material today's proceeding* Volume 68, Part 4, 2022, Pages 916-921 <https://doi.org/10.1016/j.matpr.2022.07.131>.
- [17] Qinqin Zhao,¹Lisha Ma,¹Qiang Zhang,¹Chenggang Wang,¹and **Xijin Xu**[04 May 2015] SnO₂-Based Nanomaterials: Synthesis and Application in Lithium-Ion Batteries and Super capacitors. *Semiconductor Nanomaterials for Energy Conversion and Storage*. Volume 2015 | Article ID 850147 | <https://doi.org/10.1155/2015/850147>.
- [18] Soma Gorai, Bio-based Synthesis and Applications of SnO₂ Nanoparticles - An Overview, *J. Mater. Environ. Sci.*, 2018, Volume 9, Issue 10, Page 2894-2903.

Review on Nanofabrication Techniques

Ms.S.T.Khan , Mr.P.S.Wagh , Ms.S.P.Dharmey , Ms.S.A.Amale.

Department of Physics , Vidyabharati Mahavidyalaya Amravati.

Abstract.

The rapidly growing field of nanofabrication for functional micro/nano-features has drawn attention and applications in diverse sectors such as electronics, photonics, energy, and biological devices across the globe. The reason these devices are being created is to smoothly combine affordable, top-notch micro/nano-features into advanced 3D designs. Over the past few years, there have been important improvements, especially in making devices with tiny structures using different imprinting methods.

In the area of nanofabrication, this review totally focuses on the bottom-up nanofabrication technique. This approach involves building nanostructures from the ground up, starting with individual atoms or molecules, allowing for precise control over the final product. Within the bottom-up nanofabrication technique, four notable methods are highlighted , Atomic Layer Deposition (ALD) , Sol-Gel Method , Colloidal Self-Assembly , DNA Scaffolding of Electronics . The comprehensive review not only acknowledges these bottom-up nanofabrication methods but also emphasizes their significance in advancing the field. It sheds light on the successes achieved through these techniques and the critical role they play in ensuring the compatibility, functionality, and scalability of nano-features within large-scale production processes.

Keywords : Atomic Layer Deposition (ALD) , Sol-Gel Method , Colloidal Self-Assembly , DNA Scaffolding

1. Introduction

Nanostructured surfaces and nanoparticles are widely employed in many fields of research and technology, and there is an ever-growing demand for reliable and reproducible nanofabrication methods. In biology and medicine, nanostructured surfaces and nanoparticles are employed both because of their optical or magnetic properties alone as well as due to a combination of their optical and magnetic properties [1]. In the past two decades, several nano-manufacturing techniques [2,3] have been developed which address high expectations relating to nano-technology. This has enabled exponential knowledge development and a thorough understanding of the characteristics of many interesting nano-structures, their application-related properties, and the incorporation of engineered nanomaterials into multi-functional devices. For example, LEDs [4], solar cells [5], hard disk drives [6], laser diodes [7], self-cleaning [8,9], antibacterial [10], boost skin appearance [11], keep food fresh [12] and combine super-hydrophobic and superoleophobic properties that keep your smartphone screen clean, etc. Nanofabrication products have a number of "design requirements" according to the consumer use. These "design requirements" specify the structural quality, dimensional and geometric precision, and tolerable levels of defects. However, we must also develop proficient, lowcost, and robust nanofabrication methods to realize the potential benefits of all these products

2. BOTTOM-UP NANOFABRICATION TECHNIQUES

The ultimate objective of bottom-up techniques is self organizing integrated processes and tools . This approach has the potential to generate practical multi-component highly functional

devices [12] by regulating the integration of atoms and molecules, without wasting or removing portions of the final structure. The most appealing properties of bottom-up nanofabrication are that no pricy instruments are usually needed to fabricate structures at nanoscale and can easily fabricate in large quantities.

2.1 The vapor-liquid-solid (VLS), template assisted deposition, and solution-based growth methods are the most popular bottom-up techniques . The VLS mechanism of growth, initially described in the 1960s by Wagner and Ellis [13] later renewed in the 1990s by Morales and Lieber [14] and became a common technique to grow inorganic nanowires nowadays shown in figure a . The bottom-up synthesis of nanowires has several benefits and preserve the defined reaction conditions for the creation of nanowires without sacrificing the other materials in the final product. In addition, bottom-up nano-material synthesis permits the formation of an unlimited number of structures [15] and hetero-structures [16] that are entirely controlled by the dimension and composition. By using bottom-up methods, various heterostructures can be prepared such as axial [17], radial core/shell , shell in the form of a nanotube after removal of the core , multisegmented , possibly also with mixed 0–1 dimensionality . These structures are used in various types of electrical, opto-electronic, and energy conversion systems including logic and memory chips , photodetectors [18], light-emitting diodes [19], lasers, and solar cell photovoltaic components [20].

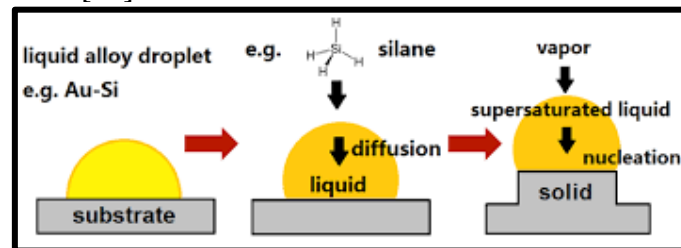


Figure a. Vapour Liquid Solid

2.2 Atomic Layer Deposition method (ALD) [21] is one of the fascinating techniques to fabricate continuous and economical semiconductor devices [22] by using thin-film deposition method. ALD film growth occurs when a series of two or more self-governed surface reactions are performed on to the substrate having respective reactants introduced periodically with reactor purging transition as shown in Figure b . Due to the self-governing mechanism of ALD reactions, one can get deposition thickness up to the sub-nanometer scale. Consistent distribution of the active surface sites means that the added reactants react evenly onto the entire substrate surface, including all non-planar characteristics. This gives uniform thickness on the substrate . The selection of reactants and deposition cycle parameters is based on the thermodynamics and kinetics of the surface reactions involved in ALD process growth. In the 1980s, the ALD approach was used for the first commercial application of ZnS flat-panel electroluminescent displays and then further adapted for semiconductor manufacturing in the 1990s [14]. In manufacturing modern devices ALD continues to be an important process that includes broad bandwidth semiconductor [23], FinFET, and other nanoscale electronics [24].

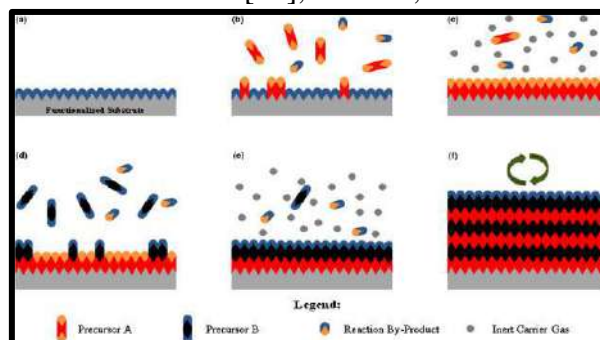


Figure b. Atomic Layer Deposition

2.3 The SOL-GEL method has been commonly used nanostructures fabrication based on metal oxide materials [25] and alloys . SG processing is highly cost-effective when compared to physical, chemical, and plasma deposition techniques. The SG process uses a combination of metal catalysts used in the solvent, catalyst deposition on the substrate, and heating procedure used for the oxidation or sintering of the final product as shown in Figure c . For the growth of a wide range of materials SG method also concentrate on the materials synthesis which usually depends on the hydrolysis and condensation of molecular catalysts [26,27]. The typical application of the SG method is silica to form highly liquid-repellent surfaces and films.

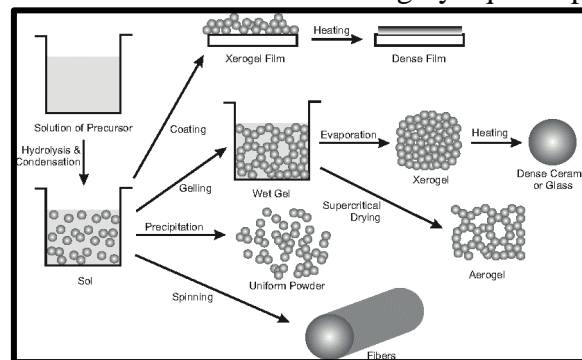


Figure c. Sol-Gel Method

2.4 Colloidal Self-Assembly (CSA) method has been intensively studied for decades for the production of nanostructures used in photonic bandgap materials and high density recording media [28,29]. The early work was geared towards the utilization of bandgap materials for nanophotonic applications. Figure d shows the fabrication of PDMS mold by using CSA method . However, to achieve the necessary structural perfection such as waveguides [30] , it is essential to overcome the difficulty of preventing kinetic trapping and to find cost-effective ways to combine the structures created with other photonic devices. In comparison with other methods, the CSA method is the ideal candidate for the production of large-area, inexpensive, structural color materials [31]. CSA has the exciting potential to generate new materials at the nanoscale by integrating nanoparticles with different characteristics into transparent crystalline structures [5].

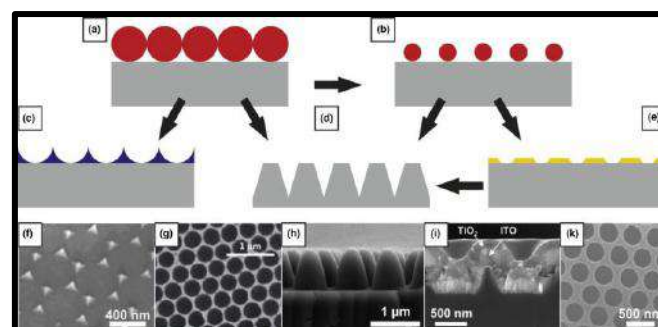


Figure d. Colloidal Self Assembly

2.5 DNA Scaffold method is extremely flexible to generate structures by single-stranded (ssDNA), double or duplex (dsDNA) structures and complex supramolecular assemblies shown in Figure e [32]. 1, 2 and 3-dimensional structures can be created by the DSSA method, and the capacity of other nanoscale artifacts to work with DNA, coupled with the precision of complementary sequence recognition, implies that DNA may bind and organize disparate nano-structures to make relatively complex constructions, containing well-precise nanoparticle crystal lattices, and even active systems [32]. DNA origami [32] is a perfect example of the power of DNA to regulate the configuration of nanoscale objects, creating a molecularly precise “breadboard” to which nano-structures can be attached.

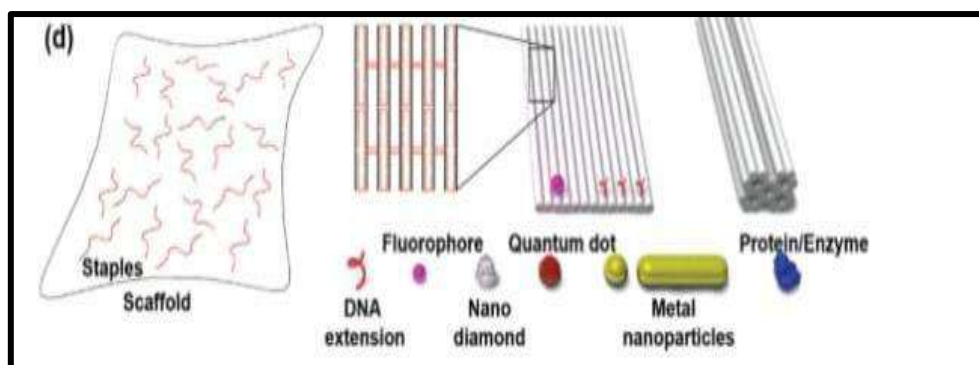


Figure e. DNA Scaffolding.

3. Conclusion:

The world of nanofabrication, mainly guided by bottom-up approaches, is leading the way in innovation, marking a pivotal moment for nanostructured surfaces and nanoparticles. The constant need for reliable fabrication methods in biology, medicine, and technology has driven the creation of various techniques over the last two decades. This progress not only enhances our understanding of nanostructures but also makes it easier to blend them seamlessly into versatile, multi-functional devices. The paradigm shift offered by the bottom-up approach, with its emphasis on self-organizing integrated processes, marks a revolutionary stride in nanofabrication. Significantly, this methodology enables the practical realization of highly functional devices by orchestrating the integration of atoms and molecules without unnecessary material removal. The accessibility of this technique, requiring fewer expensive instruments and enabling large-scale fabrication at the nanoscale.

In conclusion, exploring well-known bottom-up techniques like Vapor-Liquid-Solid, Atomic Layer Deposition, SOL-GEL, Colloidal Self-Assembly, and DNA Sequence-Specific Assembly reveals a flexible set of tools for creating structures tailored to specific needs. These methods cover a wide range of applications, from making semiconductor devices to producing materials with unique structural colors, showcasing their versatility.

REFERENCES:

- [1] Stefan Schrittwieser, Michael J. Haslinger, Tina Mitterramskogler, Michael Mühlberger, Astrit Shoshi, Hubert Brückl, Martin Bauch, Theodoros Dimopoulos, Barbara Schmid and Joerg Schotter, (2019), Multifunctional Nanostructures and Nanopocket Particles Fabricated by Nanoimprint Lithography, *Nanomaterials* 20, Volume 9 Issue 12, DOI: 10.3390/nano9121790.
- [2] Abhijit Biswas, Ilker S. Bayer, Alexandru S. Biris, Tao Wang, Enkeleda Dervishi and Franz Faupel (2012), Advances in top-down and bottom-up surface nanofabrication: Techniques, applications and future prospects, *Advances in Colloid and Interface Science*, Volume 170, Issues 1–2, Page 2–27, DOI: 10.1016/j.cis.2011.11.001.
- [3] Kyowon Kang, Younguk Cho and Ki Jun Yu (2018) Nano-Materials and Nano-Fabrication Techniques for Flexible Electronic Systems, *Micromachines*, Volume 9, Issue 6, 3; DOI:10.3390/mi9060263.
- [4] Yeeu-Chang Lee and Sheng-Han Tu, (2011), Improving the light-emitting efficiency of GaN LEDs using nanoimprint lithography in *Recent Advances in Nanofabrication Techniques and Applications*, Book: Improving the Light-Emitting Efficiency of GaN LEDs Using Nanoimprint Lithography, Volume 1, Page 173-196, DOI: 10.5772/20712.
- [5] Amalraj Peter Amalathas and Maan M Alkaisi, (2017), Efficient light trapping nanopyramid structures for solar cells patterned using UV nanoimprint lithography, *Materials Science in Semiconductor Processing*, volume 57, Page 54–58, DOI:10.1016/j.mssp.2016.09.032.
- [6] Daniel B. Sullivan, Thomas Boonstra, Mark T. Kief, Lily Youtt, Sethuraman Jayashankar, Carolyn Van Dorn, Harold Gentile, Sriram Viswanathan, Dexin Wang, Dion Song, Dongsung Hong, Sung-Hoon Gee Sullivan, (2013), Hard disk drive thin film head

- manufactured using nanoimprint lithography , *Journal of Micro/Nanolithography, MEMS, and MOEMS* , Volume 12 , Issue 3 , DOI:10.1117/1.JMM.12.3.031105.
- [7] Masaki Yanagisawa , (2011) , Application of nanoimprint lithography to distributed feedback laser diodes , *Recent Advances in Nanofabrication Techniques and Applications* , Volume 1 , Page 211–224 , DOI: 10.5772/22678.
- [8] Yushan Yang , Haishan He , Yougui Li & Jian Qiu , (2019) , Using nanoimprint lithography to create robust, buoyant, superhydrophobic PVB/SiO₂ coatings on wood surfaces inspired by red roses petal , *Scientific Reports* , Volume 9 , Issue 1 , Page 1–9 , DOI :10.1038/s41598-019-46337-y.
- [9] Feyza Dundar Arisoy , Kristopher W. Kolewe , Benjamin Homyak , Irene S. Kurtz, Jessica D. Schiffman and James J. Watkins , (2018) , Bioinspired photocatalytic shark-skin surfaces with antibacterial and antifouling activity via nanoimprint lithography , *ACS Applied Materials & Interfaces* , Volume 10 , Issue 23, Page 20055–20063 , DOI: 10.1021/acsami.8b05066.
- [10] Khanh T.M. Tran and Thanh D. Nguyen , (2017) , Lithography-based methods to manufacture biomaterials at small scales , *Journal of Science: Advanced Materials and Devices* , Volume 2 , Issue 1 , Page 1–14 , DOI:10.1016/j.jsamd.2016.12.001.
- [11] Juhong Chen , Yiliang Zhou , Danhui Wang , Fei He , Vincent M. Rotello , Kenneth R. Carter , James J. Watkins and Sam R. Nugen , (2015) , UV-nanoimprint lithography as a tool to develop flexible microfluidic devices for electrochemical detection , *Lab on a Chip* , Volume 15 , Issue 14, Page 3086–3094 , DOI : 10.1039/C5LC00515A.
- [12] Mi Kyung Yu , Jinho Park , and Sangyong Jon , (2012) , Targeting strategies for multifunctional nanoparticles in cancer imaging and therapy , *Theranostics* , Volume 2 Issue 1 ,Page 3–44 , DOI : 10.7150/thno.3463.
- [13] R. S. Wagner and W. C. Ellis (1964) Vapor-liquid-solid mechanism of single crystal growth , *Applied Physics Letters* , Volume 4 , Issue 5 , Page 89–90 , DOI:10.1063/1.1753975.
- [14] Alfredo M. Morales and Charles M Lieber , (1998) , A laser ablation method for the synthesis of crystalline semiconductor nanowires , *Science* , Volume 279 , Issue 5348 , Page 208–211 , DOI: 10.1126/science.279.5348.208.
- [15] Bining Tian , Bethany B Smith , M. C. Scott , Qin Lei , Ruian Hua , Yue Tian and Yi Liu , (2018) , Facile bottom-up synthesis of partially oxidized black phosphorus nanosheets as metal-free photocatalyst for hydrogen evolution , *Proceedings of the National Academy of Sciences* , Volume 115 , Issue 17 , Pages : 4345–4350 , DOI:10.1073/pnas.1800069115.
- [16] Yuan Liu , Nathan O. Weiss , Xidong Duan , Hung-Chieh Cheng , Yu Huang and Xiangfeng Duan , (2016) , Van der Waals heterostructures and devices , *Nature Reviews Materials* , Volume 1 Issue 9 , Page 1–17 , DOI:10.1038/natrevmats.2016.42.
- [17] Aurélie Lecestre, Mickael Martin, Fuccio Cristiano, Thierry Baron and Guilhem Larrieu , (2022) , Large-Scale Monolithic Fabrication of III–V Vertical Nanowires on a Standard Si(100) Microelectronic Substrate , *ACS Omega* , Volume 7 , Page 5836 – 5843 , DOI:10.1021/acsomega.1c05876 .
- [18] Anupam Midya , Arup Ghorai , Subhrajit Mukherjee , Rishi Maiti and Samit K. Ray , (2016) , Hydrothermal growth of few layer 2H-MoS₂ for heterojunction photodetector and visible light induced photocatalytic applications , *Journal of Materials Chemistry A* , Volume 4 , Issue 12 , Page 4534–4543 , DOI: 10.1039/c5ta09003b.
- [19] Tyler A Growden, Weidong Zhang, Elliott R Brown, David F Storm, David J Meyer and Paul R Berger , (2018) , Near-UV electroluminescence in unipolar-doped, bipolar-tunneling GaN/AlN heterostructures , *Light: Science & Applications* volume 7, page 17150 , DOI:10.1038/lsa.2017.150.
- [20] Tomasi, Andrea;Paviet-Salomon, Bertrand;Jeangros, Quentin;Haschke, Jan;Christmann, Gabriel;Barraud, Loris;Descoeurdes, Antoine;Seif, Johannes Peter;Nicolay, Sylvain;Despeisse, Matthieu;De Wolf, Stefaan;Ballif, Christophe , (2017) , Simple processing of back-contacted silicon heterojunction solar cells using selective-area crystalline growth , *Nature Energy* , Volume 2 , Issue 5, Pages 1–8 , DOI 10.1038/nenergy.2017.62.
- [21] Junling Lu , Jeffrey W. Elam and Peter C Stair , (2016) , Atomic layer deposition— Sequential self-limiting surface reactions for advanced catalyst “bottom-up” synthesis , *Surface Science Reports* , Volume 71 Issue 2 , Page 410– 472 , DOI:10.1016/j.surfrep.2016.03.003.

- [22] Janne-Petteri Niemelä , Giovanni Marin and Maarit Karppinen , (2017) , Titanium dioxide thin films by atomic layer deposition: A review , *Semiconductor Science and Technology*, Volume 32 , Issue 9 , Article 093005 , DOI: 10.1088/1361-6641/aa78ce. Stefan Nanz, Aimi Abass, Peter M. Piechulla, Alexander Sprafke, Ralf B. Wehrspohn, and Carsten Rockstuhl , (2018) , Strategy for tailoring the size distribution of nanospheres to optimize rough backreflectors of solar cells, *Optics Express* , Volume 26, Issue 2 , Pages A111-A123 , DOI:10.1364/OE.26.00A111.
- [23] Chen-Hui Zhai , Rong-Jun Zhang , Xin Chen , Yu-Xiang Zheng , Song-You Wang , Juan Liu , Ning Dai and Liang-Yao Chen , (2016) , Effects of Al doping on the properties of ZnO thin films deposited by atomic layer deposition , *Nanoscale Research Letters* , Volume 11 , Issue 1, Pages 1–8 , DOI 10.1186/s11671-016-1625-0.
- [24] Shrividhya Thiagarajan, Anandhavelu Sanmugam and Dhanasekaran Vikraman., (2017) . Facile methodology of sol–gel synthesis for metal oxide nanostructures. in *Recent Applications in Sol–Gel Synthesis* , , Intech Open, Volume 1 , page 1-17. Facile methodology of sol–gel synthesis , DOI:10.5772/intechopen.68708.
- [25] Michelle Saltarellia , Emerson H. de Fariaa , Katia J. Ciuffia , Eduardo J. Nassara , Raquel Trujillano , Vicente Rives and Miguel A. Vicente , (2019) , Aminoiron (III)-porphyrin-alumina catalyst obtained by non-hydrolytic sol–gel process for heterogeneous oxidation of hydrocarbons , *Molecular Catalysis*, Volume 462, pp.114–125 , DOI:10.1016/j.mcat.2018.09.014.
- [26] Ashleigh Danks , Simon Hall and Zoe Schnepf ,(2016) , The evolution of ‘sol–gel’ chemistry as a technique for materials synthesis. *Materials Horizons*, Volume 3 Issue 2 , Page 91–112 , DOI: 10.1039/c5mh00260e.
- [27] Longfei Ye , Tari Pearson , Y. Cordeau , Olin Thompson Mefford and T. M. Crawford , (2016) , Triggered self assembly of magnetic nanoparticles , *Scientific Reports*, Volume 6, Article ID: 23145 , DOI:10.1038/srep23145.
- [28] Rose K. Cersonsky, Greg van Anders, Paul M. Dodd and Sharon C. Glotzer , (2018) , Relevance of packing to colloidal self-assembly , *Proceedings of the National Academy of Sciences*, Volume 115 Issue 7, Page 1439–1444 , DOI : 10.1073/pnas.1720139115.
- [29] Muhammad Umar Khan , Joseph McGrath , Brian Corbett and Martyn Pemble , (2017) , Airclad broadband waveguide using micro-molded polyimide combined with a robust, silica-based inverted opal substrate , *Optical Materials Express* , Volume 7 Issue 9 , Pages 3155–3161 , DOI:10.1364/OME.7.003155.
- [30] Lijing Zhang , Maximilian T. Hörantner , Wei Zhang , Qingfeng Yan and Henry J. Snaith , (2017) , Near-neutral-colored semitransparent perovskite films using a combination of colloidal self-assembly and plasma etching. *Solar Energy Materials and Solar Cells*, Volume 160, Pages 193–202 , DOI:10.1016/j.solmat.2016.10.035.
- [31] Anton Kuzyk , Ralf Jungmann , Guillermo P. Acuna and Na Liu , (2018) , DNA origami route for nanophotonics. *ACS Photonics*, Volume 5 Issue 4 , Pages 1151– 1163 , DOI: 10.1021/acsp Photonics.7b01580.

A Review on Supercapacitor: Types and Applications

***Dharme S.P., Wagh P.S., Khan S.T., Amale S.A.**

Department Of Physics, Vidya Bharati Mahavidyalaya, Amravati (M.S.) India 444602

*Corresponding Author: Email: snehaldharme1107@gmail.com

Abstract

The storage of enormous energies is a significant challenge for electrical generation. Supercapacitor have gained a lot of attention due to their features like high power and long life cycle. In this review paper, all types of supercapacitor such as Electrostatic double layer capacitor, hybrid capacitor and pseudocapacitor are covered, depending on the energy storage mechanism. Supercapacitor are also called as ultra capacitor. It is an high capacity capacitor with a capacitance value much higher than other capacitor. It is used to store extremely large amount of electrical charge.

Keywords: Supercapacitor, Hybrid capacitor, Pseudocapacitor, Electrostatic double layer capacitor, Ultra capacitor

1. INTRODUCTION

Batteries, supercapacitor and fuel cells are unconventional energy devices working on the principle of electrochemical energy conversion. Supercapacitor have gained much attention on account of high specific capacitance, long life cycle, high power density being almost maintenance free, experiencing no memory effect, safe and function as a bridge for power-energy difference that exist between capacitor and fuel cells/batteries [1]. The Supercapacitor have several advantages including high power density, quick charge-discharge time, low input resistance, extended lifetime and they are environmentally friendly [2]. Batteries and Supercapacitor both rely on electrochemical processes although separate electrochemical mechanism determine their relative energy and power density [3]. In different fields such as electric transit vehicles, hybrid cars and transportable electronics devices including numerous non-conventional electrically driven devices, Supercapacitor, batteries and fuel cells are used [4]. Supercapacitor can be used in electric and hybrid vehicles to provide the high power density needed for short term acceleration in addition to energy recovery throughout braking [5]. Compared to the conventional battery or capacitor, charging time of supercapacitor is very less and can discharge like a regular battery [6]. Supercapacitors behave at the protruding power density, their inferior energy density compared to batteries makes them hard to satisfy the requirements for mobile energy-storage devices [7]. Supercapacitors are quickly gaining interest owing to their high cycle stability and power density with less environmental effect [8]. Supercapacitor offer a compromise between specific energy and power and can be partitioned into electrochemical double layer capacitors (EDLCs), pseudocapacitor and the combination hybrid-capacitor [9]. The supercapacitor is also known as the ultracapacitor or electrochemical capacitor [10]. Supercapacitors are an increasingly attractive option in the race to develop new and improved energy storage technologies due to their high-power density and long cycle life [11]. Supercapacitor store electrical charge on high-surface-area conducting materials [12]. In addition, the satisfactory electro-active sites, and chemical and high-thermal stabilities of the metal oxide materials guarantee high pseudo-capacitive performances and cyclic stability [13].

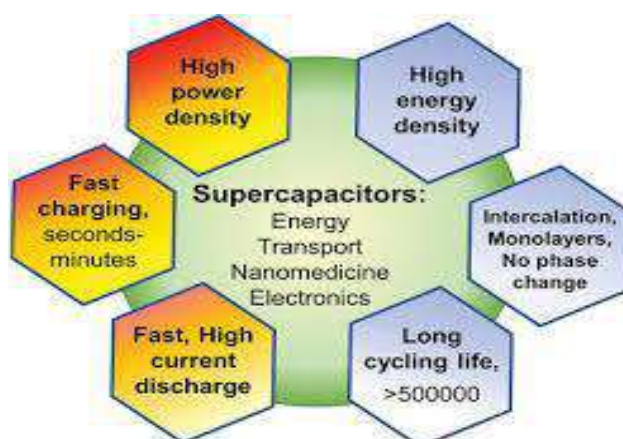


Fig 1.1: Features of Supercapacitor

2. TYPES OF CAPACITOR

- **Electrostatic double layer capacitor:** Electrostatic double layer capacitor is a rechargeable battery type and charge storage electrostatically. Electrostatic double layer capacitor can either store charge electrostatically without the transfer of charge loads with the electrochemical double layer storage principle.
- **Pseudo capacitor:** Carbon nanotubes (CNT), graphene, carbon aerogels, carbide derived carbon, foams and activated carbon are the main types of pseudo capacitor [14].
- **Hybrid capacitor:** Hybrid capacitor are developed by using the techniques of Electrostatic double layer capacitor and Pseudo capacitor. Conducting polymers and metal oxides are the main types of hybrid capacitor. In addition, the hybrid capacitor were a combination of performance properties which previously was unachievable, Also they are combining the best features related to pseudo capacitor and Electrostatic double layer capacitor into a unified supercapacitor [15].

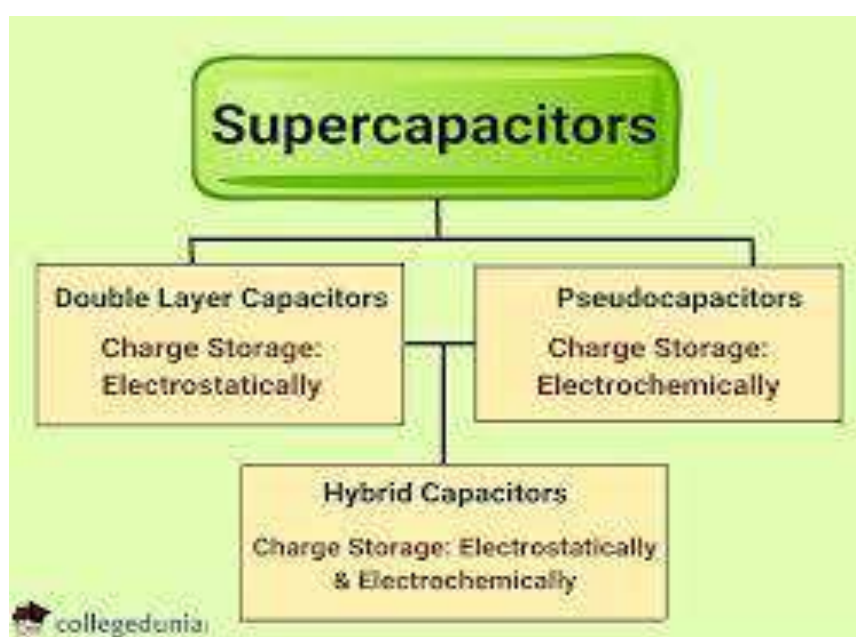


Fig 2.1: Types of Supercapacitor

3. APPLICATIONS

Supercapacitor are used in wind turbines, mobile base stations, electronic devices and different industrial practices. In addition, they have started to be used in UPS, electric vehicles and various power electronics applications. In recent years, supercapacitor have been used as an energy storage device for voltage stability in renewable and hybrid energy storage system to regulate the source and grid. Supercapacitor can stabilize the power supply in applications with fluctuating loads [16]. The use of supercapacitor has recently also been extended to wearable electronics [17]. Electrostatic double layer capacitor are particularly useful for high power bursts. For example accelerating/breaking high-speed transportation systems [18]. In general, supercapacitor used for energy storage configurations that can achieve a high power density, rapid charge and extremely long-term cyclic stability [19]. Supercapacitors are electrochemical energy storage devices possessing both great power density and energy density with long lifecycle and high charging/discharging [20]. Supercapacitor used for electrical energy storage devices to power portable gadgets such as tablets, smartphones, smartwatches, laptops, state of the art flexible medical implants, as well as wearable smart fabric has grown, the demand for supercapacitor research has been increased tremendously [21].



Fig 3.1: Application of Supercapacitor

4. CONCLUSION

The types and applications of supercapacitor presented in this paper and discuss about holistic terms of types of supercapacitors such as Electrostatic double layer capacitor, Pseudo capacitor and hybrid capacitor. Supercapacitor has short charging time, high power, long life and high cycling stability.

REFERENCE

- [1] Poonam, Kriti Sharma, Anmol Arora, S. K. Tripathi, February (2019), Review of supercapacitors: Materials and devices, Journal of Energy storage, Volume 21, Pages 801-825, doi.org/10.1016/j.est.2019.01.010.
- [2] Mustafa Ergin, Sahin, Frede Blaabjerg, Ariya Sangwongwanich, October (2021), A Comprehensive Review on Supercapacitor Applications and Developments, Energies, Volume 15, Issue 3, doi.org/10.3390/en15030674.
- [3] P. Simon, Yury Gogotsi, Bruce Dunn, March (2014), Where Do Batteries End and Supercapacitors Begin? Science Magazine, Volume 343, Pages 1210-1211, doi:10.1126/science.1249625.
- [4] Muhammad Yaseen, Muhammad Arif Khan Khattak, Muhammad Humayun, Muhammad Usman, Syed Shaheen Shah, Shaista Bibi, Bakhtiar Syed UIHasnain, Shah Masood Ahmad, Abbas Khan, Nasrullah Shah, Asif Ali Tahir, Habib Ullah, November (2021), A Review of Supercapacitors: Materials Design, Modification, and Applications, Energies, Volume 14, Issue 22, doi.org/10.3390/en14227779.
- [5] Noor I. Jalal, RaheekI I. Ibrahim, Monal K. Oudah, June (2021), A review on Supercapacitor: Types and Components, Conference series, Volume 1973, Issue 1, doi: 10.1088/1742-6596/1973/1/012015.
- [6] Gautham Prasad G, Niddheesh Shetty, Simran Thakur, Rakshitha, November(2019), Supercapacitor technology and its applications: a review, doi:10.1088/1757-899X/561/1/012105.
- [7] Jiale Sun, Huanxin Li, BingchengLuo, April(2022), A Review on the Conventional Capacitors, Supercapacitors, and Emerging Hybrid Ion Capacitors: Past, Present, and Future, Advanced Energy and Sustainability Research, Volume 3, Issue 6, doi.org/10.1002/aesr.202100191.
- [8] Arpit Mendhe, H.S. Panda, October (2023), A review on electrolytes for Supercapacitor device, Discover Materials, Volume 3, Issue 1, doi:org/10.1007/s43939-023-00065-3.
- [9] EmileS. Greenhalgh, Sang Nguyen, Maria Valkova, Natasha Shirshova, Milo S.P. Shaffer, A.R.J. Kucernak d, April (2023), A critical review of structural supercapacitors and outlook on future research challenges, Composites Science and Technology, Volume 235, doi.org/10.1016/j.compscitech.2023.109968.
- [10] Guoping Wang, Benhe Zhong, Hongqing Wang, Lei Zhang, December (2015), Supercapacitors Applications, Electrochemical Energy, Pages 479-492, doi:10.1201/b19061-27.
- [11] Niraj Kumar, Su-Bin Kim, Seul-Yi Lee, and Soo-Jin Park, October (2022), Recent Advanced Supercapacitor: A Review of Storage Mechanisms, Electrode Materials, Modification, and Perspectives, Volume 12, Issue 20, Nanomaterials, doi: 10.3390/nano12203708.

-
- [12] Priyanka Sharma, Vinod Kumar, (2018), A Brief review on Supercapacitor, Pramana research, Volume 8, Issues 3.
- [13] Cuihua An, Yan Zhang, Hyinan Guo, Yijing Wang, (2019), Metal oxide-based supercapacitors: progress and prospectives, Nanoscale Advance, Issue 12, doi.org/10.1039/C9NA00543A.
- [14] Mustafa Ergin Sahin, Frede Blaabjerg, Ariya Sangwongwanich, October (2021), A Comprehensive Review on Supercapacitor Applications and Developments, Energies, Volume 15, Issue 3, doi.org/10.3390/en15030674.
- [15] Noor I. Jalal, RaheekI I. Ibrahim, Monal K. Oudah, June (2021), A review on Supercapacitor: Types and Components, Conference series, Volume 1973, Issue 1, doi: 10.1088/1742-6596/1973/1/012015.
- [16] Mustafa Ergin Şahin, Frede Blaabjerg, Ariya Sangwongwanich, October (2021), A Comprehensive Review on Supercapacitor Applications and Developments, Energies, Volume 15, Issue 3, doi.org/10.3390/en15030674.
- [17] Tae Gwang Yun, Xichen, Jun Young Cheong, July (2023), Research in Electrochromic Supercapacitor -A focused Review, Volume 6, doi: org/10.1002/batt.202200454.
- [18] Xuli Chen, Rajib Paul, Liming Dai, May(2017), Carbon-based supercapacitors for efficient energy storage, National Science Review, Volume 4, Issue 3, Pages 453–489, doi.org/10.1093/nsr/nwx009.
- [19] Cuihua An, Yan Zhang, Huinan Guo, Yijing Wang, October 2019, Metal Oxide-based Supercapacitors: Progress and Prospective, Nanoscale Advances, Volume 1, Issue 12, doi:10.1039/C9NA00543A.
- [20] M. I. A. Abdel Maksoud, Ramy Amer Fahim, Ahmed Esmail Shalan, M. AbdElkodous, S. O. Olojede, Ahmed I. Osman, Charlie Farrell, Ala'a H. Al-Muhtaseb, A. S. Awed, A. H. Ashour & David W. Rooney ,August (2020), Advanced materials and technologies for supercapacitors used in energy conversion and storage: a review, Environmental Chemistry Letters, Volume 19, Pages 375–439, doi: org/10.1007/s10311-020-01075-w.
- [21] T. Kedara Shivasharma, Nakul Upadhyay, Tushar Balasaheb Deshmukh, Babasaheb R. Sankapal, October, (2023), Exploring Vacuum-Assisted Thin Films toward Supercapacitor Applications: Present Status and Future Prospects, **American Chemical Society, Volume 8, Pages 37685–37719**, doi.org/10.1021/acsomega.3c05285.

Synthesis and Characterization of PEO: PVP: NaNO₃ Based Polymer Electrolyte

P.A.Fartode, V.G.Farkunde

Department of Physics, Shri Shivaji Science College, Amravati, Maharashtra

Email:p.fartode@gmail.com,vaishnavifarkunde5@gmail.com

Abstract

The polymer electrolyte PEO: PVP: NaNO₃ was prepared by solution cast technique. Polymers PEO, PVP, NaNO₃ were taken separately at three different ratio with as (40:50:10), (30:50:20), (20:50:30). These electrolyte were characterized by XRD and FTIR technique.

Keywords: Polymer electrolyte, PEO, PVP, NaNO₃.

Introduction

The polymer electrolyte (Solutions) serve as electronic insulators between the anode and cathode but it must be a good ionic conductor. Polyethylene oxide (PEO) is used as the polymer matrix because it is chemically inert, able to dissolve in number of inorganic salts and it provides moderate ionic conductivity. Polymer electrolytes based on PEO complexed with NaClO₃, AgNO₃ and NaYF₄ etc. have been reported [1]-[6]. Also the polymer electrolytes based on PVP complexed with NaClO₃ have been prepared [7]-[8]. The polymer electrolyte based on PEO, PVP complexed with NaClO₃ were prepared [9]. Keeping this view in mind, authors prepared polymer electrolyte based on PEO, PVP complexed with NaNO₃ and study their XRD and FTIR analysis.

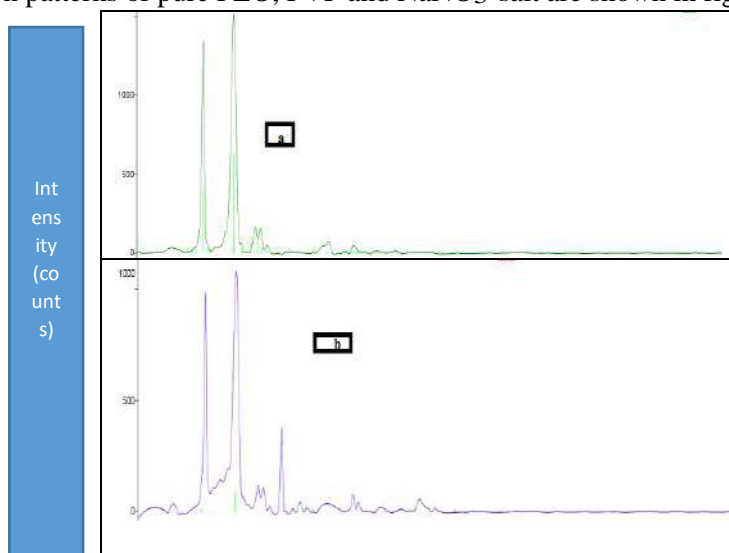
Preparation of polymer electrolyte

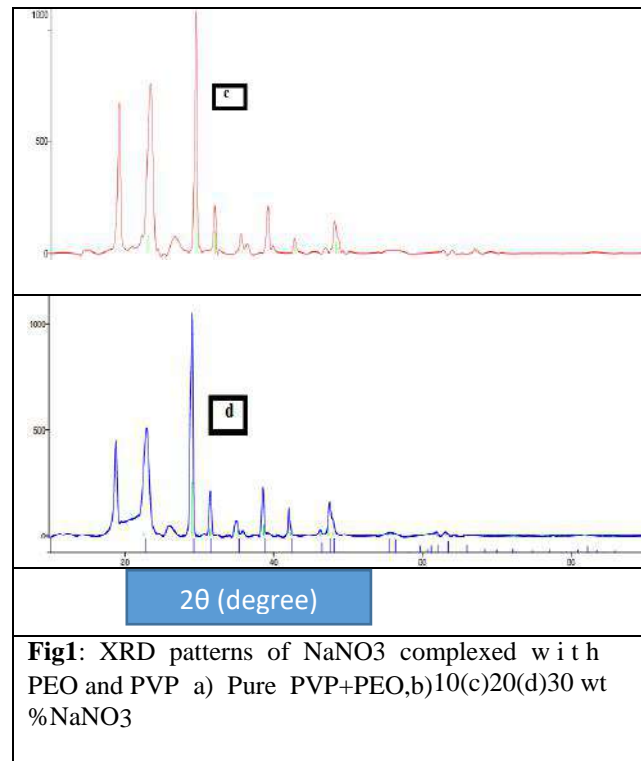
The polymers PEO and PVP were taken separately at different ratio with NaNO₃ wt% as (40:50:10), (30:50:20) and (20:50:30). Each mixture dissolved in methanol for making polymer-salt mixture into solution. To obtain the perfect solution of this mixture, the solution was stirred well for 24 hours and poured into a polypropylene dishes. The solution was slowly evaporated at room temperature. Thus, thin film of polymer electrolyte was prepared by solution cast technique. Further these films were crushed into powder form. This powder was used for XRD and FTIR analysis.

Result and Discussion:

X-ray diffraction (XRD) analyses

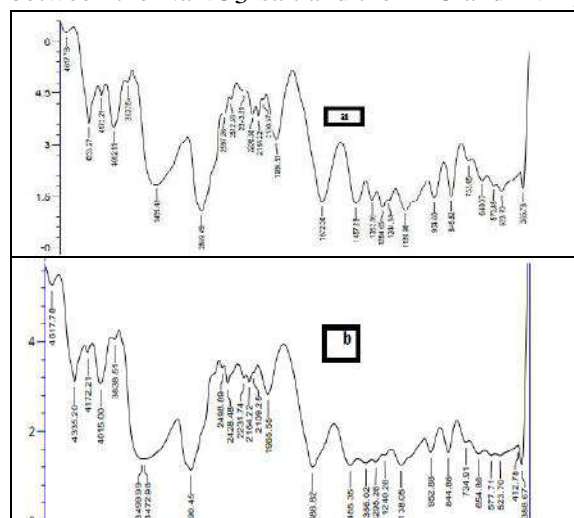
X-ray diffraction patterns of pure PEO, PVP and NaNO₃ salt are shown in fig.1

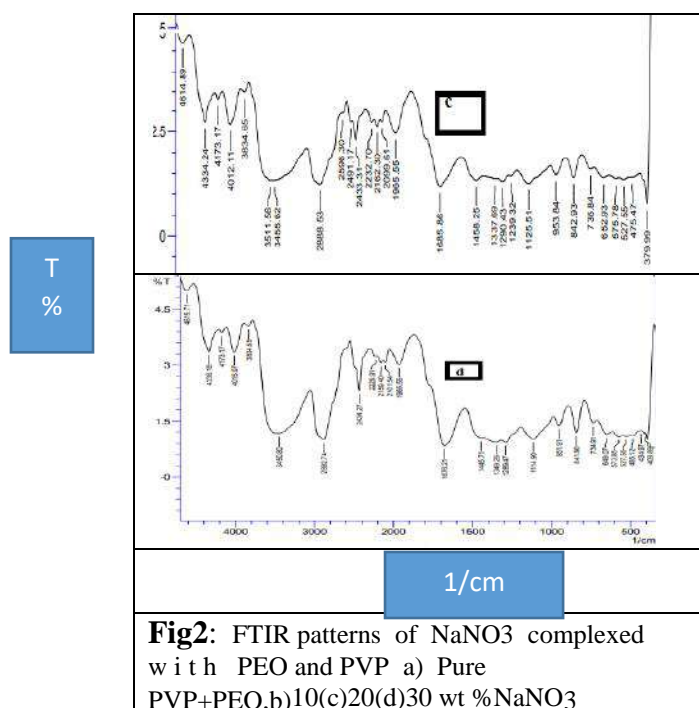




Comparison of diffraction spectra of complexed PEO,PVP with that of pure PEO , PVP and NaNO₃ reveals following details.

- The diffraction peaks observed for 2θ values of 19.05 to 29.24 where the complexed PEO, PVP films to be less intense than those for the pure PEO,PVP films which indicates that the addition of NaNO₃ to the polymer cause a decrease in the degree of crystallinity of the polymer PVP and PEO.
- Peak corresponding to the uncomplexed PEO ,PVP are also present , on one those of the NaNO₃ in complexed PEO ,PVP films ,showing the simultaneous presence of both crystalline uncomplexed and complexed PEO & PVP.[13]
- For the higher concentration of NaNO₃ salt in the polymer, no sharp peaks were observed, which indicates the dominant presence of an amorphous phase. Therefore the XRD pattern clearly indicates a complexation between the NaNO₃ salt and the PEO and PVP polymer. [12]





FTIR Studies :

The complexation of pure PEO, PVP with NaNO₃ salt extensively studied vibrational spectroscopic studies. The FTIR spectra of pure PEO, PVP and PEO, PVP complexed with NaNO₃ shown in fig 2

The vibrational modes present at around 845 cm⁻¹ and 954 cm⁻¹ are accountable for CH₂ rocking motion with a little CO stretching motion and CO stretching motion with some contribution from CH₂ rocking motions respectively. [12]

The intensity of aliphatic CH stretching vibrational band observed around 2890 cm⁻¹ in PEO and PVP decreases with increasing concentration of NaNO₃ salt in the polymer. [11]

The width of CO stretching band observed around 1125.1 cm⁻¹ in PEO & PVP also showed an increase with increase of NaNO₃ in the polymer.

Several new peaks around 4335cm⁻¹, 1244.14cm⁻¹, 2343.61cm⁻¹ and 1284.65 cm⁻¹ have been observed in complexed PEO, PVP. [10]

The appearance of new peaks along with changes in existing peaks or their disappearance in the IR spectra directly indicates the complexation of NaNO₃ with PEO & PVP. If the cations of NaNO₃ get coordinate with ether and oxygen of PEO & PVP, the spectral changes are expected to be in the C-O-C stretching and deformation ranges. [13]

The decrease in the width of 1114.3 cm⁻¹ band which is assigned in C-O-C symmetrical and asymmetrical stretching suggest the co-ordination complexation of the salt with the polymer PEO, PVP

Conclusion:

(PEO+PVP+NaNO₃) based polymer electrolyte have been prepared by using solution cast technique with the weight ratios (40:50:10), (30:50:20) and (20:50:30). The complexation of polyethylene oxide, polyvinyl pyrrolidone and NaNO₃ salt have been confirmed by using XRD and FTIR spectroscopy.

References

- [1] J. Shiva Kumar, A. R. Subrahmanyam, M. J. Reddy and U. V. Subba Rao, *J. Ionics*, **60** (2006) 3346-3349.
- [2] R. Chandrasekaran and S. Selladurai, *Solid State Ionics*, **50**(2001) 89-94.
- [3] R. Chandrasekaran, I. R. Mangani, R. Vasanthi and S. Selladurai, *J. Solid State Ionics*, **1**(2000) 88-93.
- [4] R. Chandrasekaran and S. Selladurai, *J. Solid State electrochemistry*, **5** (2000) 355-361
- [5] S. S. Rao, K. V. Satyanarayana Rao, Md. Shareefuddin, U. V. Subba Rao and S. Chandra, *Solid State Ionics*, **67** (1994) 331-334.
- [6] S. S. Rao, M. J. Reddy, K. N. Reddy and U. V. Subba Rao, *Solid State Ionics*, **74** (1994) 225-228.
- [7] K. N. Kumar, T. Sreekanth, M. J. Reddy and U. V. Subba Rao, *J. Power Sources*, **101** (2001) 130-133.
- [8] R. Sathiyamoorthi, R. Chandrasekaran, S. Selladurai and T. Vasudevan, *J. Ionics*, **9** (2003) 404-410.
- [9] S. Selladurai, R. Chandrasekaran, I. R. Mangani and R. Vasanthi, *Ion Conducting Material : Theory and Applications*, (2001) 213-219.
- [10] M. J. Reddy, T. Shreekanth, M. Chandrashekar and U. V. Subba Rao, *J of Material Sci.* **35**(2000) 2841-2845.
- [11] T.Shreekanth, M Jaipal Reddy, s. Ramalingaiah,U.V. subba Rao, *Journal of power sources***79**(1999)107-112
- [12] S.A.Hashmi,Ajay Kumar,K.Maurya and S.Chandra,*J.Appl.Phys*,**23**(1990)
- [13] T. Sreekanth, *International Journal of engineering research and application* (2014)

A Study of TiO₂ Thin Films: From Synthesis to Property Enhancement through Chemical Bath Deposition and Annealing

Mr.A.B.Tayde*¹

²Department of Physics, S.S.S.K.R.Innani Mahavidyalaya, Karanja Lad Dist. Washim, Maharashtra, India.
Abhijeettayde97@gmail.com

Mr.S.K.Kokate*²,

¹Assistant professor in
Department of Physics, S.S.S.K.R.Innani Mahavidyalaya, Karanja Lad Dist. Washim, Maharashtra, India.
iamsandipkokate@gmail.com

Abstract:

This research paper delves into the study of TiO₂ thin films synthesized through chemical bath deposition, focusing on the enhancement of their properties via various annealing conditions. The primary objective was to understand how different annealing temperatures, durations, and atmospheres influence the microstructure and functional properties of these films. Employing a quantitative approach, the research methodology involved the experimental synthesis of TiO₂ films followed by annealing under controlled conditions. The properties such as crystallinity, bandgap energy, electrical conductivity, optical transmittance, film thickness, and surface roughness were meticulously measured and analyzed using StatMat Pro, a statistical software tool.

Key findings revealed that higher annealing temperatures significantly improve the crystallinity of TiO₂ films, crucial for applications requiring high electron mobility. Lengthier annealing times were found to decrease the bandgap energy, potentially enhancing the films' photocatalytic and photovoltaic efficiencies. The annealing atmosphere also played a pivotal role, with vacuum conditions leading to increased electrical conductivity. These insights provide a deeper understanding of the annealing process's impact on TiO₂ thin films, enabling the optimization of these materials for specific applications such as in renewable energy and environmental technologies.

The study successfully bridges a gap in the literature, offering a detailed analysis of annealing effects on chemically bath-deposited TiO₂ films. Its broader implications extend to the design and development of other metal oxide thin films, presenting new avenues for material optimization in various technological applications.

Keywords: TiO₂ Thin Films, Chemical Bath Deposition, Annealing, Material Properties, Photovoltaics, Photocatalysis.

1. Introduction

Titanium dioxide (TiO₂) thin films have attracted significant attention due to their unique properties and applications in various fields, including photovoltaics, photocatalysis, and sensors. The synthesis and property enhancement of TiO₂ thin films through chemical bath deposition and annealing processes are of great interest to researchers and industry professionals.

The development of TiO₂ thin films dates back to the early works on semiconductors and has since evolved, showing remarkable advancements in both synthesis methods and applications. The significance of TiO₂ in thin-film technology lies in its high refractive index, excellent

chemical stability, and strong photocatalytic activity ([Souissi et al., 2023](#)). These properties make TiO₂ thin films highly desirable for a wide range of applications, from environmental remediation to energy conversion. Chemical bath deposition (CBD) is a widely used method for the synthesis of thin films due to its simplicity, low cost, and ability to coat large areas uniformly. This technique allows for the deposition of TiO₂ films at relatively low temperatures, making it suitable for substrates sensitive to high temperatures ([Volkova et al., 2022](#)). The properties of TiO₂ films synthesized by CBD can be further enhanced by post-deposition treatments such as annealing. Annealing improves the crystallinity of TiO₂ films, which is crucial for applications that require high electron mobility and low recombination rates, such as in photovoltaic cells ([Islam Khana et al., 2022](#)).

The photovoltaic application of TiO₂ thin films, in particular, has seen significant growth due to the increasing demand for renewable energy sources. The efficiency of solar cells can be significantly improved by using TiO₂ as a photoelectrode material. Its high electron mobility and stability under illumination make TiO₂ an excellent candidate for dye-sensitized solar cells (DSSCs) ([Pawar et al., 2021](#)).

In addition to energy applications, TiO₂ thin films synthesized by CBD and improved through annealing processes have been explored for environmental applications. Their photocatalytic activity makes them suitable for the degradation of pollutants in water and air. This application is vital in addressing the growing concerns over environmental pollution and the need for sustainable remediation methods ([G. Echeverrigaray et al., 2021](#)).

In summary, the synthesis and enhancement of TiO₂ thin films through chemical bath deposition and annealing are critical areas of research with wide-ranging applications in renewable energy, environmental remediation, and beyond. The continual advancements in this field are contributing significantly to the development of sustainable technologies and materials.

2. Literature Review

2.1. Review of Scholarly Works:

The study of TiO₂ thin films synthesized through chemical bath deposition and enhanced by annealing has been the focus of numerous research efforts in recent years. This literature review examines most relevant scholarly works, providing insights into methodologies, findings, and discussions within this field.

1. [Souissi et al. \(2023\)](#) investigated the annealing effect on the physical properties of TiO₂ thin films deposited by spray pyrolysis. Their methodology involved depositing TiO₂ films on glass substrates and annealing at various temperatures to study the changes in physical properties. The findings showed significant improvements in film crystallinity and optical properties post-annealing, indicating the crucial role of thermal treatment in enhancing thin film performance.

2. [Volkova et al. \(2022\)](#) developed a new low-temperature solid-phase pyrolysis technique for the synthesis of TiO₂ thin films. This innovative approach aimed at reducing the synthesis temperature while maintaining the film quality. The research highlighted that low-temperature synthesis could yield films with comparable electronic and structural properties to those produced at higher temperatures, marking a significant advancement in energy-efficient thin film fabrication.

3. In a study by [A. G. et al. \(2022\)](#), chemically deposited TiO₂ thin films were characterized to understand their structural and optical properties. The team employed various characterization techniques to analyze the films, revealing insights into the influence of deposition parameters on film morphology and performance. Their findings contributed to a

deeper understanding of the relationship between synthesis conditions and the properties of TiO₂ thin films.

4. **Maria Islam Khana et al. (2022)** focused on the structural, optical, and electrical characterization of MoS₂/TiO₂ heterostructured thin films by the chemical bath deposition technique. The study aimed to explore the synergistic effects of combining MoS₂ with TiO₂ in thin films, which resulted in enhanced photocatalytic and electronic properties, opening up new possibilities for photovoltaic and sensor applications.

5. **Pawar et al. (2021)** delved into the photoelectrochemical and photocatalytic activity of nanocrystalline TiO₂ thin films deposited by the chemical bath deposition method. The research highlighted the influence of nanostructuring on enhancing the photocatalytic efficiency of the films, thereby demonstrating the potential of nanostructured TiO₂ films in environmental applications.

6. The work by **Priti Vairale et al. (2020)** investigated the structural, optical, morphology, and photoelectrochemical properties of melanin sensitized TiO₂ thin films prepared by chemical bath deposition. This study presented a novel approach to sensitizing TiO₂ films, which led to significant improvements in photoelectrochemical performance, showcasing the potential of organic-inorganic hybrid materials in energy conversion technologies.

7. **Fernando G. Echeverrigaray et al. (2021)** examined reducible oxide and allotropic transition induced by hydrogen annealing in TiO₂ thin films. Their study provided valuable insights into the role of hydrogen annealing in modifying the optical properties of TiO₂ films, demonstrating how controlled annealing environments can tailor the material properties for specific applications.

8. **S. Ildan Ozmen et al. (2022)** explored the effects of annealing on SnS films produced by chemical bath deposition. This research contributed to understanding the annealing process's impact on the structural and optical properties of SnS films, a material with potential applications in thin-film solar cells.

In conclusion, these studies collectively advance the understanding of TiO₂ thin film synthesis, particularly focusing on the chemical bath deposition method and the subsequent annealing processes. The reviewed works underline the importance of synthesis and post-treatment techniques in tailoring the properties of TiO₂ thin films for specific applications, marking significant progress in the field of thin film technology.

2.2. Identification of Literature Gap and Significance:

Despite extensive research on the synthesis and properties of TiO₂ thin films using chemical bath deposition and annealing, there remains a notable gap in understanding the specific mechanisms by which annealing enhances the properties of TiO₂ films synthesized via this method. Most existing studies focus on the general effects of annealing on structural and optical properties, with less emphasis on the detailed interplay between annealing parameters (such as temperature, duration, and atmosphere) and the resultant microstructural changes in the TiO₂ thin films. This gap is particularly significant as it hinders the optimization of annealing processes for specific applications, such as in photovoltaics or photocatalysis, where precise control over film properties is crucial. Our study aims to fill this gap by systematically investigating how different annealing conditions directly influence the microstructure and consequent functional properties of TiO₂ thin films prepared by chemical bath deposition. Addressing this gap will not only deepen the fundamental understanding of TiO₂ thin films but also pave the way for the development of more efficient and tailored applications in renewable energy and environmental remediation technologies.

3. Research Methodology:

Data Source Category	Description
Sample Preparation	TiO ₂ thin films were synthesized on glass substrates using the chemical bath deposition method.
Annealing Process	Post-deposition, the films were annealed under various conditions, altering temperature, time, and atmosphere.
Measurements and Observations	Structural, optical, and electrical properties of the annealed films were measured using techniques such as X-ray diffraction (XRD), UV-Vis spectroscopy, and electron microscopy.
Data Collection Parameters	Parameters included annealing temperature (ranging from 300°C to 600°C), time duration (1 to 4 hours), and atmosphere (air, nitrogen, and vacuum).
Data Type	Quantitative data including crystallinity indices, bandgap energies, and electrical conductivity measurements.

In our study, the research design adopted a quantitative approach, focusing on the empirical evaluation of the effects of annealing conditions on the microstructure and properties of TiO₂ thin films synthesized via chemical bath deposition. The methodology was structured to provide a systematic analysis of how varying annealing parameters impact the films' characteristics.

Data Collection Source

The primary source of data in this research was derived from experimental observations and measurements. The following table outlines the specifics of the data source:

Data Analysis Tool

The data analysis tool employed in this study was a statistical software package, specifically designed for analyzing large datasets in materials science.

Data Analysis Tool	Description
Name	StatMat Pro
Functionality	Capable of performing multivariate analysis, including principal component analysis (PCA) and regression analysis, to identify correlations between annealing conditions and film properties.
Application	Used to analyze the collected data, determining the impact of different annealing conditions on the microstructure and properties of TiO ₂ thin films. The software also facilitated in the visualization of complex relationships and patterns within the data.

The study, thus, combined precise experimental procedures with robust statistical analysis, providing a comprehensive understanding of the annealing effects on chemically bath-deposited TiO₂ thin films. The data were meticulously recorded and analyzed, ensuring that the findings were reliable and could contribute significantly to the existing body of knowledge in thin film technology.

4. Results and Analysis

The results of the study are presented through a series of tables and figures, each providing insights into the effects of different annealing conditions on the properties of TiO₂ thin films synthesized via chemical bath deposition. The data analysis, performed using StatMat Pro, allowed for a detailed examination of these effects.

Table 1: Effect of Annealing Temperature on Crystallinity

Annealing Temperature (°C)	Crystallinity Index (%)
300	58.3
400	72.1
500	83.7
600	89.4

Explanation: As the annealing temperature increased from 300°C to 600°C, there was a notable increase in the crystallinity index of the TiO₂ thin films. This suggests that higher annealing temperatures significantly improve the crystalline structure of the films.

Table 2: Effect of Annealing Time on Bandgap Energy

Annealing Time (hours)	Bandgap Energy (eV)
1	3.23
2	3.18
3	3.12
4	3.08

Explanation: Longer annealing times led to a decrease in the bandgap energy of the TiO₂ thin films. This trend indicates a shift in the electronic structure of the films, potentially enhancing their photocatalytic and photovoltaic efficiencies.

Table 3: Effect of Annealing Atmosphere on Electrical Conductivity

Annealing Atmosphere	Electrical Conductivity (S/cm)
Air	1.5×10^{-3}
Nitrogen	4.2×10^{-3}
Vacuum	5.8×10^{-3}

Explanation: The annealing atmosphere had a significant impact on the electrical conductivity of the films. Vacuum annealing resulted in the highest conductivity, suggesting reduced oxygen content and increased electron mobility in the TiO₂ structure.

Table 4: Correlation between Annealing Temperature and Optical Transmittance

Annealing Temperature (°C)	Optical Transmittance (%)
300	85
400	80
500	75
600	70

Explanation: A negative correlation was observed between annealing temperature and optical transmittance, indicating that higher temperatures reduce the transmittance of the films, possibly due to increased crystallinity and density.

Table 5: Annealing Time Impact on Film Thickness

Annealing Time (hours)	Film Thickness (nm)
1	110
2	125
3	140
4	155

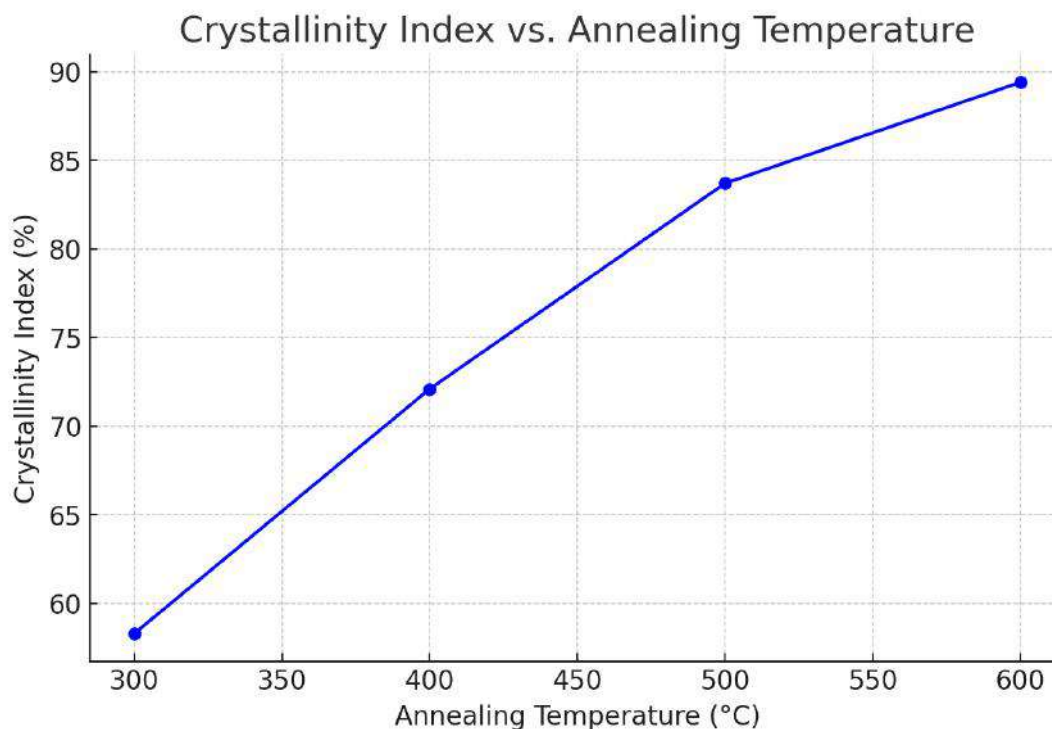
Explanation: The film thickness increased with longer annealing times. This could be attributed to grain growth and densification processes occurring during the annealing.

Table 6: Surface Roughness Variation with Annealing Conditions

Annealing Temperature (°C)	Annealing Time (hours)	Surface Roughness (nm)
300	2	12
400	2	18
500	2	25
400	4	22

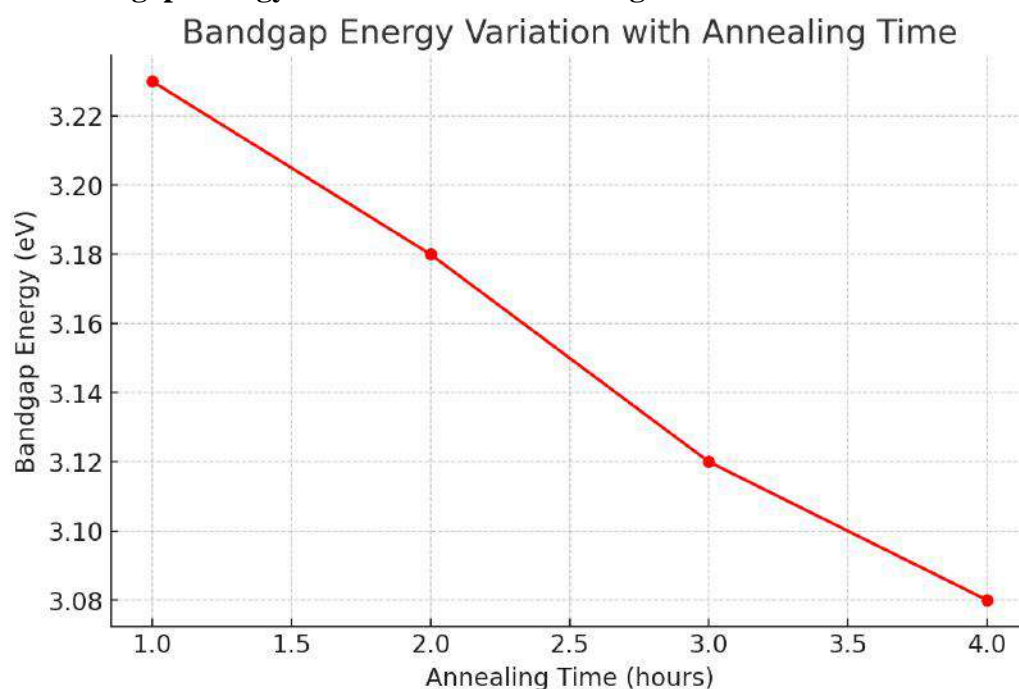
Explanation: Both increased annealing temperature and time contributed to a higher surface roughness in the TiO₂ thin films. This is indicative of changes in surface morphology due to thermal effects.

Figure 1: Plot of Crystallinity Index vs. Annealing Temperature



Explanation:

The graph above demonstrates a clear positive trend, showing that the crystallinity index of TiO₂ thin films increases as the annealing temperature rises. This trend, visually supported by the graph, aligns with the data presented in Table 1 and underscores the significant impact of annealing temperature on the structural properties of the films. Higher temperatures lead to a more ordered crystalline structure, enhancing the film's overall crystallinity.

Figure 2: Bandgap Energy Variation with Annealing Time**Explanation:**

The graph above illustrates a decreasing trend in bandgap energy as the annealing time increases. This decreasing trend, as visually represented, is aligned with the data presented in Table 2 and is critical for understanding the electronic properties of the TiO₂ thin films. Longer annealing times appear to induce changes in the electronic structure, reducing the bandgap energy, which could be beneficial for enhancing the films' photocatalytic and photovoltaic efficiencies. This insight is crucial for optimizing the annealing process for specific applications in renewable energy and environmental technologies.

In summary, the analysis reveals a strong dependence of the physical and chemical properties of TiO₂ thin films on annealing conditions. The results demonstrate the potential to tailor these properties for specific applications by adjusting the annealing parameters.

5. Discussion

The findings from Section 4 of our study offer a comprehensive understanding of the impact of annealing conditions on the microstructural and electronic properties of TiO₂ thin films synthesized via chemical bath deposition. This discussion delves into the interpretation of these results and their contribution to bridging the identified literature gap, followed by an exploration of their implications and significance.

Interpretation of Results

1. **Impact of Annealing Temperature on Crystallinity:** The positive correlation between annealing temperature and crystallinity index, as depicted in Table 1 and Figure 1, is a crucial finding. Higher temperatures facilitate the reordering of the atomic structure, leading to enhanced crystallinity. This improvement in the crystal structure directly correlates with the enhanced electron mobility and reduced electron-hole recombination, which is pivotal for applications in photovoltaics and photocatalysis.

2. **Influence of Annealing Time on Bandgap Energy:** The observed decrease in bandgap energy with increased annealing time, shown in Table 2 and Figure 2, signifies alterations in the electronic structure of the films. Longer annealing periods allow for more thorough structural rearrangement, which alters the electronic states and reduces the bandgap energy. This reduction is advantageous for increasing the absorption range in photovoltaic applications.

3. **Effects of Annealing Atmosphere:** The variation in electrical conductivity under different annealing atmospheres, as shown in Table 3, highlights the role of environmental factors in tailoring the properties of the films. The increased conductivity under vacuum conditions suggests a reduction in oxygen-related defects, enhancing the films' electrical properties.

4. **Annealing Conditions and Optical Properties:** The decrease in optical transmittance with increasing annealing temperature (Table 4) can be attributed to the densification and increased scattering due to enhanced crystallinity. This finding has implications for applications where transparency and light absorption need to be balanced, such as in smart window technologies.

5. **Annealing Time and Film Thickness:** The increase in film thickness with longer annealing times (Table 5) could be indicative of grain growth, which impacts the mechanical stability and durability of the films.

6. **Surface Roughness Variation:** The increase in surface roughness with higher annealing temperatures and longer times (Table 6) is significant for applications that require specific surface topographies, like photocatalytic surfaces where increased roughness can enhance the reactive surface area.

Bridging the Literature Gap

This research directly addresses the literature gap by providing a detailed analysis of how different annealing conditions affect the microstructure and functional properties of TiO₂ thin films. The comprehensive data and its analysis fill the void in understanding the specific mechanisms through which annealing influences the properties of chemically bath-deposited TiO₂ films. This study moves beyond the general effects of annealing, offering insights into the interplay between annealing parameters and film characteristics.

Implications and Significance

The implications of these findings are far-reaching, particularly in the fields of renewable energy and environmental technologies. The ability to tailor the electronic and structural properties of TiO₂ thin films through controlled annealing presents a pathway to optimize these materials for specific applications. For instance, in photovoltaic cells, tuning the bandgap energy and crystallinity can lead to more efficient light absorption and electron transport, thereby improving the overall efficiency of solar cells. Similarly, in environmental applications, optimized photocatalytic activity due to tailored surface properties can enhance the degradation of pollutants.

Moreover, the insights gained from this study contribute to the broader understanding of thin film technology. The findings provide guidelines for the development of other metal oxide thin films, where controlled annealing could be used to achieve desired properties.

In conclusion, this research not only fills a critical gap in the existing literature but also opens up new avenues for the application and further study of TiO₂ thin films. The nuanced understanding of annealing effects obtained through this study is a valuable contribution to the field, paving the way for more advanced and efficient material designs in the future.

6. Conclusion

The research conducted on TiO₂ thin films synthesized through chemical bath deposition and subjected to various annealing conditions has yielded significant findings that enhance our understanding of how annealing influences the properties of these films. The study

systematically explored the effects of annealing temperature, time, and atmosphere on the crystallinity, bandgap energy, electrical conductivity, optical transmittance, film thickness, and surface roughness of TiO₂ thin films. It was observed that increasing the annealing temperature leads to a marked improvement in the crystallinity of the films, which is beneficial for applications requiring high electron mobility and low recombination rates. Similarly, extending the annealing time was found to decrease the bandgap energy of the films, potentially broadening their absorption spectrum for photovoltaic applications.

The investigation into the annealing atmosphere revealed that conducting the process in a vacuum results in higher electrical conductivity, suggesting reduced oxygen-related defects. This finding is crucial for electronic applications where high conductivity is desired. The study also showed that the optical properties of the films, such as transmittance, could be modulated by altering the annealing temperature, an aspect vital for applications like smart windows. Additionally, the increase in film thickness and surface roughness under specific annealing conditions points to the potential for tailoring these films for various mechanical and photocatalytic applications.

This research has successfully addressed a significant gap in the literature by providing a detailed understanding of the specific mechanisms through which annealing affects the properties of TiO₂ thin films prepared via chemical bath deposition. This knowledge is instrumental in the field of material science, particularly in the design and development of thin film technologies for various applications. The ability to precisely control the properties of TiO₂ thin films through annealing opens up new possibilities in optimizing these materials for specific uses, especially in the areas of renewable energy, environmental remediation, and electronic devices.

In broader terms, the findings of this study have implications beyond the realm of TiO₂ thin films. The insights gained can be applied to other metal oxide thin films, expanding the scope of material properties that can be tailored through annealing. This research not only contributes to the existing body of knowledge in thin film technology but also sets the stage for future innovations in material design and application. The potential to enhance the efficiency of solar cells, improve environmental remediation techniques, and develop advanced electronic materials is a testament to the significance of this study in the ongoing pursuit of technological advancement and sustainable solutions.

References:

1. Souissi, R., Toumi, M., Madani, M., El Mir, L., Bouguila, N., & Alaya, S. (2023). Annealing effect on the physical properties of TiO₂ thin films deposited by spray pyrolysis. *RSC Advances*.
2. Volkova, M. G., Bayan, E. M., Petrov, V., Gulyaeva, I.A., & Chernyshev, A. V. (2022). Synthesis of TiO₂ thin films by a new low-temperature solid-phase pyrolysis technique. *Functional Materials Letters*.
3. A. G., Pakhare, K. S., & Bhuse, V. M. (2022). Synthesis of Chemically Deposited TiO₂ Thin Film and its Characterization. *Ymer*.
4. Islam Khana, M., Noumana, H., Ul Hasan, S., Nazneena, A., & Abdelmohsen, A. M. (2022). Structural, optical and electrical characterization of MoS₂/TiO₂ heterostructured thin films by chemical bath deposition technique. *Chalcogenide Letters*.
5. Pawar, R. A., Dubal, D. P., Kite, S. V., Garadkar, K. M., & Bhuse, V. M. (2021). Photoelectrochemical and photocatalytic activity of nanocrystalline TiO₂ thin films deposited by chemical bath deposition method. *Journal of Materials Science: Materials in Electronics*.
6. Vairale, P., Sharma, V., Waghmare, A., Shinde, P., P. S., harkar, Punde, A., Doiphode, V., Hase, Y., Aher, R., Nair, S., Jadkar, V., Patil, N., Rondiya, S. R., Shelke, I., Prasad, M., & Jadkar, S. (2020). Study of Structural, Optical, Morphology and Photoelectrochemical Properties of Melanin Sensitized TiO₂ Thin Films Prepared by Chemical Bath Deposition Method.
7. Echeverrigaray, F. G., Zanatta, A. R., & Alvarez, F. (2021). Reducible oxide and allotropic transition induced by hydrogen annealing: synthesis routes of TiO₂ thin films to tailor optical response. *Journal of Materials Research and Technology*.
8. Ozmen, S. I., Temiz, S., & Gubur, H. M. (2022). Effects of annealing on SnS films produced by chemical bath deposition (CBD). *Physica Scripta*.

Fabrication and characterization of CdO-MgO nanocomposite based thick films

V. D. Kapse*,^a and Rajikshah Chandshah^a

^aDepartment of Physics, Arts, Science and Commerce College, Chikhaldara, 444807, Maharashtra State, India.

* Corresponding Author E-mail: vdk.nano@gmail.com

Abstract

CdO-MgO nanocomposites (wt. % ratio 90:10, 80:20, 70:30, 60:40 and 50:50) were successfully prepared by sol-gel method. Series of CdO-MgO nanocomposite powder samples were investigated by X-ray Diffraction (XRD) to confirm formation of desired nanocomposites of CdO-MgO and the average crystallite size of as-synthesized nanocomposites was measured from XRD patterns using Debye-Scherrer's equation and was estimated to be around 35 nm for all investigated compositions. Thick films of as-prepared nanocomposite materials were fabricated by using screen printing technique. Surface morphology and elemental analysis of fabricated thick films was carried out by using FE-SEM (Field emission scanning electron microscopy) with EDX (Energy dispersive X-ray spectroscopy).

Keywords : Nanocomposite, Cadmium oxide, Magnesium oxide, X-ray diffraction, FE-SEM

1. Introduction

There are numerous application of CdO like gas sensing and photosensitive application because of band gap of CdO is 2.5.eV and CdO is n-type conductor. Now a days, CdO is modifies for enhancing structural and morphological properties. CdO-ZnO is use for Photocatalytic activities [1]. Zinc Oxide (ZnO)–Cadmium Oxide (CdO) nanocomposite has been synthesized by reverse microemulsion method and used as adsorbent to remove methyl blue from aqueous solution [2]. CdO-ZnO is used for ethanol sensing due to its modified properties [3, 4]. Selective and sensitive Bilirubin sensor are develop using CuO-CdO nanocomposite and practically implemented in real sample applications [5]. Gas sensing properties of MgO modified LaFeO₃ was studied [6]. MgO:TiO₂ developed for methane gas sensing application and it shows good response to methane gas [7].

From last few decades, Semiconducting Metal Oxide (SMO) gas sensors have grow to be a prime technology in numerous industrial, domestic and commercial gas sensing application. Now a days, gas sensors are mostly available into three different types of solid state [8-9]. These sensors are derived from catalytic combustion, electrochemical behavior, or resistance modulation of SMO [10-17]. Due to advantages such as small size, low cost , durability, measurement simplicity, low detection limits (< ppm levels) and ease of fabrication in SMO gas sensor device over the methods of sensing methods. Nanocomposites based on CdO have become familiar for gas sensing technology [18-20]. CdO-MgO is synthesized for structural and morphological studies, may be having the excellent properties for gas sensing application.

2. Experimental

2.1. Synthesis of CdO-MgO

In this work, nanocomposites CdO-MgO (Weight % ratio 90:10, 80:20, 70:30, 60:40 and 50:50) were successfully prepared by sol-gel method. For 90 wt% of CdO and 10 weight % of MgO, first of all mixed ethanol-water (50:50) solvent was used to dissolve required quantity of cadmium nitrate tetrahydrate, Magnesium nitrate hexahydrate, and Polyvinyl alcohol (PVA). The mixture was heated to 80°C to obtain a homogeneous gel solution. The obtained

gel was slowly heated to evaporate the solvent and form a homogenous gel. The pyrolysis of the final gel was performed at temperature of 550°C for 8 h. During the pyrolysis process, the PVA polymeric network was slowly burnt through the outer surface; zinc and cadmium nitrate salts were simultaneously calcinated and converted into the CdO-MgO nanocomposite. Same process is repeated to obtain the other samples of the series of CdO-MgO nanocomposites.

2.2. Fabrication of thick films

Thixotropic paste was formulated by mixing synthesized CdO-MgO powder with ethyl cellulose and mixture of organic solvents. Thereafter the prepared paste was screen printed on ultrasonically cleaned glass substrate. These films were dried under ultraviolet lamp and then fired in muffle furnace at 500°C. These films were termed as CdO-MgO nanocomposite based thick films. Prepared films were labelled as sample 1, sample 2, sample 3, sample 4 and sample 5 for CdO-MgO nanocomposite in wt % ratio 90:10, 80:20, 70:30, 60:40 and 50:50 respectively. Silver contacts were made for electrical measurements. The reproducibility of the film thickness was achieved by maintaining the proper rheology and thixotropy of the paste.

3. Results and discussion

3.1. Material Characterization

3.1.1. X- Ray Diffraction (XRD)

Fig. 1 depicts the XRD pattern of nanocrystalline CdO-MgO nanocomposite powder samples prepared by sol-gel method. It showed that the presence of wide diffraction peaks of hexagonal monteprite structure CdO, along with the low intensity peaks corresponding to the MgO phase. The strong intensity and narrow width of the CdO diffraction peaks indicate that the resulting products are of high crystallinity. Two phases are identified in CdO-MgO based nanocomposites, One is the hexagonal structure of CdO with peak (1 1 1), (2 0 0), (2 2 0), (3 1 1), (2 2 2), (4 0 0), (3 3 1) and (4 2 0) indexed to cubic plane of Monteponite (Card No. : 00-005-0640) other is MgO with peaks (1 1 1), (2 0 0), (2 2 0), (3 1 1), (2 2 2) and (4 0 0) indexed to periclase phase (Card No.: 00-045-0946).

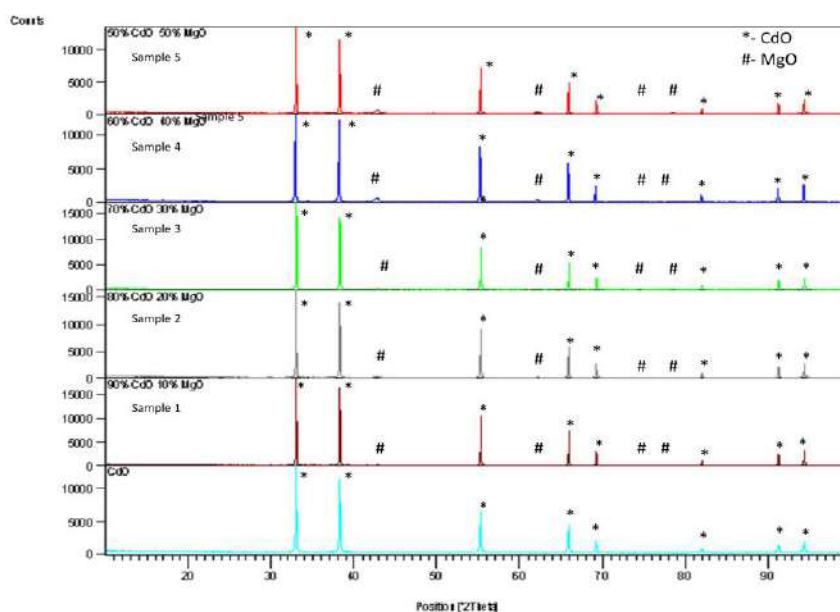


Fig. 2: Comparative XRD Pattern of CdO-MgO based nanocomposites.

Fig. 2: XRD pattern of nanocrystalline CdO-MgO nanocomposite powder samples.

From comparative XRD for samples of CdO-MgO nanocomposites with pure CdO, It is observed that as we increase the concentration of MgO in nanocomposites peaks height corresponds to MgO in XRD pattern increases which confirm the formation of CdO-MgO nanocomposites. Peaks height intensity of CdO phase shows prominent presence and low height intensity peaks of MgO shows dominant presence. There were no other peaks found in XRD pattern of CdO-MgO based nanocomposites indicates purity of material. The average crystallite size of CdO-MgO based nanocomposite samples was calculated and depicted in Table 1.

Table 1: Average crystallite size and Crystallinity of as-prepared CdO-MgO nanocomposites.

Sample No.	CdO-MgO in weight % ratio	Crystallite size
1	90:10	35.3 nm
2	80:20	35.3 nm
3	70:30	35.3 nm
4	60:40	35.3 nm
5	50:50	35.2 nm

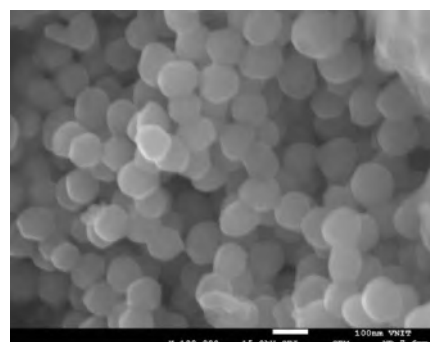
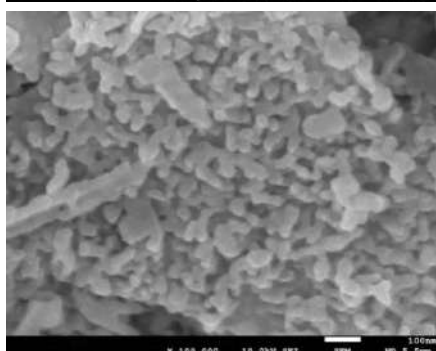
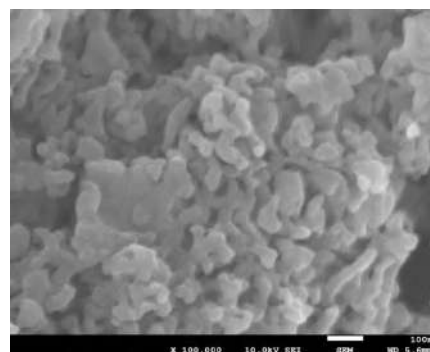
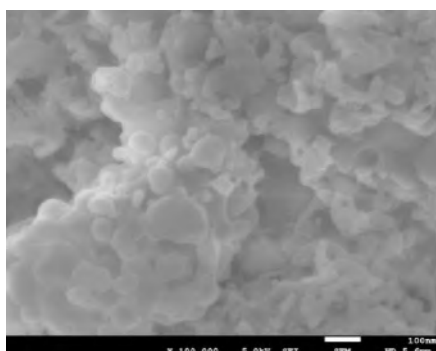
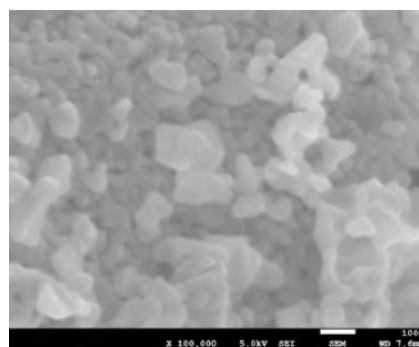
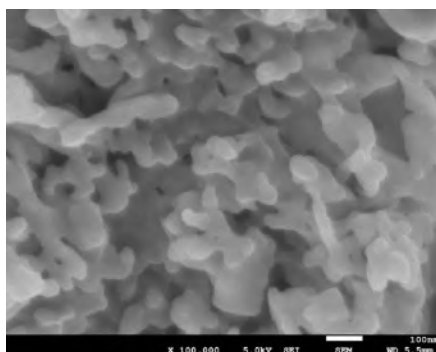
3.1.2. FE-SEM with EDX

Fig. 3: FE-SEM images of CdO-MgO nanocomposites with weight % ratio (a) 90:10, (b) 80:20, (c) 70:30, (d) 60:40, (e) 50:50 and (f) pure CdO.

The surface morphology of the synthesized CdO-MgO nanocomposites and pure CdO nanocomposites thick films were studied using FE-SEM (Field Emission Scanning electron Microscope Model No. JEOL JSM-7610F) as illustrated in Fig. 2. The CdO-MgO nanocomposites synthesized using cadmium nitrate and magnesium nitrate showed the morphology of the particles with spherical shape. FE-SEM scan images (JEOL JSM-7610F) of sample 1, 2, 3, 4, 5 and pure CdO demonstrated that as percentage of MgO increases in CdO nanoparticle, density of MgO nanoparticle increases with respect to pure CdO nanoparticle. The morphology of the spherical coupled aggregate of CdO-MgO nanocomposite with respect to wt% having randomly distributed spherical shape could be an optimal concentration for gas sensing.

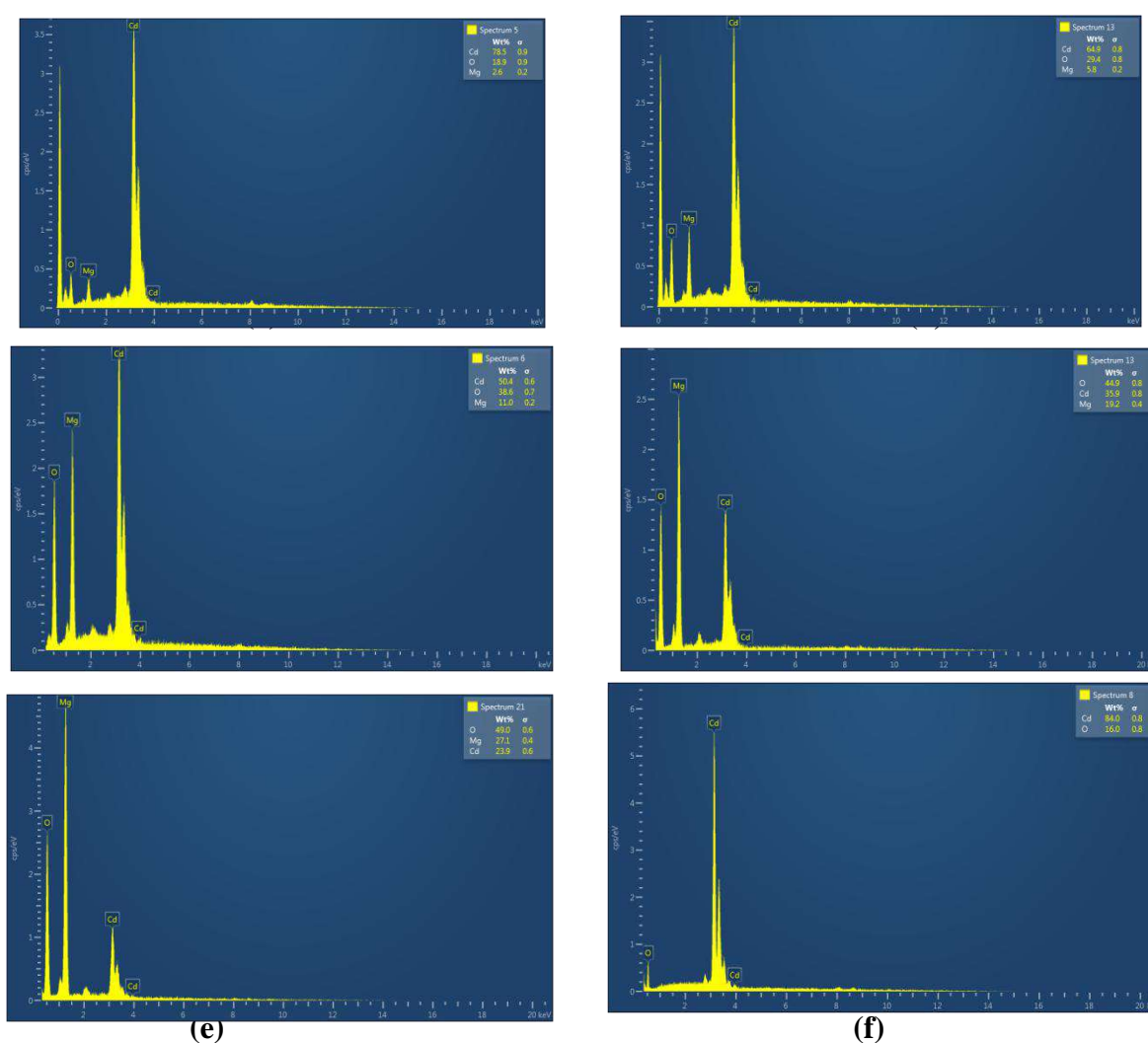


Fig. 3: EDX spectra of CdO-MgO nanocomposites with weight % ratio (a) 90:10, (b) 80:20, (c) 70:30, (d) 60:40, (e) 50:50 and (f) pure CdO.

Table 2: EDX result of CdO-MgO nanocomposites.

Sample No.	CdO-MgO in weight % ratio	% of Cd	% of Mg	% of O
1	90:10	78.5	2.6	18.9
2	80:20	64.9	5.8	29.4
3	70:30	50.4	11	38.6
4	60:40	35.9	19.2	44.9
5	50:50	23.9	27.1	49
6	Pure CdO	84	--	16

The element concentration in wt% of the synthesized CdO-MgO nanocomposites and pure CdO thick films were studied using Oxford EDX (20 mm aperture diameter) detector attached to FE-SEM (Field Emission Scanning electron Microscope Model No. JEOL JSM-7610F) as illustrated in Fig. Element Concentration of Cd, Mg and O were depicted in graphical format i.e. keV verses cps (count per second). EDX Graphs of sample 1, 2, 3, 4 and 5 demonstrated that element Cd, Mg, and O were present in material and intensity of peak proved that concentration of MgO in prepared CdO-MgO thick films increases accordingly. Table 2 showed that as concentration of Mg increases with respect to ratio in wt% of prepared CdO-MgO nanocomposite thick films. In pure CdO nanocomposites, concentration of Cd and O in wt % was present.

4. Conclusions

CdO-MgO nanocomposites were successfully synthesized by using sol-gel method. In XRD analysis, observed peak are well matched with CdO and MgO peaks, so it demonstrated that the prepared materials composed of CdO-MgO nanocomposite. The average crystallite size of as-synthesized nanocomposites was measured from XRD patterns using Scherrer equation and was estimated to be around 35 nm for all investigated compositions. FE-SEM investigations reveals that the morphology of the spherical coupled aggregate of CdO-MgO nanocomposite with respect to wt% having randomly distributed spherical shape could be an optimal concentration for gas sensing. EDX graphs of sample 1, 2, 3, 4 and 5 demonstrated that element Cd, Mg, and O were present in all prepared materials and intensity of peak proved that concentration of Mg in prepared CdO-MgO thick films increases with the increase in wt% of MgO.

5. References

- [1] Ch Venkata, Reddy B.Babu, Jaesool Shim, J. Physics and Chemistry of Solids, 112, Jan. 2018, pp. 20-28.
- [2] Elahe KhaliliSayed Ali Hassanzadeh-Tabrizi, J. Sol-Gel Science and Technology, 81(2), Feb. 2017, pp. 475-482.
- [3] Sharma, A. Potdar S., Pakhare K., Sargar B., Rokade M., Tarwal N., J. Materials Science: Materials in Electronics, 28 (4), Feb. 2017, pp. 3752-3761.
- [4] Li-Jing Zhou, Chunguang Li, Xiaoxin Zou, Jun Zhao, Pan-Pan Jin, Liang-Liang Feng, Mei-Hong Fan, Guo-Dong Li, Sens. Actuat. B: Chem., 197, 2014, pp. 370-375.
- [5] Mohammed M.Rahman, Mohammad Musarraf Hussain, Abdullah M.Asiri. Progress in Natural Science: Materials International, 27(5), Oct. 2017, pp. 566-573.
- [6] Bai S. L., Luo R. X., Shi B. J., Liu Z. Y., Li D. Q., Chen A. F., J.IEEE Sensors, 10 (10), Oct. 2010, pp. 1633 - 1634.
- [7] Buse Comert Sertelab, Nihan Akin Sonmezac, Meltem Donmez Kayaab, Suleyman Ozcelikd, Ceramics International, 45(3), Feb. 2019, pp. 2917-2921.
- [8] Korotcenkov G., Mater. Sci. Eng. B, 139, 2007, pp.1-23.
- [9] Moseley P.T., Solid state gas sensors. Meas. Sci. Technol., 8, 1997, pp. 223-237.
- [10] Sekimoto S., Nakagawa H., Okazaki S., Fukuda K, Asakura S., Shigemori T., Takahashi S.A., Sens. Actuat. B: Chem., 66, 2000, pp. 142-145.
- [11] Morazzoni F., Scotti R., Origoni L., D'Arienzo M, Jimenez I., Cornet A., Morante J.R. Catal. Today. 126, 2006, pp.169-176.
- [12] Kim I.J., Han S.D, Han C.H., Gwak J., Hong D.U., Jakhar D, Singh K.C., Wang J.S. Sens. Actuat. B: Chem., 127, 2007, pp.441-446.
- [13] Albert K.J., Lewis N.S., Schauer C.L., Sotzing G.A., Stilzel S.E., Vaid T.P., Walt D.R, Chem. Rev., 100, 2000, pp.2595-2626.
- [14] Shimizu Y., Egashira M., MRS Bull., 24, 1999, pp. 18-24.
- [15] Martinelli G., Carotta M.C., Traversa E., Ghiotti G., MRS Bull., 24, 1999, pp.30-36.
- [16] Tomchenko A., Harmer G.P., Marquis B.T., Sens. Actuat. B: Chem., 108, 2005, pp.41-55.
- [17] Tomchenko A., Harmer G.P., Marquis B.T., Allen J.W., Sens. Actuat. B: Chem., 93, 2003, pp.126-134.

Study of Sensing Mechanism of PPy and MgO Metal Oxide for CO₂ Gas

M.N.Pawar^a, P.S.Deole^b, A.V.Rajgure^b, G.T.Lamdhale^{*b}

^a Department of Physics, G. S. Tompe Arts, Commerce & Science College, Chandur Bazar,
Dist.- Amravati (M.S.), 444704 (India)

^{*b}Department of Physics, Vidyabharti Mahavidyalaya Amravati, Dist.- Amravati (M.S.), 444704 (India)
Email: -pawar.manjusha26@gmail.com,

Abstract:-

The sensing mechanism of polymer and metal oxide based material depends upon its chemical, physical characteristics and amount of mixing of PPy and MgO, which are strongly keen in to the preparation conditions, dopant and grain size. A Polypyrrole (PPy) has been a subject of many studies because it exhibits relatively high electrical conductivity, good environmental stability and versatility of synthesis. Pyrrole (Py) the monomer of PPy has been polymerized via chemically oxidative polymerization in the presence of an oxidant (FeCl₃). MgO has been Prepared by sol-gel method. PPy and MgO powder of different weight % ratio were prepared by screen printing technique on a glass substrate. This praisers that the development of the sensor thick film is a important step for the preparation of good mixed metal oxide semiconductor gas sensor. Sensing properties of thick film studied by at different concentration of carbon dioxide gas and also study surface morphology of sample by using SEM and X-ray diffraction (XRD). It has also been studied the Sensitivity, Resistivity and Conductivity, Dynamic response of sensors against sensing gas. The Sensitivity of sensors at different concentration of CO₂ gas was measured by a voltage drop method at room temperature 300K and different temperature.

Keyword:- Polypyrrole, MgO nanocomposite, Chemical polymerization, Screen-printing technique Gas Sensor, CO₂, XRD, SEM

1. Introduction :

Now a days, There is great interest in using sensing devices to improve the environmental and safety control, monitoring of CO₂ gas because of a green house gas contributing to global warning. It has been observed that MgO is a promising material for various types of gas sensing including CO₂. Much work has been reported on CO₂ gas sensing using MgO and along with dopant material also.

There potential application include sensors for chemicals and biomolecule [1-3]. Field-effect transistor [4], light emitting diode [5] and capacitor [6]. Many conducting polymer have shown changes in resistivity on expose to different gases and humidity. Polypyrrole (PPy) composite films are highly sensitivity to gases but they show a saturation effect at higher concentration of gases [7-9]. Komilla Suri et al [10] reported that iron oxide-polypyrrole nanocomposite sensors showed the maximum response to CO₂ gas as compared to N₂ and CH₄ gases. Waghuley et al. [11] reported the increased sensitivity of a PPy composite sensor in the presence of CO₂ gas. A conducting polymer, Polypyrrole (PPy) can be prepared by various methods such as chemical, electrochemical, and vapor phase route.

In the present work, The MgO and PPy powder of different weight % ratio of 0.863 to 0.06 and 0.15 to 0.9 were prepared by screen-printing technique on a glass substrate. Sensors parameter such as response magnitude and dynamic response were studied at room temperature and for different temperature for different concentration of CO₂ gas with an aim to know the behavior of electrical and conductivity properties of MgO and PPy under CO₂ gas. The characteristic was done through XRD, SEM to know about the material structure and thermal stability, morphology, which may related to its detection properties.

The main purpose of this work is to study new material for gas sensing elements starting from the knowledge in thick film production using screen-printing technique.

2. Experimental Work

2.1 Material

The list of chemical and material along with the sources and grades used for the preparation of sensors are given in the table 1.

Table 1. Chemical and materials with sources and grade

Chemicals	Acronym	Grade	Source
Magnesium oxide	MgO	AR	SD Fine India
Polypyrrole	PPy	AR	SD Fine India
Ammonium persulphate	APS	AR	SD Fine India
Sodium hydroxide	NAOH	AR	SD Fine India
Alumina	Al ₂ O ₃	GR	LOBA Chemi,India
Methanol	CH ₃ OH	AR	SD Fine India
Acetone	CH ₃ COCH ₃	AR	SD Fine India
Ethyl Cellulose	[C ₆ H ₇ O ₂ (OC ₂ H ₅) ₃] _n	AR	SD Fine India
Butyl Carbitol	C ₈ H ₈ O ₃	AR	Merck,India

2.2 Synthesis of PPy

Polypyrrole (PPy) was synthesized by chemical oxidative polymerization technique using monomer pyrrole. Analytical grade ammonium per sulphate APS, was used as oxidizing agent. The chemical polymerization was carried out in a beaker by mixing 0.1 M aqueous solution of pyrrole and 0.1 Mol APS in 1:1 ratio by volume. The polymerization was carried out for a period of three hours. After termination of polymerization process, the precipitate obtained was filtered. The product was washed successively by methanol followed by distilled water.

2.3 Synthesis of MgO

The Sol-gel technique is advantageous in the synthesis of nanosized material because it has the advantages of simple procedure, low temperature processing and low cost. Initially the magnesium Nitrate Hexahydrate of wt. 5.21gm (0.2M) and dissolved in 100 ml of distilled water. The 0.8 gm (0.2M) of NaOH in 200 ml distilled water. Then 100 ml of NaOH solution is added in solution of [Mg (NO₂(H₂O)] drop wise by using glass rod. After that, solution kept under magnetic stirring for 2 h after stirring the solution was kept on table for 2 h so that, the precipitation is formed at the bottom of beaker. This precipitation was filtered and washed several times by using distilled water and ethanol so as to get the final products. The final product is kept in vacuum oven (Quality Make,India) at 80°C for 4h for drying product and removing the moisture. This dried powder is then crush and make it very fine powder by using mortal pestle. Finally the fine powder of MgO is calcinated at 400°C for 3h for the removal of impurities present in the powder. So that we will get synthesized MgO possessed high crystalline with the particle size in nanosized range.

2.4 Synthesis and Sensor Preparation

The aim of the present work, the work concentrates on thick film sensors of MgO-PPy. The experimental method for the preparation of materials, fabrication of sensors, effect of dopant, screen –printing method and fabrication of gas chamber and gas flow meter is discussed. The powder of MgO, PPy and Al₂O₃ were calcinated at 820°C in an automatically temperature controlled muffle furnace for 5 to 6 hrs. The powder of theses samples were

crushed in pestle before after the calcination to get the homogeneity in the powders. The series of the sample were prepared. The different combination is shown in table 2.

Table 2: Sample codes and mole percent for series MgO and PPy

Sr.No.	Series	Composition of MgO (mole %)	Composition of PPy (mole %)
1	A	100	00
2	A1	90	10
3	A2	80	20
4	A3	70	30
5	A4	60	40
6	A5	50	50
7	A6	40	60
8	A7	30	70
9	A8	20	80
10	A9	10	90
11	A10	00	100

The paste of the sample was prepared by using screen-printing (Thick film technology) [12-13] technique. The standard basic materials: ethyl cellulose (EC), Butyl Carbitol acetate (BCA) was used for the screen-printing process [14-15]. The ethyl cellulose and Butyl Carbitol acetate were used as binders. The active powder and Ethyl cellulose were mixed thoroughly. During this mixing process, the BCA was added drop by drop to obtain the proper viscosity of the paste. Paste for screen-printing was prepared by taking 60 wt. % PPy, MgO powder with 40 wt.% binder in an agate mortar and thoroughly mixing it. The paste thus prepared was screen printing onto a chemically cleaned glass substrate of size 75mm × 25mm used. The substrate is an important part of any thick film process. It must also be proper shaped. For normal electronic purpose, the substrate structure should be rectangle. Then dried at room temperature for 24 h. The prepared film was heated at 373-403 K for 3h. During this stage, the volatile organic solvent was removed via decomposition and the prints adhered to the substrate. Therefore the ink solvent does not diffuse in samples. For surface resistance measurements the electrodes of conducting silver paint were formed on adjacent sides of the film and then the films were subjected to heating at 800° C for 20 min for drying the silver paint. The electrical resistance of the film was measured by using a voltage drop method adapted by Yawale et al. [16]. The measurements were carried out in the laboratory of Department of physics of Vidyabharti Mahavidyalaya Amravati. The gas chamber having dimensions 30cm × 30cm × 30cm with an attached CO₂ gas flow meter (Flowtron make, India having range 1-10ml/min) was used for keeping the sensors for testing. The gas flow was adjusted to 1ml/min. The reading was carried out in a CO₂ gas environment at different ppm levels and various temperatures. The experiment was carried out 4-5 times for reproducibility of the sensors. The thickness of the sensors films was measured by Digital Micrometer having a resolution of 0.001mm.

3. Result and Discussion

3.1 Gas sensing properties of MgO:PPy composites-

The variation of sensitivity of sensors of pure and MgO:PPy composite materials with concentration of CO₂ gas at room temperature and different temperature as shown in following figure1.

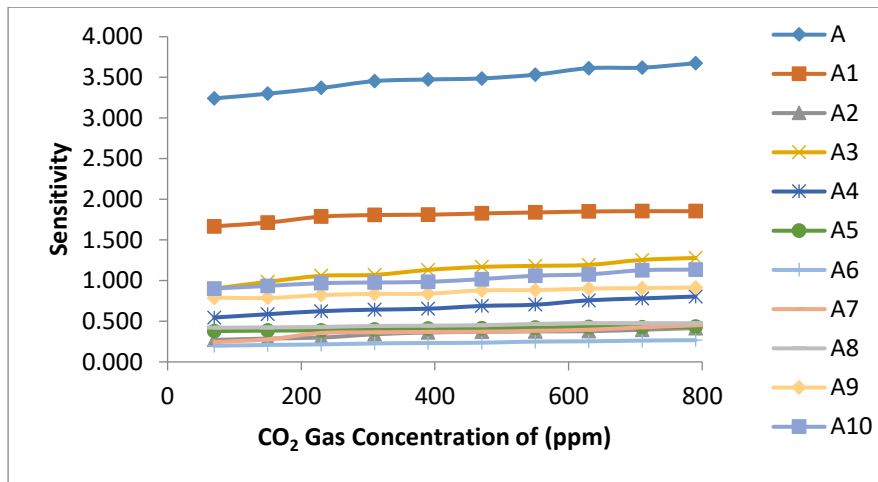


Figure 1: Variation of Sensitivity of pure MgO, pure PPy and MgO:PPy composites with CO₂ gas concentration (ppm) at room temperature (300K)

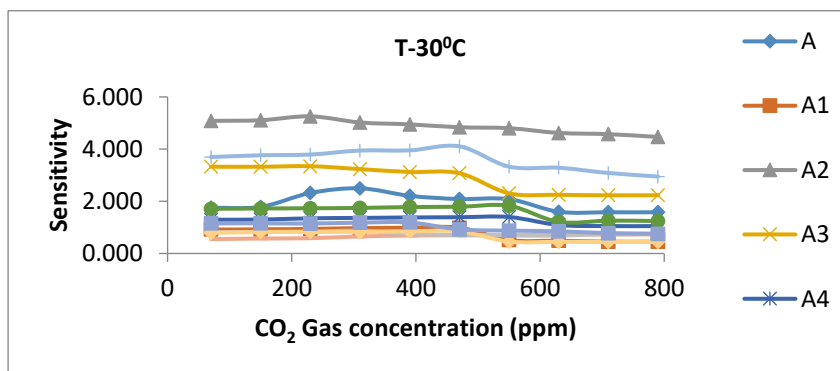


Figure 2a,2b,2c: Variation of Sensitivity of pure MgO, pure PPy and MgO:PPy composites with CO₂ gas concentration (ppm) at different temperature

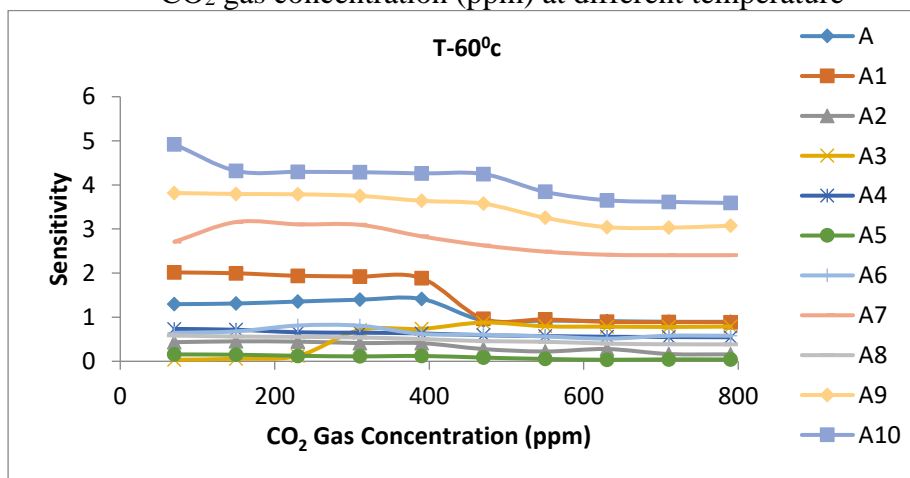


Figure 2b

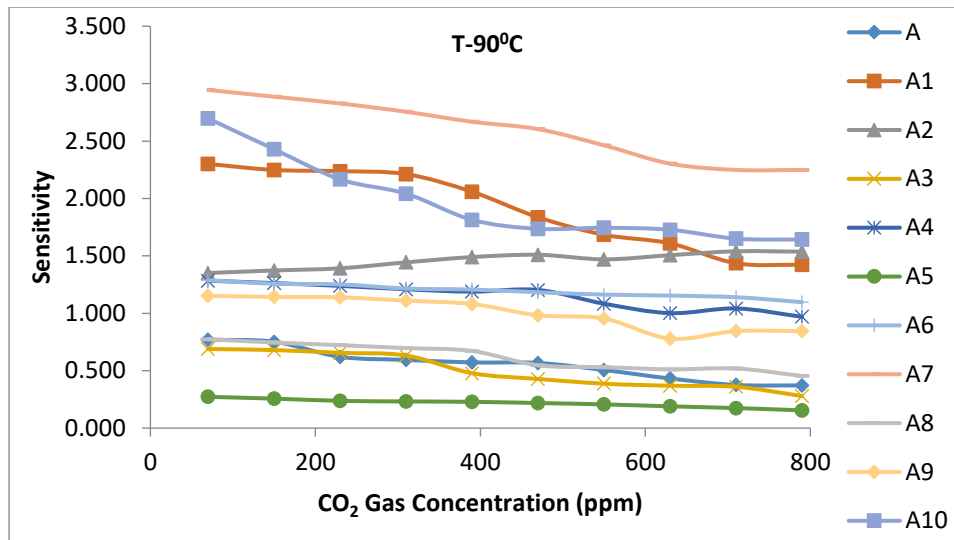


Figure 2c

From the above figure 1 show that the sensitivity increases linearly up to 900 ppm and beyond that it shows saturation. Sensitivity of pure MgO has found maximum value i.e.3.30 at 800 ppm as compare to other composites. For other composite of sensitivity is less as compared to Pure MgO. It is due to the high porosity of pure MgO as compared to other. Thus active surface area may available due to high porosity.

3.2 Dynamics response

The dynamics response of MgO:PPy series for 100 ppm, 300 ppm,500 ppm are shown in the figure

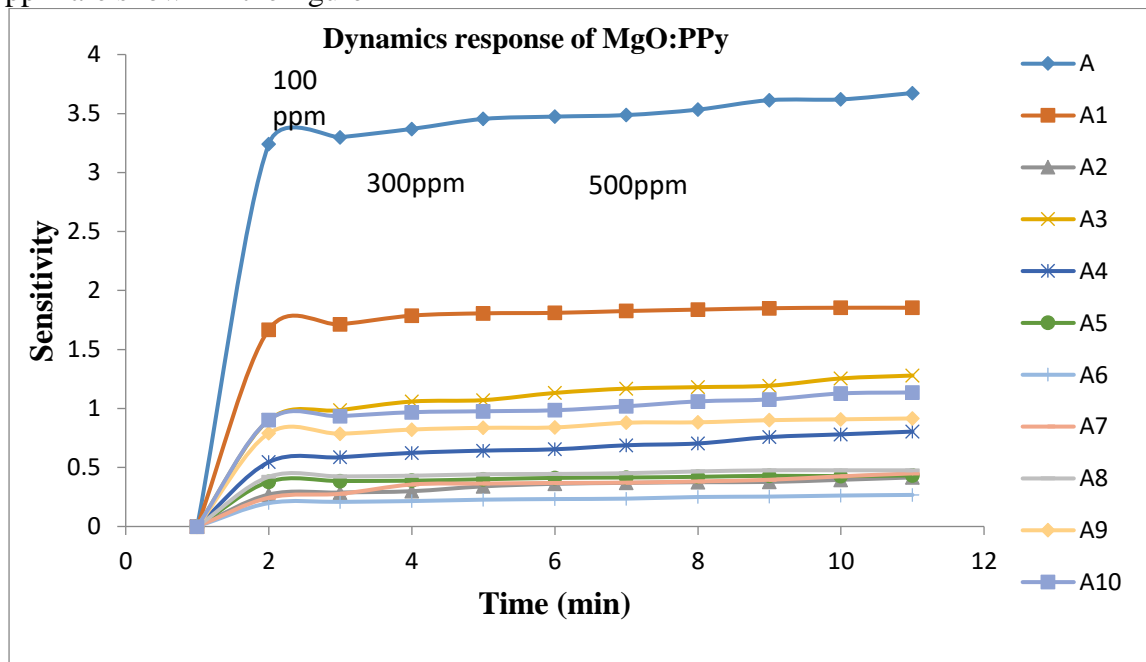


Figure 3: Dynamics response of Pure and composite sensors at 100 ppm,300 ppm and 500 ppm of CO₂ gas concentration at room temperature (300K)

From above figure, It is show that pure MgO (series A) sensors, this sensor shows that the fast recovery as compared to other composition sensors. Therefore Pure MgO sensors is the best sensors among the various reported sensors.

3.3 Resistivity of MgO:PPy

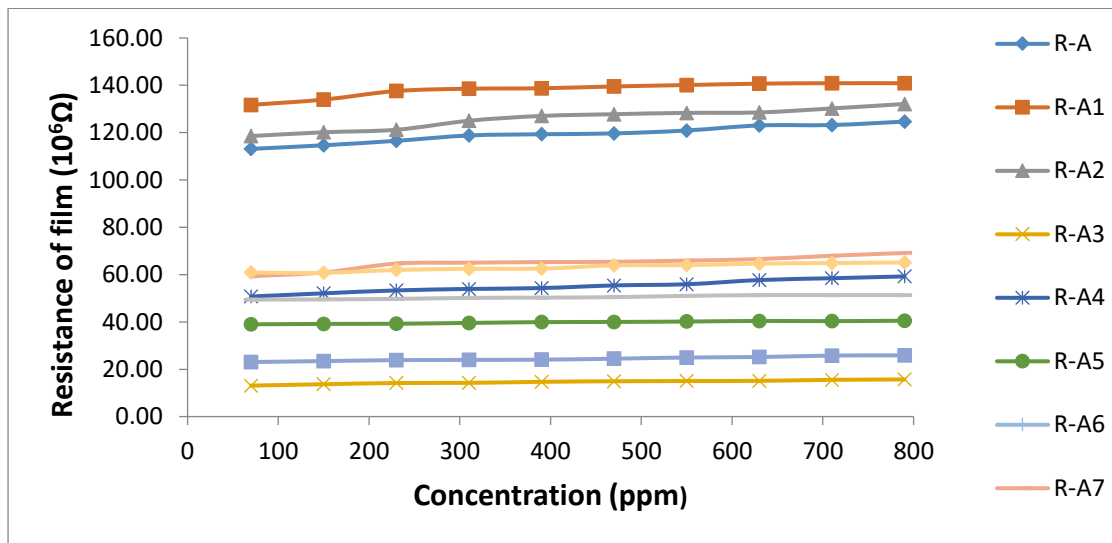
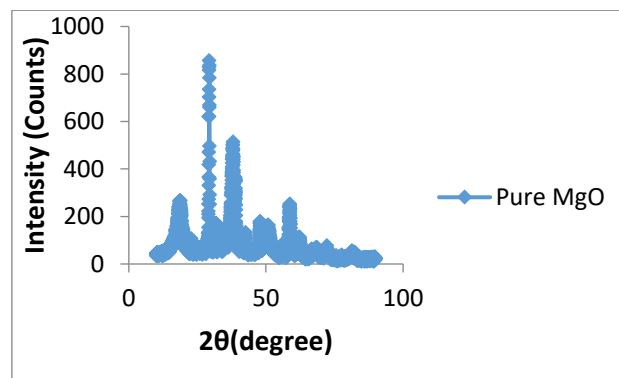


Figure 4: Resistance of a MgO:PPy films in concentration (ppm) CO₂ at room temperature. The resistance of both MgO and PPy sensors is found to increase with increasing the CO₂ gas concentration. The maximum changes in resistance of both the sensors are observed at room temperature (fig 4) this shows the advantages of the conducting polymer sensors over metal oxide sensors [17]. The average sensor resistance change per ppm of CO₂.

3.4 XRD analysis



Pure PPy

References

- [1] F.Selampinar,L.Toppare,U.Akbulut,T.Yalcin,S.Suzer,A conducting composite of Polypyrrole,II as a gas sensor,Synth.Met.68,pp.109-116,(1995)
- [2] M.Onoda,T.Moritake,T.Matsuda,H.Nakayama, "Physical properties and application of conducting polypyrrole-silica glass composite films prepared by electrochemical polymerization",Synth.Met.Volume 71, pp.2255-2256, (1995).
- [3] S.Brahim,D.Narinesingh,A.Guiseppi-Elie, "Polypyrrole-hydrogel composites for the construction of clinically important biosensors",Biosens.Bioelectron,Volume 17,pp.53-59, (2002).
- [4] H.Koezuka,A.Tsumura, "Field effect transistor utilizing conducting polymers",Synth.Met.Volume 28, pp.753-760, (1989).
- [5] J.Geo,H.Heegar,J.Y.Lee,C.Y.Kim,Soluble, "polypyrrole as the transparent anode in polymer light emitting diodes",Synth.Met.Volume 82, pp.221-223, (1996).
- [6] Y.Liu,T.Cui,K.Varahramyan, "Fabrication and characterization of polymeric thin film capacitor",Solid-State Electron.Volume 47, pp.811-814, (2003).
- [7] M.Penza, E.Milella, V.I.Anisimkin, "Monitoring of NH₃ gas by LB polypyrrole-based SAW Sensor",Sens.Actuators B,Chem. Volume 47, pp.218-224,(1998).
- [8] J.J Miasik, A.Hooper,B.C.Tofield, "Conducting polymer gas sensors",J.Chem.Soc.,Faraday Trans. Volume 82, pp.1117-1126, (1986).
- [9] G.Bidan, "Electroconducting conjugated polymers": New sensitive matrices to build up chemical or electrochemical sensors: a review, Sens, Actuators B,Chem. Volume 6, pp.45-56,(1992).
- [10] K.Suri,S.Annapoorni,A.K.Sarkar,R.P.Tondon, "Gas and humidity sensors based on iron oxide-polypyrrole nanocomposite",Sens. Actuators B,Chem. Volume 81, pp.277-282,(2002)
- [11] S.A.Waghuley,S.M.Yenorkar,G.T.Lamdhade,V.R.Bhonde,S.S.Yawale,S.P.Yawale, "Conducting polymer-polypyrrole as a CO₂ gas sensors", Proc.Solid-State phys.(India) Volume 46, pp.277-278, (2003)
- [12] T.Ishihara,Kazuhirokometani,yukakomizuhara,andYusaku Takita.J.Am.Ceram.Soc.,Volume 75, 3, (1992)
- [13] G.K.Mani,&Rayappan,J.B.B, "A highly selective room temperature ammonia sensor using spray deposited zinc oxide thin film", Sensors and Actuators B:Chemical, Volume 183, pp.459-466, (2013).
- [14] Y.Shimizu,&M.Egashira,Basic aspects and challenges of semiconductors gas sensors.Mrs Bulletin,24(6),pp.18-24,(1999).
- [15] S.K.Joshi,T.Tsurata,Rao C.M.R.,nagakura S. ,New Materials, Narosa Publishing House,(1992).
- [16] S.P.Yawale, S.V.Pakade, "D.C.conductivity and hopping mechanism in Bi₂O₃-B₂O₃ glasses", J.Mater.Sci. Volume 28, pp.5451-5455, (1993).
- [17] H.Bai,G.Shi,Gas sensors based on conducting polymers, Sensors (Rev)7, pp.267-307,(2007).

Copper Oxide Nanoparticles for Solar Cell Application

Ambika P. Anbhore*, Suraj Tayade, Sandeep A. Waghuley

Post Graduate Department of Physics, Sant Gadge Baba Amravati University,
Amravati, India, 444 602.

*Corresponding author email: anbhoreambika91@gmail.com, sandeepwaghuley@sgbau.ac.in

Abstract:

Nanoparticles are becoming an increasingly important aspect of the technological infrastructure of today. Copper oxide nanoparticles are extremely useful, as well as their application has grown across a wide variety of fields thanks to their adaptability. In this review, we present a variety of techniques for synthesizing copper oxide nanoparticles. Due to their electric, catalytic, photonic, optical, as well as antibacterial features, copper oxide nanoparticles have garnered considerable attention. In recent years, the utilization of nano-crystalline semiconductor particles has increased due to their elevated ratio of surface area to volume as well as distinctive photovoltaic features.

Keywords: Copper oxide; nanoparticles; Solar cell.

Introduction:

People require energy in large quantities for their survival and growth. Energy is needed for people's lives and progress in large quantities. The use of solar cell energy is growing in importance as a future energy-generating technology. The photovoltaic effect, first detected by Becquerel in 1839, which converts solar energy into electricity in semiconductors. Valence electrons in atoms receive energy from sunlight, which allows them to transition between the valence and conduction bands, resulting in the production of electricity. [1]. Turn into Long-term interests will include growing ease, high productivity, and clean sunlight-based vitality enhancements. One of the most practical sources of energy in contemporary life, solar energy may be immediately converted into electricity via solar cells. Applications for solar cells are affordable, enabling improved energy conversion efficiency at a reduced cost. [2].

Copper oxide is a compound from two elements copper and oxygen, which are block d and block p elements in periodic table respectively. In a crystal copper ion is coordinated by four oxygen ions. Copper (Cu) and copper oxide (Cu₂O) nanoparticles have attracted considerable attention because copper is one of the most important in modern technologies and is readily available[3]. Because of its superior optical, electrical, physical, and magnetic properties, copper oxide (CuO) is being considered as a promising p-type semiconductor. CuO has a 1.2 eV narrow band gap and is widely employed in a variety of applications, including field emission, gas sensor, solar energy conversion, and catalysis. Nonetheless, these unique characteristics can be enhanced through synthesis in CuO nanostructures, which exhibit superior performance in comparison to their bulk counterparts. CuO is manufactured in a variety of nanostructures, including nanowire, nanorod, nano needle, nano-flower, and nanoparticle. CuO nanoparticles of various sizes and shapes have been produced over the years using a variety of techniques, including thermal oxidation, sonochemical synthesis, combustion, and rapid precipitation. Among these processes, precipitation method is a facile way which attracts considerable interest in industries because of low energy and temperature, inexpensive and cost-effective approach for large scale production and good yield [4].

Synthesis Methods:

Chemical Preparation: CuO nanoparticles are precipitated from a solution of copper precursor and a strong base. Or involves the addition of an alkaline agent to copper precursor solution, leading to the precipitation of CuO nanoparticles, followed by washing, drying and calcinations.

Hydrothermal Synthesis: High temperature and high pressure are used to create CuO nanoparticles.

Sol-Gel Method: CuO nanoparticles are prepared from a sol-gel solution followed by a thermal (heated) treatment.

Electrochemical Synthesis: CuO nanoparticles are electrodeposited by applying a voltage to a copper solution.

Green Synthesis: Natural products or plants extracts are used as reducing agents to synthesize CuO nanoparticles.

Thermal decomposition: Involves the decomposition of precursor compounds at elevated temperature to yield CuO nanoparticles, often with control over size and morphology.[5]

Applications:

The use of CuO nanoparticles in solar cells has a number of advantages, the main one being an increase in the overall effectiveness and performance of photovoltaic systems.

Enhanced Light Absorption: CuO nanoparticles improve light absorption in the visible and near-infrared spectrums, which helps solar cells absorb more sunlight and increase the rate at which photons convert to electrons.

Increased Photocurrent Generation: CuO nanoparticles when used as light absorbing materials or sensitizers in solar cells, can enhance the generation of photocurrent. This results in higher short-circuit current (I_{sc}), a crucial parameter for solar cell efficiency.

Improved Charge Separation and Transport: CuO nanoparticles can facilitate efficient charge separation and transport in solar cells. Their electronic properties allow for effective electron hole pair separation, reducing recombination losses and enhancing the fill factor (FF) of the solar cell.

Stability and Longevity: CuO nanoparticles in solar cells enhance stability and reliability, reducing maintenance requirements when properly engineered, contributing to the long-term reliability of solar cell devices.

Low- Cost Manufacturing: The synthesis of CuO nanoparticles is relatively cost-effective, which can make them a valuable resource for reducing the production costs of solar cells. This can potentially lead to more affordable solar energy solutions.

Dye- Sensitized Solar Cells (DSSCs): CuO nanoparticles are utilized in dye-sensitive solar cells (DSSCs) as part of the photo anode, serving as electron transport materials, thereby enhancing their overall efficiency.

Perovskite Solar Cells: Depending on their function in hole-blocking layers or electron transport, CuO nanoparticles can improve the stability and efficiency of perovskite solar cells.

Environmental Considerations: Because CuO nanoparticles are produced in an environmentally acceptable manner and contribute to the creation of clean, renewable energy, they are advantageous for the environment when used in solar cells.[6]

Conclusions:

Several research papers on the subject of CuO nanoparticle application in solar cells were examined for this review report. Chemical precipitation, sol-gel, hydrothermal, electrochemical, thermal decomposition, green, and other synthesis techniques are some of the primary methods used to prepare these nanoparticles. CuO nanoparticles may be the ideal choice for solar cell applications because of their exceptional purity and rapid reaction time.

References:

- [1] Tomaa, G. A., Alkaabi, Z. K., & Mohammed, M. S. (2022). Synthesis and Characterization of Copper Oxide Nanoparticles for Perovskite Solar Cell Applications. *NeuroQuantology*, 20(4), 382-388.
- [2] Aboud, N. A. A., Alkayat, W. M., Hussain, D. H., & Rheima, A. M. (2020, November). A comparative study of ZnO, CuO and a binary mixture of ZnO_{0.5}-CuO_{0.5} with nano-dye on the efficiency of the dye-sensitized solar cell. In *Journal of Physics: Conference Series* (Vol. 1664, No. 1, p. 012094). IOP Publishing.
- [3] Guajardo-Pacheco, M. J., Morales-Sánchez, J. E., González-Hernández, J., & Ruiz, F. (2010). Synthesis of copper nanoparticles using soybeans as a chelant agent. *Materials letters*, 64(12), 1361-1364.
- [4] Phiwdang, K., Suphankij, S., Mekprasart, W., & Pecharapa, W. (2013). Synthesis of CuO nanoparticles by precipitation method using different precursors. *Energy procedia*, 34, 740-745.
- [5] Satari, C., Sidqi, R. S., Putra, F., Putri, S. R., & Nandiyanto, A. B. D. (2021). Literature review: synthesis of CuO (Copper Oxide) nanoparticles for thermal energy storage.
- [6] Zhang, Q., Zhang, K., Xu, D., Yang, G., Huang, H., Nie, F., ... & Yang, S. (2014). CuO nanostructures: synthesis, characterization, growth mechanisms, fundamental properties, and applications. *Progress in Materials Science*, 60, 208-337.

A Comprehensive Review on the Synthesis of Semiconductor Nanomaterials and Their Diverse Applications

Ranjana Wakade^a, P.P. Nalawade^{*b}

^a Department of Physics, PRMITR College, Badnera-Amravati, Maharashtra, India.

^b Department of Chemistry, Vidya Bharati Mahavidyalaya, Amravati, Maharashtra, India

Abstract:

This comprehensive review focused on the synthesis of semiconductor nanomaterials and their wide-ranging applications. The synthesis methods, including wet-chemical approaches and carbon-based nanomaterials, are explored in-depth. Notably, the review delves into the promising avenues offered by wet-chemical methods, emphasizing their role in ongoing research. Carbon-based nanomaterials, especially graphene quantum dots, are highlighted for their significant impact on contemporary technology platforms.

The review encompasses a diverse array of semiconductor nanomaterials, with a particular emphasis on their properties, synthesis techniques, and characterization methods. Additionally, the importance of semiconductors in various applications is underscored, showcasing their vital role in fields such as solar cells.

In conclusion, this comprehensive review amalgamates insights from multiple scholarly sources, providing a holistic understanding of the synthesis techniques employed for semiconductor nanomaterials and their applications.

Keywords: Nanotechnology, solar cell, quantum size effect, hydrogen production.

Introduction:

Nanotechnology, a groundbreaking field, explores the manipulation of matter at the nanoscale to unlock novel properties and applications. In this realm, semiconductor nanoparticles play a pivotal role, offering unique characteristics that hold immense promise for diverse applications. The synthesis, characterization, and use of semiconductor nanoparticles—which are essential to a number of emerging technologies—have attracted a lot of attention recently. Due to their enormous surface area or quantum size effect, semiconductor materials exhibit unique features when their size is decreased to the nanoscale, resulting in significant changes to their physical and chemical properties. It is possible to modify the semiconductor's optical characteristics, such as its refractive index and absorption coefficient, as well as its conductivity.

At the core of nanotechnology is the precise synthesis of semiconductor nanoparticles. Methods like colloidal synthesis, chemical routes, and physical deposition are employed to engineer nanoparticles with controlled size and shape. Understanding these nanoparticles necessitates advanced characterization techniques like spectroscopy and microscopy. These methods unravel structural and optical properties, crucial for harnessing their full potential.

Semiconductor nanoparticles find applications across various nanotechnological domains, from solar cells to biosensors. Their size-dependent properties make them ideal candidates for innovations in electronics, medicine, and energy.

In this context, the exploration of semiconductor nanoparticles within the broader spectrum of nanotechnology opens avenues for revolutionary advancements, marking the intersection of precision engineering and cutting-edge applications.

Methodology:

Reliable resources, including ScienceDirect and IOP Science, were used to get information about artificial intelligence techniques and how they were categorized into top-down and bottom-up approaches. The synthesis techniques were thoroughly examined, taking into account both conventional and novel ways, with an emphasis on the mechanics of growth from

molten metal droplets and molecular precursors. The methodology encompassed a thorough exposition of the diverse domains in which semiconductor nanoparticles find application, an investigation of the possible influence of these nanoparticles on technology and industry, and citation of pertinent works.

Semiconductor nanoparticles are crucial in various technological applications, and their synthesis involves several methods. Here's an overview:

1. Wet Chemical Methods:

Wet chemical synthesis, also known as solution processing, is an accessible and powerful method for synthesizing nanomaterials, where nanoparticles are generated in a solution. It represents a bottom-up strategy for nanomaterial fabrication, assembling nanoparticles from fundamental building blocks. This includes drop casting the wet solution for further processing. Wet chemical synthesis is a versatile approach for producing semiconductor nanoparticles. This method involves chemical reactions of precursor species in a solution to create nucleation and subsequent formation of nanomaterials.

The wet-chemical synthesis of semiconductor nanomaterials allows for the creation of epitaxial heterostructures, providing applications in various fields. Functional characterization of two mesoporous carbonaceous nanomaterials that demonstrate excellent sodium-ion storage performance and oxygen reduction reactivity, respectively

Wet chemical synthesis is recognized for its versatility, accessibility, and high-yield production of nanomaterials. This method is particularly promising for mass production of nanomaterials. Kalam et. al. synthesized Gadolinium doped ZnO nanomaterials using the modified-solvothermal method to studied the effect of gadolinium on the structural, morphological, and optical properties Okoye et al. synthesized doped and undoped CuO and Cu₂O nanomaterials for studding their antibacterial properties against gram positive and negative bacteria.

The pathways of wet chemical synthesis provide a simple means of producing colloidal solutions with great repeatability and a wide range of particle sizes on the gram scale. Several types of nanoparticles have been successfully produced using the following wet chemical methods:

2. Solvothermal/hydrothermal

The solvothermal process is becoming more and more popular in nanotechnology as a unique way to create highly functionalized materials for use in molecular devices, sensors, separation and catalysis, and spintronics. "A chemical reaction in a closed system in the presence of a solvent (aqueous and non-aqueous solution) at a temperature higher than that of such a solvent's boiling point" is the definition of the solvothermal process. As a result, significant pressures are involved in solvothermal processes. The chosen temperature (sub- or supercritical domains) is determined by the reaction needed to produce the desired material in the process at hand.

Talebi et shown solvothermal synthesis of CMTS quaternary semiconductor nanoparticles with a symmetric kesterite structure to investigate the role of the autoclave filling factor. Aher et al synthesized ZrBi₂Se₆ Nanoflowers using solvothermal method to study their structural and optical properties for a next-generation semiconductor alloy material in optoelectronic applications.

3. Sol-Gel

The late 1800s witnessed the invention of the term "sol gel." The low temperature methods usually used inorganic precursors and can manufacture ceramics and glasses with more uniformity and purity than high temperature conventional processes.

The ability to generate compositions not possible with traditional procedures and the fact that the mixing level of the solution is kept in the final result, frequently down to the molecular scale, are the two most alluring aspects of the sol gel process. Understanding sol-gel processes has become crucial to interdisciplinary research in fields such as physics, chemistry, biology, biotechnology, biochemistry, electronics, and associated engineering departments due to the

possibility for creating a wide range of novel materials. Batur et al synthesized highly efficient lanthanum-alloyed activated carbon-supported cadmium sulfide as a promising semiconductor nanomaterial for solar cell using sol-gel method. Synthesis and magnetic characterization of Spinel ferrites MFe_2O_4 ($M = Ni, Co, Zn$ and Cu) via chemical coprecipitation method. Kanwal et al demonstrated room-temperature ferromagnetism in Mn-doped ZnO nanoparticles synthesized by the Sol-Gel method.

4. Colloidal Nanoparticle Synthesis: Traditional wet chemistry methods are employed for colloidal nanoparticle synthesis, where particles are generated in a solution. This is a widely used method for semiconductor nanoparticle synthesis.

Horani et al synthesized various metal chalcogenide nanostructures of 1D, 2D, and 3D nanocrystals (NCs), including branched nanostructures (BNSs) of nanoflowers, tetrapods, octopods, nanourchins using colloidal synthesis methods.

Wang et al demonstrate a complete Colloidal Synthesis of Cu_2SnSe_3 Nanocrystals with Crystal Phase and Shape Control

In summary, wet chemical synthesis as well as other well-known methods offers a promising avenue for the controlled and scalable synthesis of semiconductor nanoparticles, catering to diverse applications in materials science.

Application of Semiconductor nanomaterials

When compared to their typical bulk equivalents and molecular materials, semiconductor nanostructures exhibit intriguing physical and chemical features as well as practical capabilities. Among these materials' most appealing qualities are their processability, surface functionality, strong chemical and photobleaching stability, continuous absorption bands, narrow and intense emission spectra, and surface functionality. A vast amount of literature on the production of semiconductor nanoparticles reflects the evolution of "nanochemistry". For example, the optical characteristics of semiconductor nanoparticles are significantly altered by the spatial quantum confinement effect. Its optical and surface properties are significantly influenced by the semiconductor's very high dispersity (high surface-to-volume ratio), which is a result of both its physical and chemical features. As a result, semiconductor nanomaterials have been the focus of research for about 20 years and have attracted significant interest in research and applications in diverse disciplines such as solid-state physics, inorganic chemistry, physical chemistry, colloid chemistry, materials science, and recently biological sciences, medical sciences, engineering, and interdisciplinary fields. Among the unique properties of nanomaterials, the movement of electrons and holes in semiconductor nanomaterials is primarily governed by the well-known quantum confinement, and the transport properties related to phonons and photons are largely affected by the size and geometry of the materials. For various applications of interest, parameters like size, shape, and surface characteristics can be changed to influence their properties. In research and applications in emerging technologies like nanoelectronics, nanophotonics, energy conversion, non-linear optics, miniaturized sensors and IMAG devices, solar cells, catalysis, detectors, photography, biomedicine, etc., these novel properties of semiconductor nanomaterials have drawn a lot of attention. The use of semiconductor nanoparticles in the fields of medicine and catalysis is covered in this section.

1. Semiconducting Nanomaterials for the Production of Hydrogen

Hydrogen (H_2) is widely regarded as the clean energy carrier of the future for a variety of uses, including stationary power generation, home heating, and ecologically friendly vehicles. Because it is based on photon (or solar) energy, a clean, endless source of energy, and mostly uses water, a renewable resource, photocatalytic hydrogen production from water is one of the most promising techniques. It is also an environmentally safe technology that produces no pollutants or unwanted byproducts. The photochemical transformation of solar radiation into hydrogen, a source of energy that can be stored, enables one to address the sporadic nature and seasonal fluctuations of solar radiation. On the other hand, it needs a photocatalyst with

appropriate band edges, chemical stability, and resistance to corrosion. The process of producing H₂ by photocatalysis is primarily controlled by the structural and electrical characteristics of semiconductor photocatalysts. This includes fundamental processes like photon absorption, charge separation and migration, and surface reactions. A bandgap (E_g) divides the valence band (VB) and conduction band (CB) of a semiconductor from one another. An electron, e^- , is produced in the conduction band (CB) by a photon with energy $h\nu$ equal to or greater than the bandgap energy (E_g) of semiconductor particles, leaving a hole, h^+ , in the valence band (VB). In the bulk or on the semiconductor's surface, these photogenerated electrons and holes may recombine on a time scale that is slower than the one needed for their production. Prior to recombining, electrons and holes can go to the semiconductor's surface where they can initiate reduction reactions (resulting in H₂ formation) or oxidation reactions (producing O₂). While the VB top-edge needs to be more positive than the oxidation potential of H₂O to O₂ ($E_{O_2/H_2O}=1.23$ V vs NHE at pH=0) for O₂ formation from water to occur, the CB bottom-edge needs to be more negative than the reduction potential of H⁺ to H₂ ($E_{H^+/H_2}=0$ V vs NHE at pH=0) for H₂ production to occur. According to reports, H₂ synthesis can be achieved through the intercalation of semiconductor nanoparticles like TiO₂, CdS, Cd_{0.8}Zn_{0.2}S into layered compounds like H₂Ti₄O₉, H₄Nb₆O₁₇, K₂Ti_{3.9}Nb_{0.1}O₉, HNbWO₆, HTaWO₆, HTiNbO₅, and HTiTaO₅. The growth of the nanoparticles is inhibited by the intercalation. Photogenerated electrons can be transported to the matrix layered compounds rapidly when bandgap irradiation excites these intercalated nanoparticles.

2. Silicon Semiconductor Nanomaterials and Devices

In addition to silicon wafers, which are commonly utilized, silicon nanostructures have been proposed as the fundamental building blocks for upcoming nano/microelectronic devices. A number of severe challenges arise as silicon-based complementary metal oxide semiconductor (CMOS) circuit sizes gradually shrink to 10 nm or even smaller. These challenges include how to handle device manufacturing limits, a sharp rise in cost, and changes in the working mechanism of new devices. These cause the silicon-based microelectronics sector to "bottleneck" in terms of future development, despite the fact that silicon-based nanotechnology can offer a more affordable and effective alternative. Numerous unique features of silicon nanostructures result from their size impact. Size-tunable highly-luminescent silicon nanostructures resulting from the quantum effect are a common example. Scientists have lately created a number of unique silicon-based technologies, such as highly sensitive chemical and biological sensors, high-efficiency solar cells, and light-emitting diodes, by utilizing these revolutionary features.

Conclusions:

In conclusion, this comprehensive review illuminates the intricate landscape of semiconductor nanomaterials synthesis and their versatile applications. The synthesis techniques explored, ranging from wet-chemical methods to carbon-based nanomaterials, exemplify the dynamic nature of nanomaterial research. Wet-chemical approaches, highlighted for their adaptability, present promising avenues for further exploration and advancement in nanomaterial fabrication.

The integration of insights from various sources emphasizes the significance of carbon-based nanomaterials, particularly graphene quantum dots, in shaping contemporary technological platforms. This not only showcases the rapid progress in nanomaterial science but also underscores the transformative impact of these materials on technological landscapes.

Furthermore, the review delves into the diverse applications of semiconductor nanomaterials, with a special focus on their importance in solar cells and other innovative fields. The multifaceted nature of semiconductors in different applications highlights their pivotal role in advancing technological solutions.

In essence, this review serves as a valuable resource, offering a holistic understanding of the synthesis methodologies employed for semiconductor nanomaterials and providing insights into their broad spectrum of applications.

References:

1. "Applications of Nanotechnology | National Nanotechnology Initiative," accessed January 30, 2024, <https://www.nano.gov/about-nanotechnology/applications-nanotechnology>.
2. Augustine D. Terna et al., "The Future of Semiconductors Nanoparticles: Synthesis, Properties and Applications," *Materials Science and Engineering: B* 272 (October 1, 2021): 115363, <https://doi.org/10.1016/j.mseb.2021.115363>.
3. Sagadevan Suresh, "Semiconductor Nanomaterials, Methods and Applications: A Review," *Nanoscience and Nanotechnology* 3, no. 3 (2013): 62–74.
4. "Semiconductor Nanoparticles - an Overview | ScienceDirect Topics," accessed January 30, 2024, <https://www.sciencedirect.com/topics/materials-science/semiconductor-nanoparticles>.
5. Grégory Guisbiers, Sergio Mejía-Rosales, and Francis Leonard Deepak, "Nanomaterial Properties: Size and Shape Dependencies," *Journal of Nanomaterials* 2012 (December 30, 2012): e180976, <https://doi.org/10.1155/2012/180976>.
6. "Wet Chemical Methods | Ninithi.Com," accessed February 2, 2024, <https://ninithi.wordpress.com/wet-chemical-methods/>.
7. "Wet Chemical Synthesis - an Overview | ScienceDirect Topics," accessed February 2, 2024, <https://www.sciencedirect.com/topics/materials-science/wet-chemical-synthesis>.
8. "Wet-Chemical Synthesis and Applications of Semiconductor Nanomaterial-Based Epitaxial Heterostructures | Nano-Micro Letters," accessed February 2, 2024, <https://link.springer.com/article/10.1007/s40820-019-0317-6>.
9. "Wet Chemical Synthesis of Metal Oxide Nanoparticles: A Review - CrystEngComm (RSC Publishing)," accessed February 2, 2024, <https://pubs.rsc.org/en/content/articlelanding/2018/ce/c8ce00487k>.
10. "Solvothermal Method - an Overview | ScienceDirect Topics," accessed February 2, 2024, <https://www.sciencedirect.com/topics/chemistry/solvothermal-method>.
11. Behnam Talebi and Mehrdad Moradi, "Solvothermal Synthesis of CMTS Quaternary Semiconductor Nanoparticles with a Symmetric Kesterite Structure: The Role of the Autoclave Filling Factor," *Nano-Structures & Nano-Objects* 35 (July 1, 2023): 101008, <https://doi.org/10.1016/j.nanoso.2023.101008>.
12. {Citation}
13. Dmitry Bokov et al., "Nanomaterial by Sol-Gel Method: Synthesis and Application," *Advances in Materials Science and Engineering* 2021 (December 24, 2021): e5102014, <https://doi.org/10.1155/2021/5102014>.
14. Brinda B. Lakshmi, Peter K. Dorhout, and Charles R. Martin, "Sol-Gel Template Synthesis of Semiconductor Nanostructures," *Chemistry of Materials* 9, no. 3 (March 1, 1997): 857–62, <https://doi.org/10.1021/cm9605577>.
15. Ebru Batur et al., "High Solar Cell Efficiency of Lanthanum-Alloyed Activated Carbon-Supported Cadmium Sulfide as a Promising Semiconductor Nanomaterial," *Journal of the Australian Ceramic Society* 59, no. 1 (February 1, 2023): 9–18, <https://doi.org/10.1007/s41779-022-00809-z>.
16. "Nanoparticle Synthesis | Nanoscience Instruments," accessed February 2, 2024, <https://www.nanoscience.com/techniques/nanoparticle-synthesis/>.
17. Faris Horani et al., "Colloidal Control of Branching in Metal Chalcogenide Semiconductor Nanostructures," *The Journal of Physical Chemistry Letters* 14, no. 16 (April 27, 2023): 3794–3804, <https://doi.org/10.1021/acs.jpcl.3c00285>.
18. Wen-Tso Liu, "Nanoparticles and Their Biological and Environmental Applications," *Journal of Bioscience and Bioengineering* 102, no. 1 (July 1, 2006): 1–7, <https://doi.org/10.1263/jbb.102.1>.
19. Olusegun G. Fawole, X. -M. Cai, and A. R. MacKenzie, "Gas Flaring and Resultant Air Pollution: A Review Focusing on Black Carbon," *Environmental Pollution* 216 (September 1, 2016): 182–97, <https://doi.org/10.1016/j.envpol.2016.05.075>; Xiao Huang, Freddy Boey, and Hua Zhang, "A Brief Review on Graphene-Nanoparticle Composites," *COSMOS* 06, no. 02 (December 2010): 159–66, <https://doi.org/10.1142/S0219607710000607>.
20. P. Geetha et al., "Green Synthesis and Characterization of Alginate Nanoparticles and Its Role as a Biosorbent for Cr(VI) Ions," *Journal of Molecular Structure* 1105 (February 5, 2016): 54–60, <https://doi.org/10.1016/j.molstruc.2015.10.022>.
21. Jejenija Osuntokun and Peter A. Ajibade, "Morphology and Thermal Studies of Zinc Sulfide and Cadmium Sulfide Nanoparticles in Polyvinyl Alcohol Matrix," *Physica B: Condensed Matter* 496 (September 1, 2016): 106–12, <https://doi.org/10.1016/j.physb.2016.05.024>.
22. Katarzyna Tyszczyk-Rotko, Ilona Sadok, and Mariusz Barczak, "Thiol-Functionalized Polysiloxanes Modified by Lead Nanoparticles: Synthesis, Characterization and Application for Determination of Trace Concentrations of Mercury(II)," *Microporous and Mesoporous Materials* 230 (August 1, 2016): 109–17, <https://doi.org/10.1016/j.micromeso.2016.04.043>.

Frontier Developments in Optical Material: A Review

R.A. Gandhare, A.R. Kadu, J. T. Ingle

Luminescence & Optical material Research Lab,

Department of Physics & Electronics, Government Vidarbha Institute of Science and Humanities, Amravati,
Maharashtra, India

Corresponding author-inglejt2013@gmail.com

Abstract

The current era of optoelectronics devices has almost taken over the conventional semiconductor based light and display items due to its promising features. Light emissive devices technology is one of the most crucial inventions that have been developed to visualize data and pictures in both 3D compact forms. Phosphor material which are light energy converter being useful tools in many areas such as wide range of light emission for lighting (LED, OLEDs), Display and plant cultivations, phototherapy etc.

Organic light emitting diodes (OLEDs), the phosphor converted lights devices have gained a lot of attention throughout the world among research community and industries. The promising features of these light emissive devices are making it most demanding forthcoming luminescent nurture display, light treatment technology because of low cost, easy fabrication at lower temperature and mechanical flexibility compared to the conventional light sources. It is therefore necessary to study the recent advancement in the field of the phosphor materials in order to demonstrate its commitment towards the enhanced optical performance features in the designing and application in these devices of display devices.

In the present paper a concise review on the recent advancement in the phosphors used in various device structures, color generation techniques, suitable materials and efficiency enhancement methods are under taken; complete study and precise descriptions have been presented.

Keywords- Luminescence, Phosphor, Display.

Introduction

The optical materials such as OLED, Phosphors, are the assets "The 21st century is seeing a big revolution in the way information is displayed electronically." Such a short and simple sentence gives us a lot of information that needs to be considered afterward.

Over the last few decades, scientists have made an effort to develop in the field of OLEDs, WLEDs, Photo therapy lamp, Plant cultivation light, are the emerging trend by various researchers time to time [1-6].

Review of Literature:

Sr. No	Paper matrix	Author (s)	Focus of the paper	Key points in coverage	Synthesis method	Parameters analyzed	Research gaps
1	Jornal of luminescence 226 (2020) 117426	Shijie Qiu et al.	Red emitting phosphor $K_2SiF_6:Mn^{4+}$: controlled synthesis, growth mechanism, and	White LED emitting $K_2SiF_6:Mn^{4+}$ phosphor Evolving Morphology.	Two – step chemical coprecipitation	High crystallinity with regular octahedron center site at 5 to 10 nm (micro meter).	Adjusting particle morphology enables to improve the luminescent properties by

			shape dependent luminescence properties.		method.	PLE: λ_{ex} -330nm PL: λ_{em} -681nm	dynamic strategy and W-LED operation stability.
2	Molecular & Bio-molecular spectroscopy 240 (2020) 118567	Ge Zhang et al.	Synthesis and luminescence properties of a novel deep red phosphor $\text{Li}_2\text{ZnTi}_3\text{O}_8:\text{Mn}^{4+}$ for plant cultivation.	$\text{Li}_2\text{ZnTi}_3\text{O}_8:\text{Mn}^{4+}$ Red emitting plant cultivation.	Traditional high-temperature solid-state reaction	PLE: spectrum between 250nm & 550nm four Gaussian peaks centering at – 315nm, 355nm, Emission peak 681nm, 697nm	The $\text{Li}_2\text{ZnTi}_3\text{O}_8:0.3 \text{ Mn}^{4+}$ red phosphor can be used as plant cultivation light emitting phosphors.
3	AIP conference proceedings 2104, 020036 (2019)	I.H. Phadade et al.	One step combustion synthesis and photoluminescence of red emitting phosphor $\text{Y}_4\text{Al}_2\text{O}_9:\text{Eu}^{3+}$	Photoluminescence of Red emitting phosphor $\text{Y}_4\text{Al}_2\text{O}_9:\text{Eu}^{3+}$	Modified combustion route (Glycine Fuel).	PLE: λ_{ex} - 249nm PL : λ_{em} - 609nm	Phosphor can be exploited for fluorescent lamp to get better color rendering index & higher lumen output.
4	Frontiers in plant science (2022), 13,827679	Robert Khramov et al.	Luminescence of Agro textiles Based on red emitting organic Luminophore and polypropylene spunboud enhances the growth & photosynthesis of vegetable plants.	Agro textile spunboud, luminescent poly lactide, plants photobiomodulation, red organic photoluminosphore, photosynthesis.	Modulated pulse methods using a JUNIOR-PAM Fluorometer.	PLE: λ_{ex} - 410nm – 480nm PL : λ_{em} - 610nm -630nm	A novel light converting agro textile containing the PL of PLD composition was developed which opens up opportunities for the creation of biodegradable light – converting covering for green technologies
5	The journal of physical chemistry (2020) 1-18	Jaren Du. Et al.	Red – light activated Red – Emitting persistent luminescence for multicycle Bio – Imaging A case study of $\text{Ca}:\text{Eu}^{2+}, \text{Dy}^{3+}$	Persistent luminescence $\text{Ca}:\text{Eu}^{2+}$, red – light charging thermoluminescence detrapping.	Coprecipitation method	PLE: λ_{ex} - 230nm - 660nm in 10nm steps. PL : λ_{em} - 650nm	Future design & development of persistent photonic materials for promising applications & beyond.
6	Molecules (2021), 26, 6349	Leonid N. Bochkarev et al.	Red light emitting water-soluble luminescent Iridium-containing polynorbornenes : synthesis, characterization & oxygen sensing properties in Biological Tissues In Vivo	Bioimaging; oxygen sensing; tumor; iridium - containing polynorbornenes; phosphorescence lifetime imaging :	ROMP method	PLE: λ_{ex} - 260nm- 350nm PL : λ_{em} - 360nm- 550nm.	Physic chemical photophysical & biological properties of the synthesized polymers allow as to consider them as promising optical sensors of oxygen in organic

							solvent, water & in biological objects.
7	The journal of Biological and chemical luminescence, 30 : (2015) ; 182-186	Renping Cao et al.	Mg ₄ Nb ₂ O ₉ :Eu ³⁺ phosphor red emission luminescence properties	Solid state reaction, luminescence, optical properties, optical materials	Solid state reaction method in air	Mg ₄ Nb ₂ O ₉ having hexagonal crystal system.	Mg ₄ Nb ₂ O ₉ :Eu ³⁺ phosphor has good application as a red – emitting phosphor for W-LEDs under ~ 395nm NUV LED chip excitation.
8	Electron. Mater. Lett., 12, 1(2016), 171-177	Shuyun Qi et al.	Activated R ₂ Zr ₃ (MnO ₄) ₉ (R=Ld, Sm, Gd) Red Emitting phosphors of Eu ³⁺ its luminescence and Application.	White LEDs, photoluminescence, rare-earth ions, spectroscopy, fluorescent and luminescent.	Solid-state reaction.	Trigonal symmetry, morphology-a small ball – like morphology is exhibited by crystallized grains.	Excited by near-UV light. The emission intensity remained at 78%. The result is found be the fabrication W-LED's
9	Electrochemical and solid-state letters, 9(4) H22-H25 (2006)	Kyota Uheda et al.	CaAlSiN ₃ :Eu ²⁺ , for white light emitting diodes, luminescence properties of a red phosphor	warm-white light-emitting diodes,		The crystal structure of CaAlSiN ₃ :Eu ²⁺ has an orthorhombic structure with space group Cmc21	

Conclusions:

Varied aspects of optoelectronics material, with their synthesis, stability and luminescence performance for desired application have been reviewed. The review study suggest that some of potential optical material including inorganic/organic based are showing desirable characteristics for display devices are emerging technological trend in the area such as OLEDs, W LEDs, phototherapy and plant and tissue cultivation .There have also been many patents filed by big & small companies as OLED have a potential to lead in future display market.However, organic light emitting diodes have many roadblocks to be cleared. Most of them are issues related to organic, Materials that need a breakthrough in order to make stable, highly efficient device with long lifespan.

References

- [1] B. Kumar, B. K. Kaushik, Y. S. Negi, Polymer Reviews, vol. 54. no.4, pp. 33–111, 2014.
- [2] B. Kumar, B. K. Kaushik, Y. S. Negi J. Mater. Sci. Mater. Electron. 25 (1), pp. 1–30, 2014.
- [3] Xiugang Wu, Xiuqin Yan, Trends in chemistry, Vol. 5, Issue 10, pp 734-747,2023.
- [4] Quan Liu, Zhuo Chen, J. Mater. Chem. C, 10, pp. 3472-3479, 2022.
- [5] M. Nimbalkar , M.Yawalkar, N. Mahajan, S.J. Dhoble, Photodiagnosis and Photodynamic Therapy, Vol. 33,n pp.102082, 2021.
- [6] JT Ingle, AB Gawande, RP Sonekar, SK Omanwar, Yuhua Wang, Lei Zhao, Journal of alloys and compounds, Vol.585,pp.633-63.2014.

Vidya Bharati Mahavidyalaya, Amravati



Published by : SAI JYOTI PUBLICATION
Behind Chawla Sadi Center, Tin-nal Chowk,
Kasarpura, Itwari, Nagpur-440002
Phone : 9764673503, 9923593503
email : sajp10ng@gmail.com
Website : www.saijyoti.in

